Modelling of Human Control and Performance Evaluation using Artificial Neural Network and Brainwave

Keattikorn Samarnggoon

A thesis submitted in partial fulfilment of the requirement of Staffordshire University for the degree of Doctor of Philosophy

February 2016

Abstract

Conventionally, a human has to learn to operate a machine by himself / herself. Human Adaptive Mechatronics (HAM) aims to investigate a machine that has the capability to learn its operator skills in order to provide assistance and guidance appropriately. Therefore, the understanding of human behaviour during the human-machine interaction (HMI) from the machine's side is essential. The focus of this research is to propose a model of human-machine control strategy and performance evaluation from the machine's point of view. Various HAM simulation scenarios are developed for the investigations of the HMI.

The first case study that utilises the classic pendulum-driven capsule system reveals that a human can learn to control the unfamiliar system and summarise the control strategy as a set of rules. Further investigation of the case study is conducted with nine participants to explore the performance differences and control characteristics among them. High performers tend to control the pendulum at high frequency in the right portion of the angle range while the low performers perform inconsistent control behaviour. This control information is used to develop a human-machine control model by adopting an Artificial Neural Network (ANN) and 10-time-10-fold cross-validation. Two models of capsule direction and position predictions are obtained with 88.3% and 79.1% accuracies, respectively.

An Electroencephalogram (EEG) headset is integrated into the platform for monitoring brain activity during HMI. A number of preliminary studies reveal that the brain has a specific response pattern to particular stimuli compared to normal brainwaves. A novel human-machine performance evaluation based on the EEG brainwaves is developed by utilising a classical target hitting task as a case study of HMI. Six models are obtained for the evaluation of the corresponding performance aspects including the Fitts index of performance. The averaged evaluation accuracy of the models is 72.35%. However, the accuracy drops to 65.81% when the models are applied to unseen data. In general, it can be claimed that the accuracy is satisfactory since it is very challenging to evaluate the HMI performance based only on the EEG brainwave activity.

Acknowledgement

Table of Contents

List of Figures

List of Tables

Glossary

Term	Descriptions	Appearance
2D	Two dimensional	Section 2.13.5.2, 4.3.2, 5.5.2, 5.7.2, 6.6
3D	Three dimensional	Section 1.6, 2.6.2.1, 2.3.1, 2.13.5.3, 4.3.2
ABS	Anti-lock brake system	Section 1.2
AC	Accuracy	Section 2.8.3, 4.4.2.1
AE	Absolute error	Section 2.5.2
AI	Artificial intelligence	Section 2.2.1
ANN	Artificial neural network	Section 1.8, 2.9, 2.13.4.6, 2.14, 3.6, 3.7, 4.4, 4.4.1, 4.4.2.1, 4.4.2.2, 4.5, 4.6, 6.6, 7.7
API	Application programming interface	Section 3.4, 5.3, 5.4.1, 6.3, 6.7.2
AR	Autoregressive	Section 2.13.4.6
AUC	Area under a curve	Section 2.8.3, 4.4.2.1, 6.7.5.1 Appendix I.1, I.2, I.3, I.4, I.5, I.6
BCI	Brain computer interface	Section 2.13.2, 2.13.4.1, 2.13.6
CE	Constant error	Section 2.5.2
CMS	Common mode sense	Section 2.13.6
CNS	Central nervous system	Section 2.12

COE	Centre of excellence	Section 2.2.1
CSP	Common spatial pattern	Section 2.13.4.6
CSV	Comma separated value	Section 5.4.1, 5.4.2, 5.6
DOF	Degree of freedom	Section 2.4.1
DPI	Dot per inch	Section 6.4
DRL	Driven right leg	Section 2.13.6
ECG	Electrocardiography	Section 2.13.1.2
EEG	Electroencephalography	Section 1.4, 1.6, 1.8, 2.13, 2.13.1, 2.13.1.1, 2.13.1.2, 2.13.2, 2.13.3, 2.13.3.1, 2.13.4.2, 2.13.4.3, 2.13.4.4, 2.13.4.5, 2.13.4.6, 2.13.5.2, 2.13.5.3, 2.13.6, 2.14, 3.3, 3.7, 5.1, 5.2, 5.3, 5.4.1, 5.4.2, 5.4.3, 5.5.1, 5.6, 5.7.2, 5.8, 6.1, 6.3, 6.6, 6.7.2, 6.7.4.1, 6.7.4.2, 6.7.5, 6.7.6, 6.8, 7.3, 7.4, 7.7 Appendix B
EMG	Electromyography	Section 2.13.1.2
ERD	Event-related desynchronisation	Section 2.13.1.1
ERP	Event related potential	Section 2.13.3, 2.13.3.1, 2.13.4.6, 2.13.5.1, 2.13.6, 3.7, 5.4.2, 5.4.3, 5.5.1, 5.6, 5.7.1, 5.7.2, 5.8, 6.6, 6.7.4, 6.7.4.1, 6.7.4.2, 6.7.4.3, 6.7.5, 7.3
FCM	Fuzzy C-Means	Section 2.13.4.6

FFT	Fast Fourier Transform	Section 2.13.4.3, 2.13.4.6
fMRI	functional magnetic resonance imaging	Section 2.13.2
FT	Fourier transform	Section 2.13.4.3
GPA	Grading point average	Section 2.5.6
GUI	Graphic user interface	Section 1.6
HAI	Human automation interaction	Section 2.2, 2.14
HAM	Human adaptive mechatronics	Section 1.3, 1.4, 1.8, 1.8, 2.1, 2.2.1, 2.2.2, 2.7.5, 2.13.2, 2.14, 3.1, 3.4, 3.4.1, 3.8, 5.3, 5.4.1, 5.5.1, 5.6, 5.8, 6.2, Appendix A, B
HCI	Human computer interaction	Section 2.2.1, 2.7.4, 2.5.3.1, 6.1
HHMM	Hierarchy hidden Markov model	Section 2.3.1
HMI	Human machine interaction	Section 1.3, 1.4, 1.5, 2.1, 2.5.8, 2.5, 2.7.1, 2.5, 2.5.8, 2.8, 2.9, 2.14, 3.2, 3.3, 4.1, 4.5, 6.1, 6.7.6, 6.8, 7.2
HMM	Hidden Markov model	Section 2.3.1, 2.3.2, 3.6
HPI	Human performance index	Section 2.5.6
HRI	Human robot interaction	Section 1.8, 2.2.3, 2.4, 2.4.1, 2.4.2, 2.4.3.1, 2.4.3.3, 2.4.3.4, 2.7.5, 2.14

HSC	Haptic shared control	Section 1.8, 2.2.3, 2.4, 2.4.1, 2.4.2, 2.4.3.1, 2.4.3.3, 2.4.3.4, 2.7.5, 2.14
HT	Headset timeline	Section 6.3, 6.7.2
IC	Independent components	Section 6.6
ICA	Independent component analysis	Section 2.13.1.2, 2.13.3, 2.13.4.5, 5.6, 5.8, 6.6
ID	index of difficulty	Section 6.2.1
IPD	Inverted pendulum-driven	Section 2.10.1
K-means	Statistical cluster analysis	Section 2.3.1
k-NN	k-nearest neighbour	Section 2.13.4.6
LHMM	Layered hidden Markov model	Section 2.3.1
LoA	Level of automation	Section 2.4.3.2
LoHA	Level of haptic authority	Section 2.4.3.2
LW	local weight matrix for the ANN	Section 4.4.2.1, 4.4.2.2, 4.4.2.2
MAP	Maximum a Posteriori	Section 2.13.4.6
MEG	Magneto-encephalography	Section 2.13.2
MMI	Man-machine interface	Section 3.2
NES	Nintendo entertainment system	Section 2.5.6
NIRS	Optical topography	Section 2.13.2
NR	Not ready	Section 2.5.6

ODE	Ordinary differential equations	Section 3.4.1, 3.5.1
P300	Positive deflection of EEG around 300ms	Section 2.13.3.1, 2.13.4.1, 2.13.6
PARAFAC	Parallel factor analysis	Section 2.13.4.6
PC	principal component	Section 2.8.1, 6.7.5
PCA	principal component analysis	Section 2.8.1, 6.6, 6.7.5
PD	proportional-derivative	Section 2.7.2
PET	positron emission tomography	Section 2.13.2
PhD	Doctor of Philosophy	Section 1.2
PID	Proportional Integral Differential controller	Section 3.5.2, 3.5.3, 3.7, 4.3, 4.3.2, 4.4, 4.5, 7.2
PNS	Peripheral system	Section 2.12
PR	Precision-recall	Section 2.8.3, 4.4.2, 6.7.5 Appendix I.1, I.2, I.3, I.4, I.5, I.6
PSD	Power spectral density	Section 2.13.4.6
R	Ready	Section 2.5.6
ROC	receiver operating characteristic	Section 2.8.3, 3.6, 4.4.2.1, 4.5, 4.6, 6.7.5.1, 7.2 Appendix I.1, I.2, I.3, I.4, I.5, I.6
SA	Situation Awareness	Section 2.6.2.1, 2.4.3.3
SDK	Software development kit	Section 1.6
SMR	Sensorimotor rhythm	Section 6.6

SOM	Self-organized mapping	Section 2.3.2
SRK	Skill, rule, and knowledge	Section 2.5.4, 2.14, 4.5, 7.2
ST	Simulation timeline	Section 6.3, 6.7.2
STAT-PCA	Statistical principal component analysis	Section 2.13.4.6
STFT	Short time Fourier transform	Section 2.13.4.3
SVM	Support vector machine	Section 2.3.1, 2.13.4.6
TDP	Time domain parameters	Section 2.13.4.6
THT	Target hitting task	Section 6.2, 6.3, 6.4, 6.5, 6.5.3, 6.7.2
TP	Task pattern	Section 6.2.1
USAR	Urban search and rescue	Section 2.2.1, 2.2.2, 2.6.2
USB	Universal serial bus	Section 2.13.2, 5.3, 6.4
VE	Variable error	Section 2.5.2
XNA	XNA is a framework for cross-platform managed libraries for game development.	Section 1.6, 3.4.1

List of Symbols

Symbol	Description
θ	Angle
μ	Friction constant
τ	Torque
ω	Angular velocity of the pendulum
AE	Absolute error
AF3, AF4, F3, F4, F7, F8, FC5, FC6, P7, P8, O1, O2, T7, T8, CMS, DRL	The location names of the Emotiv EPOC electrodes on the scalp
b	Bias
CE	Constant error
CH4P1, CH4P2, …, CH4P9	Participant identifier used in Chapter 4

CH5P1, CH5P2	Participant identifier used in Section 5.7
DT	Duration time
F	Force
f	Friction
f_{AN}	Activation function
FN	False negative
FNR	False negative rate
FP	False positive
FPR	False positive rate
g	Earth gravity constant which is equal to 9.81 m/s^2
H	Entropy
HA	Hit accuracy
I	Information capacity
ID	Fitts index of difficulty
IP	Fitts index of performance
kD	Derivative constant
kI	Integral constant
kP	Proportional constant
L	Length of a pendulum shaft
M	A mass of the cart / capsule body

m	A mass of the ball attached to the end of pendulum shaft
MA	Movement accuracy
MP(x,y)	Mouse position
MT	Movement time
N	Noise
P	Precision
P1, P2, P3, P4	Participant identifier used in Chapter 6
PT_1 - PT_4	Point in space
RT	Reaction time
S	Signal
SEG_A	Position vector
SEG_B	Position vector
sk	Number of samples
TN	True negative
TNR	True negative rate
TOC	Trial outcome
TP	True positive
TP(x,y)	Target position
TPR	True positive rate
TT	Trial target

TW	Target width
t_x	Time at point x
T_{xy}	Time difference between point x and y
v	Velocity of capsule
VE	Variable error
X	X-axis
x	Pendulum ball position on x-axis
Y	Y-axis
y	Pendulum ball position on y-axis
Z	Neuron input vector

Chapter 1 Introduction

1.1 Background

Automated robots have been embraced unconsciously in day-to-day life. There are a growing number of intelligent domestic appliances, smart cars, prostheses, smart organs, robotic furniture, and robots for traffic monitoring that designed to improve quality of living and to make life easier [1], [2], including co-working or co-inhabiting robots in the home environment that are a promising prospect for elderly care [3].

Artificial intelligence is technologically advanced. An arm prosthesis, illustrated in Figure 1.1, is a benchmark of a novel human re-engineering, the disabled can efficiently utilise it with confident. The future of human re-engineering has been projected in [4], for instance; soft robot actuators, modular prosthesis, artificial white blood cell, printed bones, bionic lens, lab-grown liver etc. Humanoid robots in many science fiction are not so imaginative at all in the not-too-distance future.

Figure 1.1 The robot arm prosthesis [4].

In terms of developing human-friendly and safe robots, the interaction is considerable concern as humans are expected to participate in many critical applications such as medical applications or dexterous machine controls. A real benefit is to have a surgeon who holds not only knowledge but also knows how to apply a robot device that has high accuracy. Nevertheless, these robots need to interact considerately and appropriately to various types of users and must be practically adaptable according to spontaneous situations in order to achieve the overall optimum system performance.

1.2 Motivation

The author completed a BSc in Computer Engineering with the project "3D Solar System Simulator". The project and personal interests in the field of graphics programming have driven the author to game development. After several years in the game development business, the author has been recruited as a game development lecturer in the Department of Animation, College of Arts, Media and Technology, Chiang Mai University, Thailand. While being a lecturer, the author completed an MSc in Software Engineering in order to improve the knowledge in systematic software development and the MSc project was on the design aspect of computer games. The author also conducted the research in common elements in a game design and produced a conference paper which is [5]. The inspiration of [5] is the design and development of the adaptive game based on a player skill level. The adaptive gaming balances the amount of challenge to match the player skill to improve the player experience by avoiding too much boredom or anxiety. This balance would maximise the enjoyment experienced by a player. The concept of this balancing is known as 'flow', the psychology of optimal experience [6].

The nature of a lecturer career has encouraged the author to pursue further education to improve the maturity in a specific domain of knowledge. Therefore, the author has secured the offer for pursuing a Doctor of Philosophy (Ph.D.) in the United Kingdom at Staffordshire University provided by the Erasmus-Mundus Sustainable eTourism.

The connection and motivation between the previous knowledge and experiences of the author to the Ph.D. study is the adaptive manner of the software and machine intelligence. The concept of Human Adaptive Mechatronics (HAM) is similar to adaptive game development that aims to produce adaptive behaviour according to the individual human skill.

Although steady advances in technology continue to evolve a machine to become more automated, some machines still require a human for the operation and interaction. The interaction can be roughly categorised into fully manual, semi-manual, supervisory, regulatory, attached interaction etc. Despite the types of interaction, there has been an increasing improvement on the interaction ergonomics, especially in the adaptive manner. The examples of adaptive interaction come from a variety of applications including anti-locked brake (ABS) system, traction control system, car driving assistance, vehicle manipulation assistance, a computer mouse cursor aiming or snapping system, smart watch, adaptive wheelchair, adaptive prosthesis, human walking support system etc.

To provide an adaptable interactive machine, the machine is required to understand the human operator as shown in Figure 1.2. It does need to recognise the current state of the human action. It does need to know the competency of the action i.e. performance evaluation model. It does require understanding the model of the interaction.
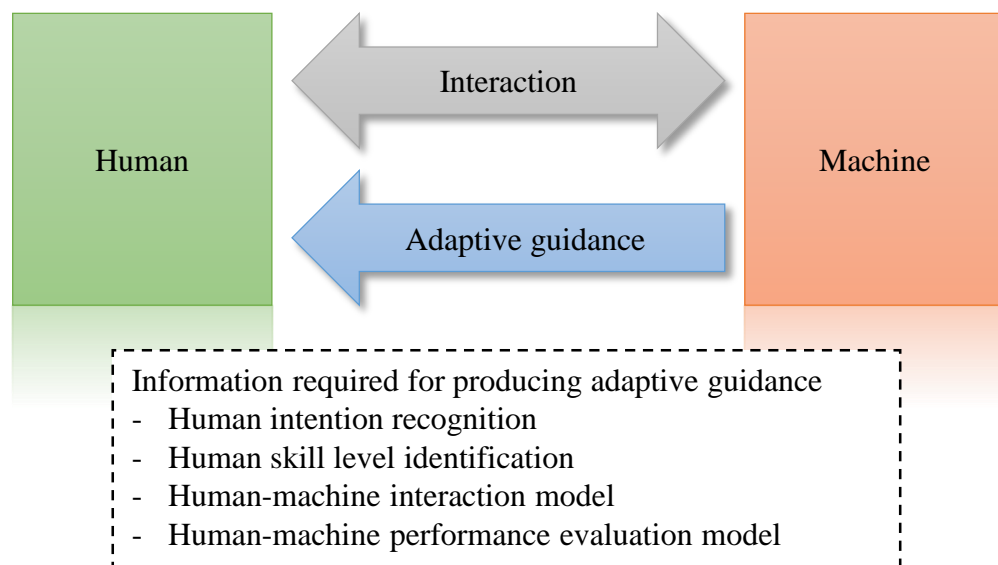
Figure 1.2 The requirements for a human-machine adaptive interaction system.

Hence, the understanding of HMI to provide the adaptive interaction is the particular interest of this research especially the modelling and performance evaluation of the interaction. Considering an example of a walking support system for an elderly or disabled person as shown in Figure 1.3, the system needs to understand the interaction behaviour of the human wearing it in order to provide the intuitive assisting interaction.

Figure 1.3 A fully lower limbs exoskeleton support system [3], [4].

1.3 Aim

The aim of this research is to investigate a Human Adaptive Mechatronics (HAM) based HMI system by focusing on the understanding of human heuristic learning, human-machine control modelling, and human-machine performance evaluation modelling from the human brainwave using Artificial Neural Network.

1.4 Objectives and deliverables

The objectives with the corresponding deliverables are summarised in Table 1.1.

Table 1.1 Research objectives and deliverables.

Objective 1. To investigate the concept, component and mechanism of the HAM particularly on the HMI and performance evaluation modelling.

Deliverable 1. The literature review and this research documentation (This Ph.D. thesis).

Objective 2. To set up a human-machine interaction environment for the investigations and data acquisitions for model developments.

Deliverable 2. A HAM simulation platform that provides the interaction environment and models a case study machine for human participants to perform a given scenario to evaluate and model performance (Chapter 3).

Objective 3. To study a human heuristic control and learning transformation according to the Rasmussen's skills, rules, and knowledge model.

Deliverable 3. The investigation on a human heuristic learning control with an unfamiliar machine system for control strategy identification and transformation into a set of rules and knowledge (Chapter 4).

Objective 4. To study human-machine control skills, and characteristics by comparing the performance outcome from a number of participants and developing a model from the control information.

Deliverable 4. The development of a model for the human-machine interaction and control information with a case study of an inverted pendulum-driven capsule system (Chapter 4).

Objective 5. To develop a model of human-machine interaction performance evaluation based on the human brainwave.

Deliverable 5. A proposed model of HMI performance evaluation that links between the control performance and the EEG brainwave. (Chapter 5, Chapter 6)

1.5 Ethical issue

This research carries out an in-depth analysis of HMI. Experiments are confidentially conducted with a number of participants in a suitable environment. Preliminarily, the participants have informed a detailed explanation about the purpose and nature of the experiment(s) and volunteered to participate. Participants have the right to end the participation at any time. Participants' personal information is recorded and treated as confidential information. A university's fast track ethical form has been submitted to and officially approved by the corresponding committee. All the relevant documents e.g. consent form template etc. can be found in the Appendix A and B.

1.6 Resources

The listings below are the resources used in this research.

- A personal computer that can support running of the interactive simulation platform in 3D.
    - Microsoft Visual Studio 2010.
    - Microsoft XNA Game Studio 4.0.
    - DigitalRune engine for graphic user interface (GUI) within the simulation.
    - A joystick control interfaces i.e. Microsoft XBOX Joystick, Logitech 3D Force Feedback.
- An Emotiv EPOC headset for the brain activity measurement (Electroencephalogram, EEG).
    - Emotiv EPOC software development kit (SDK).
- MathWorks MATLAB for data analysis.
    - EEGLAB – an open source software package for electrophysiological signal processing.
- Access to Staffordshire University's library resources.
- Access to Chiang Mai University's on-line research library resources.
- Documentation

- o Microsoft Word and Excel.

- o Zotero for reference management.

- o Apache OpenOffice Draw.

- o Adobe Photoshop and Adobe Illustrator.

- o FreeMind – an open source mind map drawing.

- A digital camera for taking photographs of devices and experiment settings.

1.7 Project plan

This research outlines a modified waterfall project plan as shown in Figure 1.4. The corresponding timeline of the project plan is shown in Table 1.2.
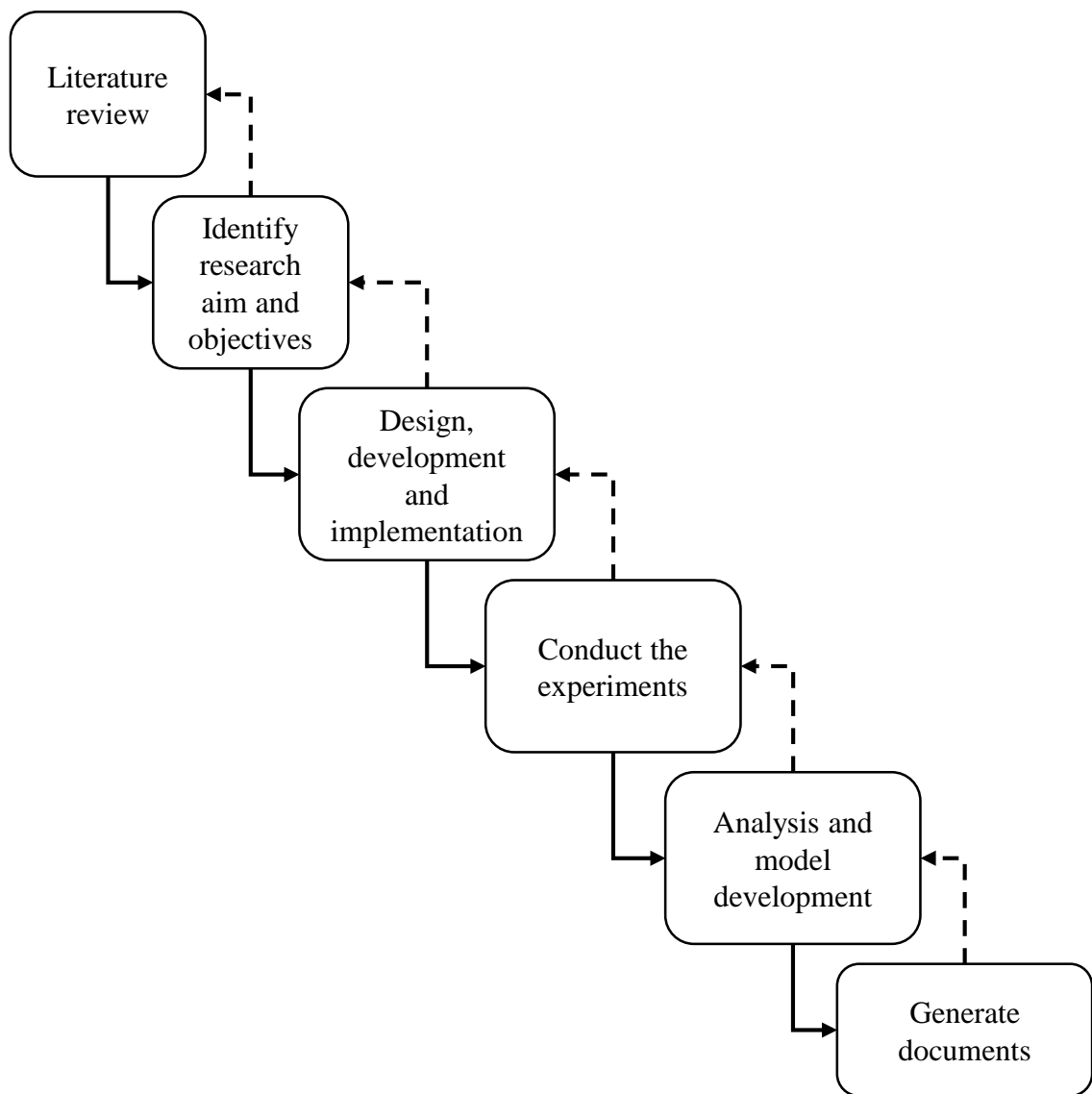
Figure 1.4 A modified waterfall project plan.

Table 1.2 A timeline of the project plan.

Task	2011	2012				2013				2014				2015			
	Q4	Q1	Q2	Q3	Q4	Q1	Q2	Q3	Q4	Q1	Q2	Q3	Q4	Q1	Q2	Q3	Q4
Literature review	▓	▓	▓	▓	▓	▓	▓	▓	▓	▓	▓	▓	▓	▓	▓	▓	▓
Identify research aim and objectives			▓	▓													
Design, development, and implementation					▓	▓	▓	▓	▓	▓	▓	▓					
Conduct the experiments						▓	▓	▓	▓	▓	▓	▓					
Analysis and model developments											▓	▓	▓	▓	▓		
Generate documents					▓	▓	▓	▓	▓	▓	▓	▓	▓	▓	▓	▓	▓

1.8 Contributions

The contributions of this thesis are listed underneath.

- A review of the human interaction with the man-made systems i.e. HAM, HRI, HSC etc. that leads to the importance of human-machine interaction performance modelling and evaluation. To develop the interaction performance model between human and machine, a review of model development approaches, perspectives, and the modelling algorithm is given. The human EEG brain activity monitoring system is reviewed in order to develop a novel model of human-machine performance evaluation based on the EEG brain activity – 1.10.

- The design, development and implementation of the human adaptive mechatronics (HAM) simulation platform to conduct the investigations on the human interaction with the case study scenarios. The design and implementation of the descriptive-predictive 10-time-10-fold cross-validation model development procedure – Chapter 3.

- The investigation of human heuristic learning that emphasises the concept of skills, rules, and knowledge (SRK). The analysis for the extension of the SRK to include wisdom into the cycle of human heuristic learning – Chapter 4.

- The analysis of human-machine control performance and model developments by applying the descriptive-predictive approach and artificial neural network (ANN) – Chapter 4.

- The studies and implementations of the HMI scenarios simultaneously with the human brainwave monitoring system that lead to the development of a novel performance evaluation models based on the human brainwave – Chapter 5, Chapter 6.

1.9 Organisation of the thesis

The thesis is organised into chapters as follows.

Chapter 2 reviews the importance of human existence in man-made systems. A human and a machine are becoming close by the advancement of innovative technology. Nevertheless, a human is still the primary entity who makes use of the machine. To develop the HMI and performance evaluation model, the review related to human skill, performance, and machine are given. Moreover, a deep understanding of the HMI behaviour can be gained by the investigation of the human brain activity from the Electroencephalography (EEG) system. Many investigations related to EEG are reviewed with the primary objective of modelling an HMI performance evaluation based on the brain activity.

Chapter 3 gives the focus and methodology adopted in this research. The HAM platform, design, and implementation of the investigations are described. The model development procedure is employed in the latter chapters for the development of human-machine control model and the six EEG-based human-machine performance evaluation models.

Chapter 4 primarily provides the investigations on the human-machine heuristic learning, skill acquisition, rule formulation, performance differences, and control model development.

Chapter 5 presents the preliminary studies on the EEG brain monitoring based human-machine interaction.

Chapter 6 provides the development of a novel EEG-based human-machine performance evaluation models.

Chapter 7 draws conclusions from each of the investigations, states the research limitation, and suggests possible future works after the completion.

1.10 List of publications

- K. Samarnggoon, S. Cang, H. Yu, M. S. Hasan, and T. Flämig, "Human Skill Performance to Control an Underactuated Pendulum-Driven Capsule System," in *Control (CONTROL), 2014 UKACC International Conference on*, Loughborough, United Kingdom, 2014, pp. 731–736 [7].

- K. Samarnggoon and H. Yu, "Real-time Virtual Simulation of an Underactuated Pendulum-Driven Capsule System," in *Control (CONTROL), 2012 UKACC International Conference on*, Cardiff, United Kingdom, 2012, vol. 2012, pp. 568–573 [8].

Chapter 2 Literature review

2.1 Introduction

This chapter reviews related literature rooted from the concept of HAM by focusing on the human interaction, learning and modelling of the human behaviour in a system. A human is the most difficult part to understand because of the unpredictable behaviour. Therefore, several aspects and research projects relating to the human interaction with a system are carried out in order to identify the approach and the model development methodology aimed at understanding HMI. Moreover, the innovation of the affordable human brainwave monitoring system has made the possibility to study the human interaction behaviour with a machine system from the brainwave aspect. The related literature is given in the latter part of the chapter.

Figure 2.1 shows a mind map of the literature review in this chapter. The review starts with the motivation mentioned in Section 1.2 i.e. a human-machine adaptive interaction. A generic view of the interaction between a human and a man-made system is introduced in Section 2.2 to support the reason for the emergence of many HMI research fields. However, a HAM is the root motivation of this research because of its attractive concept. The literature is reviewed and categorised by the three key components of the HAM based HMI concept as shown in Figure 2.1. Then, the review is extended to the other relevant areas that are required to fulfil the objectives and the aim of this research.
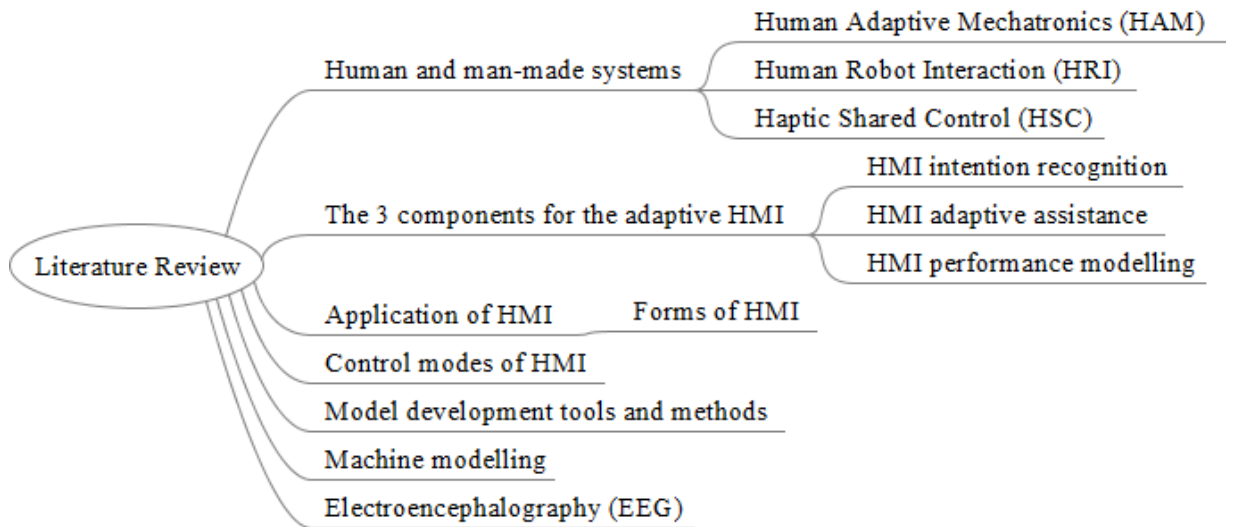
Figure 2.1 A mind map of the literature review.

The review extends to the areas of the application that would benefit from the improvement of the adaptive HMI in various forms of interaction i.e. the Forms of HMI. A review of control modes of the HMI provides various types of machine control activity that can be located and can be studied for the improvement of HMI e.g. pursuit tracking, balancing control, target hitting control etc. Furthermore, the review covers the model development, machine modelling, and the human EEG brainwaves monitoring that are applied in this research.

2.2 Human and man-made systems

Modern concepts such as HAI [9], HMI [10], HRI [11], and HAM [12] regularly use the word 'human', additionally with other words like 'machine', 'automation', 'robot', and 'mechatronics' to refer to a human in relation to a man-made system. These additional words are defined with some subtly different meanings by the Oxford dictionary [13] as follows.

Machine: (noun)   *"An apparatus using mechanical power and having several parts, each with a definite function and together performing a particular task."*

Automation: (noun)   *"The use or introduction of automatic equipment in a manufacturing or other process or facility."*

Robot: (noun)	*"A machine capable of carrying out a complex series of actions automatically, especially one programmable by a computer."*
Mechatronics (noun)	*"Technology combining electronics and mechanical engineering."*

Despite the subtle different meaning of these additional words, the HRI, HMI, HAI, and HAM concepts always strive for a common goal i.e. the interaction between human and a man-made system.

To avoid ambiguity, the term human-machine interaction (HMI) will be used to refer to the human interaction with a man-made system. Otherwise, a specific term will be clearly stated.

2.2.1 Human adaptive mechatronics (HAM)

A human adaptive mechatronics (HAM) is a concept that originated from the Centre of Excellence (COE) Tokyo Denki University Japan in 2005 [14]. In a conventional human-machine system, learning and skill expertise are the sole responsibility of a human. A HAM introduces an intelligent concept of adaptive capability that assists operators to learn and improve, based on individual skill level and environment to achieve the optimum system performance [12], [15]–[20].

The holistic view of HAM as depicted in Figure 2.2, demonstrates the major disciplines and their relationships required to convey the HAM ideas. Each pair of the disciplines, including 'human', 'mechatronics', 'intelligent control', and 'computer network', forms cross-related disciplines that require further study to understand the collaboration and application between them. Human and mechatronics form a human-machine system or human-in-the-loop system. Human-computer interaction (HCI) is established between human and computer network. The mechatronics controlled by intelligence makes an ordinary machine into a robotic one. In an attempt to mimic human intelligence and knowledge, cognitive science is applied to machine intelligence. The dashed line between mechatronics and computer network composes the network facility for the machine to be monitored and controlled over the network systems.

As a human-in-the-loop machine system, the human is considered the main beneficiary during operation. Mechatronics, itself, is a relatively vast research area including many system-

modelling studies from a simple pendulum to a complicated vehicular model. Intelligence and control mechanisms function as a brain behind all the system. Computer and network participate in remote controlling over an underlying infrastructure, e.g. urban search and rescue (USAR), supervisory and monitoring, off-site control, remote laboratory etc.
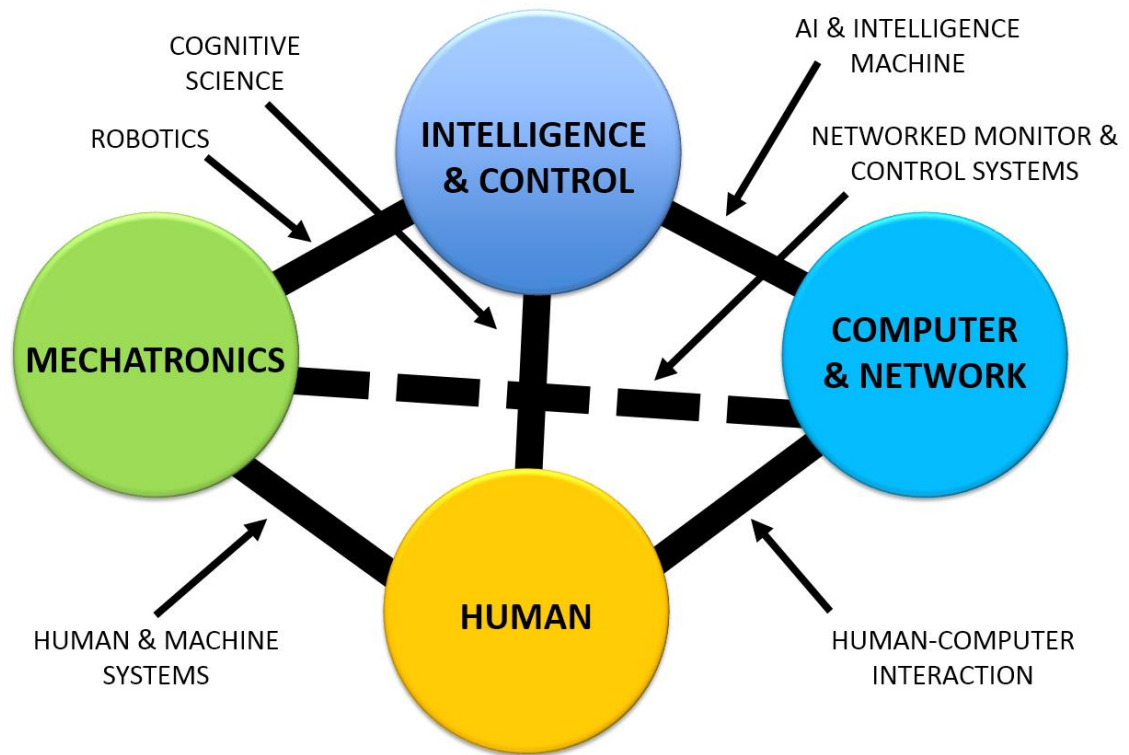
Figure 2.2 The holistic view of HAM multi-disciplinary [19].

2.2.2 Human-robot interaction (HRI)

Human-robot interaction (HRI) is a multidisciplinary research for investigating the interaction between a human and a robot. Similarly to the HAM, the HRI incorporates multiple disciplines such as engineering, computer science, artificial intelligence, robotics, social science, and humanities [11]. The challenging issues of HRI are the intuitive and safe interaction between these pairs of the interacting agent; human and robot, robot and robot, or both pairs simultaneously [21]–[24]. Furthermore, the survey in [25] shows a growing trend towards the interaction in dynamic environments rather than a stationary one. The design of HRI needs to be suitable for the particular applications. For examples, an autonomous robot should take a

little effort to operate. In contrast with a robot in a serious application such as USAR, medical surgery application, or nuclear handling etc., the interaction should be designed by focusing on speed, efficiency, accuracy, reliability etc. Furthermore, a robot task may be dissimilar to human's task for the same type of operation. For example, a vacuum cleaner robot needs a clear space to operate properly whereas a human can do the same operation without the space clearance [26].

2.2.3 Haptic shared control (HSC)

Haptic shared control (HSC) is an approach that combines a force feedback device to an active assistive system in a shared control manner [27]. The shared control between human and machine means that the control authority could be taken from both the operator and machine depended on a certain circumstance. As illustrated in Figure 2.3, in one particular task, the operator exert force F_O to a special designed haptic device, concurrently the device estimates and balances active force feedback back to the operator to assist with the operation. For instance, a force feedback steering wheel for a lane-keeping task renders assistance to a driver based on the error of a car heading direction. This seamless assistance has managed to reduce the effort for steering, stress, attention demand, and improve safety and accuracy of the driving by 16% [28].
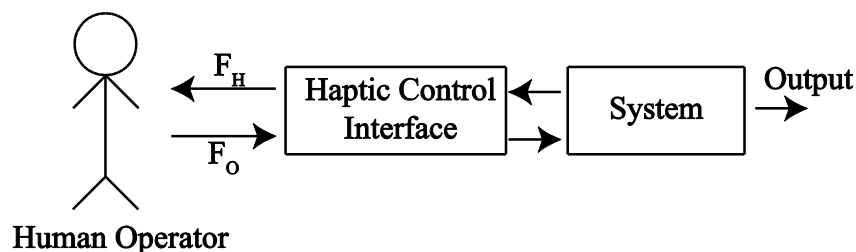
Figure 2.3 A haptic shared control approach.

2.2.4 The evaluation of the HMI

Section 2.2 introduces some concepts that aim to improve the quality of HMI using different approaches. An HSC focuses on utilising a haptic device that actively assists a human during HMI. An HRI gives a top view and general idea of the interaction improvement and awareness

between a human and a machine. A HAM based HMI aims to provide a machine adaptability in active, passive or in a combined manner. However, in practical, there are three key components in order to realise the HAM conceptual machine i.e. intention recognition, performance evaluation and adaptive assistance. The following sections review literature that corresponded to the three components i.e. Section 2.3 HMI intention recognition, Section 2.4 HMI adaptive assistance and Section 2.5 HMI performance modelling.

2.3 HMI intention recognition

Since HMI is a human-in-the-loop system, the intention of the interaction from a human is one of the important components in achieving the improvement of HMI. For a machine to assist the human operator appropriately, the recognition of a human's intentions is considered necessary. Although a human behavioural intention is rather difficult to predict, it is possible to recognise and estimate the HMI intention from a goal-oriented task by applying a pattern recognition technique.

An example of the pattern recognition applied to decode and estimate a covert human intention is studied in neuroscience [29]–[32]. The use of spatial information from various section shows the improvement in the recognition accuracy compared to the usage of a single spatial information. This improvement conforms to the fact that the human brain utilises several sections cooperatively to perform a task. Another interesting human intention study shows that the behavioural intention is influenced by a human's personal experiences [33]. There are convincing pieces of evidence that the human brain simulates internal motions after the observation of biological motions. Consequently, the subsequent intentions of actions are the result of the internal imagination of motions.

2.3.1 Hidden Markov Model based intention recognition

A Hidden Markov Model (HMM) has been applied to discriminate the state of human intentions in order to improve the HMI performance in [34]–[40]. The states of unconscious hand touching on the desk during a pattern drawing task are classified using HMM. The hand states are the

indications of fine and rough movements of pattern drawing modes. Therefore, the classified state is used to improve the micro teleoperation performance by automatic switching between fine and rough movement modes [34].

Active cooperation between a human and a robot arm has been realised using the recognition of human intention by applying the HMM to learn the characteristic of forces exerted on the robot arm gripper [35]. The scenario has been applied to a transportation task in which a human control to balance the payload during the human-robot arm cooperation. There are three stages in this active cooperation system; force-torque signal processing, force pattern recognition using HMM, and the cooperative trajectories generation. The experimental result suggests that both time and frequency domain information should be taken into account to obtain the most out of system robustness.

Telemanipulation with virtual fixture assistance also has benefited from knowing the intentions of the working operator. A virtual fixture is a form of constraint that is applied to limit the range of e.g. movements, paths, or angles to guide the operator. An HMM model is used to classify the human intentions from motion and velocity profile in [36]. As a consequence of the intention classification outcomes, one of three types of the virtual fixture is activated. Path following with virtual fixture direction, aiming at the target with helping of attractive force field, and obstacles avoidance with the help of repulsive force field are the examples of the task with guidance. Combined recognition of intention and appropriate activation of guidance has proved improvements in both less operation execution time and less error during the teleoperation. Furthermore, suggestions for improving the accuracy of intention recognition could be done by giving sufficient training data, expanding the dimension of states in HMM, which only increase linear time complexity as long as the states are independent from each other.

Although the use of virtual fixtures helps the overall teleoperation system's performance in both time and accuracy, a typical virtual fixture is inflexible. An adaptive virtual fixture is introduced which can be adapted by tuning the fixture factor according to operator current estimated trajectories or intentions [37]. The algorithms such as K-means clustering, HMM, and Support Vector Machines (SVMs) are used in combination in the proposed system. The system shows an acceptable tolerance to the untrained situations.

A Layered Hidden Markov Model (LHMM) is used for intention recognition systems based on the motion of robot-assisted applications [38], [39]. This type of HMM has several HMMs running concurrently with their corresponding purpose for each level of HMMs. For example, the lowest level HMM may correspond to estimate primitive motions such as translation or rotation of robot manipulator while the higher level HMM is responsible for aggregate recognition from the primitive actions i.e. task level recognition. Two more advantages over a typical HMM are the smaller amount of training data and the independence of training for each level of HMM. In conclusion, it is stated that the LHMM has more recognition power than a typical HMM and has more robustness in case that misclassification occurred in the lower level but the overall system still able to recognise the tasks.

An HHMM, i.e. a hierarchy of multiple HMMs is used to implement smart assisted living systems for elderly [40]. Information used to identify intention is obtained from a single inertial sensor worn on a finger, which can provide several data for intention identification such as 3D acceleration, orientation (gyro), magnetic data, and temperature. Five types of hand gesture are being recognised and mapped to command the robot actions for elderly people. The comparison between normal HMM and HHMM shows that the latter has more accuracy. This is because HHMM contains multi-level recognition steps.

2.3.2 Self-organising map (SOM) based intention recognition

A type of ANN called self-organising map (SOM) combined with Bayesian filtering technique is applied to estimate human intention [41]–[45]. The justification for applying SOM can be explained as follows. Firstly, there is no need to define finite automata states like other graph-based models e.g. HMMs. Secondly, it is stated that a human intention should be recognised from inside the human brain activity rather than the recognition of the external activity of the human behaviour. Thus, the use of SOM in this work is claimed to be a model of the cerebral cortex area in the human brain. Besides, SOM is able to map a relatively large amount of dimensional data to much lesser dimensional data and with no loss of topology information. As a result, the computation complexity is decreased. Finally, the advantage of Bayes filtering algorithm over other methods is the ability to handle non-Gaussian data distribution of human

intention. Implementation of Bayes filtering is done by a statistical particle filtering algorithm. The test bed based on this proposed method is a remote operation task where the operator has to control two types of the truck in a miniature environment via remote interfaces and control panels. Large amounts of information are monitored during the operation, for example, infrared light markers for truck position tracking, potentiometers for rotations tracking and control panel switches etc.

2.3.3 The evaluation of the HMI intention recognition

Section 2.3 reviews some of the literature relating to HMI intention recognition. Several studies show that HMI improvement can be achieved by applying the knowledge of the human's intention to provide assistance and adaptation. However, most of the works has weaknesses e.g. lack of performance evaluation related to the corresponding intention, fine tuning of the provided assistance etc. The only the work that tries to introduce an adaptive virtual fixture based on the current operator's intended trajectory is proposed by [37].

2.4 HMI adaptive assistance

The aim of adaptive assistance is to achieve the optimum system performance by providing help to a human operator. The assistance can be divided into passive and active. A direct assistance such as a physically assistive movement is considered as the active one [20], [46]. There are proofs that show the improvement in learning efficiency from the system's active force assistance during the HMI task performed in many research experiments [47]–[50]. The HSC is one of the active assistance methods, which is introduced in Section 2.2.3. Passive assistance, on the other hand, is an internal adaptation of a system i.e. an automated system's parameter tuning [51], [52].

2.4.1 Dynamic system with virtual fixture and shared control guidance

The effectiveness of the active assistance for performance and training enhancements has been studied [27]. As experimented in [53], the dynamic system is a mass-spring–damper as shown in Figure 2.4. This dynamic system can be controlled and moved in a two-dimensional space with 4 Degrees of Freedom (DOF) i.e. (x_1, y_1) and (x_2, y_2). A 2-DOF force feedback joystick is used to control the system's dynamic. A direction and magnitude are directly applied to the mass m_1 to force the mass m_2 at the other end to move and reach a target. The system is classified as an underactuated system since the mass m_2 is moved involuntarily.
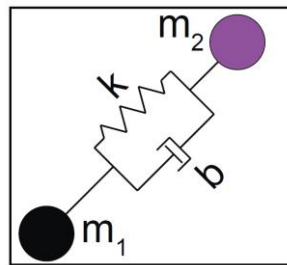
Figure 2.4 A two-mass spring damper dynamic system [53].

There are three scenarios compared in this classical target-hitting/reaching i.e. no assistance, virtual fixture assistance, and shared control. For virtual fixture assistance, a pair of virtual walls, modelled as a spring and damper, would automatically give feedback via the joystick to put the operator back on track when the mass tends to stray from the path. This kind of penalty-based passive assistance does nothing unless the object position is out of range. The virtual fixture could be either repulsive or attractive depended on the design, while the shared control scenario is implemented based on the HSC concept.

Both virtual fixture and shared control assistance obviously boost the performance of the operation but the latter is in the lead because of its generality. However, they are inapplicable in the case of training enhancement. The effectiveness of training enhancement is equivalent in all of the three scenarios [27], [53].

2.4.2 Confliction among the interacting agents

A conflict commonly occurs when two or more agents participated in any cooperative task. It has been shown that one prefers to control the operation by himself/herself without interference [54], [55]. In the case of active assistance from an HSC machine, this conflict becomes unavoidable. Therefore, it is a good idea to pay more attention to the detail of the operator. Neuromuscular information from the operator leads to a real understanding of the operator control behaviour such as in a car lane-changing task [56].

Humans learn to cooperate and share intention with each other since the beginning of life and a set of intuitive cooperation behaviours are developed during this time. Based on this fact, it is an attractive idea to identify these learning ways and mimic them for the development of an intuitive human-robot cooperation [55]. This kind of study gives mutual benefit to at least two research fields i.e. developmental psychology and robotics. Developmental psychology requires the experimental testing scenario for its human-being related theories whilst the research in robotics gains psychological knowledge to implement a robot that accurately mimics the human behaviour since it is impossible to develop a robot that behaves like a human being based solely on an ordinary sequential programming.

2.4.3 Challenging issues in shared control

2.4.3.1 <u>Degree of support</u>

Although HSC has been proven in training improvement, a degree of assistance in HSC system should be carefully tuned because an excessive amount of support is likely to result in a lacklustre performance, worse than a task without any HSC support. This issue has to be clarified in the long run [27], [57].

2.4.3.2 <u>Authority</u>

Apart from the comfort derived from the autonomy, the authority to take control is critical [57]. Policy must be explicitly formulated over a level of automation (LoA) and a level of haptic authority (LoHA) on any certain circumstances.

There are two approaches to shared control in [58], "input-mixing shared control" and "haptic shared control". The former allows mixing of control inputs from machine intelligence and human before evaluating the final control outcome to the actuators. The latter allows either a human or a machine to take over the machine simultaneously with a degree of negotiable authority through the haptic control interface. The "haptic shared control" shows better design potential over the "input-mixing shared control" because the operator stands in the loop constantly to overrule the elaborate system and to evaluate some erratic situation [28].

Instead of giving full authority to an actual haptic device to calculate and return force feedback to the operator, a study alters the human-robot shared control situation with two human participants. The two participants mutually control an on-screen object and obtain force feedback from each other via the haptic devices. Unfortunately, the result suggests that a human prefers to make a control decision solely on his/her own without interference from the partner [54].

2.4.3.3 <u>Overreliance</u>

A machine is a man-made tool or a piece of equipment with limitations covered by its design and functionality. It is at risk of relying merely on the autonomous machine. Overreliance or over trust on autonomous systems could be a problem. Appreciating natural human ability of learning and problem solving, the system needs to be kept under the supervision of the operator. To avoid the overreliance or over trust issue, an HSC design should come up with situation awareness (SA) alerts at regular intervals.

2.4.3.4 <u>Dependency and skill retention</u>

In spite of experimental evidence indicating benefit over tradition manual control, the HSC experiments provide too small sample sizes compared to the real world. Overdependence of the system tends to confront with a long-term problem in which the operator would be unable to work without any support and influences to retention of skill as well [57]. There are many aspects of the HSC system still to be experimented in a long-term usage.

2.4.4 The evaluation of the HMI adaptive assistance

Section 2.4 reviews the adaptive assistance component of the HAM concept. Apparently, HSC appears to be the concept that plays the major role in this component because of its active assistance mode by the utilisation of a haptic force feedback device. Many investigations e.g. [27], [53] etc. show that the HMI enhancement can be achieved when the active assistance is applied. However, it is not effective in some situations e.g. the case of training enhancement. However, there are still gaps and challenging issues in this particular aspect of HMI to be improved. These issues are the degree of support, the authority, the overreliance, the dependency and retention. All of the four issues may be solved by the investigation to the degree of support. The reason is that the degree of skill performance of each individual human operator is unique. Therefore, it is vital to evaluate an HMI performance prior to fine tuning of the degree of support. This reason is also applicable to the authority as the individual performance can vary, therefore, the offered authority must be adjusted accordingly. The aspect of overreliance may be improved by applying a different degree of active support to a human. The dependency and retention of skill would be improved by providing a different degree of support according to each stage of learning and performance levels of a human operator e.g. the support might be high at the beginning of the learning to use a machine, then it is gradually decreased. In summary, the basis of all aspects comes from the performance evaluation.

2.5 HMI performance modelling

A HMI performance modelling can provide valuable information for the enhancement and evaluation of the system design prior to the actual system implementation [59]–[61]. In addition to the pre-implementation benefit, with recent advancements in sensor and actuator technologies, a HMI performance model can be used in an online manner to provide adaptive guidance and assistance [12], [20], [51]. To understand the HMI performance model, many research projects have attempted to investigate the HMI aspects such as human skills, human sensory-motor skill performance, human skill learning stages, skills-rules-knowledge, human capacity etc.

2.5.1 Definition of human skill performance

Over the decades, continued studies of human skill performance in various features take place in areas of research including psychology, sports, human factor engineering, cognitive science etc. [62]–[64]. Human skills can be described by two following perspectives [65]. In the first perspective, 'skills' is an ability to repeatedly perform sequences of action in the same task and similar environment with maximum certainty, minimal visual attention, and highly predictable pattern. Ideally, the outcome performance is identical from trial to trial. This skill perspective is also known as 'open-loop skills'. It is commonly found in skilled workers in an assembly line, musician performance and vehicle manipulation skills etc.

The next is a human skill in a dynamic system. A dynamic system is uncertain in both time and space of environment. Control in dynamic system requires tracking information for an operator therefore; it can be viewed as 'closed-loop skills'. Examples of a tracking control task in dynamic environment are vehicle road driving and computer-based cursor positioning. As compared to the former definition, it can be noted that good vehicle manipulation skill does not necessary mean good driving on a road.

The characteristics of open loop and closed loop skills are summarised in Table 2.1.

Table 2.1 Characteristics of 'open-loop' and 'closed-loop' skills.

Characteristic of skills	
Open-loop	**Closed-loop**
- High level of practice - Low attention demand - Single-response selection - Consistency of outcome	- Processing time - Bandwidth - A rate of information transmission - Prediction and anticipation - Resources processing and management

In general, a skilled operator performs a task with intimate knowledge [66]. A sequence of actions is formulated beforehand and is able to be adapted according to a change of circumstances. Controversially, an unskilled performer tends to perform the task without the knowledge and is likely to result in a disappointing performance.

Ability to extract only useful information by ignoring any redundant piece of information is another personal characteristic of a skilful person. For example, a skilful restaurant server is able to take a long verbal order that at times includes irrelevant information.

It is commonly mentioned that 'skill learning years' is in the ages between eight to twelve years old [63]. In fact, this statement is not necessarily true. A person can acquire a new skill through a learning process at any ages. Skills such as car driving, skiing, riding a motorcycle etc. can be learned at any ages. It is a term 'skill acquisition' typically used in traditional psychology, philosophy, education, movement science, and performance development [67].

2.5.2 Human sensory-motor skill performance

Measurement of human sensory-motor skill performance is scaled by three general metrics i.e. time, magnitude, and accuracy. Timing is designed to evaluate reaction speed of perception in a task that related to sensory and reaction response. According to [64], motor timing measurement used especially in laboratory setting is the total 'response time' which is a period begun from the first appearance of stimuli appearance until the end of the task. The response time is divided into reaction time (RT) and movement time (MT) as shown in Figure 2.5. An RT starts from an appearance of stimuli until responding movement takes place and an MT starts from the movement to task completion.
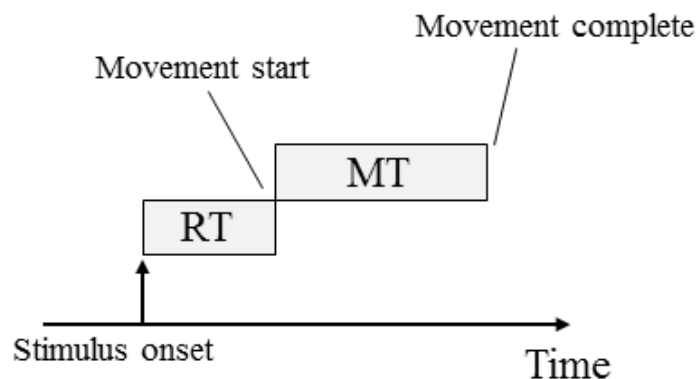
Figure 2.5 A diagram of reaction time (RT) and movement time (MT).

The magnitude aspect of skill performance is measured in terms of distance, weight, force and height etc. The magnitude appears inconsistent for the sensory-motor skill measurement because

accumulation tends to appear from trial to trial depending on personal ergonomics such as body strength, body size, body weight, etc.

According to [64], there are three terms of accuracy measurement - absolute error (AE), constant error (CE) and variable error (VE). The number of samples is denoted by *sk*. A trail of each performance outcome i.e. the outcome of an action is denoted by *TOC*. A trial target is denoted by *TT*.

Absolute error (AE) is computed by averaging error values from trials out, disregarding a sign by applying an absolute mathematic operator. The *AE* calculation shows average error without direction, which is given by (2.1).

$$AE = \frac{\sum |TOC - TT|}{sk} \tag{2.1}$$

Constant error (CE), as given by (2.2), is quite similar to *AE* except for the absolute mathematical operator i.e. a sign of each error is taken into account. The metric indicates average and direction of error from the trials.

$$CE = \frac{\sum (TOC - TT)}{sk} \tag{2.2}$$

Variable error (VE), as named, gives a variability value of the performance trials i.e. a consistency of the outcomes. The *VE* can be calculated by (2.3). A low variable error does not confirm high accuracy as consistency may occur at either low or high accuracy.

$$VE = \sqrt{\frac{\sum (TOC - TT)^2}{sk} - CE^2} \tag{2.3}$$

2.5.3 Fitts and Posner three stages model of skill learning

Fitts and Posner [68] suggest a three-stage model of skill learning, consisting of the cognitive stage, associative stage, and autonomous stage as depicted in Figure 2.6. At a cognitive stage that is the lowest stage of the model, a learner develops the basic movement necessary to accomplish a task. A learner is still consciously aware of every movement. The movements are finely tuned and become smoother. Skill is developed to a middle stage of the model called the

associative stage. At the highest stage of the model, the autonomous stage, the movements become virtually automatic. The skill for a particular task is fully acquired.
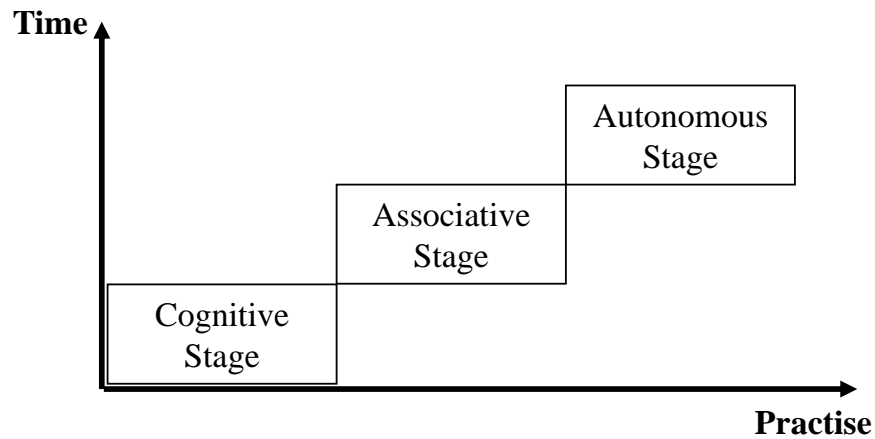
Figure 2.6 Fitts 3 stages model of skill learning.

2.5.3.1 Fitts' law

Fitts' law is a well-known method for quantitative measurement to evaluate the capacity of the human motor system associated with the amplitude movement control [69]. It is used as a performance indicator for pointing devices [70] and HCI research [71]. A formulation of Fitts' law can be expressed as follows.

$$Movement\ Time\ (MT) = a + b \log_2 \left(\frac{2D}{W}\right)\ seconds \qquad (2.4)$$

$$Index\ of\ difficulty\ (ID) = \log_2 \left(\frac{2D}{W}\right)\ bits \qquad (2.5)$$

$$Index\ of\ performance\ (IP) = \frac{ID}{MT}\ bits/second \qquad (2.6)$$

Equation (2.4) defines movement time (MT) where D is an amplitude or a distance of movement and W is a target width. Figure 2.7 shows an example of the scenario. The term $\log_2 \left(\frac{2D}{W}\right)$ is defined as an "index of difficulty" (ID) of the task (2.5). This formula shows a speed-accuracy trade-off for a target reaching/hitting task. An index of performance (IP) can be calculated with (2.6). Equation (2.5) is basically the same as (A.1) in Appendix F, which is the amount of

information conveyed in binary format. By dividing (2.5) with MT, Equation (2.6) becomes similar to (A.4) in Appendix F which is the information capacity of a communication channel.
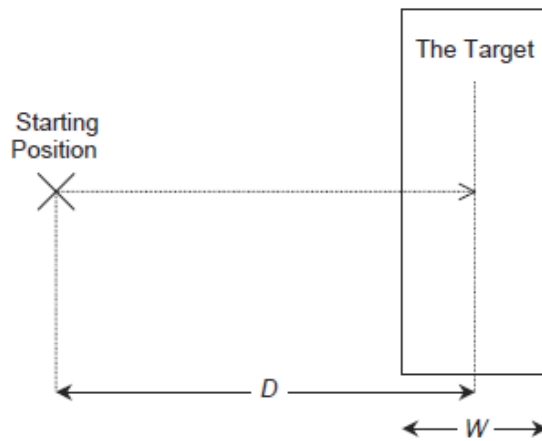
(a)
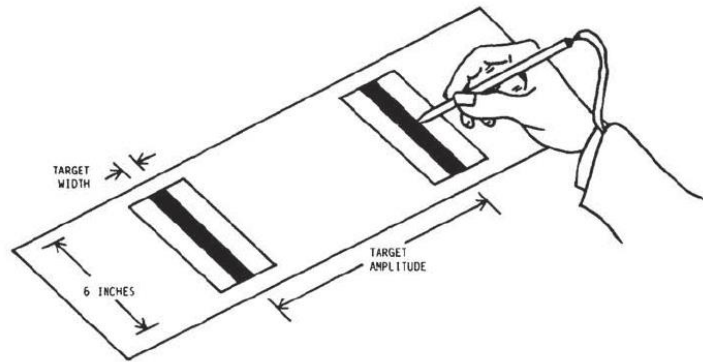
(b)

Figure 2.7 Fitts' law target hitting task [70].

2.5.4 Skills, rules and knowledge (SRK)

Rasmussen divides human behaviour into 3 levels; skill, rule, and knowledge [72]. First, the skill level behaviour is the low-level behaviour. An action is voluntary and automated without consciousness. The movement is seamlessly integrated, smooth, and hardly to be decomposed without unwanted attention. Musical performance is considered a low-level skill behaviour as professional musicians such as violinist, guitarist, and cellist cannot give precise detail of their

performance [73]. The skilled behaviour is directly influenced by repetitive practising and can be described by the Fitts and Posner model (Section 2.5.3).

Secondly, the rule level behaviour, a human adheres to rules, know-how, or instructions learned from previous experience either in person or from others.

Thirdly, the highest level, known as knowledge behaviour, occurs in an unfamiliar situation since rules and know-how is impractical. The situation leads to "trial and error" learning where critical thinking and plan modifying is tested. These suggested three levels of behaviour indicate personal capability and draw up guidelines for human-machine performance development model.

A signal, sign, and symbol are type of information flowing amongst the three levels of behaviour. A signal is continuous sensory raw data from any interested matter, for example; room temperature, ambient light, dust level, humidity etc. Sign is an indicator associated with a certain signal to inform or suggest the corresponding actions to deal with. A symbol is a conceptual information used for further reasoning. The symbol differentiates from the sign as described in the following statement, "a sign is part of the physical world of being while a symbol is part of the human world of meaning". These concepts of information flow are useful for modelling human performance.

2.5.5 Human capacity

The idea of human perception capacity borrows a formulation from an information theory. Figure 2.8 shows measurement of perception capacity using a concept of transmitted information. An intersection between the input and the output is used to refer to an amount of information transmitted from the input to the output. In other words, it measures a degree of recognition according to the given samples. The intersection could cover a fragment or the entirety of the input depends on the perception. Experimentally, a number of samples are given to a person for a particular aspect to be perceived i.e. the input circle in Figure 2.8. Later, a perceptive judgement i.e. the output circle in Figure 2.8 is obtained from him/her. By doing this repeatedly on a number of human subjects, the covariance of the input and the output is

calculated (the intersection in Figure 2.8) which is an indicator of an amount of information transmitted in a particular experiment.
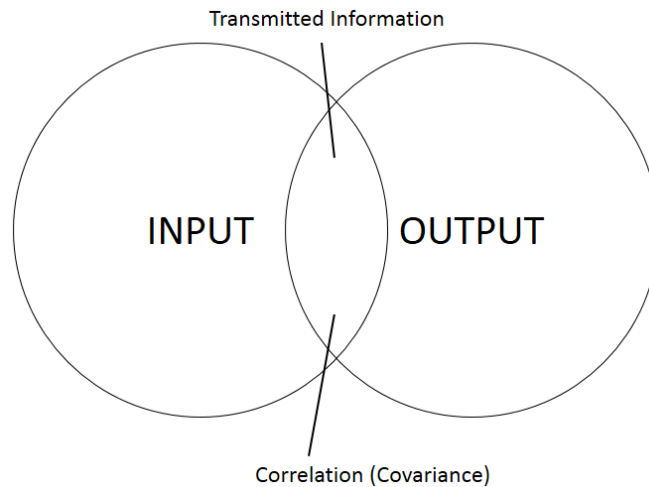
Figure 2.8 Transmitted information between input and output.

2.5.5.1 Human perceptions capacity

An absolute perception judgement on a particular aspect is made by human capacity [74]. Unit of measurement is in bit or entropy as in the information theory (Appendix F). Table 2.2 summarises human perception capacity on the one-dimensional variable. Experimentally, capacity for each aspect of human perception e.g. visual, hearing, and tasting is calculated from the ability to spot differences. These human capacities are measured for a single aspect without any extra information.

Table 2.2 Channel capacity of a human absolute judgement on the one-dimensional variable.

Aspect	Capacity (bits)
Visual	
Points presented on a line interval	3.25
Area	2.6
Angle	3
Hue	3.1
Curvature	2.2
Square size	2.2
Brightness	2.3
Size	2.8
Hearing	
Pitch tone	2.5
Loudness	2.3
Tasting	
Taste intensity (of salt solution)	1.9

The capacity of human perception is increased when supplied with extra information and more variables for the judgement. As summarised in Table 2.3 there are two variables at the time of the judgement.

Table 2.3 Channel capacity of a human absolute judgement on the two-dimensional variable.

Aspect	Capacity (bits)
Visual	
Position of a dot in a square	4.6
Colours	3.6
Hearing	
Loudness and pitch	3.1
Tasting	
Intensity of mixed salt and sugar	2.3

In fact, human beings are able to discriminate things more accurately and more efficiently than the capacity values shown in Table 2.3. In real life, there exists multiple supplement information or contexts that help improve the human perception. As a multi-dimensional confirmation, the surrounding information help ensures the judgement.

Furthermore, a special experiment with six variables of frequency, intensity, rate of interruption on time fraction, total duration, and spatial location is set up. Approximately 150 different variations are discriminated with 7.2 bits capacity. It is able to conclude that the variables help represent features or properties of objects and provide relevant for the perception judgement.

The more the number of variables raises, the more the capacity increase and tends towards the real human-being world.

2.5.5.2 Redundancy of information for human perception

The redundancy of information is occasionally necessary for human perception. An example, shown in Figure 2.9, illustrates a monitor display of a single decimal number. Apparently, an additional bar graph under an identical number affects clear and easy perception for human eyes.

Alternative example is a pixel containing $2^8 = 256$ bits of information on a colour display monitor. Human eyes are likely to encounter difficulty in perceiving and working with a single pixel although it supplies plenty amount of information.

<p align="center">(a)   (b)</p>
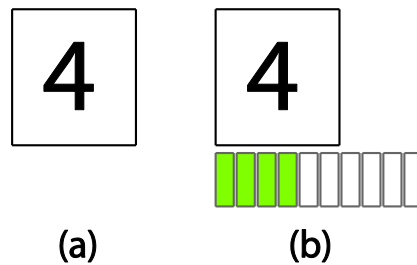
Figure 2.9 A single decimal number monitoring (a) a single number (b) a single number with an additional bar graph.

2.5.6 Human performance index (HPI)

[75] proposes a human performance index (HPI) as a generic performance evaluation framework. The framework consists of two layers of evaluation. The first layer is a collection of performance variables that evaluate the raw competency of actions. The second layer, so called performance criterions, is a weighted condition integrated to variables in the first layer. Ordinarily, performance criteria such as speed and accuracy are used in competency measurement metric.

The weighted concept of HPI measurement can be simplified as grading evaluation in school. Scores from paper works, examinations, and attendance are weighted with different percentage values according to an importance of each piece of work separately in the subject. Grading point

average (GPA) is finally calculated from weighted credits of each subject. Therefore, the HPI is the final result of GPA while performance criterions are subjects, and raw evaluations are scoring.

In addition, HPI framework could be used in two modes; open and closed form. The open form is located at the second layer i.e. performance criterions which are able to use in any applicable closed form. The closed form is located at the final accumulation evaluations i.e. the HPI.

2.5.7 Human-robot information pipeline

A human-robot information model or HRI based on a pipeline of information exchange has been proposed by [76]. A robot equipped with a colour web-camera, which has the capability to record a video at 640*480 resolutions. Each pixel in a recorded frame consists of three colours with eight bits of the colour intensity scale. The robot is used to report the status of a cup of coffee from one room to another room i.e. the coffee monitoring task. This scenario is an example of the information exchange pipeline. The camera can transfer $640*480*3*8 = 921,600$ bytes of information per second. However, the task requires only 1 bit to report the status i.e. ready (R) or not ready (NR). The value is calculated from standard entropy equation in (2.7).

$$H = -0.5 \log_2 0.5 - 0.5 \log_2 0.5 = 1 \; bit \; of \; entropy \tag{2.7}$$

It is denoted from (2.7) that the two statuses are equally occurred with 50% probability. If the coffee is likely to be ready (R) than not ready (NR) with 75% of probability, the conveyed information can be calculated from (2.8).

$$H = -0.75 \log_2 0.75 - 0.25 \log_2 0.25 = 0.8113 \; bit \; of \; entropy \tag{2.8}$$

It is clear that only the relevant information is needed for the coffee monitoring task. The information for the coffee status indicator is relatively small when compared to the robot that equipped with a high capacity of information from the camera. It is indicated a redundancy of information for a robot for this type of task. However, this redundancy of information is required for a human as discussed in Section 2.5.5.2.

The information exchange is partially restricted to the capacity of the control interface. For instance, Atari gaming joystick has a single fire button and an eight-direction movement control

as demonstrated in Figure 2.10 (a). The Atari joystick provides $\log_2(8) + 1$ equals to 4 bits of information per sample.

NES (Nintendo Entertainment System) gamepad, in Figure 2.10 (b), consists of four directional navigators, two fire buttons which could be pressed either separately or simultaneously and two middle 'select' and 'start' buttons have to be pressed separately. The NES gamepad has $3 + \log_2(2^2 + 2)$ equals to 5.6 bits per sample.
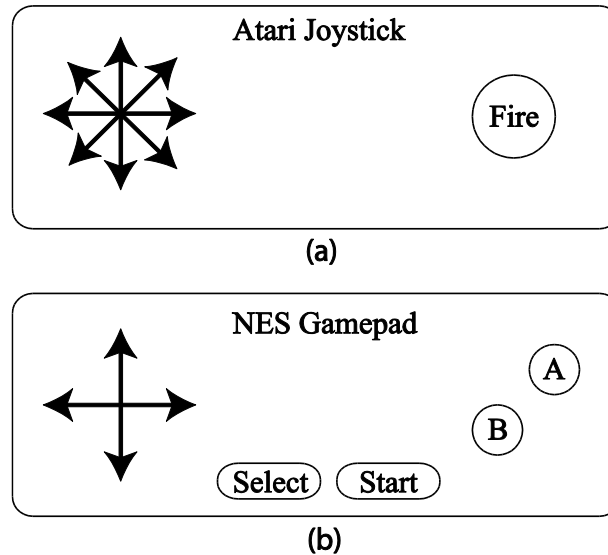
Figure 2.10 The layout of (a) Atari joystick, and (b) NES gamepad.

2.5.8 HMI modelling perspectives and approaches

There exist four perspectives in modelling human interaction with a machine as described in [61] i.e. control theoretic, task network, information processing, and knowledge base. Description of the four perspectives is given in Table 2.4.

Table 2.4 The four perspectives in HMI performance modelling.

Perspective	Description
Knowledge base	The knowledge base perspective models HMI based on the human ability to solve a problem at hands especially in the occurrence of an unfamiliar situation. A human needs to apply knowledge to interact and solve a problem heuristically.
Information processing	This perspective models HMI based on the human ability to identify a problem from the surrounding information. For example, an operator ability to diagnose a problem from the huge amount of information from monitoring consoles.
Task network	The task network models HMI based on the ability to formulate a sequence of actions to accomplish a particular task. For instance, an expert has the ability to perform a sequence of actions without a wrong order of actions. As oppose, a novice could perform a sequence of actions chaotically.
Control theoretic	This control theoretic perspective models HMI based on ability to perform certain action skilfully. This approach can be compared to a human skill modelling.

Apart from the above four perspectives in HMI performance modelling, a model development approach should also be in consideration. Several approaches in model development can be applied e.g. descriptive, predictive, top down, bottom up etc. A pair of model development approaches and description is shown in Table 2.5 [61].

Table 2.5 A list of pairing between the model development approaches.

Model development approach	Description
Process vs. Output	The process modelling focuses on modelling the activity within a process while the output modelling focuses on the relationship between input-output of a system.
Predictive vs. Descriptive	The predictive modelling anticipates the output from a certain circumstance while the descriptive modelling describes the existing data with a model.
Prescriptive vs. Descriptive	The prescriptive modelling explains instructively how ones should perform a system task while the descriptive modelling tells that how the operator is likely to perform a system task.
Top-down vs. Bottom-up	The top-down views from the overall system goal to the primitive activities while the bottom-up is vice versa i.e. modelling from primitive elements and actions up to the overall system goal.
Single task vs. Multitask	Model for a single specific task versus general modelling that can universally apply to multiple types of task.

2.5.9 The evaluation of HMI performance modelling

Section 2.5 reviews the literature related to HMI performance modelling. This topic is an extensive research area that incorporates many human-related disciplines such as the study of human skill and learning, the study of human capacity and performance, the study of HMI performance etc. A few of the research projects have focused on the development of online performance model which is considered to be the mandatory factor for achieving improvement of adaptive HMI.

2.6 Forms of HMI

This section presents three forms of HMI i.e. proximity interaction, remote interaction, and wearable robotics as illustrated in Figure 2.11. These three forms of HMI can be considered as the application that would benefit from the HMI improvement in both practical and academic aspects.
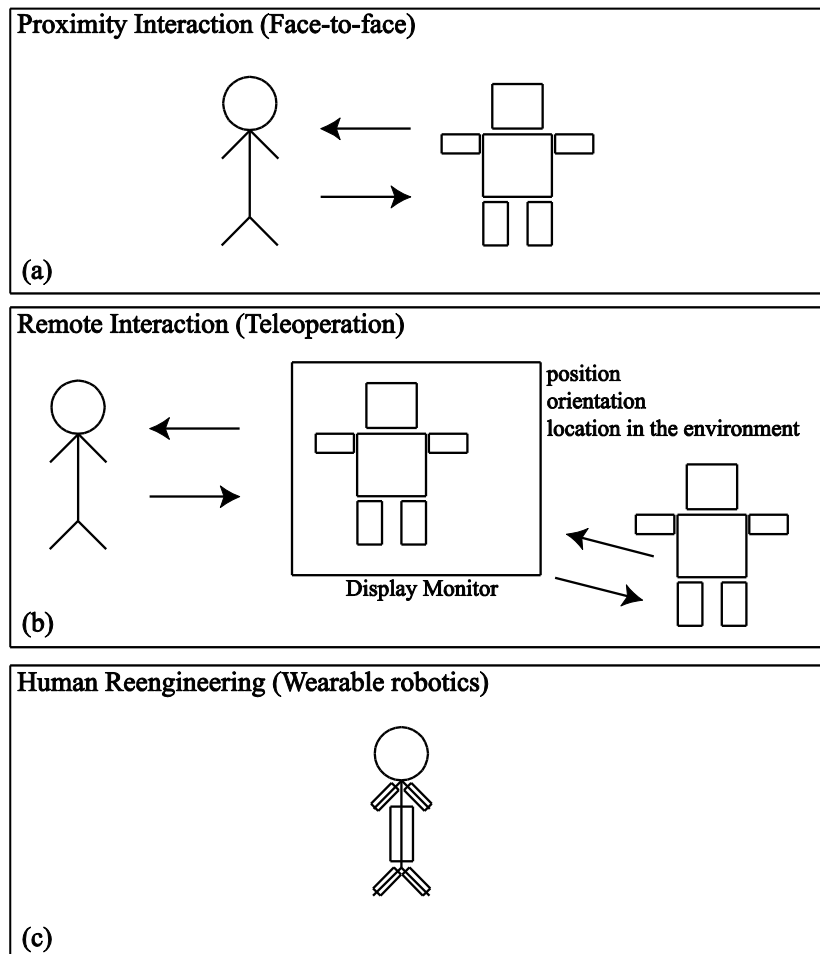
Figure 2.11 The three forms of HMI.

2.6.1 Proximity interaction

Figure 2.11(a) shows the proximity or face-to-face interaction that arises directly and physically within close range and immediate environment. A service robot with some kind of physical

interacting medium like a robotic arm or hand is one of the examples of a robot that can interact with a proximity range.

2.6.2 Remote interaction

A remote controlled interaction, also called telerobotics, teleoperation, or telemanipulation, occurs between an operator and robot situated in distant sites such as USAR and telemedicine. Depicted in Figure 2.11(b), a robot is remotely operated through a communication network via a local control interface. The interaction has to deal with time delay, telepresence, and situation awareness on a control screen over the network.

2.6.2.1 <u>Telerobotics</u>

Telerobotics is the study of robots that can be interacted with from a remote environment. Many terms can refer to the same as telerobotics including teleoperated robots, robot telemanipulation, and robot teleoperations.

According to a distinguishing characteristic and its usefulness, remotely operated robots have been utilised in many applications. This remote indirect interaction (Figure 2.11 (b)) has emerged over decades for nuclear material handling operations [77] and space exploration. In a life-saving situation where every minute is counted, rescuers capably attempt a rescue from a remote site, exert less energy, and stay completely safe [24], [78]. Medical applications are greatly contributed by teleoperated robotics. In telesurgery, telemedicine, telehealthcare, and teleexamination, experts or doctors are able to perform operations from a physical distance [79], [80]. The teleoperations are employed in military battlefields in the same way. Hazardous operations such as explosive ordinance disposal [81], radioactive material handling [82] and operations in a poisonous environment, which are considered exceedingly dangerous for the human operators, demands control with dexterity and precision from teleoperations. Exploration tasks in inaccessible or hardly accessible areas such as space [83]–[86], underwater [87], [88], underground [89], and those relatively different in size of the operating environment compared to a human [90]–[96] (i.e. different in scale, either smaller or bigger) can be accomplished by teleoperated robotics. To reduce cost and to avoid loss of life, teleoperated vehicles are

frequently used in harsh terrain or environments [97]. These telerobotics applications help to enhance human capabilities.

Besides the potential advantages, a remote connection poses problems of time delays, information loss, and distortion in the communication channel. A feeling of control is also problematic. As compensation, numerous control strategies are surveyed, compared, and summarised [98]–[100] e.g. force reflection, shared compliance control, predictive control etc. For example, bilateral teleoperations are the master controller and slave actuator systems that render force feedback over a transmission channel feeling from master to slave and vice versa.

Advances in technologies have made hard tasks easier. For instance, the introduction of touch-screen interfaces makes a teleoperated mobile control possible with just a fingertip by touching and specifying a robot's trajectory through a touch panel [101]. To gain better teleoperations, telerobotics is facilitated by developments in 3D real time rendering hardware, computer graphics software, gaming industries [78], [102] and highly integrated technologies such as Nintendo Wii [103] and Microsoft Kinect [104]–[106].

Situation awareness (SA) is a significant aspect of display interface design e.g. teleoperator interfaces, interfaces for aeroplanes, interfaces for power plants, and manufacturing [107], [108]. The experiment conducted in [102] is the comparative experiments between novice and expert users using altered 3D teleoperation interfaces for general domestic duties. There is a confirmation from the experiments that the novel mixed perspective visual display, designed to improve the SA, help to improve novice performance. The SA can be viewed as one of the assistive information provided to improve the efficiency of the operation.

2.6.3 Wearable robotics

Wearable robotics as shown in Figure 2.11(c) is an emerging technology of an intelligent device which is constituted as a part of the wearer as a prosthesis or a supportive device [109]. As a prosthetic device, it is used to replace amputated limbs. A supportive device is a device that aids the wearer in walking, carrying heavy loads, improving accuracy etc.

2.7 Control modes of HMI

There exist several control modes depending on the situation and design of the control task e.g. pursuit tracking, balancing, on-off intermittent, aiming, and oscillatory control etc. Some of the daily life activities such as riding a bicycle require several control modes acting simultaneously. The rider has to maintain balance and turn the pedals to move forward simultaneously while the hands control the handlebar to keep the bicycle on track.

2.7.1 Pursuit tracking and compensatory control

A characteristic of human operators in manual control systems is identified by a simple pursuit and compensatory control. When a human functions as a servo, it can be modelled by families of quasi-linear transfer functions and other functions of frequency [110].

In [111], a human-to-human interaction study has been conducted to examine a relationship between the sharing control of a pursuit tracking task. The approach extends the McRuer's cross-over model [112], [113] to cope with two operators. Undertaking the cooperative task, a result concludes that each of the operators tends to adapt to the other. The explored relationship is established to advance a natural and intuitive HMI.

2.7.2 Balancing control

A mop or an inverted pendulum balancing is the example of this type of control mode that can be extended to the studies such as a study of human posture balancing, development of a robot arm posture, development of a crane vehicle etc. Many investigations have applied this type of control mode to study human control behaviour [16], [114], [115]. It is found that a skilful operator exhibits an on-off intermittency control strategy in balancing an inverted pendulum task. This intermittent control can be described by a linear model of time and velocity shifts [16]. Likewise, a human balancing control strategy is turned towards a discrete like control strategy when delay is introduced, also known as the bang-bang strategy [114]. This bang-bang control strategy is considerable to be a proportional-derivative (PD) type of automatic controller.

2.7.3 Oscillatory control

An oscillatory control mode happens when there is a vibrating element with a damping ratio below 0.35 [116]. This oscillation limits a human ability to track the position of the system while operating it. To recover the tracking ability, a technique called 'input shaping' is enabled to suppress the oscillations. A crane system is an example that is likely to have the oscillatory dynamics while the human operator controls the payload through the obstacles as shown in Figure 2.12 [117], [118].
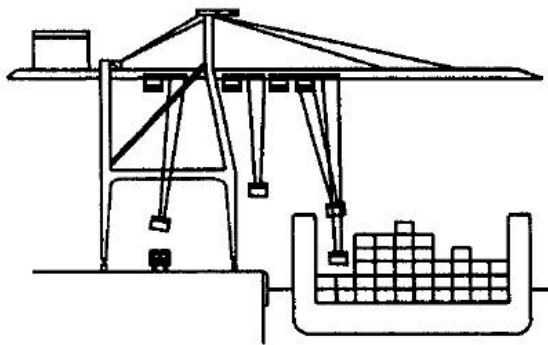
Figure 2.12 A crane system [117], [118].

2.7.4 Target hitting/reaching control

Target hitting or reaching is a simple control task that comprises of reaching or moving from one target to another target. The task can be either in the physical or virtual worlds. One examples of a physical target reaching task is to move a physical object from one position to another. In a virtual world, an example is the manipulation of a mouse cursor from one position to another. Fitts' law (which is discussed in Section 2.5.3.1) is usually the formulation for performance measurement in a target hitting task, especially for a pointing device in HCI research [70], [119]. The target hitting task based on Fitts' law definition is shown in Figure 2.7 in Section 2.5.3.1.

2.7.5 Other studies

The human control strategies discussed in the previous sections are considered as basic control tasks that are less complicated than a task in real life situations. Human control for a virtual ball juggling task is studied under the HAM assisting control [46], [120]. Car driving behaviour is particularly interested in the HSC research [28], [121].

2.8 Descriptive and predictive model developments

It is well-known that human behaviour is complicated and unpredictable. Therefore, it is difficult to develop a model analytically. A descriptive model development seems to be an appropriate approach for the model development of HMI performance modelling because it creates a model based on the observations.

The descriptive approach is successfully applied in a number of HMI studies including a human car control strategy study [122], a crane control operation [117], a set of rules to control the level of a water tank [123], balancing an inverted pendulum under time delay [114].

According to Table 2.5, opposition to the descriptive approach is a predictive modelling approach, which anticipates output from a given set of observations. The example of the predictive modelling approach can be found in [124], [125] for the modelling of human control in pursuit tracking task. The two opposite approaches can be developed in combination in order to obtain a reliable model. The combination is proceeded by dividing the observation data into two datasets. One part is used for the descriptive model development and another part is used to test the validity of the obtained descriptive model i.e. the predictive approach.

2.8.1 Model development procedure

A generic descriptive model development procedure is shown in Figure 2.13. The procedure consists of four main steps with one optional step. First, raw data is obtained from an experimental observation. Secondly, the raw data is segmented into an object of interest.

Thirdly, features are extracted from the segmented data. Then, the feature can be transformed if necessary depended on circumstances such as dimensionality reduction. Finally, the dataset is ready for a model development for a selection of modelling algorithms.

At the optional block in Figure 2.13, the following data transformation technique could be applied. The principal component analysis (PCA) is a statistical technique for data or feature transformation into another space of an equal number of variables i.e. principal component (PC). However, the PCs in the principal component space is ranged from high to low importance in term of redundancy of information linearly combined from the original feature space i.e. each PC is a linear combination of the original space variables. That is, the variance among the PCs is maximised [126].
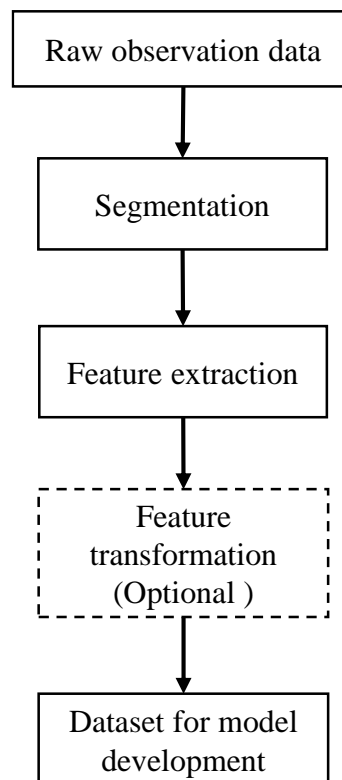
Figure 2.13 The generic descriptive model development procedure.

2.8.2 Cross-validation

The descriptive modelling approach utilises data obtained from an empirical observation to develop a model. It is obvious that there is a limitation of the data samples for the model

development. A cross-validation method is often applied for model training with this limitation [127]. The method divides data into two parts i.e. training and testing datasets. Obviously, the training dataset is used for training a model. The testing dataset is used to test the obtained model from the training. The model performance is evaluated from the testing result. By proceeding this model development for one time, it is a single fold cross-validation.

Although there is some debates on the division ratio between training and testing datasets, a tenfold cross-validation seems to be the standard in practical applications [127]. The tenfold cross-validation separates data into two parts at a time i.e. 90% for training and 10% for testing. The tenfold procedure proceeds for ten times i.e. ten folds by rotating the parts accounted for training and testing. The model performance is measured from averaging the ten testing outcomes. Furthermore, to obtain a reliable result, the overall tenfold procedure is repeated for ten iterations i.e. ten times. Therefore, the name of the entire procedure is ten times ten folds cross-validation.

2.8.3 Model performance evaluation

A model evaluation by a single dimension may not adequate and could mislead the interpretation of the performance [128]. The additional metric can be produced to support the single dimension evaluation such as confusion matrix [129], receiver operating characteristic (ROC) curve [130], precision-recall (PR) curve [131].

A confusion matrix or contingency table for a two-class prediction problem is given in Table 2.6. The two classes are denoted by positive and negative. The table shows the four possible prediction outcomes which are true positive (TP), false positive (FP), false negative (FN), and true negative (TN). Equation (2.9) indicates the overall accuracy of the prediction. The true positive rate (TPR) is the proportion where positives are correctly predicted. The TPR is also known as recall or sensitivity. The false positive rate (FPR) is the proportion where negatives are incorrectly classified as positives. The TPR and FPR are calculated using (2.10) and (2.11), respectively. The true negative rate (TNR) is the proportion where negatives are classified correctly and the false negative rate (FNR) is the proportion where positives are incorrectly classified as negatives. They are calculated using (2.12) and (2.13), respectively. Finally, a

precision which is the proportion of predicted positives that are correct. The precision (P) is calculated using (2.14).

Table 2.6 A two-class confusion matrix.

		Predicted Class	
		Positive	Negative
Actual Class	Positive	True positive (TP)	False negative (FN)
	Negative	False positive (FP)	True negative (TN)

$$Accuracy\ (AC) = \frac{TP + TN}{TP + TN + FP + FN} \tag{2.9}$$

$$True\ Positive\ Rate\ (TPR)\ or\ Recall = \frac{TP}{TP + FN} \tag{2.10}$$

$$False\ Positive\ Rate\ (FPR) = \frac{FP}{FP + TN} \tag{2.11}$$

$$False\ Negative\ Rate\ (FNR) = \frac{FN}{TP + FN} \tag{2.12}$$

$$True\ Negative\ Rate\ (TNR) = \frac{TN}{FP + TN} \tag{2.13}$$

$$Precision\ (P) = \frac{TP}{TP + FP} \tag{2.14}$$

These additional evaluations provide a deeper understanding of the classifier performance instead of a single dimension evaluation. Additionally, a plot between precision and recall i.e. PR curve can reveal the analytical performance of a classifier ability to predict certain positive cases with a particular precision.

An ROC curve is another addition metric for model performance evaluation adopted from signal detection theory. ROC curve is a plot between TPR and FPR on y and x axes, respectively. A curve characteristic and an area under an ROC curve (AUC) reveal the performance of a classifier [132], [133]. The area closer to 1.0 is the ideal classifier performance.

2.9 Artificial neural network (ANN)

Artificial neural network (ANN) is a statistical learning model inspired by a nervous system of the brain. Dating back to the 1940s, a nervous system is first mathematically modelled by McCulloch and Pitts [134]. Followed by the perceptron invented by Rosenblatt in 1962 [135], it is the less complicated by receiving one or more inputs and producing a single output.

As stated in [136], "even though a computer is a million times faster in raw switching speed, the brain ends up being a billion times faster at what it does", that because of the massiveness of concurrent function of the brain. A complex task, for example, face or speech recognition requires less than a second to perform by the brain. Comparing to a computer, there are billions of cycle needed to be completed. In human-like tasks, a neural network model represents remarkable achievement over other traditional artificial intelligence techniques. In addition, the neural network is an inductive learning algorithm meaning that parameters are modifiable during training.

As a classification and pattern recognition model, an ANN is applied in plenty areas of research including assessment of HMI flight operation [137], control systems and applications [138]–[141], modelling and optimisation of human car control strategy [122], modelling human decision making [142], [143], predicting human trajectories in a novel vision-based robotic [144], a control of nonlinear structural systems [145], a tracking control of underactuated surface vessels [146] etc.

An ANN mainly consists of interconnected entities, inputs, and outputs. The interconnected entities, called neurons or units U, mimic the biological neurons the human brain. An illustration of a neuron in neural network is shown in Figure 2.14.
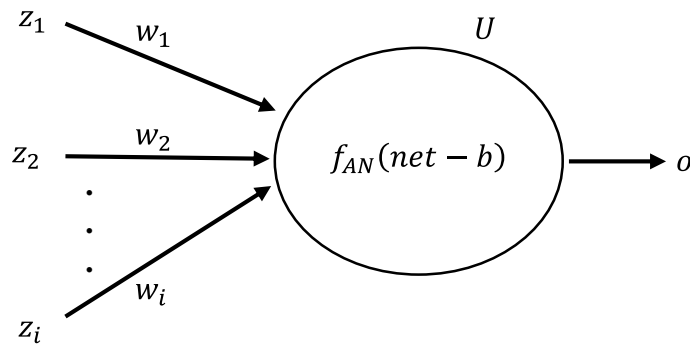
Figure 2.14 A single neuron in a neural network [147].

An input vector Z has an associated weight vector W that represents strength of each input i. A net input at each neuron is computed by $net = \sum z_i w_i$. An output o of each neuron is a calculation of the activation function f_{AN} given the net input and a bias value b. The simplest activation function is a linear function $f_{AN}(net - b) = \lambda(net - b)$ where λ is a constant slope of a function. There are other frequently used functions e.g. step function, ramp function that is a combination of linear and step function, sigmoid function, hyperbolic tangent, and Gaussian function.

An adaptive learning rule is a prominent component of the ANN. During training, the input vector is provided repetitively. The weight and bias value is allowed to adjust according to the learning rule to meet criterion until the best weight and bias value is retrieved corresponding to the output vector.

There are three strategies for learning; supervised, unsupervised and reinforcement learning. In supervised learning, a labelled dataset with known answers, so called a training dataset, is used in the training process to infer prediction functions for a new test dataset. Instead, the training dataset of unsupervised learning is supplied without labels. The model tries to extract patterns or features of the dataset from the environment without any supervision. It is widely known as cluster analysis. Lastly, the reinforcement learning is an intuitive trial and error paradigm of learning from previous experiences. Actions are rewarded or penalised from the feedback of the environment. Without prior knowledge, the paradigm aims to take actions that gain the highest reward.

2.10 Machine modelling

2.10.1 An inverted pendulum-driven (IPD) capsule system

An inverted pendulum is a classic dynamical system. Several studies have been conducted on the mechanism of the inverted pendulum-driven cart pole [148]–[150]. The IPD capsule is generally the same as IPD cart in which the inverted pendulum is enclosed by a capsule body. Applications of the capsule type of IPD systems are intestine diagnosis and tube inspection etc.

The schematic diagram of IPD systems is shown in Figure 2.15(a) and Figure 2.15(b) for IPD cart pole and IPD capsule, respectively. The system consists of a body of mass M, a shaft of negligible mass attached via a rotatable joint to the upper midpoint of the body with length L, and a small mass m attached to the end of the shaft. With proper rotation of the upper shaft, the system can be displaced. An input torque τ applied to the joint causes the rotation of the shaft. θ is an angle between y-axis and the shaft. The displacement is measured in x direction that has surface friction f. The mathematical model in this section is adopted from [148].
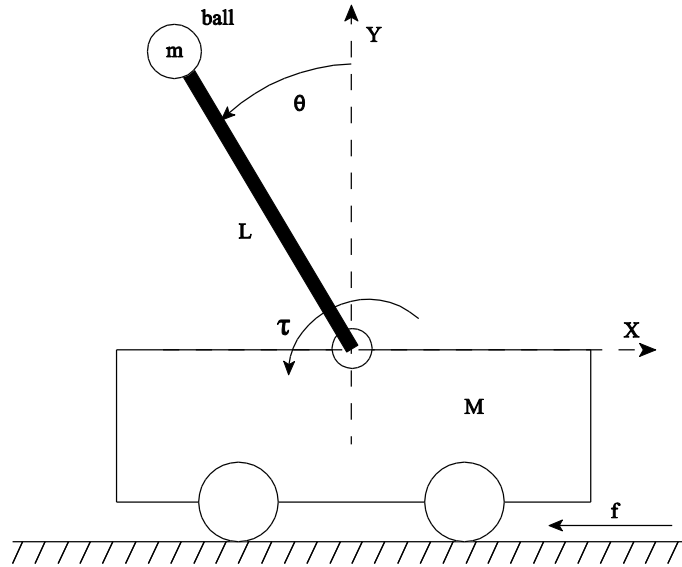
(a) Inverted Pendulum-Driven Cart Pole System
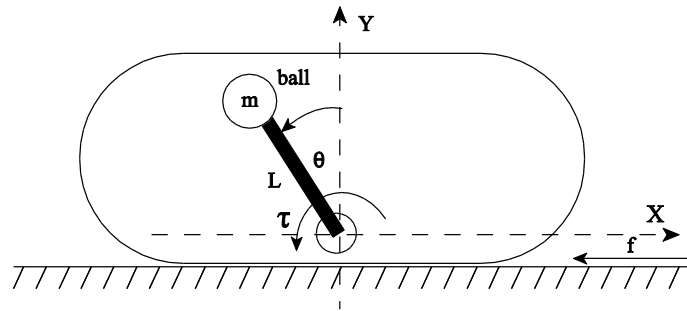
(b) Inverted Pendulum-Driven Capsule System

Figure 2.15 The inverted pendulum-driven cart-pole system and inverted pendulum-driven capsule system.

According to Figure 2.15, the equations for ball position, velocity, and acceleration can be expressed by (2.15), (2.16), and (2.17) respectively. The subscription b stands for ball.

$$\begin{bmatrix} x_b \\ y_b \end{bmatrix} = \begin{bmatrix} x - L\sin\theta \\ L\cos\theta \end{bmatrix} \tag{2.15}$$

$$\begin{bmatrix} \dot{x}_b \\ \dot{y}_b \end{bmatrix} = \begin{bmatrix} \dot{x} - L\dot{\theta}\cos\theta \\ L\dot{\theta}\sin\theta \end{bmatrix} \tag{2.16}$$

$$\begin{bmatrix} \ddot{x}_b \\ \ddot{y}_b \end{bmatrix} = \begin{bmatrix} \ddot{x} - L\ddot{\theta}\cos\theta + L\dot{\theta}^2\sin\theta \\ -(L\ddot{\theta}\sin\theta + L\dot{\theta}^2\cos\theta) \end{bmatrix} \tag{2.17}$$

The forces resulted from the small mass m movement in x and y directions can be formulated by (2.18) and (2.19), respectively. By putting (2.17) into (2.18) and (2.19), the equation of motion and force from the ball mass i.e. (2.20) can be derived.

$$F_{bx} = -m\ddot{x}_b \tag{2.18}$$

$$F_{by} - mg = m\ddot{y}_b \tag{2.19}$$

$$F_b = \begin{bmatrix} F_{bx} \\ F_{by} \end{bmatrix} = \begin{bmatrix} -m\ddot{x} + mL\ddot{\theta}cos\theta - mL\dot{\theta}^2 sin\theta \\ mg - mL\ddot{\theta}sin\theta - mL\dot{\theta}^2 cos\theta \end{bmatrix} \tag{2.20}$$

According to [148], the input torque at the joint is calculated as follows.

$$\tau = (-mLcos\theta)\ddot{x} + (mL^2)\ddot{\theta} - mgLsin\theta \tag{2.21}$$

$$F_{bx} - f = M\ddot{x}; \quad \text{where} \quad f = \mu N sgn(\dot{x}) \tag{2.22}$$

$$N = Mg + F_{by} \tag{2.23}$$

From equation (2.21), (2.22) and (2.23), the (2.24) and (2.25) can be obtained

$$\ddot{x} = \frac{f\sigma_1 + \ddot{\theta}Lmcos\theta - \dot{\theta}Lmsin\theta}{M + m} \tag{2.24}$$

where $\sigma_1 = -g(M + m) + \dot{\theta}^2 Lmcos\theta + \ddot{\theta}Lmsin\theta$

$$\ddot{\theta} = \frac{Lmcos\theta\ddot{x} + \tau + gLmsin\theta}{L^2 m} \tag{2.25}$$

2.11 Inclusion of human brain monitoring system

It is a reasonable idea to include the knowledge of the human brain into the investigation for a better understanding of the human operator and thus can provide proper assistance based on this knowledge. It is proposed that an internal model exists inside human brain [151]. The role of the internal model is that the brain inside is adapting iteratively to model the interaction with the outside world. The adaptation makes the human motor skill progressive from feedback control towards feed-forward control once the brain mastered the skill. When a skill is mastered, the prediction and anticipation come into play for the feedforward control strategy. This existence of the internal model conforms with the evidence from neuroscientist that human

internally learns to simulate motion and reveal to the actual action in the future consequences [33]. Likewise, it is found that the human brain behaves like a Smith predictor which is agreed with the feed forward anticipation behaviour [152]. Furthermore, the researchers from neuroscience show that the internal brain activities can be decoded to understand a human intention from the spatial location of brain images [29], [31], [153].

2.12 Human brain regions and functions

The human brain is a living organ located in a head of a body that plays major roles in the central nervous system. As depicted in Figure 2.16(a), there are two principle components of the nervous system; the central nervous system (CNS) consists of the brain and spinal cord and the peripheral system (PNS) consists of sensory and motor nerve cells (neurons). Outside the brain and spinal cord, widespread networks of PNS nerve cells are built up across the body. Two-way communication from receptors in skins, motor connections in body muscles, and sensors in internal body organs to the brain are established through the networks. Sensory and motor information are gathered and delivered to the brain. A tremendous amount of the information is transmitted along the specialised plasma membranes of nerve cells through synapses in the form of electrical signals called nerve impulses. Subsequent to the interpretation of the information by the brain, instructions are sent back to the target parts of our body about how to react.
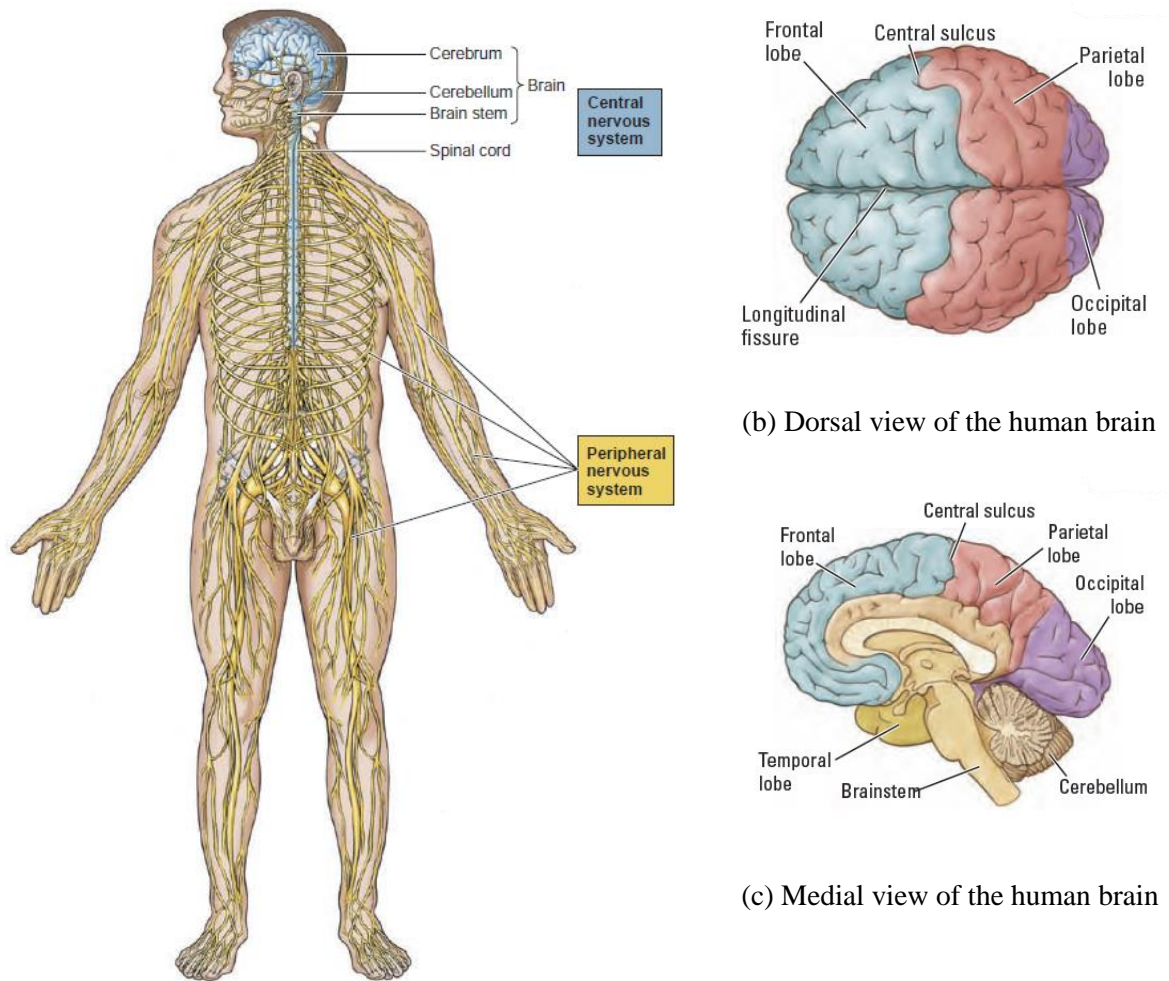
Frontal lobe
Central sulcus
Parietal lobe
Longitudinal fissure
Occipital lobe

(b) Dorsal view of the human brain

Central sulcus
Frontal lobe
Parietal lobe
Occipital lobe
Temporal lobe
Brainstem
Cerebellum

(c) Medial view of the human brain

Cerebrum
Cerebellum
Brain stem
Spinal cord
Brain
Central nervous system
Peripheral nervous system

(a) The human nervous system

Figure 2.16 The human nervous system and the brain structure [154], [155].

The nerve cell is the basic unit of the whole nervous system. A complex tissue structure of the brain is estimated to be made up of 100 billion nerve cells [155]. There are two particular regions of a nerve cell, cell body and extensions, as shown in Figure 2.17(a). The cell body, so called a soma, a core region of a nerve cell, contains nucleus and organelles of an endomembrane system, like another ordinary cell cytoplasm. The extensions or processes are subdivided into two types, dendrites and axon. The dendrites are small tubular branches extended from the cell body that collects impulses from other cells. The axon is a lengthy single fibre connected to the cell body at an axon hillock like a root, responded for an impulse conduction. A nerve cell has many

dendrites but only one axon. The end of each axon is divided into branch structures. The branch termination has a knob called synaptic bouton or synaptic knob. These knobs locate relatively close to dendrites of other cells that form almost-connected junctions, called synapses, as depicted in Figure 2.17(b). The nerve impulses are transmitted toward the axon to the nearby cells through these knobs.
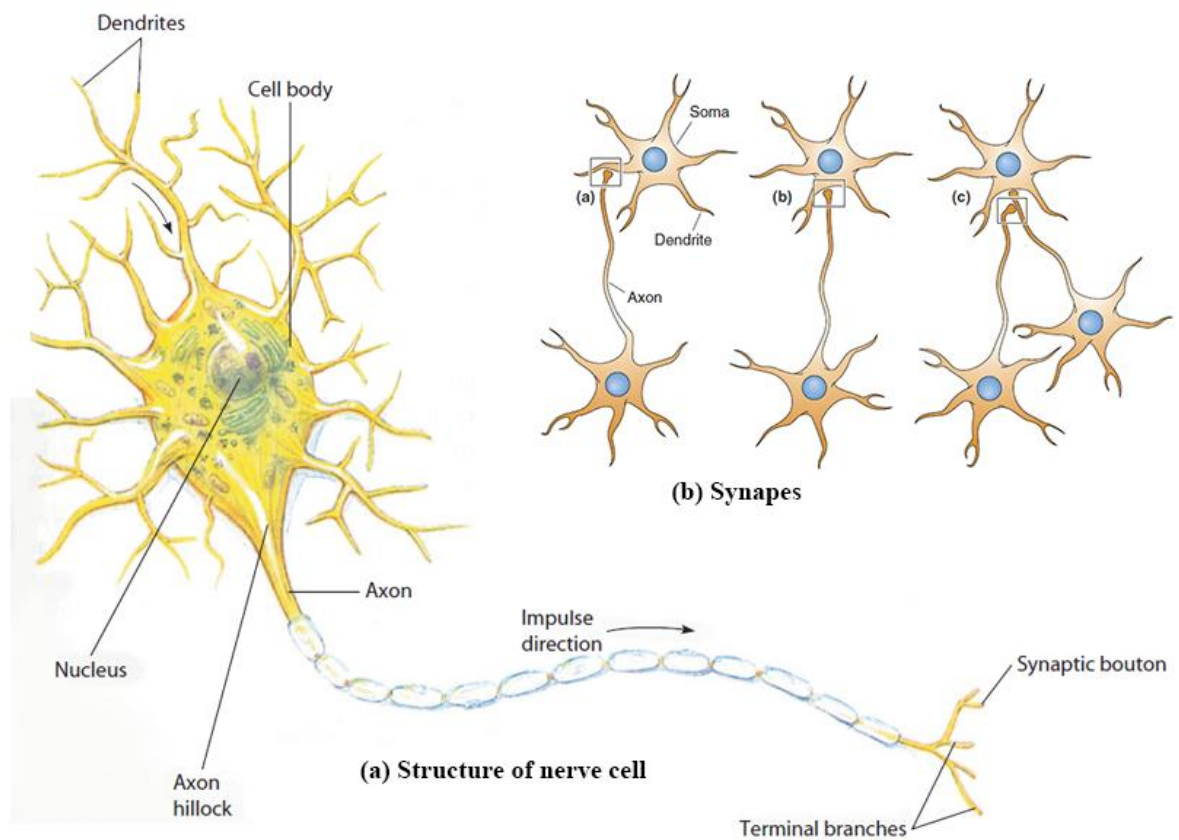
Figure 2.17 Structure of nerve cell and synapse sites [154], [156].

The human brain composes of three major parts: the cerebrum, the cerebellum, and the brainstem. The cerebrum (the forebrain), the biggest and most developed part of the brain, influences in conscious behaviours, whereas the brainstem influences in most unconscious behaviours [155]. The second largest part in the back of the brain is the cerebellum. It is utilised in learning skill and movement control. Movement control of the body is direct to the side of the cerebellum. The right size of the cerebellum controls the right side of the body while the left side of the cerebellum controls the left side [154].

The cerebrum (the forebrain), itself, as the biggest and most developed part of the brain, is evenly divided by a longitudinal fissure into left and right cerebral hemispheres as shown in Figure 2.16(b). The hemispheres are covered by cerebral cortex that is a thin layer of nervous tissue. Each hemisphere is subdivided into four lobes: frontal lobe, parietal lobe, temporal lobe, and occipital lobe as shown in Figure 2.16(c). They are named after skull bones that they lie underneath [154]. The frontal lobe locates at the front of the brain. The parietal lobe is at the top of the brain behind the frontal lobe. The temporal lobe locates under the parietal lobe at the side of the brain. The occipital lobe is at the back. The frontal lobe involves in motor function, executive function, attention, memory, language, emotion, and personality [157]. On the other hand, the other three lobes serve mostly in sensory function, the parietal lobe serves in tactile functions, the temporal lobe functions in visual, auditory, and gustatory and the occipital functions in visual. Unlike the cerebellum, control of the body is opposite to the side of the hemisphere. The right size of the hemisphere controls the left side of the body, while the left side of the hemisphere controls the right side [154].

Together with the spinal cord, the brain entirely dominates personalities, body functions, physical abilities, sensing, behaviours, automatic functions such as the heart beating, digestion, blood circulation, and lung inflation and much more. The spinal cord is cylindrical tissue enveloped in vertebrae, lying along the backbone of the body. Serving as a normal channel of communication between the brain and the rest of the body, information from skin, tissue, muscles and internal organ are relayed through the spinal cord. Apart from the relay duties, some of the movement instructions such as reflex are operated independently by the spinal cord. In the case of spinal cord injuries, there could be effects on bodily functions according to position and severity of injuries such as breathing, food digestion, leg paralysis, and temperature and pain sensation.

2.13 Electroencephalography (EEG)

An electroencephalography (EEG) is a non-invasive measurement of electrical activities of the cerebral cortex, familiarly known as brainwaves. It is considered to be a macroscopic measurement. Figure 2.18 shows an example of EEG signal recorded from a 12-channel headset.

The x-axis is time measured in seconds while the y-axis is the electrical voltage that is usually measured in microvolts (µV).
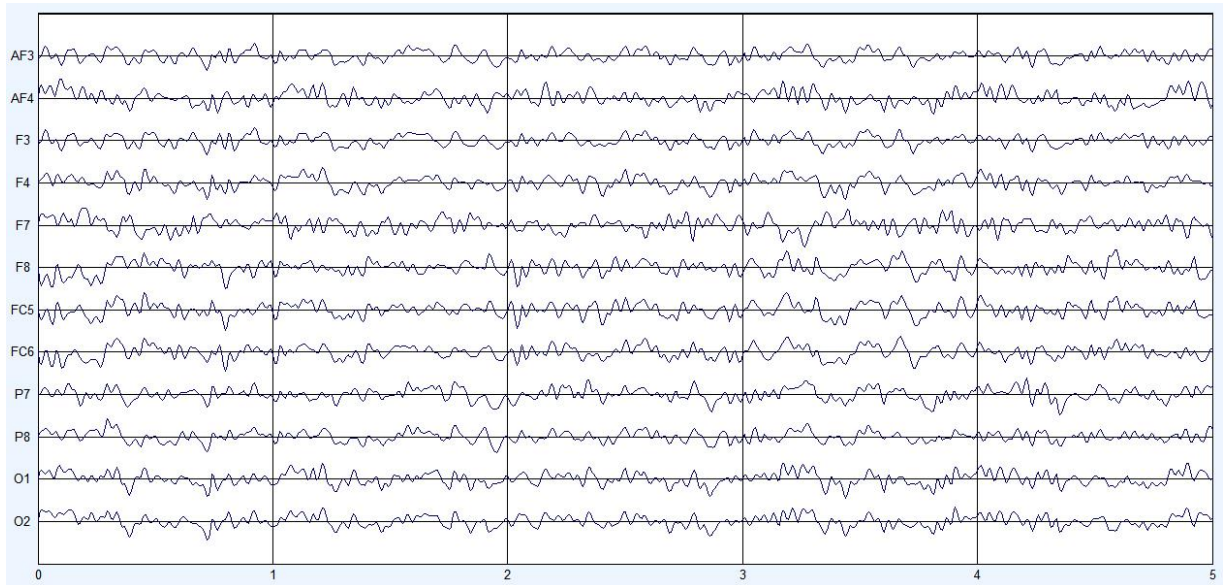
Figure 2.18 An example of 12 channels EEG signal.

The prior EEG research is conducted on animals by Richard Caton in 1875 [158], [159]. In 1929, the first human EEG was contributed by German psychiatrist Hans Berger [160]. The electrical activities are record of information transmission in the human brain neuron networks during synaptic excitation by placing the electrodes on a head scalp [154]. The EEG pattern significantly changes as behaviour or mental attitude changes. Despite a sleep mode, the signal still changes dramatically [155]. For decades, the EEG has been used to study human brain functions by psychologists, neuroscientists, physiologists etc. [161]–[163]. Also, it has been applied for the continuous monitoring of the cerebral cortex activity of a patient suffered from symptoms such as obtund and comatose [164]. The experimental report of the EEG for functional localisation of brain regions mentions that the left frontal hemisphere has a higher level of activity while listening to joy and happy musical excerpt. In contrast, a level of activity of the right frontal hemisphere rises when subjects listen to frightened and sad music excerpts [165].

2.13.1 The 10-20 international system

The standard 10-20 international system is the specification for theplacement of electrodes. The electrodes are placed radially around the scalp surface to cover spatial areas across the cerebral cortex regions. The examples of electrodes and cap used for EEG signal recording are shown in Figure 2.19.

Figure 2.19 The electrodes and caps for EEG data acquisition [166].

The distances between adjacent electrodes are 10% or 20% of the front-to-back or left-to-right point of the skull, as depicted in Figure 2.20. Each electrode is labelled with an alphabet and a number associated with the cerebral hemisphere lobe underneath the areas. The label 'F', 'P', 'T' and 'O' are used as the prefix for frontal lobe, parietal lobe, temporal lobe, and occipital lobe, respectively. The label 'C' stands for the centre and 'Z' means zero, used to refer to the electrodes along the nasion-inion line. The 'A1' and 'A2' are usually used as the ground i.e. the point of voltage reference for the other electrodes.
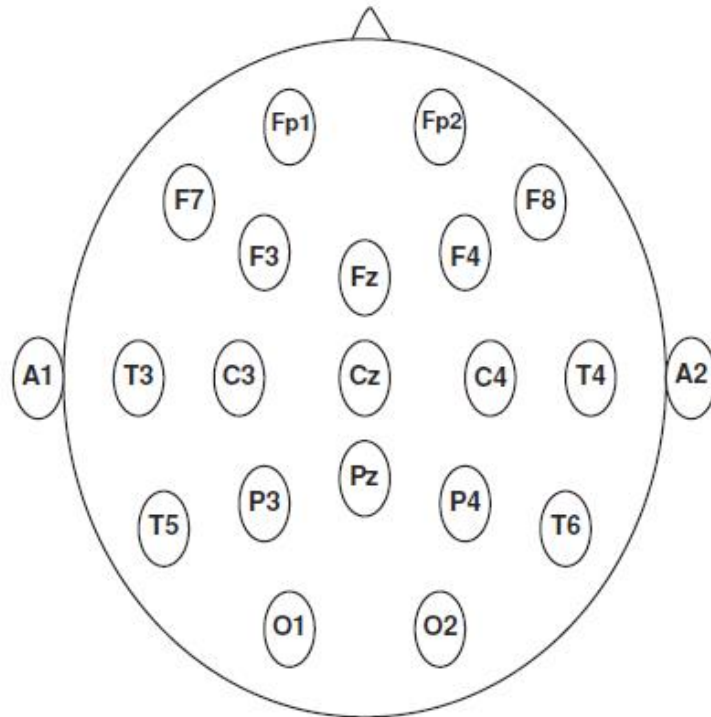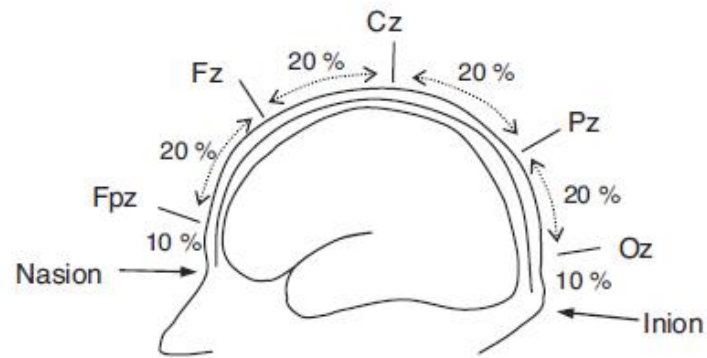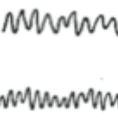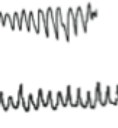
Figure 2.20 the 10-20 international system of electrode placements [166].

2.13.1.1 EEG rhythms

Within 1-30 Hz range, the EEG brainwave can be categorised into rhythms of interests corresponding to a particular brain activity, frequency, amplitude, shape, and the location of the electrode. The frequency rhythms are specified as shown in Table 2.7 [166].

Table 2.7 EEG rhythms [166].

Rhythm name	Example of signal within 1-second window	Frequency band range	Amplitude (µV)	Locations	Example of activity
Delta		< 4 Hz	50-350	Vary	Deep sleep, drowsiness
Theta		4 – 8 Hz	10-150	Vary	Deep sleep, drowsiness
Alpha		8 - 13 Hz	20-100	Posterior	Relaxed wakefulness with eyes closed.
Beta		13 – 30 Hz	10-30	Frontal or diffuse	Cognitive activities
Mu		7-12 Hz	10-50	Central	Relaxed and wakefulness with either both eyes open or close. The mu rhythm is then blocked (event related desynchronisation or ERD) by limb movements such as hand movement.
Lambda		Sharp transients of 200-300ms duration	Below 50	Occipital	Visual exploration

The Delta rhythms are the slowest signal oscillation below 4 Hz. The Delta rhythms are usually occurred during a deep sleep state. During a normal sleep or a drowsiness activity, the signal is categorised as the Theta rhythms. The Alpha rhythms of the brainwave oscillate around 8-13 Hz at the posterior region during relaxed and wakefulness states with eyes closed. The Beta rhythms are categorised by the brainwave oscillated around 13-30 Hz and occurred during the cognitively oriented activities.

Mu rhythms are a subset of the Alpha rhythms that are associated with limb movements during relaxed and wakefulness state [167], [168]. The Mu rhythms block or desynchronise the ongoing brainwaves. In other words, there is the identifiable change in the ongoing train of the signal [169]–[171].

2.13.1.2 <u>EEG artefacts</u>

Due to the very low electric voltages on the scalp surface, the signal contamination tends to happen easily by many non-brain sources [172] such as eyes blinks, eyes movements, muscle movements, head movements, body movements, electrode defect etc. The sources of EEG artefacts can be divided into two categories biological and technical sources, as summarised in Table 2.8 [166]. Some examples of the EEG artefacts are shown in Figure 2.21. Distinctly from the typical EEG signal, some abnormal characteristics of the signal are obviously shown in the artefacts. These artefacts need to be identified and dealt before any meaningful analyses. Fortunately, some research projects have been accounted for these artefacts [173]–[175] e.g. the wavelet analysis for artefact removal, the independent component analysis (ICA) etc. These techniques are fully discussed in Section 2.13.4.

Table 2.8 The sources of EEG artefacts [166].

Source of EEG artefacts	
Biological	Technical
Muscle activity (EMG)	Defective electrodes, wires, ground
Electrocardiogram (ECG)	Loose electrodes
Heartbeat/pulse	Electrostatic disturbances
Eye movements	Electromagnetic interference
Wet skin (sweating)	A/C power sources (50/60 Hz)
Body movements, breathing	
Tongue movements	

| normal EEG | epileptiform activity | spike wave | temporal sharp wave | wet skin | light switch | ECG | muscle activity |
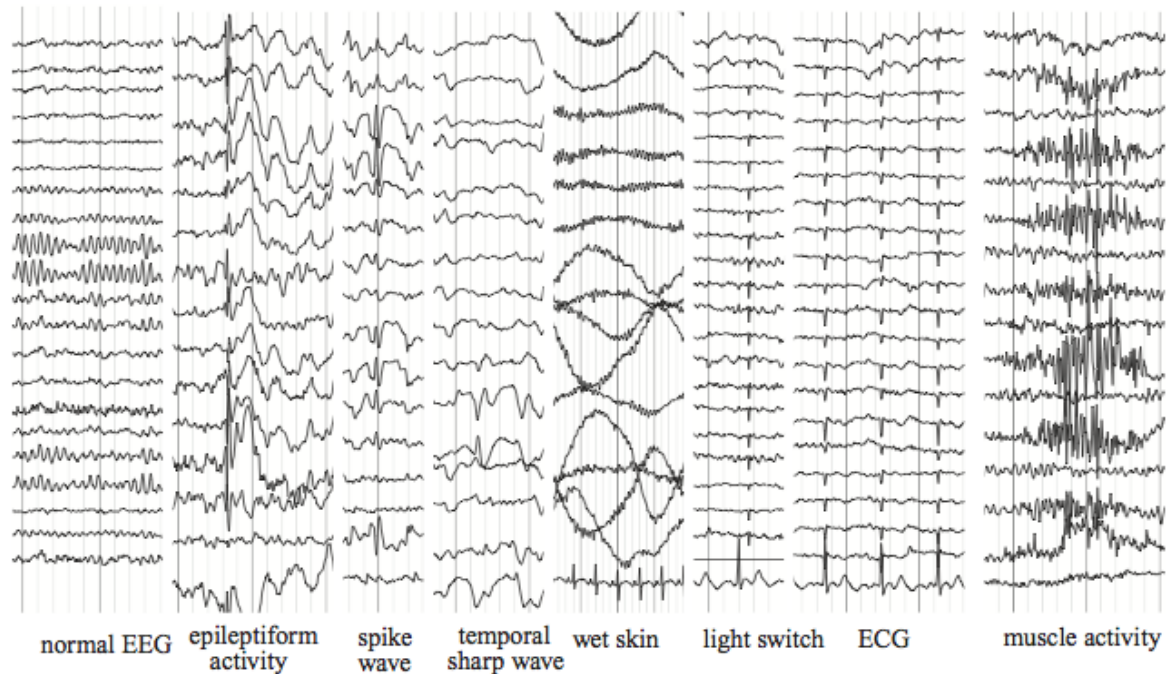
Figure 2.21 The examples of EEG artefact [166].

2.13.2 Advantages and disadvantages of EEG

The fact that the weakness of the signals retrieved from the human scalp, which is likely to be contaminated, is considered as one of the disadvantages of the EEG recording. An amplifier is usually utilised to boost the relatively weak electric potential to gain the useable signal [154].

The advantages of an EEG monitoring system outweigh its downside. The cost of EEG recording is rather low. The method is non-invasive. Although the EEG's spatial resolution is low, the temporal resolution of the EEG is high.

The advancement in headset technologies makes the EEG monitoring processes easier and more comfortable especially for patients such as children and elderly [176], [177]. The Emotiv EPOC is an example of a lightweight and wireless headset, as shown in Figure 2.22. The felt sensors, as shown in Figure 2.23, are moistened with saline solution and attached to the headset's placeholders. The headset sends signals through a wireless USB dongle shown in Figure 2.24 to a computer. The sampling interval depends on a headset. The Emotiv EPOC headset can

provide 128 Hz of the sampling rate (2048 Hz internal) while the Biosemi Active can give 2048 Hz of sampling rate [178]. The 128 Hz is a reasonable sample rate because the oscillation of the EEG brain activity falls between 1 Hz to approximately 30 Hz. Therefore, the acquired signal is typically band-pass filtered to a range of the interested frequencies e.g. 1-30 Hz, or 1-60 Hz.

Besides the general advantages, the number of brain monitoring systems and techniques including positron emission tomography (PET), functional magnetic resonance imaging (fMRI), magneto-encephalography (MEG), optical topography (NIRS) is compared and criticised in HAM studies together with the EEG [16].

The reliability of the EEG method in brain activity measurements has been proven over a period of months on many types of subjects [179]–[181]. In disabled subjects, the EEG is effectively utilised as a brain-computer interface (BCI) to help subject with limbs movement problem to control an object without any physical limb movements [178], [182].

Figure 2.22 The Emotiv EPOC headset.

Figure 2.23 Felt sensors.

Figure 2.24 USB dongle for wireless data acquisition with the Emotiv EPOC headset.

2.13.3 Stimulus-locked event or event-related potential (ERP)

An event-related potential (ERP) or a stimulus-locked event is an identifiable change of ongoing EEG signals reacting to given stimulus events e.g. visual, auditory, imagery, sensorimotor, etc. [172], [183], [184]. Figure 2.25 demonstrates the ERP that takes place at the time of the onset of the stimuli within the reading window of -500ms to 1500ms. The ERP signals or voltages are quite small e.g. around 1 to 30 microvolts compared to the background EEG signals [185].

By a low signal-to-noise ratio of the EEG signal, the conventional method to detect the ERP is to average the EEG signal out around the stimulus onset time. To the event of interest, mental

preparation and response are expressed in the averaged ERP. The noises or artefacts are deadened, and the signal-to-noise is improved as well. Still, some cancellation of important brain related activities are revealed in this averaging method [186], [187]. That makes this method unsuitable for a research project that bases on a single trial brain response analysis.

During the analysis, it is important to eliminate interferences from other sources e.g. eye blinks, heartbeats etc. For example, an independent component analysis (ICA) in EEGLAB [188] is used to remove those artefacts in [189].
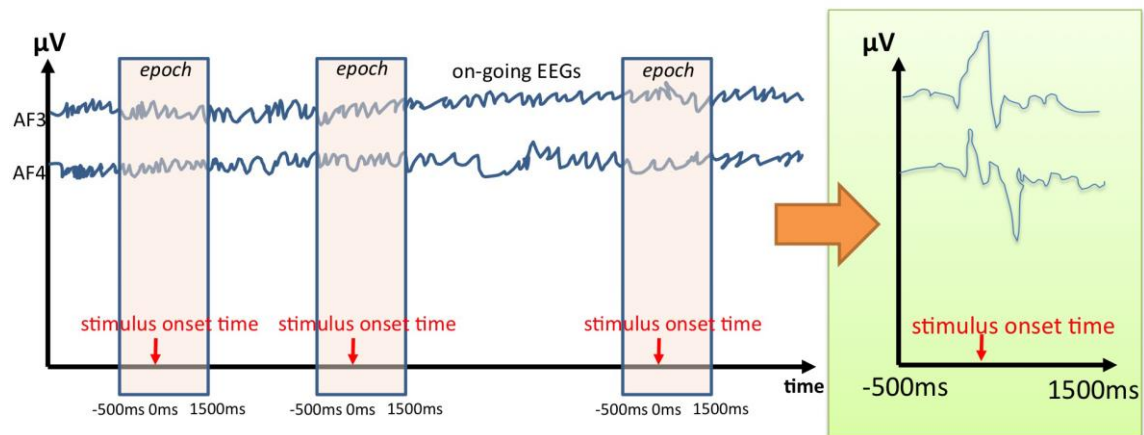
Figure 2.25 Event-related potential (ERP) averaging method.

There is a study using the ERP to investigate the origins of memory sources [162]. The study uses an old-new discrimination scenario to differentiate the ERPs from the occipital lobe and the frontal lobe. It has been concluded that the frontal lobe is the important region for memory source monitoring.

2.13.3.1 P300 speller ERP

A P300 speller is human-brain-thinking spelling based on the ERP brain responses [177], [178], [190]. Regularly, a P300 ERP can be interpreted from the central-parietal lobe of the brain. The common features of ERP waveform are the amplitude, the latency, and the scalp distribution. The letter 'P' refers to a positive deflection of the EEG signal after stimulated and the number

'300' is the latency of the deflection measured in milliseconds. If a deflection is bounced back towards the negative scale then a letter 'N' is used instead.

An example of P300 is depicted in a graph in Figure 2.26. The Emotiv EPOC headset is used in a P300 ERP experiment in [177], [190]. The wave is returned from an electrode Cz at the centre of a human head shown in Figure 2.20. The P300 ERP shows five deflections from an onset of a stimulus. The first deflection is a positive deflection P1 occurring around 100ms, followed by a negative deflection N1. Around 200ms after the stimulus, another positive deflection P2 occurs. The signal bounces towards negative scale again at N2 and gradually moves towards positive at P3 at around 400ms.
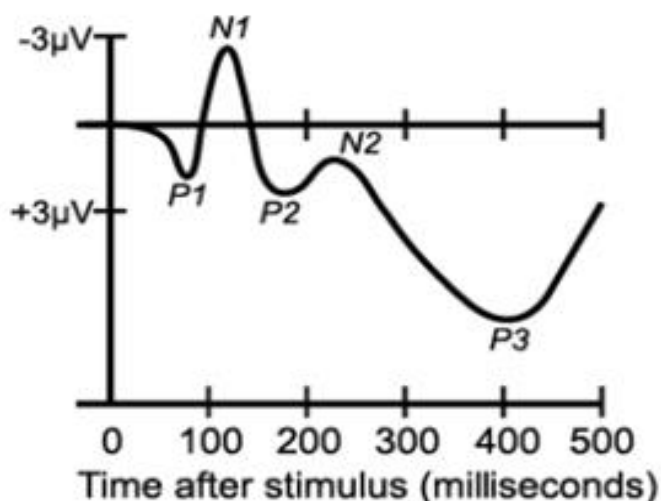
Figure 2.26 P300 event-related potential [190].

2.13.4 Analysis and signal processing methods

2.13.4.1 Filtering

In most cases, the frequency of the brainwaves falls between 1 Hz to 30 Hz agreeing to the rhythms definition, as summarised in Table 2.7 in Section 2.13.1.1. Therefore, it is mandatory to band pass filter the signals to the frequency range of interest. For example, the Butterworth band-pass filter is applied to limit the acquired signals to fall between 1 Hz to 12 Hz in a study of P300-based BCI for disabled subjects [178]. The immediate effect of filtering is that power line frequency, which normally is 50/60 Hz, is cancelled out as well.

2.13.4.2 <u>Windsorisation</u>

Windsorisation is an amplitude trimmings or truncation during pre-processing to make the EEG signal stay within the range of interest. Spikes, unwanted, and extreme amplitude caused by strange noise or artefact are eliminated. This technique is employed in pre-processing of [178]. Figure 2.27 shows truncated boundary of the method. The signals that exceed the two red lines are clipped off.
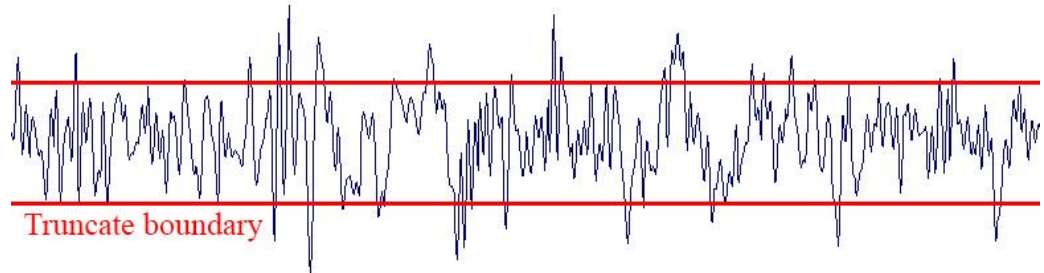
Figure 2.27 The example of windsorisation or truncation.

2.13.4.3 <u>Time and frequency domain analysis</u>

The extraction of frequencies from a time series signal provides the extra dimension of data inthe time domain signal analysis. Fourier Transform (FT) is a method used for transforming data from time domain to frequency domain. The transformation extracts frequency and amplitude information from the periodic data. The process is reversible, so it is possible to transform from the time domain to the frequency domain and vice versa. The advantage of the analysis in the frequency domain is that the filtering is performed faster and sometimes the noise is easier to be filtered out. Therefore, the method is frequently applied to the EEG study [180], [191]–[195].

Any periodic sequence $f(t)$ can be defined in terms of a linear combination of sines and cosines of different frequency. It is known as a Fourier series (2.26).

$$f(t) = \sum_{k=1}^{n} A_k \cos(2\pi\omega_k t) + B_k \sin(2\pi\omega_k t) \tag{2.26}$$

Where A is an amplitude, ω is a frequency.

The Fourier transform of $f(t)$ is defined as (2.27)

$$F(\omega) = \int_{-\infty}^{\infty} f(t)e^{-2\pi i \omega t} dt \tag{2.27}$$

And the inverse Fourier transform is defined as (2.28)

$$f(t) = \int_{-\infty}^{\infty} F(\omega)e^{2\pi i \omega t} d\omega \tag{2.28}$$

In case of a discrete periodic sequence $f(k)$ where k is an integer at a period N.

A Discrete Fourier Transform (DFT) can be defined as (2.29)

$$F(j) = \sum_{k=0}^{N-1} f(k)e^{-2\pi i k j / N} \qquad\qquad 0 \le j \le N-1 \tag{2.29}$$

The inverse Discrete Fourier Transform is defined by (2.30)

$$f(k) = \frac{1}{N}\sum_{j=0}^{N-1} F(j)e^{2\pi i k j / N} \qquad\qquad 0 \le k \le N-1 \tag{2.30}$$

The faster algorithm to the Discrete Fourier Transform is the Fast Fourier Transform (FFT), which uses $O(N \log N)$ instead of $O(N^2)$ operations [196], [197].

The major drawback of the Fourier Transform is that the time domain information is completely lost after the transformation. The other drawback of the Fourier Transform is that it works well only with the stationarysignal. The Fourier Transform produces decent results when it is applied to stationary data, unfortunately, the EEG signal is non-stationary. Hence, the alternative version of the Fourier Transform called Short-Time Fourier Transform (STFT) or Gabor transform [198] is invented to deal with the mentioned drawback. The STFT method pays more attention to the time window of a local segment of the signal. Although the STFT has overcome the stationary problem, it is still lack of time resolution.

2.13.4.4 <u>Wavelet Analysis</u>

Wavelet analysis is an alternative to the shortcomings of the Fourier analysis. A basic concept of the wavelet analysis and a tutorial on application to the neuroelectric or EEG data are supplied in [199]. The wavelet has a time-varying shape that can be stretched, shrunk or translated over a time scale. Figure 2.28 shows a B-spline wavelet and its variations. Various works in the EEG including de-noising [187], ocular artefacts removal [174], [175], feature extraction [200], [201] etc. has applied the analysis in many ways.
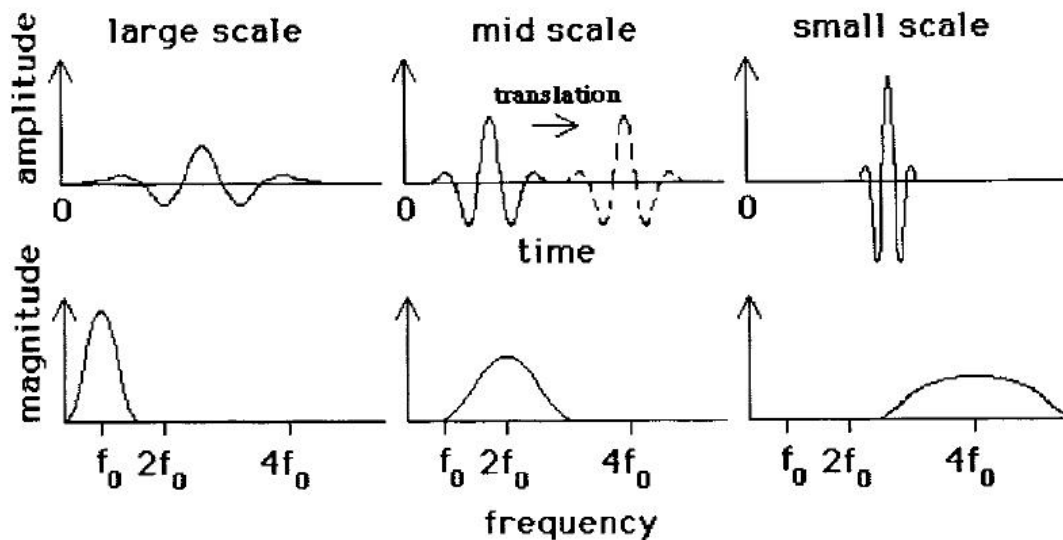
Figure 2.28 A B-spline wavelet stretching, shrinking, translation and the corresponding frequency spectrum [199].

The potential advantage of the wavelet analysis is that it maintains both frequency and time domain data of the transformed signal. Basically, in the Fourier Transform, the sine and cosine waves are used for sampling the signal of interest. The sine and cosine waves are localised in a frequency domain but spread infinitely in a time domain. Conversely, the wavelet transformation utilises a wavelet shape instead of the sine/cosine waves to transform the signal of interest. A set of variations of a wavelet shape is called a wavelet family. The examples of well-known wavelet shapes are shown in Figure 2.29. By utilising a wavelet family, the wavelet transformation is localised in both time and frequency domain. In theory, scale and translation are infinite, but practically it is limited to particular levels.
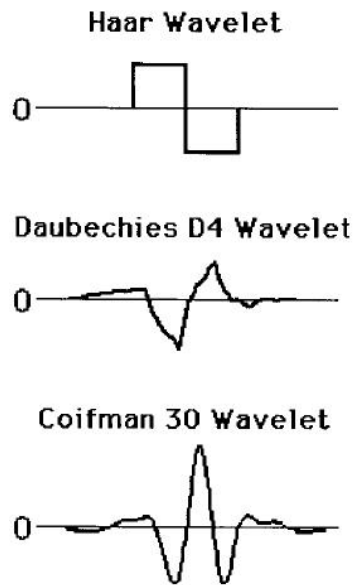
Figure 2.29 Some of the wavelet shapes [199].

2.13.4.5 Independent component analysis (ICA)

The independent component analysis (ICA) is a method for training or learning spatial filters that focuses on one source of information in the data while processing the data collected from many scalp locations [172], [188], [202]. It is a statistical blind source separation problem. Figure 2.30 shows the basic illustration of the ICA. Given that there are two sinusoidal signals A and B, which have different frequency and phase, Figure 2.30(a). They are linearly mixed using equations (2.31) and (2.32). The mixed signals are shown in Figure 2.30(b). By applying the ICA algorithm to M1 and M2, the sources A and B can be revealed. The revealed signals are shown in Figure 2.30(c), which are approximately the same as the sources. The amplitude of both uncovered signals is slightly different from the sources. It is required to invert the phase of the revealed signal that seems to be the source B.

$$M1 = A - 2B \qquad\qquad (2.31)$$

$$M2 = 1.73A + 3.41B \qquad\qquad (2.32)$$
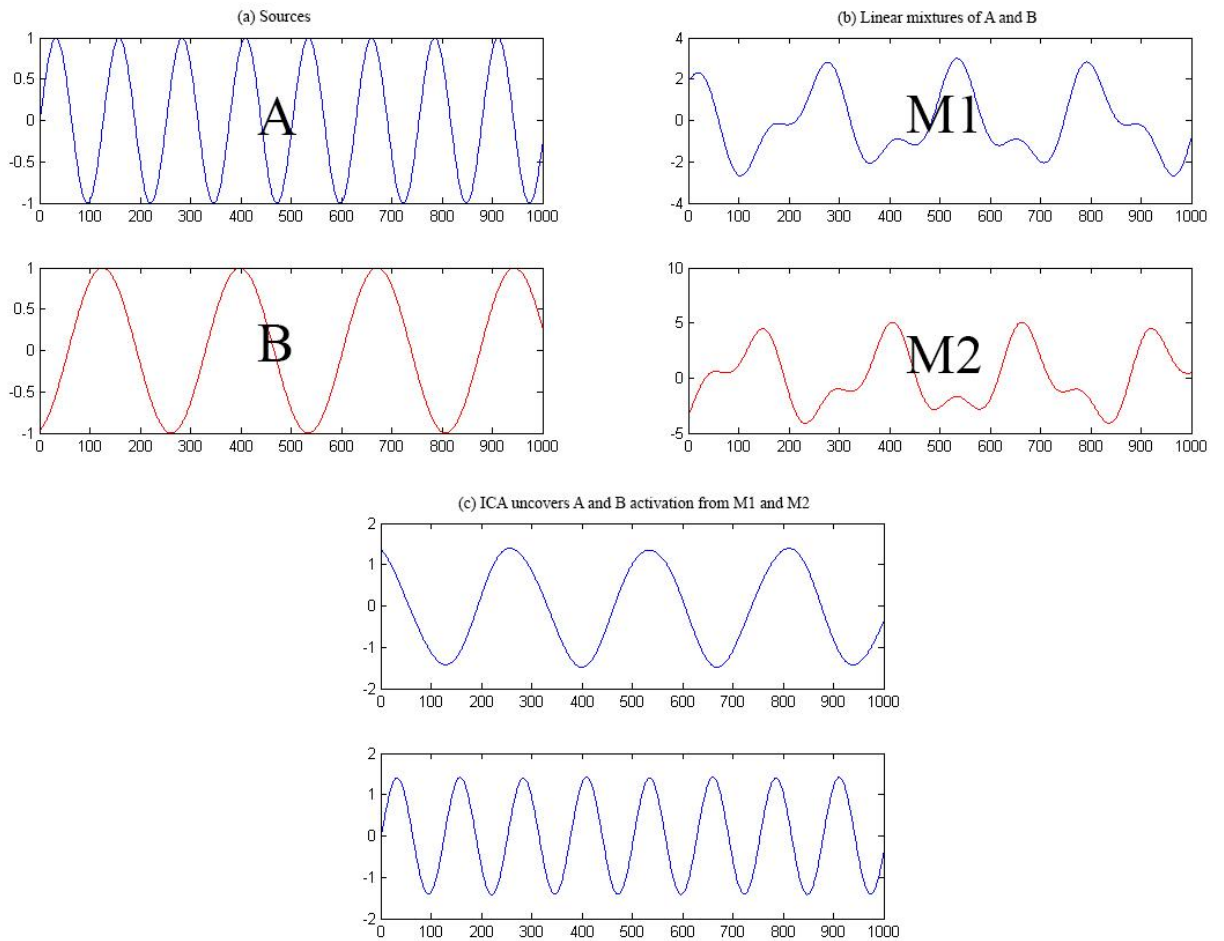
Figure 2.30 The ICA process.

The ICA can be applied for removal of eye activity artefacts as explained in [203]. The process of eye artefact removal using ICA is shown in Figure 2.31. A multiple channels of EEG data is unmixed into independent component Figure 2.31(a). The suspicious eye activity artefactual components are marked for exclusion, then the remaining components are mixed in order to form the original EEG signal without the eye activity artefacts.

(a) ICA decomposition

Independent Components

EEG Scalp Channels

VEOG
F3
FC5
Cz
Pz

100 µV

20
0
-20
µV

unmixing
(W)

IC1
20
0
-20
µV

IC2
0.2
0
-0.2

IC3
2
0
-2

IC4
0.5
0
-0.5

1 sec

activations   scalp maps
(u=WX)   (W⁻¹)
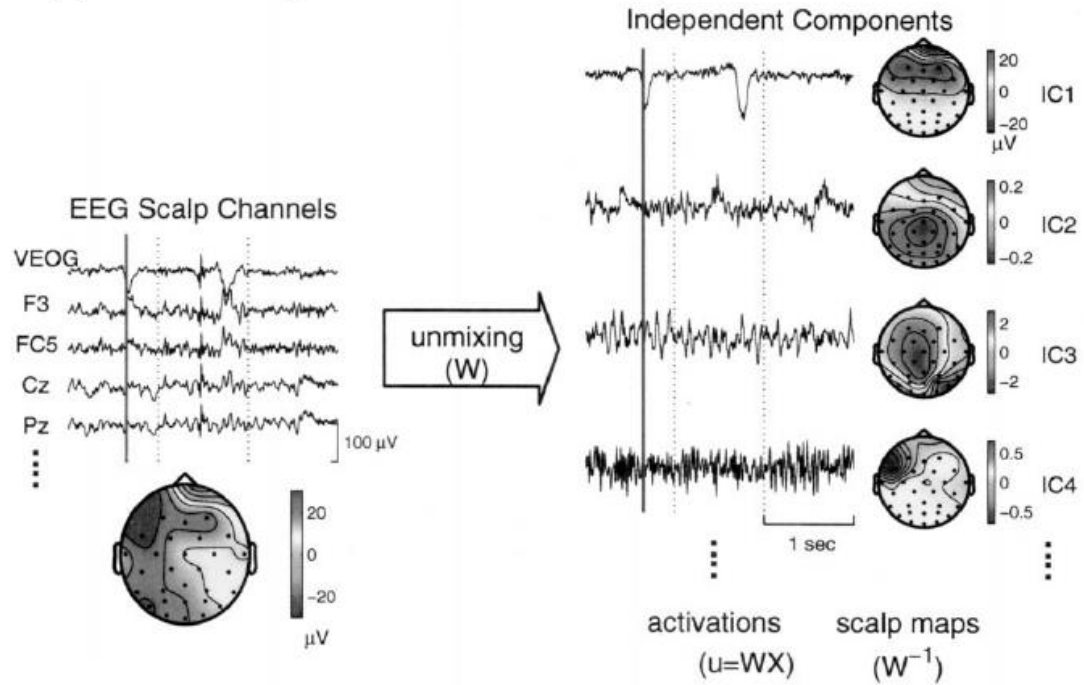
(b) Summed projection of selected components

Artifact–corrected EEG

VEOG
F3
FC5
Cz
Pz

100 µV

mixing
(W⁻¹)

20
0
-20
µV

$(x_0=W^{-1}u_0)$

IC1
IC2
IC3
IC4

1 sec
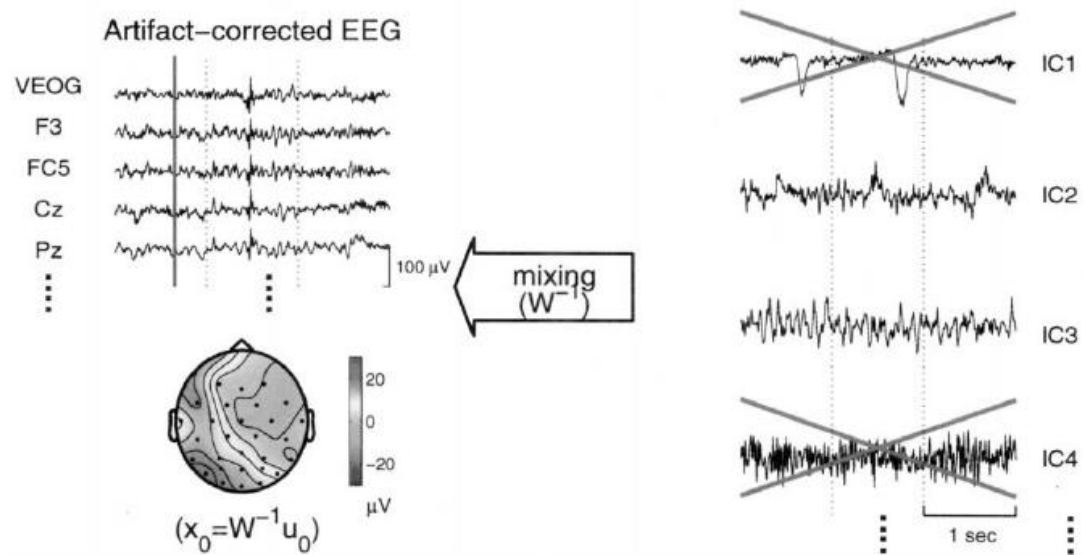
Figure 2.31 ICA applied for eye activity artefact removal [203].

2.13.4.6 <u>EEG feature extraction</u>

In order to be able to create a model from EEG brainwaves, it is required to analyse the characteristic / feature of the EEG signals. Several analysis perspectives can be applied to extract features from the EEG signal including statistical analysis [191], [204], [205], time domain analysis, ERP analysis [172], frequency domain analysis [191]–[193], time-frequency domain analysis [194], [195], wavelet transform [199]–[201] etc. Summaries of EEG feature extraction domains and algorithms are given in Table 2.9. Some of the reviewed works for human emotion recognition by applying statistical features is given in Table 2.10. Most of the works apply six statistical features referred from [192]. The advantage of using statistical features is that it can be computed online with less calculation effort.

Table 2.9 The EEG feature extraction domains and algorithms.

Feature extraction domain	Algorithms	Related works
Statistical	Means, median, standard deviation, root mean square, skewness, kurtosis, minimum, maximum, peak-to-peak	[191], [192], [195], [204]–[206]
Time domain	Event related potential (ERP), Time domain parameters (TDP)	[172], [193], [207], [208]
Frequency domain	Fast Fourier transform (FFT), Power spectral density (PSD), autoregressive (AR), Eigenvector	[191]–[193]
Time-frequency domain	Wavelet transform, Common spatial pattern (CSP), Time frequency distribution	[194], [199]–[201]
Space-time-frequency domain	Parallel factor analysis (PARAFAC), STAT-PCA	[209]–[211]

Table 2.10 Reviewed works on human emotion recognition based on statistical features.

Reviewed work	Recognition	Signals / data size	Statistical analysis	Time domain analysis	Frequency domain analysis	Time-frequency domain analysis	Classifier algorithms	Accuracy	Additional information
[204]	5 emotions	- 6 subjects, 64 channels EEG, 256 Hz sampling rate - 150 for training	6 statistical features plus 5 transformation of statistical features	N/A	N/A	N/A	Back propagation ANN	95%	N/A
[206]	5 emotions	- multi-modal 3 bio-potential sensors (EEG, pulse, skin conductance) - 12 subjects	6 statistical features	N/A	N/A	N/A	SVM	41.7%	N/A
[192]	8 emotions recognition from	- single subject - 5 physiological states; electromyogram, blood-volume pressure, heart rate, skin conductivity, respiration	6 statistical features	N/A	4 features of power spectral density (PSD)	N/A	k-NN, MAP	81%	features transformation: sequential floating forward search (SFFS) and fisher projection (FP)
[191]	7 emotions	- 3 subjects - EEG BIOPAC with 3 electrodes	min, max, skewness, kurtosis, peak-to-peak, median, standard deviation	N/A	FFT for frequency spectrum	N/A	N/A	N/A	salient features Only provide an analysis no conclusion accuracy

[205]	Parkinson diseases classification	- 11 subjects - EEG 9 channels	baseline, standard deviation, means	N/A	FFT	N/A	Simplecart	84.42%	Parkinson disease WEKA software 11 folds cross-validation
[195]	6 emotions detection	- EEG 63 biosensors - 6 healthy subjects - 256 Hz sampling rate	energy, recoursing energy efficiency, root mean square	N/A	N/A	discrete wavelet transform	Fuzzy C-Means (FCM)	N/A	Cluster analysis

Remarks: k-nearest neighbour (k-NN) classifier, Maximum a Posteriori (MAP) classifier, support vector machine (SVM), artificial neural network (ANN).

2.13.5 Visualisation

2.13.5.1 <u>ERP image</u>

An ERP image is a single-trial visualisation tool which is drawn alongside with the averaged ERP to show every trial that is averaged for the ERP [212]. The example of the ERP image from an electrode AF3 is shown in Figure 2.32. The averaged ERP graph is shown at the bottom of Figure 2.32. The ERP is averaged from 293 epochs. All of the 293 epochs is shown by the colour-coded value of amplitude as shown at the top of Figure 2.32. The colour-code is shown on the right side of Figure 2.32.
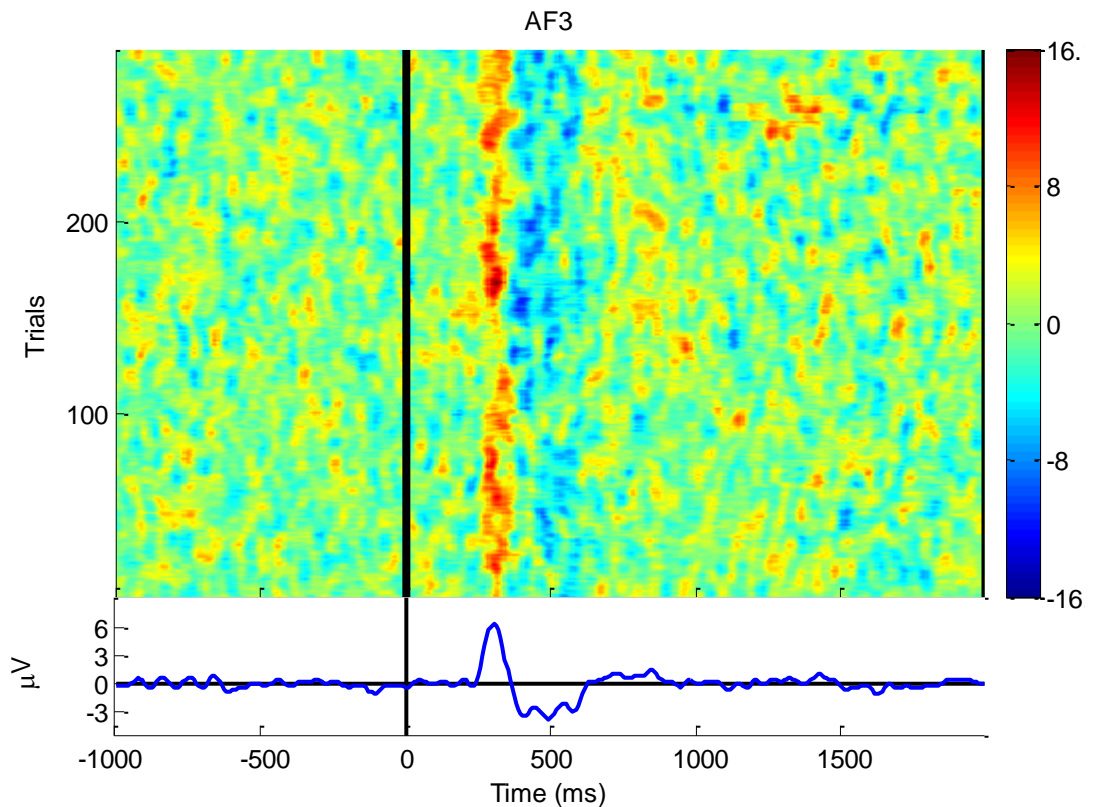
Figure 2.32 An example of ERP image.

2.13.5.2 <u>2D topography map</u>

A 2D topography is an EEG activation mapping across the scalp surface. It is represented in a colour-coded scale from the top view. The colour gradation expresses amplitude of the brain activity at the given time. An example of 2D topography is shown in Figure 2.33. The figure shows an EEG activation at 200ms, 300ms, 400ms, and 500ms, respectively. The colour-coded scale ranges from -7.2 to 7.2 µV in blue to red colour.
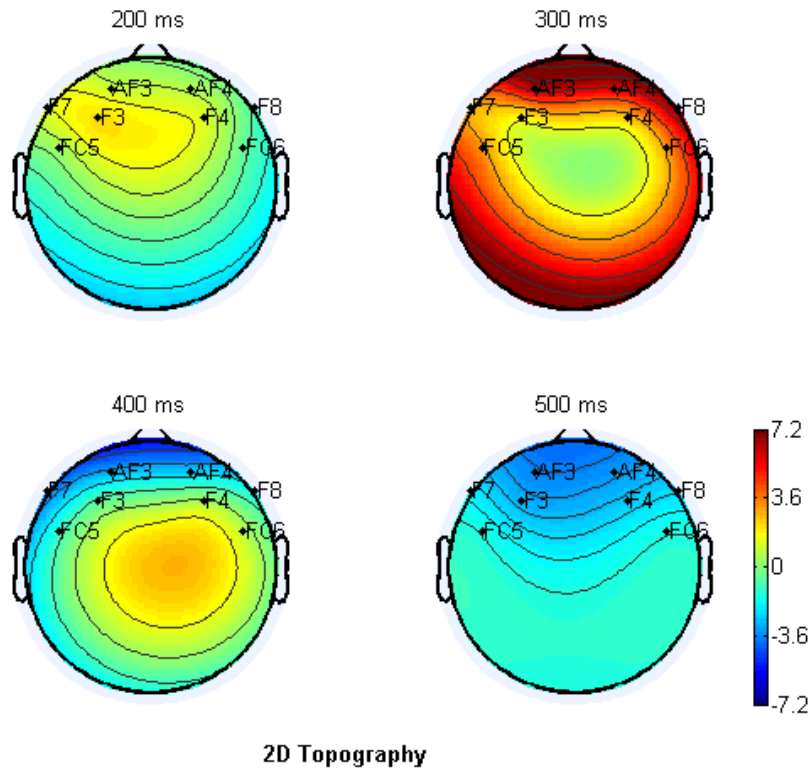
Figure 2.33 An example of 2D topography.

2.13.5.3 <u>3D topography map</u>

Likewise, a 3D topography represents a three-dimensional mapping of EEG activations across the scalp. An example of 3D topography is shown in Figure 2.34. The figure shows colour-coded EEG activation in 3D scalp head at 200ms, 300ms, 400ms, and 500ms. The voltage code is range from -7.9 to 7.9 µV from blue to red colour. The colours that represented EEG activation are derived from the voltage value at the location of the sensor on the scalp at the specified time. The colour of the topography other than the exact sensor location is interpolated.
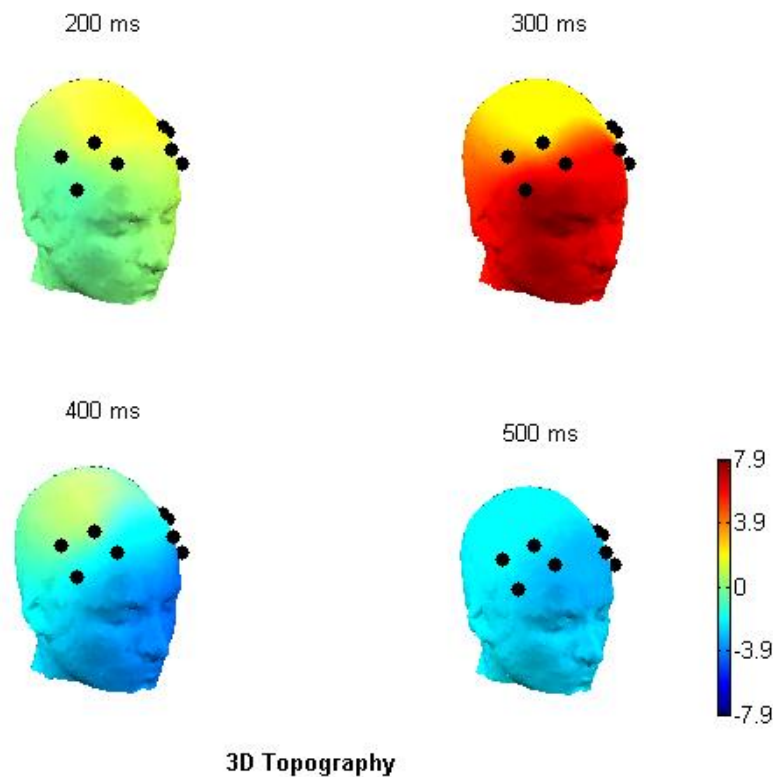
Figure 2.34 An example of 3D topography.

2.13.6 Apparatus

The Emotiv EPOC is a wireless EEG headset as shown in Figure 2.35. The headset has 16 electrodes, as depicted in Figure 2.35. Fourteen electrodes are used for the EEG recording while the other two i.e. CMS and DRL are used as the reference. The CMS and DRL stand for "Common Mode Sense" and "Driven Right Leg", respectively. The sampling rate of the headset is 128 Hz (2048 Hz internal).

Some literature has proven that the Emotiv EPOC headset can provide a good quality of EEG brain activity signal for various applications including a replication of visual P300 ERP speller [190], an auditory ERP study [189], and mental actions BCI classification [213]. A study by [189] compares the Emotiv headset simultaneously with a research grade Neuroscan 4.3 headset by placing them on top of each other while subjects listen to the auditory stimuli to capture the auditory ERP and can be concluded that the Emotiv headset can record a reliable EEG signal. The portability of the headset provides flexibility for EEG recording. Children and cognitive

disorder adults benefit from this advantage. The outdoor EEG recording also benefits from this advantage [176]. The wireless capability of the headset makes it possible to integrate the headset to a mobile phone for a novel phone BCI dialling application by adopting a P300 speller paradigm with a lightweight classifier running on the phone [177].
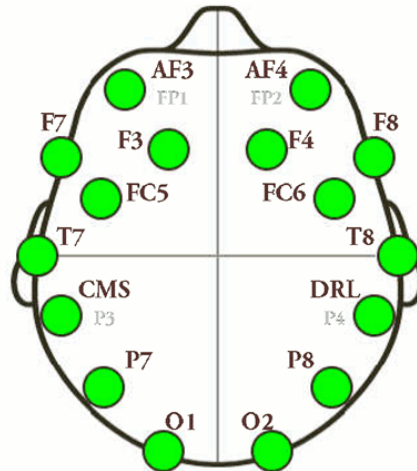
Figure 2.35 The locations of Emotiv EPOC electrodes on the scalp [190].

The localisation or coordinates of the electrodes of the Emotiv EPOC headset can be found in Appendix C. These values can be used with EEGLAB [188], [214], [215] or other software for a plotting of scalp topography maps.

2.14 The analysis and the identification of research gap

It is found from the literature review that most of the research projects are lacks of the important component i.e. the online HMI performance modelling and evaluation. This component is the centre of the machine's capability to give the adaptive assistance based on the individual performance level. Although the study related to a human performance has been investigated for decades, it is rather different from the HMI performance modelling point of view. It is the performance of the interaction between a human and a machine that is the basis for the adaptive capability of a machine.

There exist some of the recent research projects on the analysis and understanding of HMI performance in various type of applications such as forestry manipulation [216], air traffic control [217]. The work in [216] focuses on the performance analysis of a hydraulic manipulator's trajectories operated by two different operators. It is the offline performance analysis of the manipulation trajectory that would be useful in the future for the implementation of an adaptive machine. The work in [217] proposes a model of human performance from the perspective of decision-making ability i.e. the decision of a sequence of actions from the air traffic control application. Apparently, it is a study of human performance models from the task network perspective of HMI performance modelling [61].

Recent work based on the HAM concept implements an assistive steering wheel from a driving simulation scenario [218]. The assistive controller is adjusted based on the classification of the driving behaviours of an expert and a non-expert drivers. A classifier is used to compare the similarity distance between them in order to adjust the parameter of the assistive controller. There is no apparent performance evaluation model but the comparison between the two different drivers by using a classifier. It is lack of a performance evaluation method. Another HAM based research work focuses on a comparison of skill index algorithms for the evaluation of human operator performance on the driving skill [219]. However, the comparison is rather brief, unclear, and there exists the limitation mentioned on the paper i.e. it is subject-dependent.

The improvement of HMI requires multiple studies in the related fields e.g. a machine, a human, interaction, intention recognition etc. However, a human can be considered as the main body who uses a machine, and it is the most unpredictable part of an HMI system. Hence, the inclusion of an EEG device to record the internal inherent of the human brain processing activity could reveal the relationship of the HMI activity and provide the establishment to create a model of HMI performance evaluation. This establishment can be considered as the bridge between the internal of a human intention to the outcome of the HMI actions.

2.15 Summary

This chapter reviews research works related to human and machine interaction especially the HAM concept. The HAM concept has emerged from a simple idea of machine intelligent and

learning i.e. the machine capability to give the assistance or guidance to its user. The HAM realisation requires knowledge and methodology from many research fields. However, the HAM research is still in its infancy stage. It still has many challenging issues to be addressed such as human-machine interaction modelling, human-machine performance evaluation modelling, human intention modelling etc.

A review on HRI, HMI, HAI, HSC, and HAM reveals the important similarity among these man-made systems i.e. the human interaction with them. Although the interaction may be slightly different, a human is a primary body within these human-in-the-loop systems.

There exist several forms of human-machine interaction (HMI) including proximity, remote, and wearable. A control interface is the mandatory interacting medium in any forms of the interaction. The advancements of the human-machine control interface have improved the many aspects the interaction e.g. performance, ergonomic, efficiency, energy conservation etc. A brief review of telerobotics is given to addressing the importance of the remote controlled robot applications that could be accomplished by the improvement from human-machine interaction research.

An adaptive interaction requires several components working as a system; recognition of human intention, human-machine performance evaluation, adaptive assistance, shared control etc. The details and reviews of these components are given.

Although the concept of adaptive and shared control interaction would successfully improve the quality of interaction towards the positive direction, this is idealistic. Many issues regarding the conflict, degree of sharing, authority in control, overreliances etc. have been discussed.

It is vital to understand a model of human performance since the human is the primary beneficial body of the interaction. Various aspects of human performance modelling including the definition of human skill, characteristic of the skilful operator, human capacity, stages of skill learning, Fitts' law, and Rasmussen model of SRK etc. have been given.

A review of some particular aspects of human control modes e.g. pursuit tracking, compensatory control, balancing control, oscillatory control, target hitting control etc. have been given. These control strategies can be thought as a primitive human-machine interaction.

Several perspectives can be adopted in the HMI model development. The selection of perspectives depends on the particular level of interaction. For example, a supervisory interaction can apply the knowledge base perspective while a low level of interaction can apply the control-theoretic perspective for HMI performance modelling. Apart from the perspective selection, a choice of modelling approaches depends on the available data. The descriptive modelling approach is often used for human modelling since the human behaviour is relatively difficult to model analytically. The review of these perspectives and approaches are presented.

Particularly, the descriptive and predictive approaches are suitable for the development of HMI model. A cross-validation method ensures the consistency of the modelling outcome. Additional model performance evaluation methods are reviewed to confirm the validity of the model accuracy. The bio-inspired artificial neural networks (ANN) machine learning is reviewed for using along with the selected perspective and approach.

To conduct the investigation on HMI, a model of a pendulum-driven capsule system is reviewed, and the mathematical model is examined for the simulation platform.

In order to achieve in depth understanding to HMI, the introduction of brain monitoring system can be employed. The brain regions and functions are reviewed in conjunction with a non-invasive measurement of brain electrical activity of cerebral cortex, EEG. Some technical aspects related to the EEG system, fundamental, analysis methods etc. are introduced. Finally, the apparatus used in this research i.e. the Emotiv EPOC headset is investigated.

Chapter 3 Method of investigation, platform design and implementation

3.1 Introduction

This chapter describes the investigation method, design, and implementation in order to fulfil the aim and objectives of this research. Since this research aims at studying human interaction with a machine under the motivation from the HAM concept, two main stakeholders are obviously involved i.e. a human and a machine. A human can be any person who can interact with a robot / machine in order to accomplish a certain task. It is well known that to conduct research on an actual machine can cost tremendous budget, time, and effort. Also, a physical machine requires a certain amount of effort from a human participant to conduct an experiment. Safety is also a serious issue that needs to be taken into account to a physically based research. Alternatively, simulation is a powerful method that can help avoid the previously mentioned issues and can give an accurate result before a physically based research. Hence, this research is based on the simulation where a machine is simulated using a mathematical model. However, the operator side is still performed by an actual human rather than a simulated one. Consequently, a hardware interfacing between a simulated machine and a human is still required in order to acquire the interaction behaviour.

A HAM simulation platform is developed by this research in order to conduct the investigations. The platform is responsible for simulating a machine model, interface with external hardware, and handle the interaction between the machine and a human. The design, architecture, and implementation of the platform are discussed in Section 3.4.

3.2 Focus of the research

To describe the focus of this research, the four approaches of human performance modelling from a review in Section 2.5.8 is used to clarify the focus area of the investigation. The approaches can be hierarchically represented by the arrangement from low to high level of HMI as shown in Figure 3.1. The 'knowledge base' circle can be considered as a high level of interaction to a machine such as supervisory control. The 'information processing' involves the processing of information and notification of any occurrences of a meaningful signal from a machine system i.e. monitoring. The 'task network' requires a human to interact with a machine in a correct sequence of actions in order to achieve the best performance e.g. a sequence of making a dish of salad. The 'control theoretic' is the focus of this research in which the interaction is focused on the low-level interaction with a machine e.g. vegetable chopping.

It can be noted from Figure 3.1 that it is possible to develop the corresponding performance and control model at each level. Since this research focuses at the low level, the design and method of investigation are proposed to develop control and performance model at this level.
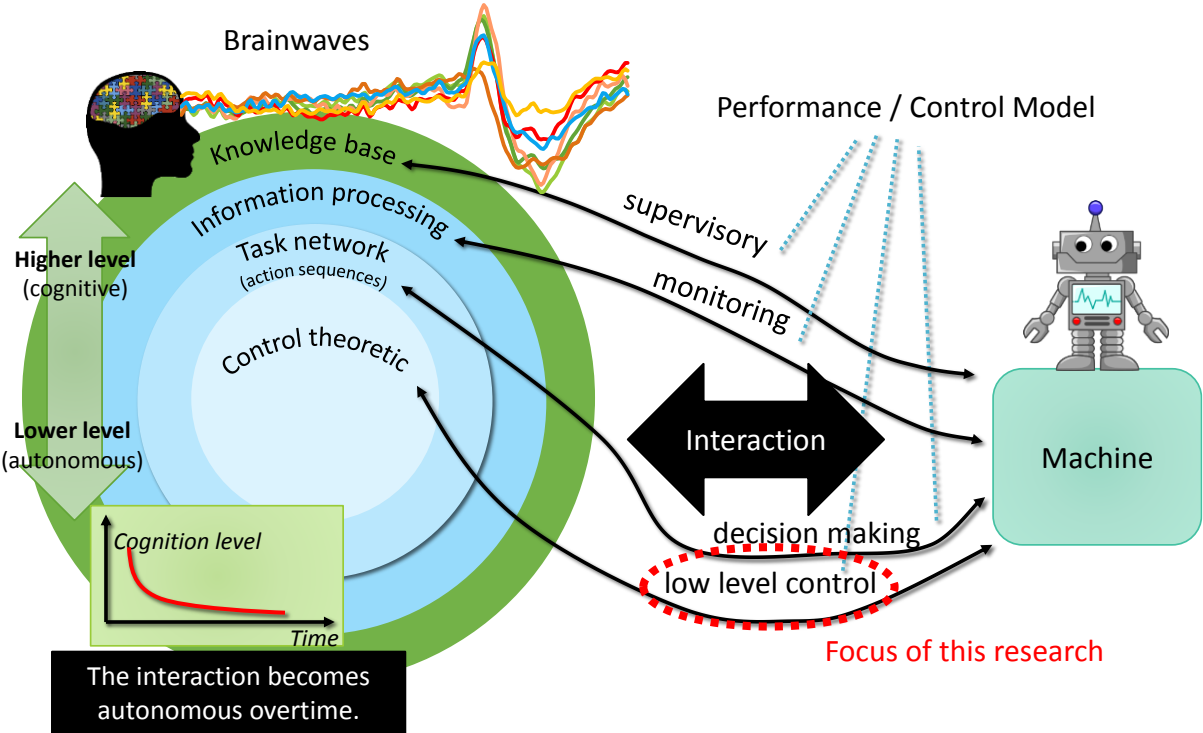
Figure 3.1 Hierarchical of approaches for a modelling of HMI.

Although HMI modelling can be defined in a number of ways, this research develops a view on the perspective of HMI modelling which is shown in Figure 3.2. A human can be modelled in terms of e.g. mental model, cognition model, and human physical attributes etc. A system can be anysystems such as a robot, a car, a factory plant, a computer etc. A task can be designed based on the goal of a particular problem. The intersections of each pair form a meaningful relationship. A 'human-system' forms a human machine interface or man-machine interface (MMI) which defines ergonomic and interaction between human and machine. A 'human-task' forms a relation for a task understanding. A 'system-task' forms a relation that specifies the capability of the system to do a task. The centre of the three blocks forms the HMI modelling. Also, the environment modelling is an inevitable part that covers all of the blocks because the participating bodies have to work within an environment.
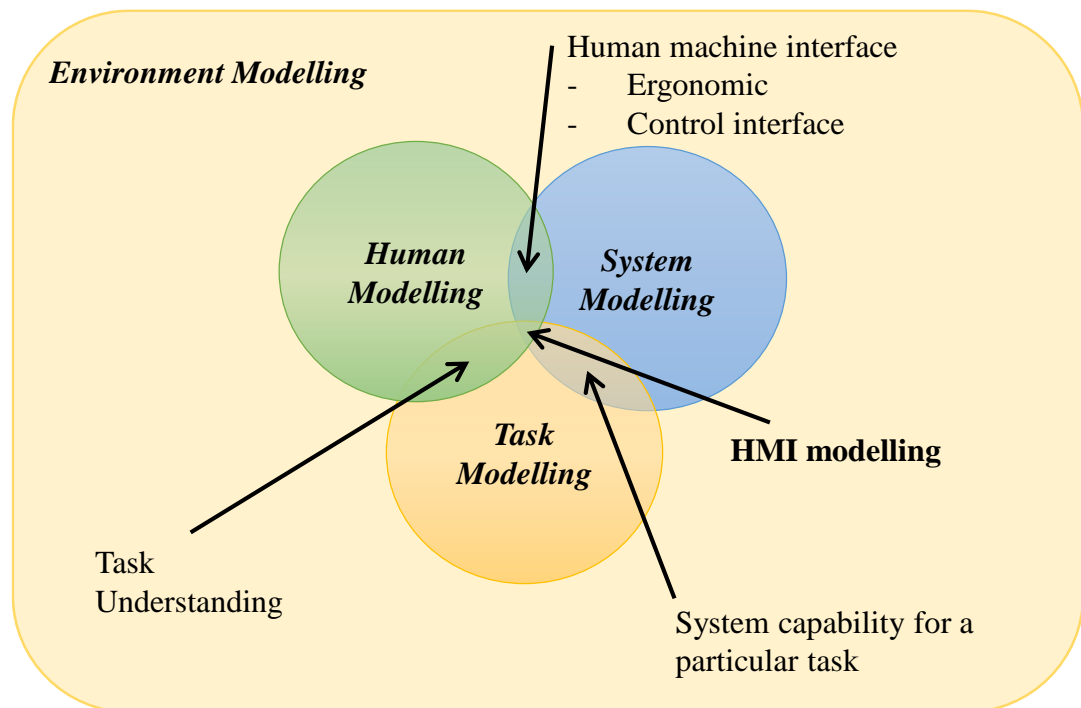
Figure 3.2 This research view on the perspective of HMI modelling.

3.3 Research methodology and design of the investigations

This research is based on a positivism research paradigm/philosophy where the research approach is to investigate, analyse, and develop a model based on conductions of an empirical study. An experimental scenario is designed and developed in order to execute an empirical study by enquiring a human participant to perform the scenario on a simulation platform. The data acquired during the experimental scenario is used for analysis, deductive reasoning and development of a model. The establishment of a relationship between a human-machine interaction performance and the scenarios is drawn from these analysis and model development.

A systematic research onion model has been presented in [220]. This research has adopted some parts of the onion model which are shown by the red dashed lines in Figure 3.3. The justification for choosing the onion components are given below.
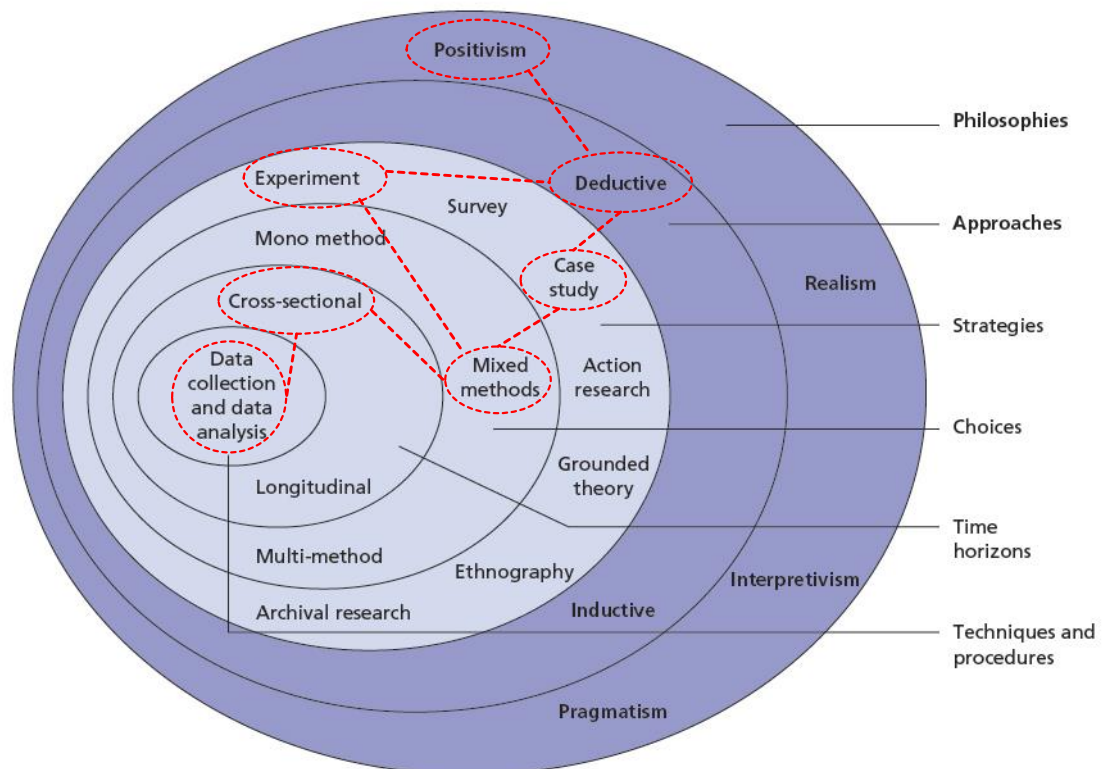
Figure 3.3 The research methods applied in this research are indicated by the red dashed lines from the view of research onion [220].

- **Philosophies**
  - Positivism - The nature of this research is a multidiscipline science based on the observation of the phenomena of HMI.

- **Approaches**
  - Deductive - the investigations are designed to fulfil the research aim and objectives.

- **Strategies**
  - Experiment and case study - the strategy of this research is to design case studies and experiments to fulfil the research aim and objectives.

- **Choices**
  - Mixed methods - both qualitative and quantitative methods are applied. However, the quantitative is the key method because the main motive is to obtain and analyse data from the empirical experiments.

- **Time horizons** (Cross-sectional)
  - Cross sectional - this research is conducted based on short periods in time horizon because of the constraints of the Ph.D. duration and resources.

- **Techniques and procedures**
  - Data collection and analysis - this research obtains data empirically from the experimentation which are performed by participants.

Figure 3.4 shows a simplified diagram of the focus of the investigation from Figure 3.1.
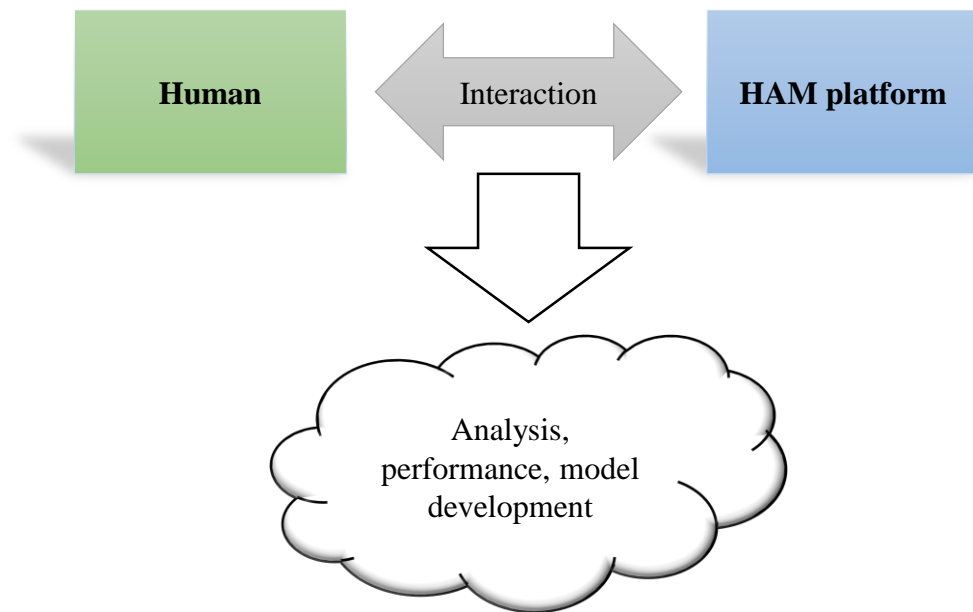
Figure 3.4 A simplified diagram of the investigation.

According to the paradigm and methods of the research, there are three main scenarios designed for the empirical investigations.

1. A human heuristic learning to control and identify a machine control rule.
2. A human heuristic learning and control performance analysis.
    a. Development of a human-machine control model based on the data observation.
3. A development of HMI performance evaluation model based on the features of EEG brainwaves.

3.4 HAM simulation platform

A simulation is a powerful tool for realising a system prior to an actual development, implementation, and deployment. Therefore, to study the HAM concept, a virtual platform is developed which provides an environment for a robot / machine simulation based on a mathematical model. In addition, the platform intends to provide real-time interaction with a human operator / participant in order to acquire their control information.

A diagram of interconnection blocks between a human and the platform is shown in Figure 3.5. A human operates a machine with the platform via an interface device such as a joystick,

keyboard, mouse, etc. The operator perceives a feedback and interact by their intention and turns out to be an action based on his/her skills and knowledge. It is noted that the operation is driven by a task goal. The process is reciprocal as a learning cycle. The action is based on skill. A human has the capability to learn to operate a machine by training until a particular skill is acquired. The skill is transformed into a set of rules. Eventually, a set of rules is formulated into knowledge. Ultimately, knowledge revolutionises into wisdom.

The HAM simulation platform is responsible for providing a simulation environment that is including a machine model simulation, a scenario based on a task, data acquisition, interface management, rendering the virtual appearance of the simulation etc. It is noted that the platform wirelessly acquires data from the Emotiv EPOC headset through the manufacturer provided API.
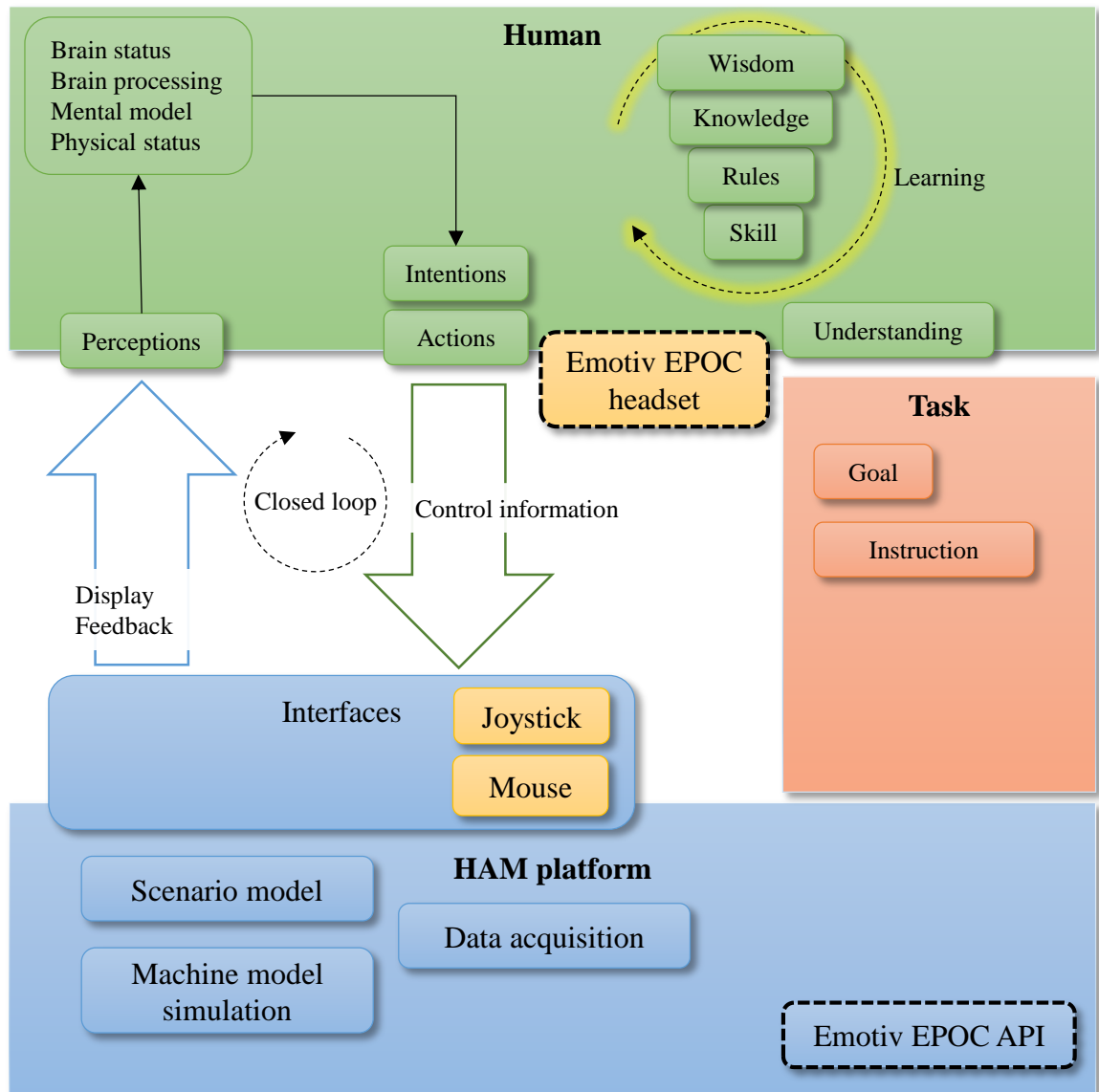
Figure 3.5 A building block of the platform.

3.4.1 The internal architecture of the platform

An internal architecture of the simulation platform is shown in Figure 3.6. The simulation begins with the specified initial conditions such as an initial pendulum angle, a zero model velocity, etc. Then, it enters the loop that sequentially processes the blocks inside the loop. The loop is aimed to maintain the specified time step. However, this depends on many factors e.g. complexity of the model and the simulation calculation method, speed of the computer etc. The simulation loop contains the equation solver, input management, graphic rendering, on-screen

graph drawing, a logging system, and the optional adaptation computation for active / passive assistance. The equation solver is implemented with ordinary differential equation (ODE) solver using 4th Order Runge-Kutta numerical method [221], [222]. After the simulation is completed, the platform saves logged data to files for further analysis.
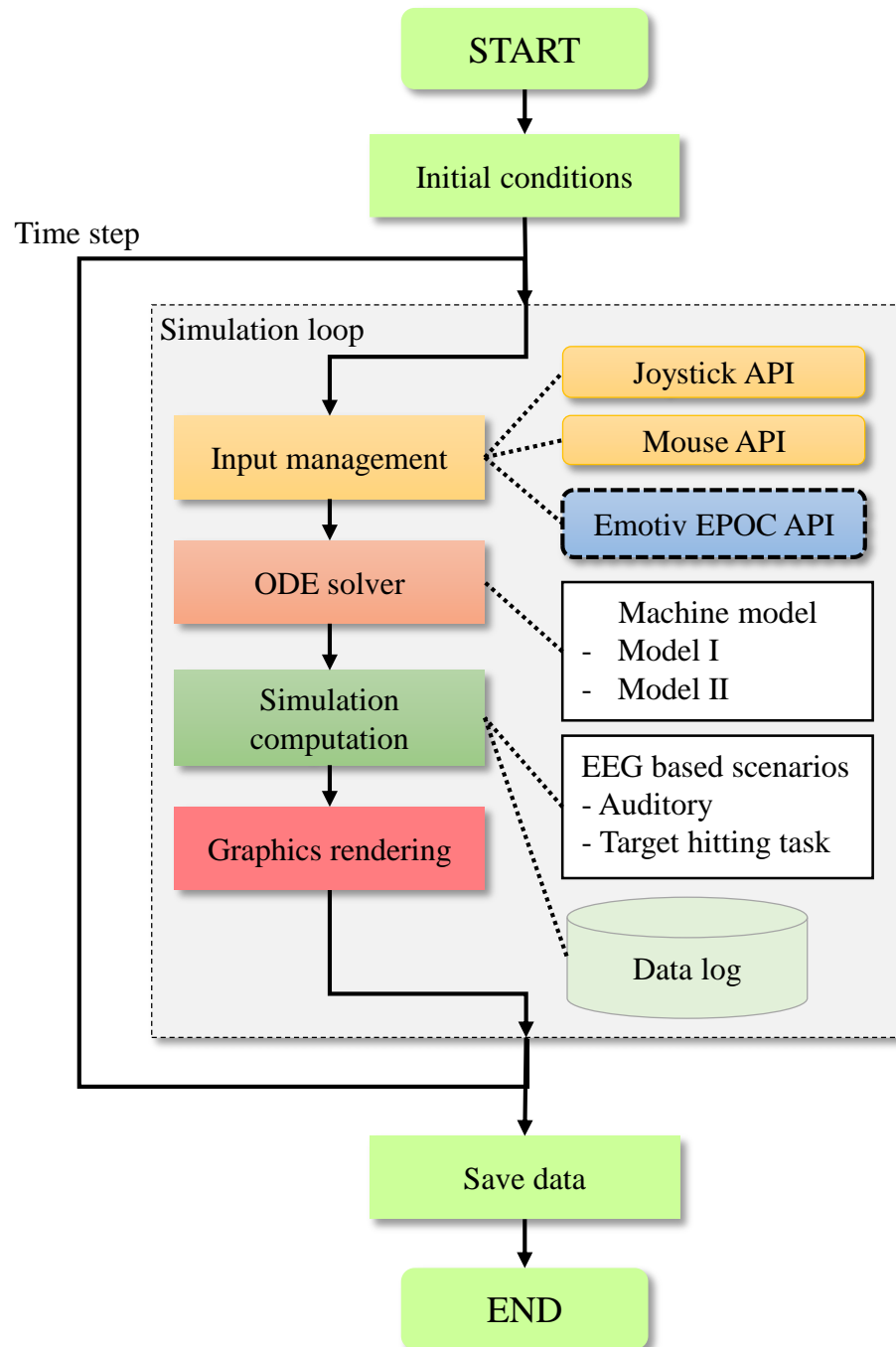
Figure 3.6 The HAM simulation platform internal architecture.

The platform is implemented using Microsoft C# programming language and the XNA as the graphical rendering package. The XNA is a powerful cross-platform library for graphics and game development.

3.5 Variations of pendulum-driven capsule models

A pendulum-driven capsule model explained in Section 2.10.1 is chosen as the case study because of its dynamics and challenges to control by a human. The study of the pendulum control mechanism is useful in many applications such as a human standing posture, an excavator arm structure etc. Furthermore, the pendulum-driven capsule is an underactuated mechanical system that required the particular level of skill, rule, and knowledge to learn to control it. There are two variations of the pendulum-driven model in this research i.e. Model I in Section 3.5.1 and Model II in Section 3.5.2.

3.5.1 Model I: A pendulum-driven capsule

A mathematical model of the pendulum-driven capsule Model I is obtained from the modelling explained in section 2.10.1. The model is required to be in a proper form for the numerical simulation by the platform. Thereby, the equations of motion (2.24) and (2.25) need to be transformed into the state-space form as follows.

$$\dot{v} = \frac{(2M + 2m)(\sigma_2 + \mu S\sigma_3) - \omega^2 Lmsin(\theta)}{(M + m)(2M + m - mcos(2\theta) - \mu Smsin(2\theta))} \tag{3.1}$$

$$where \ \sigma_2 = \frac{cos(\theta)(\tau + gLmsin(\theta))}{L}$$

$$and \ \sigma_3 = \frac{gLmsin^2(\theta) + \tau sin(\theta)}{L} - g(M + m) + \omega^2 Lmcos(\theta)$$

$$\dot{\omega} = \frac{(2M + 2m)(\tau + gLmsin(\theta) - \sigma_4)}{L^2 m(2M + m - mcos(2\theta) - \mu Smsin(2\theta))} \tag{3.2}$$

$$where \ \sigma_4$$

$$= \frac{Lmcos(\theta)(\mu S(Mg + mg - \omega^2 Lmcos(\theta)) + \omega^2 Lmsin(\theta))}{M + m}$$

$$\dot{x} = v \tag{3.3}$$

$$\dot{\theta} = \omega \tag{3.4}$$

The equations (3.1), (3.2), (3.3), and (3.4) are in the appropriate form for the numerical simulation using the implemented ODE solver in the platform simulation loop. A diagram of the pendulum-driven capsule input / output is shown in Figure 3.7. Input is the torque τ that controls the pendulum at the joint attached to the capsule body as illustrated in Figure 2.15. The outputs are the pendulum rotation angle and the capsule position according to the underactuated mechanism.
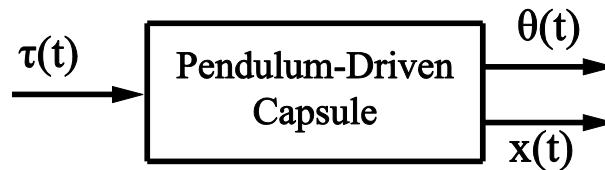
Figure 3.7 Input / output of pendulum-driven capsule model.

3.5.2 Model II: A PID controlled inverted pendulum-driven capsule

In this section, the model in Section 3.5.1 is modified to integrate an additional proportional-integral-differential (PID) i.e. Model II. A diagram of the modified model is shown in Figure 3.8. The PID controller is used to control the amount of torque required to maintain the pendulum angle at the desired value θ_d. Therefore, a pendulum-driven capsule becomes an inverted pendulum-driven capsule system by applying the PID controller to maintain the pendulum angle at the upright position ($\theta=0$) while there is no control input from a human operator. The simulation for this model is programmed to limit the range of pendulum angle to match the physical appearance of the capsule i.e. $90 < \theta < -90$. Unlike the model in Section 3.5.1 where the raw control input is the amount of torque. The raw input for the Model II is the desired angle θ. In other words, a human operator can concentrate on the pendulum angle to underactuate the capsule system to move in desired directions. The amount of torque is automatically computed by the PID controller to rotate the pendulum to the target angle.
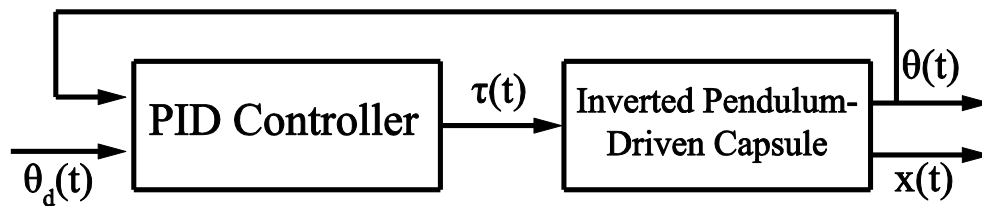
Figure 3.8 Input / output of PID controlled inverted pendulum-driven capsule model.

The justification for utilising a PID controller is explained here. The PID controller closely mimics the control behaviour of a human in balancing an inverted pendulum which is discussed in Section 2.7.2. A human can compensate the control in only two aspects i.e. the instantaneous compensation (proportional component) and the compensation over short consecutive actions (derivative component). The extra integral controller component is responsible for compensating the accumulated error over a period of time which is hardly achievable by a human being. Therefore, the use of PID controller can provide a smooth control to a human participant with the additional benefit of the integral component.

3.5.3 Human interaction with the machine models

The models described in Section 3.5.1 and 3.5.2 can be illustrated when they are operated by a human participant as shown in Figure 3.9 and Figure 3.10, respectively. The human operator is given the goal of the task that acts as the reference. The human brain processes the information and takes the action via the joystick interface to control the pendulum-driven capsule system. Then, the joystick action is transformed into the input to control the pendulum model. The Model I is controlled directly via the joystick output that is mapped into the amount of torque. The Model II has the PID controller to transform the desired pendulum angle into the amount of torque required to control the pendulum angle. A proper rotation of the inverted pendulum can drive the capsule system towards the desired direction. This rotation strategy is the control task that the human operator needs to learn. The appearance of pendulum orientation and capsule position on the display acts as feedback information to the human operator. Then, the loop is iterated aim at completing the task goal.

The models contain time-varying variables that pass the information throughout the system loop. The signal $r(t)$ is the reference or the given task goal. The $p(t)$ is the internal processing of the

individual human brain. The *h(t)* is the result of an internal brain processing output as a hand motion to control the joystick interface. The signal *j(t)* is the output from the joystick that is generated by the human operator's hand movement. *u(t)* is the control output from the PID controller to the pendulum-driven capsule simulation to achieve the desired angle. The *θ(t)* and *x(t)* are the outputs from the simulation model that appear on the screen of the virtual simulation platform. These outputs act as the feedback to the human operator's visual perception. The signal *ep(t)* is the simulation output information plus any external disturbances such as environmental distractions and unrelated activities on the screen.
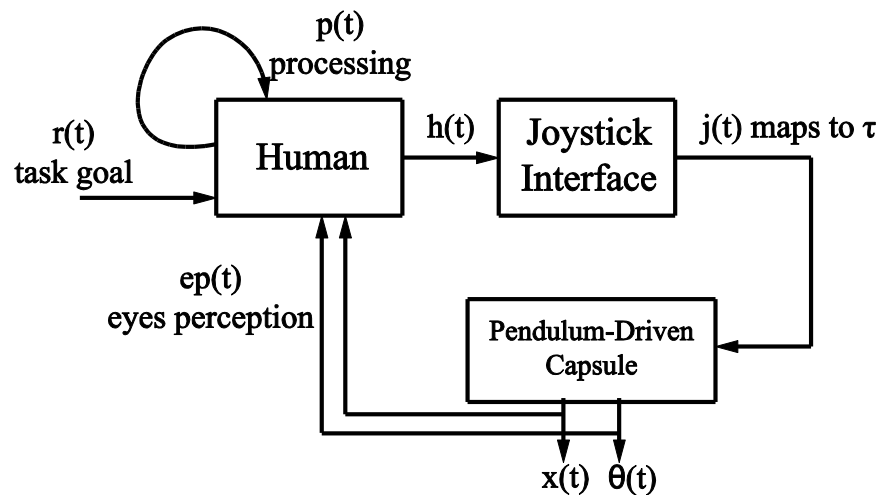
Figure 3.9 A human interaction with the pendulum-driven capsule system (Model I).
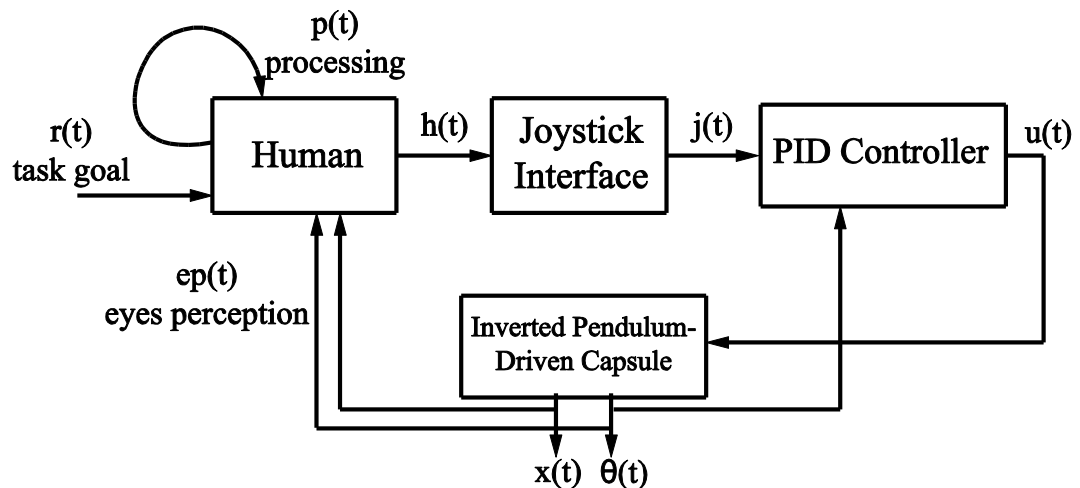
Figure 3.10 A human interaction with the PID controlled inverted pendulum-driven capsule system (Model II).

3.6 10-time-10-fold cross-validation

It is mentioned in Section 3.3 that the investigation includes a model development. The model development requires dataset acquired from the empirical experimentation. Then, the dataset is developed into a model by one of the modelling algorithms such as ANN, SVM, HMM, linear regression etc. In this research, an ANN is adopted as a model development tool because of its flexibility and the ability to solve both linear and nonlinear problems. Furthermore, the structure of an ANN is the artificial resemblance of the human's brain. Also, a review of several machine learning algorithms in [223] indicates that the ANN is the most suitable and widely adopted over the other methods for the EEG brainwave model development such as BCI.

The procedure shown in Figure 3.11 proceeds to ensure the consistency and validity of the model development. Firstly, the dataset is divided into two parts i.e. training and blind test datasets. The condition for dataset dividing depends on the application. Then step 1, the training dataset is fed into the 10-time-10-fold cross-validation procedure as shown in details in a flowchart in Figure 3.13. The procedure is adopted from Section 2.8.1. The training dataset is shuffled and partitioned into ten equal portions as shown in Figure 3.12. It is noted that the partitioning is done along with stratification. The stratification distributes the equal number of types of class into each portion to avoid the situation where there is a single type of class in a portion. Then, the 1st portion out of ten portions is preserved for testing while the rest is used for training a model. This process is the 1st fold. The 2nd fold is continued by using the 2nd portion as the testing and the rest as the training. This process is repeated for ten folds. Then, this entire process is repeated for ten times i.e. 10-time-10-fold cross validation. It is noted that the previous training is for a single configuration of a model. In order to find the optimal model configuration, several of model configuration and parameter need to be put into the procedure e.g. number of hidden neurons.

The purpose of the 10-time-10-fold cross-validation procedure is to locate the best model configuration and parameter, given the training dataset. It is noted that configuration and parameter can be anything that affects the performance of the developing model e.g. number of hidden neurons in an ANN, training algorithm, initial condition etc. In this research, the configuration is determined only by a number hidden neuron within a single hidden layer design

of an ANN. A single hidden layer with the proper number of hidden neurons and activation function is sufficient to solve both linear and non-linear problems [224], [225]. The 10-time-10-fold cross-validation loops 100 iterations for each configuration. This method ensures the consistency of the outcome since the best model is selected from the averaged performance of this procedure that is indicated by step 2 of Figure 3.11. Then, the selected best model is trained with the entire training dataset. This is the outcome of the model development. The final model is tested with unseen dataset i.e. the blind test dataset in order to test the effectiveness of the model when it is applied in general.
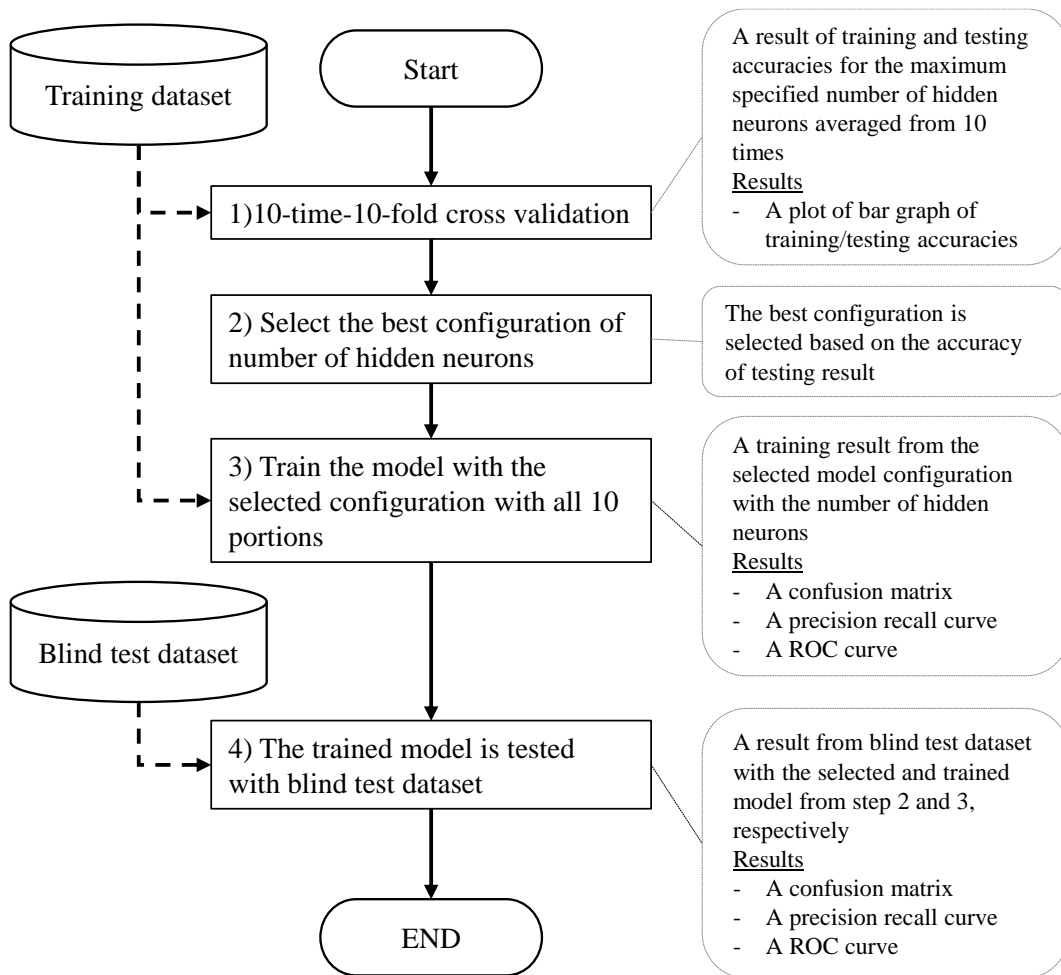
Figure 3.11 An overall process of training and blind testing with 10-time-10-fold cross validation.
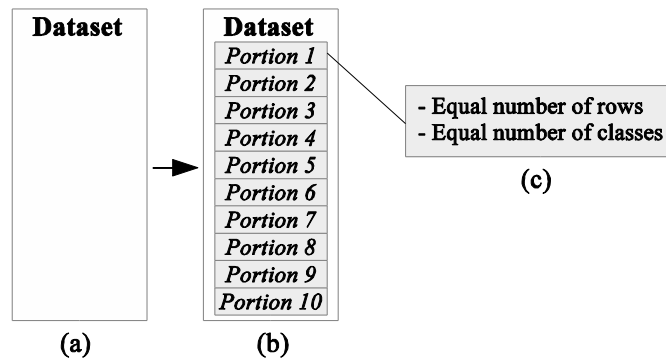
Figure 3.12 Dataset partitioning and stratification (a) the entire dataset (b) the dataset partitioned into ten portions (c) each portion contains an equal number of rows and equal type of classes.

10-Time-10-Fold Cross Validation

Input Dataset → Start

Start → *Time* = 1

Time = 1 → *Time* <=10

Dataset
| Portion 1 |
| Portion 2 |
| Portion 3 |
| Portion 4 |
| Portion 5 |
| Portion 6 |
| Portion 7 |
| Portion 8 |
| Portion 9 |
| Portion 10 |

Time <=10 — No → End

Time <=10 — Yes → Shuffle Dataset rows

Shuffle Dataset rows → Partition and stratify Dataset rows into 10 equal portions

→ *Neuron* = 1

Time = *Time*+1

Neuron <= **H**[1] — No → *Time* = *Time*+1

Neuron <= **H**[1] — Yes → *Fold* = 1

Neuron = *Neuron*+1

Fold = 1 → *Fold* <=10

Fold <=10 — No → *Neuron* = *Neuron*+1

Fold <=10 — Yes → Set *ANN* hidden neuron = *Neuron*

Set *ANN* hidden neuron = *Neuron* → *ANN* (Training and Testing) Train with 9 *Portions* != *Fold* Test with *Portion* = *Fold*

→ Save training and testing results

Fold = *Fold*+1

Result table
Time #
Fold #   *Fold* 10
Neuron #
.
.
.
Neuron **H**

[1]**H**=(Number of ANN input features)*2

Figure 3.13 A flow chart of 10-time-10-fold cross-validation procedure.

3.7 List of the investigations

This section summarises the investigations have been completed in this research. A list of the investigation is shown in Table 3.1.

Table 3.1 List of the investigations completed in this research.

No.	Description	Chapter /Section	Objectives fulfilment
1	**Single participant learning to control pendulum-driven capsule system (Model I)** o Identification of a set of rules to control the system	4.2	1, 2, 4
2	**Nine participants learning to control a PID controlled pendulum-driven capsule system (Model II)** o Nine participants o A comparison of performance outcome between participants in terms of final capsule displacement o A characteristic of low and high performance control signals are identified	4.3	1, 2, 4, 5
3	**Development of a human-machine control model based on the control data and information from the investigation No. 2** o A set of rules of capsule control law from human control information is developed into a model. o Feature extraction from the control information o Develop two model by adopting ANN as the modelling algorithm o The procedure in Section 3.6 is applied.	4.4	1, 2, 3, 4

4	**A study on brainwaves from EEG measurement**	Chapter 5	2
	o Preliminary study on EEG with the Emotiv EPOC headset o The main investigation is the ERP for certain stimuli e.g. auditory, click, simple target hitting task.		
5	**A human EEG brainwaves and human-machine interaction performance evaluation** o A target hitting task is adopted as the investigation scenario to capture the human EEG brainwaves. o The corresponding target hitting task performance metrics are RT, MT, DT, MA, HA and the Fitts IP. o Development of 6 ANN models which can be used to evaluate a human-machine interaction performance based on the EEG brainwaves. ▪ Six ANN models are obtained corresponding to each performance indicator. o The procedure in Section 3.6 is applied.	Chapter 6	1, 2, 3, 4, 5
6	**An implementation of hardware inverted pendulum driven-capsule system**	Appendix J	Not applicable

3.8 Summary

This chapter presents a research methodology adopted in this research i.e. positivism paradigm with quantitative approach. The focus area of the research has been clarified that is the investigation at the lowest level of the four approaches to hierarchical modelling of human-machine performance. Then, the paradigm and the focus are formulated into the method and design of the investigations that are realised by the implementation of the HAM simulation platform. The platform is functioned as a machine simulation and the interaction interface between human and machine instead of using a physical machine.

The experiment data of each scenario are acquired via the platform. The analysis and model development of the acquired data is done offline. The model development procedures that ensure the consistency of the obtained model has presented i.e. the 10-time-10-fold cross validation. A table that summarises all of the investigations completed in this research is given along with a reference to the corresponding sections of this thesis.

Chapter 4 Human-machine interaction – learning, performance, and model development

4.1 Introduction

This chapter presents the investigation on an HMI with the two machine models presented in Section 3.5 i.e. Model I and II. The Model I is applied in the study of heuristic learning to control the machine in Section 4.2. The Model II is applied in the investigation with nine participants in Section 4.3. The control information from Section 4.3 is further analysed in order to develop a human-machine control model in Section 4.4.

4.2 A heuristic learning to control the pendulum-driven capsule system

The Model I in Section 3.5.1 is applied in order to understand a heuristic learning of a human. A participant is asked to learn and figure out how to control the machine according to the given instruction.

A sampling rate or the simulation time step is 100Hz or 10ms per loop. The only input of Model I is the torque at the joint as shown in Figure 2.15 which is mapped directly to the movement of a thumbstick of the joystick to control the amount of torque. A photo of the thumb stick is shown in Figure 4.1. It can be noted that the system time step is 10ms. Therefore, the torque pushed by the joystick in real time is applied to the system at every step of the simulation loop.

Figure 4.1 A photo of the joystick which indicates the thumbstick.

4.2.1 Heuristic learning and identification of control strategy

Apparently, one of the advantages of a real-time interactive simulation is that it is useful for heuristic learning and practising. The underactuated nature of the pendulum-driven capsule system is rather challenging for a human operator to learn to control especially the control of a capsule body movement rather than the pendulum itself.

The experimentation is conducted by having a participant try to control the capsule system to move the capsule body to the desired direction either left or right. The interaction loop is shown in Figure 3.9 which diagrams transfer of control information around the system loop. A participant needs to interact with the system by the mentioned control mechanisms i.e. control of a thumb stick to actuate the amount of torque at the pendulum joint. The outputs of the system are the pendulum angle $\theta(t)$ and the capsule body movement $x(t)$. These outputs act as feedback to a human, and the overall system becomes closed loop.

The capsule system parameters are configured as follows; M=0.5kg, m=0.05kg, L=0.3m, g=9.81 m/s², μ=0.01 N*m/s. The initial conditions – θ, ω, x, v, and τ are 180 degrees, 0 rad/s, 0 m, 0 m/s, and 0 N.m/s respectively. The illustration of the system configurations and the initial conditions are shown in Figure 4.2.
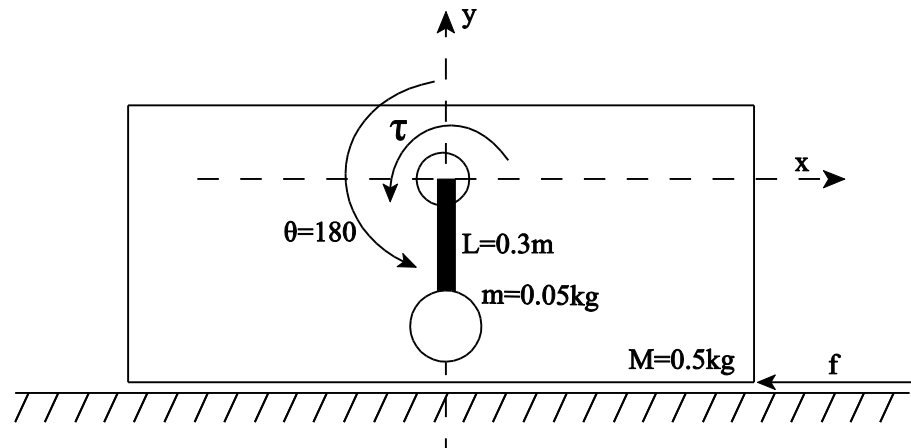
Figure 4.2 The system configuration, parameters, and initial conditions.

In the beginning, the system stays still with the pendulum shaft and the ball lying straight down because of the gravity and the absence of any disturbances. The pendulum start to swing when a small torque is applied by a user via the joystick as shown by the short-time downward impulse of the blue dashed line in Figure 4.3 (a). The capsule body starts to move to the left and the right repeatedly according to the forces produced from the pendulum ball movements and the surface friction as shown in Figure 4.3 (b). The capsule is unintentionally displaced to the right after it finally comes to the steady state as indicated by the ending position at approximately 0.15m of the capsule body position graph in Figure 4.3 (b). A screenshot of the simulation and the experiment is shown in Figure 4.4. A human participant learns to control the simulated machine by control the amount of torque via the joystick as shown in Figure 4.4.
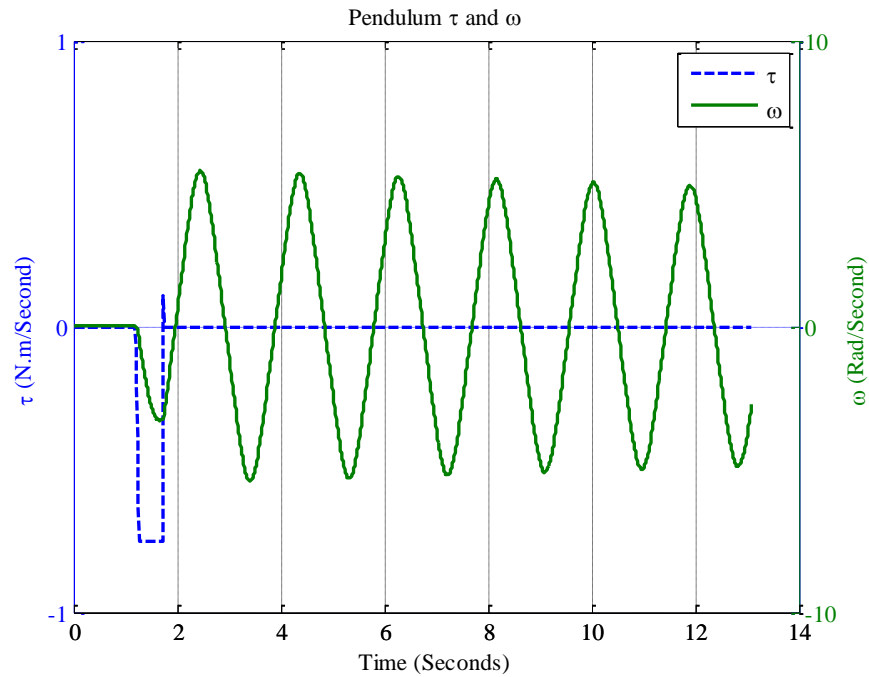
(a) A small activation of torque and the pendulum angular velocity.
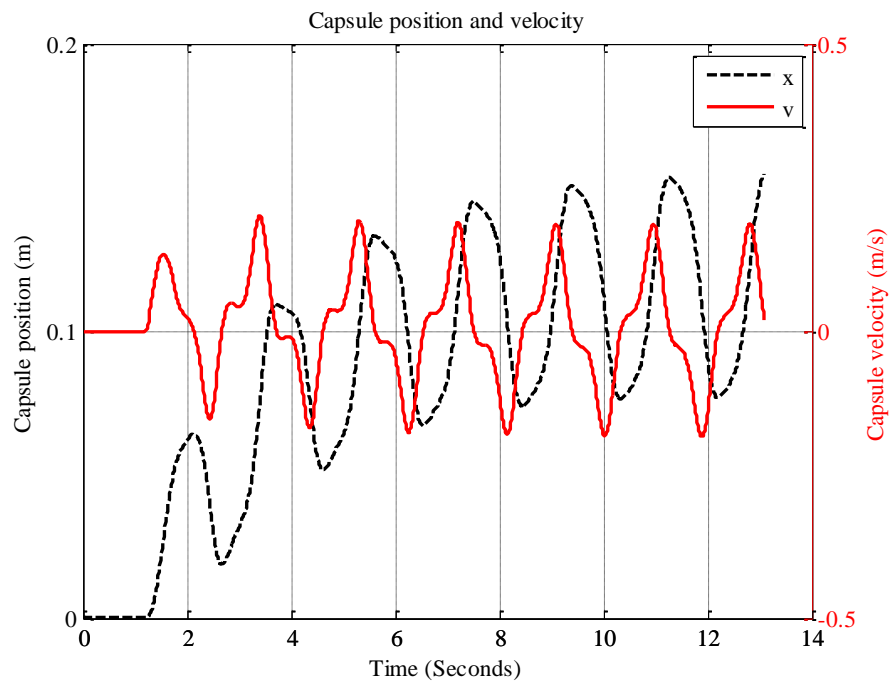
(b) The capsule body position (black dashed line) and velocity (solid red line) when the small amount of torque is activated.

Figure 4.3 A small activation of torque τ at near the 2nd second (blue dashed line) causes the pendulum to swing, and the capsule starts to move.
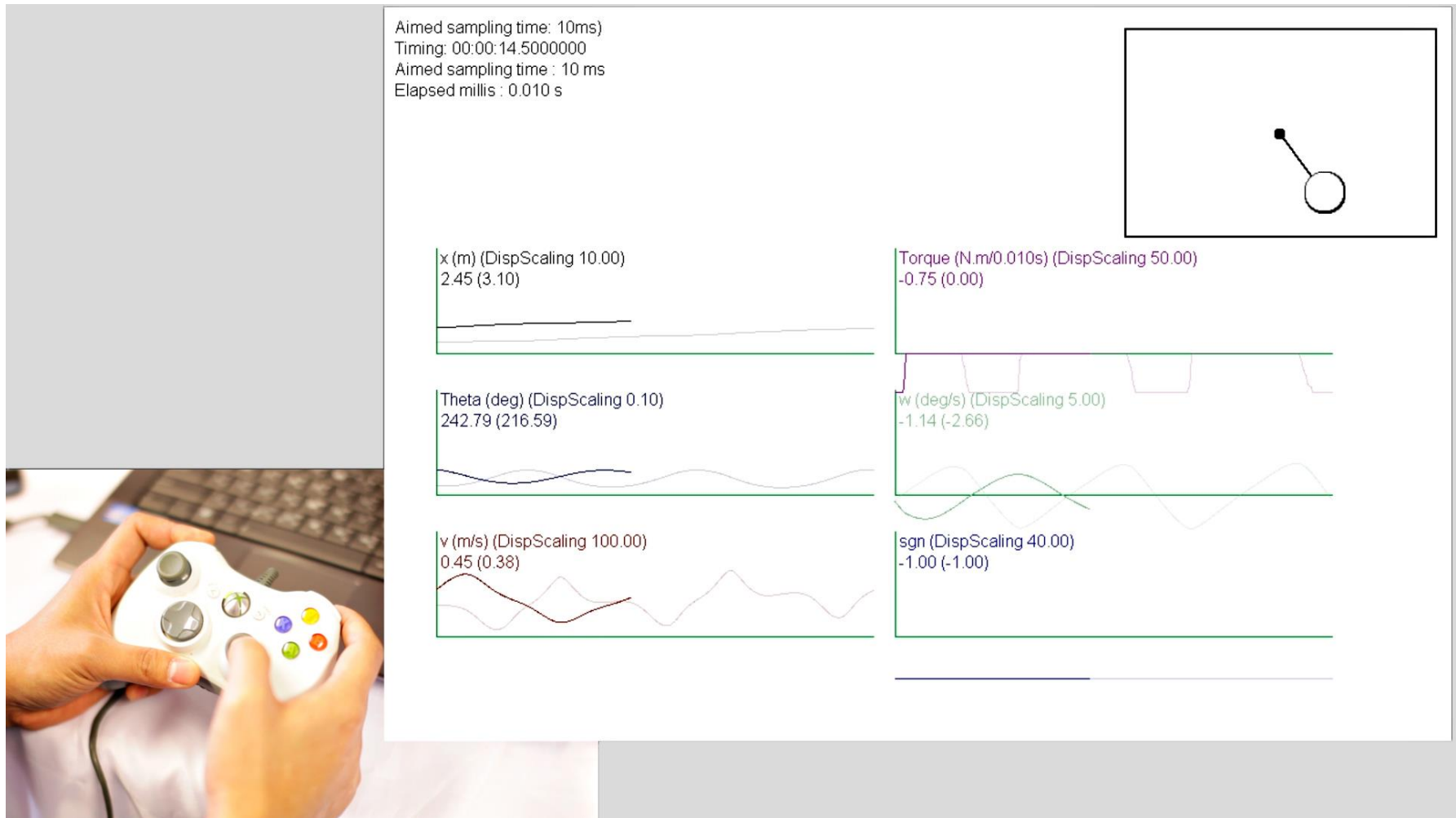
Figure 4.4 A screenshot of a human heuristic learning to control a pendulum-driven capsule system.

4.2.2 The identification of rules for the machine control

After several tries of control the movement of the pendulum to drive the capsule into the desired direction, a set of control rules is developed. Figure 4.5 shows the identified control rules of the capsule system. The identified control rules can be summarised and explained by the following steps.

Step 1) Generate a pulse of torque by pushing the joystick to allow the pendulum to swing freely and then release the joystick as shown at approximately around the 1st second in Figure 4.5(a). Figure 4.6(a) shows the close-up moment where a small impulse of torque is generated (solid red line), and the angular velocity of the pendulum starts to accelerate (solid green line). Then, the pendulum freely oscillates in the same behaviour as shown in Figure 4.3(a).

Step 2) If an operator wants to control the capsule to the left direction. The human operator needs to push the torque backwards suddenly and only in a short period (impulse liked) while the pendulum is freely swinging back to the left side as shown at the approximately 3rd second of Figure 4.5(a), technically at the middle of the swinging back. The close-up detail of this moment is shown in Figure 4.6(b). The instructions for moving the capsule body to the right direction can be achieved in a similar way.

A general description can be explained as follows. In order to control the capsule to the left, a human operator needs to push the torque in the middle of the rising or falling of the pendulum angular velocity. In other words, the operator needs to push the torque at the middle edge of the sine curves. These rules torque control strategy allow the user to control the capsule body to the desired directions.
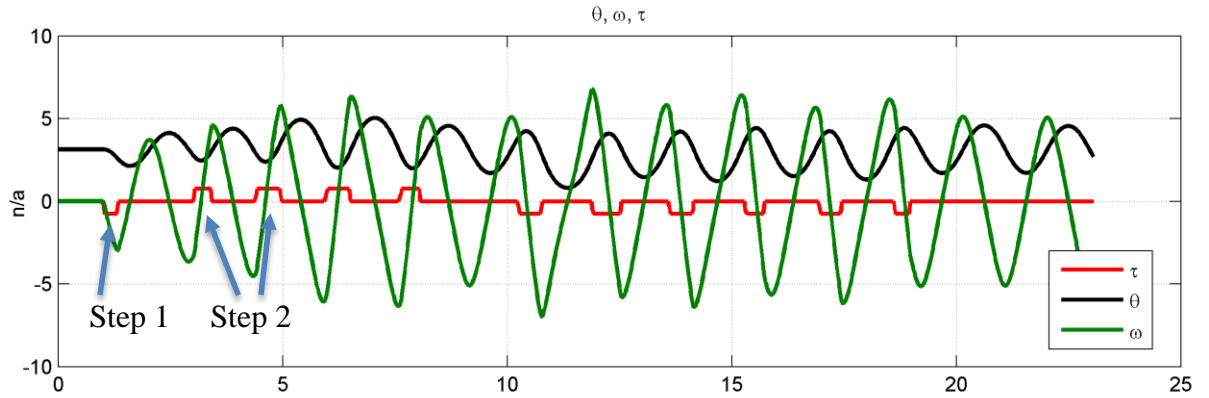
(a) The graphs of torque (τ), pendulum angle (θ), and angular velocity (ω) during control of the pendulum to the left (from 0 to 10s) and the right directions (from 10s to 20s).
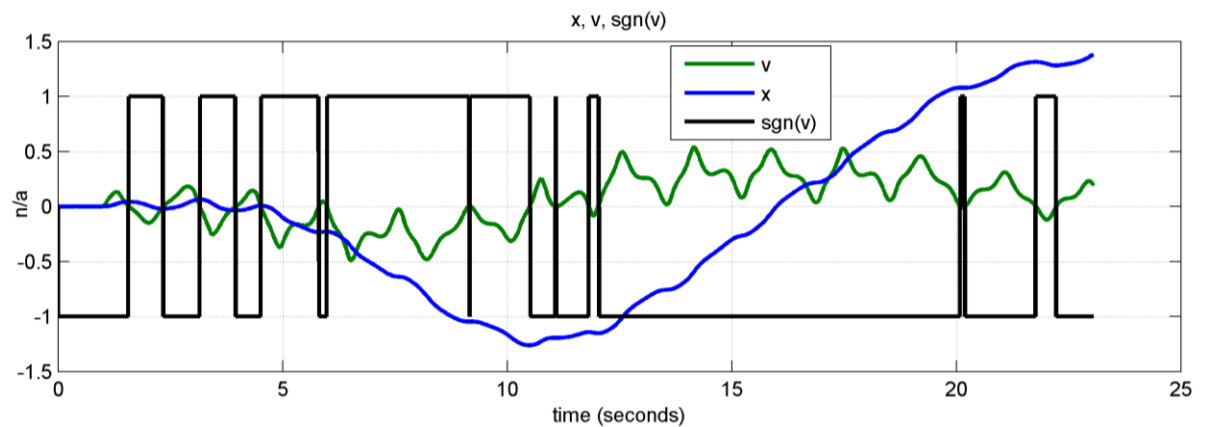
(b) The graphs of capsule body position (x), velocity (v), and the sign of surface friction, sgn(v).

Figure 4.5 The scaled control signals from the heuristic learning to control the system by a human operator.
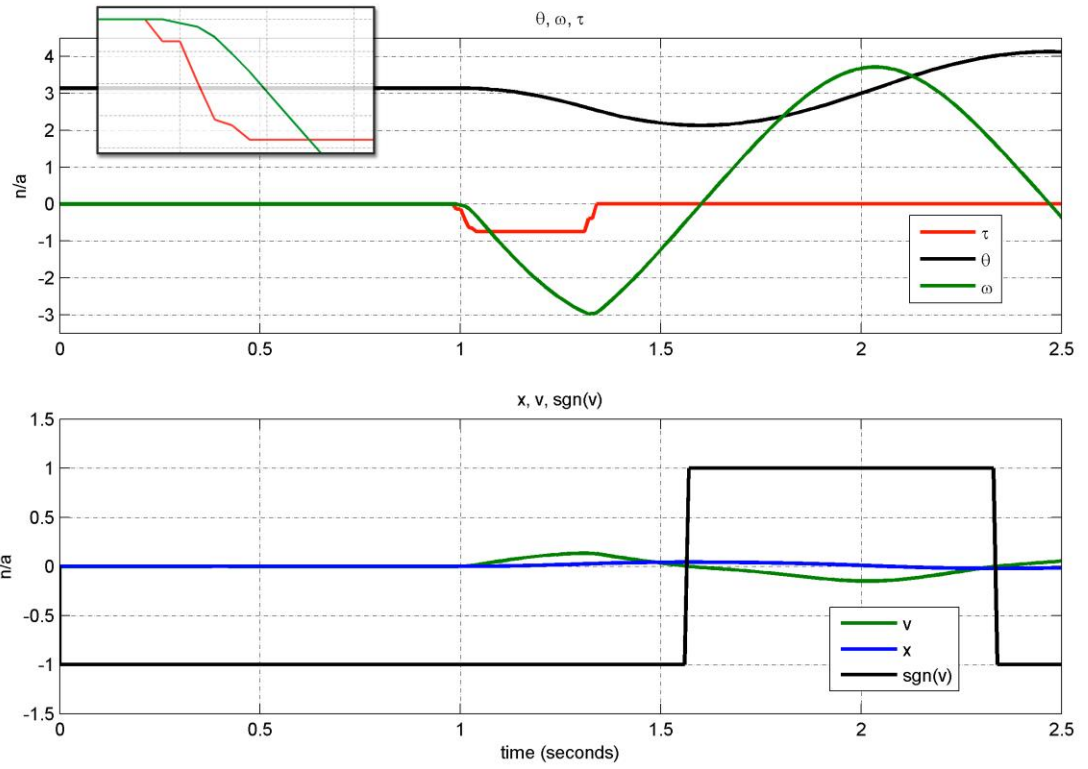
(a) The control characteristics for step 1.
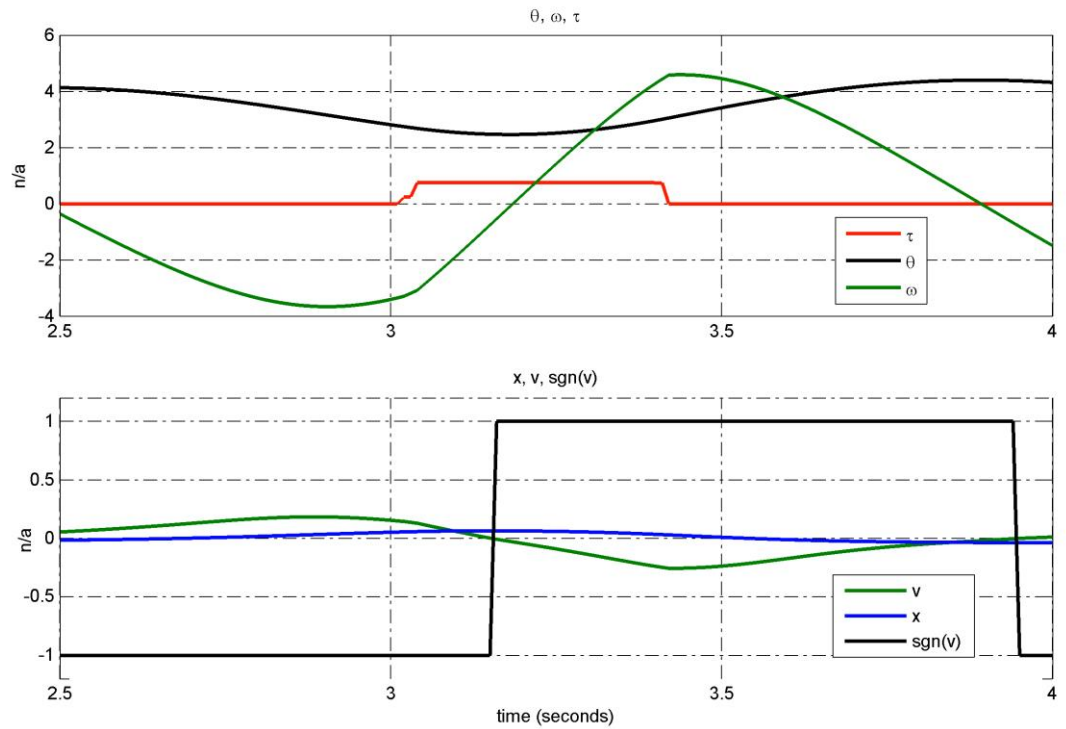
(b) The control characteristics for step 2.

Figure 4.6 The control characteristics for (a) step 1 and (b) step 2.

Conclusion remarks to the investigation on a human heuristic learning to control the pendulum-driven capsule system, the identified rules of the control seem similar to a walking cycle of a human that can be illustrated by Figure 4.7 i.e. an inverted bottom half of a circle of leg movements. Given that the desired movement is to move to the right, firstly it is needed to push the pendulum to swing freely from A to B reciprocally. At the moment where the pendulum ball is reaching the point B, the torque must be pushed in the opposite way. This will make the capsule move to the right because of both the pushed torque and the surface friction effects. This mechanism is working in the same way as a human walking cycle.
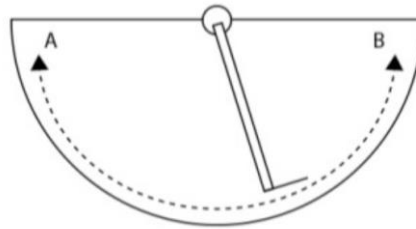
Figure 4.7 A simple human walking cycle by swinging a leg from point A to point B.

4.3 Human learning skill and performance to control an underactuated inverted pendulum-driven capsule system

The investigation in this section is based on the Model II, a PID controlled inverted pendulum-driven capsule system as explained in Section 3.5.2.

4.3.1 Participants

Nine participants age between 21 and 50 attend this experiment. Each of them agreed and signed the consent form before the investigation. The consent form template can be found in Appendix A. The participants have different personal attributes such as ages, handedness, and knowledge about principles related to the machine that could influence the control learning and performance. The participants are labelled as CH4P1 to CH4P9. The detail of the participants attributes and knowledge is shown in Table 4.1. One of them is female. Eight of them are right-handed while two of them are left-handed. All of them know the knowledge on Newtons law of

motion. Only one of them does not know the pendulum mechanism. Almost half of the participants do not know the inverted pendulum mechanism. Three out of nine know the principle of an inverted pendulum. None of them has tried this experiment before this investigation.

Table 4.1 The participants' attributes and knowledge.

P	G	A	H	N	Pe	IPe	IpeP	TBF
CH4P1	Male	31-35	Right	Yes	Yes	No	No	No
CH4P2	Male	36-40	Right	Yes	Yes	Yes	No	No
CH4P3	Female	31-35	Right	Yes	Yes	No	No	No
CH4P4	Male	21-25	Right	Yes	No	No	No	No
CH4P5	Male	26-30	Left	Yes	Yes	No	No	No
CH4P6	Male	26-30	Right	Yes	Yes	Yes	No	No
CH4P7	Male	41-45	Left	Yes	Yes	Yes	Yes	No
CH4P8	Male	46-50	Right	Yes	Yes	Yes	Yes	No
CH4P9	Male	26-30	Right	Yes	Yes	Yes	Yes	No

P=Participant Identity, G=Gender, A=Ages, H=Handedness, N=Knowledge on Newton law of motion, Pe=Knowledge on pendulum, IPe=Knowledge on inverted pendulum, IPeP=Knowledge on inverted pendulum principle, TBF=Has the participant tried this experiment before

4.3.2 The investigation

The experiment is designed to investigate the human operator learning and skill performance when operating the underactuated inverted pendulum-driven capsule system i.e. the Model II in Section 3.5.2. The PID controlled inverted pendulum-driven capsule system allowed the participants to concentrate on controlling the pendulum angle rather than the torque. A proper rotation of the pendulum can underactuate the capsule body to move in the desired direction. However, it requires both learning and skill to operate and identify the correct control strategy. The interaction model is shown in Figure 3.10. The simulation appearance in this section has been upgraded from 2D to 3D simulation as shown in Figure 4.8. However, the model is basically the model presented in Section 3.5.2. The underlying mathematical model is the one-dimensional system that can move in either positive or negative x-axis. The 3D appearance makes the system easy for the operator perceptions.

The joystick axis is mapped to control the angle of the pendulum directly. The mapping means that when the joystick is pushed towards negative PovX direction (Figure 4.9) it can rotate the

pendulum angle of the capsule system to left-hand side which means toward the positive 90 degrees of the pendulum-driven capsule model (refer to Figure 2.15).
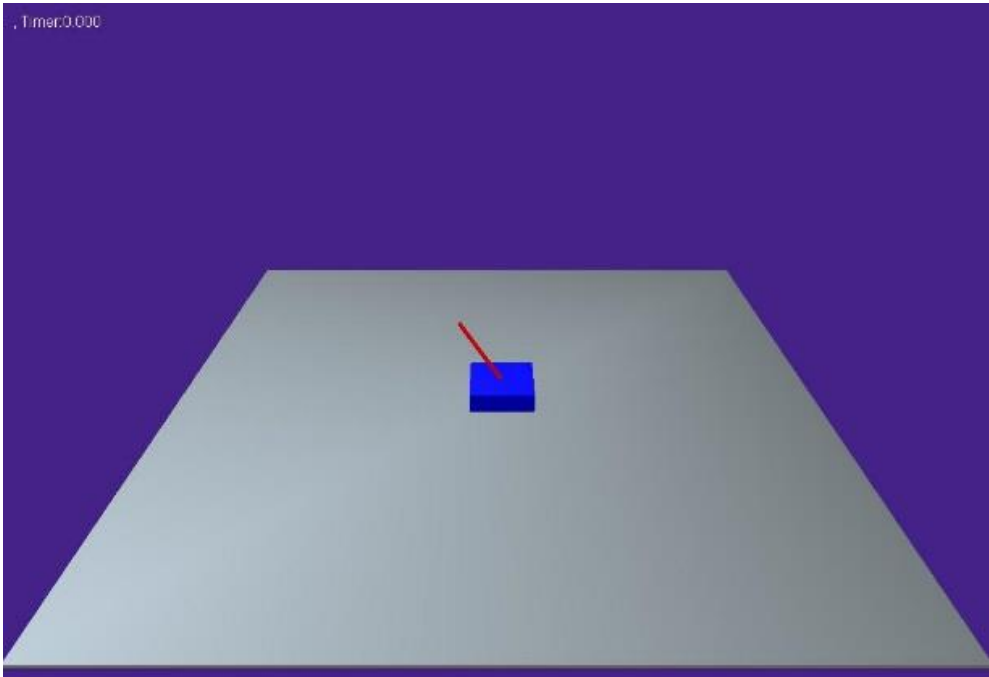
Figure 4.8 The screenshot of the 3D interactive simulation.

Figure 4.9 The joystick and the axis mapping to the pendulum angle.

The PID controller constants – kP, kI, kD are 0.7, 0.7, and 6.0, respectively. The control output gain factor is 10. The constants and the gain are heuristically tuned so that the maximum pendulum angle overshoot is achieved as shown in Figure 4.10. Table 4.2 shows the parameters for the capsule system.

Table 4.2 The capsule system parameters.

Ball mass (kg)	Capsule mass (kg)	Shaft length (m)	Surface friction coefficient	Gravity constant (m/s²)
0.2	0.5	0.3	0.5	9.81
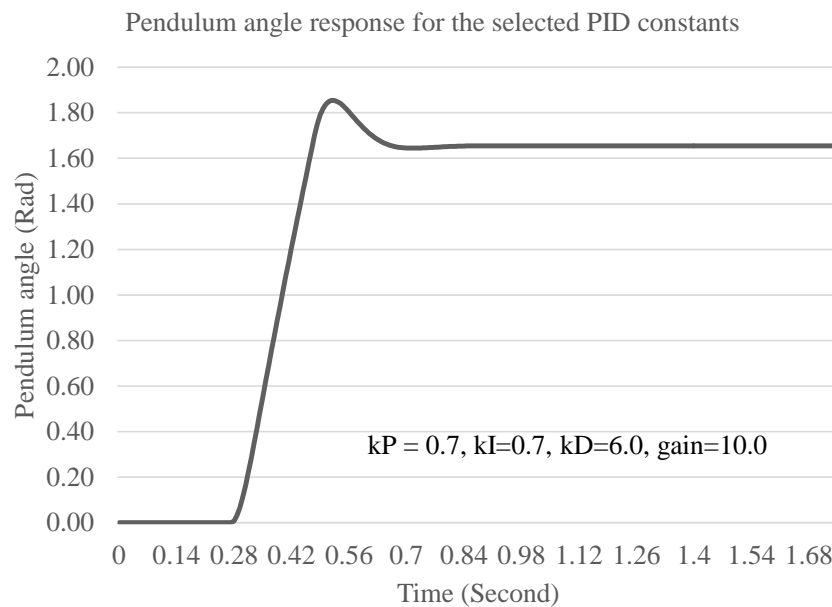
Figure 4.10 The pendulum angle response for the selected PID constants.

4.3.3 Task

The control task in this experiment is a direct control of the pendulum angle to displace the capsule body to the specified direction i.e. left or right. A participant has full control over the desired angle of the pendulum by pushing the joystick handle. The effect of pendulum rotation can cause the capsule to move erratically back and forth. This is a normal condition because of the mechanism of the inverted pendulum-driven capsule system. Nonetheless, it is controllable for the intended displacement direction.

Each session of the experiment for each participant contains a learning session before the actual performance trials. The actual trials consist of 6 trials separated into three trials for right and three trials for left movement. There is no time limitation for the learning session while the actual trial is limited to 20 seconds per session which means a participant has to control the capsule to the specified direction as far as possible within the given time limitation.

4.3.4 Performance analysis

This section summarises the results from the experimentation conducted by the nine participants. The 'R' and 'L' letters are used to indicate right or left movement task followed by a trial number as shown in Figure 4.11. For examples, 'R1' stands for the first right trial, 'R2' for the second right trial, and so on. Each of the participants performs the experiment for 'R1' to 'R3' and 'L1' to 'L3' which produces a total of 54 trials for the entire investigation.

Figure 4.12 shows the amount of learning time used by each participant before the actual performance tracked trials. According to Figure 4.12, the amount of learning time (LT) does not reflect the performance of the actual trials since the best performance is achieved by 'CH4P3' who takes 212.9s learning time while 'CH4P9' uses 586.88s to learn to control the capsule system but achieves the worst outcomes. It is indicated that the participant 'CH4P9' spends a large amount of time to figure out how the capsule system works but could not acquire sufficient skill to control the capsule system.

The performance is indicated by the final capsule position i.e. the horizontal distance measured from the start position of the capsule body. The top two high performance trials belong to 'CH4P2' and 'CH4P3' with their 3rd and 2nd left trials, respectively. They are denoted by 'CH4P2-L3' and 'CH4P3-L2' as shown in Figure 4.11. It is apparent that the best performer is 'CH4P2' which is shown by the highest amount of accumulated capsule distance as shown in Figure 4.13.The highest average speed at 2.10 cm/s is also from 'CH4P2' as shown in Figure 4.14. At the low ends, it is clear that the lowest performance trial is achieved by 'CH4P4-R2' i.e. 0.26 cm. However, 'CH4P4' is not the lowest performer because the total accumulated distance and capsule average speed are still higher than 'CH4P9'. It is concluded that 'CH4P9' achieves the worst performance which is agreed with the statement in the previous paragraph that the 'CH4P9' could not figure out how to control the capsule system.
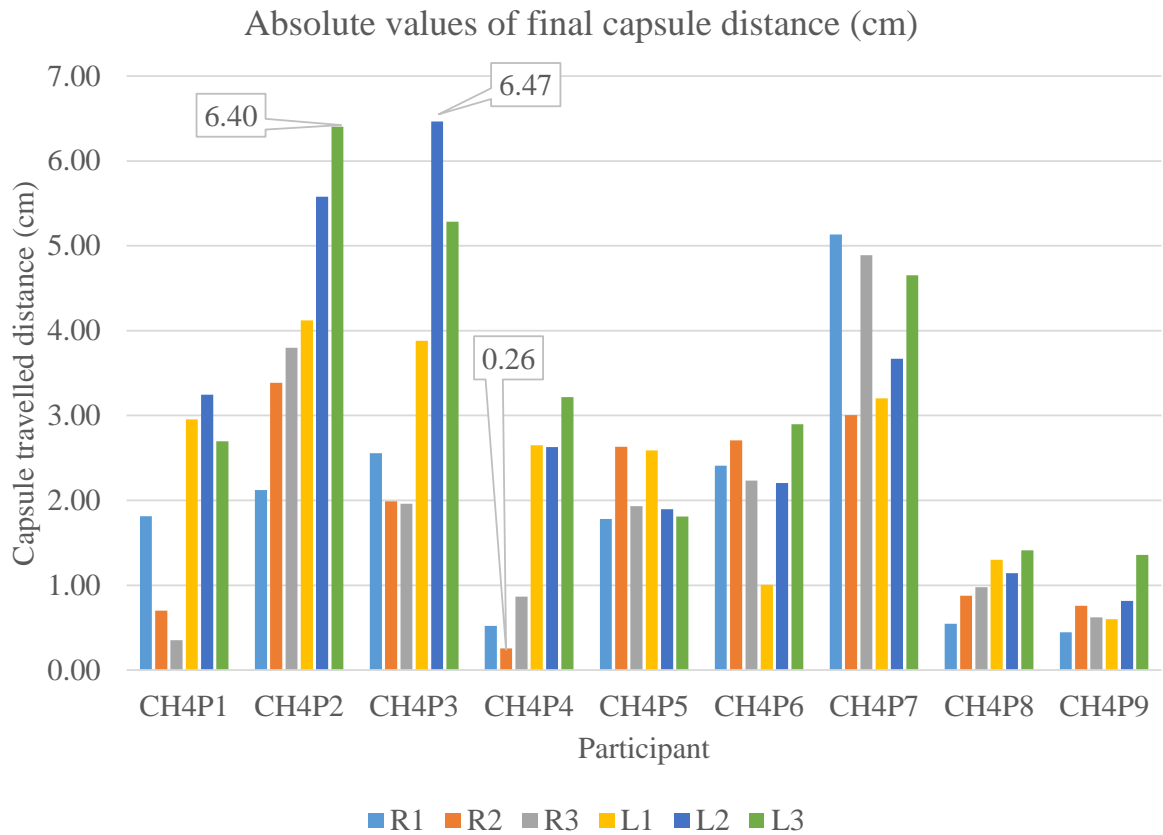
Figure 4.11 The absolute values of final capsule position.
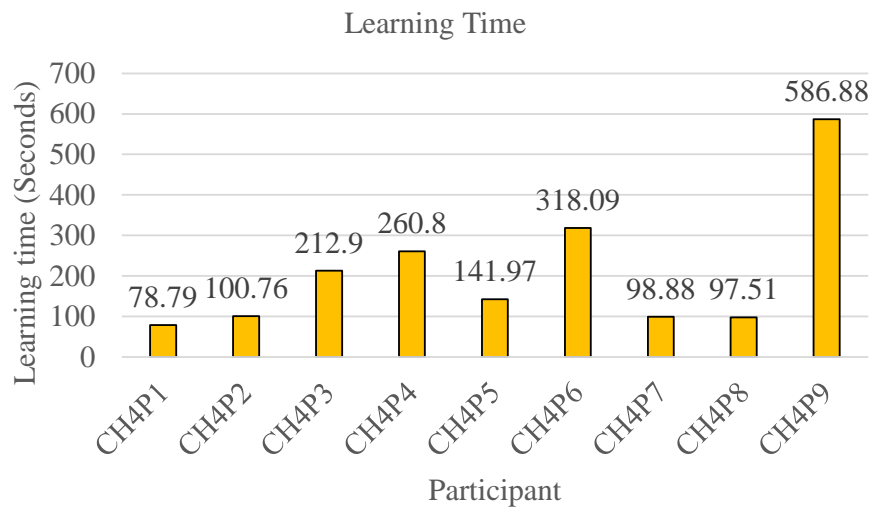
Figure 4.12 The time used for learning from the nine participants.
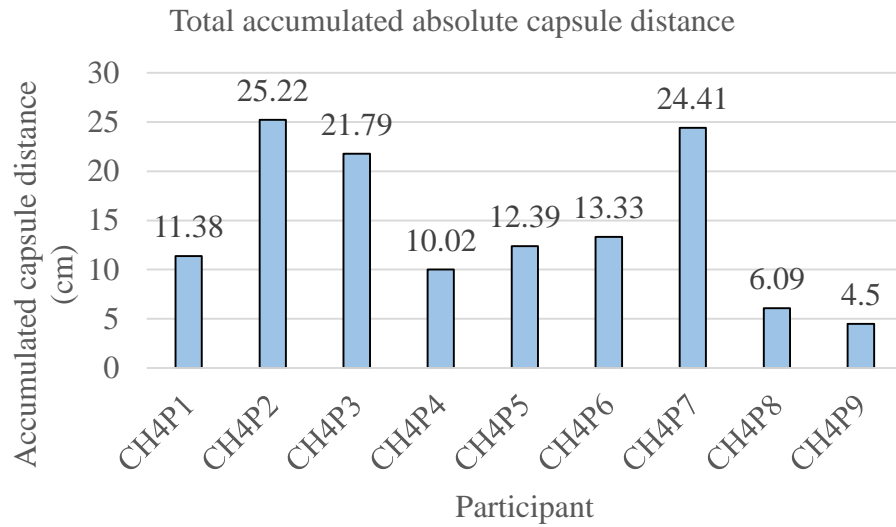
Figure 4.13 The total capsule distances accumulate from all trials.
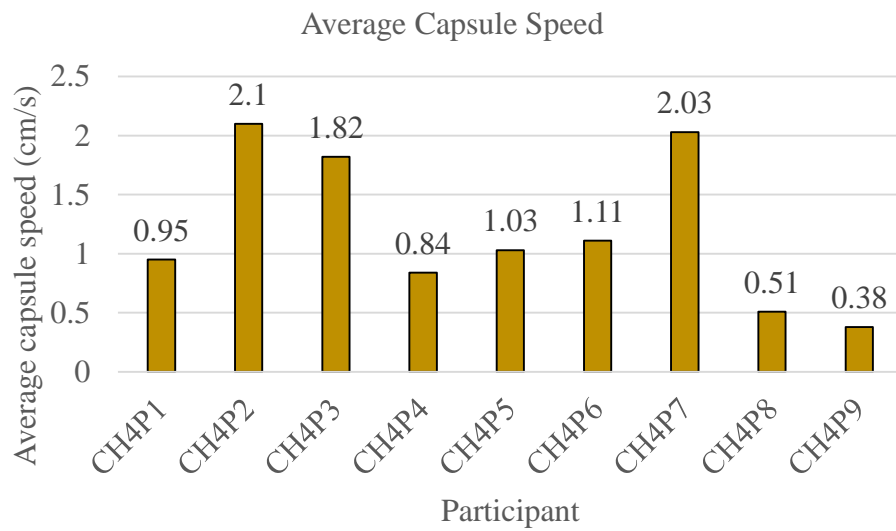
Figure 4.14 The average capsule speeds accumulate from all trials.
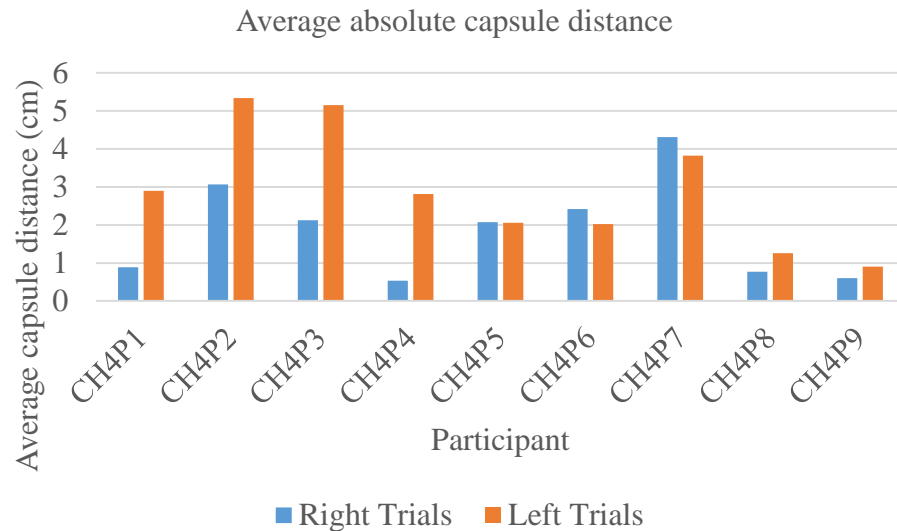
Figure 4.15 The average capsule distance from the right trials and left trials of the nine participants.

It is interesting that almost all of the right-handed participants achieve higher left performance than right performance as shown in Figure 4.15. Likewise, the left-handed participants, 'CH4P5' and 'CH4P7' achieve higher performance in their right direction. This phenomenon could be an effect of a hand grasping orientation on the joystick and the fact of the human brain activation. A left human brain is activated when the right parts of the body are in action, and vice versa. This is confirmed from the pieces of evidence from the experimental results as follows. The highest left direction performance is from the participant 'CH4P2' who is right-handed (CH4P2-L3). The highest right direction performance is from the participant 'CH4P7' who is left-handed (CH4P7-R1).

The variance of the final capsule distance is shown in Figure 4.16. This value indicates the consistency of performance of each participant across all of their performance trials. It could be used as a learning index. For example, the participant 'CH4P3' gained the highest learning performance since the three right trials are not performed very well but in the remaining left trials the participant achieves rather higher performances. Outcomes from 'CH4P2' follow the same trend with slightly less variance. This interpretation is also applied to 'CH4P1' and 'CH4P4' who gain high learning performance indicator or variance. Although the participant

'CH4P7' achieves good performance across all of the trials, the variance is relatively low. This means there is a low learning achieved by this participant.
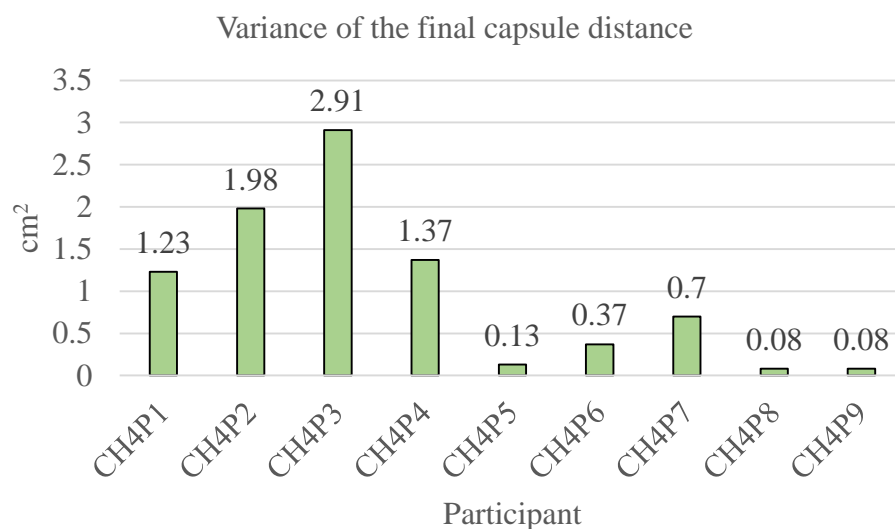
Figure 4.16 The variance of the absolute displacement for each participant.

4.3.4.1 <u>Control characteristics of low and high performers</u>

Figure 4.17 shows characteristics of the control input from two of the best and worst trials. Obviously, the two best trials are from 'CH4P2-L3' and 'CH4P3-L2' as shown in Figure 4.17 (a) and Figure 4.17 (b), respectively. The worst two performance trials are 'CH4P4-R2' and 'CH4P1-R3' as shown in Figure 4.17 (c) and Figure 4.17 (d), respectively. The figures also show a periodogram or frequency characteristic of the corresponding graphs of control input. The analysis shows that the control input with high frequency i.e. around 5 Hz are from both of the best trials, 'CH4P2-L3' and 'CH4P3-L2'. This frequency of control input oscillation is performed and maintained across the performance trials. In other words, the oscillation is performed at consistent frequency across the trials. In contrast, the low skill performers show rather low frequency of input oscillation and inconsistent across the trial. These control input characteristics are performed by 'CH4P4-R2' and 'CH4P1-R3'.
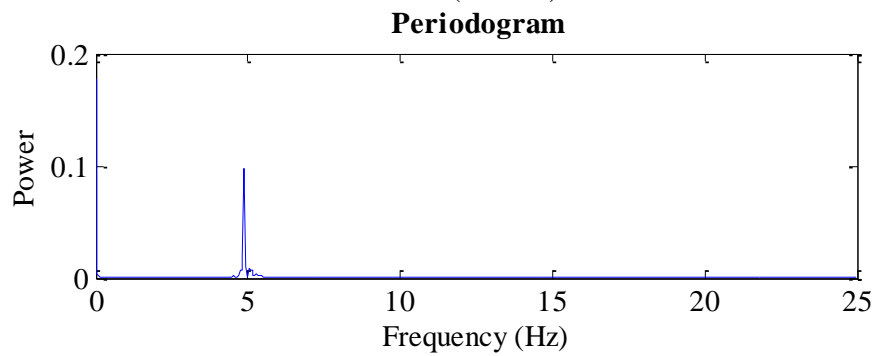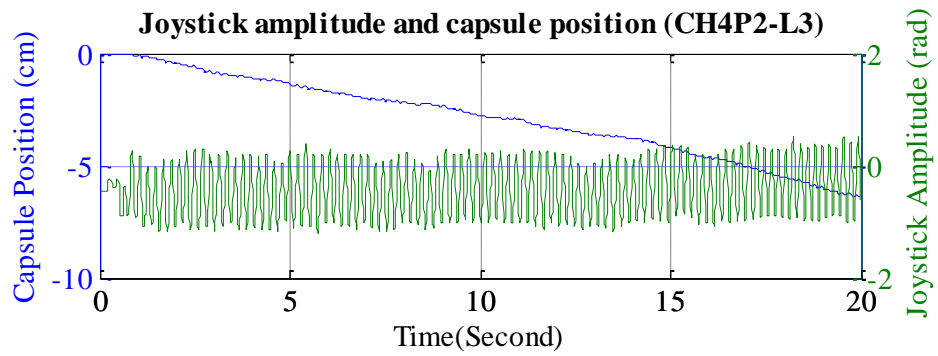
(a)
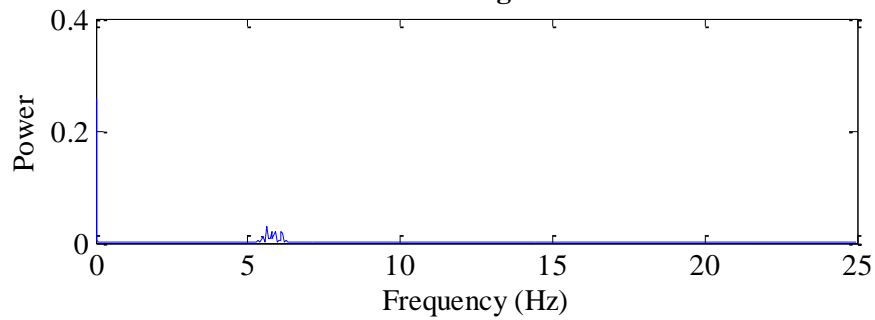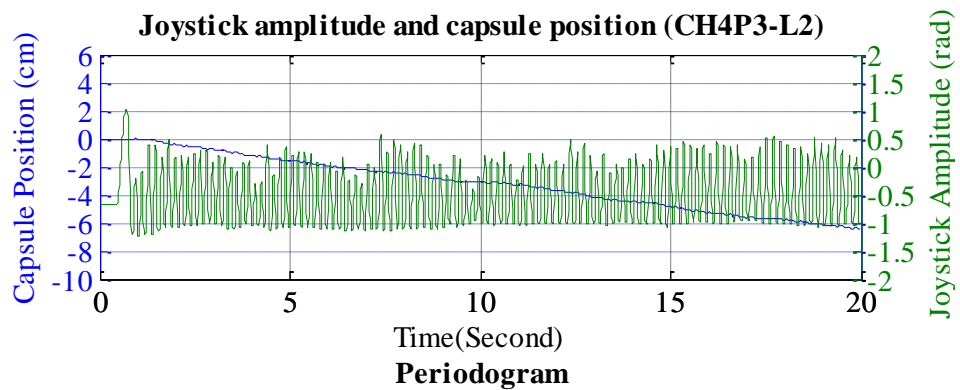
(b)
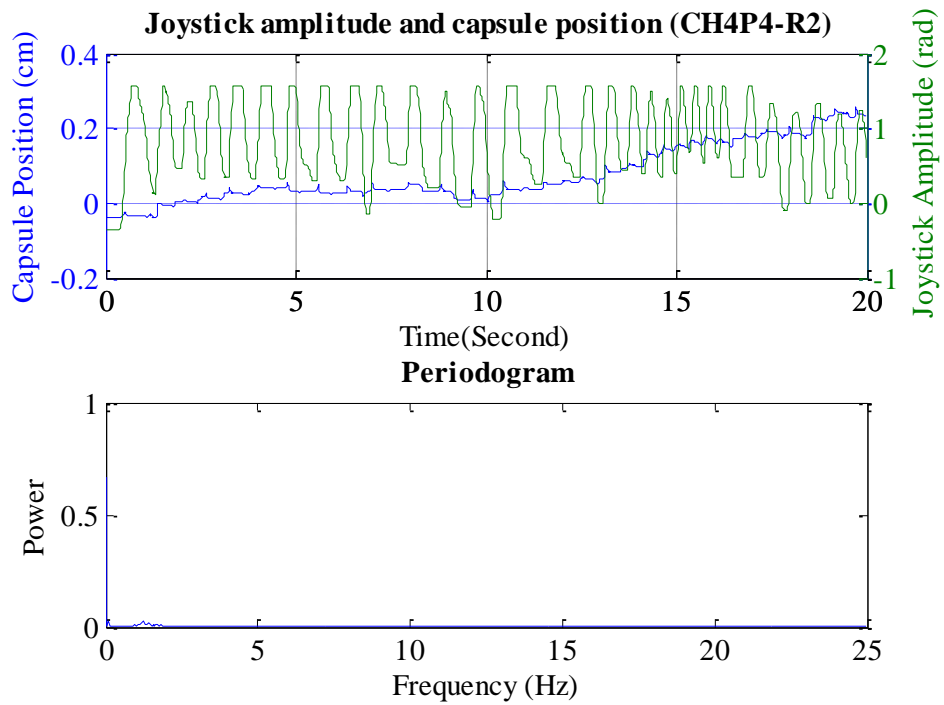
(c)
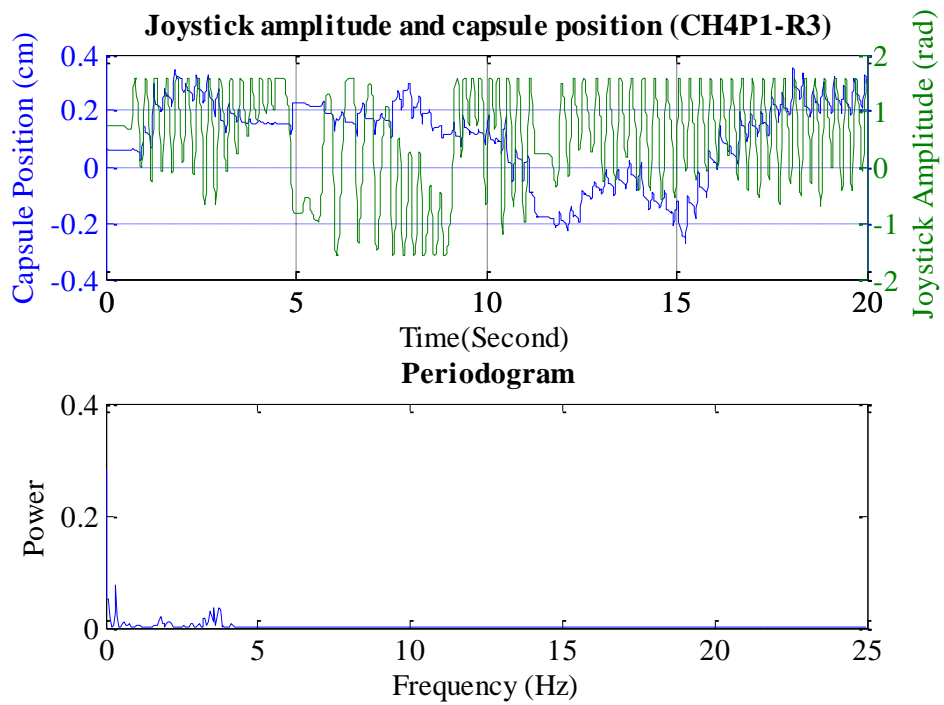
(d)

Figure 4.17 The graphs show control amplitude from the joystick, frequency characteristics, and the capsule displacement.

4.3.5 Low-level analysis

In the previous section, skill performance of the human operator to control the capsule is measured from the final capsule distance. It is interesting to analyse the details of the control input i.e. the raw control input from the joystick that produces the desired angle of the inverted pendulum and causes the capsule to displace. From theoretical and mathematical control points of view [148], [149], [226], the studies are sought to create a profile of pendulum angles which tend to underactuate a capsule body to displace. These control profiles are designed to be performed automatically by a machine controller. The rotation profiles are perfect in both time and frequency of control oscillation. As opposed to a human operator is not a perfect machine who can reproduce the control profile from the theory although it could be used as purpose guideline.

Obviously, the underlying outcome of the final performance is from the manual control of the joystick as indicated in Section 4.3.4.1. The detailed analysis of this manual control signal could reveal the information which can be used to create a human-machine control model. One of the detailed analysis is the identification of a control cycle which mimicries the automatic control profile from [148], [149], [226]. The identification can be accomplished by applying an approximation algorithm to the control input i.e. a local minimum and maximum as shown in Figure 4.18. The algorithm finds the peaks and bottoms of sinusoidal waves which are the approximation as a control cycle. This cycle information can be used to develop a model in Section 4.4.
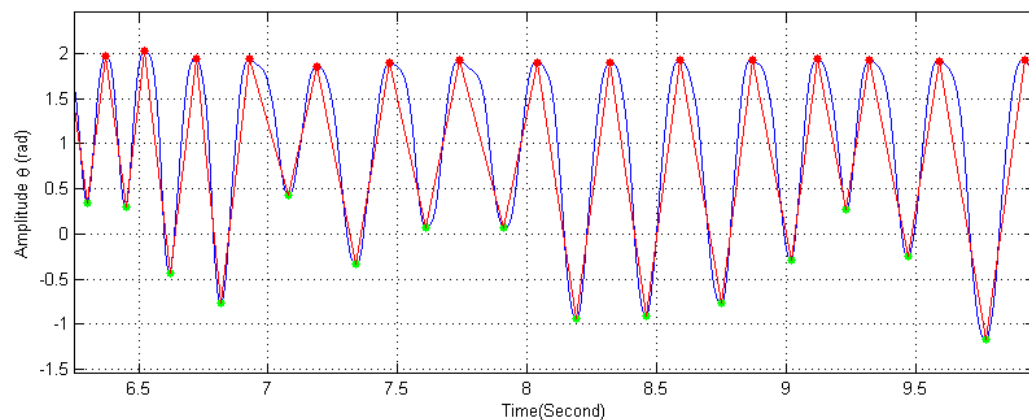
Figure 4.18 An example of the identification of cycles from the joystick control input.

4.4 Development of human-machine control model using ANN

In this section, a human-machine control model is investigated based on the control information from Section 4.3. In Section 4.3, nine participants have been instructed to learn to control a PID controlled inverted pendulum-driven capsule system. A joystick is the input device which controls the pendulum angle. Hence, the control information is the time-varying angle of the inverted pendulum.

The time-varying angle of the inverted pendulum contains a human control strategy that rules the movement of the capsule body. Therefore, it is required to extract the information from these control signals in order to develop a control model. According to the literature review, there exist several approaches for a model development as reviewed in Section 2.5.8. Since a human control strategy is rather difficult to obtain analytically, a descriptive modelling approach appears to be a suitable method to develop a model from the given control information. The opposition is a predictive modelling approach where it makes a prediction based on a set of given inputs.

Although the two approaches are in opposition, they are often developed simultaneously to ensure that the obtained descriptive model performance is truly effective.

4.4.1 Model development

An ANN is adopted as a modelling tool in order to develop the model of human-machine control. Two types of ANN modelling are employed i.e. classification and regression neural networks, as shown in Figure 4.19. The classification model produces a discrete output that indicates a class of capsule movements i.e. backward and forward. The regression model generates a continuous output which is a capsule displacement. The inputs or features are extracted from the control information in Section 4.3.
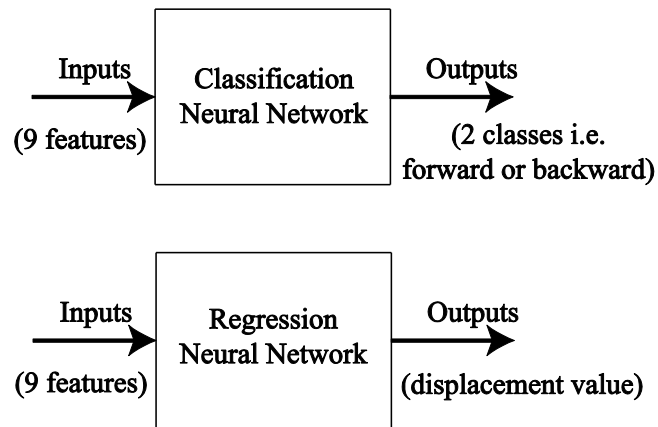
Figure 4.19 The block diagrams of ANN classification and regression.

4.4.1.1 <u>Signal segmentation and feature extraction</u>

The procedure to extract control information from a sinusoidal like control signal is shown in Figure 4.20. It is noted that a trial of the experiment lasts 20 seconds with a sampling rate of 100 Hz. Therefore, the joystick control signal is the equal length. On the right side of the 'Joystick Control Signal' from the dashed line is a graph of an example of the control signal produced by a participant. The graph conveys control information that can be approximated into a train of simple switch control cycles [226]. The control signal can be approximated i.e. segmentation by applying local minima and local maxima algorithms as described in Appendix G. The algorithms find peaks and bottoms of the sinusoidal like control signal as shown by the dashed line from the 'Control Cycle Approximation' block. Any three adjacent bottom-peak-bottom points form the triangle of a control cycle. A triangle conforms to the stereotype of the simple switch control profile [226]. The process is repeated until all of the trials are processed.

The graph on the right of the 'Extract feature' in Figure 4.20 is the example of an identified control cycle. A, B and C are the amplitude parameters at each of the corresponding time t_A, t_B and t_C, respectively. These parameters are used to create features of a control cycle as shown in Table 4.3. It is noted that the output for a cycle is the net displacement of a capsule measured from the start to the end of the cycle timing period i.e. t_A to t_C.
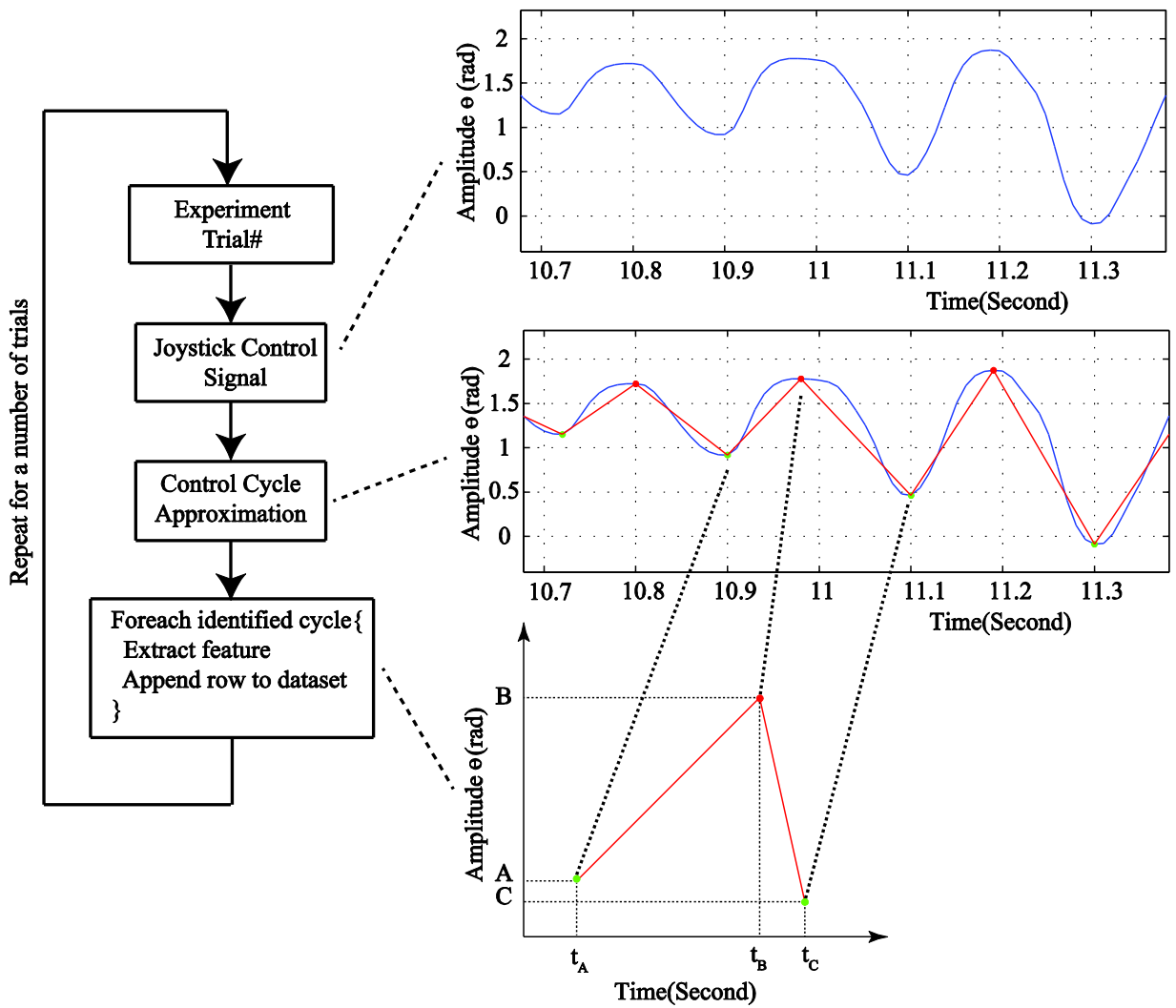
Figure 4.20 The flow chart of the signal processing procedure to extract the control features.

Table 4.3 The nine features of a control cycle and description.

Feature No.	Cycle Parameter	Description
1	A	Amplitude value at point A
2	B	Amplitude value at point B
3	C	Amplitude value at point C
4	$T_{CA} = t_C - t_A$	Time difference between point C and A
5	$T_{BA} = t_B - t_A$	Time difference between point B and A
6	$T_{CB} = t_C - t_B$	Time difference between point C and B
7	$CA = C - A$	Amplitude difference from point C and A
8	$BA = B - A$	Amplitude difference from point B and A
9	$CB = C - B$	Amplitude difference from point C and B

4.4.1.2 <u>Datasets preparation</u>

After completing the process of segmentation and feature extraction as explained in Section 4.4.1.1, the datasets are obtained as shown in Table 4.4 and Table 4.5. It is noted that the data is normalised and shown only in 3 rows. The tables expand to K=3,685 rows which are the size of the extracted control cycles from the entire 54 trials.

The procedure in Section 3.4 is applied for models development. Since the procedure requires two datasets i.e. training and blind test datasets, the control cycles extracted from the best performance trial from each of the participants are preserved as the blind test dataset which is equal to 683 rows of the K. Therefore; the remaining 3,002 is for the training dataset as shown in Figure 4.21.
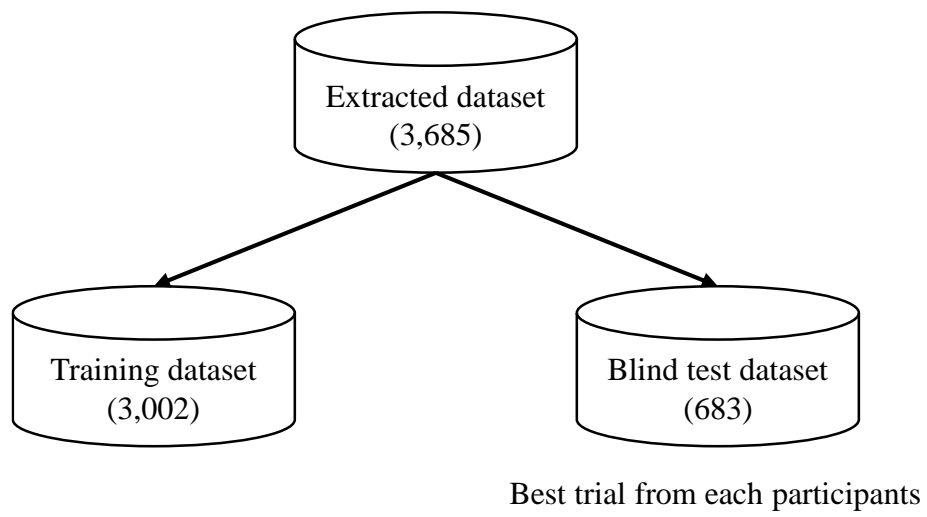
Figure 4.21 The datasets preparation for human-machine control modelling.

Table 4.4 The example of normalised dataset rows for the neural network classification.

Cycle No.	Features / Inputs									Outputs	
	A	B	C	T_{CA}	T_{BA}	T_{CB}	CA	BA	CB	Forward	Backward
1	0.6514	0.0197	0.5655	0.1157	0.4688	0.3612	0.4284	0.0935	0.8569	1	0
2	0.5655	0.0314	0.4363	0.0992	0.4688	0.3524	0.3924	0.1478	0.7776	0	1
3	0.4363	0.0432	0.3618	0.1074	0.4648	0.3612	0.4379	0.2261	0.7290	0	1
…	…	…	…	…	…	…	…	…	…	…	…
K											

Table 4.5 The example of normalised dataset rows for the Neural Network Regression.

Cycle No.	Features / Inputs									Output
	A	B	C	T_{CA}	T_{BA}	T_{CB}	CA	BA	CB	Displacement value
1	0.3284	0.0314	0.4167	0.0909	0.4609	0.3568	0.5735	0.2794	0.7665	0.4735
2	0.4167	0.0314	0.4363	0.0992	0.4609	0.3612	0.5163	0.2304	0.7776	0.3341
3	0.4363	0.0236	0.6319	0.1074	0.4609	0.3656	0.6630	0.2152	0.8921	0.3292
…	…	…	…	…	…	…	…	…	…	…
K										

4.4.2 Modelling results

The results are delivered separately for classification and regression models in Section 4.4.2.1 and 4.4.2.2, respectively.

4.4.2.1 <u>Classification model</u>

The classification model training result is shown in Figure 4.22. The figure shows the result from step 1 of Figure 3.11 i.e. averaged training and testing accuracies from 10 times of running with a number of hidden neurons range from 1 to 18. The overall trend of the averaged training accuracies is in an increasing trend as the number of hidden neurons increased. However, the averaged testing accuracies do not follow the same trend. The best model is selected based on the best average testing accuracy. Therefore, it is found that a model with seven hidden neurons gives the best averaged testing accuracy at 86.94%. The structure of the seven hidden neurons ANN model is shown in Figure 4.23. The corresponding input weight, local weight, and bias are given in Table 4.6, Table 4.7, and Table 4.8, respectively.
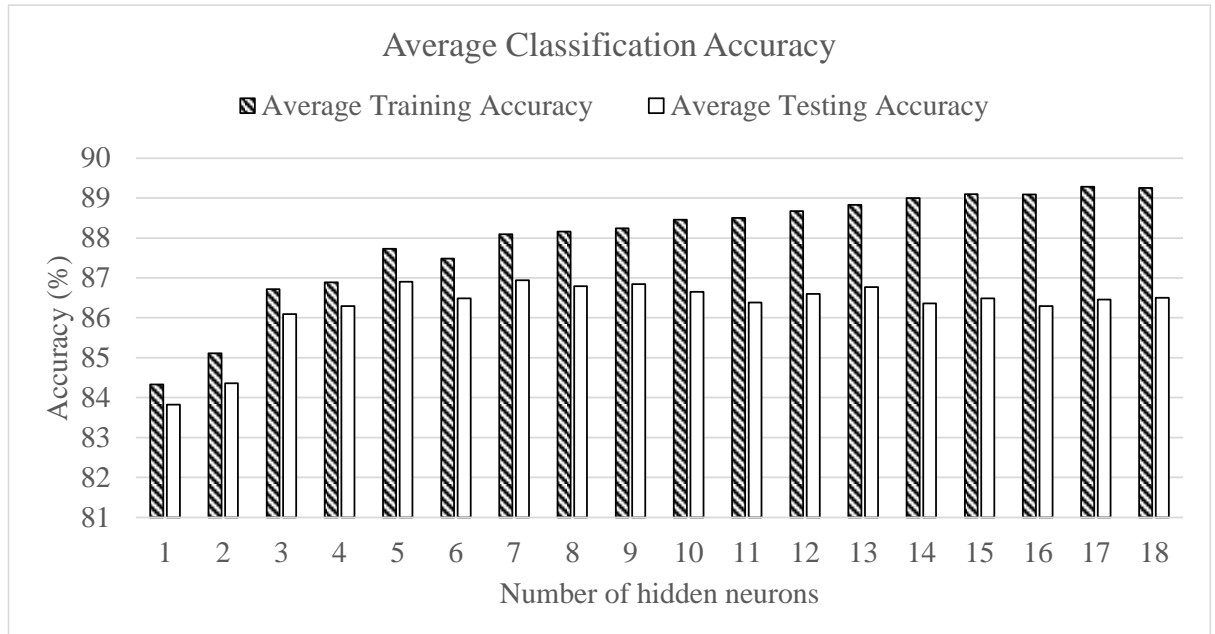
Figure 4.22 The classification result using the 10-time-10-fold validation.

Classification Neural Network

f_1 : sigmoid function   f_2 : threshold function
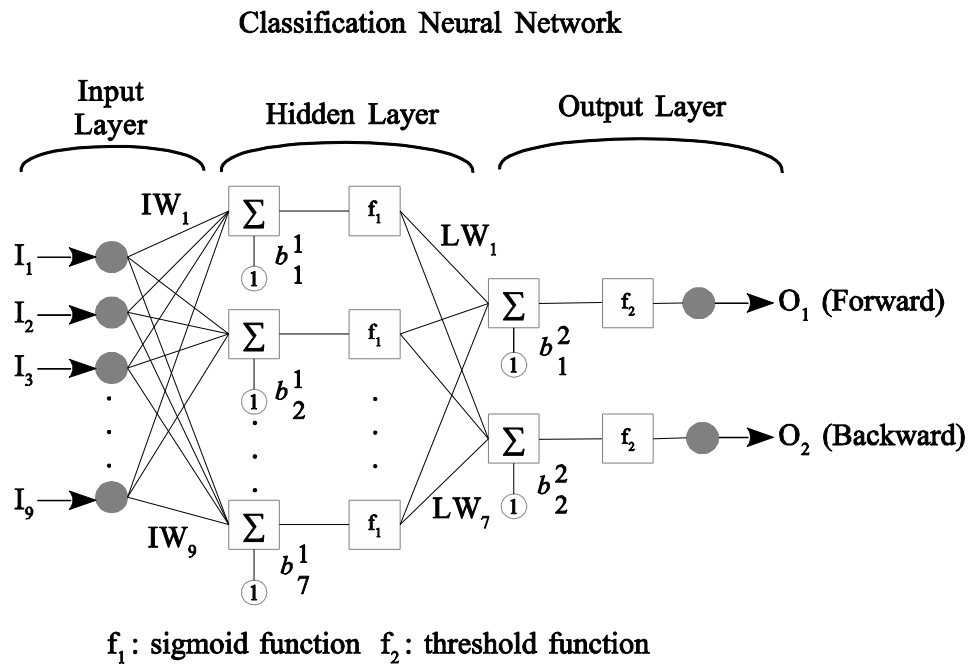
Figure 4.23 The classification ANN with seven hidden neurons.

Table 4.6 The input weight (IW) matrix for the ANN classification model.

IW								
1.398	0.141	0.914	0.542	1.744	-0.691	-1.237	-0.494	-0.379
0.793	-1.479	-0.590	0.814	-0.648	-0.064	-0.039	-0.969	0.106
2.533	1.737	0.361	-1.142	0.768	-0.692	0.194	0.742	-0.625
2.156	-0.500	0.661	0.969	1.734	-1.626	-1.633	-1.289	-0.755
-3.707	-4.354	-2.809	3.342	-1.029	3.205	1.181	0.093	2.422
5.421	1.670	1.522	-1.491	-1.846	-0.340	-3.459	-1.566	-0.382
-1.040	-3.458	-0.715	0.331	-1.786	1.783	-0.383	-1.541	1.063

Table 4.7 The local weight (LW) matrix for the ANN classification model.

LW						
4.981	-2.542	-4.699	-4.565	-2.000	1.523	2.589
-4.575	3.564	4.596	2.825	2.620	-1.395	-2.512

Table 4.8 The bias matrix for the ANN classification model.

b^1	b^2
-0.1589	-2.1565
-1.2782	0.8545
-3.0643	
0.3230	
7.7591	
1.1063	
-3.4729	

Following step 2 in Figure 3.11, the best model is selected i.e. the model with seven hidden neurons. Then, the selected configuration is trained with the entire data to obtain the optimum model. A confusion matrix of the optimum model is shown in Table 4.9. The overall classification accuracy is 88.3%. A TPR or recall of 'Forward' and 'Backward' is 86.2% and 89.9%, respectively. The total numbers of 'Forward' and 'Backward' instances are 1287 and 1715, respectively. The model can retrieve or recall the 'Forward' instances equal to 1109 out of 1287 (86.2%) whereas in the 'Backward' case it recalls 1541 instances out of 1715 (89.9%). An FPR of 'Forward' and 'Backward' is 13.6% and 10.4%, respectively. It means that 174 instances of 'Backward' are incorrectly classified as 'Forward' while 178 instances of 'Forward' are incorrectly classified as 'Backward'. A TNR of 'Forward' and 'Backward' is 86.4% and 89.6%, respectively. It shows that 1109 instances of 'Forward' are correctly classified out of the mixing of 1109 'Forward' and 174 'Backward' instances. An FNR of 'Forward' and 'Backward' is 13.8% and 10.1%, respectively. The rate shows that 178 of 'Forward' instances are incorrectly classified as 'Backward' and 174 of 'Backward' instances are incorrectly classified as 'Forward' in proportion to the class instances i.e. 1287 and 1715, respectively.

Then, the trained optimum model is tested with an unseen data which is the process of a blind test. The preserved 683 data rows are used for this purpose. A confusion matrix of the blind testing is given in Table 4.10. The overall accuracy is 92.2%. A TPR for 'Forward' and 'Backward' are 80.0% (144 out of 180 instances) and 96.6% (486 out of 504 instances), respectively. An FPR is 10.6% and 6.9% for 'Forward' and 'Backward', respectively. An FNR is 20.0% and 3.4% for forward and backward, respectively. A TNR is 89.4% and 93.1% for forward and backward, respectively.

Table 4.9 The confusion matrix of the classification model with the seven hidden neurons.

		Predicted Class		
		Forward	Backward	
Actual Class	Forward	1109 (TP) 36.9%	178 (FN) 5.9%	86.2% (TPR) 13.8% (FNR)
	Backward	174 (FP) 5.8%	1541 (TN) 51.3%	89.9% (TPR) 10.1 (FNR)
		86.4% (TNR) 13.6% (FPR)	89.6% (TNR) 10.4% (FPR)	88.3% (AC) 11.7% (Error)

Table 4.10 The confusion matrix of the blind test process tested with the seven hidden neurons model.

		Predicted Class		
		Forward	Backward	
Actual Class	Forward	144 (TP) 21.1%	36 (FN) 5.3%	80.0% (TPR) 20.0% (FNR)
	Backward	17 (FP) 2.5%	486 (TN) 71.2%	96.6% (TPR) 3.4% (FNR)
		89.4% (TNR) 10.6% (FPR)	93.1% (TNR) 6.9% (FPR)	92.2% (AC) 7.8% (Error)

Both the optimum model training and blind testing results provide a rather high performance of classification. However, in some cases, a single value of performance indication e.g. TPR or

TNR might be misleading. Therefore, precision-recall (PR) and receiver operating characteristic (ROC) graphs are produced to provide further analysis. The PR and ROC curves from the seven hidden neurons training i.e. the optimum model are shown in Figure 4.24. The curves confirm a good classification performance with the area under a curve (AUC) equal to 0.9338 of the ROC curve. The PR curve is slightly different. The PR curve shows 'Backward' marginally better than the 'Forward' case. This is because the actual population of 'Backward' class is higher than the 'Forward' class (1715 versus 1287, a summation of the population in each of the class row).

For blind testing, the AUC of ROC curve is 0.9314 which also confirms the excellence of the model performance. Nonetheless, PR curve in Figure 4.25 shows that the 'Backward' case performs better than the 'Forward' case with the black dotted line closer to the upper right corner. It is noted that the reason could be the greater number of 'Backward' population for blind testing. The population is calculated by adding the number of populations in the same row of actual class. The population of 'Backward' class is 503 compared to 180 for 'Forward' class.
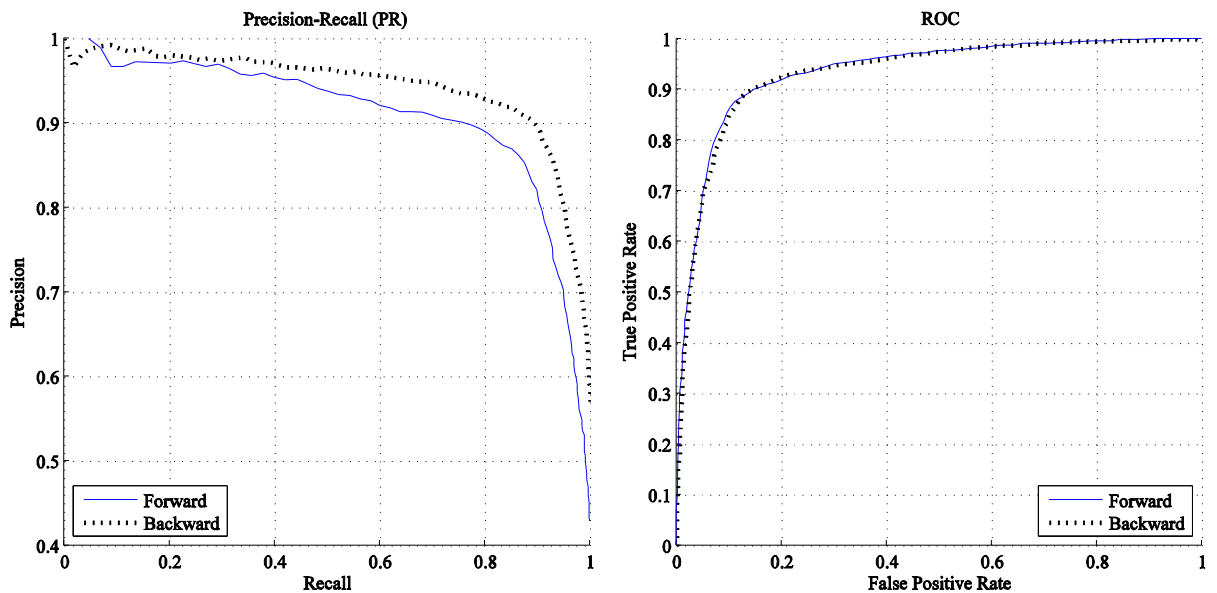
Figure 4.24 The Precision-Recall (PR) and Receiver Operating Characteristic (ROC) curves of the optimum classification model with seven hidden neurons.
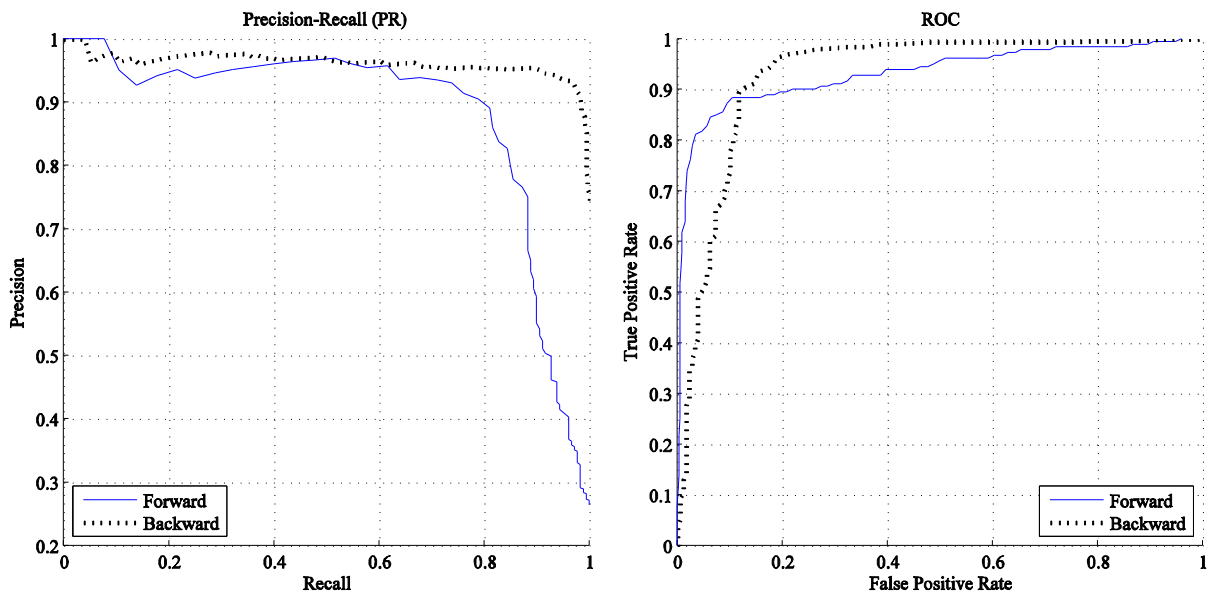
Figure 4.25 The Precision-Recall (PR) and Receiver Operating Characteristic (ROC) curves of the classification model applied to blind test dataset.

4.4.2.2 Regression model

A regression model follows the same procedure in Section 3.4. Figure 4.26 shows the averaged training and testing results referring to step 1 of Figure 3.11. The result is similar to the classification modelling in the sense that the accuracy increases as the number of hidden neurons grow. The best testing accuracy of 73.16% is produced by the model with 14 hidden neurons. Figure 4.27 shows the structure of the regression model with 14 hidden neurons. The input weights, local weights and biases are given in Table 4.11, Table 4.12, and Table 4.13, respectively. Then, 100% of data are used to train the 14-hidden neuron model i.e. the optimum regression model. By training with 100% of data, the optimum regression model is obtained with 79.10%. Then, the accuracy is 77.01% when the model is applied to the preserved blind test dataset.

The regression model is further applied to predict the capsule position using the preserved best trials for each of the participants. Figure 4.28 shows the capsule position predictions. The x-axis shows the sequence of the identified control cycles. Most of the capsule position predictions are fairly accurate except the 'CH4P6-L3' and 'CH4P8-L3'.
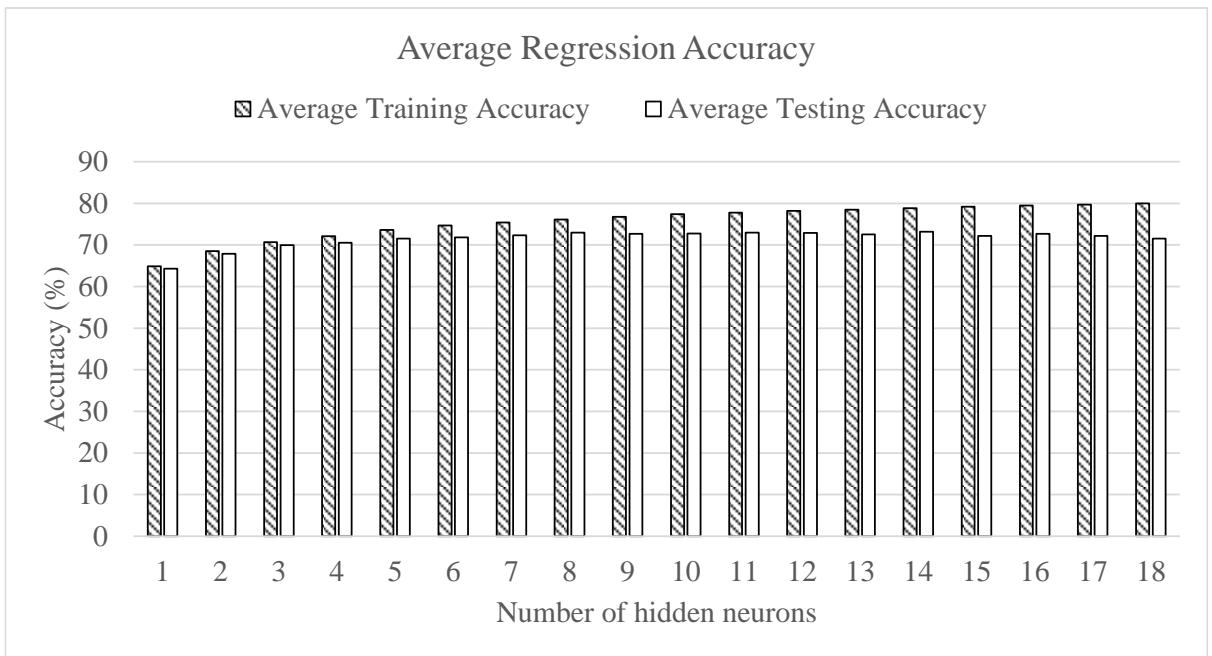
Figure 4.26 The regression result using the 10-time-10-fold cross validation.

f_1 : sigmoid function f_2 : linear function
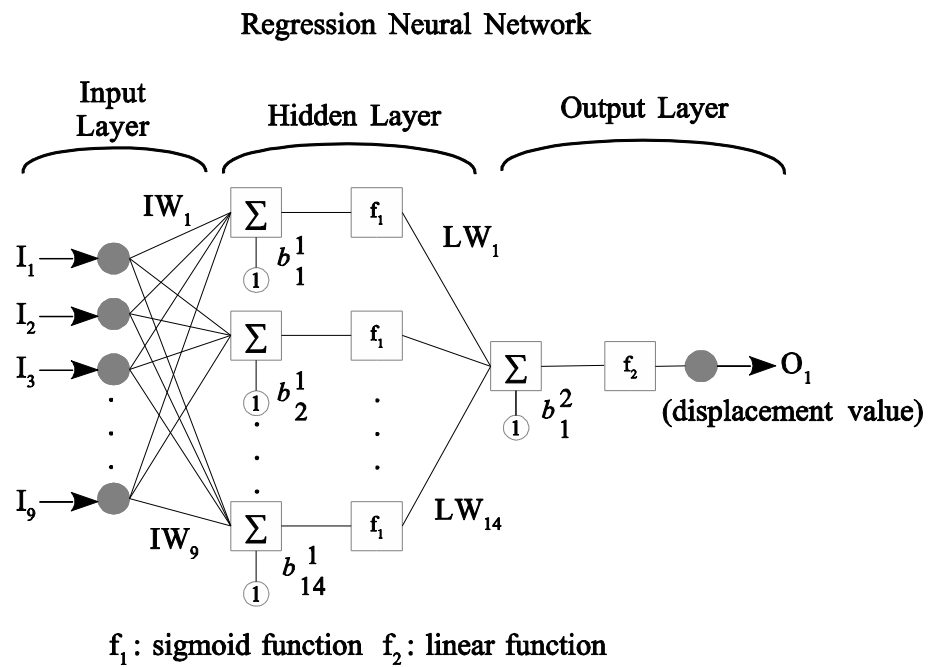
Figure 4.27 The ANN regression structure with 14 hidden neurons.

Table 4.11 The input weight (IW) matrix for the ANN regression model.

IW								
0.093	-1.263	0.359	0.153	0.225	-0.493	-0.597	-1.494	1.050
0.756	0.473	3.168	-2.591	-2.875	3.628	1.484	-0.322	2.123
-5.313	-0.849	-3.514	-2.801	-4.569	1.781	1.195	2.778	-2.419
-1.437	0.609	2.855	3.806	4.534	-2.353	2.733	0.724	1.994
0.118	-2.097	-1.491	1.006	1.032	-1.968	-1.963	-1.354	0.400
0.438	-2.619	-1.298	0.444	2.173	-0.900	-1.930	-0.863	0.020
28.708	4.339	-102.359	-6.705	28.300	-25.699	-108.932	-27.757	-48.703
2.246	0.798	1.389	-0.010	-1.654	1.001	-2.089	0.493	-0.682
1.731	1.484	1.158	-0.230	-1.153	1.354	-1.684	-0.971	-0.899
-0.636	0.615	-1.050	0.749	-0.491	-0.696	0.305	-0.391	-0.681
-0.606	-0.281	0.501	0.104	-1.053	-0.520	0.541	0.012	-0.993
1.250	-0.917	0.897	-0.281	1.151	0.002	-0.490	0.104	-0.010
-1.822	-6.108	-3.485	-0.624	-6.016	7.917	-1.093	-2.949	1.499
1.910	0.671	-0.854	10.068	10.485	-5.778	-0.115	0.023	-0.164

Table 4.12 The local weight (LW) matrix for the ANN regression model.

LW													
0.887	0.323	-0.132	-0.055	-9.769	9.767	0.174	-9.285	9.384	2.720	4.629	1.842	0.071	0.058

Table 4.13 The bias matrix for the ANN regression model.

b1	b2
3.625	3.757
4.349	
3.383	
1.230	
0.191	
0.225	
122.839	
-0.729	
-0.877	
-1.860	
-1.560	
1.680	
-4.667	
5.494	
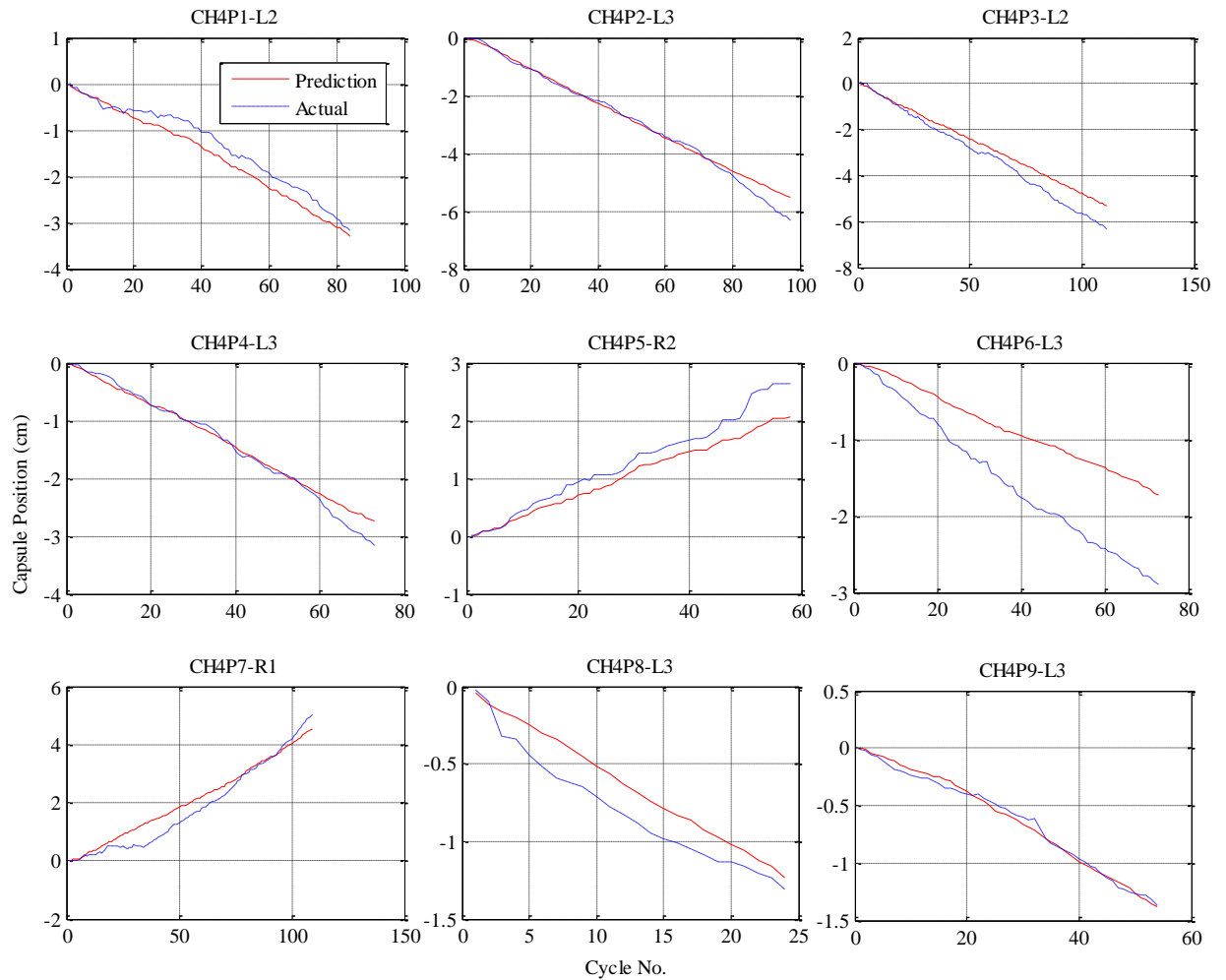
Figure 4.28 The capsule position prediction using the regression model applied to the preserved trials.

4.5 Analysis

The Model I in Section 3.5 is learned heuristically by an operator in order to discover a control law of the model. A set of control rules is identified after several attempts. Apparently, a human can learn heuristically although the system is rather challenging to manipulate because of the dynamic behaviour of the pendulum. This identification of control rules obeys Fitts three stages of learning and the Rasmussen model SRK. The skill to control the dynamic of pendulum via the joystick is developed into a set of rules. Then, the set of rules is developed into knowledge when it is applied to compare with a human walking cycle. These skills and rules can be

developed into the knowledge for the specific machine operation. The knowledge can be revolutionised and generalised into wisdom over time by applying particular domain of knowledge into other domains as shown in Figure 4.29.
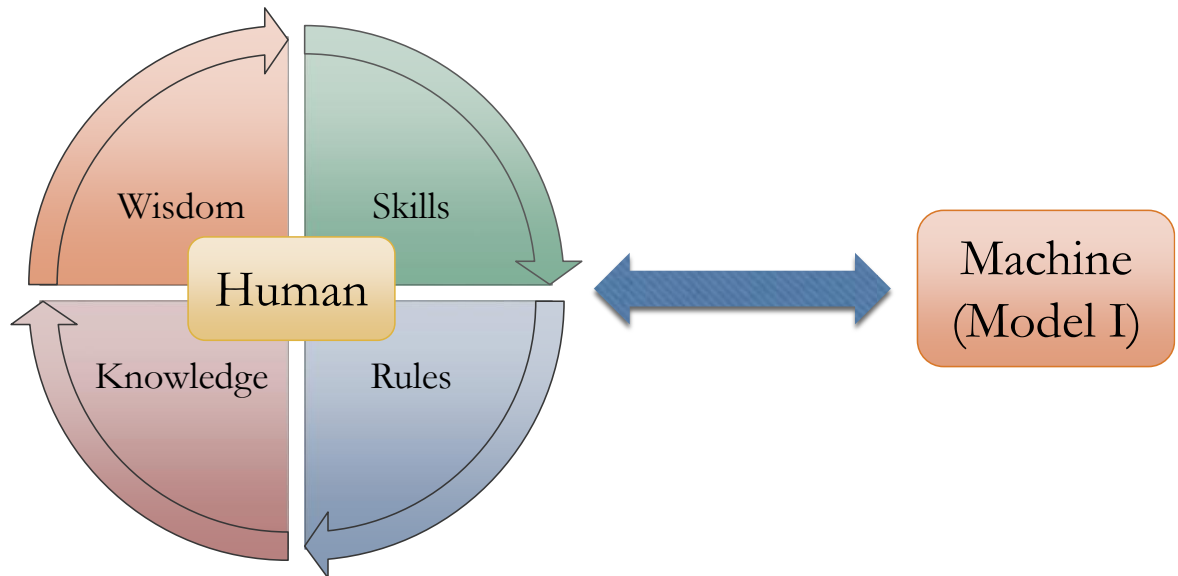
Figure 4.29 The cycle of skills-rules-knowledge-wisdom.

It can be noted that the Model I is not an inverted pendulum. It is a hanging pendulum attached to the capsule body. Therefore, it is practically impossible for a human to control the pendulum to stay upright while managing to underactuate the capsule body movement. A pendulum balancing alone is one of the classical challenging problems of the investigation in many research projects [16], [47], [114], [227].

The Model II is an inverted pendulum-driven capsule system. The model includes a PID controller in order to control the pendulum angle to stay upright. As a consequence, a human participant can concentrate to control the pendulum rotation rather concentrate on the dynamic of pendulum balancing. Nine participants are recruited to participate this scenario of the investigation. The results indicate that the nine participants show different learning time and performance outcomes. The performance is indicated by e.g. an amount of absolute value of final capsule distance, accumulated absolute final capsule distance, average capsule speed etc. It is interesting that the right-handed and left-handed participants achieve their best performance on the opposite side of their handed-ness. The variance of the final capsule distance seems to

indicate a learning index in this investigation. The characteristic of a high and a low performer is differentiated by the input oscillation frequency, correctness of the oscillation etc.

Although the pendulum rotation angle control profile generated by a human operator differs from the six steps control strategy in [148] the profile successfully drives the capsule system forward. The manual control profile is not identical to the automatic control profile. This is normal as a human being who can heuristically learn and apply knowledge to the facing circumstance to solve the problem but does not need to be mathematically / objectively perfect as in the same as the automation.

Further, the manual control information is analysed by the identification of a control cycle which mimicries the theoretical control profile. The extremum is applied in order to approximate the manual control signal. These control signals are developed into a model of human-machine control in Section 4.4.

A coupling of descriptive and predictive modelling approaches is utilised with an ANN for the model developments. The data of human-machine control information is obtained from the investigation in Section 4.3. The data is analysed, segmented, and features extracted in order to develop an ANN model. Two types of ANN i.e. classification and regression models are developed by applying the 10-time-10-fold cross-validation procedure from Section 3.4. The procedure reveals that the optimum ANN configurations for classification and regression models are 7 and 14 number of hidden neurons, respectively. The overall accuracies of the models are 88.3% and 79.1%, respectively. These accuracies are additionally confirmed by a plot of precision-recall and ROC curves.

Moreover, the two models are tested with an unseen data i.e. blind test dataset. The blind test outcomes are 92.2% and 77.01% for classification and regression models, respectively. Once more, the accuracies are double confirmed by a plot of precision-recall and ROC curves.

Since the regression model gives a continuous output of capsule displacement, therefore, it is applied to predict a capsule displacement. The prediction results are fairly accurate.

4.6 Summary

In this chapter, a human-machine heuristic learning and human-machine control model development have been investigated based on a case study machine i.e. the pendulum-driven capsule system. It can be concluded from the investigation in Section 4.2 that a human can learn to control an unfamiliar system and formulate a set of control rules for it. Moreover, these rules of machine control can be developed into knowledge that can be applied to other similar mechanisms. From time to time, the knowledge can be evolved into wisdom that can be applied to other domains. The investigation in Section 4.3 has been conducted with nine participants which provide more variety of information on the human-machine control. Various performance aspects have been produced to compare and to identify the differences in the control characteristics among the participants. Further development has been investigated in Section 4.4, the human raw control information from Section 4.3 is extracted in order to develop a human-machine control model. As a result, two ANN models are obtained with relatively high accuracy. The classification model is possible to be applied to predict the human-machine control behaviour i.e. the human operator intention to control the machine to the desired direction.

Chapter 5 Electroencephalography – preliminary investigations

5.1 Introduction

This chapter introduces a new hardware interface into the platform i.e. the Emotiv EPOC headset. The headset is used to record brainwave activity in the form of electroencephalogram (EEG) which is the electrical neuro-activity generated from the brain neural system as discussed in Section 2.13. The chapter conducts preliminary investigations on the fundamental of EEG recording, EEG data processing, EEG artefacts removal, and to formulate a workflow for the EEG analysis. In order to perform these investigations, three scenarios are designed and implemented i.e. 1) Study on brain response to an auditory event, 2) Study on brain response to a finger movement, and 3) Study on brain response to target hitting task.

5.2 The investigations

The three investigations can be divided into two categories according to the eyes opening condition i.e. eye closed, and eyes opened. The investigation 1 and 2 are conducted while the participant eyes are closed. The investigation 3, a simple scenario of a target hitting task is required that the participant eyes be opened during the experiment. A list of the EEG preliminary investigation is summarised in Table 5.1

Table 5.1 A list of the EEG preliminary investigations.

Investigation	Description	Eyes status	Section
1	Study on brain response to an auditory event	Closed	Section 5.4
2	Study on brain response to a finger movement	Closed	Section 5.5
3	Study on brain response to target hitting task	Opened	Section 5.7

5.3 The integration of EEG brain monitoring system to the HAM simulation platform

To acquire EEG brain activity data, the HAM platform building block in Figure 3.5 Section 3.4 includes the dashed block diagram where the Emotiv EPOC headset and the API are implemented for the EEG data acquisition. It can be noted that the communication between the platform and the headset is wireless via the USB dongle. The platform can acquire the EEG data simultaneously with the other simulation data via the manufacturer provided API.

5.4 Study on brain response to an auditory event

A brain response to an auditory event is investigated in this section. Previously, it has been reported that the brain is responded to an auditory by the frontal area of the human's scalp [189]. Therefore, the AF3 and AF4 (Figure 2.35) electrodes of the Emotiv EPOC are the focus of this investigation. The investigation consists of a single participant with four experiments.

5.4.1 Experiment procedure

A participant sits in a comfortable chair with both eyes closed while wearing the headset and earphones. The HAM platform runs and plays a sound effect at certain time intervals while the headset is recording the EEG brainwave. The markers denoted as '1' are inserted into the marker channel of the headset when the sound effect 'Windows Critical Stop.wav' is played. The sound effect is played randomly at every 2,000ms to 3,000ms intervals. The marker '1' is a target event i.e. the event of interest. In this case, it is the brain response to the sound. The markers denoted as '2' are inserted randomly at every 1,000ms to 5,000ms intervals. The marker '2' is a non-target event which is used to compare with the target response. Figure 5.1 depicts the insertion process of the two markers during the experiment timeline. It can be noted that the HAM platform is programmed to prevent the chance of the two events from happening at the same time.
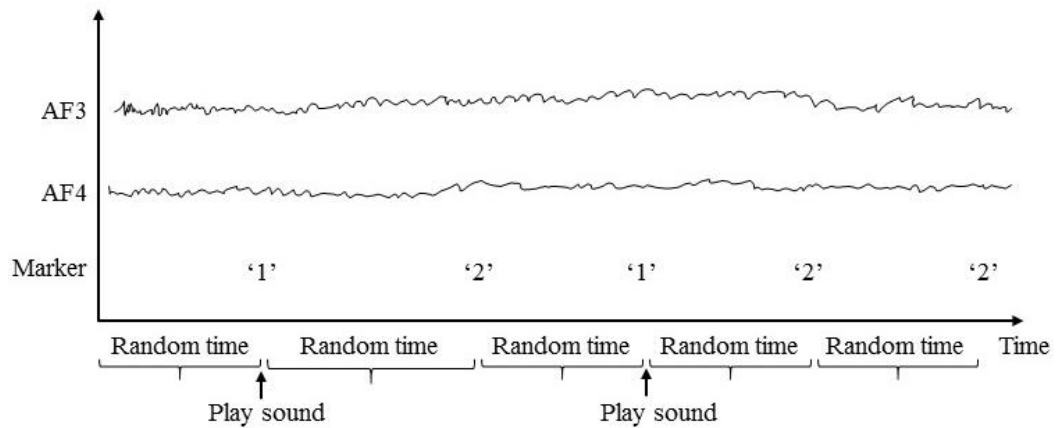
Figure 5.1 The markers insertion for the auditory experiment.

The participant is instructed to keep the body movement as low as possible to keep the noises at the minimum level. However, eyes opening, mouth water swallow, head muscle movement, coughing, and other activities can happen randomly. These activities cause the unrelated brain activity signal which is known as artefacts. The artefacts need to be removed in the post-processing analysis of the recorded data.

A recording session lasts for approximately 3-10 minutes and produces a comma-separated value (CSV) file. Each experiment repeats for a number of sessions until the headset is removed.

5.4.2 Data processing

Each of the CSV files is imported into MATLAB for processing with the EEGLAB software toolbox. Each file contains the 14 channels of EEG brainwave plus an additional marker channel. However, only AF3 and AF4 are selected for the analysis according to [189] for the study of the brain responded to the auditory stimulus. The data from AF3 and AF4 is band pass filtered to 1-20 Hz. Then, the epochs i.e. a segment of the two brainwaves at the event markers are extracted. The major artefacts are manually inspected and the contaminated epochs are rejected using the epoch rejection tools provided in the EEGLAB. This means some of the extracted epochs are excluded from the ERP calculation. This processing procedure is shown in Figure 5.2. This data processing procedure is applied to each experiment session one at a time. Once all the sessions within the same experiment are processed, they are merged for the ERP calculation. Then, the ERP and ERP images are produced. The ERP image shows the strength

of the signal from all epochs within one plot. Each epoch is plotted with the colour-coded value of amplitude over time along the horizontal view. The entire epochs plot is stacked vertically.
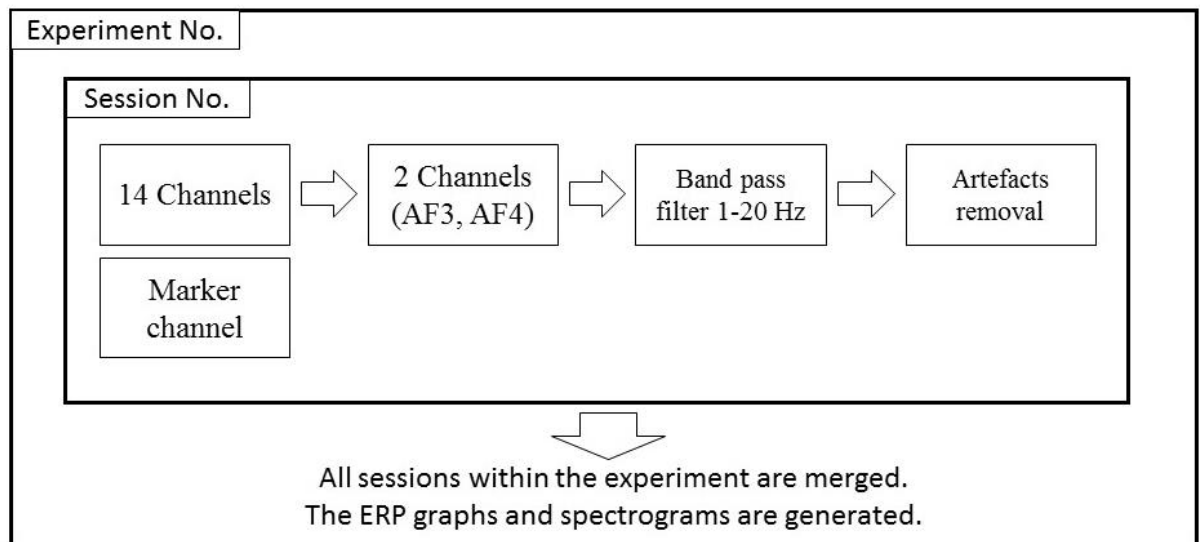
Figure 5.2 The processing procedure of the auditory ERP data.

5.4.3 Results

The detail of the four experiments is shown in Table 5.2. All of the four experiments have been conducted with one participant who is at age 33, male, and right-handed. Three experiments are performed in a quiet environment while the experiment number 2 is performed in an office environment. Each of the experiments contains an unequal amount of sessions because the time used for each session is not the same due to the discomfort of the headset. Therefore, the amount of extracted events (target and non-target) from the marked marker is not the same for each experiment. After artefact removal, the total number of artefact-free target and non-target epochs is remained as shown in Table 5.2.

Table 5.2 The summary of experiment details for the four experiments.

Experiment No.	1	2	3	4	All Experiments
Number of sessions	8	10	3	4	Not applicable
Experiment Environment	Quiet	Office	Quiet	Quiet	Not applicable
Number of target epochs	267	622	393	429	1711
Number of non-target epochs	164	518	344	51	1414
Target and non-target ERPs comparison	Figure Appendix.4	Figure Appendix.5	Figure Appendix.6	Figure Appendix.7	Figure Appendix.8

Experiment 1

Session 1, 2, 3, 4, 5, 6, 8 are merged to calculate the ERP graph. It can be noted that session 7 is excluded from the calculation because it contains few events and most of them are noisy. Figure Appendix.4 shows the comparison of the ERP from AF3 and AF4 for target and non-target. It is obvious that the target ERP shows a brain response to the sound effect event. Both AF3 and AF4 potentials are decreasing (approximately at N200) and then increasing (approximately at P400).

Experiment 2

All 10 sessions are included in the data processing. The number of extracted target events (with marker '1') is 622 epochs. Figure Appendix.5 shows the comparison of channels ERP from AF3 and AF4 electrodes in response to target and non-target events. Although the result from experiment 2 is not very clear for the ERP responses to the target event when compared to the experiment 1, the graphs still show the similar pattern with a relatively weak response to the target sound. This could be the result of the signal recording in an office environment which has many non-related distractions. However, the non-target ERP obviously shows random brainwave.

Experiment 3

Figure Appendix.6 shows the comparison of the channels ERP for the brain AF3 and AF4 electrodes to the target and non-target events. The target ERP shows an identifiable pattern of the brain response when compared to the non-target response which has no pattern.

Experiment 4

Figure Appendix.7 shows the comparison of channel ERP for the target and non-target events. Although in this experiment the signals corresponding to target events are not clearly distinguishable, but it still shows the clearer pattern than the non-target ERP, which shows random waveforms.

All Experiments

All in all, some of the experiment within this investigation does not show any obvious auditory ERP e.g. experiment 2 and 3. However, the ERP is highly obvious when all of the 4 experiments are combined to generate the ERP as shown in Figure Appendix.8. The target EEG deflects toward negative at around 250ms then bounces back immediately before the 500ms of the event onset latency. The non-target does not show a significant brain response.

5.5 Study on brain response to a finger movement

This section presents the study of a human brain response when a human participant clicks on a computer mouse at his / her intention while both eyes are closed to keep artefacts to the minimum level.

5.5.1 Experimental procedure

In this study, all of the frontal electrodes – AF3, AF4, F7, F8, F3, F4, FC5, FC6 are included in the analysis of the ERP. A human participant sits on a comfortable chair in front of a computer

and grasps a mouse. The participant is instructed to close both eyes and to keep the other activities to a minimum. The participant can click a mouse at any time at his / her intention when the HAM platform is running while recording the EEG data. A target marker '1' is marked when the participant clicks the mouse. A non-target marker '2' is inserted at random intervals in order to be used as a comparison between the ERP of click event and the human normal ongoing brain event. The marking procedure is depicted in Figure 5.3.
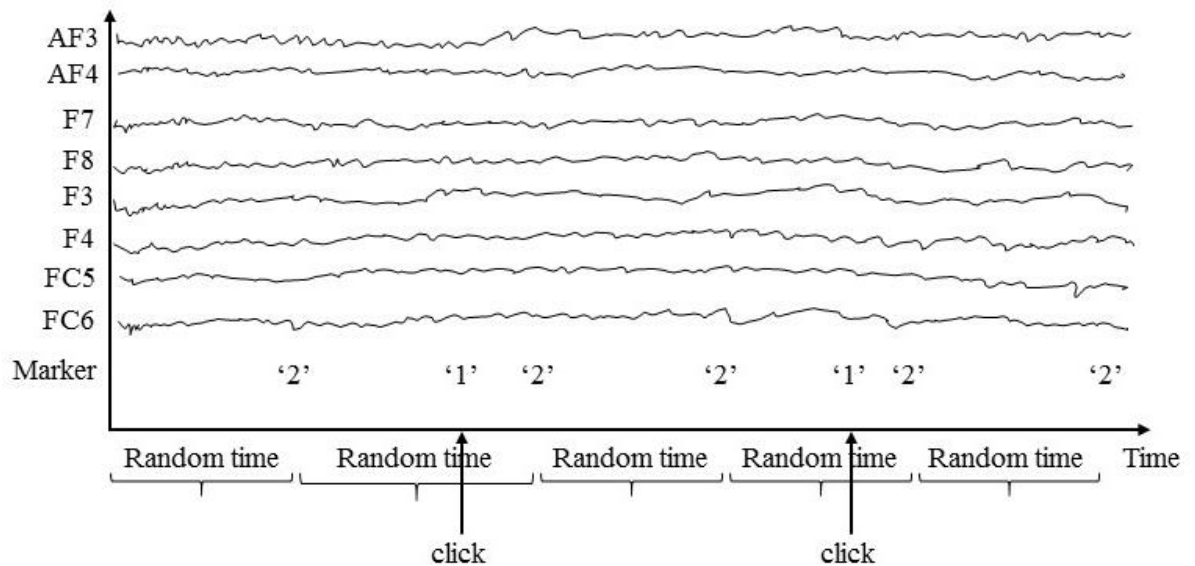
Figure 5.3 The event marking procedure of the study on brain response to a mouse click.

5.5.2 Results

The investigation contains four experiments as shown in Table 5.3. The participant is male aged 33 with right-handedness. Three experiments are performed with the right hand while experiment 4 is performed with the left hand. The number of target and non-target epochs is shown in the table. The numbers are not equal because it depends on the amount of time the participant spends on each session. The ERP graphs for the four experiments are calculated and shown in Figure Appendix.9, Figure Appendix.10, Figure Appendix.11, and Figure Appendix.12, sequentially.

Table 5.3 Summary of the four experiments of the study on brain response to a mouse click.

Experiment No.	1	2	3	4
Number of target epochs (click)	545	270	359	372
Number of non-target epochs (random)	493	200	295	272
Target and non-target ERPs comparison	Figure Appendix.9	Figure Appendix.10	Figure Appendix.11	Figure Appendix.12

It can be noted from all of the four experiments that the ERP of a finger movement is clearly visible. The brain responds to the voluntary mouse click at around 200ms. For example, Figure Appendix.9 (a) shows the ERP graph and 2D topography. The 2D topography shows at 244ms after a mouse click. The brain at the F3 electrodes (refer to Figure 2.35 for the F3 location) shows the darkest red colour of positive deflection with the surrounding areas having the same colour fading away. This type of response is the same that is found in experiment 1, 2, and 3. However, the experiment 4 is different. The right parts around F4 of the brain are activated as shown in Figure Appendix.12 (a). It is commonly known that when the right parts of the human body are in use, the left brain takes responsibility to process the action, and vice versa. Therefore, the study on the brain response to a mouse click confirms this knowledge.

5.6 A workflow for eye opened experiments

In Section 5.7, the investigation on a simple target hitting task is conducted. It is obvious that this type of operation is a vision based operation. Therefore, both eyes are required to be open during the operation. As a consequence, it is necessary to have a workflow which includes a method to handle the eye related artefacts. The ICA discussed in Section 2.13.4.5 is a technique that can be used to deal with this type of artefacts. Figure 5.4 shows a workflow for the investigation in Section 5.7 which includes the ICA analysis which has the capability to remove eye artefacts.

The process starts with data acquisition via the HAM platform. The HAM platform generates a CSV file for each session which can be imported directly into MATLAB for further post-processing. The CSV file contains the EEG signals, marker channel, task-specific data etc. The EEGLAB toolbox in MATLAB is used to band pass filter the EEG data into the range of brain normal rhythms i.e. 1-30 Hz. Then, the continuous EEG waves are extracted into epochs by the specified marker name e.g. '5', '10' etc. The epoch duration can be specified to be e.g. from -500ms to 1500ms centred at the marker onset time for the ERP analysis. Normally, the EEG data falls into the particular amplitude range e.g. 10-30 μV of Beta brain rhythm (Table 2.7). Therefore, the epoch that contains the signal that exceeds the range can be removed. After that, a manual inspection is performed to exclude the abnormal epochs. Then, the ICA algorithm is executed on the EEG data to extract the ICA components. After the ICA components have been extracted, an analysis of the independent component to find the suspicious artefactual components are performed. Thereby, the suspicious component which contributes to the eyes or other artefacts is marked to be removed. The marked components are removed in order to obtain the remaining EEG data without artefacts. The process of ICA for artefact removal can be found in Section 2.13.4.5. Finally, the cleaned EEG data is ready for the analysis.
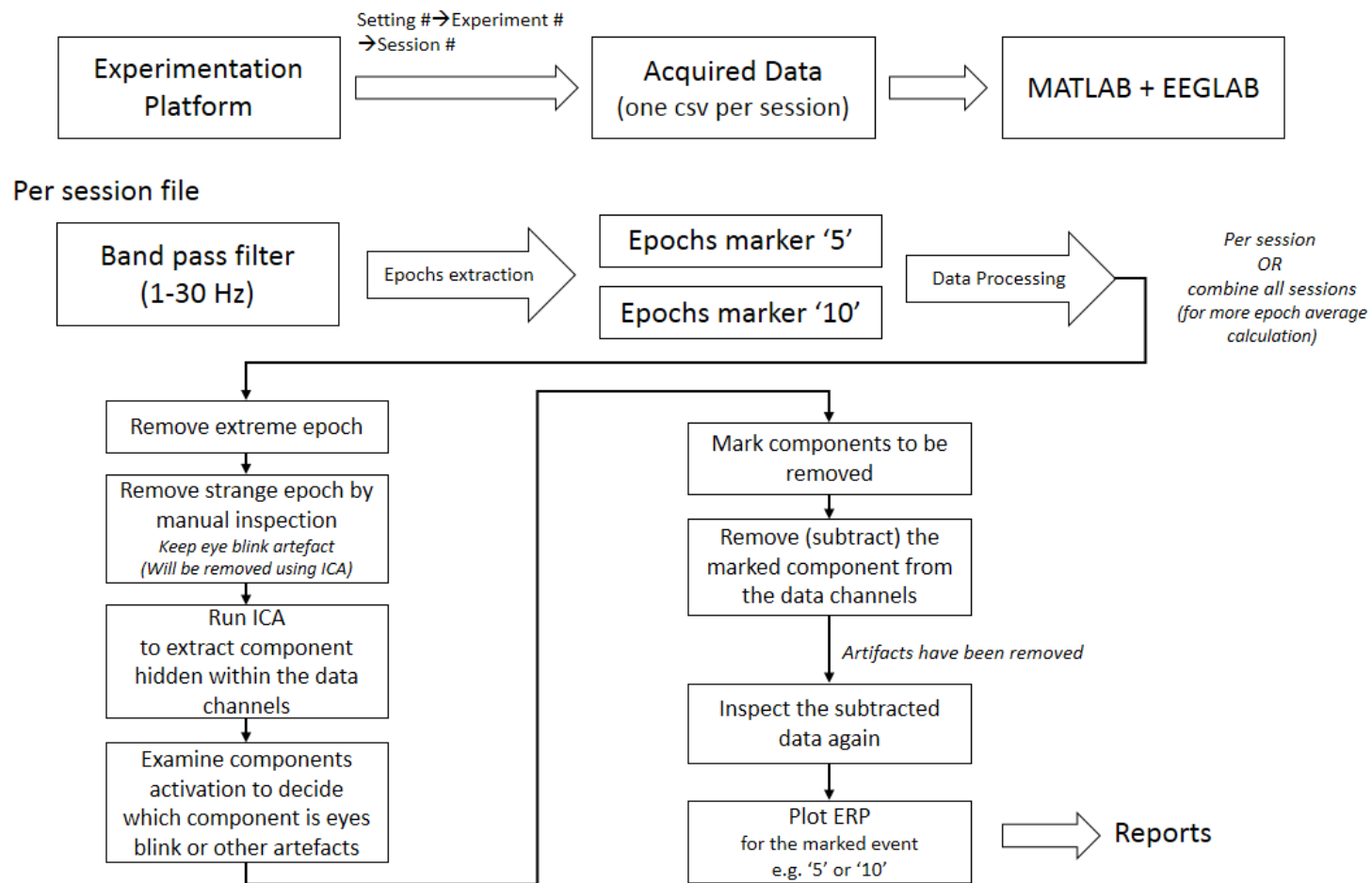
Figure 5.4 A workflow that can deal with eye artefacts by utilising the ICA.

5.7 Study on brain response to target hitting task

In this section a study on brain response when a participant performs a simple target hitting task is reported. This type of task has been discussed in Section 2.7.4.

5.7.1 Experimental procedure

A black target circle is programmed to appear on screen at random positions and time intervals. A human participant has to move the mouse to click on the appeared target as quick as possible. A screenshot of the scenario is shown in Figure 5.5. It can be noted that a participant has been instructed to keep mouse stationary while waiting for a target to appear on the screen. The target disappears after it has been clicked and the process is repeated. The process lasts for 30 repetitions for each session for each participant. There are two types of event marker in this experiment for the ERP calculation i.e. 1) target appear, 2) target click.
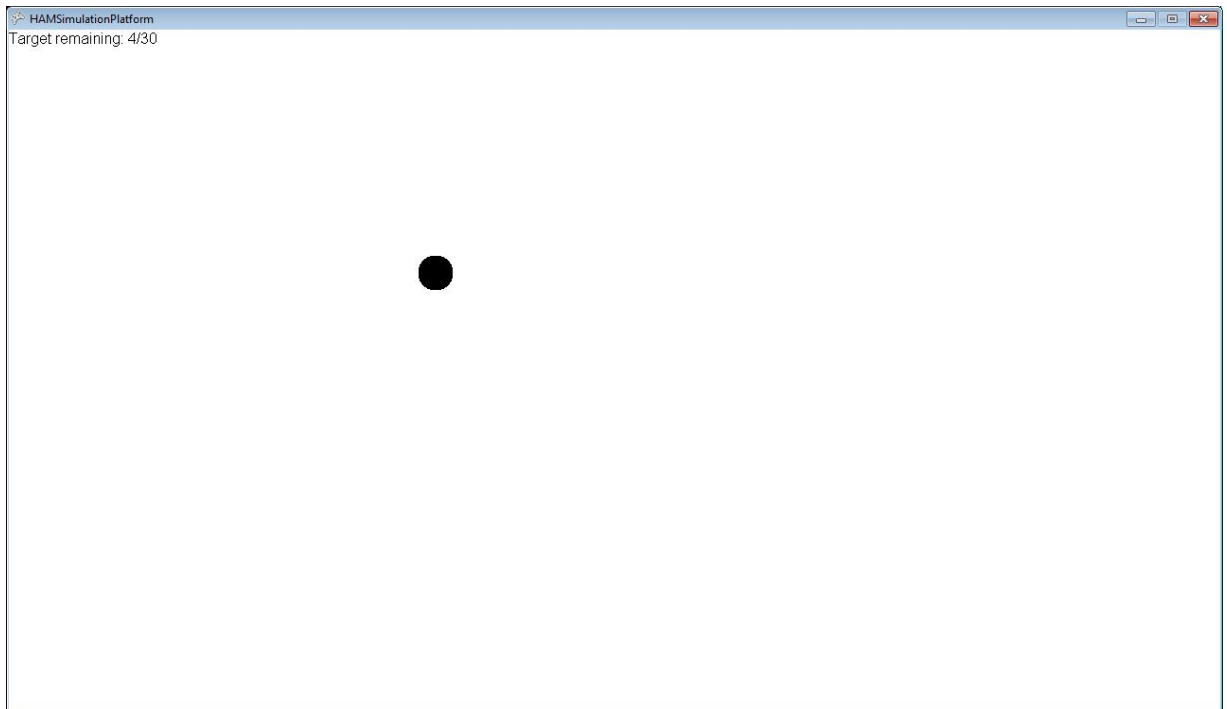
Figure 5.5 A screenshot of the simple target hitting task scenario.

5.7.2 Results

The ERP analysis is focused on the two events i.e. 1) when a black target circle has appeared on the screen 2) when the target has been clicked. The investigation in this section has been conducted by two participants as shown in Table 5.4 for the participant and experiment details. Each participant conducts 10 sessions while each session has been programmed to have 30 appearances of the black circle target. However, some of the epochs have to be excluded due to artefacts. The number of epochs after the exclusion of artefactual epochs is shown in Table 5.4. Figure 5.6 and Figure 5.7 show the ERP response to the two events i.e. target appear and target click, for participant CH5P1 and CH5P2, respectively.

Table 5.4 The participants and experiment details.

	Participant CH5P1	Participant CH5P2
Age	34	35
Handedness	Right	Right
Number of epochs for target appear event	259	293
Number of epochs for target click event	267	306

The ERP results clearly show that the brain responds to the target appearance events as shown in (b) and (c) of Figure 5.6 and Figure 5.7. However, it is relatively difficult to differentiate the ERP at the click event because the ERP is not very clear as shown in (e) and (f) of Figure 5.6 and Figure 5.7. The 2D topography maps of the brain areas activation have been produced as shown in (d) and (g) of Figure 5.6 and Figure 5.7 for some of the interesting latency after the events onset time i.e. from 250ms to 360ms with 10ms interval. The 2D topography maps of the target appear event from participant CH5P1 shows that both frontal and posterior areas activate downward negative value of EEG. In contrast, frontal and posterior brain areas from participant CH5P2 are activated in the opposite direction i.e. the frontal towards positive while the posterior towards the negative value of EEG. Nevertheless, the posterior ERP from both participants are identical in which the brainwaves are deflected downward negative and then bounce back toward positive at around 250ms and 500ms, respectively. It is clear that this is the effect of the function of the posterior area which functions for visual processing while the frontal areas can be functioned for multiple types of task.

Snapshots of display monitor

click

Target has appeared   Target has been clicked
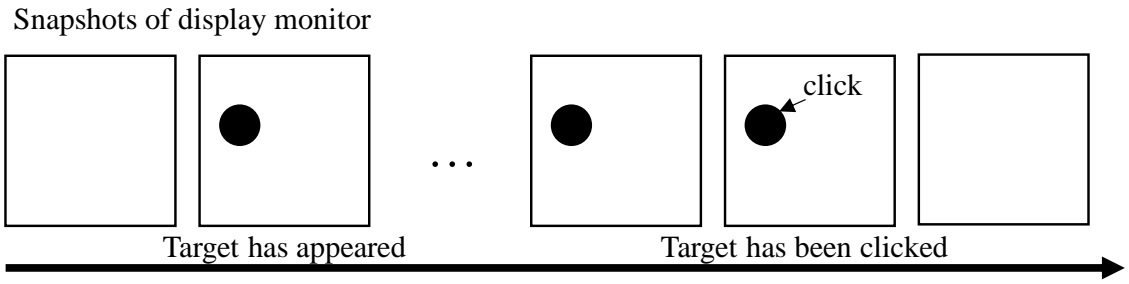
(a) Time line
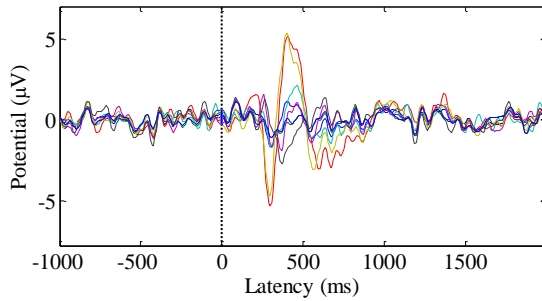
(b) Target appear ERP from frontal electrodes

(e) Target click ERP from frontal electrodes
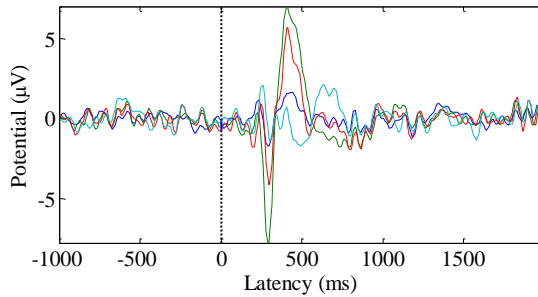
(c) Target appear ERP
from posterior electrodes
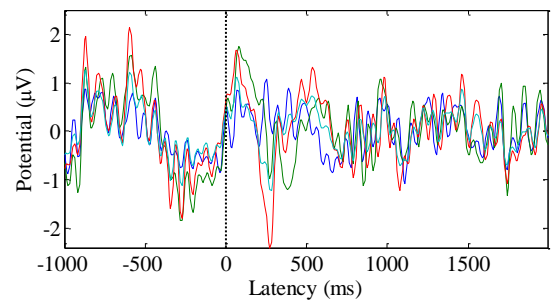
(f) Target click ERP
from posterior electrodes
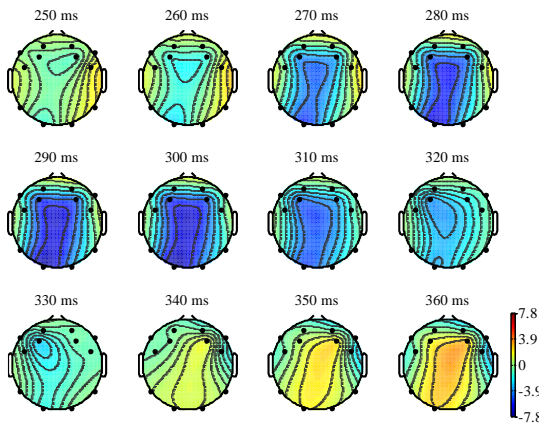
(d) 2D topography maps of target appear
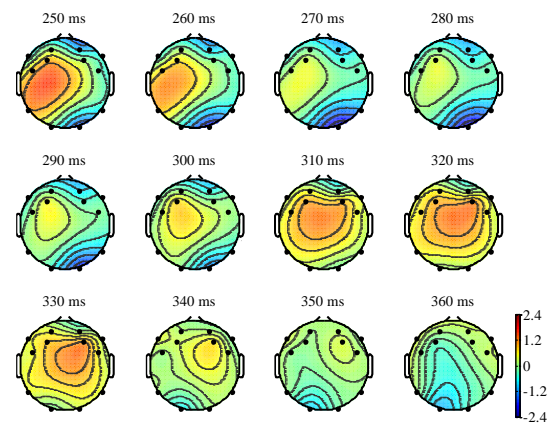
(g) 2D topography maps of target click

Frontal electrodes: AF3 AF4 F7 F8 FC5 FC6 F3 F4   Posterior electrodes: P7 O1 O2 P8

Figure 5.6 The brain responses at target-appear and target-click events from Participant CH5P1.

(a) Time line

(b) Target appear ERP from frontal electrodes

(c) Target appear ERP from posterior electrodes
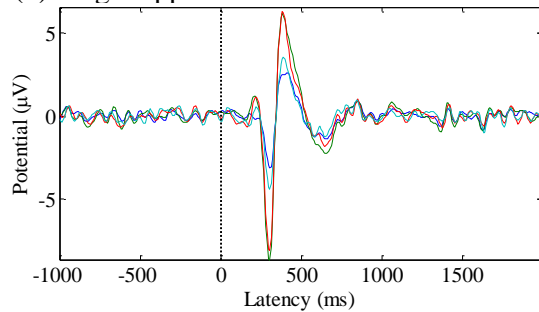
(e) Target click ERP from frontal electrodes
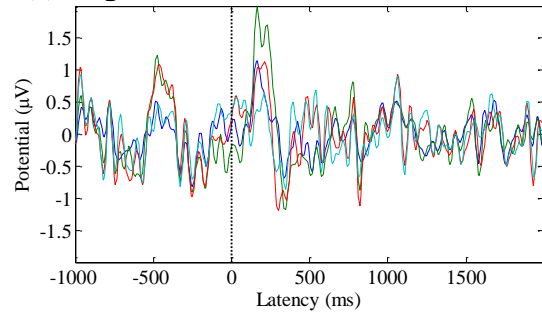
(f) Target click ERP from posterior electrodes

(d) 2D topography maps of target appear
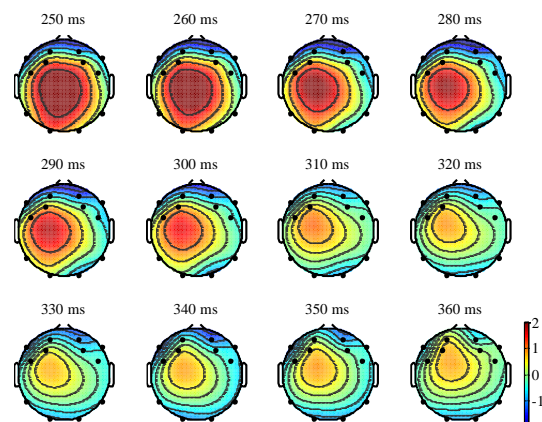
(g) 2D topography maps of target click

Frontal electrodes: AF3 AF4 F7 F8 FC5 FC6 F3 F4   Posterior electrodes: P7 O1 O2 P8

Figure 5.7 The brain responses at target-appear and target-click events from Participant CH5P2.

5.8 Summary

The investigations in this chapter are mainly the study of the fundamental of EEG brainwaves data acquisition, data processing, workflow, ERP analysis etc. New hardware for the EEG recording has been introduced and integrated into the HAM platform in order to perform the investigations. Three investigations are presented based on the study of the brain response to a particular stimulus i.e. audio, finger movement, and a simple target hitting task. The first two of them are performed while the participant's eyes are closed in order to minimise noises. The last one requires participant eyes opened in order to perform the task.

The ERP from the particular target stimuli i.e. audio and finger movement are obviously identifiable. A comparison between the ERP from the target and non-target events reveal that the brain EEG has a specific response to the stimulus by having a transient spike immediately after the stimulus onset time.

A simple target hitting task has been implemented in order to study the brain response to the task events i.e. target appear and click events. This type of task is visually based operation. Therefore, a workflow for eyes opened EEG analysis is needed. The independent component analysis (ICA) is an effective method which can deal with this artefactual EEG. The result shows that the brain responds to the target appearance and the click events differently. The evidence from these investigations confirms that the Emotiv EPOC headset is able to record a brain-related activity.

Chapter 6 Human-machine interaction performance evaluation based on brainwave

6.1 Introduction

This chapter presents the investigation of a human-machine operation simultaneously with the EEG data acquisition system to establish a relationship between task actions and the human brainwave functions. A target hitting / reaching operation is adopted as a case study for this investigation based on the following justifications.

1. The task is simple.
2. It is a primitive task that can be in any part of HMI which involves reaching from one point to another point.
3. The simplicity of the task allows analysis of the EEG brainwaves with a clear focus on a particular type of action by having a minimum amount of distractions.
4. An aspect of the task and the corresponding performance indicator is well established by a renowned Fitts and Posner study and a number of followed studies e.g. in HCI research.

6.2 Experiment design

The experiment is designed to replicate a target hitting task (THT) and is integrated into the existing HAM platform. THT is simply a task of moving a mouse cursor to reach and hit a target as fast and as accurate as possible. A literature review of THT is discussed in Section 2.7.4 and 2.5.3.1.

In this study, a THT is designed and explained as follows. A target and mouse cursor are spawned at a certain time and position within the screen boundary as shown in Figure 6.1 and

are represented by *TP(x,y)* and *MP(x,y)*, respectively. They are settled apart at a certain distance. A target has a diameter of *W*. The screen has a fixed dimension of 1280 by 720 pixels i.e. width and height, respectively. The coordinate of the screen is depicted in the figure and can be noted that the positive *X* axis is pointed toward the right, and the positive *Y* is pointed downward.
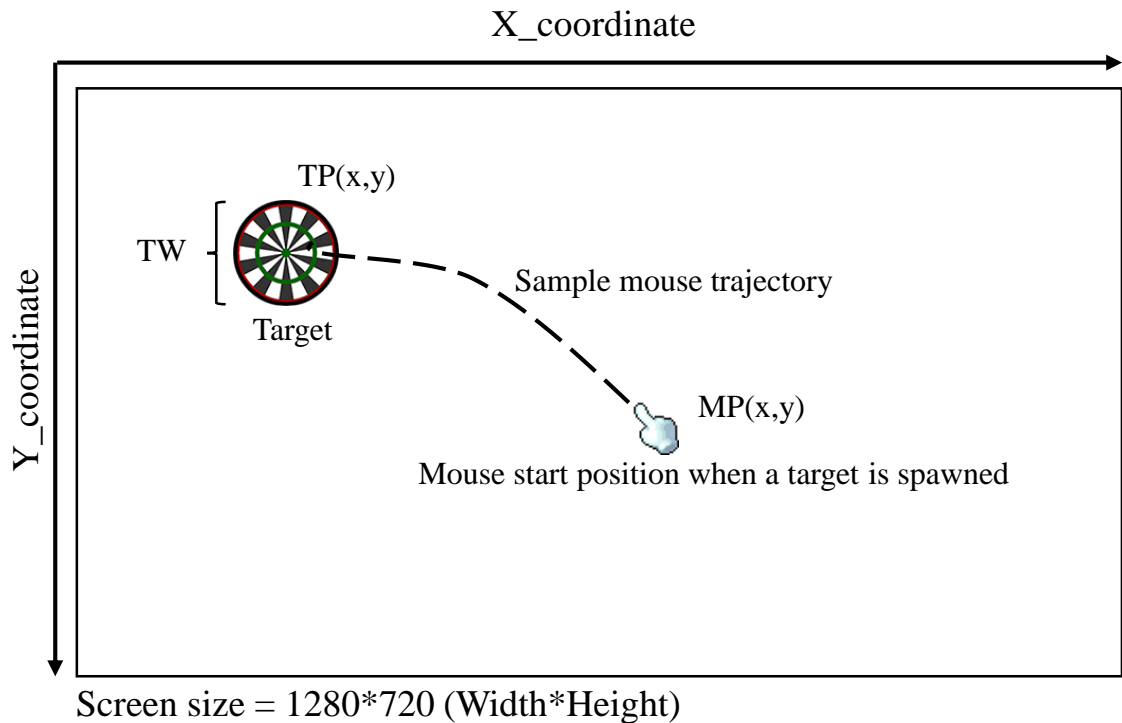
Figure 6.1 A design of target hitting task.

6.2.1 Task pattern

A set of delay spawn time, mouse cursor start position, and the target position is defined as a set of "task pattern" (TP) initialisation parameters. Fourteen task patterns and a set of initialisation parameters are pseudos pre-designed as shown in Table 6.1. According to Fitts index of difficulty (ID) which is defined by (2.5), each task pattern has a certain index of difficulty that is shown in the last column of Table 6.1. For simplicity, it can be noted that the target size is the same for all fourteen task patterns i.e. 100 pixels diameter.

Table 6.1 The pseudo pre-generated 'task pattern' with targets delay to spawn with its position, and mouse start position.

Task pattern number	Delay spawn time (Milliseconds)	Mouse position, MP		Target position, TP		Target diameter TW (pixels)	Target distance (pixels)	Fitts index of difficulty, ID (bits)
		x	y	x	y			
1	2108	640	360	320	180	100	367.15	2.88
2	1190	640	360	960	180	100	367.15	2.88
3	2174	640	360	960	540	100	367.15	2.88
4	1490	640	360	320	540	100	367.15	2.88
5	2014	640	360	640	620	100	260.00	2.38
6	2055	640	360	640	100	100	260.00	2.38
7	1634	640	360	100	360	100	540.00	3.43
8	1969	640	360	1180	360	100	540.00	3.43
9	1552	30	30	1180	620	100	1292.52	4.69
10	1508	30	690	1180	100	100	1292.52	4.69
11	2082	1250	690	100	100	100	1292.52	4.69
12	2349	1250	30	100	620	100	1292.52	4.69
13	1345	30	360	640	360	100	610.00	3.61
14	2627	1250	360	640	360	100	610.00	3.61

A list of task patterns on Table 6.1 is sequentially spawned one by one. For example, once the simulation is started. 2,108milliseconds are delayed before the first task pattern is spawned on the screen concurrently with the specified mouse cursor start position. The human participant moves the mouse to click on a target as fast and accurately as possible. The timeline in Figure 6.2 shows a sequence of fixation and spawn-reaction-click events of a task pattern. Reaction event is measured from the moment where a target is spawned to the first voluntary reaction of the participant to move the mouse. The duration of a task pattern is completed with a hit click on the target within the boundary *TW*. Then, the next queued task pattern is scheduled to be spawned by the delay / fixation time. A 'session' is completed when all of the 14 task patterns are spawned and clicked.

A timeline of task pattern with its delay fixation and events
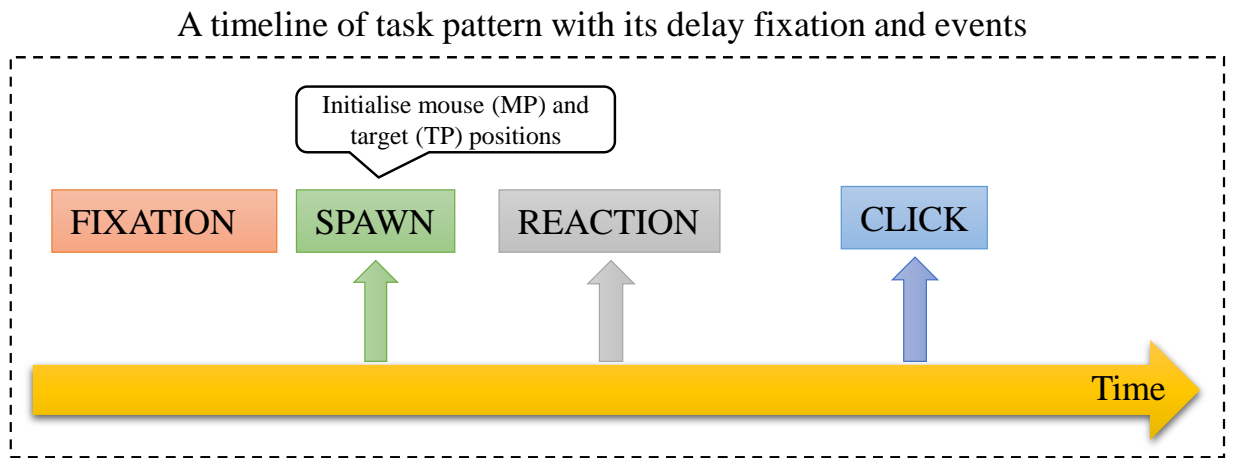
Figure 6.2 A timeline shows the sequence of task pattern fixation and events - spawn, reaction, and click.

6.3 EEG data acquisition and synchronisation

The Emotiv EPOC headset (Section 2.13.6) is used to record the EEG signals from scalp locations across a participant's head. It is noted that T7 and T8 are excluded from the context of this investigation since the main focus is in the frontal and posterior region of the human brain function. The frontal of the brain region is responsible for decision making, planning of movement etc. The posterior is functioned for visual processing. Therefore, the remaining 12 electrodes are AF3, AF4, F7, F8, F3, F4, FC5, FC6, P7, P8, O1, and O2 as shown in Figure 6.3.
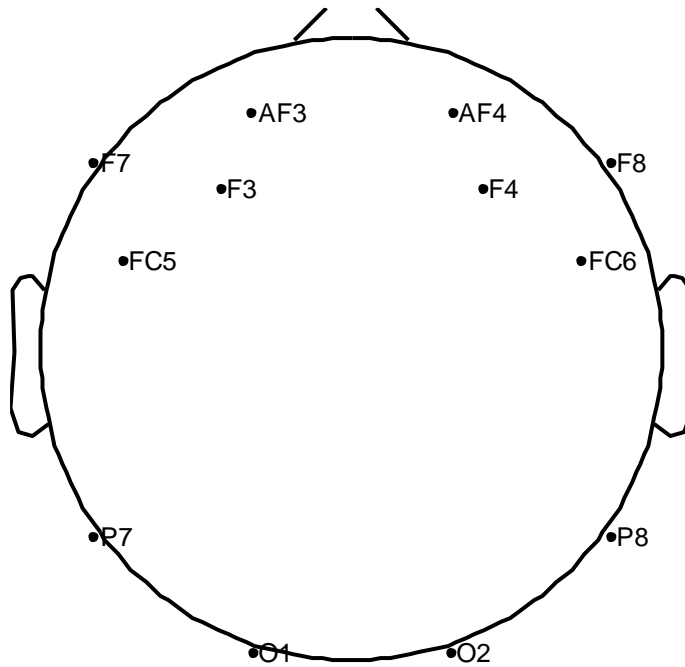
Figure 6.3 The 12 electrode locations focused in the THT investigation.

The EEG signals are recorded simultaneously with the simulation of the experiment described in Section 6.2. An event marker of spawn, reaction, and click is invoked to be inserted via the headset API to be used as the synchronisation points between the brainwave recording and the simulation system on a computer as shown in Figure 6.4. A simulation of the THT while having the headset turned on for EEG data acquisition simultaneously can be considered as having two systems running concurrently i.e. simulation on the computer and the headset. Thus, there is two timelines i.e. simulation timeline (ST) and headset timeline (HT). The simulation is directly interacted with a participant while collecting the task information such as a mouse cursor start position, a target spawn position, a mouse trajectory, a mouse click, and the three main task events – spawn, reaction, and click. The simulation time is kept track by the high precision clock on the computer while the headset has its clock for the acquisition of the 12 channels EEG signals.
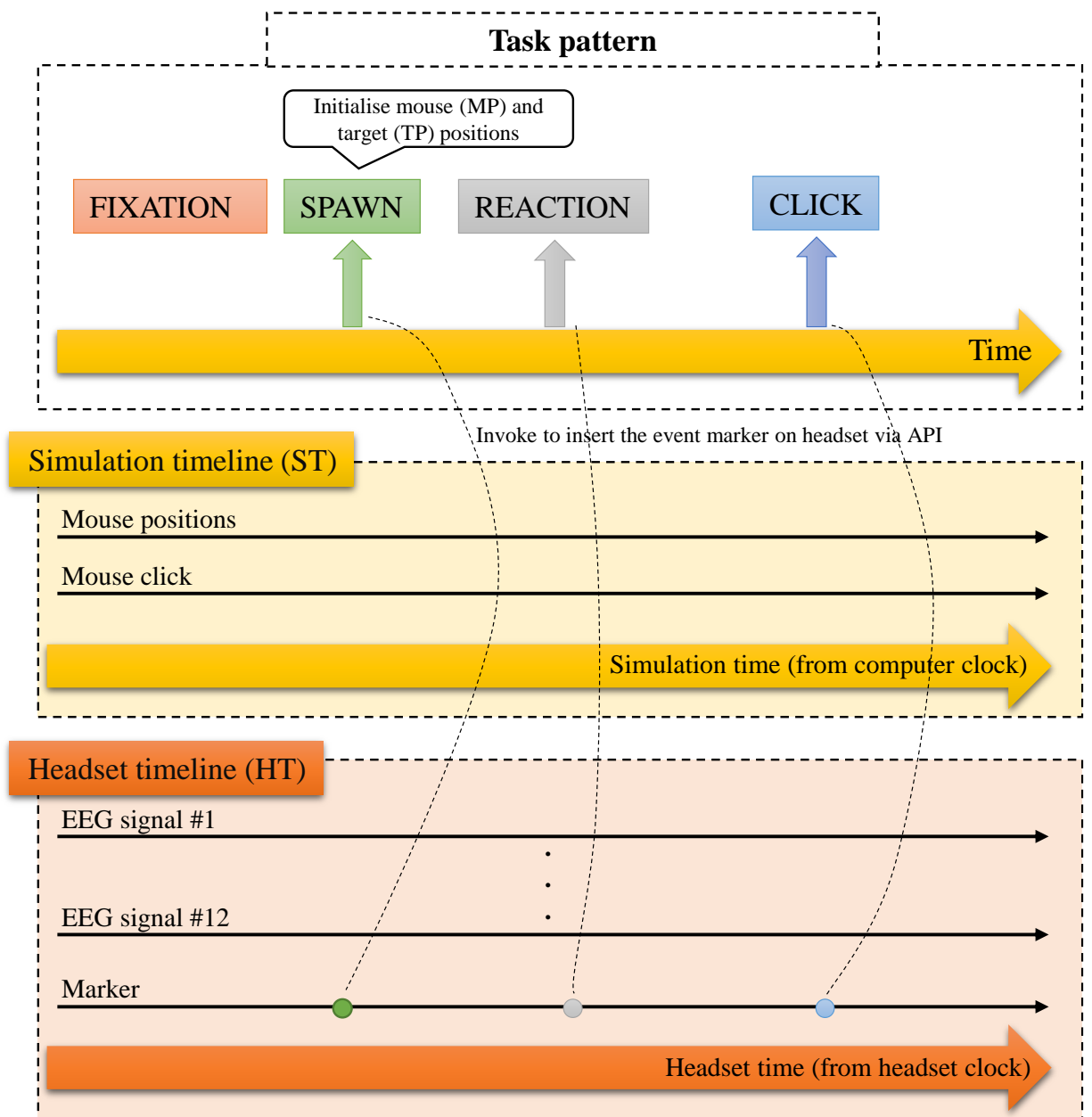
Figure 6.4 The task pattern events, simulation timeline (ST), and headset timeline (HT).

6.4 Experiment procedure

An experiment starts with a brief demonstration to perform the THT operation and the purpose of the experiment. A participant is instructed as follows.

- To perform the THT by moving the mouse to click on a spawned target as fast and accurate as possible.
- To react and move a mouse only when a target is spawned and ready on screen otherwise keep the mouse at stationary.
- To keep other body part movements and eye blinks at a minimum. However, a participant is informed and allowed to relax during the delay time since the main focus of the analysis is from the start of a target spawn, during the movement, and a click moment of task pattern.

Then, the following sequences of procedure are executed.

1. The 14 electrodes are moistened with saline solution as recommended by the manual. It is noted that T7 and T8 are recorded but are not used for the analysis.
2. The headset is placed on a participant scalp according to 10-20 international system and the headset instruction manual.
3. Each electrode is inspected individually to ensure that it is properly contacted with the participant's scalp.
4. The headset is switched on to start communication wirelessly with its accompanying USB data receiver.
5. A "TestBench" software which is provided by the headset manufacturer is launched to show the brainwaves in real-time.
6. The brainwaves are examined to ensure that the recording contains minimum unrelated brain activities.

Then, a "session" is started which contains 14 task patterns (Table 6.1). Each participant performs 15 sessions per "experiment". Each participant completes 3 experiments.

Furthermore, the following conditions are always met.

1. The same cursor pointing device is used for each participant which is a Logitech G600 with a sensitivity configured to 3100 dots per inch (DPI) and a report rate of 1000 Hz by default.
2. For each of the 'experiment', the headset is removed for relaxation for 10-15 minutes. Then, the process is repeated from the sequences above.

6.5 Task performance metrics

A number of aspects of the evaluation of the THT performance can be assessed including speed, accuracy, Fitts and Posner formulation etc.

6.5.1 Speed

An aspect of speed performance is obviously the evaluation based on time measurements. In this case of the design and implementation, the speed aspect is divided into two metrics i.e. reaction time (RT) and movement time (MT). Summation between the two is duration time (DT) of a task pattern measured from spawn to click.

6.5.2 Accuracy

An accuracy aspect of a task pattern can be assessed from two perspectives i.e. a mouse movement accuracy and a click on target accuracy.

6.5.2.1 <u>Movement accuracy</u>

The mouse movement accuracy can be explained by Figure 6.5 with an example of task pattern. A mouse cursor and a target are spawned at position PT_1 and PT_3, respectively. A mouse movement is captured by a discrete sampling time of the simulation e.g. a sampling frequency of 128 Hz means that the movement is captured 128 times in one second. An example of a single captured mouse position is shown as P_2 in Figure 6.5. It can be noted that the best movement trajectory is a straight line between the two position of the mouse start and the target centre. Therefore, a relative movement error can be calculated from the perpendicular distance deviated from the best movement trajectory.

Figure 6.5 The analysis diagram of target hitting task trajectory.

A detail of the calculation is described as follows. Vector SEG_A is a vector of segment PT_1 to PT_2. Vector SEG_B is a vector segment PT_1 to PT_3. Therefore, SEG_A and SEG_B can be formulated by (6.1) and (6.2).

$$SEG\_A = PT_2 - PT_1 \tag{6.1}$$

$$SEG\_B = PT_3 - PT_1 \tag{6.2}$$

Vector dot product between two vectors can be calculated algebraically and geometrically by (6.3) and (6.4), respectively. Therefore, the angle θ_1 can be calculated by (6.5).

$$SEG\_A.SEG\_B = \sum_{i=1}^{n} SEG\_A_i SEG\_B_i \tag{6.3}$$

$$SEG\_A.SEG\_B = |SEG\_A||SEG\_B| \cos \theta_1 \tag{6.4}$$

$$\theta_1 = \cos^{-1}\left(\frac{SEG\_A.SEG\_B}{|SEG\_A||SEG\_B|}\right) \tag{6.5}$$

Thus, a movement error for the case of Figure 6.5 can be calculated by (6.6)

$$An\ error\ at\ each\ point\ of\ discrete\ movement = |SEG\_A| \sin \theta_1 \tag{6.6}$$

All in all, the accumulate movement error for the entire task pattern duration can be calculated by (6.7).

$$Accumulate\ movement\ error = \sum_{k=1}^{n} |\boldsymbol{SEG\_A}|_k \sin\theta_k \qquad (6.7)$$

6.5.2.2 <u>Hit accuracy</u>

A hit accuracy can be calculated by (6.8).

$$Hit\ accuracy\ (\%) = \left(1 - \frac{|\boldsymbol{PT_4} - \boldsymbol{PT_3}|}{0.5TW}\right) * 100 \qquad (6.8)$$

6.5.3 Calculation of task performance

To summarise, the performance metrics for the THT can be categorised as shown in Table 6.2. The accuracy aspects are measured in pixel and percentage for the MA and HA, respectively. The aspects of speed are measured in a unit of time i.e. second.

Table 6.2 A summary of the performance metrics for the THT.

Aspect	Measurement	Unit of measurement	Performance indication direction
Speed	Reaction time (RT)	Second	lower is better
	Movement time (MT)	Second	lower is better
	Duration time (DT)	Second	lower is better
Accuracy	Movement accuracy (MA)	Pixel	lower is better
	Hitting accuracy (HA)	Percentage	higher is better
Rate of information processing	Index of performance (IP)	Bits/Seconds	higher is better

6.6 The establishment of EEG brainwaves and task performances

In order to establish a relationship between EEG brainwaves and task performances, a sequence of steps in Figure 6.10 are proceeded to develop a model. The aim is to create a model that can predict performance based on the EEG signals. Following the sequences in Figure 6.10, each step can be described as follows.

Step 1) The experiment sessions from all participants are fed into step 1.

Step 2) The independent component analysis (ICA) is applied to each session in order to extract the independent components (ICs) from the 12 channels of EEG. A measurement of EEG signal from a single electrode is considered as a resulted from multiple sources such as the brain related sources and the eyes related artefacts. The ICA tends to separate this combination into its independent source or component. As a result, the 12 ICs are obtained as shown in Figure 6.6.
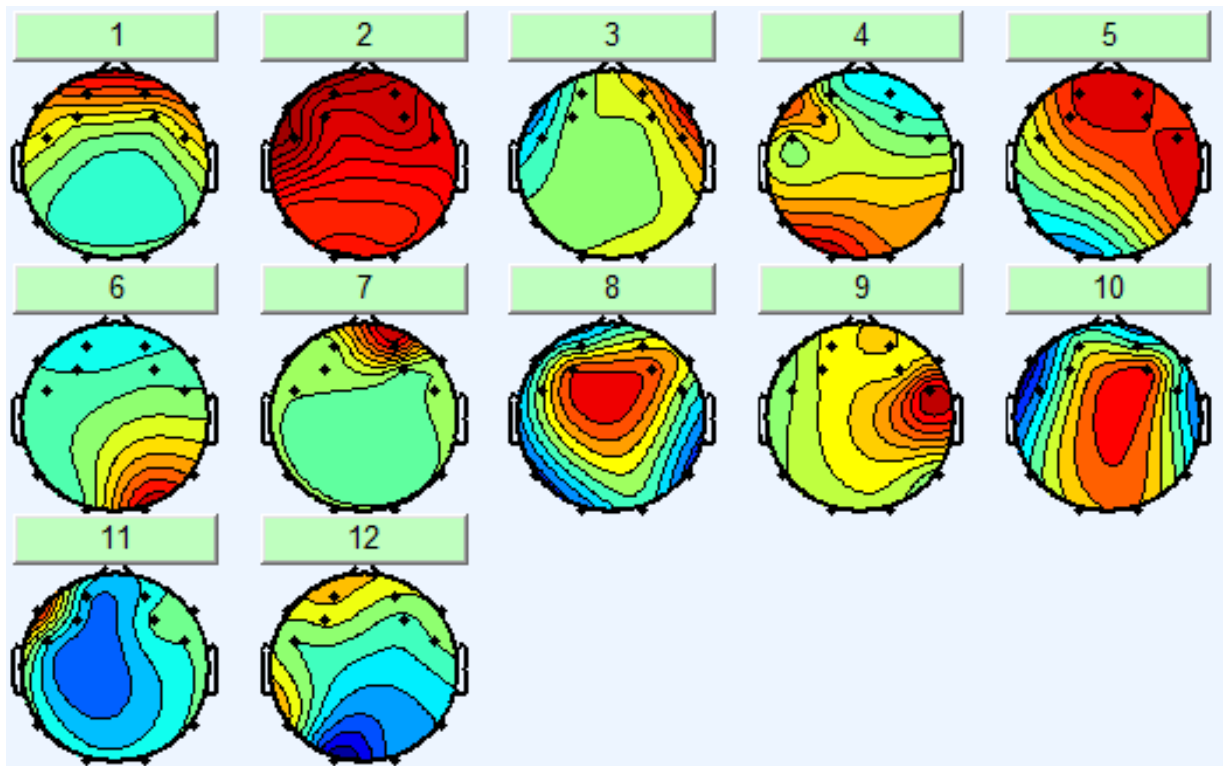
Figure 6.6 The example of 12 ICs from Participant 4 Experiment 3 Session 10 (P4E3S10).

Step 3) The 12 ICs are manually inspected in order to distinguish between brain related sources and artefacts related sources. Obviously, the eyes blink can be identified by a short spike of positive EEG amplitude as shown in Figure 6.7 while the eyes move can be identified by a short square wave of EEG amplitude either negative or positive as shown in Figure 6.8.
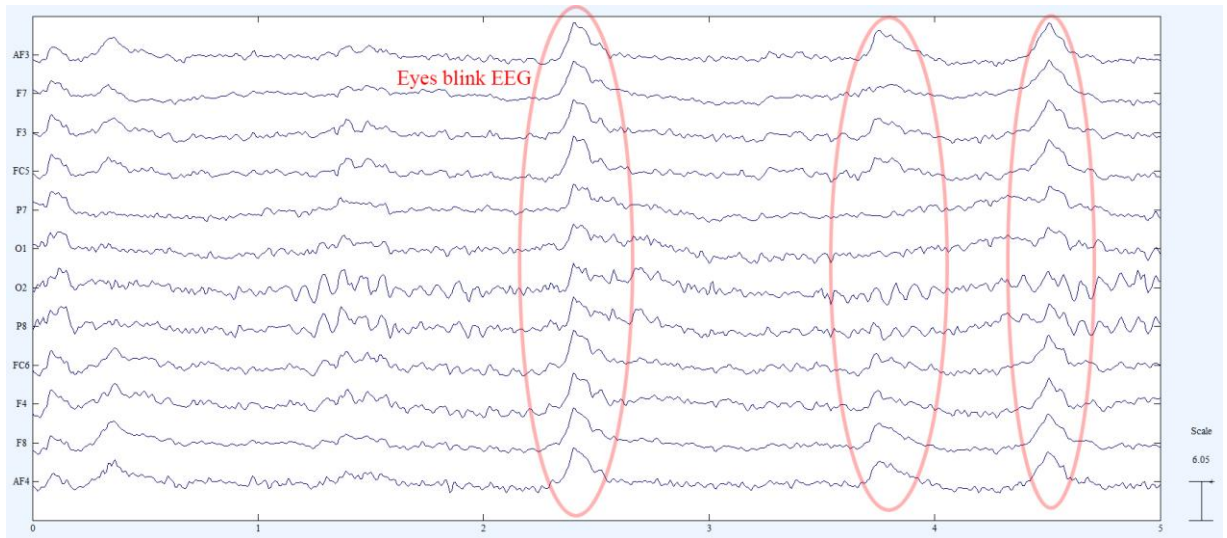
(a) The example of EEG brainwaves containing eyes blinks artefact.
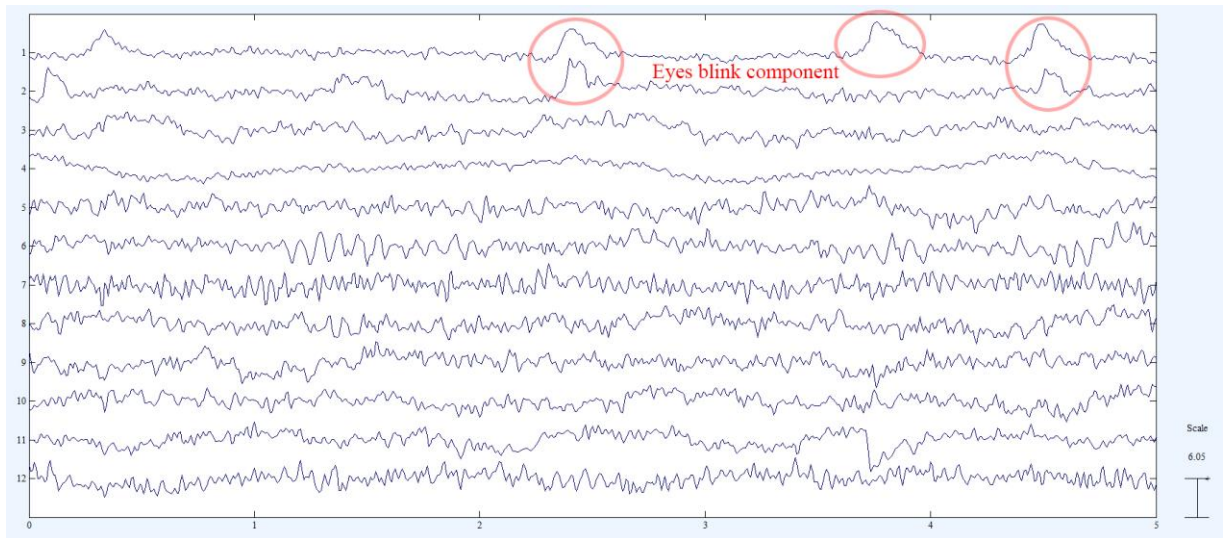
(b) The example of independent components containing eyes blinks artefact.

Figure 6.7 The example of the EEG brainwaves containing eyes blink artefact and the corresponding independent component analysis.
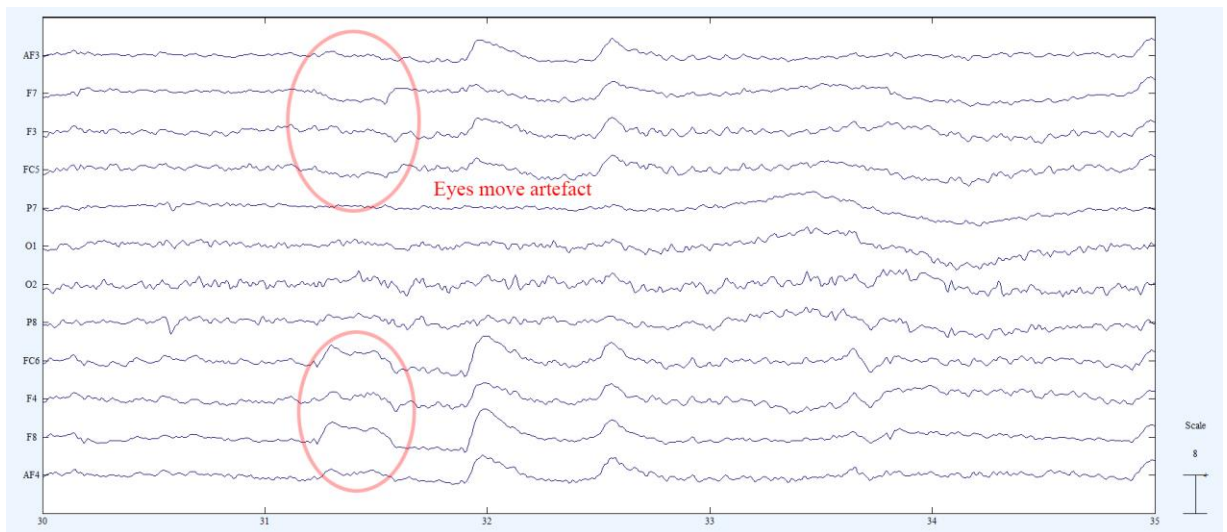
(a) The example of EEG brainwaves containing eyes moves artefact.
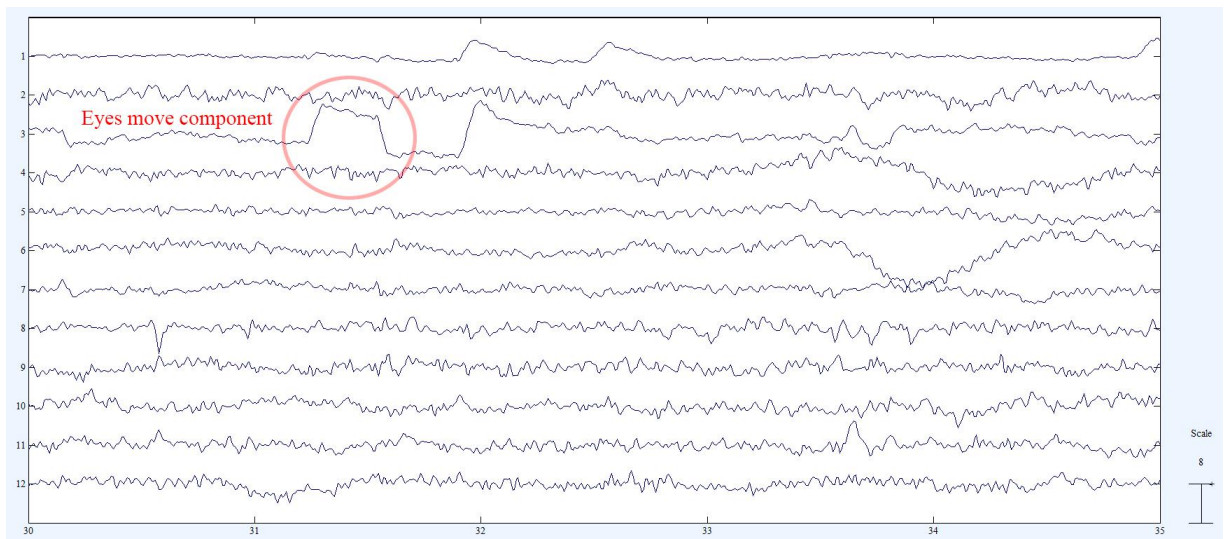
(b) The example of independent components containing eyes moves artefact.

Figure 6.8 The example of the EEG brainwaves containing eyes move artefact and the corresponding independent component analysis.

Additionally, details of the component properties as shown in Figure 6.9 can be used to identify the suspicious artefactual components. For example, Figure 6.9(a) shows an eyes blink component which is identifiable from the 2D topology scalp map where the intensity of red colour or positive spike is strong in the frontal part of the scalp map. Figure 6.9(b) shows eyes

move artefactual component where the 2D topology scalp map shows coloured blue and red on the opposite sides in the front of the scalp which is the characteristic of the eyes move artefact.
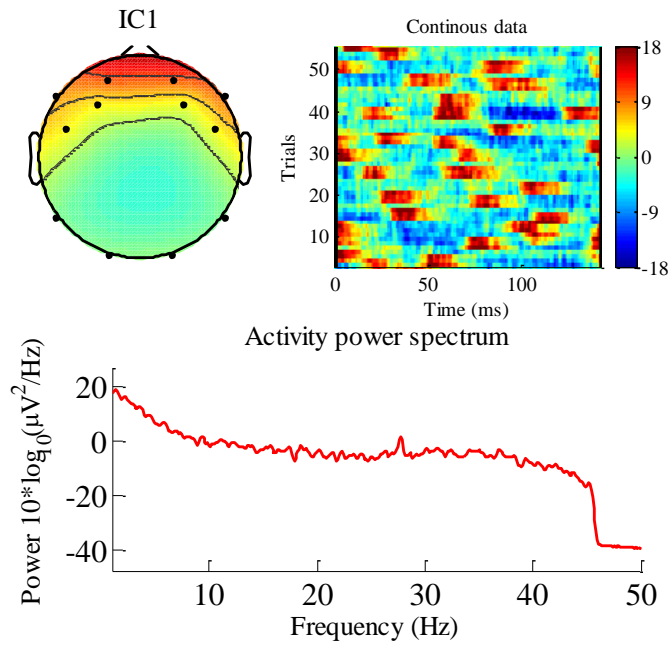
(a) The property of an independent component that contains suspicious eyes blinks artefact.
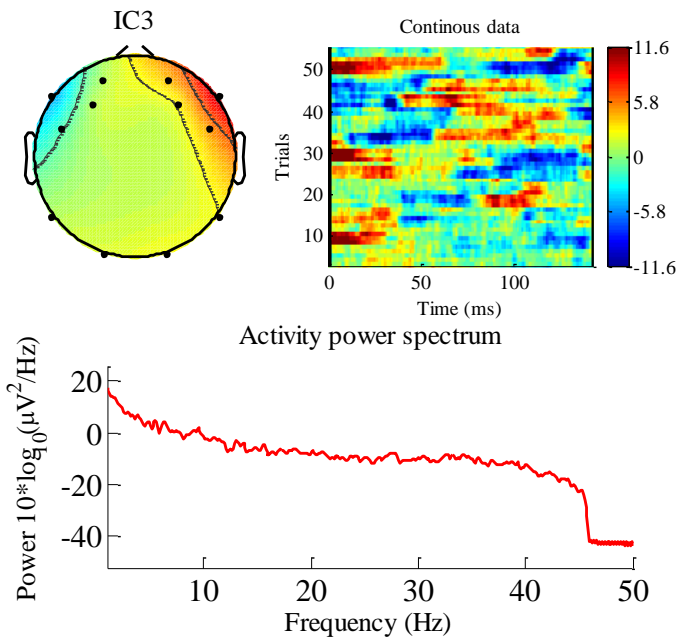
(b) The property of an independent component that contains suspicious eyes move artefact.

Figure 6.9 The examples of independent component property that contains eyes blink and eyes move artefacts.

Step 4) Once the suspicious artefactual components are identified, they are used to prune the original EEG in order to obtain the artefact-free EEG.

Step 5) The artefacts-free continuous EEG is extracted according to a task pattern boundary with the extension of 1000ms latency times around the boundary. It is because of brainwaves react to a stimulus both before and after the onset time of the presentation of the stimulus; therefore, the extension is done for this reason.

Step 6) So far, the EEG brainwaves contain the signals of the frequency range between $1 - 45$ Hz. Since the study in this context concerns about the performance of an operation which is performed during wake up state with hand movement on a computer mouse, the frequency range of interest is within the alpha rhythm especially Mu and sensorimotor rhythm (SMR). Hence, the EEG signals are band-pass filtered with 7-16 Hz using EEGLAB filtering function.

Step 7) A task pattern which contains the corresponding EEG exceeded the extreme values of the amplitude of interest is automatically excluded. The algorithm is simply a loop through all of the task patterns and detects its corresponding EEG in every channel whether the signal contains a sampling amplitude exceed a specified range e.g. -20 to 20 μV.

Step 8) The remaining task patterns are proceeded with the analysis of event-related potential (ERP) at the spawn-reaction events, and click event.

Step 9) The remaining task patterns from step 7 are used to develop a model of EEG brainwaves in association with task performance indicators.

Step 10) The remaining task patterns from step 7 are analysed with ERP method at spawn-reaction event, and click event. The information obtained from this analysis is used by EEG feature extraction in step 14.

Step 11) The task patterns are separated into two groups i.e. low and high according to the specified performance criteria / indicator. The separation point is at the median value of the criteria. Then, it is further separated into 6 sections as shown in Figure 6.10 i.e. A, B, C, D, E, and F. Sections B and E are used for training of the model. The remaining sections in each group are reserved for a blind test.

Step 12) Two group of task pattern are attained.

Step 13) The signals from frontal and posterior electrodes are averaged, respectively.

Step 14) The averaged frontal and posterior are feature extracted using the information from

      a. Local extremum information

b. Fourier transform information

c. Information from ERP analysis in step 10

Step 15) Principal component analysis (PCA) is applied in order to transform the features into an equal number of principal components as the number of features. However, variance among the principal components is maximised. Therefore, the transformed features into principal components are good to be used for training.

Step 16) The principal components are ordered from high to low important components. In other words, only a number of first few principal components can represent over 90% of the entire number of features. Therefore, the dimension of the original feature space can be reduced by selecting first few principal components.

Step 17) The selected principal components are used to develop an ANN model by training with the 10-time-10-fold cross validation method presented in Section 3.4.

Step 18) The procedure is repeated from the connector C for all of six performance indicators i.e. RT, MT, DT, MA, HA, and IP.

P1   P2   …   Pn
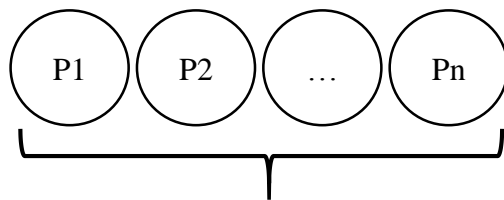
1) Experiment sessions

12 channels continuous EEG signals which are contaminated with artefacts such as eyes blink and eyes move.

2) Independent component analysis (ICA)

ICA is applied to the 12 channels EEG to extract the independent components (ICs) which linearly combined within the EEG.
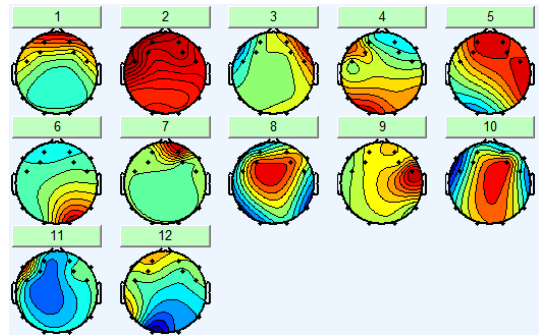
2D scalp topology maps of the 12 ICs

3) Manually inspect the ICs to identify eyes blink / move components (one session at a time)

AF3
F7
F3
FC5
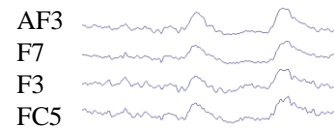
An example of eyes blink EEG for 2 times which can be noticed from frontal electrodes such as AF3, F7, F3, FC5 etc.

FC6
F4
F8
AF4

An example of eyes move which can be noticed from the end of the cut section of EEG as shown above.

Both eyes blink and eyes move can be identified by a specific 2D scalp maps of the extracted ICs as shown below.

Eyes blink   Eyes move
component (IC 1)   component (IC3)

A

A

4) Prune with the suspected artefactual ICs

After the artifactual ICs are identified. The original EEG is pruned with the suspected ICs. An example of the eyes blink removal is shown below. The blue line is the EEG before removal and the red line is the after.

Then, eyes blink and eyes move artefacts-free continuous EEG is obtained.

5) Extract continuous EEG according to a task pattern boundary minus/plus 1000ms

An example of a task pattern

1000ms   This time course is vary   1000ms
according to duration time of
each task pattern performance.

The continuous EEG is extracted into a section of EEG according to a task pattern boundary minus/plus 1000ms.

It is noted that there are task performance metrics associated with the task pattern boundary e.g. RT, MT, DT, MA, HA, IP.

6) Apply band pass filter to the extracted EEG for the range of Mu and SMR rhythm (7-16 Hz)

Apply band pass filter in order to analyse EEG in a specific band of interest i.e. alpha band in the range of Mu and SMR rhythm using EEGLAB filtering function

RT: Reaction time, MT: Movement time, DT: Duration time, MA: Movement accuracy, HA: Hit accuracy, IP: Fitts index of performance, SMR: Sensorimotor rhythm

B

```
  ( B )
    |
    v
┌─────────────────────────────────┐         Epochs which contain electrodes amplitude
│ 7) Extreme epochs are excluded  │─ ─ ─     greater or lower than the specified threshold are
└─────────────────────────────────┘         excluded.
    |         \
    |          \
    v           v
┌ ─ ─ ─ ─ ─ ─ ┐   ┌ ─ ─ ─ ─ ─ ─ ─ ─ ─ ─ ─ ─ ─ ─ ─ ─ ─ ─ ┐
  8) Event         9) Development of model of the human
  related          EEG brainwaves in association with task
  potential        performances
  (ERP) analysis
└ ─ ─ ─ ─ ─ ─ ┘   └ ─ ─ ─ ─ ─ ─ ─ ─ ─ ─ ─ ─ ─ ─ ─ ─ ─ ─ ┘
    |                                   |
    |                                   v
    |                                 ( C )
    v
┌ ─ ─ ─ ─ ─ ─ ─ ─ ─ ─ ─ ─ ┐          An analysis of event related potential (ERP) at
  10) ERP analysis at events           the events within a task pattern boundary. The
  ┌─────────────────────┐              ERP provides information for feature extraction
  │ a) SPAWN and        │              of EEG waves.
  │ REACTION ERP        │
  └─────────────────────┘
  ┌─────────────────────┐
  │ b) CLICK ERP        │
  └─────────────────────┘
└ ─ ─ ─ ─ ─ ─ ─ ─ ─ ─ ─ ─ ┘
```

C

11) Separation of task patterns and the corresponding EEG into high and low groups by a specified performance criteria / indicator

12a) High group

12b) Low group

13) Average frontal / posterior group of EEG

D

Performance criteria variable

Values

Median

5%

A

B
40%

C
5%

D
5%

E
40%

F
5%

Low group

High group

Task pattern ID

All of the remaining task patterns are sorted according to a specified performance criteria as shown in the above figure. They are separated into 6 sections A, B, C, D, E, and F. Sections B and E are used for training an ANN model while A, C, D, and F are reserved for blind test.

There are 12 channels of EEG for the corresponding task pattern boundary. Eight and four of them accounted for frontal and posterior areas, respectively. It is obvious that a single-trial EEG i.e. a single task pattern barely show identifiable pattern of response. Therefore, an averaging method of the ERP analysis is applied to the frontal and posterior areas as shown below.

Frontal Average

•AF3 •AF4

•F3 •F4 •F8

•FC5 •FC6

•T7 •T8

•P7 •P8

•O1 •O2

Posterior Average

D

14) EEG feature extraction

   14a) Local maximum / minimum information

   14b) Fourier transform information

   14c) Information from ERP analysis

Power

Frequency

Amplitude | Spawn | Click

Time

Frontal

Amplitude | Spawn | Click

Time

Posterior

15) Principal component analysis (PCA)

Transformation of features into a principal component space where the variances among components are maximised.

16) Select first few principal components which covered for most of the feature dataset representation

Reduce the dimensionality of the features into a number of principal components which is sufficient to represent the original feature space.

17) Develop an ANN model with the selected principal components by training with the 10-time-10-fold cross validation

18) Repeat from connector C for 6 performance indicators - DT, RT, MT, HA, MA, IP

D

Figure 6.10 A workflow for the establishment of a relationship of the EEG brainwaves and the task performances.

As a result of the procedure in Figure 6.10, there are six ANN models developed according to each of the performance indicators as shown in Figure 6.11. The six models take the transformed features of EEG brainwaves and evaluate performance into low and high for each of the model output.

The six artificial neural network models for performance evaluation from EEG brainwaves

EEG brainwaves

Features

RT   MT   DT   MA   HA   IP

The internal of 6 ANN models of performance predictor
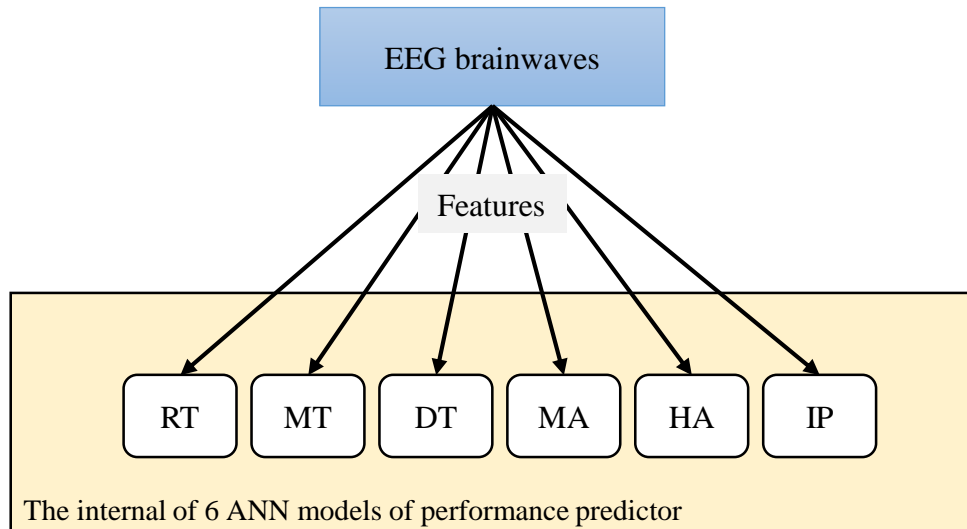
Predict performance in each aspect into low or high

RT (low/high)   MT (low/high)

MA (low/high)   DT (low/high)

HA (low/high)   IP (low/high)
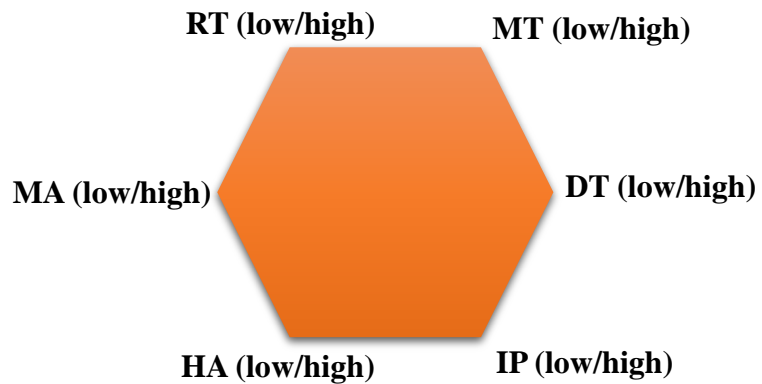
Figure 6.11 The six ANN models for performance prediction from EEG brainwaves.

6.7 Results

6.7.1 Participants and the experiment

There are 4 participants in this investigation. The participants agree to conduct the experiment by signing the consent form as shown in the Appendix B. Each of the participants completes 3 experiments, 15 sessions and 14 task patterns in each session as shown in Figure 6.12. As a result, a total of 180 sessions and 2,520 task patterns are obtained. The attribute of each participant is shown in Table 6.3. Three of the participants are male, one of them is female. Their ages are in the range of 30-35 years. One of them has left-handedness; however, the participant prefers to use right hand to perform the task.
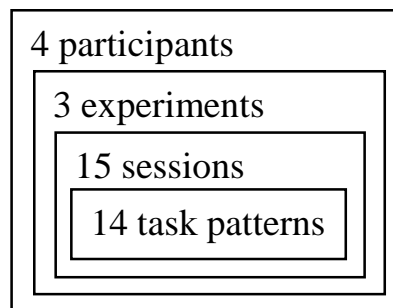
Figure 6.12 The layered blocks showing the number of participants, experiments, sessions, and task patterns.

Table 6.3 The attribute of the participants.

Participant ID	Gender	Age	Handedness	Hand used to perform an action
P1	Male	30-35	Right	Right
P2	Male	30-35	Right	Right
P3	Male	30-35	Left	Right
P4	Female	30-35	Right	Right

The setup time for each "experiment" according to the experiment procedure as explained in Section 6.4 is approximately 15 minutes including the preparation of the electrodes and the installation of the headset on the participant scalp. According to Table 6.1, a total amount of fixation time in a session excluding a participant's action time is 26.09 seconds. Thus, it is 6.52 minutes for 15 sessions provided that the experiment is performed continuously. At the end of each experiment, the headset is removed and the preparation for the next experiment starts. Therefore, an approximate total experiment time for each participant is 64.56 minutes.

6.7.1.1 <u>Naming notation</u>

To identify a specific participant, experiment, session and task pattern, a hierarchical naming notation is defined which is shown in Figure 6.13. For example, P3E2S5T2 means participant 1, experiment 2, session 5, and task pattern 1.

P#E#S#T#

Participant ID   Experiment ID   Session ID   Task pattern ID
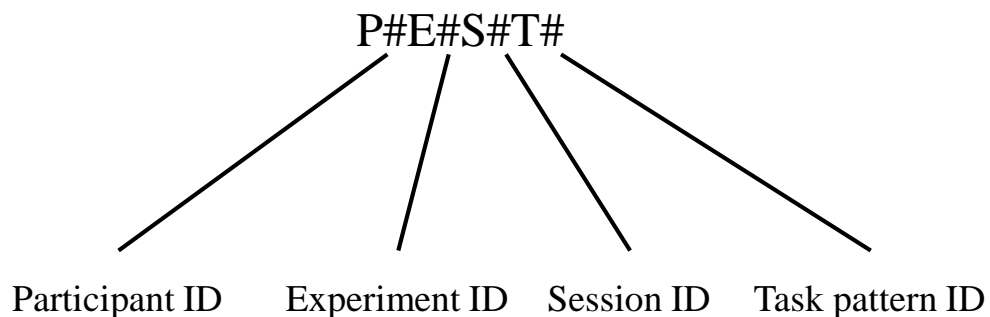
Figure 6.13 The naming notation for the identification of a participant, experiment, session, and task pattern.

6.7.2 Time synchronisation

It is important to have time synchronisation between the simulation platform and the EEG data acquisition device to ensure the validity of the timing of the human-machine operation and the brainwaves. It is mentioned in Section 6.3 that there is a marker invoked to be inserted as the synchronisation points. Although a perfect synchronisation between the simulation platform and the EEG headset system is preferable, practically, slight time drifts between the two systems do exist which can be depicted in Figure 6.14.
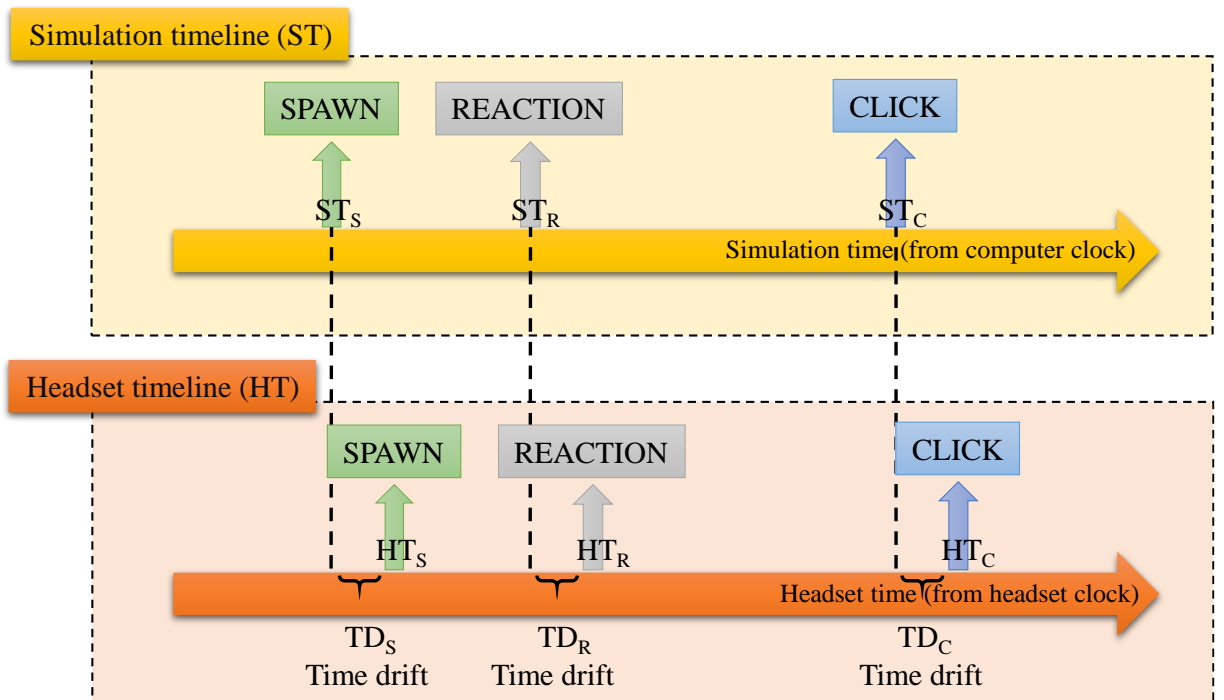
Figure 6.14 The timelines between the simulation and the Emotiv headset showing events and the time drifts.

Figure 6.14 shows the simulation timeline (ST) and headset timeline (HT) and the three main events of a task pattern. A target is spawned at time point ST_S as shown on the simulation timeline. The simulation system records a "SPAWN" event. The "REACTION" and "CLICK" events are recorded thereafter when a participant react to move and click on the target. The Emotiv EPOC API has the capability to insert an event marker for the synchronisation purpose. With an ideal condition, the appearance of the triggered marker should be fully synchronised with the simulation timeline. Unfortunately, in a practical situation, the markers appear on the headset timeline with slight time difference at HT_S, HT_R, and HT_C. The time differences are denoted as time drifts between the two systems as TD_S, TD_R, and TD_C as shown in Figure 6.14.

As an example, event timing information from the 14 task patterns from P4E3S1 is calculated as shown in Table 6.4. The table shows the corresponding time points of each of the 14 task patterns within a session. For example, the first task pattern, a target is spawned and marked as 'SPAWN' at 7.258 seconds on the simulation timeline and is also triggered to be marked on the headset timeline at the same time. However, the 'SPAWN' event marker is marked on the headset timeline at 7.225 seconds on the headset clock which is slightly early with 0.033 seconds

window of difference. With the second task pattern, a target is marked as 'SPAWN' at 11.518 seconds on the simulation timeline while it is marked on the headset timeline at 11.519 seconds which is 0.001 seconds of delay.

Time drifts information TD_S, TD_R, TD_C for all of the 14 task patterns from P4E3S1 are shown on the right side of the table. The average of time drift at spawn, reaction, and click events are 0.0174, 0.0161, 0.0166 seconds with 0.0102, 0.0113, 0.0093 deviations, respectively. Both simulation and the headset are set to sample at the same rate at 128 Hz. It is 0.0078125 seconds between two adjacent sampling windows. Therefore, the average time drift at spawn, reaction, click events are as large as 2.2272, 2.0608, and 2.1248 times compared to the sampling rate.

A solution is needed to solve the problem of time drifts between the two systems. A computer for the THT simulation is more powerful and has a higher precision clock than the headset. Also, the experiment is based on the THT simulation on a computer. The headset is an additional piece of equipment to acquire brainwave signals in relation to the task operation on the simulation on a computer. It is reasonable to use the time information of the events base from the simulation timeline and find the closest time on the headset timeline for the corresponding events. This solution of time adjustment to be based on the simulation timeline replaces the unreliable method of marker insertion via the API.

Table 6.4 The time drifts between headset and simulation from P4E3S1 before the adjustment.

| Task Pattern No. | Headset | | | Simulation | | | Time drift between simulation – headset BEFORE adjustment | | |
| | Event time (nth Second) | | | Event time (nth Second) | | | Time (Second) | | |
	HT$_S$	HT$_R$	HT$_C$	ST$_S$	ST$_R$	ST$_C$	TD$_S$	TD$_R$	TD$_C$
1	7.225	7.569	8.445	7.258	7.600	8.450	0.033	0.031	0.005
2	11.519	11.511	12.606	11.518	11.538	12.614	-0.001	0.027	0.008
3	14.763	15.107	15.827	14.771	15.109	15.847	0.008	0.002	0.020
4	18.954	19.330	20.143	18.975	19.334	20.147	0.021	0.004	0.004
5	22.583	22.927	23.615	22.601	22.959	23.634	0.018	0.032	0.019
6	26.586	26.868	27.556	26.606	26.875	27.564	0.020	0.007	0.008
7	30.559	30.778	31.716	30.576	30.803	31.720	0.017	0.025	0.004
8	34.313	34.563	35.501	34.319	34.567	35.532	0.006	0.004	0.031
9	38.441	38.817	40.067	38.461	38.820	40.088	0.020	0.003	0.021
10	42.601	42.945	44.165	42.604	42.970	44.192	0.003	0.025	0.027
11	46.636	46.855	47.794	46.666	46.879	47.818	0.030	0.024	0.024
12	50.827	51.171	52.203	50.857	51.187	52.229	0.030	0.016	0.026
13	55.519	55.831	56.519	55.531	55.834	56.544	0.012	0.003	0.025
14	58.834	59.210	59.898	58.860	59.232	59.908	0.026	0.022	0.010
				Average			0.0174	0.0161	0.0166
				Standard deviation			0.0102	0.0113	0.0093

Table 6.5 shows the events timing information from Table 6.4 after adjustment of event timing points to be based on the simulation timeline. As an example, the first task pattern, a target is spawned at 7.258 seconds on the simulation timeline. The closest time point on the headset is at 7.264 seconds which is 0.006 seconds of delay. Event timing of the second task pattern remains the same as before the adjustment. The average event time drift of all the 14 task patterns is 0.0033, 0.0034, and 0.0041 seconds of delay for spawn, reaction, and click events, respectively. They are only 0.4224, 0.4352, 0.5248 times compared to the sampling rate. Figure 6.16, Figure 6.17 show a graph of time drifts before and after adjustment for the 14 task patterns for spawn, reaction, and click events, respectively. The graphs clearly show the significant improvement of time synchronisation between the simulation timeline and the headset timeline.

Table 6.5 The time drifts between headset and simulation from P4E3S1 after the adjustment.

Task Pattern No.	Headset (adjusted time point)			Simulation			Time drift between simulation - headset AFTER adjustment		
	Event time (n^{th} Second)			Event time (n^{th} Second)			Time (Second)		
	HT_S	HT_R	HT_C	ST_S	ST_R	ST_C	TD_S	TD_R	TD_C
1	7.264	7.601	8.452	7.258	7.600	8.450	-0.006	-0.001	-0.002
2	11.519	11.542	12.614	11.518	11.538	12.614	-0.001	-0.004	0.000
3	14.771	15.115	15.85	14.771	15.109	15.847	0.000	-0.006	-0.003
4	18.978	19.338	20.151	18.975	19.334	20.147	-0.003	-0.004	-0.004
5	22.606	22.966	23.639	22.601	22.959	23.634	-0.005	-0.007	-0.005
6	26.61	26.875	27.564	26.606	26.875	27.564	-0.004	0.000	0.000
7	30.582	30.809	31.724	30.576	30.803	31.720	-0.006	-0.006	-0.004
8	34.321	34.571	35.54	34.319	34.567	35.532	-0.002	-0.004	-0.008
9	38.465	38.824	40.091	38.461	38.820	40.088	-0.004	-0.004	-0.003
10	42.609	42.976	44.196	42.604	42.970	44.192	-0.005	-0.006	-0.004
11	46.667	46.879	47.825	46.666	46.879	47.818	-0.001	0.000	-0.007
12	50.858	51.187	52.235	50.857	51.187	52.229	-0.001	0.000	-0.006
13	55.535	55.839	56.551	55.531	55.834	56.544	-0.004	-0.005	-0.007
14	58.865	59.233	59.913	58.860	59.232	59.908	-0.005	-0.001	-0.005
Average							-0.0033	-0.0034	-0.0041
Standard deviation							0.0018	0.0024	0.0023

Time drifts at SPAWN event
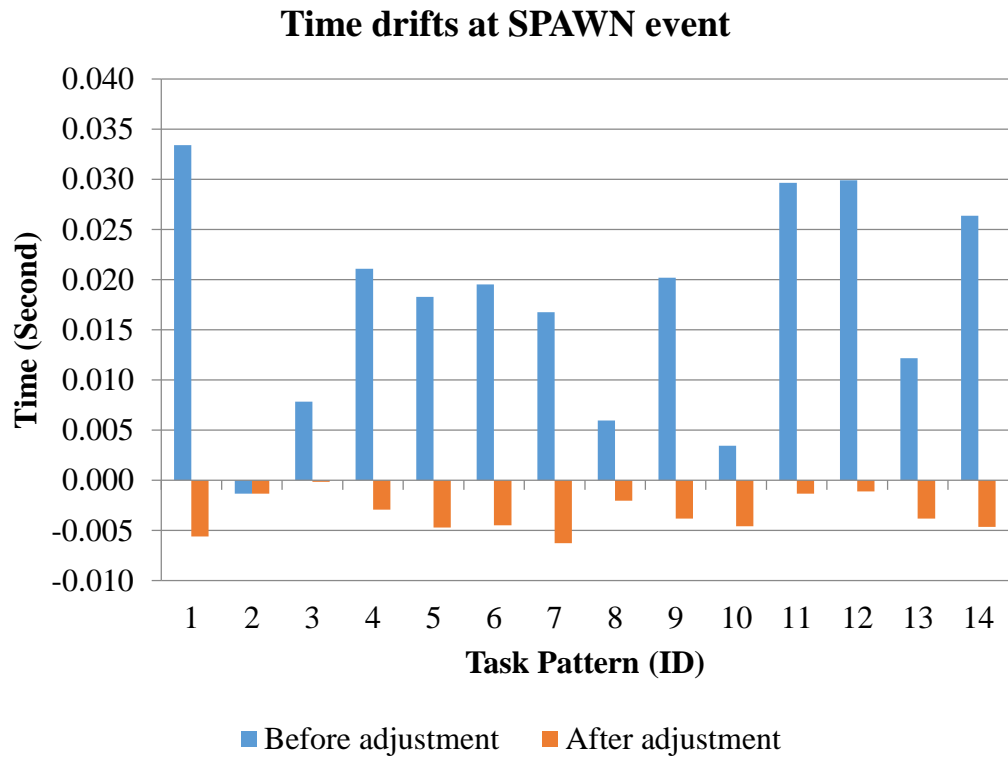
Figure 6.15 The time drifts at the SPAWN event before / after the adjustments from P4E3S1.

Time drifts at REACTION event
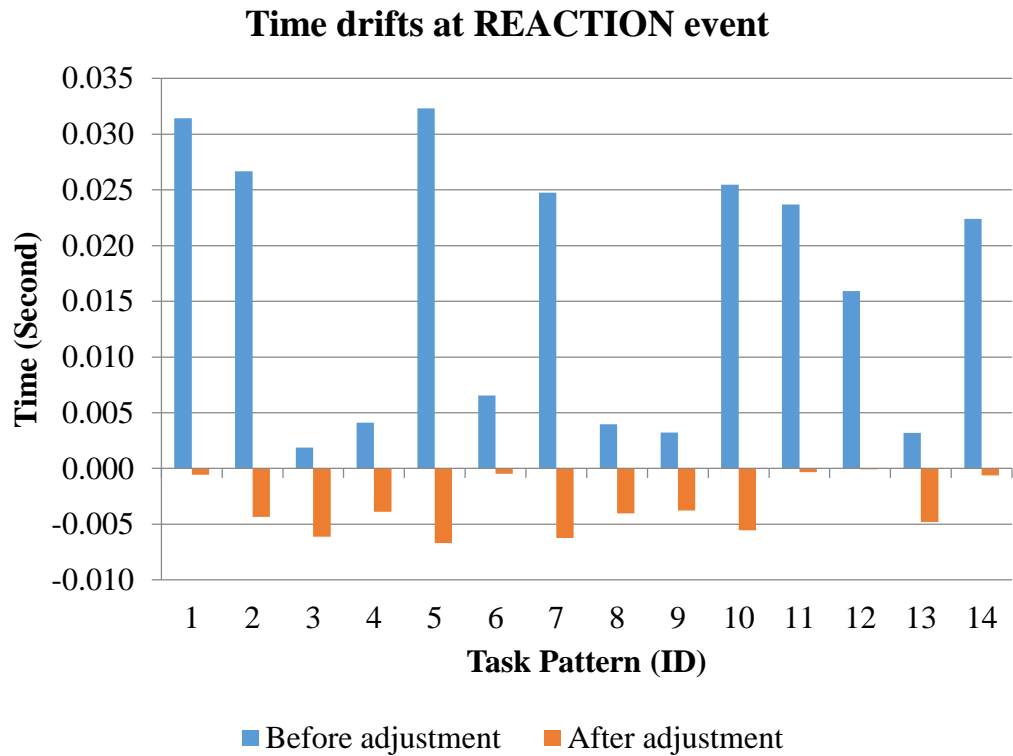
Figure 6.16 The time drifts at the REACTION event before / after the adjustments from P4E3S1.
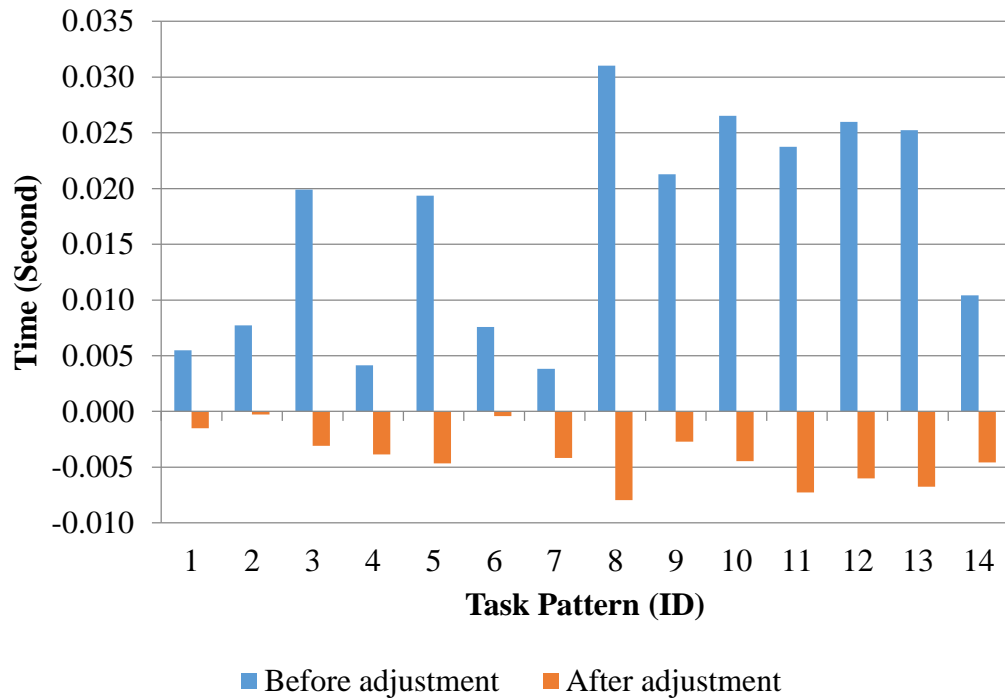
Figure 6.17 The time drifts at the CLICK event before / after the adjustments from P4E3S1.

Previously, the problem of time synchronisation and the solution to the time drift has demonstrated from a single session i.e. P4E3S1. Figure 6.18 (a) shows the averaged time drift from all of the 15 sessions in experiment 1 from participant 1 before adjustment. Figure 6.18 (b) shows the averaged time drift after adjustment. It can be noted that before adjustment all 15 sessions show averaged time drift with early marked time of the event on the headset. After adjustment, the time drifts on the headset are properly marked slightly after the simulation timeline with the very minimum amount of drift time compared to the before adjustment. Figure 6.19, Figure 6.20, and Figure 6.21 show sessions averaged time drift before / after adjustment from the first experiment of each participant.
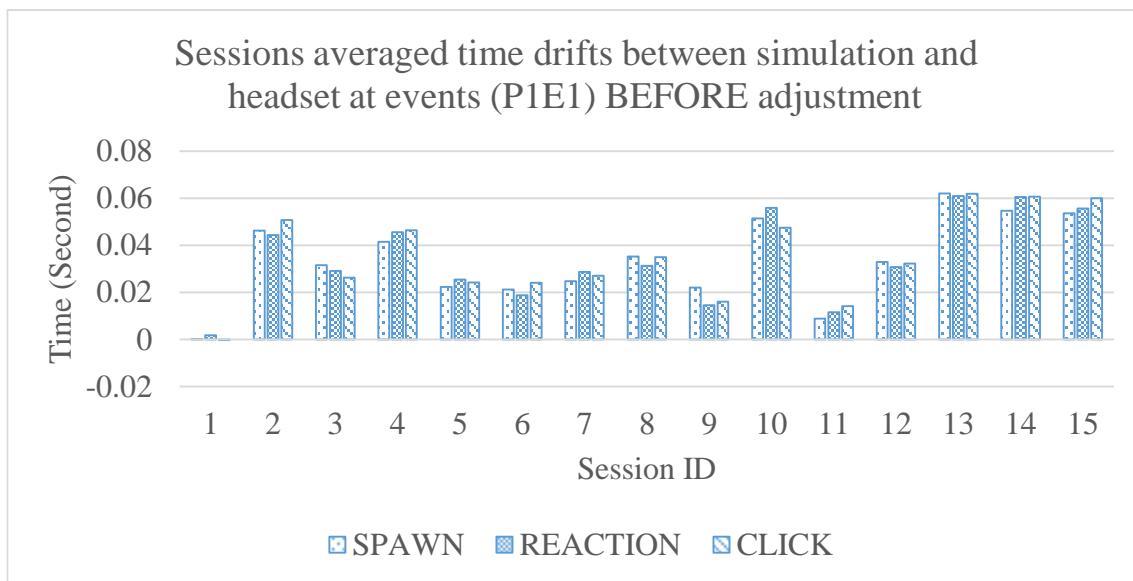
(a) Before adjustment.
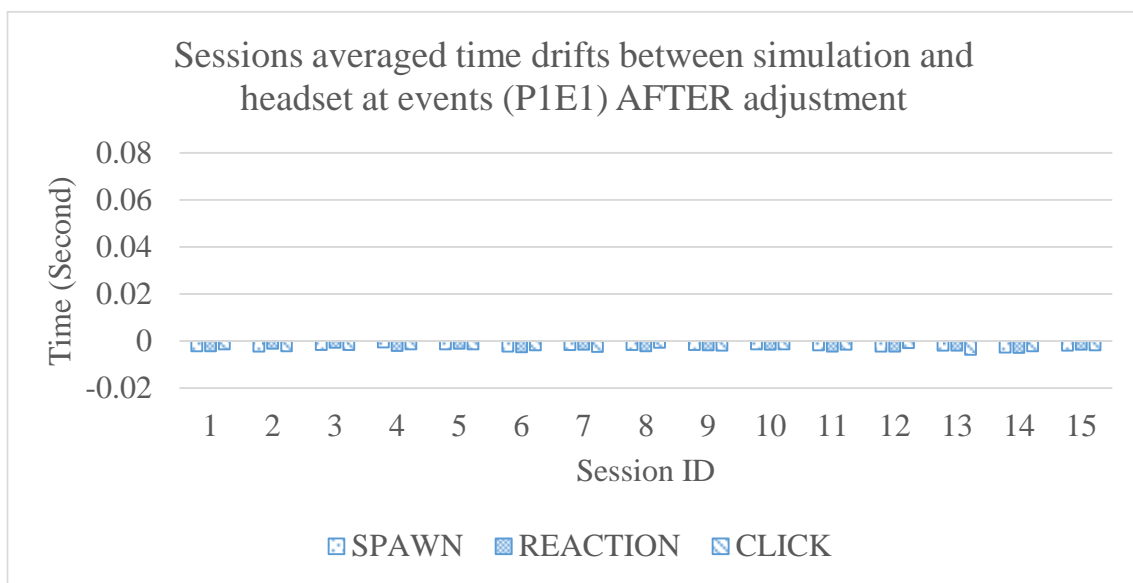
(b) After adjustment.

Figure 6.18 The sessions averaged time drifts between the simulation and the headset timelines from P1E1.
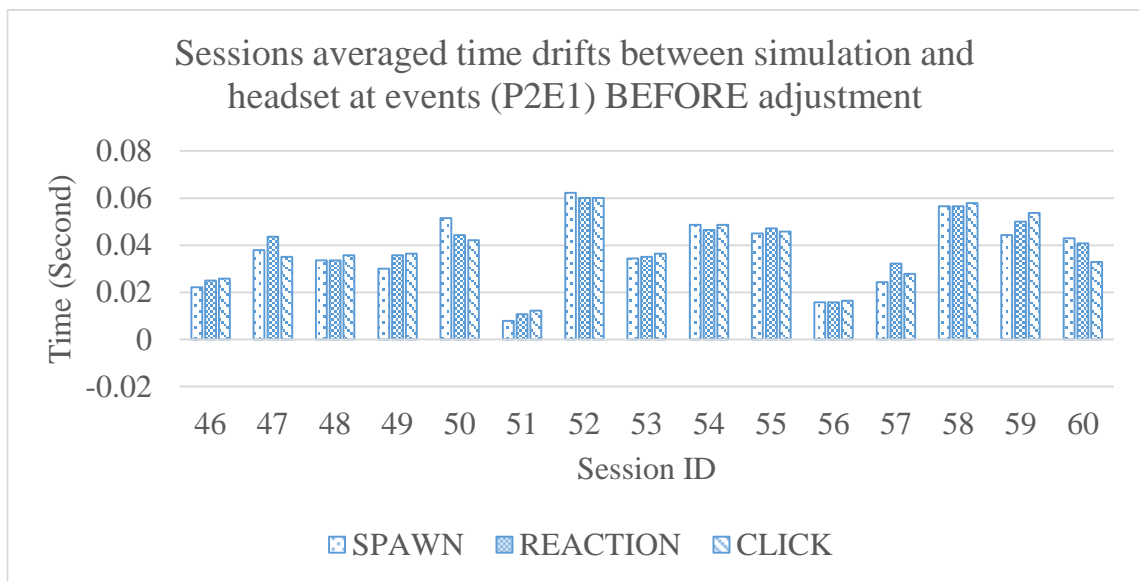
(a) Before adjustment.
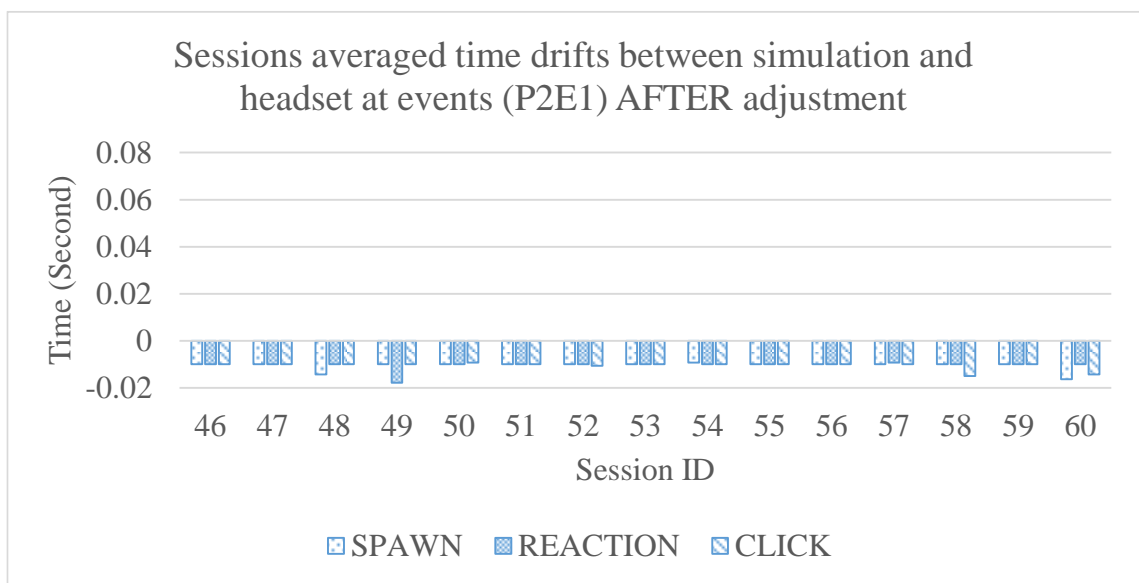
(b) After adjustment.

Figure 6.19 The sessions averaged time drifts between the simulation and the headset timelines from P2E1.
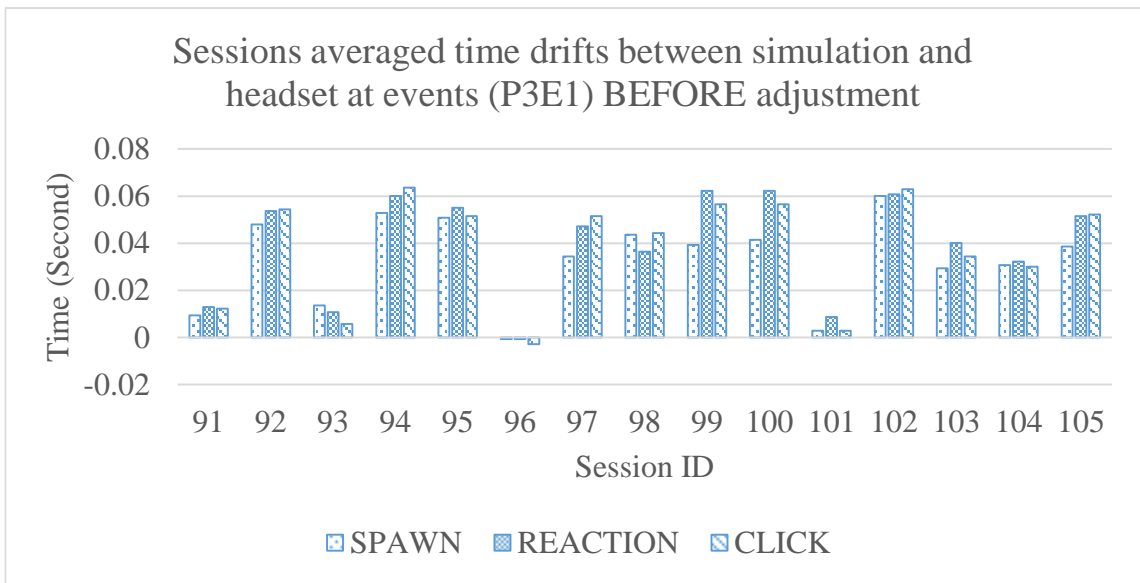
(a) Before adjustment.
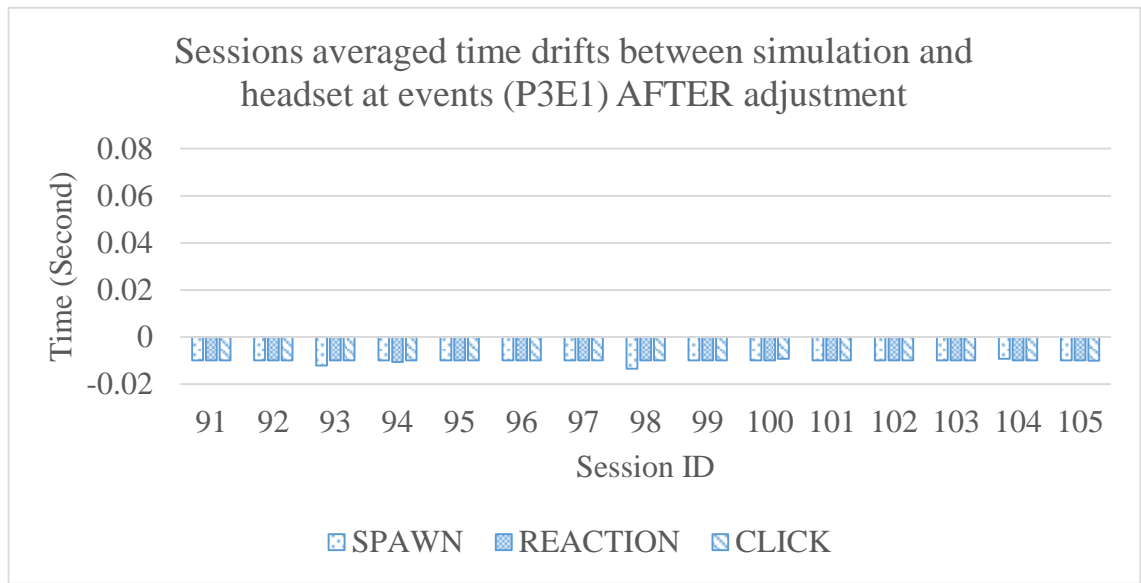
(b) After adjustment.

Figure 6.20 The sessions averaged time drifts between the simulation and the headset timelines from P3E1.
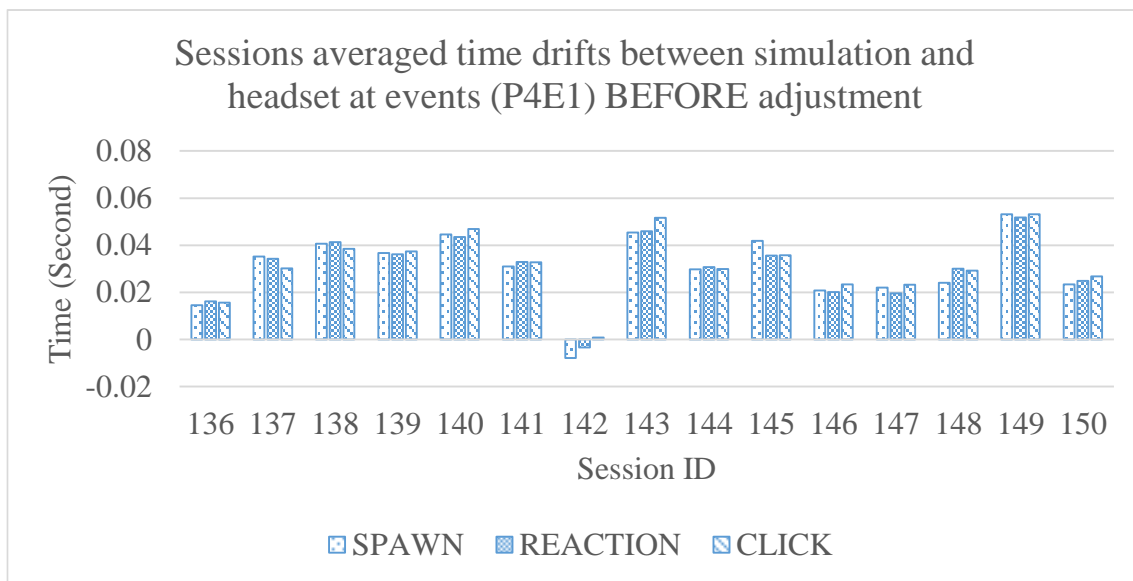
(a) Before adjustment.
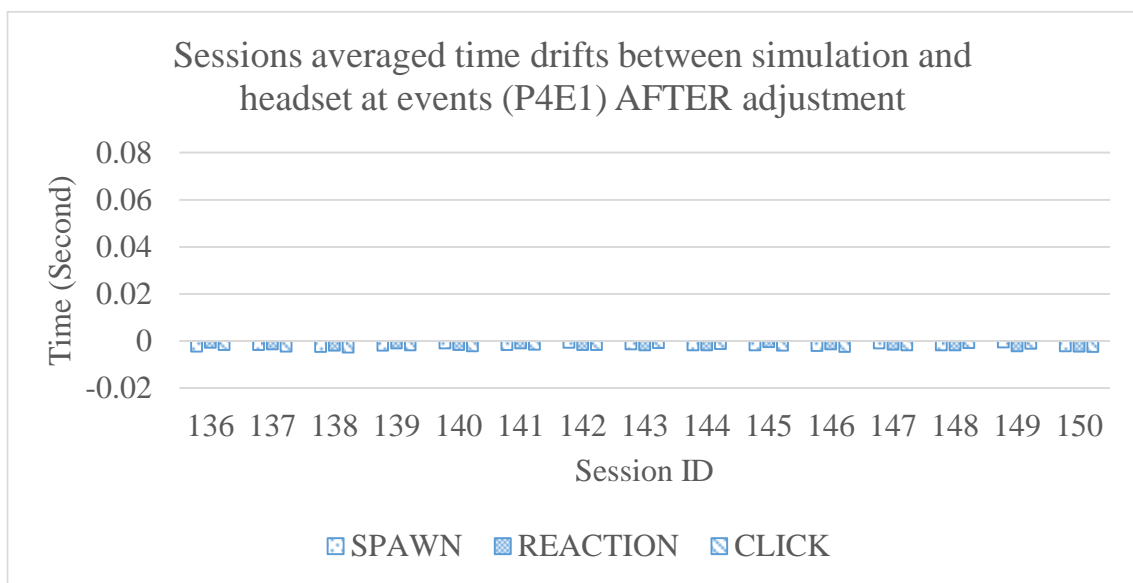
(b) After adjustment.

Figure 6.21 The sessions averaged time drifts between the simulation and the headset timelines from P4E1.

6.7.3 Analysis of task performance

In this section, an analysis of task performance is presented. Statistical information of the performance metrics in Section 6.5 are calculated and presented. A result of calculation from all participants is presented at first. Then, an individual result is presented.

6.7.3.1 <u>All participants</u>

General statistical information on the performance metrics – RT, MT, DT, MA, HA, and IP from all participants is presented in Table 6.6.

The minimum of RT is 0.0s while the maximum is 0.8s. The reason of 0.0s RT is that sometimes a participant expected a target to appear at a certain time in the incoming time point and starts to move a mouse cursor before the target is actually spawned. The biggest RT is as large as 0.8s which is slightly greater than the average of MT which is 0.79s. A box plot of RT, MT, and DT is shown in Figure 6.22. It is noted that the RT contains outliers in both lower and upper parts which are dominated in the lower part around RT 0.0s as shown in the distribution of data in Figure 6.23. MT and DT have a small number of outliers in the upper part of the box plot as shown in Figure 6.22. Therefore, the data distribution of MT and DT are reasonably a normal distribution as shown in Figure 6.24, and Figure 6.25, respectively.

A box plot of MA is shown in Figure 6.26. Although there is a huge variation in the upper outliers of the MA, most of the data are stayed within between the upper adjacent and lower adjacent as can be observed from the data distribution plot in Figure 6.27. This means although there are some movement deviations from the perfectly straight lines, most of the performances stay within the range of deviation from 0.465 pixels (minimum) to 40 pixels (upper adjacent). In contrast to MA, HA shows most of the outliers in the lower part of a box plot as shown in Figure 6.28. It is noted that there is one task pattern that contains negative HA. The negative HA is from the task pattern performed by P2E1S8T3. According to the detailed inspection, it is found that a target is located at T(960,540) while the mouse hit click moment occurs at M(996,576). The distance between these two points is 50.91 pixels. The distance is larger than the target radius, 50 pixels. This is the reason of the negative HA. It is possible to have a negative HA because of the rounding error from the algorithm used to detect a collision between the

mouse cursor and the target boundary. The algorithm is implemented by integer calculation so that an interactive simulation can run smoothly. The algorithm can be found in the Appendix C. This justification conforms to the highest accuracy of HA values where there exist 8 task patterns with 100% HA. Apart from both extreme ends, the HA data is distributed around 70-90% of HA with a standard deviation of 14.993 and the median at 81.56%.

Fitts index of performance (IP) is calculated by (2.6). Outliers of the IP belong to the high performance area or the upper end of a box plot as shown in Figure 6.30. Although there are some of the outliers, the overall distribution of IP is normal as shown in Figure 6.31. The highest performance according to the highest IP of 6.517 bits/seconds belongs to P2E2S14T14. The lowest of IP 1.565 belongs to P3E1S11T5.

Table 6.6 The performance statistics (All participants).

	Speed			Accuracy		Fitts
	RT (Seconds)	**MT (Seconds)**	**DT (Seconds)**	**MA (Pixels)**	**HA (%)**	**IP (Bits/s)**
Minimum	0.000	0.290	0.530	0.465	-1.823	1.565
Maximum	0.800	1.863	2.130	191.610	100.000	6.517
Average	0.259	0.790	1.049	17.433	77.502	3.412
Median	0.276	0.772	1.028	11.057	81.561	3.382
Standard deviation	0.106	0.252	0.239	19.653	14.993	0.724
Data distribution figure	Figure 6.23	Figure 6.24	Figure 6.25	Figure 6.27	Figure 6.29	Figure 6.31
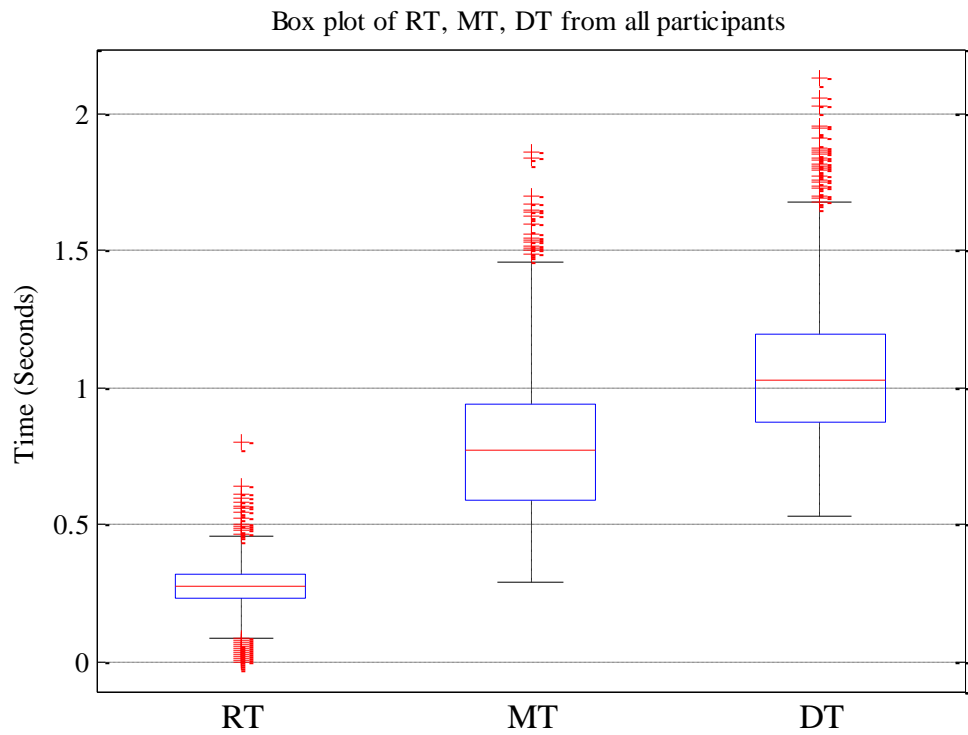
Figure 6.22 The box plot of speed aspects (RT, MT, DT) from all participants.
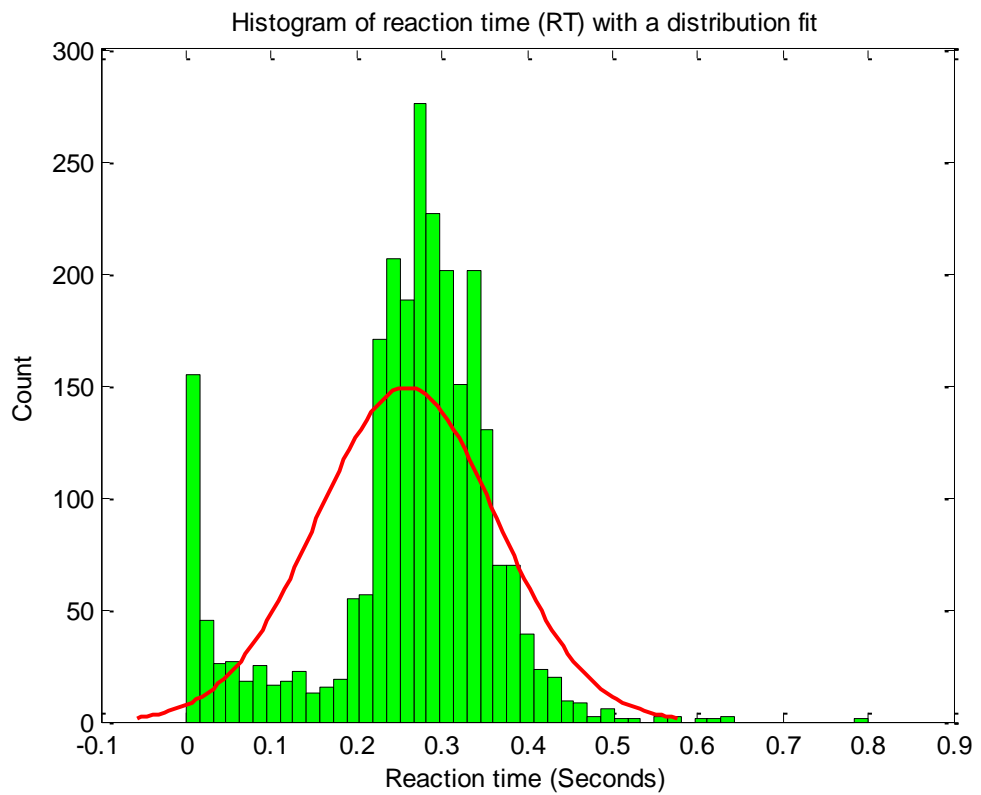
Figure 6.23 The reaction time (RT) data distribution.
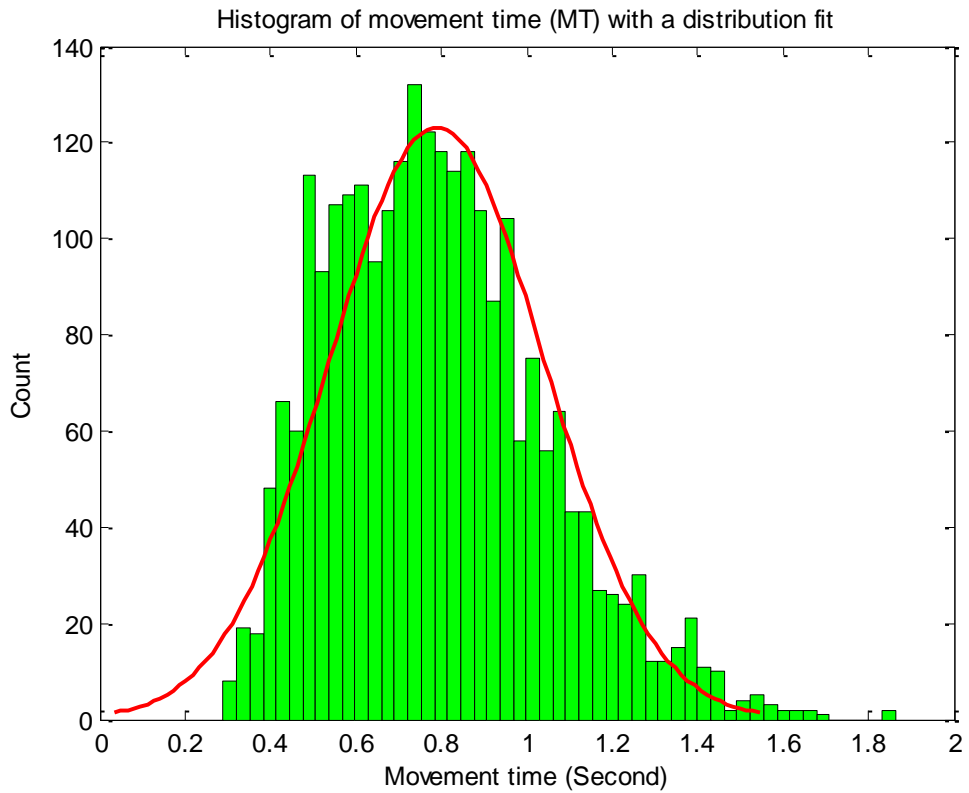
Figure 6.24 The movement time (MT) data distribution.
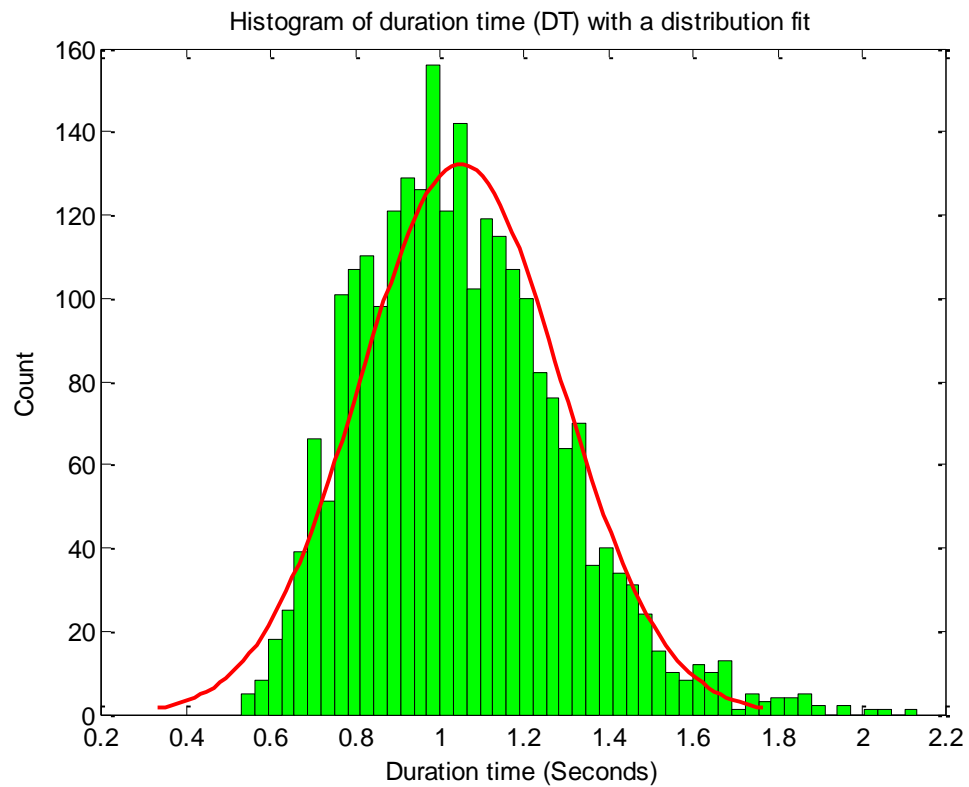
Figure 6.25 The duration time (DT) data distribution.
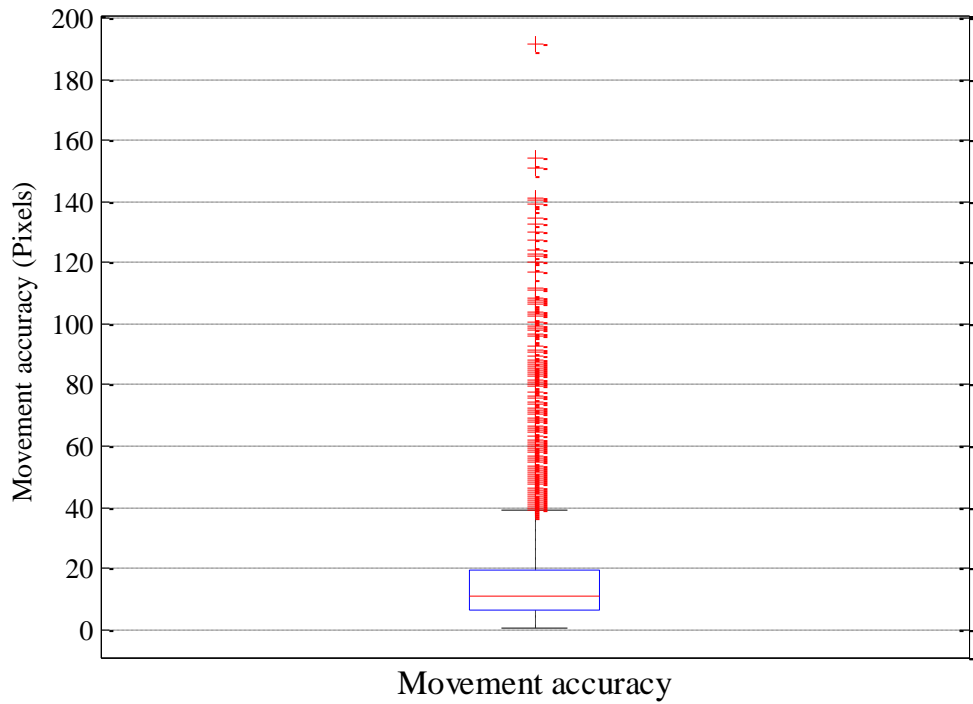
Figure 6.26 The box plot of movement accuracy (MA) from all participants.
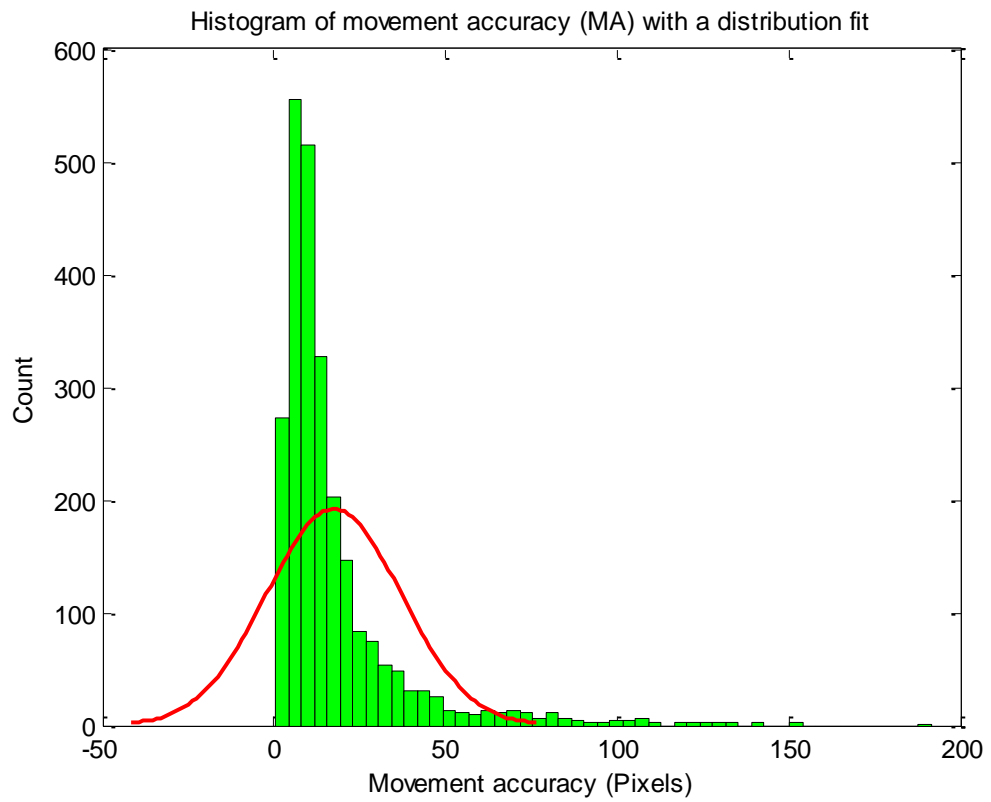
Figure 6.27 The movement accuracy (MA) data distribution.
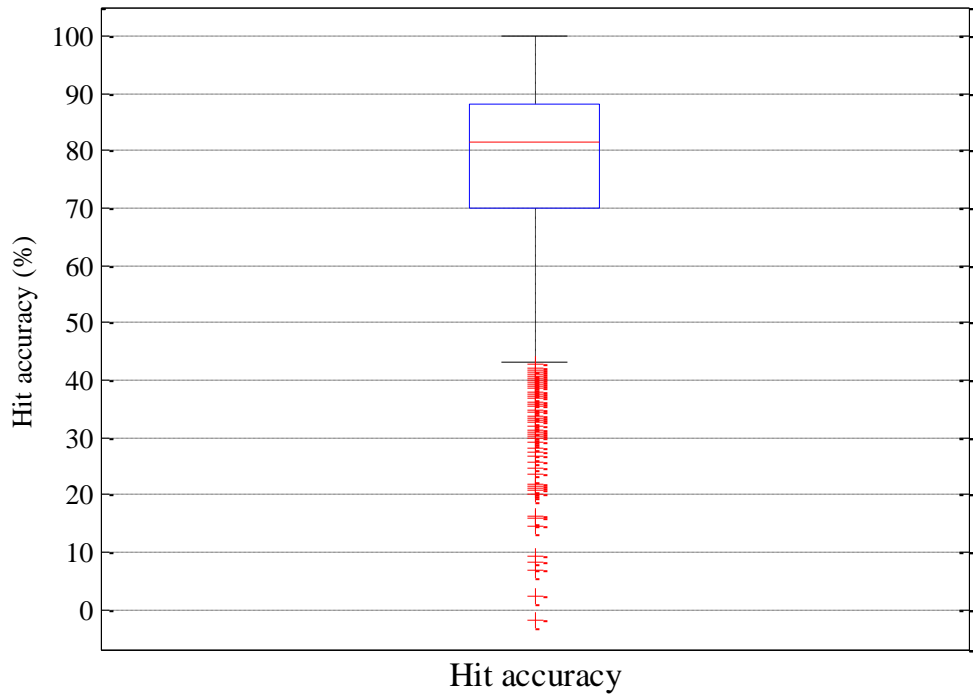
Figure 6.28 The box plot of hit accuracy (HA) from all participants.
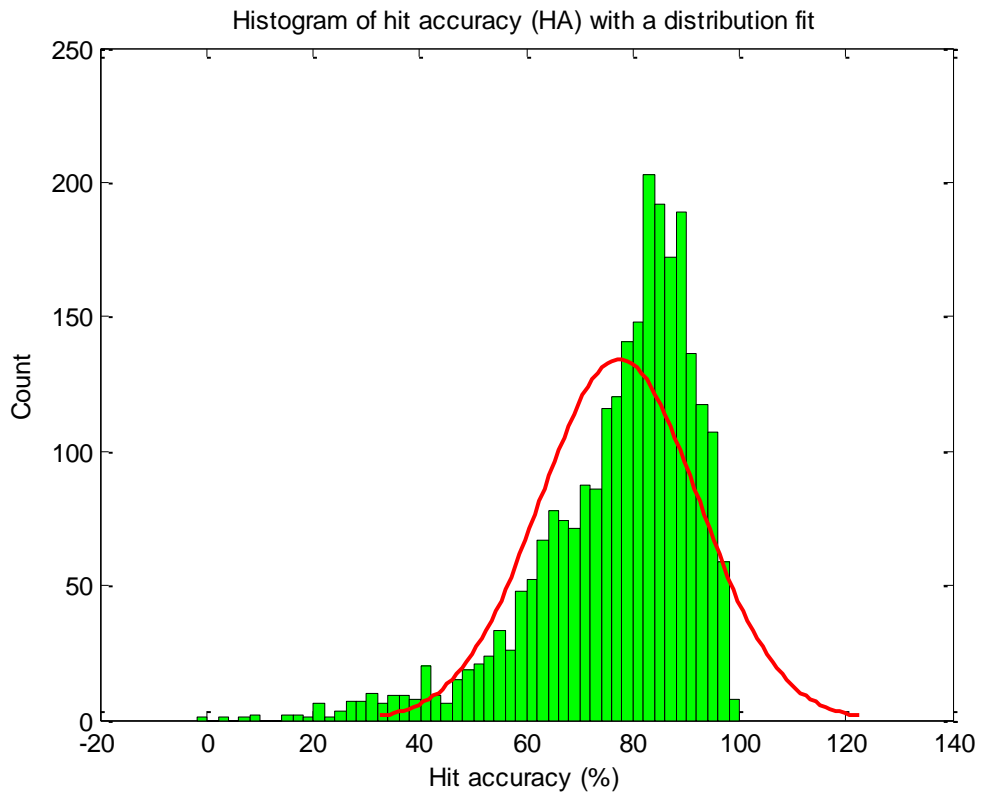
Figure 6.29 The hit accuracy (HA) data distribution.
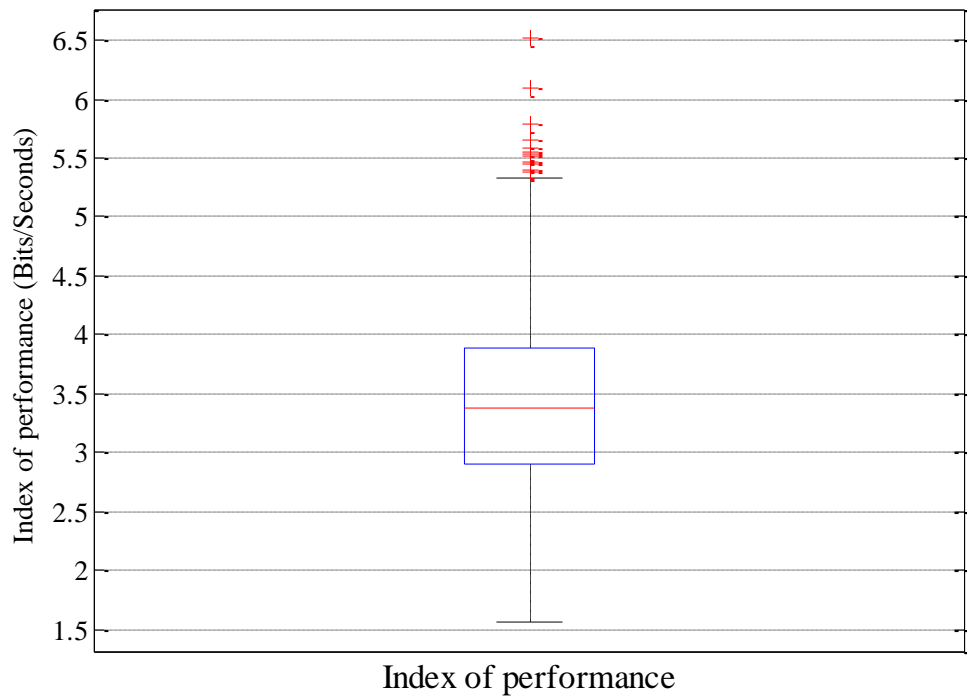
Figure 6.30 The box plot of Fitts index of performance (IP) from all participants.
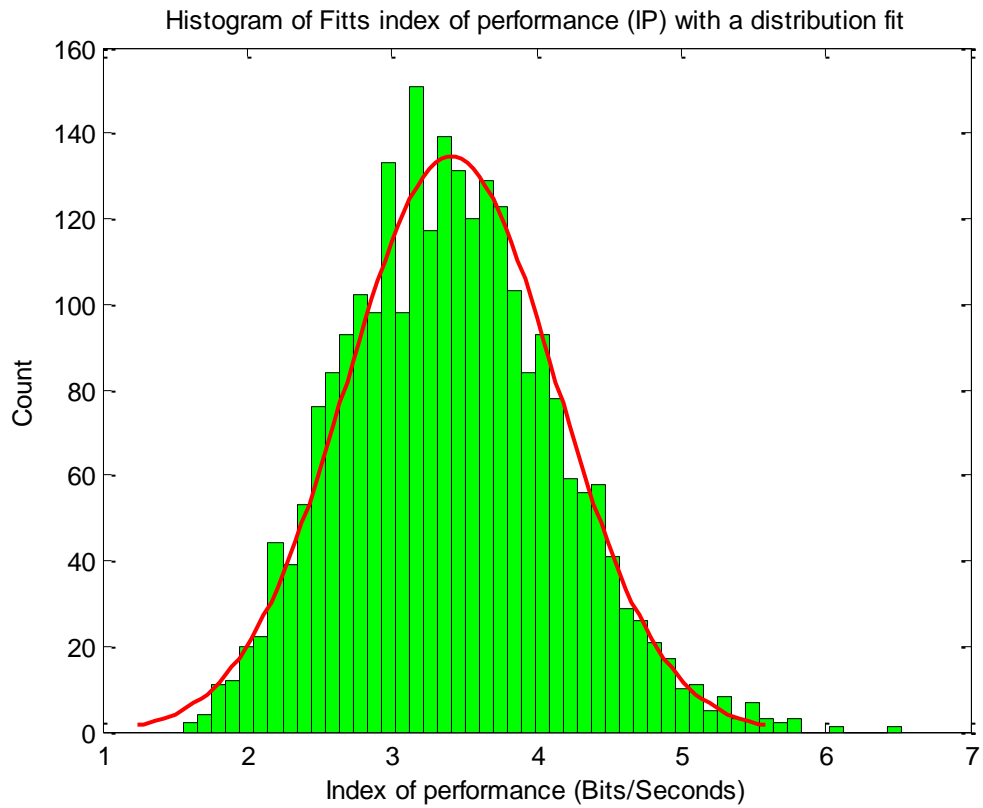
Figure 6.31 The Fitts index of performance (IP) data distribution.

6.7.3.2 <u>Comparison among participants</u>

In this section, the performance statistics are presented for each participant in order to compare the performance between them.

Table 6.7 shows the performance statistics for each participant. P3 has the fastest averaged RT of 0.188s. However, the deviation is quite large at 0.139s. This can be observed from the participant-ordered plot of RT and a box plot in Figure 6.32(a) and Figure 6.32(b), respectively. P3 also has the slowest RT of 0.8s as shown in the upper outliers in Figure 6.32(b). P1 has the slowest averaged RT of 0.309s but the RT performance is rather constant as indicated by the lowest standard deviation of 0.053s. The minimum RT from all of the participants is as low as 0s which mean there exists the anticipation behaviour for a target appearance.

Table 6.7 The performance statistics for each participant.

	Speed			Accuracy		Fitts
	RT (Seconds)	MT (Seconds)	DT (Seconds)	MA (Pixels)	HA (%)	IP (Bits/s)
P1						
Minimum	0.007	0.346	0.573	0.57	6.70	2.342
Maximum	0.469	1.110	1.541	58.98	97.17	5.276
Mean	0.309	0.633	0.941	10.46	72.31	3.727
Median	0.304	0.594	0.910	8.28	75.58	3.721
Standard deviation	0.053	0.160	0.181	8.10	15.90	0.525
P2						
Minimum	0.000	0.290	0.530	0.98	-1.82	1.698
Maximum	0.640	1.840	2.130	154.11	100.00	6.517
Mean	0.277	0.719	0.997	20.72	72.89	3.659
Median	0.280	0.686	0.960	12.29	75.95	3.641
Standard deviation	0.081	0.272	0.281	24.19	18.29	0.878
P3						
Minimum	0.000	0.448	0.593	0.86	40.33	1.565
Maximum	0.800	1.863	2.060	191.61	100.00	4.975
Mean	0.188	0.974	1.163	14.10	85.87	3.050
Median	0.210	0.950	1.146	10.03	86.58	3.072
Standard deviation	0.139	0.219	0.223	15.03	7.69	0.611
P4						
Minimum	0.006	0.400	0.655	0.46	21.89	1.822
Maximum	0.572	1.504	1.952	141.42	100.00	5.393
Mean	0.262	0.833	1.095	24.44	78.92	3.214
Median	0.276	0.794	1.062	15.78	80.20	3.181
Standard deviation	0.091	0.200	0.193	23.46	11.54	0.590
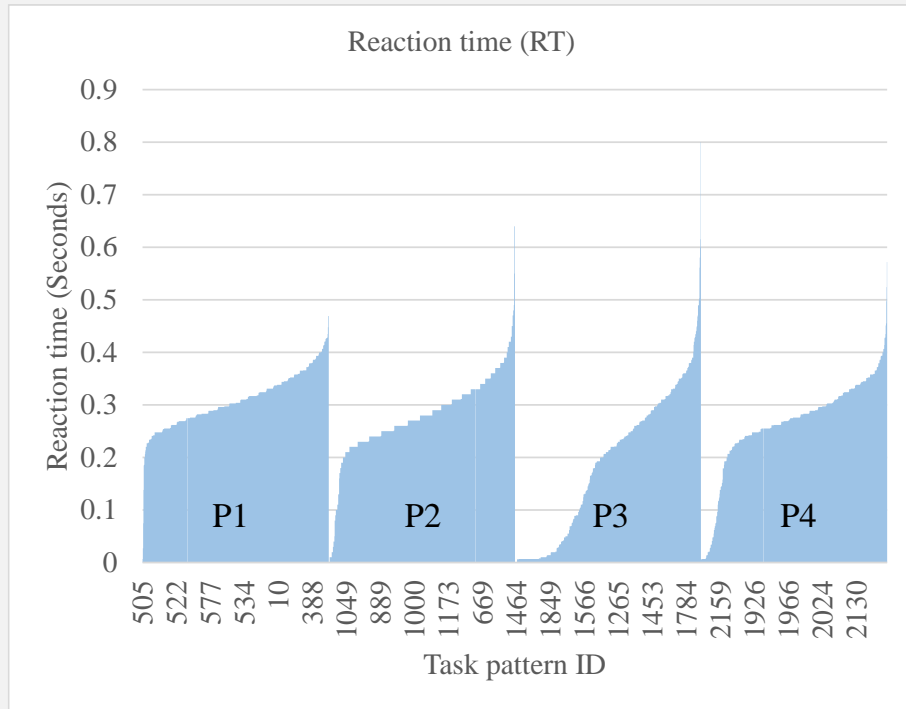
(a) The reaction time (RT) plots ordered by the participants.
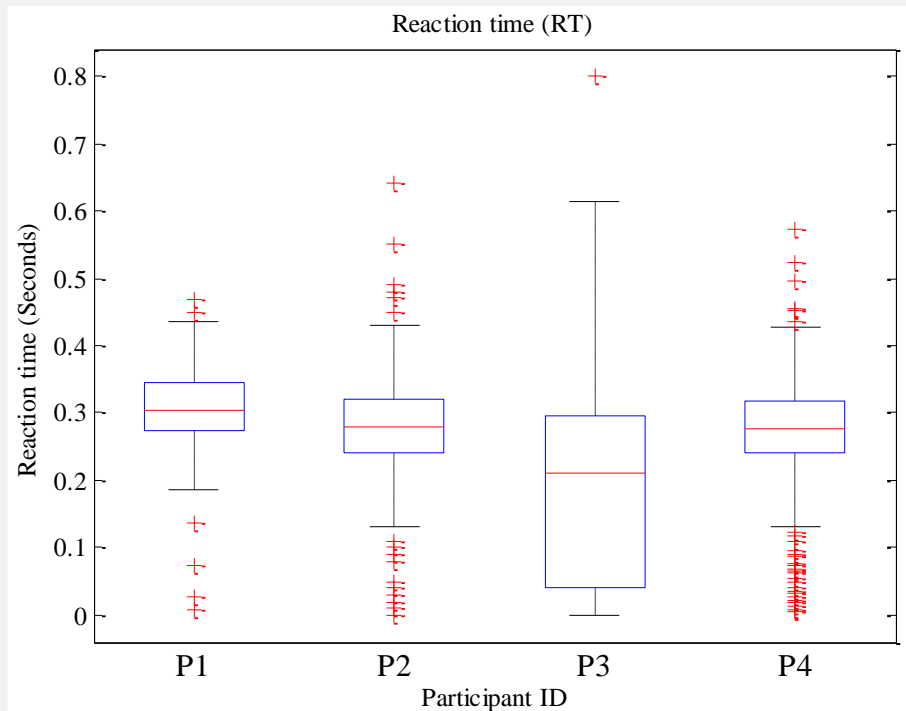
(b) The box plots of each participant reaction time (RT).

Figure 6.32 The plots of reaction time (RT) performance statistics for each participant.

The fastest MT belongs to P2 for 0.29s though the fastest averaged MT belongs to P1 for 0.633s as shown in the box plots in Figure 6.33(b). Although P2 possesses the fastest MT, the participant also exhibits the second slowest MT of 1.840s which is only 0.023s difference from the slowest one as shown in the upper outliers of the box plots in Figure 6.33(b). The averaged slowest MT belongs to P3 which is in contrast to P3's RT performance. P1 has no outliers whereas the others have outliers lie around the upper end of MT box plot as shown in Figure 6.33(a) and Figure 6.33(b).

(a) The movement time (MT) plots ordered by the participants.
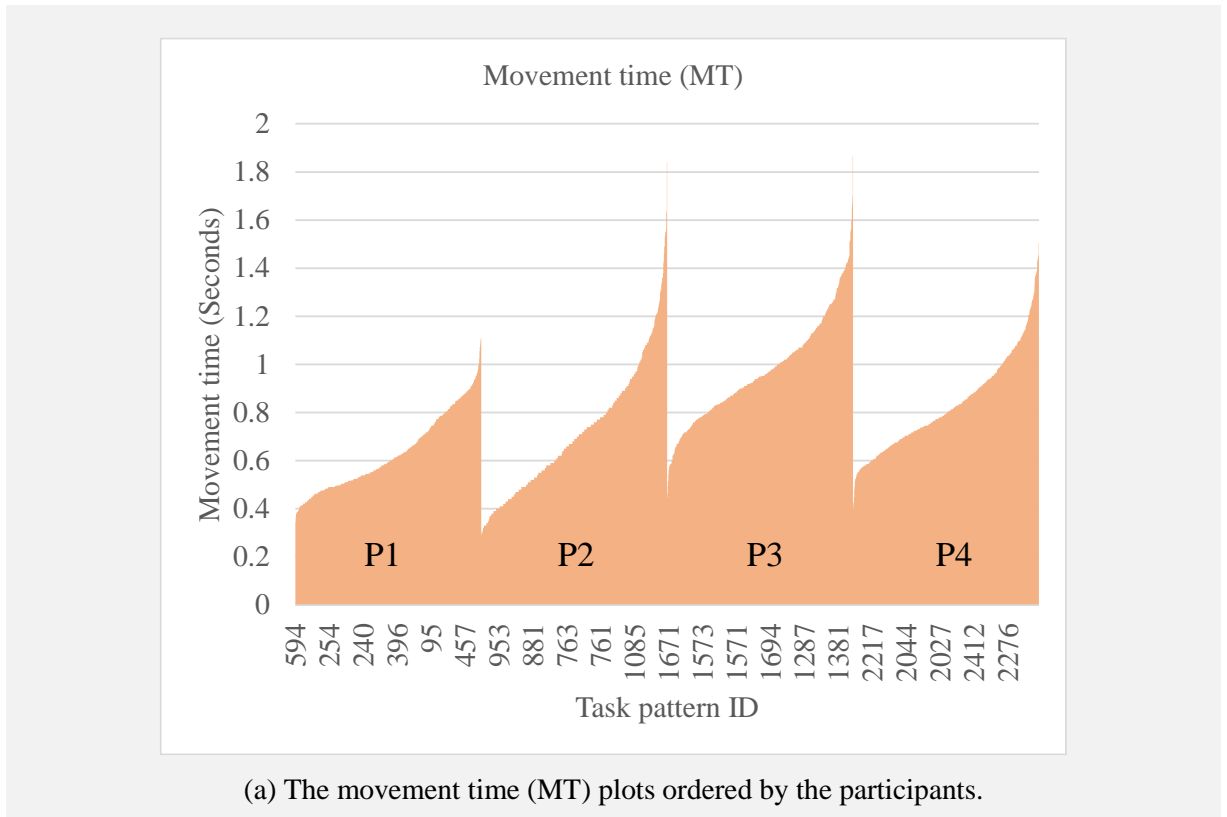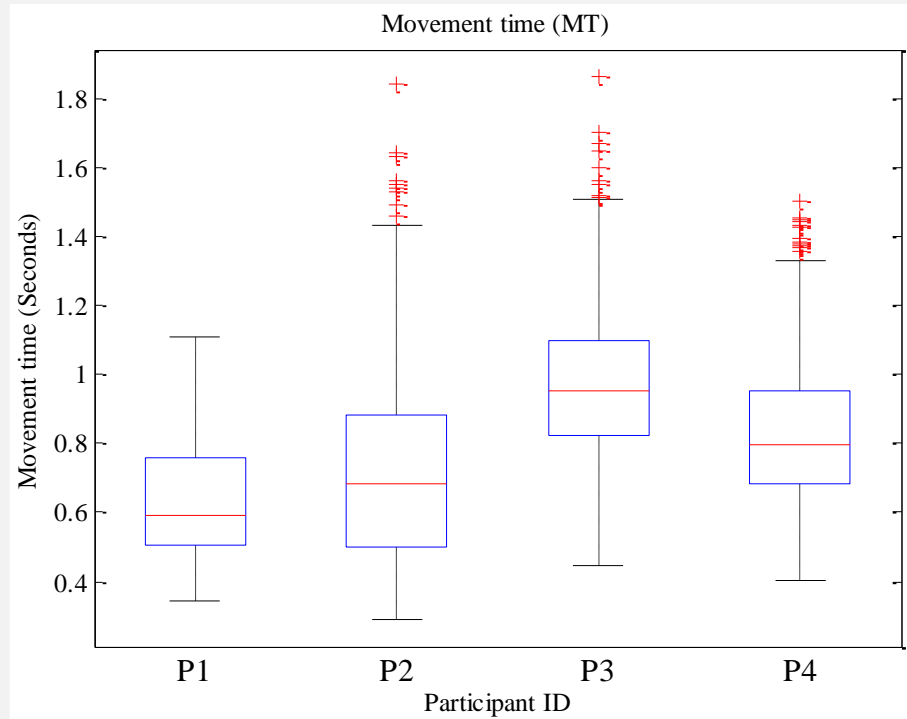
(b) The box plots of each participant movement time (MT).

Figure 6.33 The plots of movement time (MT) performance statistics for each participant.

Since DT is the sum of RT and MT, the performance aspect of DT can be largely affected by the performance of MT in addition to the RT as can be observed from Figure 6.34(b) in comparison to Figure 6.32(b) and Figure 6.33(b).
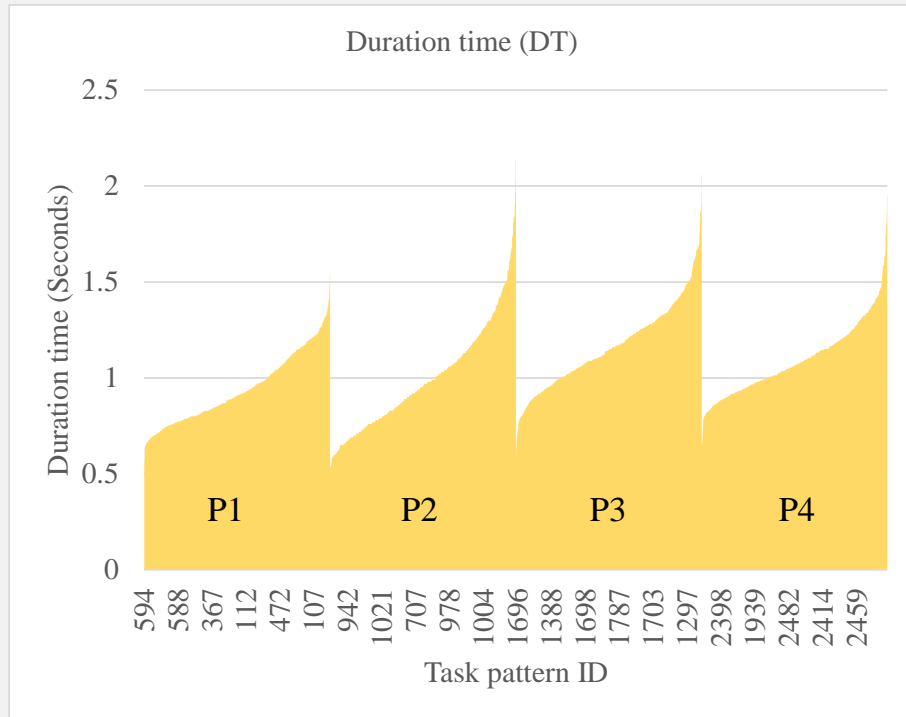
(a) The duration time (DT) plots ordered by the participants.
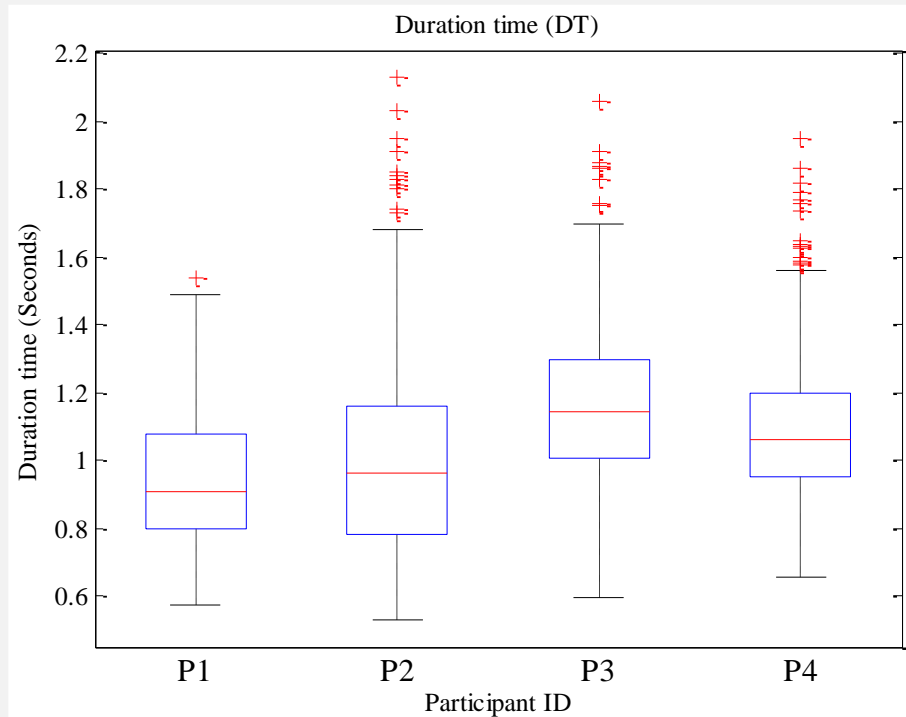
(b) The box plots of each participant duration time (DT).

Figure 6.34 The plots of duration time (DT) performance statistics for each participant.

The averaged MA from all of the participants is in the same range as shown in Figure 6.35. The maximum MA belongs to P3 with 191.61 pixels deviated from a perfect movement line as shown in the upper outlier of Figure 6.35(b) for P3. The minimum MA for each participant is as low as zero which means a perfect movement from the start position to the target click. A plot of mouse movements for each of the minimum MA from each of the participants is shown in Figure 6.36(a), Figure 6.36(b), Figure 6.36(c), and Figure 6.36(d), respectively. The plots are from task pattern P1E3S9T3, P2E2S5T1, P3E3S8T7, and P4E3S13T5, correspondingly. At the other ends, P3 has the maximum MA, then P2, P3, and P1, orderly. A plot of mouse movements of these maximums is shown in Figure 6.37(a), Figure 6.37(b), Figure 6.37(c), and Figure 6.37(d), respectively. They are illustrated from task pattern P1E3S10T10, P2E2S3T11, P3E1S1T10, and P4E1S4T10, respectively.
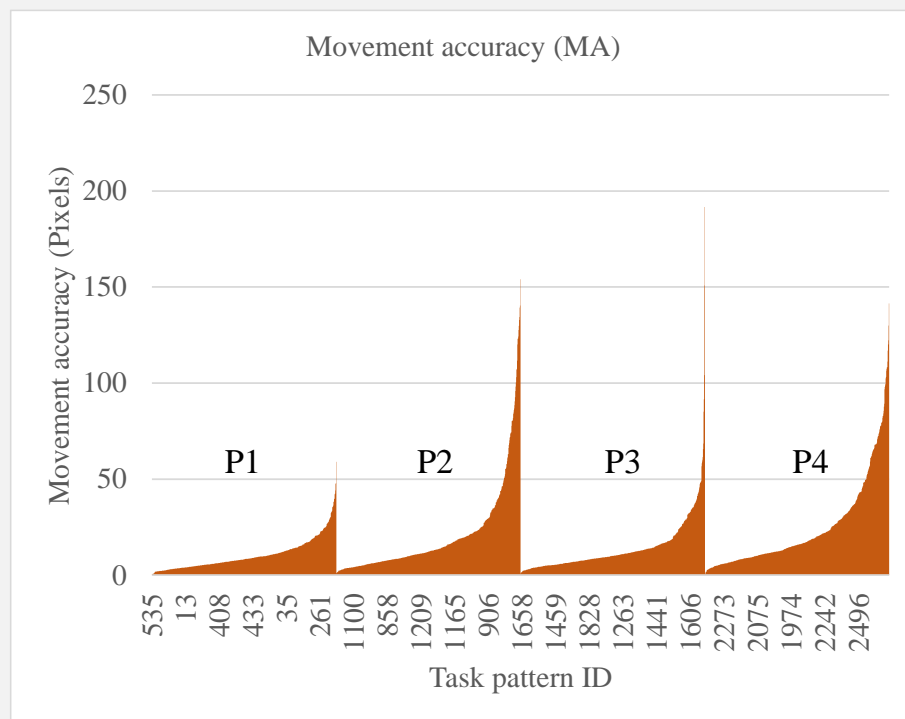
(a) The movement accuracy (MA) plots ordered by the participants.
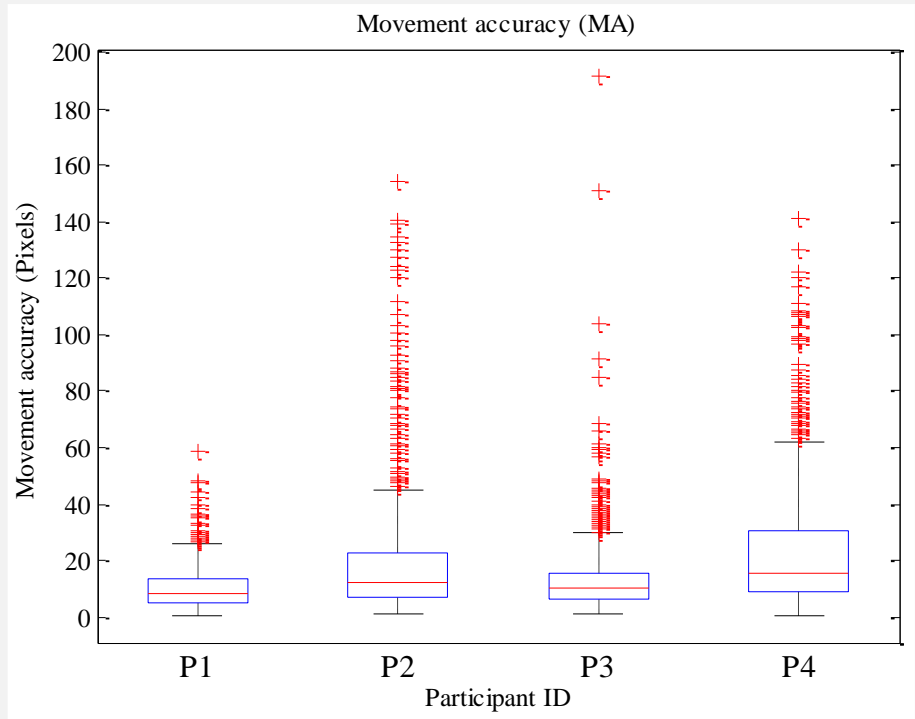
(b) The box plots of each participant movement accuracy (MA).

Figure 6.35 The plots of movement accuracy (MA) performance statistics for each participant.

P1E3S9T3
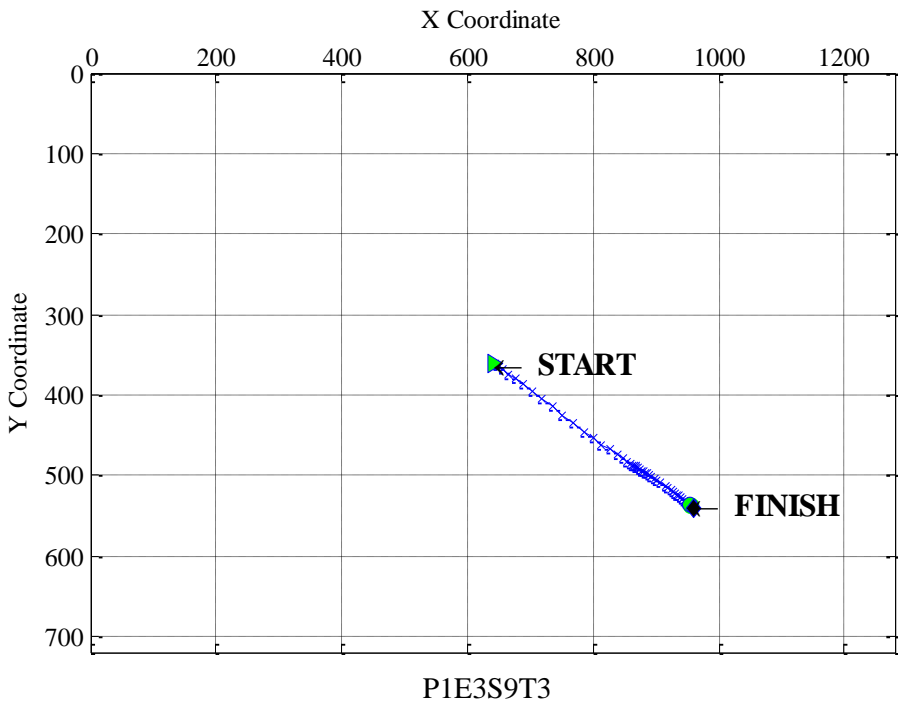
(a) The trajectory plot from the task pattern with the lowest MA from P1.

P2E2S5T1
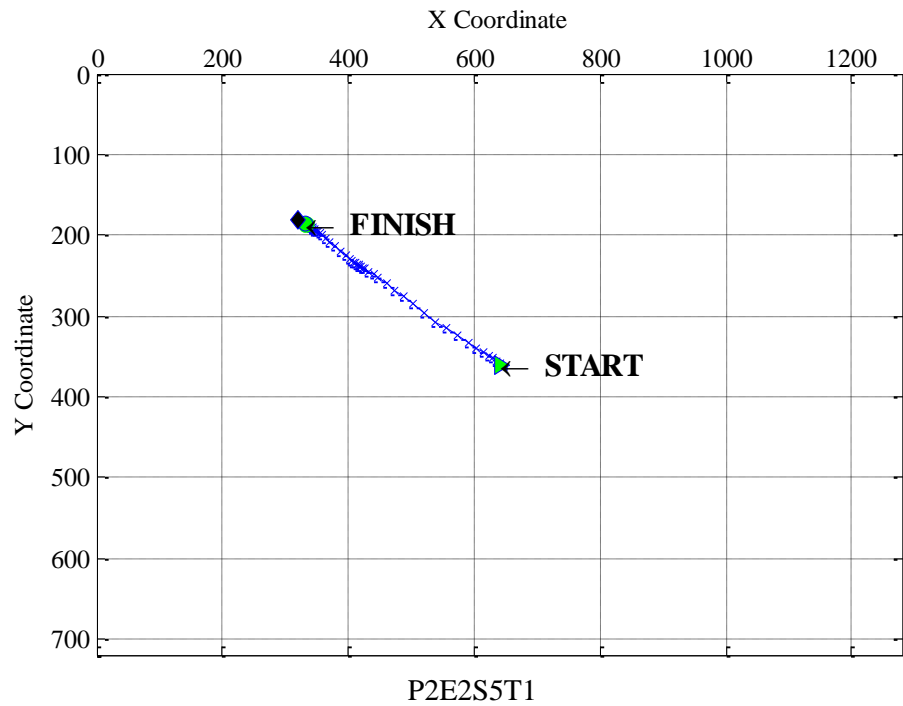
(b) The trajectory plot from the task pattern with the lowest MA from P2.

P3E3S8T7
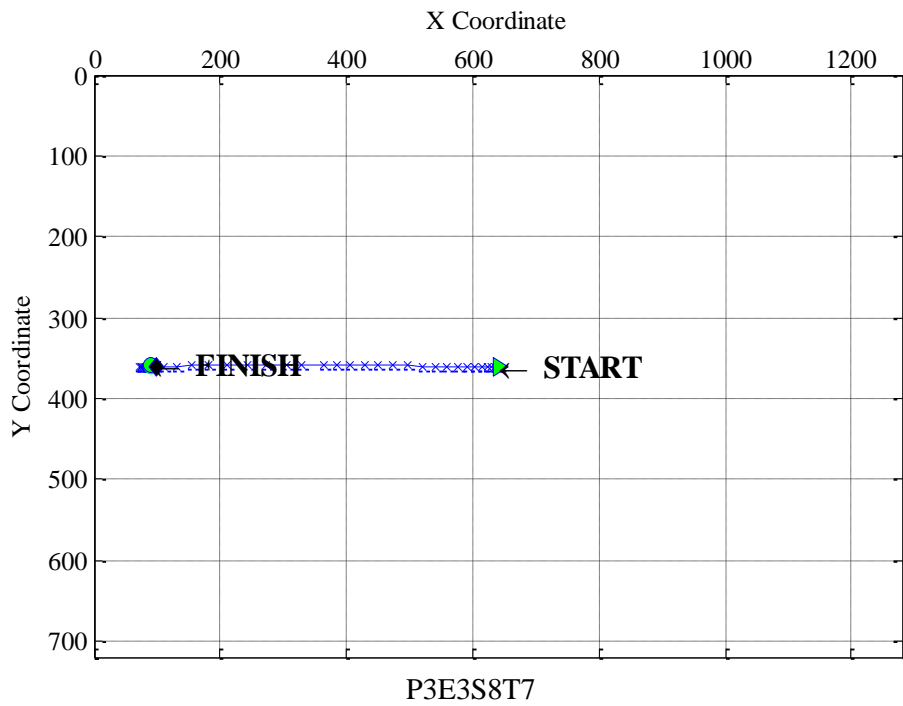
(c) The trajectory plot from the task pattern with the lowest MA from P3.

(d) The trajectory plot from the task pattern with the lowest MA from P4.

Figure 6.36 The trajectory plots from the task patterns with the lowest movement accuracy (MA) for each participant.
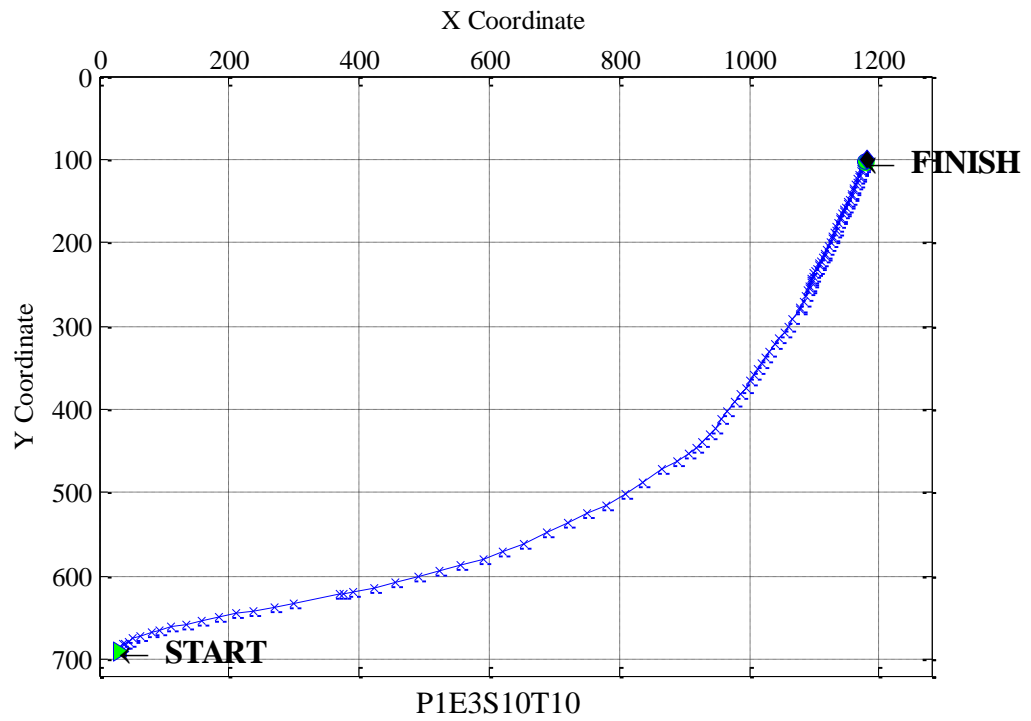
(a) The trajectory plot from the task pattern with the highest MA from P1.
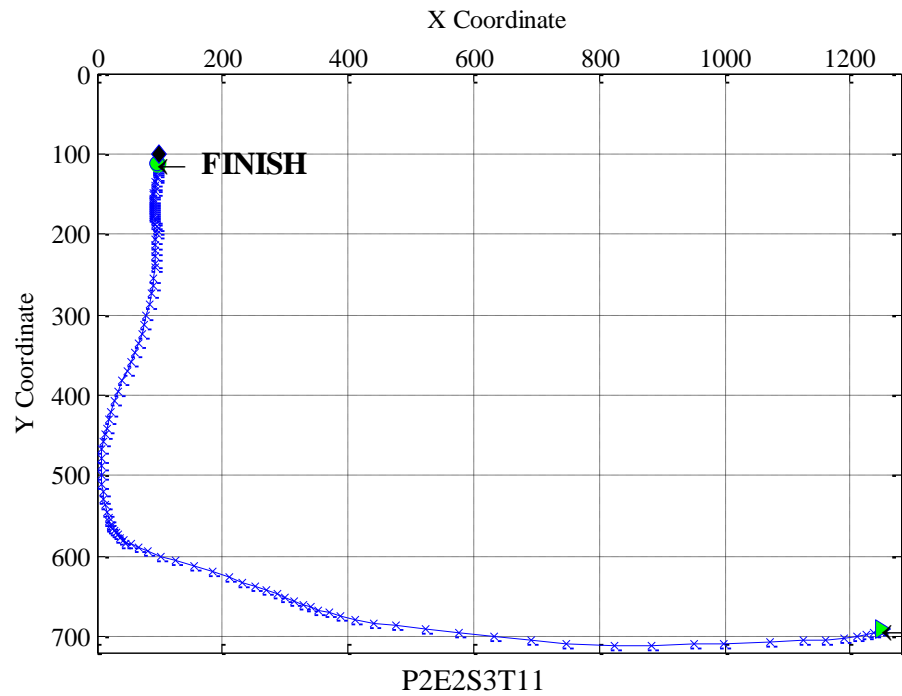
(b) The trajectory plot from the task pattern with the highest MA from P2.
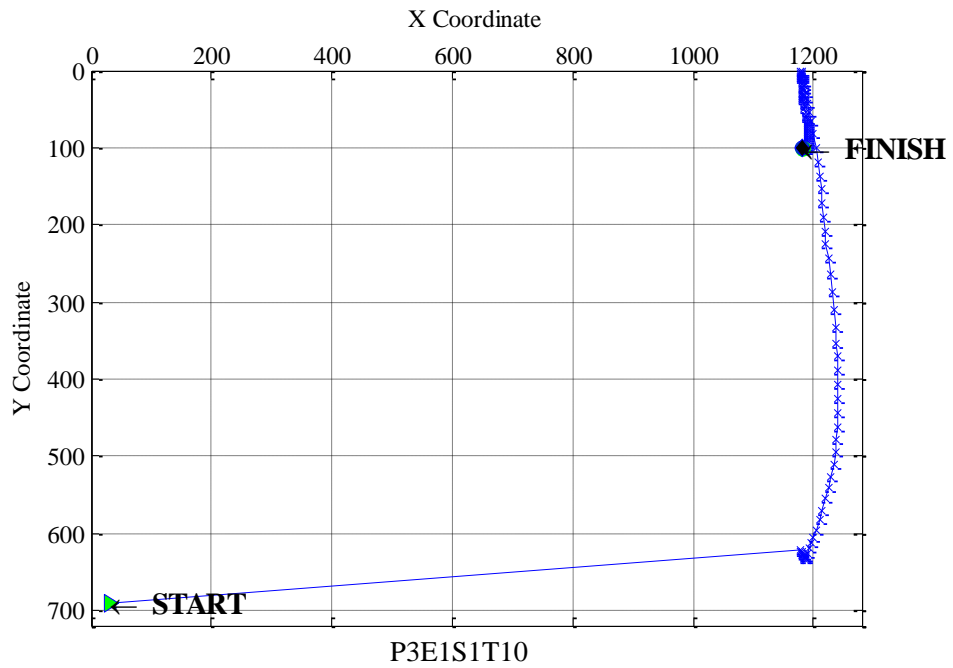
(c) The trajectory plot from the task pattern with the highest MA from P3.
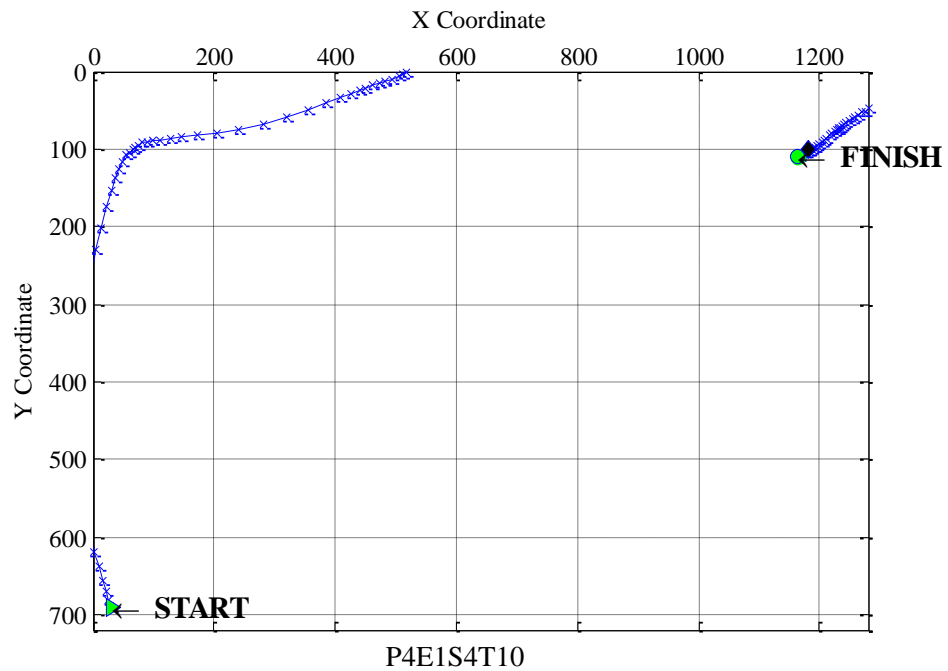
(d) The trajectory plot from the task pattern with the highest MA from P4.

Figure 6.37 The trajectory plots from the task patterns with the highest movement accuracy (MA) for each participant.

In term of hit accuracy performance i.e. HA, most participants have the maximum accuracy of 100% except P1 which has the maximum HA at 97.17%. P3 has the highest averaged HA of 85.87%. This high averaged HA conforms to a speed-accuracy trade-off since P3 has the slowest averaged DT of 1.163s. Likewise, P1 has the lowest averaged HA of 72.31% which also conforms to the trade-off by having the fastest averaged DT of 0.941s. P3 performs moderately steady as shown by the standard deviation value of HA. An ordered HA plot and the box plot of HA for the four participants are shown in Figure 6.38.
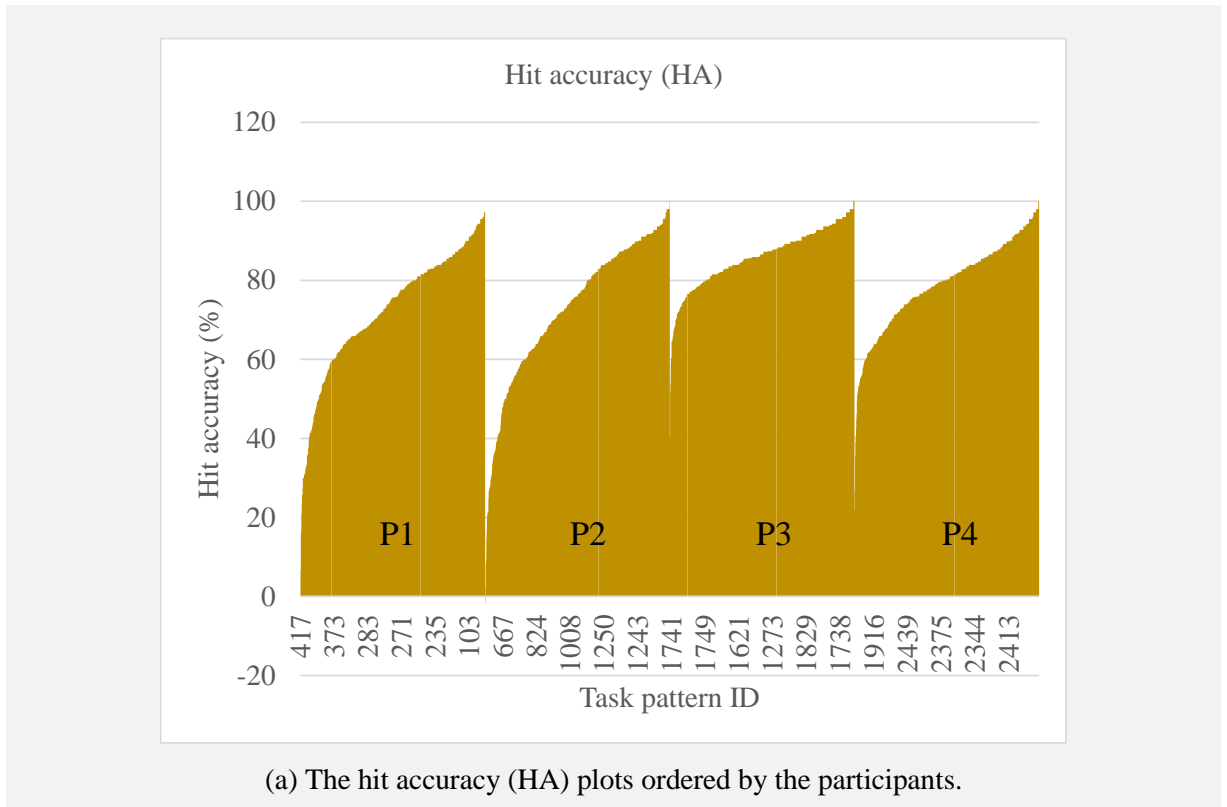
(a) The hit accuracy (HA) plots ordered by the participants.
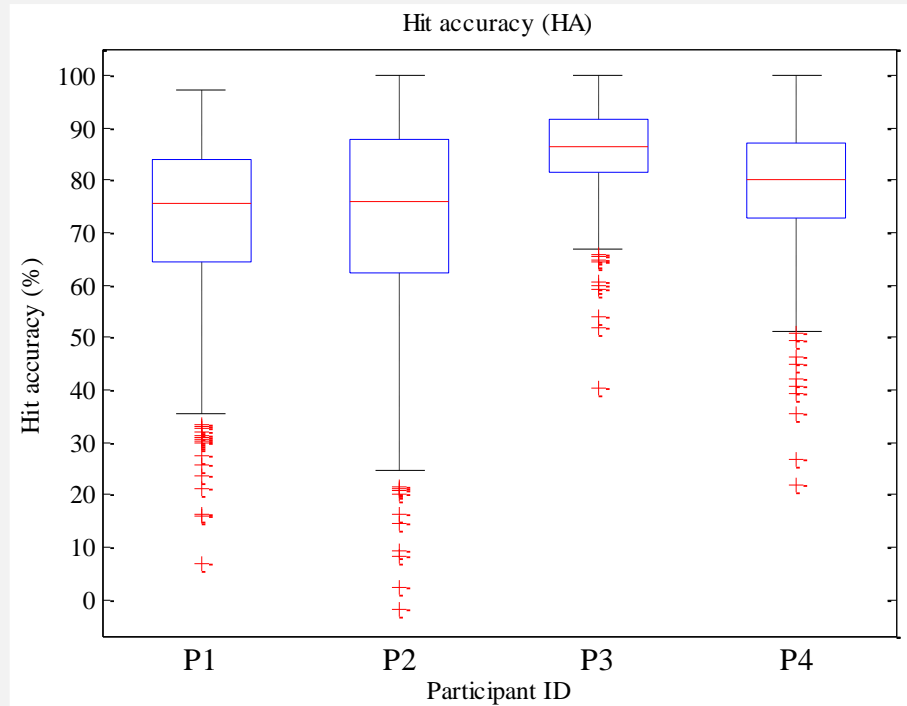
(b) The box plots of each participant hit accuracy (HA).

Figure 6.38 The plots of hit accuracy (HA) performance statistics for each participant.

Since IP is calculated based on DT and the distance between start and target positions, it is obvious that P1 has the highest averaged IP of 3.727 bits/seconds while P4 is the lowest. In contrast, the minimum and the lowest averaged IP belong to P3 who held the highest averaged HA with the value of 1.565 and 3.050 bits/seconds, respectively. A plot of ordered IP grouped by participants and box plots are shown in Figure 6.39.
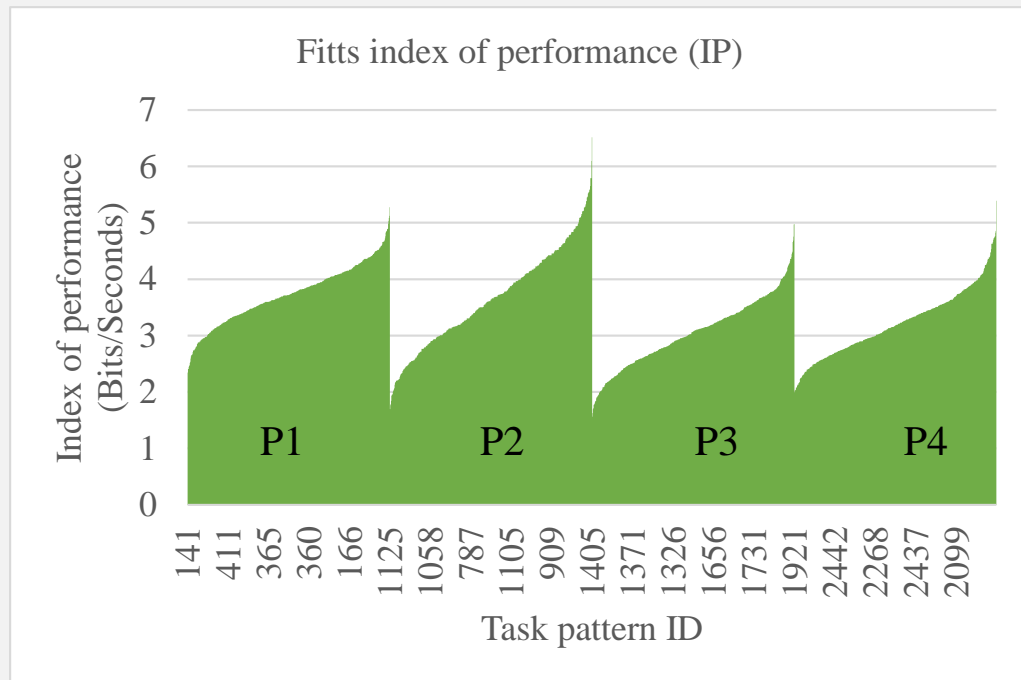
(a) The Fitts index of performance (IP) plots ordered by the participants.
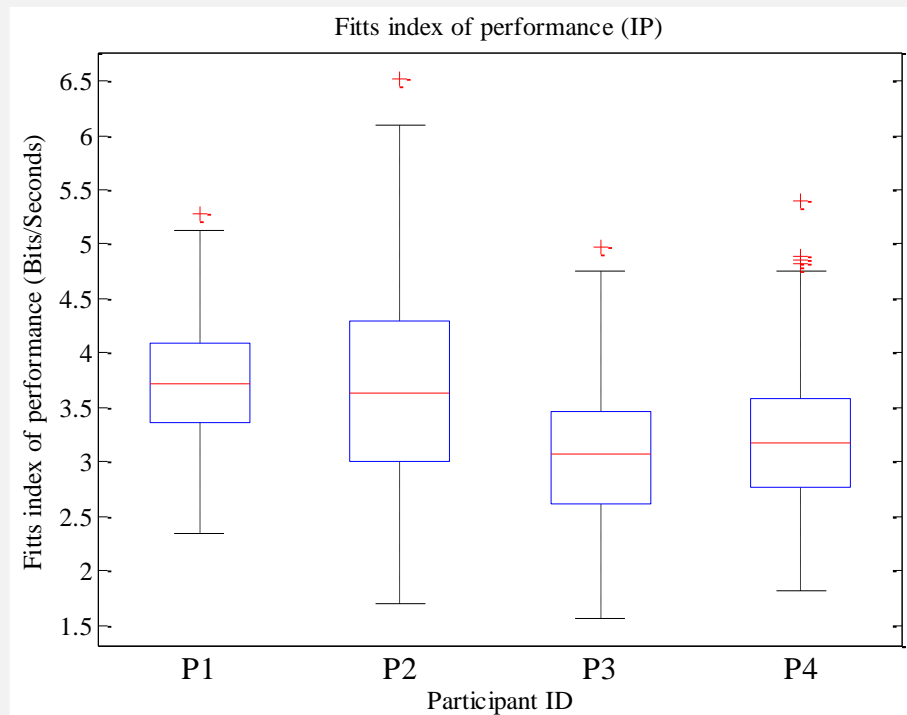
(b) The box plots of each participant Fitts index of performance (IP).

Figure 6.39 The plots of Fitts index of performance (IP) performance statistics for each participant.

6.7.4 Analysis of event-related potential (ERP)

This section presents results from analysis of the event-related potential (ERP) at the onset of the task pattern events i.e. spawn, reaction, and click. A definition and calculation method of ERP can be found in Section 2.13.3. The ERP is calculated from a total number of task patterns after exclusion of the extreme epochs as described in the 7th step of Figure 6.10. A boundary of the ERP is between -1000ms and 1000ms from the onset of the analysing event.

It is noted that a reaction event is an immediate consequence from a spawn event. The two events always come together at a fraction of seconds apart, hence, the ERP is analysed in the same section.

6.7.4.1 <u>Spawn and reaction events</u>

Figure 6.40(a) and Figure 6.40(b) show the spawn ERP for a group of frontal and posterior electrodes, respectively. Figure 6.40 shows that frontal EEG brainwaves respond to the onset of spawn event with a peak positive deflection of F4 at 164.0625ms and 0.5047 µV of amplitude. The peak deflection is followed by a deflection towards negative value at 203.125ms and -0.5821 µV of amplitude dominated by FC6 and F4. The magnitude of the amplitude is a little larger than the first deflection. The next positive deflection comes at 265.625ms at 0.541 µV dominantly at FC6. Then, the followed spikes are lowered down until back to the normal oscillation. A sequence of spawn ERP deflections is summarised in Table 6.8. In brief, all of the frontal electrodes synchronously respond to the onset of a target spawn event.

At the posterior area in Figure 6.40(b), the first deflection comes at the opposite side to the frontal area at 125ms with a slightly larger magnitude of -0.7446 µV from O1. The next distinct spike comes at 187.5ms with 1.2178 µV amplitude eminently from the same O1 electrode. It is followed by the maximum amplitude of deflection at 242.1875ms with -1.2636 µV from O1. The O1 signal bounces back once more to the positive side at 315.5ms with a reduced in magnitude at 0.7409 µV before oscillates down to the normal wave. The other posterior electrodes other than the O1 have rather normal oscillation except the O2 where it slightly follows the trend of O1 with smaller amplitudes of deflection. Table 6.9 summarises the sequence of deflections from posterior electrodes for the spawn ERP.
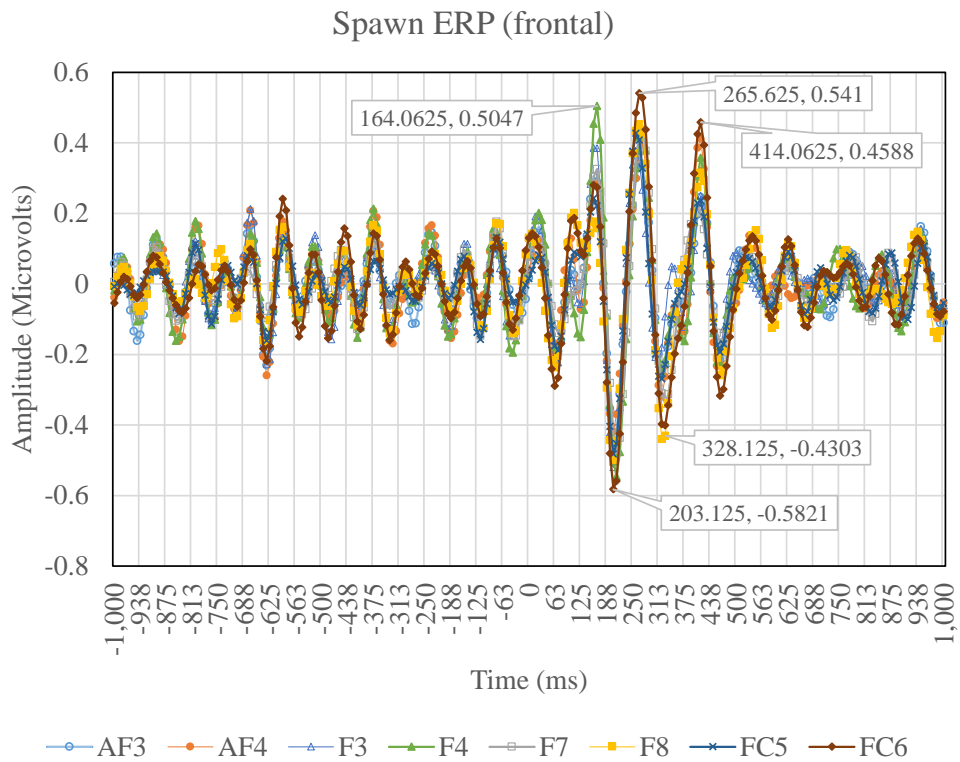
(a) The ERP at the spawn event from a group of frontal EEG electrodes.
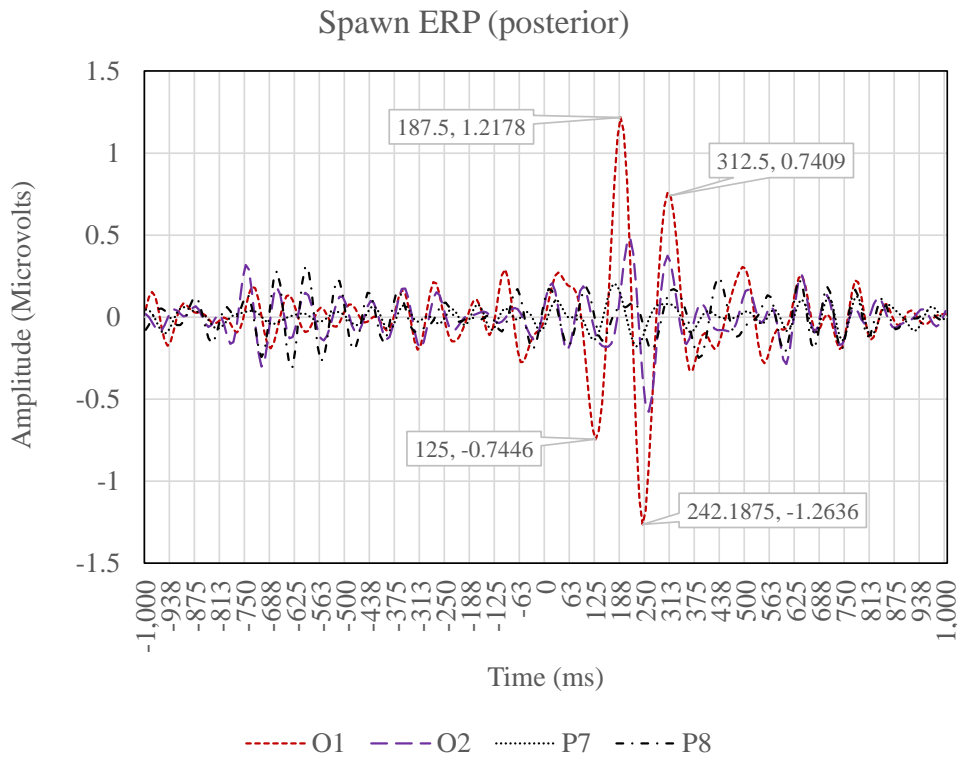
(b) The ERP at the spawn event from a group of posterior EEG electrodes.

Figure 6.40 The ERP at the spawn event.

Table 6.8 The sequence of spawn ERP deflections of frontal electrodes.

Sequence of deflections	Time (Milliseconds)	Amplitude (Microvolts)	Electrodes
1	164.0625	0.5047	F4
2	203.125	-0.5821	FC6, F4
3	265.625	0.541	FC6
4	328.125	-0.4303	F8, FC6
5	414.0625	0.4588	FC6, AF4

Table 6.9 The sequence of spawn ERP deflections of posterior electrodes.

Sequence of deflections	Time (Milliseconds)	Amplitude (Microvolts)	Electrodes
1	125	-0.7446	O1
2	187.5	1.2178	O1
3	242.1875	-1.2636	O1
4	312.5	0.7409	O1

Figure 6.41(a) and Figure 6.41(b) shows the ERP at the reaction event from frontal and posterior electrode groups, respectively. Summaries of the sequence of deflections are shown in Table 6.10 and Table 6.11 for frontal and posterior. It is obvious that although the reaction event occurs with the mean time of 259ms after the spawn event (Table 6.6), the train of deflections from the previous spawn event is missing. It means that the deviation of reaction times has cancelled out the spikes of the spawn event when the ERP is calculated at the reaction event. Nevertheless, the reaction event shows a number of spikes at latencies 109.375ms, 164.0625ms, 234.375ms, and 296.875ms with the amplitudes of -0.3434 µV, 0.3076 µV, -0.2411 µV, and 0.2008 µV, respectively. These spikes are mainly from F3, F4, and FC6. In contrast, at the posterior electrodes, the deflection is not distinguishable from the ongoing train of EEG brainwaves as shown in Figure 6.41(b).
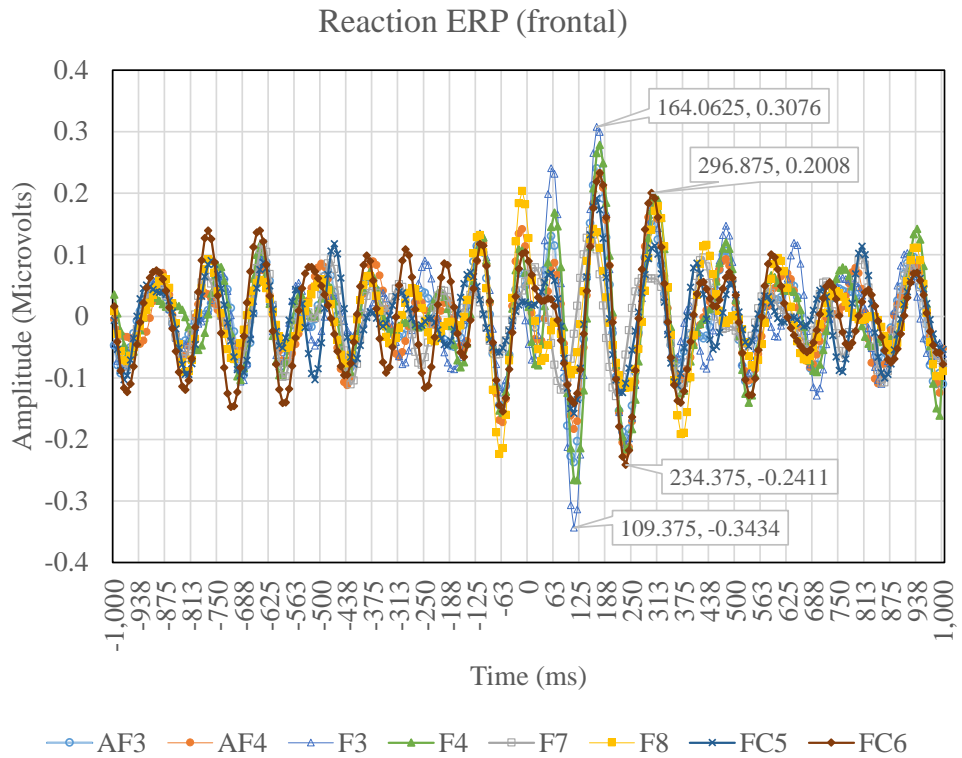
(a) The ERP at the reaction event from a group of frontal EEG electrodes.
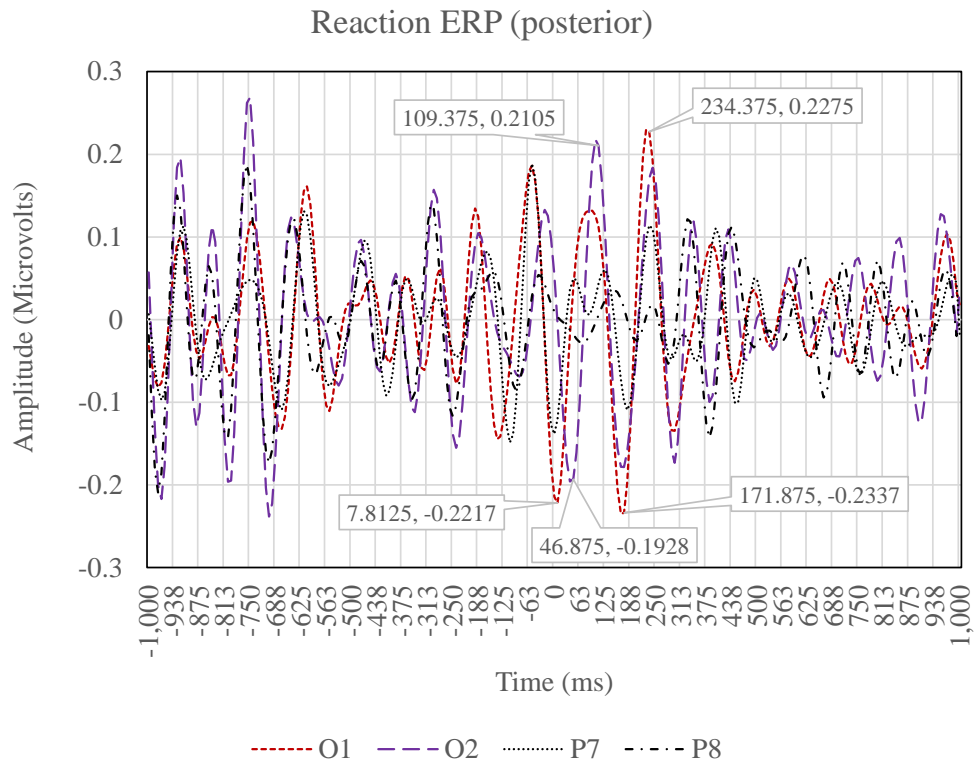
(b) The ERP at the reaction event from a group of posterior EEG electrodes.

Figure 6.41 The ERP at the reaction event.

Table 6.10 The sequence of reaction ERP deflections of frontal electrodes.

Sequence of deflections	Time (Milliseconds)	Amplitude (Microvolts)	Electrodes
1	109.375	-0.3434	F3
2	164.0625	0.3076	F3, F4
3	234.375	-0.2411	FC6
4	296.875	0.2008	FC6

Table 6.11 The sequence of reaction ERP deflections of posterior electrodes.

Sequence of deflections	Time (Milliseconds)	Amplitude (Microvolts)	Electrodes
1	7.8125	-0.2217	O1
2	46.875	-0.1928	O2
3	109.375	0.2105	O2
4	171.875	-0.2337	O1
5	234.375	0.2275	O1

6.7.4.2 <u>Click event</u>

A click event occurs after the spawn event at the mean latency of 1,049ms according to the mean duration time in Table 6.6. A trace of spawn ERP can be observed at the far left of the click ERP at the frontal group of electrodes as shown in Figure 6.42(a). In contrast, a trace of spawn ERP from posterior electrodes cannot be observed from Figure 6.42(b). From the frontal group of electrodes, the first deflection can be observed at 23.4375ms with 0.3346 µV from F3. A summary of the sequence of deflections for the frontal is shown in Table 6.12. The two dominant spikes from F3 are 0.5251 µV and -0.5217 µV at 156.25ms and 210.9375ms latencies, respectively. The frontal brainwaves of click ERP have moderate synchronisation compared to the frontal spawn ERP.

At the posterior electrodes, the synchronisation is rather chaotic but the ERP is still able to distinguish from the ongoing brainwaves. Table 6.13 summarises a sequence of deflections from posterior electrodes for the click ERP. The deflections are dominated by O1 and P8 with the bottom and peak from O1 at 304.6875ms and 359.375ms, respectively.
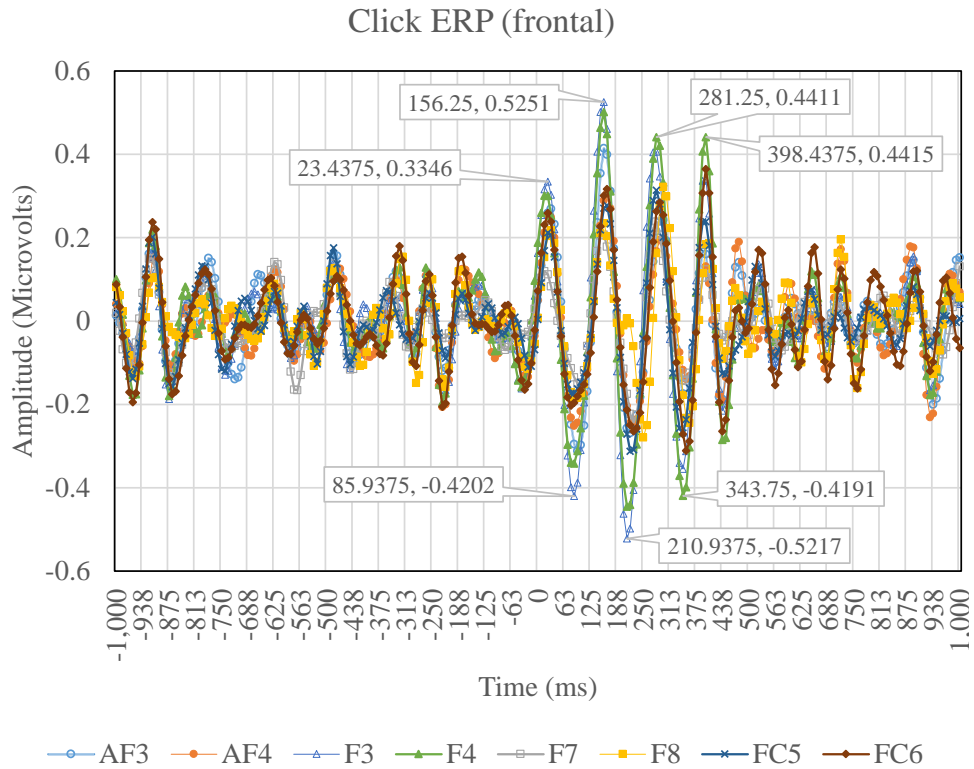
(a) The ERP at the click event from a group of frontal EEG electrodes.
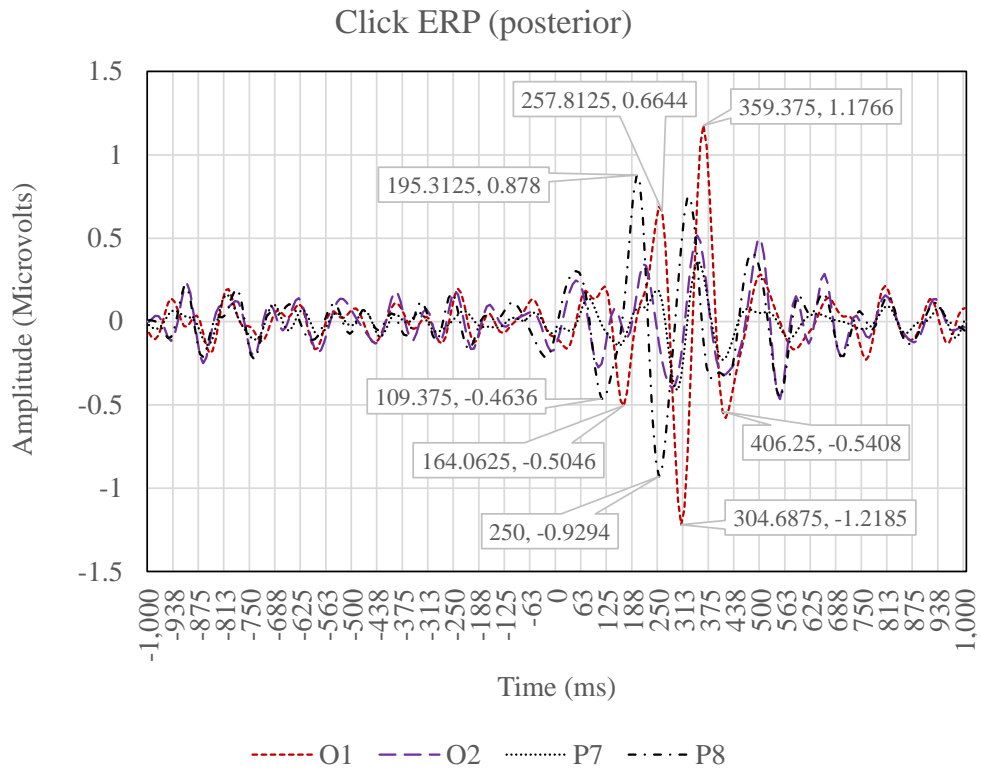
(b) The ERP at the click event from a group of posterior EEG electrodes.

Figure 6.42 The ERP at the click event.

Table 6.12 The sequence of click ERP deflections of frontal electrodes.

Sequence of deflections	Time (Milliseconds)	Amplitude (Microvolts)	Electrodes
1	23.4375	0.3346	F3
2	85.9375	-0.4202	F3
3	156.25	0.5251	F3, F4
4	210.9375	-0.5217	F3
5	281.25	0.4411	F4
6	343.75	-0.4191	F4
7	398.4375	0.4415	F4

Table 6.13 The sequence of click ERP deflections of posterior electrodes.

Sequence of deflections	Time (Milliseconds)	Amplitude (Microvolts)	Electrodes
1	109.375	-0.4636	P8
2	164.0625	-0.5046	O1
3	195.3125	0.878	P8
4	250	-0.9294	P8
5	257.8125	0.6644	O1
6	304.6875	-1.2185	O1
7	359.375	1.1766	O1
8	406.25	-0.5408	O1

6.7.4.3 <u>Region averaged ERP</u>

Figure 6.43(a), (b), (c), and (d) show the averaged ERP from the frontal and posterior group of electrodes for spawn and click events, accordingly. It is noted that the region averaged ERP makes the ERP more visible provided that the synchronisation among the brainwaves in the area are consistent.
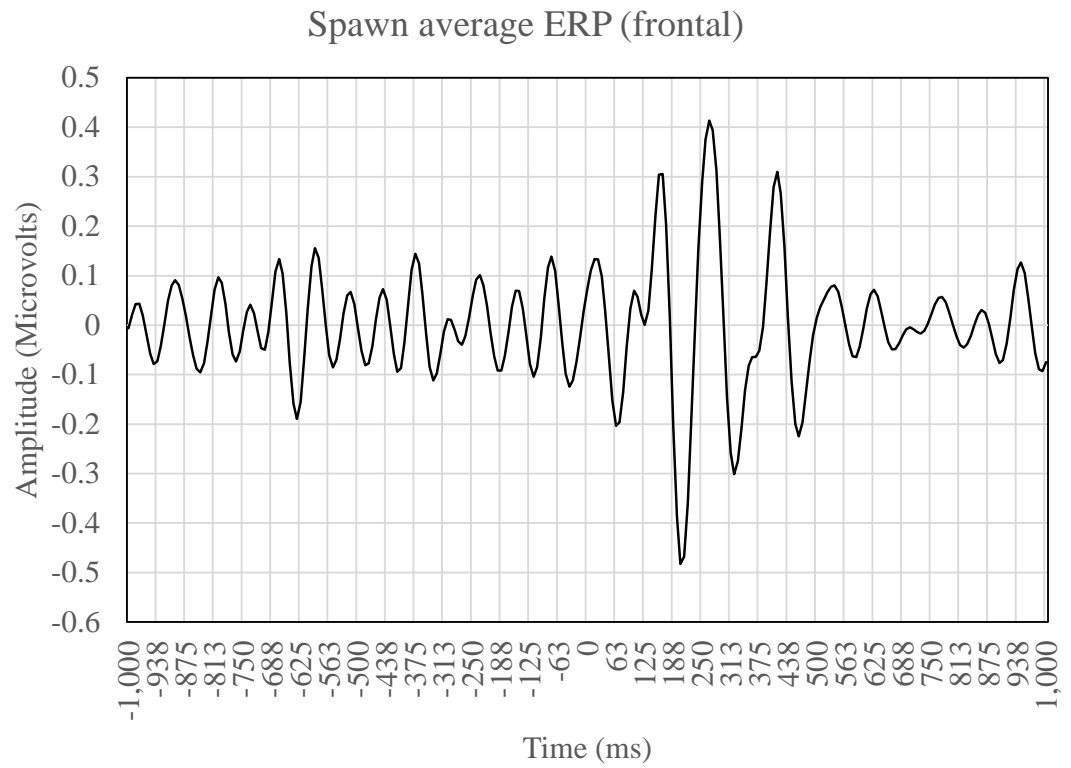
(a) The averaged ERP from the frontal group of electrodes at the spawn event.
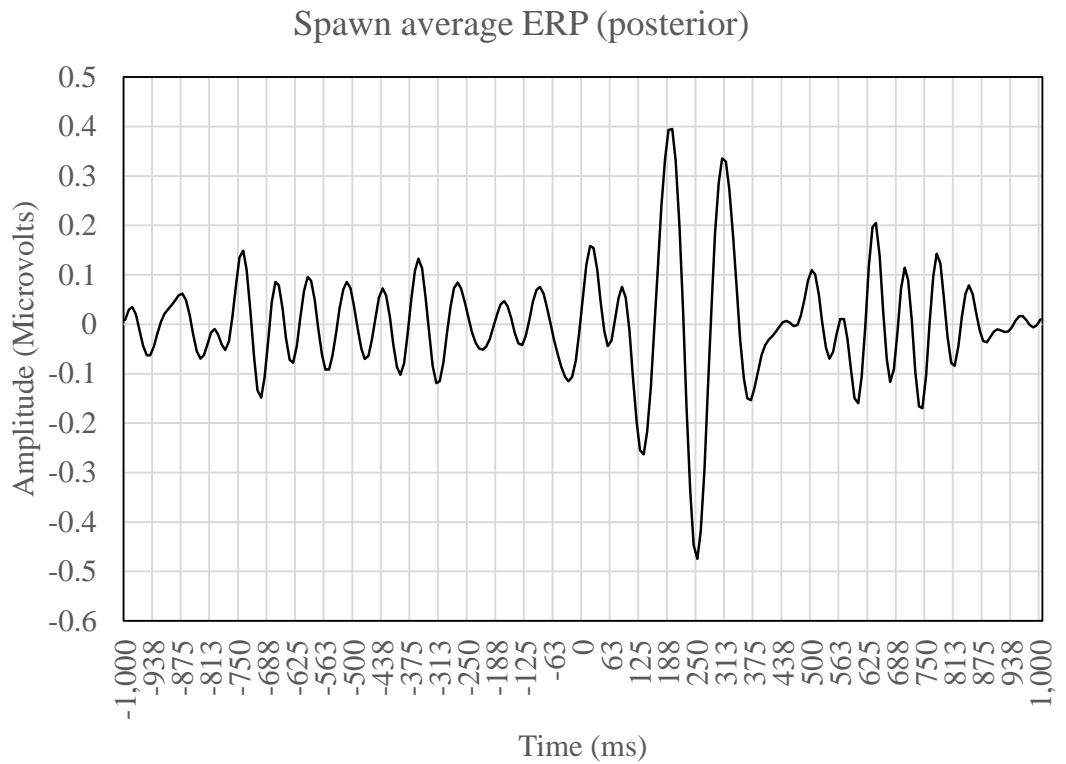
(b) The averaged ERP from the posterior group of electrodes at the spawn event.
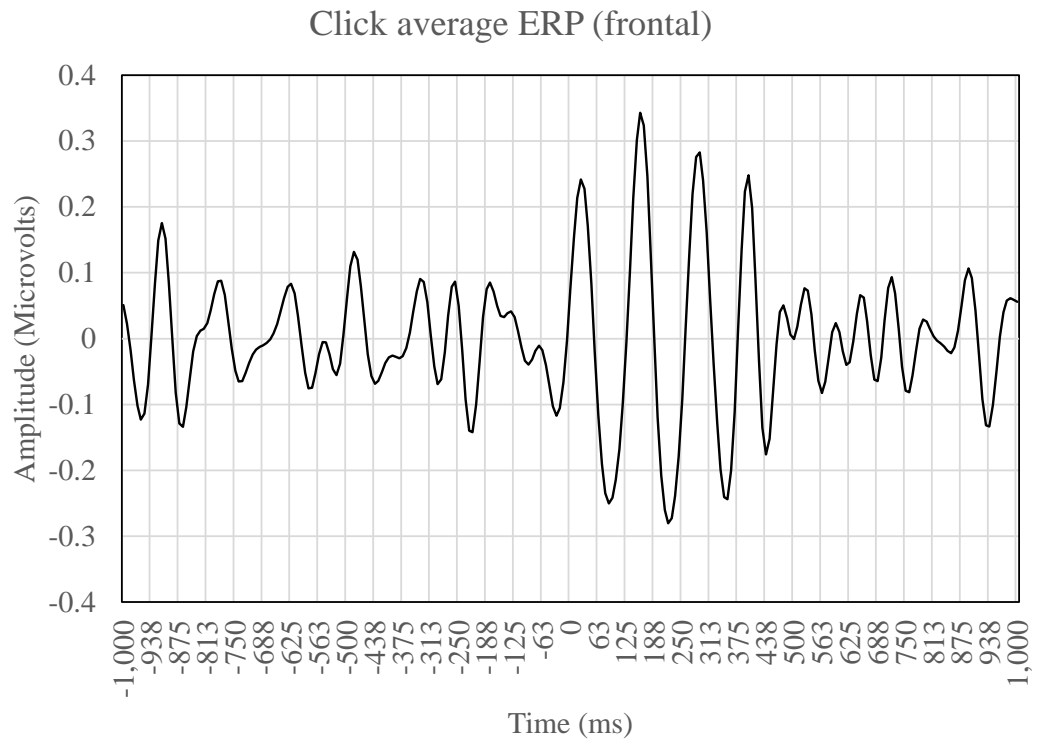
Click average ERP (frontal)

(c) The averaged ERP from the frontal group of electrodes at the click event.

Click average ERP (posterior)
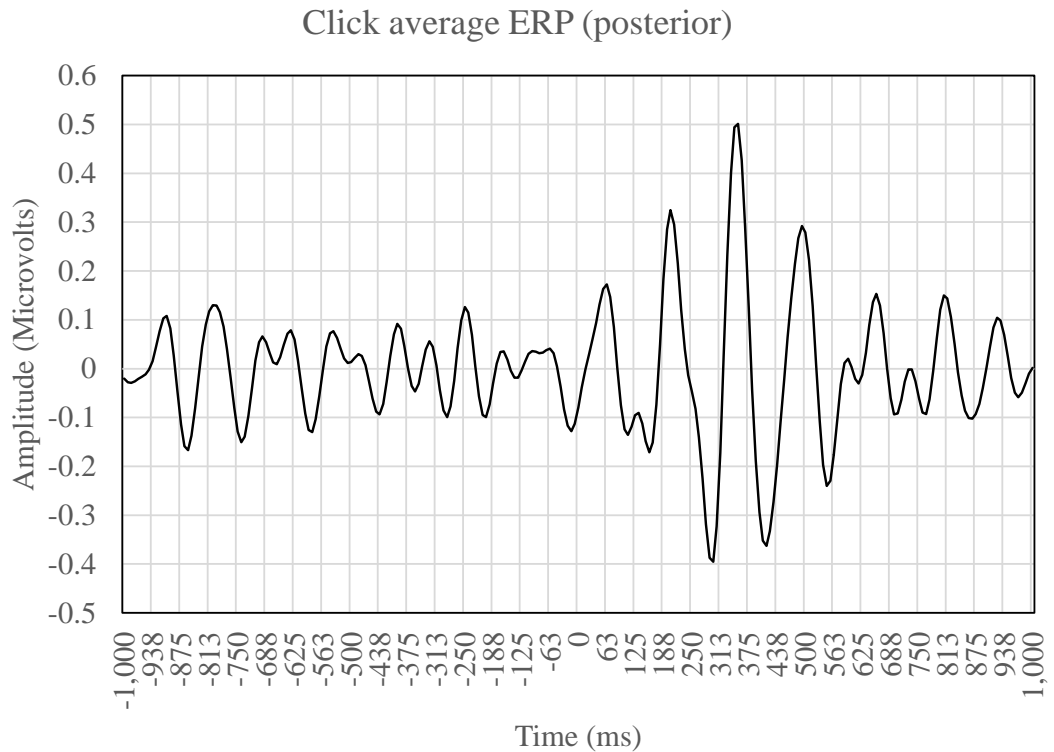
(d) The averaged ERP from the posterior group of electrodes at the click event.

Figure 6.43 The averaged ERP at the spawn and click events from the group of frontal and posterior electrodes.

6.7.5 Development of model of the human EEG brainwave in association with task performances

According to step 11 in Figure 6.10, the task patterns are sorted and separated into six sections one at a time by the particular performance criteria as shown in Figure 6.44. Table 6.14 shows the number of task patterns in each section when separates with performance criterion i.e. RT, MT, DT, MA, HA, and IP, respectively. It is noted that the separation is based solely on the value of performance criteria without the interpretation of the meaning of the value i.e. lower is better or higher is better. Therefore, the interpretation of the meaning of performance is needed after the model development.
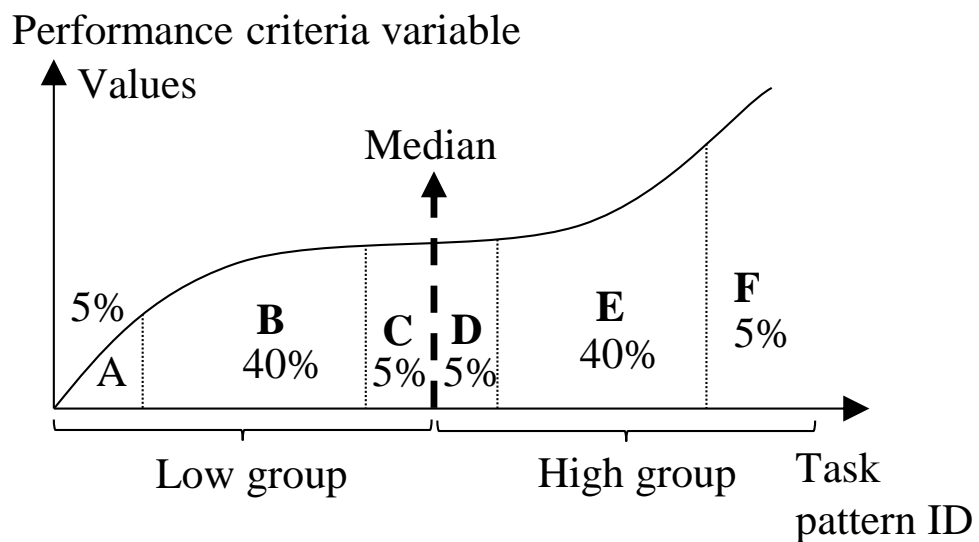
Figure 6.44 The separation of task patterns into six sections according to the performance variable.

Table 6.14 The number of task pattern in sections A, B, C, D, E, and F when separate with the particular performance variable.

Performance criteria variable	Number of task pattern in each section					
	A	B	C	D	E	F
RT	63	1126	64	63	1133	64
MT	63	1129	64	63	1130	64
DT	63	1127	64	63	1132	64
MA	63	1129	64	63	1130	64
HA	62	1122	63	63	1139	64
IP	63	1128	64	63	1131	64

According to step 14 of Figure 6.10, three areas of information are used for feature extraction i.e. local extremum, Fourier transform, and information from ERP analyses. A list of features from all three areas is shown in Table 6.15. Seven, two, and five of features are from local extremum, Fourier transform, and ERP analysis, respectively. It is noted that these features are calculated from the averaged ERP of frontal and posterior region for each single-trial of the EEG in each task pattern. Therefore, there are 28 features in total.

Table 6.15 The list of EEG features for the model development.

Frontal average EEG	Posterior average EEG
Local Extremum	
1. Number of peaks 2. Number of bottoms 3. Mean of peaks 4. Mean of bottoms 5. Standard deviation of peaks 6. Standard deviation of bottoms 7. Accumulated time different of peaks and bottoms	8. Number of peaks 9. Number of bottoms 10. Mean of peaks 11. Mean of bottoms 12. Standard deviation of peaks 13. Standard deviation of bottoms 14. Accumulated time different of peaks and bottoms
Fourier transform	
15. Averaged of 6 dominant frequencies (5% of sampling rate i.e. 128 Hz) 16. Averaged of power of the 6 dominant frequencies.	17. Averaged of 6 dominant frequencies (5% of sampling rate i.e. 128 Hz) 18. Averaged of power of the 6 dominant frequencies.
Information from ERP analyses	
19. Peak time of spawn ERP 20. Peak amplitude of spawn ERP 21. Peak time of click ERP 22. Peak amplitude of click ERP 23. (Peak time of click ERP) – (Peak time of spawn ERP)	24. Peak time of spawn ERP 25. Peak amplitude of spawn ERP 26. Peak time of click ERP 27. Peak amplitude of click ERP 28. (Peak time of click ERP) – (Peak time of spawn ERP)

Since there are 28 features in total which is a rather high dimensionality of feature space. The proposed 10-time-10-fold cross-validation requires a twice number of the input in order to train to locate the optimum number of hidden neurons. The PCA is applied in order to reduce the dimensionality of the original feature space as described in Section 2.8. Table 6.16 shows the percentages of principal component accountabilities to the original feature space range from

high to low. For example, the principal component PC1 can represent 31.46% of the whole 28 features. Therefore, the accumulated accountability from PC1 to PC28 is equal to 100%. Figure 6.45 shows the accumulated accountability percentages covered by the first 10 principal components to the 28 features. It shows that only 10 principal components can cover over 90% of the original features.

Therefore, a trade-off between percentages of coverage and number of principal components needs to be decided. The percentages of accountability for 7, 14, and 21 components are 82.94%, 97.03%, and 99.80%, respectively. According to the preliminary training of the 10-time-10-fold cross-validation for 1 time, it is shown that 7 principal components are sufficient. Furthermore, by selecting 7 principal components the maximum number of hidden neurons for training is 14 which are half the amount of hidden neurons compared to the case of 14 principal components.

Table 6.16 The percentages of variance explained for the 28 principal components (PC).

Percentages of variance explained for the 28 principal components (PC)						
PC1	**PC2**	**PC3**	**PC4**	**PC5**	**PC6**	**PC7**
31.46	23.95	9.84	5.83	4.38	3.99	3.49
PC8	**PC9**	**PC10**	**PC11**	**PC12**	**PC13**	**PC14**
3.17	2.73	2.47	2.06	1.39	1.20	1.08
PC15	**PC16**	**PC17**	**PC18**	**PC19**	**PC20**	**PC21**
0.80	0.61	0.52	0.31	0.26	0.16	0.09
PC22	**PC23**	**PC24**	**PC25**	**PC26**	**PC27**	**PC28**
0.08	0.06	0.03	0.02	0.01	0.00	0.00
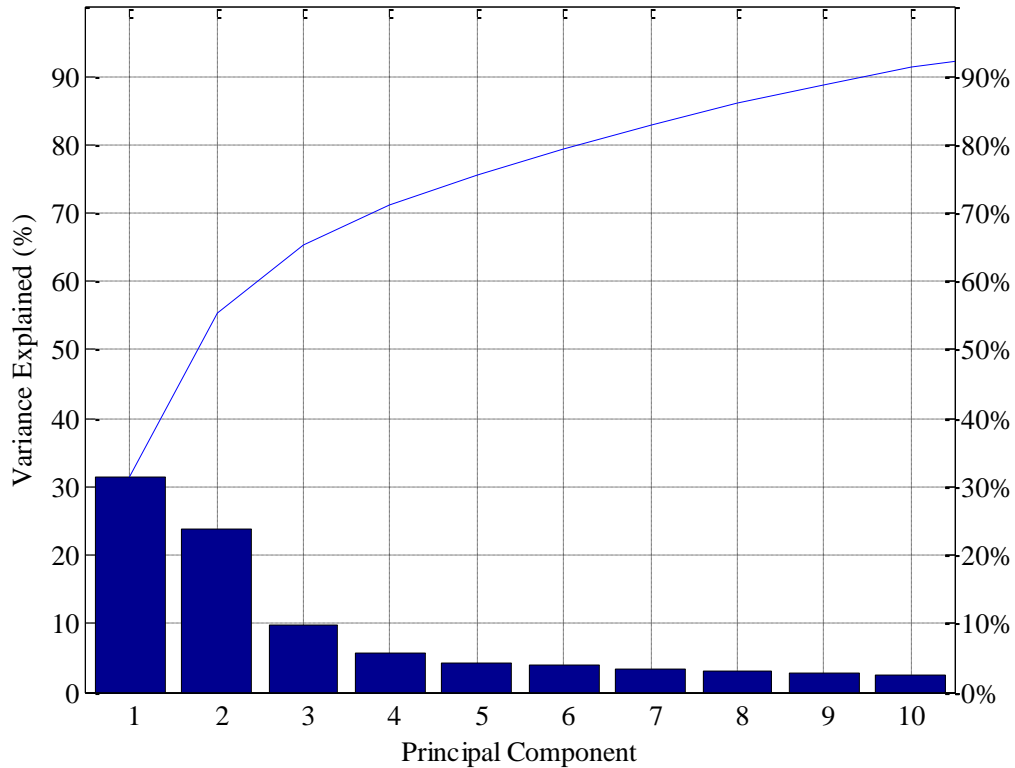
Figure 6.45 A plot of accountability percentages to the original feature space of the first 10 principal components.

6.7.5.1 <u>The modelling results</u>

The model development follows the process shown in Figure 3.11 of Section 3.4. There are six developed models i.e. the model based on each performance criteria – RT, MT, DT, MA, HA, and IP. Several of the modelling outputs are obtained during the development process. Hence, the summary of the result is presented first in this section. Then, the detailed outputs for each of the modelling process are given in Appendix I.1, I.2, I.3, I.4, I.5, and I.6 for RT, MT, DT, MA, HA, and IP, respectively.

The total running time for the 10-time-10-fold cross validation is 14.36 hours for all of the model training. Figure 6.46 shows total run times for each of the model. The average training time is 143.65 minutes. All of the models is trained with MATLAB pattern recognition neural network with a set of default training algorithms.
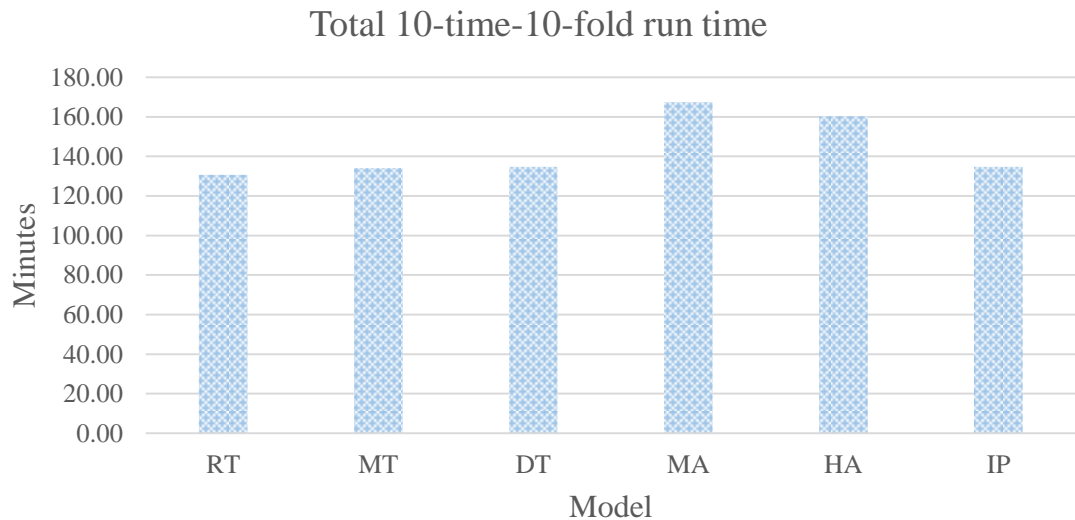
Figure 6.46 The total training run time for each model by applying the 10-time-10-fold cross validation.

Summary of the model development is shown in Table 6.17. The results can be referred to the steps in Figure 3.11. The second column of the table shows that the maximum training accuracy is 95.32% for the DT model whereas the worst is 66.56% for the HA model. All the training reaches maximum accuracy with the number of hidden neurons at twice the number of 7 principal component inputs i.e. 14 number of hidden neurons. However, the testing results are in contrast. The RT, DT, and MA models attain their best accuracy with a single hidden neuron with the accuracy of 59.87%, 85.73%, and 62.28%, respectively. The best testing accuracy is still with DT model at 91.95% which is dropped from the training by 3.37%. The worst testing remains with the HA model at 58.42%.

Table 6.17 The summary of the model development results.

| Performance indicator | Step 1 of Figure 3.11 (10-time-10-fold cross validation) | | | | Step 3 of Figure 3.11 | | Step 4 of Figure 3.11 | |
| | Best training | | Best testing | | Model training | | Blind test | |
	Acc (%)	Number of hidden neurons	Acc (%)	Number of hidden neurons	Acc (%)	AUC	Acc (%)	AUC
RT	67.01	14	59.87	1	60.3	0.63	58.3	0.59
MT	88.82	14	85.73	2	86.3	0.93	72.0	0.86
DT	95.32	14	91.95	1	92.1	0.98	74.0	0.88
MA	68.23	14	62.28	1	62.8	0.67	66.9	0.76
HA	66.56	14	58.42	8	63.2	0.69	60.7	0.62
IP	71.26	14	64.96	6	69.4	0.76	63.0	0.67
Average	76.2		70.53		72.35	0.77	65.81	0.73

According to step 2 of Figure 3.11, the best configuration for each model is located. Then, all of the training datasets is used to train the selected configuration i.e. number of hidden neurons. The result of the training accuracies is shown by the 3rd column of Table 6.17 along with the area under the curve (AUC) of ROC curve. The model training accuracies are improved by small percentages from the previous testing results. The most accurate model is the DT model with the accuracy of 92.1% and 0.98 of AUC.

After the models are trained, they are tested with the preserved blind test dataset. The results of the blind test are shown in the 4th column of Table 6.17. All of the blind testing accuracies is dropped from the model training except the MA model which gives an improvement by 4.1%.

The most accuracy drop is the DT model which is dropped by 18.1% from the model training accuracy. The second accuracy drop rate is the MT model at 14.3% while the rests are dropped by a small percentage of 2%, 2.5%, and 6.4% for RT, HA, and IP models, respectively. It is the indication of overtraining for the DT and MT models while the other models stay within the range of their training accuracy when applying to the unseen dataset.

Details of the results including the averaged classification accuracies from 10-time-10-fold cross-validation, confusion matrix, PR curve, and ROC curve from model training and blind testing for each of the model development is presented in the Appendix I.1, I.2, I.3, I.4, I.5, and I.6.

6.7.6 Evaluation of HMI performance based on the EEG brainwave

Once the six models are developed, they can be used to evaluate a task pattern performance based solely on the EEG brainwaves as mentioned at the end of Section 6.6. The diagram of the evaluation is shown in Figure 6.11. It can be noted that the models are developed by separating the data into two groups based on the value of the performance indicator. The meanings of model outcomes need to be interpreted for each of the performance indicators as shown in Table 6.18.

Table 6.18 Interpretation of the meaning of model outcomes.

Performance indicator	The interpretation of the model outcomes
RT	Class Low means high performance and vice versa
MT	Class Low means high performance and vice versa
DT	Class Low means high performance and vice versa
MA	Class Low means high performance and vice versa
HA	Class High means high performance and vice versa
IP	Class High means high performance and vice versa

The example of performance evaluation is shown in Table 6.19. It is noted that the table shows the converted interpretation of the outcomes of RT, MT, DT, and MA from 0 to 1 and vice versa. The outcomes of HA and IP remain the same as the classification model output. The values in the parenthesis of the task performance values are the median of each performance indicator. Cells of the table which are shaded with red colour mean that the outcome of the corresponding evaluation is incorrect according to the separation point at the median value.

Table 6.19 The example of performance evaluation using the six models.

P#E#S#T#	Evaluation of performance based on EEG brainwaves						Task performance values					
	RT	MT	DT	MA	HA	IP	RT (0.276)	MT (0.772)	DT (1.028)	MA (11.05)	HA (81.56)	IP (3.38)
P1E1S1T1	1	1	1	1	0	1	0.350	0.622	0.972	9.77	79.41	2.96
P1E1S1T2	0	1	0	1	0	0	0.345	0.848	1.193	16.58	75.67	2.41
P1E1S1T3	0	0	0	0	0	1	0.310	0.883	1.193	4.70	65.82	2.41
P1E1S1T4	0	1	1	1	1	0	0.255	0.655	0.910	5.32	83.03	3.16
P1E1S1T5	1	1	1	0	0	0	0.317	0.635	0.952	9.04	65.94	2.50
P2E2S8T14	1	1	1	1	0	1	0.270	0.430	0.700	8.25	58.82	5.16
P2E2S9T1	1	1	1	1	0	1	0.290	0.400	0.690	8.59	69.73	4.17
P2E2S9T2	1	1	1	1	0	1	0.280	0.370	0.650	19.43	71.36	4.43
P2E2S9T3	1	1	1	1	0	1	0.280	0.480	0.760	28.17	66.00	3.78
P2E2S9T4	1	1	1	1	0	1	0.220	0.400	0.620	15.35	56.73	4.64
P3E2S4T10	0	0	0	0	1	0	0.352	1.512	1.864	24.06	76.59	2.52
P3E2S4T11	0	0	0	0	1	0	0.007	1.601	1.608	14.03	89.80	2.92
P3E2S4T12	1	0	0	0	1	0	0.007	1.235	1.242	15.66	81.56	3.78
P3E2S4T13	0	0	0	0	1	0	0.255	0.918	1.173	6.32	77.64	3.08
P3E2S4T14	0	0	0	0	1	1	0.048	1.242	1.290	14.18	88.00	2.80
P4E1S10T7	1	1	1	0	0	0	0.048	0.869	0.917	35.81	80.00	3.74
P4E1S10T8	1	0	1	1	1	0	0.297	0.787	1.084	20.11	86.58	3.17
P4E1S10T9	0	0	0	0	0	0	0.393	1.063	1.456	26.65	67.44	3.22
P4E1S10T10	0	0	0	0	1	1	0.248	1.113	1.361	108.10	84.38	3.45
P4E1S10T11	1	0	0	0	0	0	0.296	0.780	1.076	46.55	62.42	4.36

6.8 Summary

This chapter has developed a novel human-machine performance evaluation method based on the human EEG brainwaves. A classic HMI scenario, target hitting task, is employed as a case study. The task is simple and allows the establishment of the relationship between the human EEG brainwaves and the task performance become possible with minimal disturbances. The task is designated with 14 task patterns where a participant performs the main interaction activity that is the movement of a mouse cursor to hit a target as fast and accurate as possible. The time course of a task pattern i.e. from target appear to target click, is where the establishment is taken into account. Since the performance of a task pattern is evaluated from the start of the target appearance until it is clicked by a mouse cursor. There are two main performance aspects in this type of task i.e. speed and accuracy which can be separated into more details including reaction time (RT), movement time (MT), duration time (DT), movement accuracy (MA), hit accuracy (HA), and the Fitts index of performance (IP). The establishment of the relationship between human EEG brainwaves and task performances is achieved by relating the six performance indicators to the features of the corresponding EEG signals. The models are obtained by utilising the model development methodology presented in Section 3.6 i.e. the descriptive modelling approach and the 10-time-10-fold cross-validation.

As a result, six models of task performance evaluation based solely on the EEG brainwaves are achieved. The six models are responsible for the evaluation of each aspect of the task performance. The averaged evaluation accuracy is 72.35%. The averaged evaluation accuracy when the models are applied to an unseen data is 65.81%. The overall accuracies are somewhat acceptable since it is rather challenging to establish the relationship between the human EEG brainwaves to the performances of the interaction. Furthermore, there exists a number of limitations i.e. the limitation of the number of electrodes, the limitation of the location of electrodes especially where the brain region is responsible for limbs movement. Likewise, there exist external factors other than the EEG brainwave that affects task performance e.g. other aspects of the brain processing, physical ergonomics, and spinal cord command mechanisms etc.

Chapter 7 Conclusion and future work

This chapter concludes the works completed in this research project that lead to the original contributions. Section 7.1 summarises the research in each aspect i.e. the literature review, the design and development, and the investigations. The summaries are described along with the fulfilment of the objectives presented in Chapter 1. Then, the detailed conclusions of the key investigations in this research are presented in Section 7.2 and Section 7.3. This research project has provided and improved the understanding of the author as a research student in many aspects, which can be summarised as the learning experiences in Section 7.4. Section 7.6 discusses on the known limitations and a list of future works are given in Section 7.7.

7.1 Summary of the research works

The works completed in this research project can be categorised into three parts i.e. the literature review, the design and development, the investigation and the analysis.

7.1.1 The literature review

A review of the state-of-the-art human interaction with the man-made systems has been completed. The review starts from the concept of HAM and spreads out to the related areas in order to identify / locate the gaps to improve the HAM research field. This part of the thesis can be considered as the fulfilment of Objective 1.

7.1.2 The design, development, and implementation of the HAM experimentation platform

- This research is based on a simulation because of several reasons discussed in the introduction of Chapter 3. Therefore, a HAM simulation platform has been developed to fulfil Objective 2 and is employed in all of the investigations in this research.

- The Emotiv EPOC EEG monitoring system is integrated into the HAM simulation platform for the acquisition of human brainwave simultaneously with the HMI scenarios. This expansion has been added to meet Objective 2 so that the platform can be used to conduct the experiments to fulfil Objective 5.

- The descriptive-predictive and 10-time-10-fold cross-validation model development procedures are adopted and modified to be used for the model development in this research. These parts of the research project are developed to fulfil Objective 4 and 5. The procedures are developed and applied in both the HMI control model and the performance evaluation model in Chapter 4 and Chapter 6, respectively.

- These simulation and experimentation scenarios are implemented to fulfil Objective 2.
  a. An inverted pendulum-driven capsule system i.e. the Model I and the Model II in Chapter 4.
  b. The scenarios for the EEG-based experimentation in Chapter 5.
  c. The target hitting task for the establishment of HMI performance evaluation models in Chapter 6.

7.1.3 The investigation and analysis

- The human heuristic learning control and the identification of control skills-rules-knowledge (SRK) and wisdom have been investigated in Chapter 4. This part of the investigation is conducted to fulfil Objective 3 and the outcome shows that a human follows the SRK with the addition of the wisdom i.e. the extension of the SRK.

- The establishment of human-machine control model that fulfils Objective 4 i.e. the understanding of a human from the machine side so that it can provide the appropriate assistance.

- The thesis establishes a novel HMI performance evaluation models based on the human brainwave. A target hitting task has been adopted to establish the relationship between HMI control performance and the human brainwave. This part of the research can be considered as the fulfilment of Objective 5. The concept of performance evaluation from the human brainwave from this research project could be applied to other research projects such as the adaptive adjustments of the computer game difficulty. This is the example of the application from one domain of knowledge to another.

7.2 Human-machine interaction heuristic learning and control model development

Two variations of a pendulum-driven cart pole / capsule system have been employed as a machine model for the investigation of HMI heuristic learning and control model development in Chapter 4.

From the investigation of a human heuristic learning and control in Section 4.2, it can be concluded that a human can learn to identify the control strategy of an unfamiliar machine mechanism i.e. the Model I, an underactuated pendulum-driven capsule system. A set of rules of the machine control strategy is developed during the learning stage. It is clear that this finding complies with the Fitts three stages of learning and the Rasmussen's model of SRK. The participant stays in the cognitive stage during the heuristic learning to identify the machine control mechanism. Then, the learning is transformed into the associative stage when the participant figures out the machine control mechanism. This phase of learning can be thought as the process of rules creation in the Rasmussen's SRK model. Skill is acquired during this phase of learning. The skill can be developed further by practising until the identified set of control actions becomes autonomous. These skills and rules are developed into the knowledge for the specific machine operation. The knowledge can be revolutionised and generalised into wisdom over time by applying the particular domain of knowledge into other domains.

In order to focus the study on the action of human learning and control on the inverted pendulum rotation strategy, Model I has been modified to Model II by the integration of a PID controller. Therefore, a human participant can concentrate on learning the rotation of an inverted pendulum to control the machine. The investigation with Model II has been conducted with nine human participants that provide the variations of the heuristic control and learning. As a result of the experiment, the nine participants show different characteristics of skill and strategy to control the machine e.g. high versus low oscillation of the pendulum, and the rotation range. The control characteristics and pendulum rotation profile may not be as perfect as the theoretical profile but a human can learn to identify the control strategy that can effectively produce a good performance outcome.

The control information in the investigation of Model II is further employed for the development of human-machine control model in Section 4.4. Two types of model are employed i.e. classification and regression models with the overall accuracies of 88.3% and 79.1%, respectively. The performance of the models is twofold confirmed by the plot of precision-recall and ROC curves. Furthermore, the obtained models are applied to an unseen dataset which is the blind testing process. The blind test accuracies are 92.2% and 77.01% for the classification and the regression models, respectively.

7.3 Human-machine interaction performance evaluation based on EEG brainwave

The Emotiv EPOC system has been integrated into the platform in order to simultaneously acquire the brainwave while a human participant performs the machine operation. The preliminary investigations with EEG are aimed to understand how the brain responds to a particular stimuli i.e. event-related potential (ERP) and to develop a workflow for the development of EEG-based performance evaluation models. Three preliminary investigations have been conducted which can be divided into two groups according to eyes opening conditions e.g. eyes closed, and eyes opened in Chapter 5. It can be concluded from the eyes closed investigation that the human EEG brainwave has the distinguishable responses to the stimulus e.g. the audio sound effect, and the voluntary limb movement. Moreover, the voluntary limb movements based experiment shows that the brain is activated on the opposite side of the limb movement which complies with the well-established knowledge of the human brain functions.

The preliminary study is extended to cope with eyes opened based experiment so that the workflow can be utilised in the actual HMI which essentially requires eyes to be opened during the interaction. A simple target hitting task is used to develop this pilot study. The eyes related artefacts can be removed systematically with the usage of the ICA. The ERP analysis from this pilot study shows that the human brain has a clear response when a target appears on the screen especially in the posterior region of the human brain. This region is responsible for visual processing.

In Chapter 6, a novel HMI performance evaluation model has been developed based on the features extracted from the human EEG brainwave. Six models are obtained for the six performance aspects of the target hitting task. The obtained models can be used for the prediction of operator performance that will be the guidance for the machine to provide the adaptive assistance based on the performance level.

7.4 The analysis of the chosen methods

The analysis of the chosen methods that proved to be justified is given below for each aspect.

7.4.1 The simulation

The simulation-based experimentation proves the following advantages to this research project.

- The simulation saves time and effort which allow the project to be completed in time. Moreover, the simulation unifies all of the investigations completed in this research i.e. the usage of the same environment throughout the research project.
- There is no harm to the participants with the simulation.
- Many simulation scenarios can be implemented to conduct the experiment.
- The data acquisition is convenient and effective.

7.4.2 The 10-time-10-fold cross-validation and the ANN

The limited number of dataset in this research can be problematic for the model development. However, the use of the 10-time-10-fold cross-validation can effectively utilise the dataset and can locate the best ANN model configuration because it repeatedly uses the data as explained in Section 3.6. The use of ANN in this research has proved that it can give relatively good modelling results with the case studies such as the inverted pendulum-driven capsule system and the human brainwave etc.

7.4.3 The electroencephalography brainwave monitoring system

The EEG has several advantages over the others as discussed in Section 2.13.2. This research mentions that the usage, preparation and maintenance of the EEG headset are the time-consuming process. However, it is less complicated than other brain monitoring systems. The obtained brainwave can be utilised straight away after the acquisition in the form of the computer file. Although the spatial resolution is not good, the temporal resolution is the great advantage to this research because the HMI usually uses time as the performance indicator e.g. time to react, time to complete the task etc.

7.5 Research as learning experiences

This section discusses some aspects that are learned from the research process that can be considered as the valuable experiences and knowledge.

7.5.1 Research area, scope, and focus

A research project ideally is based on the personal interest of the researcher or is generated by an organisation. A literature review is the fundamental stage that gives the exploration to the relevant area. Although it is common that the interesting literature in the research area would be attractive, the review needs to have a definite scope. It is necessary to have the focus and scope in mind so that the research project can be proceeded within the sensible period of time. The example from this research project is the multidisciplinary of the HAM. The literature review and the investigation would have easily strayed away from the focus and scope. There are many interesting literature such as machine learning methods, mathematical modelling of a machine and the simulation, the human behaviours, EEG, BCI etc.

7.5.2 Expansion of knowledge

A research project has to seek and open up to the ideas available in the related fields that would benefit to the focused area. This research starts from the HAM and expands to the related area

i.e. HRI, HSC, HAI, human intention recognition, model developments, human performance, human brainwave monitoring etc. However, the focus is maintained in the HAM area i.e. the HMI performance evaluation.

7.5.3 Know the limitations

A research project is usually bounded by some limitations such as time, resource, technical issue and budget etc. It is good to keep these limitations in mind. For example, one of the limitations of this research project is a simulation-based research that may not represent the real world situation. Furthermore, this research utilises a budget non-research-grade brainwave monitoring headset which may not give the best brainwave recording quality. The recruitment of the participants that is sometime rather difficult to access to a good sample that would represent the aimed population. The limitation of the computing resource such as the personal computer for the analysis and model development. To accelerate the research, the author uses two computers to run the analysis and model development while a laptop is used to produce the documentation simultaneously. Also, the dimensionality of the data is a considerable concern to the computing power / resource of a computer that would produce the result within the sensible computational time.

7.5.4 Time management

A good research project has to be completed within the allowed period of time. A well-defined scope, focus, and a plan of the research are the keys. A researcher would have the imagination and ambition to do a particular research. However, it is good to know the limitation of a given period of time and be reasonable for the width and the depth of the research investigations. In practical, it is needed to allocate spare times for the unforeseen circumstances e.g. the time for the administration activity, the time needed to collaborate with other people, the time for the recruitment of the sample participants, the time for the software and hardware problems etc.

7.5.5 Life and balance

It is a good practise to balance the amount of life activities such as doing a research, travelling and sightseeing, doing sports and exercises, having relaxation etc. Despite the health benefits of

doing an exercise such as running and playing football which is particularly the famous sports in the United Kingdom, these activities could help release some stresses during the intensive research activity and provide a refreshing mood to conduct a research. Moreover, during a running session, the brain is rather relaxed and there is time to think about the research problem that is being solved. This thinking might turn out to be the ultimate idea and solution of the research. Travelling and sightseeing could open up the state of mind and increase personal experiences that would benefit the research in some ways. For examples, the author thinks about the skills required to operate the car during a driving for the travelling. The skills to operate a car are different from the ability to drive carefully. Also, it does not mean that a driver has the knowledge about the traffic rules and locations etc.

7.6 Limitations in this research

- There is a known limitation of the spatial resolution of any hardware used to record the EEG brainwaves. The Emotiv EPOC has the capability to record 14 locations on the human scalp. Headsets with 256 or more electrodes are available in the market. However, these headsets are very expensive and require the wired connection rather than a wireless one which can be uncomfortable in many applications.

- The temporal resolution i.e. the sampling rate of the brainwave headset is another limitation of the research project. Although the Emotiv EPOC headset specification mentions an internal sampling rate of 256 Hz, it produces a data rate of 128 Hz only. The higher the sampling rate is, the more detail of the temporal resolution can be obtained from the recording which will be useful to produce more accurate analysis of the human brain activities.

- The use of scalp region i.e. frontal and posterior averaged brainwave may limit the spatial resolution which is already the main drawback of the EEG. However, the averaged method improves the temporal signal-to-noise ratio. This is the trade-off between the two choices i.e. spatial and temporal resolutions. This aspect may be improved in the future from the steady advancements in technology.

- The number of participants and gender i.e. male-female balance are limited because of time, effort, and ethical issues. For example, for the EEG brainwave based

investigations, a participant needs to agree to wear the headset which is moistened by saline solution. Furthermore, the investigation needs to be done in a quiet environment, takes long time to finish because of the headset preparation and the maintenance procedures during the experiment etc. However, Table 2.10 shows that the number of human participants which is 1-12 participants.

- This research adopts simulation as the primary HMI activity which may not give fully realistic situation.

7.7 Future works

A list of possible future works that can be investigated further from this research project is given below.

- An EEG headset with more electrodes and higher sampling rate could be used. Especially, the electrodes around the central area of the human scalp which are responsible for limb movements. However, the increased number of electrodes would introduce the complexity in both the acquisition and the analysis processes e.g. complexity of the headset wirings, more sensors to be moistened, more computational power etc.

- It is challenging to establish the relationship between the operation performance and the brain activity i.e. the EEG brainwaves. It might be a good idea to include another equipment to read muscle activity, spinal cord activity etc. Then, the knowledge of these muscle and spinal cord activities could be used to discover the understanding of the relationship among the brain, muscle, and spinal cord activities.

- Some other available machine learning and model development methods such as the SVM, the Genetic algorithms, and the artificial immune system etc. could be applied to make a comparison among them.

- This research project has focused on a primitive HMI task i.e. the target hitting task. It would be a good idea to extend to the other types / more complicated types of task e.g. a pendulum balancing task, a task based on the decision making etc.

- A future investigation based on a physical machine may give the more realistic HMI. However, the physical HMI may introduce some safety issues, complexities in the research procedure, efforts and time to conduct a research etc.
- A future work could increase the number of participants with the balance between the two genders i.e. male-female which may improve the investigation results.
- This research project has focused on the performance evaluation part of the HAM concept. A future work could concentrate on a closed loop HAM adaptive machine i.e. the intention recognition, the performance evaluation, and the adaptive assistance.
- A static design of the computer game difficulty may introduce boredom / anxiety to a player. The concept of the HAM adaptive machine especially the performance evaluation could be applied to make a more challenging computer game.

References

[1]   E. D. Lello, A. Loutfi, F. Pecora, and A. Saffiotti, "Robotic Furniture in a Smart Environment: The PEIS Table," in *Workshops Proceedings of the 5th International Conference on Intelligent Environments*, Barcelona, Spain, 2009, pp. 185–192.

[2]   O. Lemaire, K. Ohba, and S. Hirai, "Dynamic Integration of Ubiquitous Robotic Systems through Capability Model Processing," in *SICE-ICASE, 2006. International Joint Conference*, Busan, South Korea, 2006, pp. 1207–1211.

[3]   E. Guizzo and T. Deyle, "Robotics Trends for 2012," *IEEE Robot. Autom. Mag.*, vol. 19, no. 1, pp. 119–123, Mar. 2012.

[4]   E. Sofge, "Reengineering the Human," *Popular Mechanics*, p. 62, May-2012.

[5]   K. Samarnggoon, "An Analysis of Game Design Using Graph-based Substructure Mining Technique," presented at the 2011 3rd IEEE International Conference on Computer Research and Development, Shanghai, China, 2011, vol. 1, pp. 368–372.

[6]   J. Nakamura and M. Csikszentmihalyi, "The concept of flow," in *Flow and the Foundations of Positive Psychology*, Springer, 2014, pp. 239–263.

[7]   K. Samarnggoon, S. Cang, H. Yu, M. S. Hasan, and T. Flämig, "Human Skill Performance to Control an Underactuated Pendulum-Driven Capsule System," in *Control (CONTROL), 2014 UKACC International Conference on*, Loughborough, United Kingdom, 2014, pp. 731–736.

[8]   K. Samarnggoon and H. Yu, "Real time Virtual Simulation of an Underactuacted Pendulum-Driven Capsule System," in *Control (CONTROL), 2012 UKACC International Conference on*, Cardiff, United Kingdom, 2012, vol. 2012, pp. 568–573.

[9]   T. B. Sheridan and R. Parasuraman, "Human-Automation Interaction," *Rev. Hum. Factors Ergon.*, vol. 1, no. 1, pp. 89–129, Jun. 2005.

[10]   J. M. Hoc, "From human–machine interaction to human–machine cooperation," *Ergonomics*, vol. 43, no. 7, pp. 833–843, Jul. 2000.

[11]   D. J. Feil-Seifer and M. J. Matarić, "Human-Robot Interaction," in *Encyclopedia of Complexity and Systems Science*, R. A. Meyers, Ed. Springer New York, 2009, pp. 4643–4659.

[12]   S. Suzuki, "Human Adaptive Mechatronics," *Ind. Electron. Mag. IEEE*, vol. 4, no. 2, pp. 28–35, Jun. 2010.

[13]   O. E. Dictionary, *Oxford: Oxford university press*. 1989.

[14] S. Suzuki, K. Furuta, and F. Harashima, "Overview of Human Adaptive Mechatronics and Assist-control to Enhance Human's Proficiency," in *Proceeding of the International Conference on Control, automation, and systems*, Gyeong Gi, South Korea, 2005, pp. 2–5.

[15] S. Suzuki, H. Igarashi, H. Kobayashi, T. Yasuda, and F. Harashima, "Human Adaptive Mechatronics and Human-System Modelling," *Int. J. Adv. Robot. Syst.*, vol. 10, no. 152, Mar. 2013.

[16] S. Suzuki, F. Harashima, and K. Furuta, "Human Control Law and Brain Activity of Voluntary Motion by Utilizing a Balancing Task with an Inverted Pendulum," *Adv. Hum.-Comput. Interact.*, vol. 2010, 2010.

[17] H. Yu, "Guest Editorial," *Proc. Inst. Mech. Eng. Part J. Syst. Control Eng.*, vol. 225, no. 6, pp. 705–708, 2011.

[18] H. Yu, H. Inaba, D. H. Owens, and K. Furuta, "Editorial," *Int. J. Model. Identif. Control*, vol. 4, no. 4, pp. 299–303, 2008.

[19] H. Yu, "Overview of Human Adaptive Mechatronics," in *Proceedings of the 9th WSEAS International Conference on Mathematics & Computers In Business and Economics*, Bucharest, Romania, 2008, pp. 152–157.

[20] F. Harashima and S. Suzuki, "Human Adaptive Mechatronics-Interaction and Intelligence," in *Advanced Motion Control, 2006. 9th IEEE International Workshop on*, Istanbul, Turkey, 2006, pp. 1–8.

[21] J. Casper and R. R. Murphy, "Human-robot interactions during the robot-assisted urban search and rescue response at the world trade center," *Syst. Man Cybern. Part B Cybern. IEEE Trans. On*, vol. 33, no. 3, pp. 367–385, Jun. 2003.

[22] R. R. Murphy, "Human-Robot Interaction in Rescue Robotics," *Syst. Man Cybern. Part C Appl. Rev. IEEE Trans. On*, vol. 34, no. 2, pp. 138–153, May 2004.

[23] J. L. Burke and R. R. Murphy, "Human-robot interaction in USAR technical search: Two heads are better than one," in *Robot and Human Interactive Communication, 2004. ROMAN 2004. 13th IEEE International Workshop on*, Okayama, Japan, 2004, pp. 307–312.

[24] T. Linder, V. Tretyakov, S. Blumenthal, P. Molitor, D. Holz, R. Murphy, S. Tadokoro, and H. Surmann, "Rescue robots at the Collapse of the municipal archive of Cologne City: A field report," in *Safety Security and Rescue Robotics (SSRR), 2010 IEEE International Workshop on*, Bremen, Germany, 2010, pp. 1–6.

[25] M. A. Goodrich and A. C. Schultz, "Human-Robot Interaction: A Survey," *Found. Trends Hum.-Comput. Interact.*, vol. 1, no. 3, pp. 203–275, Feb. 2007.

[26] J. Forlizzi and C. DiSalvo, "Service robots in the domestic environment: a study of the roomba vacuum in the home," in *Proceedings of the 1st ACM SIGCHI/SIGART conference on Human-robot interaction*, Salt Lake City, Utah, 2006, pp. 258–265.

[27] M. K. O'Malley, A. Gupta, M. Gen, and Y. Li, "Shared Control in Haptic Systems for Performance Enhancement and Training," *Trans.-Am. Soc. Mech. Eng. J. Dyn. Syst. Meas. Control*, vol. 128, no. 1, pp. 75–85, 2006.

[28] M. Mulder, D. A. Abbink, and E. R. Boer, "Sharing Control With Haptics: Seamless Driver Support From Manual to Automatic Control," *Hum. Factors J. Hum. Factors Ergon. Soc.*, vol. 54, no. 5, pp. 786–798, Oct. 2012.

[29] J. D. Haynes and G. Rees, "Decoding mental states from brain activity in humans," *Nat. Rev. Neurosci.*, vol. 7, no. 7, pp. 523–534, Jul. 2006.

[30] J. D. Haynes, K. Sakai, G. Rees, S. Gilbert, C. Frith, and R. E. Passingham, "Reading Hidden Intentions in the Human Brain," *Curr. Biol.*, vol. 17, no. 4, pp. 323–328, Feb. 2007.

[31] J. D. Haynes, "Decoding and predicting intentions," *Ann. N. Y. Acad. Sci.*, vol. 1224, no. 1, pp. 9–21, Apr. 2011.

[32] M. Matsuhashi and M. Hallett, "The timing of the conscious intention to move," *Eur. J. Neurosci.*, vol. 28, no. 11, pp. 2344–2351, Dec. 2008.

[33] S. J. Blakemore and J. Decety, "From the perception of action to the understanding of intention," *Nat. Rev. Neurosci.*, vol. 2, no. 8, pp. 561–567, Aug. 2001.

[34] T. Sato, Y. Nishida, J. Ichikawa, Y. Hatamura, and H. Mizoguchi, "Active Understanding of Human Intention by a Robot through Monitoring of Human Behavior," in *Intelligent Robots and Systems' 94.'Advanced Robotic Systems and the Real World', IROS'94. Proceedings of the IEEE/RSJ/GI International Conference on*, Munich, Germany, 1994, vol. 1, pp. 405–414.

[35] V. Fernandez, C. Balaguer, D. Blanco, and M. A. Salichs, "Active Human-Mobile Manipulator Cooperation Through Intention Recognition," in *Robotics and Automation, 2001. Proceedings 2001 ICRA. IEEE International Conference on*, Seoul, South Korea, 2001, vol. 3, pp. 2668–2673.

[36] W. Yu, R. Alqasemi, R. Dubey, and N. Pernalete, "Telemanipulation Assistance Based on Motion Intention Recognition," in *Robotics and Automation, 2005. ICRA 2005. Proceedings of the 2005 IEEE International Conference on*, Barcelona, Spain, 2005, pp. 1121–1126.

[37] S. Ekvall, D. Aarno, and D. Kragic, "Online Task Recognition and Real-Time Adaptive Assistance for Computer-Aided Machine Control," *Robot. IEEE Trans. On*, vol. 22, no. 5, pp. 1029–1033, Oct. 2006.

[38] D. Aarno and D. Kragic, "Layered HMM for Motion Intention Recognition," in *Intelligent Robots and Systems, 2006 IEEE/RSJ International Conference on*, Beijing, China, 2006, pp. 5130–5135.

[39] D. Aarno and D. Kragic, "Motion intention recognition in robot assisted applications," *Robot. Auton. Syst.*, vol. 56, no. 8, pp. 692–705, Aug. 2008.

[40] C. Zhu, Q. Cheng, and W. Sheng, "Human Intention Recognition in Smart Assisted Living Systems Using A Hierarchical Hidden Markov Model," in *Automation Science and Engineering, 2008. CASE 2008. IEEE International Conference on*, Washington DC, 2008, pp. 253–258.

[41] S. Suzuki and F. Harashima, "Bayesian Intention Estimator using Self-Organizing Map and its Experimental Verification," in *RO-MAN, 2010 IEEE*, Viareggio, Italy, 2010, pp. 270–275.

[42] S. Suzuki and F. Harashima, "Context-aware Bayesian intention estimator using Self-Organizing Map and Petri net," in *RO-MAN, 2011 IEEE*, Atlanta, GA, 2011, pp. 314–320.

[43] S. Suzuki and F. Harashima, "Estimation Algorithm of Machine Operational Intention by Bayes Filtering with Self-Organizing Map," *Adv. Hum.-Comput. Interact.*, vol. 2012, pp. 1–20, 2012.

[44] S. Suzuki and F. Harashima, "Estimation of operational intentions utilizing Self-Organizing Map with Bayes filtering," in *Intelligent Robots and Systems (IROS), 2010 IEEE/RSJ International Conference on*, Taipei, Taiwan, 2010, pp. 2249–2255.

[45] S. Suzuki and F. Harashima, "Segmentation and analysis of console operation using self-organizing map with cluster growing method," in *Intelligent Robots and Systems, 2009. IROS 2009. IEEE/RSJ International Conference on*, St. Louis, MO, 2009, pp. 4875–4880.

[46] K. Furuta, Y. Kado, S. Shiratori, and S. Suzuki, "Assisting control for pendulum-like juggling in human adaptive mechatronics," *Proc. Inst. Mech. Eng. Part J. Syst. Control Eng.*, vol. 225, no. 6, pp. 709–720, Sep. 2011.

[47] Y. Kado, Y. Pan, and K. Furuta, "Control System for Skill Acquisition-Balancing Pendulum based on Human Adaptive Mechatronics," in *Systems, Man and Cybernetics, 2006. SMC'06. IEEE International Conference on*, Taipei, Taiwan, 2006, vol. 5, pp. 4040–4045.

[48] A. J. Koivo and D. W. Repperger, "Effects of force feedback on operator's skills in tele-operated systems," in *American Control Conference, 1998. Proceedings of the 1998*, Philadelphia, PA, 1998, vol. 1, pp. 447–449.

[49] A. M. Okamura, C. Richard, and M. R. Cutkosky, "Feeling is Believing: Using a Force-Feedback Joystick to Teach Dynamic Systems," *J. Eng. Educ.*, vol. 91, no. 3, pp. 345–349, Jul. 2002.

[50] A. M. Okamura, L. N. Verner, T. Yamamoto, J. C. Gwilliam, and P. G. Griffiths, "Force Feedback and Sensory Substitution for Robot-Assisted Surgery," in *Surgical Robotics : Systems Applications and Visions*, J. Rosen, B. Hannaford, and R. M. Satava, Eds. Springer US, 2011, pp. 419–448.

[51] K. Tervo and A. Rohilla, "Recursive Tuning Algorithm for Assist Controller of a Trolley Crane System," in *Applied Machine Intelligence and Informatics (SAMI), 2011 IEEE 9th International Symposium on*, Smolenice, Slovakia, 2011, pp. 61–66.

[52] K. Tervo, "Human Adaptive Mechatronics Methods for Mobile Working Machines," Doctoral dissertation, Department of Automation and Systems Technology, Aalto University, School of Science and Technology, Espoo, Finland, 2010.

[53] J. C. Huegel and M. K. O'Malley, "Progressive Haptic and Visual Guidance for Training in a Virtual Dynamic Task," in *Haptics Symposium, 2010 IEEE*, Waltham, MA, 2010, pp. 343–350.

[54] R. Groten, D. Feth, R. L. Klatzky, and A. Peer, "The Role of Haptic Feedback for the Integration of Intentions in Shared Task Execution," *Haptics IEEE Trans. On*, vol. 6, no. 1, pp. 94–105, 2013.

[55] P. F. Dominey and F. Warneken, "The basis of shared intentions in human and robot cognition," *New Ideas Psychol.*, vol. 29, no. 3, pp. 260–274, Dec. 2011.

[56] D. A. Abbink, D. Cleij, M. Mulder, and M. M. van Paassen, "The Importance of Including Knowledge of Neuromuscular Behaviour in Haptic Shared Control," in *Systems, Man, and Cybernetics (SMC), 2012 IEEE International Conference on*, Seoul, South Korea, 2012, pp. 3350–3355.

[57] D. A. Abbink, M. Mulder, and E. R. Boer, "Haptic shared control: smoothly shifting control authority?," *Cogn. Technol. Work*, vol. 14, no. 1, pp. 19–28, Mar. 2012.

[58] D. A. Abbink and M. Mulder, "Neuromuscular Analysis as a Guideline in designing Shared Control," in *Advances in Haptics*, vol. 109, M. H. Zadeh, Ed. 2010, pp. 499–516.

[59] D. B. Chaffin, "Digital Human Modeling for Workspace Design," *Rev. Hum. Factors Ergon.*, vol. 4, no. 1, pp. 41–74, Oct. 2008.

[60] G. Johannsen and E. A. Averbukh, "Human Performance Models in Control," in *Systems, Man and Cybernetics, 1993. "Systems Engineering in the Service of Humans", Conference Proceedings., International Conference on*, Le Touquet, France, 1993, vol. 4, pp. 397–402.

[61] S. Baron, D. S. Kruser, and B. M. Huey, *Quantitative Modeling of Human Performance in Complex, Dynamic Systems*. Washington DC: The National Academies Press, 1990.

[62] G. Wulf, *Attention and motor skill learning*. Human Kinetics, 2007.

[63] M. D. Robb, *The dynamics of motor-skill acquisition*. New Jersey: Prentice Hall, 1972.

[64] W. H. Edwards, *Motor Learning and Control: From Theory to Practice*, 1st ed. Cengage Learning, 2011.

[65] C. D. Wickens and J. G. Hollands, *Engineering Psychology and Human Performance*, 3rd ed. New Jersey: Prentice Hall, 1999.

[66] J. Annett and H. Kay, "'Skilled performance.,'" *Occup. Psychol.*, 1956.

[67] D. Araújo and K. Davids, "What Exactly is Acquired During Skill Acquisition?," *J. Conscious. Stud.*, vol. 18, no. 3–4, pp. 7–23, 2011.

[68] P. M. Fitts and M. I. Posner, *Human performance*. Belmont, CA: Brooks/Cole, 1967.

[69] P. M. Fitts, "The Information Capacity of the Human Motor System in Controlling the Amplitude of Movement," *J. Exp. Psychol.*, vol. 47, no. 6, pp. 381–391, Jun. 1954.

[70] R. W. Soukoreff and I. S. MacKenzie, "Towards a standard for pointing device evaluation, perspectives on 27 years of Fitts' law research in HCI," *Int. J. Hum.-Comput. Stud.*, vol. 61, no. 6, pp. 751–789, Dec. 2004.

[71] I. S. MacKenzie, "Fitts' Law as a Research and Design Tool in Human-Computer Interaction," *Hum.-Comput. Interact.*, vol. 7, no. 1, pp. 91–139, Mar. 1992.

[72] J. Rasmussen, "Skills, Rules, and Knowledge; Signals, Signs, and Symbols, and Other Distinctions in Human Performance Models," *Syst. Man Cybern. IEEE Trans. On*, vol. 13, no. 3, pp. 257–266, 1983.

[73] K. Furukawa, S. Igarashi, K. Ueno, T. Ozaki, S. Morita, N. Tamagawa, T. Okuyama, and I. Kobayashi, "Modeling Human Skill in Bayesian Network," *Linkop. Electron. Artic. Comput. Inf. Sci.*, vol. 7, p. 012, 2002.

[74] G. A. Miller, "The Magical Number Seven, Plus or Minus Two: Some Limits on Our Capacity for Processing Information," *Psychol. Rev.*, vol. 63, no. 2, pp. 81–97, Mar. 1956.

[75] T. Parthornratt, R. M. Parkin, and M. Jackson, "Human performance index – a generic performance indicator," *Proc. Inst. Mech. Eng. Part J. Syst. Control Eng.*, vol. 225, no. 6, pp. 721–734, Sep. 2011.

[76] K. Gold, "An Information Pipeline Model of Human-Robot Interaction," in *Proceedings of the 4th ACM/IEEE international conference on Human robot interaction*, La Jolla, CA, 2009, pp. 85–92.

[77] H. B. Meieran, "Mobile robots for the nuclear industry-A 1990 status report," *Trans. Am. Nucl. Soc. States*, vol. 62, no. CONF-901101–, pp. 599–600, 1990.

[78] H. Martins and R. Ventura, "Immersive 3-D teleoperation of a search and rescue robot using a head-mounted display," in *Emerging Technologies & Factory Automation, 2009. ETFA 2009. IEEE Conference on*, Mallorca, Spain, 2009, pp. 1–8.

[79] J. Zhou, X. Shen, and N. D. Georganas, "Haptic Tele-Surgery Simulation," in *Haptic, Audio and Visual Environments and Their Applications, 2004. HAVE 2004. Proceedings. The 3rd IEEE International Workshop on*, 2004, pp. 99–104.

[80] P. R. Liu, M. Q. H. Meng, F. F. L. Tong, X. J. Chen, and P. X. Liu, "A 3G based Network Solution to the Telehealthcare Robotic System," in *Intelligent Control and Automation, 2006. WCICA 2006. The Sixth World Congress on*, Dalian, China, 2006, vol. 1, pp. 381–385.

[81] D. Ryu, S. Kang, M. Kim, and J. Song, "Multi-modal user interface for teleoperation of ROBHAZ-DT2 field robot system," in *Intelligent Robots and Systems, 2004.(IROS 2004). Proceedings. 2004 IEEE/RSJ International Conference on*, Seoul, South Korea, 2004, vol. 1, pp. 168–173.

[82] D. D. Ray and M. Singh, "Development of a force reflecting Tele-robot for remote handling in nuclear installations," in *Applied Robotics for the Power Industry (CARPI), 2010 1st International Conference on*, Montreal, QC, Canada, 2010, pp. 1–6.

[83] M. Chacin, E. Rohmer, A. Mora, and K. Yoshida, "A High Level Teleoperation Platform for Space Robotic Missions," in *Space Mission Challenges for Information Technology, 2006. SMC-IT 2006. Second IEEE International Conference on*, Pasadena, CA, 2006, vol. 2006, p. 7 pp.

[84] E. Stoll, J. Letschnik, U. Walter, J. Artigas, P. Kremer, C. Preusche, and G. Hirzinger, "On-orbit servicing," *Robot. Autom. Mag. IEEE*, vol. 16, no. 4, pp. 29–33, Dec. 2009.

[85] A. Birk, N. Vaskevicius, K. Pathak, S. Schwertfeger, J. Poppinga, and H. Buelow, "3-D perception and modeling," *Robot. Autom. Mag. IEEE*, vol. 16, no. 4, pp. 53–60, Dec. 2009.

[86] L. Pedersen, D. Kortenkamp, D. Wettergreen, and I. Nourbakhsh, "A Survey of Space Robotics," in *Proceedings of the 7th International Symposium on Artificial Intelligence, Robotics and Automation in Space*, Nara, Japan, 2003, pp. 19–23.

[87] C. C. Chang, J. H. Wang, C. C. Lin, M. Der Jeng, C. Y. Chang, C. C. Wu, W. C. Hsu, C. C. Lee, and B. L. Fang, "The study of remotely teleoperated robotic manipulator system for underwater construction," in *Underwater Technology, 2004. UT'04. 2004 International Symposium on*, Taipei, Taiwan, 2004, pp. 269–276.

[88] E. Papadopoulos, E. Apostolopoulos, and P. Tsigkourakos, "Design, control, and experimental performance of a teleoperated robotic fish," in *Control and Automation, 2009. MED'09. 17th Mediterranean Conference on*, Thessaloniki, Greece, 2009, pp. 766–771.

[89] Y. Lu, T. Jin, L. Liu, and C. Yang, "Over-the-horizon teleoperation system for underground unmanned LHD," in *Mechatronics and Automation (ICMA), 2011 International Conference on*, Beijing, China, 2011, pp. 1804–1809.

[90] C. D. Onal, C. Pawashe, and M. Sitti, "A scaled bilateral control system for experimental 1-D teleoperated nanomanipulation applications," in *Intelligent Robots and Systems, 2007. IROS 2007. IEEE/RSJ International Conference on*, San Diego, CA, 2007, pp. 483–488.

[91] E. Vander Poorten, T. Kanno, and Y. Yokokohji, "Robust variable-scale bilateral control for micro teleoperation," in *Robotics and Automation, 2008. ICRA 2008. IEEE International Conference on*, Pasadena, CA, 2008, pp. 655–662.

[92] A. Bolopion, B. Cagneau, and S. Régnier, "2D micro teleoperation with force feedback," in *Intelligent Robots and Systems, 2009. IROS 2009. IEEE/RSJ International Conference on*, St. Louis, MO, 2009, pp. 3265–3270.

[93] A. Bolopion, H. Xie, D. S. Haliyo, and S. Régnier, "3D haptic handling of microspheres," in *Intelligent Robots and Systems (IROS), 2010 IEEE/RSJ International Conference on*, Taipei, Taiwan, 2010, pp. 6131–6136.

[94] N. Xiao and S. Guo, "Control modeling of a micro-manipulator for human scale tele-operation system," in *Intelligent Robots and Systems (IROS), 2010 IEEE/RSJ International Conference on*, Taipei, Taiwan, 2010, pp. 6125–6130.

[95] T. Kosugi and S. Katsura, "Experimental investigation of variable scaled bilateral control," in *Human System Interactions (HSI), 2011 4th International Conference on*, Yokohama, Japan, 2011, pp. 250–255.

[96] M. Mehrtash, N. Tsuda, and M. B. Khamesee, "Bilateral Macro-Micro Teleoperation Using Magnetic Levitation," *Mechatron. IEEEASME Trans. On*, vol. 16, no. 3, pp. 459–469, Jun. 2011.

[97] T. Fong and C. Thorpe, "Vehicle Teleoperation Interfaces," *Auton. Robots*, vol. 11, no. 1, pp. 9–18, Jul. 2001.

[98] P. Arcara and C. Melchiorri, "Control schemes for teleoperation with time delay: A comparative study," *Robot. Auton. Syst.*, vol. 38, no. 1, pp. 49–64, Jan. 2002.

[99] C. Melchiorri, "Robotic telemanipulation systems: An overview on control aspects," in *Proceedings of the 7th IFAC Symposium on Robot Control*, Wrocław, Poland, 2003, vol. 1, pp. 707–716.

[100] P. F. Hokayem and M. W. Spong, "Bilateral teleoperation: An historical survey," *Automatica*, vol. 42, no. 12, pp. 2035–2057, Dec. 2006.

[101] J. H. Hwang, R. C. Arkin, and D. S. Kwon, "Mobile robots at your fingertip: Bezier curve on-line trajectory generation for supervisory control," in *Intelligent Robots and Systems, 2003.(IROS 2003). Proceedings. 2003 IEEE/RSJ International Conference on*, Las Vegas, 2003, vol. 2, pp. 1444–1449.

[102] D. Labonte, P. Boissy, and F. Michaud, "Comparative Analysis of 3D Robot Teleoperation Interfaces with Novice Users," *Syst. Man Cybern. Part B Cybern. IEEE Trans. On*, vol. 40, no. 5, pp. 1331–1342, Oct. 2010.

[103] D. Balakrishna, P. V. Sailaja, R. V. V. Prasad Rao, and B. Indurkhya, "A novel human robot interaction using the Wiimote," in *Robotics and Biomimetics (ROBIO), 2010 IEEE International Conference on*, Tianjin, China, 2010, pp. 645–650.

[104] V. Frati and D. Prattichizzo, "Using Kinect for hand tracking and rendering in wearable haptics," in *World Haptics Conference (WHC), 2011 IEEE*, Istanbul, Turkey, 2011, pp. 317–321.

[105] E. S. Santos, E. A. Lamounier, and A. Cardoso, "Interaction in Augmented Reality Environments Using Kinect," in *Virtual Reality (SVR), 2011 XIII Symposium on*, Uberlândia, MG, Brazil, 2011, pp. 112–121.

[106] S. Waldherr, R. Romero, and S. Thrun, "A Gesture Based Interface for Human-Robot Interaction," *Auton. Robots*, vol. 9, no. 2, pp. 151–173, Sep. 2000.

[107] M. R. Endsley, "Toward a Theory of Situation Awareness in Dynamic Systems," *Hum. Factors J. Hum. Factors Ergon. Soc.*, vol. 37, no. 1, pp. 32–64, Mar. 1995.

[108] M. R. Endsley, B. Bolté, and D. G. Jones, *Designing for Situation Awareness: An Approach to User-Centered Design*. CRC Press, 2003.

[109] J. L. Pons, *Wearable Robots: Biomechatronic Exoskeletons*. John Wiley & Sons, 2008.

[110] J. I. Elkind and C. D. Forgie, "Characteristics of the Human Operator in Simple Manual Control Systems," *Autom. Control IRE Trans. On*, vol. AC-4, no. 1, pp. 44–55, May 1959.

[111] D. Feth, R. Groten, A. Peer, and M. Buss, "Control-theoretic Model of Haptic Human-Human Interaction in Pursuit Tracking Task," in *Robot and Human Interactive Communication, 2009. RO-MAN 2009. The 18th IEEE International Symposium on*, Toyama, Japan, 2009, pp. 1106–1111.

[112] D. McRuer, "Human Dynamics in Man-Machine Systems," *Automatica*, vol. 16, no. 3, pp. 237–253, May 1980.

[113] R. W. Allen and D. McRuer, "The Man/Machine Control Interface—Pursuit Control," *Automatica*, vol. 15, no. 6, pp. 683–686, Nov. 1979.

[114] M. Lupu, M. Sun, D. Askey, R. Xia, and Z. H. Mao, "Human Strategies in Balancing an Inverted Pendulum with Time Delay," in *Engineering in Medicine and Biology Society (EMBC), 2010 Annual International Conference of the IEEE*, Buenos Aires, Argentina, 2010, pp. 5246–5249.

[115] M. F. Lupu, M. Sun, R. Xia, and Z. H. Mao, "Rate of Information Transmission in Human Manual Control of an Unstable System," *Hum.-Mach. Syst. IEEE Trans. On*, vol. 43, no. 2, pp. 259–263, Mar. 2013.

[116] J. J. Potter and W. Singhose, "Improving Manual Tracking of Systems With Oscillatory Dynamics," *Hum.-Mach. Syst. IEEE Trans. On*, vol. 43, no. 1, pp. 46–52, Jan. 2013.

[117] M. R. Akbarzadeh-T and A. H. Meghdadi, "Fuzzy Modeling of Human Control Strategy for Over Head Crane," in *Fuzzy Systems, 2001. The 10th IEEE International Conference on*, Melbourne, Victoria, Australia, 2001, vol. 3, pp. 1076–1079.

[118] I. M. Rezazadeh, X. Wang, M. Firoozabadi, and M. R. Hashemi Golpayegani, "Using affective human–machine interface to increase the operation performance in virtual construction crane training system: A novel approach," *Augment. Virtual Real. Archit. Eng. Constr. CONVR2009*, vol. 20, no. 3, pp. 289–298, May 2011.

[119] I. S. MacKenzie, T. Kauppinen, and M. Silfverberg, "Accuracy Measures for Evaluating Computer Pointing Devices," in *CHI '01 Proceedings of the SIGCHI Conference on Human Factors in Computing Systems*, Seattle, Washington, 2001, pp. 9–16.

[120] K. Furuta, Y. Kado, and S. Shiratori, "Assisting Control in Human Adaptive Mechatronics - Single Ball Juggling -," in *2006 IEEE Conference on Computer Aided Control System Design, 2006 IEEE International Conference on Control Applications, 2006 IEEE International Symposium on Intelligent Control*, Munich, Germany, 2006, pp. 545–550.

[121] M. Mulder and D. A. Abbink, "Correct and Faulty Driver Support from Shared Haptic Control During Evasive Maneuvers," in *Systems, Man, and Cybernetics (SMC), 2011 IEEE International Conference on*, Anchorage, AK, 2011, pp. 1057–1062.

[122] Y. Xu, J. Song, M. C. Nechyba, and Y. Yam, "Performance evaluation and optimization of human control strategy," *Robot. Auton. Syst.*, vol. 39, no. 1, pp. 19–36, Apr. 2002.

[123] A. X. Pan and Y. Gao, "Design of an Imitating Human Controller Based on Rough Set Theory," in *Computer Science & Education, 2009. ICCSE'09. 4th International Conference on*, Nanning, China, 2009, pp. 1855–1859.

[124] S. Ertugrul, "Predictive modeling of human operators using parametric and neuro-fuzzy models by means of computer-based identification experiment," *Eng. Appl. Artif. Intell.*, vol. 21, no. 2, pp. 259–268, Mar. 2008.

[125] O. Celik and S. Ertugrul, "Predictive human operator model to be utilized as a controller using linear, neuro-fuzzy and fuzzy-ARX modeling techniques," *Eng. Appl. Artif. Intell.*, vol. 23, no. 4, pp. 595–603, Jun. 2010.

[126] I. Jolliffe, "Principal Component Analysis," in *Encyclopedia of Statistics in Behavioral Science*, Wiley Online Library, 2005.

[127] I. H. Witten, E. Frank, and M. A. Hall, *Data Mining: Practical Machine Learning Tools and Techniques*, 3rd ed. San Francisco, CA: Morgan Kaufmann Publishers Inc., 2011.

[128] F. J. Provost, T. Fawcett, and others, "Analysis and Visualization of Classifier Performance: Comparison under Imprecise Class and Cost Distributions," in *Proceedings*

of the 3rd International Conference on Knowledge Discovery and Data Mining, Newport Beach, CA, 1997, vol. 97, pp. 43–48.

[129] R. Kohavi and F. Provost, "Confusion matrix," *Mach. Learn.*, vol. 30, no. 2–3, pp. 271–274, 1998.

[130] T. Fawcett, "An introduction to ROC analysis," *Pattern Recognit. Lett.*, vol. 27, no. 8, pp. 861–874, Jun. 2006.

[131] J. Davis and M. Goodrich, "The relationship between Precision-Recall and ROC curves," in *Proceedings of the 23rd international conference on Machine learning*, Pittsburgh, PA, 2006, pp. 233–240.

[132] A. P. Bradley, "The use of the area under the ROC curve in the evaluation of machine learning algorithms," *Pattern Recognit.*, vol. 30, no. 7, pp. 1145–1159, Jul. 1997.

[133] J. A. Hanley and B. J. McNeil, "The Meaning and Use of the Area under a Receiver Operating Characteristic (ROC) Curve," *Radiology*, vol. 143, no. 1, pp. 29–36, Apr. 1982.

[134] W. S. McCulloch and W. Pitts, "A logical calculus of the ideas immanent in nervous activity," *Bull. Math. Biophys.*, vol. 5, no. 4, pp. 115–133, Dec. 1943.

[135] F. Rosenblatt, "The perceptron: A probabilistic model for information storage and organization in the brain.," *Psychol. Rev.*, vol. 65, no. 6, pp. 386–408, Nov. 1958.

[136] S. J. Russell and P. Norvig, *Artificial Intelligence: A Modern Approach*, 3rd ed. Prentice Hall, 2010.

[137] K. B. Sullivan, K. M. Feigh, R. Mappus IV, F. T. Durso, U. Fischer, V. Pop, K. L. Mosier, and D. G. Morrow, "Using neural networks to assess flight deck human–automation interaction," *Reliab. Eng. Syst. Saf.*, vol. 114, pp. 26–35, Jun. 2013.

[138] E. F. Camacho and M. R. Arahal, "Neural network based adaptive control," *Annu. Rev. Autom. Program.*, vol. 19, pp. 13–24, 1994.

[139] M. J. Willis, G. A. Montague, C. Di Massimo, M. T. Tham, and A. J. Morris, "Artificial neural networks in process estimation and control," *Automatica*, vol. 28, no. 6, pp. 1181–1187, Nov. 1992.

[140] J. W. Lee and J. H. Oh, "Time delay control of nonlinear systems with neural network modeling," *Mechatronics*, vol. 7, no. 7, pp. 613–640, Oct. 1997.

[141] V. Vemuri, "Artificial Neural Networks in Control Applications," *Adv. Comput.*, vol. 36, pp. 203–254, 1993.

[142] B. Couraud and P. Liu, "Use of neural networks as decision makers in strategic situations," in *Machine Learning and Cybernetics, 2009 International Conference on*, Baoding, Hebei, China, 2009, vol. 3, pp. 1280–1285.

[143] C. L. Tan, T. S. Quah, and H. H. Teh, "An Artificial Neural Network that Models Human Decision Making," *Computer*, vol. 29, no. 3, pp. 64–70, Mar. 1996.

[144] S. Soyguder, "Intelligent control based on wavelet decomposition and neural network for predicting of human trajectories with a novel vision-based robotic," *Expert Syst. Appl.*, vol. 38, no. 11, pp. 13994–14000, Oct. 2011.

[145] C. W. Chen, "Modeling and control for nonlinear structural systems via a NN-based approach," *Expert Syst. Appl.*, vol. 36, no. 3, pp. 4765–4772, Apr. 2009.

[146] C. Z. Pan, X. Z. Lai, S. X. Yang, and M. Wu, "A biologically inspired approach to tracking control of underactuated surface vessels subject to unknown dynamics," *Expert Syst. Appl.*, vol. 42, no. 4, pp. 2153–2161, Mar. 2015.

[147] A. P. Engelbrecht, *Computational Intelligence: An Introduction*, 2nd ed. John Wiley & Sons, 2007.

[148] H. Yu, Y. Liu, and T. Yang, "Closed-loop tracking control of a pendulum-driven cart-pole underactuated system," *Proc. Inst. Mech. Eng. Part J. Syst. Control Eng.*, vol. 222, no. 2, pp. 109–125, Mar. 2008.

[149] Y. Liu, H. Yu, S. Wane, and T. Yang, "On tracking control of a pendulum-driven cart-pole underactuated system," *Int. J. Model. Identif. Control*, vol. 4, no. 4, pp. 357–372, 2008.

[150] Y. Liu, H. Yu, and S. Cang, "Modelling and motion control of a double-pendulum driven cart," *Proc. Inst. Mech. Eng. Part J. Syst. Control Eng.*, vol. 226, no. 2, pp. 175–187, Feb. 2012.

[151] M. Kawato, "Internal models for motor control and trajectory planning," *Curr. Opin. Neurobiol.*, vol. 9, no. 6, pp. 718–727, 1999.

[152] R. C. Miall, D. J. Weir, D. M. Wolpert, and J. F. Stein, "Is the Cerebellum a Smith Predictor?," *J. Mot. Behav.*, vol. 25, no. 3, pp. 203–216, Sep. 1993.

[153] S. T. Grafton and C. M. Tipper, "Decoding intention: A neuroergonomic perspective," *NeuroImage*, vol. 59, no. 1, pp. 14–24, Jan. 2012.

[154] M. F. Bear, B. W. Connors, and M. A. Paradiso, *Neuroscience: Exploring the Brain*, 3rd ed. Lippincott Williams & Wilkins, 2007.

[155] B. Kolb and I. Q. Whishaw, *An Introduction to Brain and Behavior*, 4th ed. Worth Publishers, 2013.

[156] J. Hardin, G. Bertoni, and L. J. Kleinsmith, *Becker's World of the Cell*, 8th ed. Benjamin Cummings, 2012.

[157] C. Chayer and M. Freedman, "Frontal Lobe Functions," *Curr. Neurol. Neurosci. Rep.*, vol. 1, no. 6, pp. 547–552, 2001.

[158] R. Caton, "The Electric Currents of the Brain," *Br. Med. J.*, vol. 2, Aug. 1875.

[159] R. Caton, "Electrical Currents of the Brain.," *Chic. J. Nerv. Ment. Dis.*, vol. 2, no. 4, p. 610, Oct. 1875.

[160] L. F. Haas, "Hans Berger (1873–1941), Richard Caton (1842–1926), and electroencephalography," *J. Neurol. Neurosurg. Psychiatry*, vol. 74, no. 1, p. 9, Jan. 2003.

[161] A. Gale, "The psychophysiology of individual differences: Studies of extraversion and the EEG," *New Approaches Psychol. Meas.*, pp. 211–256, 1973.

[162] M. K. Johnson, J. Kounios, and S. F. Nolde, "Electrophysiological brain activity and memory source monitoring," *NeuroReport*, vol. 8, no. 5, pp. 1317–1320, Mar. 1997.

[163] P. C. Gram, B. R. Dunn, and D. Ellis, "Relationship Between EEG and Psychological Type," *J. Psychol. Type*, vol. 65, no. 5, pp. 33–46, Nov. 2005.

[164] M. L. Scheuer, "Continuous EEG Monitoring in the Intensive Care Unit," *Epilepsia*, vol. 43, no. s3, pp. 114–127, 2002.

[165] L. A. Schmidt and L. J. Trainor, "Frontal brain electrical activity (EEG) distinguishes valence and intensity of musical emotions," *Cogn. Emot.*, vol. 15, no. 4, pp. 487–500, 2001.

[166] N. Boutros, S. Galderisi, O. Pogarell, and S. Riggio, Eds., *Standard electroencephalography in clinical psychiatry: a practical handbook*. John Wiley & Sons, 2011.

[167] G. Pfurtscheller, R. Scherer, R. Leeb, C. Keinrath, C. Neuper, F. Lee, and H. Bischof, "Viewing Moving Objects in Virtual Reality Can Change the Dynamics of Sensorimotor EEG Rhythms," *Presence Teleoperators Virtual Environ.*, vol. 16, no. 1, pp. 111–118, Feb. 2007.

[168] P. Avanzini, M. Fabbri-Destro, R. Dalla Volta, E. Daprati, G. Rizzolatti, and G. Cantalupo, "The Dynamics of Sensorimotor Cortical Oscillations during the Observation of Hand Movements: An EEG Study," *PLoS ONE*, vol. 7, no. 5, p. e37534, 2012.

[169] D. J. McFarland, L. A. Miner, T. M. Vaughan, and J. R. Wolpaw, "Mu and Beta Rhythm Topographies During Motor Imagery and Actual Movements," *Brain Topogr.*, vol. 12, no. 3, pp. 177–186, 2000.

[170] G. Pfurtscheller, C. Brunner, A. Schlögl, and F. H. Lopes da Silva, "Mu rhythm (de)synchronization and EEG single-trial classification of different motor imagery tasks," *NeuroImage*, vol. 31, no. 1, pp. 153–159, May 2006.

[171] J. A. Pineda, B. Z. Allison, and A. Vankov, "The Effects of Self-Movement, Observation, and Imagination on Rhythms and Readiness Potentials (RP's): Toward a Brain–Computer Interface (BCI)," *Rehabil. Eng. IEEE Trans. On*, vol. 8, no. 2, pp. 219–222, Jun. 2000.

[172] S. Makeig and J. Onton, "ERP features and EEG dynamics: an ICA perspective," in *The Oxford Handbook of Event-Related Potential Components*, E. S. Kappenman and S. J. Luck, Eds. New York: Oxford University Press, 2009, pp. 51–86.

[173] R. J. Croft and R. J. Barry, "Removal of ocular artifact from the EEG: a review," *Neurophysiol. Clin. Neurophysiol.*, vol. 30, no. 1, pp. 5–19, Feb. 2000.

[174] V. Krishnaveni, S. Jayaraman, S. Aravind, V. Hariharasudhan, and K. Ramadoss, "Automatic Identification and Removal of Ocular Artifacts from EEG using Wavelet Transform," *Meas. Sci. Rev.*, vol. 6, no. 4, pp. 45–57, 2006.

[175] P. S. Kumar, R. Arumuganathan, K. Sivakumar, and C. Vimal, "Removal of Ocular Artifacts in the EEG through Wavelet Transform without using an EOG Reference Channel," *Int. J. Open Probl. Comput. Sci. Math. IJOPCM*, vol. 1, no. 3, pp. 189–200, 2008.

[176] S. Debener, F. Minow, R. Emkes, K. Gandras, and M. Vos, "How about taking a low-cost, small, and wireless EEG for a walk?," *Psychophysiology*, vol. 49, no. 11, pp. 1617–1621, Nov. 2012.

[177] A. T. Campbell, T. Choudhury, S. Hu, H. Lu, M. K. Mukerjee, M. Rabbi, and R. D. S. Raizada, "NeuroPhone: Brain-Mobile Phone Interface using a Wireless EEG Headset," presented at the Proceedings of the second ACM SIGCOMM workshop on Networking, systems, and applications on mobile handhelds, New Delhi, India, 2010, pp. 3–8.

[178] U. Hoffmann, J. M. Vesin, T. Ebrahimi, and K. Diserens, "An efficient P300-based brain–computer interface for disabled subjects," *J. Neurosci. Methods*, vol. 167, no. 1, pp. 115–125, Jan. 2008.

[179] V. E. Pollock, L. S. Schneider, and S. A. Lyness, "Reliability of topographic quantitative EEG amplitude in healthy late-middle-aged and elderly subjects," *Electroencephalogr. Clin. Neurophysiol.*, vol. 79, no. 1, pp. 20–26, Jul. 1991.

[180] M. C. Salinsky, B. S. Oken, and L. Morehead, "Test-retest reliability in EEG frequency analysis," *Electroencephalogr. Clin. Neurophysiol.*, vol. 79, no. 5, pp. 382–392, Nov. 1991.

[181] V. E. Pollock, L. S. Schneider, and S. A. Lyness, "EEG amplitudes in healthy, late-middle-aged and elderly adults: normality of the distributions and correlations with age," *Electroencephalogr. Clin. Neurophysiol.*, vol. 75, no. 4, pp. 276–288, Apr. 1990.

[182] D. Huang, K. Qian, D. Y. Fei, W. Jia, X. Chen, and O. Bai, "Electroencephalography (EEG)-Based Brain–Computer Interface (BCI): A 2-D Virtual Wheelchair Control Based on Event-Related Desynchronization/Synchronization and State Control," *Neural Syst. Rehabil. Eng. IEEE Trans. On*, vol. 20, no. 3, pp. 379–388, May 2012.

[183] M. M. Bradley and A. Keil, "Event-Related Potentials (ERPs)," in *Encyclopedia of Human Behavior*, 2nd ed., V. S. Ramachandran, Ed. San Diego: Academic Press, 2012, pp. 79–85.

[184] S. A. Hillyard, "Event-Related Potentials (ERPs) and Cognitive Processing," in *Encyclopedia of Neuroscience*, L. R. Squire, Ed. Oxford: Academic Press, 2009, pp. 13–18.

[185] S. Sanei and J. A. Chambers, *EEG signal processing*. John Wiley & Sons, 2007.

[186] R. Q. Quiroga, M. Atienza, J. L. Cantero, and M. L. A. Jongsma, "What can we learn from single-trial event-related potentials?," *Chaos Complex. Lett.*, vol. 2, no. 2/3, pp. 345–363, 2007.

[187] R. Q. Quiroga and H. Garcia, "Single-trial event-related potentials with wavelet denoising," *Clin. Neurophysiol.*, vol. 114, no. 2, pp. 376–390, Feb. 2003.

[188] A. Delorme and S. Makeig, "EEGLAB: an open source toolbox for analysis of single-trial EEG dynamics including independent component analysis," *J. Neurosci. Methods*, vol. 134, no. 1, pp. 9–21, Mar. 2004.

[189] N. A. Badcock, P. Mousikou, Y. Mahajan, P. de Lissa, J. Thie, and G. McArthur, "Validation of the Emotiv EPOC® EEG gaming system for measuring research quality auditory ERPs," *PeerJ*, vol. 1, p. e38, Feb. 2013.

[190] H. Ekanayake, "P300 and Emotiv EPOC: Does Emotiv EPOC capture real EEG?" The Solution Available: http://neurofeedback.visaduma.info/emotivresearch.htm, 2010.

[191] M. Islam, T. Ahmed, S. S. Mostafa, M. S. U. Yusuf, and M. Ahmad, "Human Emotion Recognition using Frequency & Statistical Measures of EEG Signal," in *Informatics, Electronics & Vision (ICIEV), 2013 International Conference on*, Dhaka, Bangladesh, 2013, pp. 1–6.

[192] R. W. Picard, E. Vyzas, and J. Healey, "Toward Machine Emotional Intelligence: Analysis of Affective Physiological State," *Pattern Anal. Mach. Intell. IEEE Trans. On*, vol. 23, no. 10, pp. 1175–1191, Oct. 2001.

[193] V. Srinivasan, C. Eswaran, and N. Sriraam, "Artificial neural network based epileptic detection using time-domain and frequency-domain features," *J. Med. Syst.*, vol. 29, no. 6, pp. 647–660, Dec. 2005.

[194] A. S. Al-Fahoum and A. A. Al-Fraihat, "Methods of EEG Signal Features Extraction Using Linear Analysis in Frequency and Time-Frequency Domains," *ISRN Neurosci.*, vol. 2014, 2014.

[195] M. Murugappan, M. Rizon, R. Nagarajan, S. Yaacob, D. Hazry, and I. Zunaidi, "Time-Frequency Analysis of EEG Signals for Human Emotion Detection," in *4th Kuala Lumpur International Conference on Biomedical Engineering 2008*, Kuala Lumpur, Malaysia, 2008, vol. 21, pp. 262–265.

[196] W. T. Cochran, J. W. Cooley, D. L. Favin, H. D. Helms, R. A. Kaenel, W. W. Lang, G. C. Maling Jr, D. E. Nelson, C. M. Rader, and P. D. Welch, "What is the fast Fourier transform?," *Proc. IEEE*, vol. 55, no. 10, pp. 1664–1674, Oct. 1967.

[197] H. Shatkay, "The Fourier transform-A primer." Brown University, Nov-1995.

[198] D. Gabor, "Theory of communication. Part 1: The analysis of information," *Electr. Eng. - Part III Radio Commun. Eng. J. Inst. Of*, vol. 93, no. 26, pp. 429–441, Nov. 1946.

[199] V. J. Samar, A. Bopardikar, R. Rao, and K. Swartz, "Wavelet Analysis of Neuroelectric Waveforms: A Conceptual Tutorial," *Brain Lang.*, vol. 66, no. 1, pp. 7–60, Jan. 1999.

[200] A. Procházka, J. Kukal, and O. Vyšata, "Wavelet Transform Use for Feature Extraction and EEG Signal Segments Classification," in *Communications, Control and Signal Processing, 2008. ISCCSP 2008. 3rd International Symposium on*, St Julians, Malta, 2008, pp. 719–722.

[201] A. Subasi, "EEG signal classification using wavelet feature extraction and a mixture of expert model," *Expert Syst. Appl.*, vol. 32, no. 4, pp. 1084–1093, May 2007.

[202] T. P. Jung, S. Makeig, M. Westerfield, J. Townsend, E. Courchesne, and T. J. Sejnowski, "Independent component analysis of single-trial event-related potentials," in *Proc. ICA*, Aussois, France, 1999, vol. 99, pp. 173–178.

[203] T. P. Jung, S. Makeig, M. Westerfield, J. Townsend, E. Courchesne, and T. J. Sejnowski, "Removal of eye activity artifacts from visual event-related potentials in normal and clinical subjects," *Clin. Neurophysiol.*, vol. 111, no. 10, pp. 1745–1758, Oct. 2000.

[204] T. Y. Chai, S. S. Woo, Mohamed Rizon, and C. S. Tan, "Classification of human emotions from EEG signals using statistical features and neural network," in *International Journal of Integrated Engineering*, 2010, vol. 1, pp. 1–6.

[205] N. MAHFUZ, W. ISMAIL, Z. JALI, K. ANUAR, and M. J. NORDIN, "Classification of brainwave using data mining in producing an emotional model," *J. Theor. Appl. Inf. Technol.*, vol. 75, no. 2, 2015.

[206] K. Takahashi, "Remarks on Emotion Recognition from Bio-Potential Signals," in *2nd International Conference on Autonomous Robots and Agents*, Palmerston North, New Zealand, 2004, vol. 3, pp. 186–191.

[207] S. Makeig, S. Debener, J. Onton, and A. Delorme, "Mining event-related brain dynamics," *Trends Cogn. Sci.*, vol. 8, no. 5, pp. 204–210, May 2004.

[208] C. Vidaurre, N. Krämer, B. Blankertz, and A. Schlögl, "Time Domain Parameters as a feature for EEG-based Brain–Computer Interfaces," *Neural Netw.*, vol. 22, no. 9, pp. 1313–1319, Nov. 2009.

[209] Y. Wongsawat, S. Oraintara, and K. R. Rao, "Reduced Complexity Space-Time-Frequency Model for Multi-Channel EEG and Its Applications," in *Circuits and Systems,*

2007. ISCAS 2007. IEEE International Symposium on, New Orleans, LA, 2007, pp. 1305–1308.

[210] K. Nazarpour, S. Sanei, L. Shoker, and J. A. Chambers, "Parallel space-time-frequency decomposition of EEG signals for brain computer interfacing," in *Signal Processing Conference, 2006 14th European*, Florence, Italy, 2006, pp. 1–4.

[211] T. C. Ferree, M. R. Brier, J. Hart Jr, and M. A. Kraut, "Space–time–frequency analysis of EEG data using within-subject statistical tests followed by sequential PCA," *NeuroImage*, vol. 45, no. 1, pp. 109–121, Mar. 2009.

[212] T. P. Jung, S. Makeig, M. Westerfield, J. Townsend, E. Courchesne, and T. J. Sejnowski, "Analyzing and Visualizing Single-Trial Event-Related Potentials," *Adv. Neural Inf. Process. Syst.*, vol. 11, pp. 118–124, 1999.

[213] G. S. Taylor and C. Schmidt, "Empirical Evaluation of the Emotiv EPOC BCI Headset for the Detection of Mental Actions," in *Proceedings of the Human Factors and Ergonomics Society Annual Meeting*, Boston, 2012, vol. 56, pp. 193–197.

[214] A. Delorme, T. Fernsler, H. Serby, and S. Makeig, "EEGLAB Tutorial." University of San Diego California, 2006.

[215] T. Mullen, A. Delorme, C. Kothe, and S. Makeig, "An Electrophysiological Information Flow Toolbox for EEGLAB," *Biol Cybern*, vol. 83, pp. 34–45, 2010.

[216] D. O. Morales, P. L. Hera, S. Westerberg, L. B. Freidovich, and A. S. Shiriaev, "Path-Constrained Motion Analysis: An Algorithm to Understand Human Performance on Hydraulic Manipulators," *IEEE Trans. Hum.-Mach. Syst.*, vol. 45, no. 2, pp. 187–199, Apr. 2015.

[217] A. Hasselberg and D. Söffker, "Petri-Net-Based Modeling of Human Operator's Planning for the Evaluation of Task Performance Using the Example of Air Traffic Control," *IEEE Trans. Hum.-Mach. Syst.*, vol. 45, no. 6, pp. 676–685, Dec. 2015.

[218] R. C. S. Antunes, L. B. Palma, F. V. Coito, and H. Duarte-Ramos, "Inductive transfer assist-control for human-interface steering device," in *Evolving and Adaptive Intelligent Systems (EAIS), 2015 IEEE International Conference on*, 2015, pp. 1–8.

[219] A. â€™ B. Hisham, M. H. I. Ishak, M. F. A. M. Kasai, and N. H. Idris, "Comparisons of skill index algorithm in driving for human adaptive mechatronics," in *Control Conference (ASCC), 2015 10th Asian Conference on*, 2015, pp. 1–6.

[220] M. Saunders, P. Lewis, and A. Thornhill, *Research Methods for Business Students*. Financial Times Prentice Hall, 2009.

[221] J. C. Butcher, *Numerical Methods for Ordinary Differential Equations*, 2nd ed. Wiley Online Library, 2008.

[222] D. F. Griffiths and D. J. Higham, *Numerical Methods for Ordinary Differential Equations: Initial Value Problems*, 1st ed. Springer-Verlag London, 2010.

[223] F. Lotte, M. Congedo, A. Lécuyer, F. Lamarche, and B. Arnaldi, "A review of classification algorithms for EEG-based brain–computer interfaces," *J. Neural Eng.*, vol. 4, no. 2, p. R1, 2007.

[224] S. Chen, S. A. Billings, and P. M. Grant, "Non-linear system identification using neural networks," *Int. J. Control*, vol. 51, no. 6, pp. 1191–1214, 1990.

[225] G. B. Huang, Y. Q. Chen, and H. A. Babri, "Classification Ability of Single Hidden Layer Feedforward Neural Networks," *Neural Netw. IEEE Trans. On*, vol. 11, no. 3, pp. 799–801, May 2000.

[226] H. Yu, T. Yang, Y. Liu, and S. Wane, "A further study of control for a pendulum-driven cart," *Int. J. Adv. Mechatron. Syst.*, vol. 1, no. 1, pp. 44–52, 2008.

[227] C. W. Anderson, "Learning to Control an Inverted Pendulum Using Neural Networks," *Control Syst. Mag. IEEE*, vol. 9, no. 3, pp. 31–37, Apr. 1989.

[228] T. M. Cover and J. A. Thomas, *Elements of information theory*, 2nd ed. John Wiley & Sons, 2006.

[229] C. E. Shannon and W. Weaver, *The mathematical theory of communication*. University of Illinois press, 1998.

[230] C. E. Shannon, "A Mathematical Theory of Communication," *Bell Syst. Tech. J.*, vol. 27, no. 3, pp. 379–423, 623–656, Jul. 1948.

[231] R. T. Smith and R. B. Minton, *Calculus*, 4th ed. McGraw-Hill Higher Education, 2011.

Appendix

A. Consent form for a low level control of pendulum-driven robot to measure performance among participants

<div style="text-align: center">**Research Ethics Consent Form**</div>

Project title: Human adaptive mechatronics (HAM) based human robot interactions (HRI) through an adaptive virtual simulation platform

Name of the researcher: Keattikorn Samarnggoon, Research Student, Faculty of Computing, Engineering and Technology

Name of the experiment: A low level control of pendulum-driven robot to measure performance among participants

The experiment:

Description

A participant will be asked to conduct a low level control of the pendulum-driven robot in a virtual environment platform using the provided joystick interface. The control information and internal parameters of the simulation will be collected for further analyses. Video recording of the participant during the experiment will be made and it will be used as a reference when analysing the acquired data.

Task

A simple target reaching task will be given to the participant. The participant will learn to control the pendulum-driven robot in virtual environment.

Protocol
1. The participant read and signs the consent form.

2. The experiment environment is set up and prepared.
3. The participant answers pre-experiment questionnaires.
4. The participant will be explained and demonstrated about the simulation software and the interface that will be used.
5. The first trial, 20 seconds will be given to familiarize with the platform and learn to control the robot.
6. Main trials will last 20 seconds for each trial, the participant will be asked to control the robot to the right/left as far as possible within 20 seconds.
7. 3 trials for right side, 3 trials for left side

Please tick in the boxes below:

☐ I have read all the information provided regarding the experiment description, task, and protocol which will be conducted during your participation.

☐ I agree to participate in this experiment.

Name of participant:

………………………………………………………………………Signature………………………
……Date…………….

Name of researcher:

………………………………………………………………………Signature………………………
……Date…………….

Please answer to the questionnaires behind this page.

Pre-experiment questionnaires

1. What is gender?
   ☐ Male
   ☐ Female
   ☐ Not applicable
2. How old are you?
   ☐ Below 20
   ☐ 21-25
   ☐ 26-30
   ☐ 31-35
   ☐ 36-40
   ☐ 41-45
   ☐ 46-50
   ☐ Above 50

3. What is your handedness? (Choose one)
   - ☐ Righty
   - ☐ Lefty
   - ☐ Comfortable with either side
4. Do you know Physics like Newton laws of motion?

   ☐ Yes ☐ No

5. Do you know pendulum?

   ☐ Yes ☐ No

6. Do you know inverted pendulum?

   ☐ Yes ☐ No ☐

7. Do you know the principle behind the inverted pendulum-driven robot?

   ☐ Yes ☐ No

8. Have you conducted this experiment before?

   ☐ Yes ☐ No
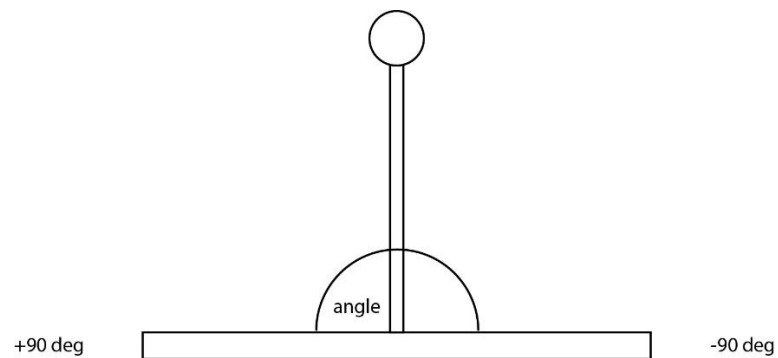
B. Consent form for EEG target hitting task experiment

Research Ethics Consent Form

Project title: Human adaptive mechatronics (HAM) based human robot interactions (HRI) through an adaptive virtual simulation platform

Name of the researcher: Keattikorn Samarnggoon, Research Student, Faculty of Computing, Engineering and Technology

Name of the experiment: An EEG based experimentation conduct on a HAM simulation platform

The experiment:

  Description

   A participant will be asked to conduct the given experiment e.g. target hitting task while having an Emotiv EPOC headset installed on his / her head in order to record the EEG brainwaves during the interaction with the given task / operation.

Please tick in the boxes below:

  ☐ I have read all the information provided regarding the experiment and task description which will be conducted during your participation.
  ☐ I agree to participate in this experiment.

Name of participant:
……………………………………………………………………Signature………………………
……Date…………….

Name of researcher:

……………………………………………………………………Signature………………………
……Date…………….

C. Emotiv EPOC electrode placement coordinates

The localisation or coordinates of the electrodes of the Emotiv EPOC headset.

Number	labels	ref	theta	radius	X	Y	Z	sph_theta	sph_phi	sph_radius	type
1	AF3	-23	0.411	0.885	0.376	0.276	23	16	1	1	1
2	F7	-54	0.511	0.587	0.809	-0.0349	54	-2	1	2	1
3	F3	-39	0.333	0.673	0.545	0.5	39	30	1	3	1
4	FC5	-69	0.394	0.339	0.883	0.326	69	19	1	4	1
5	T7	-90	0.511	0	0.999	-0.0349	90	-2	1	5	1
6	P7	-126	0.511	-0.59	0.809	-0.0349	126	-2	1	6	1
7	O1	-162	0.511	-0.95	0.309	-0.0349	162	-2	1	7	1
8	O2	162	0.511	-0.95	-0.309	-0.0349	-162	-2	1	8	1
9	P8	126	0.511	-0.59	-0.809	-0.0349	-126	-2	1	9	1
10	T8	90	0.511	0	0.999	-0.0349	-90	-2	1	10	1
11	FC6	69	0.394	0.34	-0.883	0.326	-69	19	1	11	1
12	F4	39	0.333	0.67	-0.545	0.5	-39	30	1	12	1
13	F8	54	0.511	0.59	-0.809	-0.0349	-54	-2	1	13	1
14	AF4	23	0.411	0.89	-0.376	0.276	-23	16	1	14	1

D. Circle to circle intersection algorithm

```
Boolean CircleCircleIntersection ( int c1x , int c1y ,
int r1 ,
int c2x , int c2y , int r2 )
{
    int lx = c1x - c2x ;
    int ly = c1y - c2y ;
    int ll = lx * lx + ly * ly ;
    int r1_plus_r2 = r1 + r2 ;

    if ( ll > ( ( r1_plus_r2 ) * ( r1_plus_r2 ) ) )
    {
        return false ;
    }
    return true ;
}
```

E. Box plot

A box plot in this research is based on boxplot function from MATLAB. The elements of a box plot are shown in Figure Appendix.1 . The centre mark in the box is the median. The edges of the box are 25th and 75th percentiles. Red crossed points outside the box are outliers.
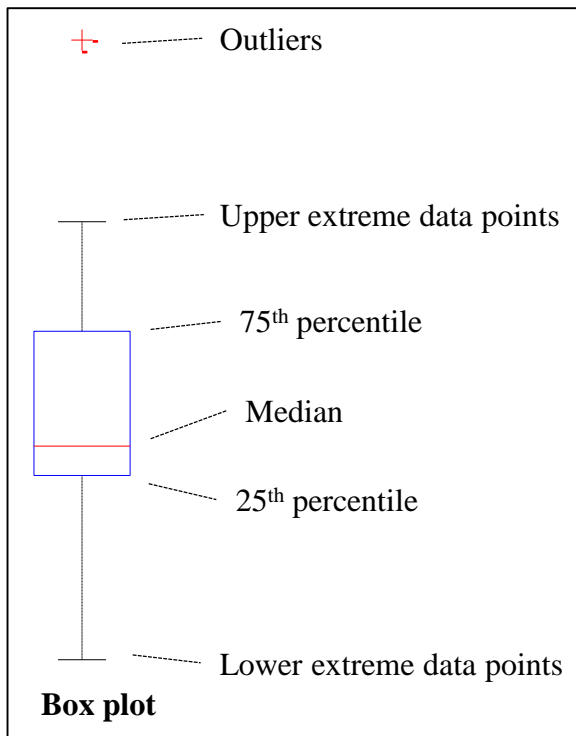
Figure Appendix.1 Box plot elements.

F. Information theory

The information theory is used to calculate the amount of information transfer / convey from one place to another e.g. the concept of human-robot information pipeline in Section 2.5.6. The amount of information, conveyed by the probability of events having the same degree of occurrence , equals to $\log_2 N$ where N is number of the events [228]. The amount of information is expressed in *bits*. The information transmission rate is expressed in *bits/second*. In other words, this information conveying can be described in computing science using a binary representation where 1 bit of binary digit can convey two possible outcomes which are 0 or 1.

In general, 2^n different possibilities (equally-likely of occurrence) can be expressed using n bits of binary digits.

$$H_s = \log_2 N \ bits \tag{A.1}$$

For the case of unequal probability events, the information convey is calculated using the inverse of the corresponding probability.

$$H_s = \log_2 \frac{1}{P} \ bits \tag{A.2}$$

For a series of information, the average information conveyed can be computed using summation of the above equation multiply by the corresponding probability.

$$H_{average} = \sum_{i=1}^{n} P_i \left[\log_2 \frac{1}{P_i} \right] \ bits \tag{A.3}$$

Information capacity of a channel

The information capacity I of a communication channel is defined as (A.4) where W is a bandwidth, S is a signal, and N is a noise [71], [229], [230].

$$I = W \log_2 \frac{S + N}{N} \ bits/second \tag{A.4}$$

Entropy of information

An entropy of information is a measure of uncertainty of the information given the probability of the events. A standard entropy calculation is defined as follows.

$$H(X) = E_X[I(x)] = \sum_{x \in X} -p(x) \log p(x) \tag{A.5}$$

In the case of binary information representation, entropy can be calculated as follows.

$$H(X) = - \sum_{x \in X} p(x) \log_2 p(x) - (1 - p(x)) \log_2 1 - p(x) \tag{A.6}$$

The information transmission rate is defined as follows.

Base equation
$$I = W \log_2 \left[1 + \frac{S(f)}{N(f)} \right] \qquad (A.7)$$

Continuous
$$I = \int_0^W \log_2 \left[1 + \frac{S(f)}{N(f)} \right] df \qquad (A.8)$$

Discrete
$$I = \sum_{i=0}^W \log_2 \left[1 + \frac{S_i(f)}{N_i(f)} \right] \qquad (A.9)$$

S is a signal spectrum while N is a noise spectrum. W is a channel capacity, or bandwidth.

G. Extremum – local minima and maxima

An absolute maximum or an absolute minimum is an absolute extremum of a function. Sometimes they are referred to as a global maximum or a global minimum, respectively. Not every function has both an absolute maximum and an absolute minimum. As shown in Figure Appendix.2, a function in Figure Appendix.2 (a) has only an absolute minimum whilst a function in Figure Appendix.2 (b) has only an absolute maximum.

(a)   (b)
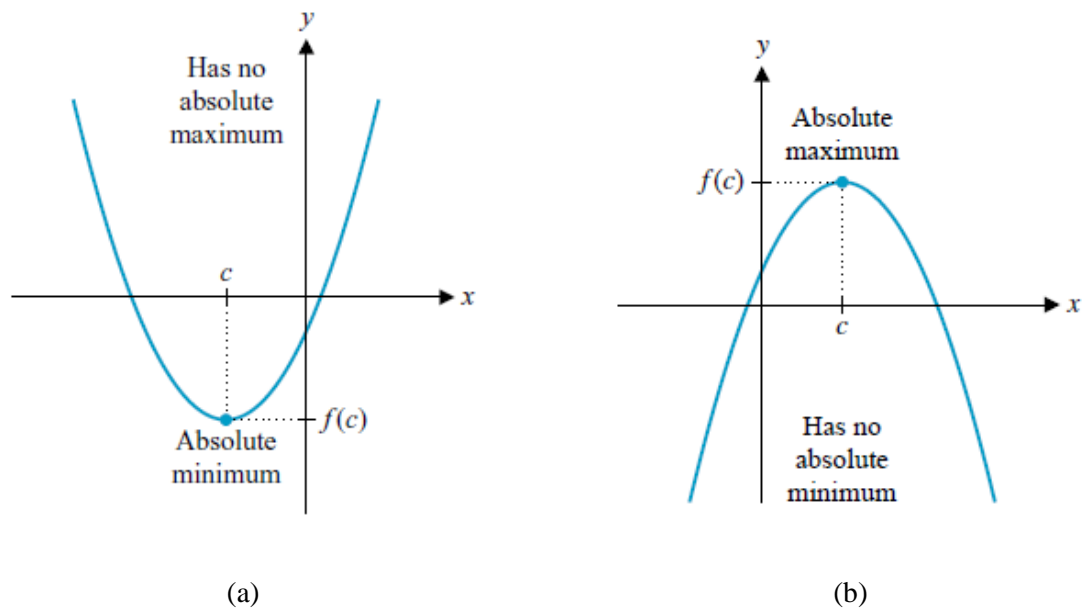
Figure Appendix.2 Functions with no absolute extremum [231].

For a function f defined on a set S of real numbers and a number $c \in S$.

The absolute maximum and absolute minimum can be defined as

$f(c)$ is the absolute maximum of f on S if $f(c) \geq f(x)$ for all $x \in S$ and

$f(c)$ is the absolute minimum of f on S if $f(c) \leq f(x)$ for all $x \in S$

A local maximum or a local minimum, sometimes referred to as a relative maximum or a relative minimum, respectively, is a local extremum in a given neighbourhood, as shown in Figure Appendix.3.

The local maximum and local minimum can be defined as $f(c)$ is the local maximum of f if $f(c) \geq f(x)$ for all x in some open interval containing C. $f(c)$ is the local minimum of f if $f(c) \leq f(x)$ for all x in some open interval containing C.

A point c where its derivative $f'(c)$ is zero or undefinable is called a critical point of the function. The local extrema always occur at the critical point. A local extremum is not necessary to be equal to an absolute extremum of a function, whereas an absolute extremum and a local extremum are the same value in the given neighbourhood.

If a continuous function is defined in a closed interval $[a, b]$, an absolute extremum must be occurred at a boundary point of the interval (at point a or b) or a critical point.

If a function is a piecewise-defined function, all of the absolute extrema must be defined and then compared for the absolute largest or smallest value.
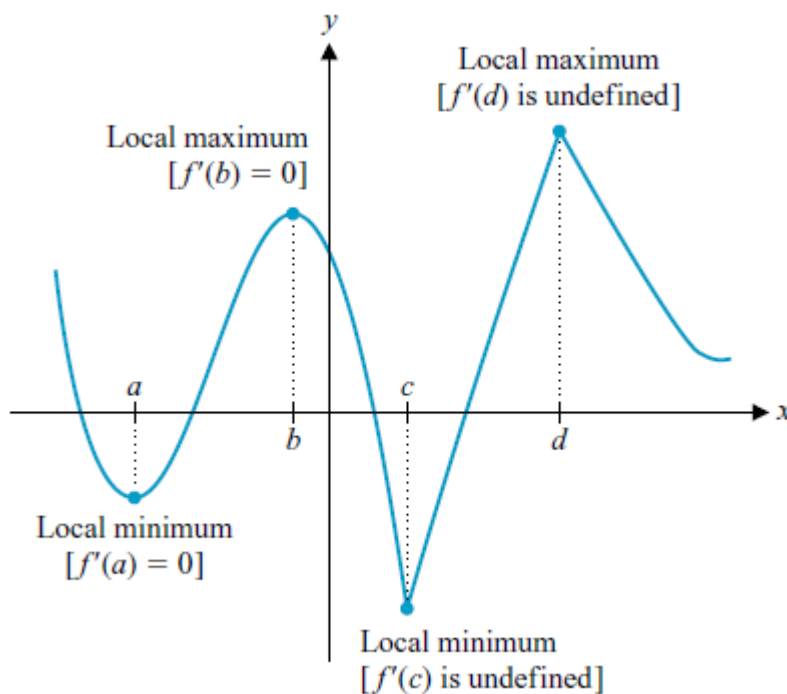
Figure Appendix.3 Local extrema of a function [231].

H. Preliminary EEG investigation results

Target
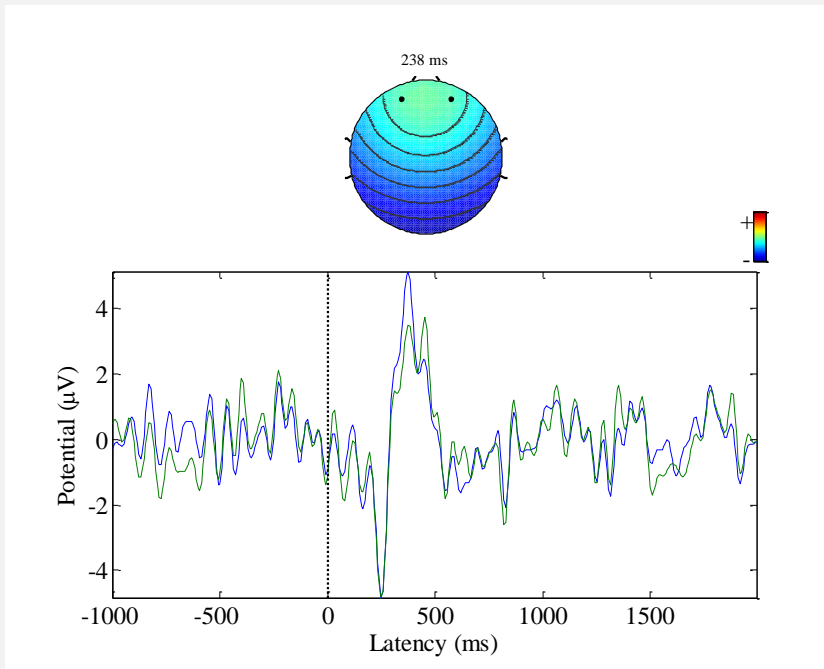
Non-target
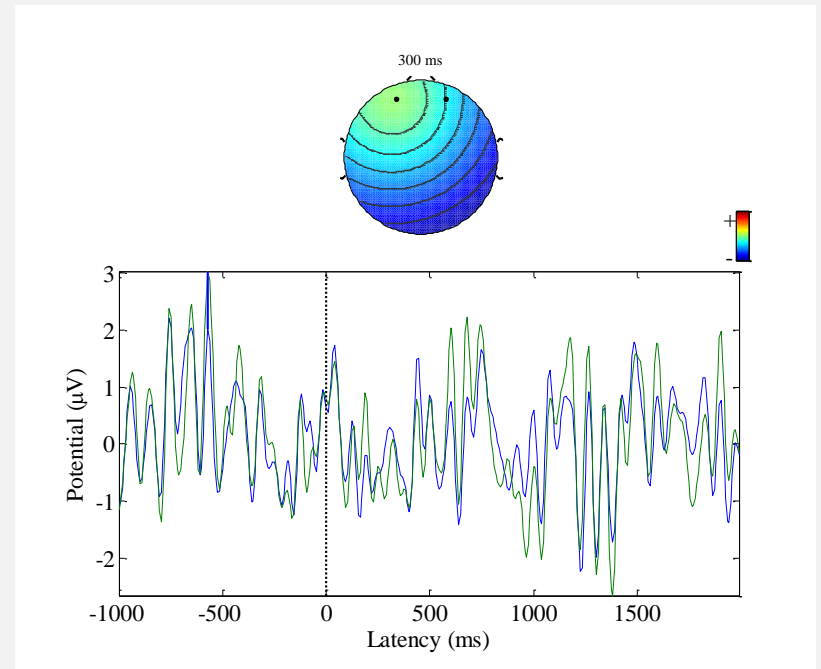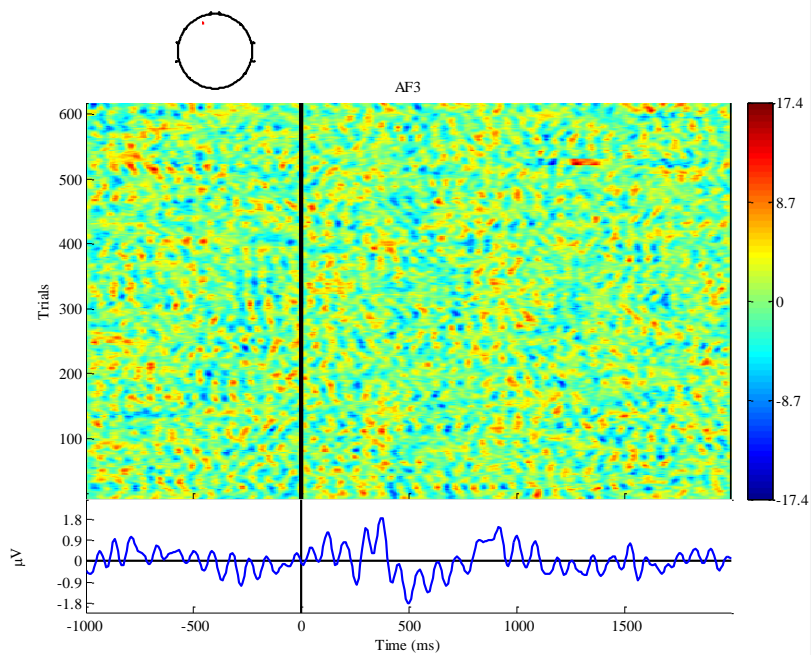
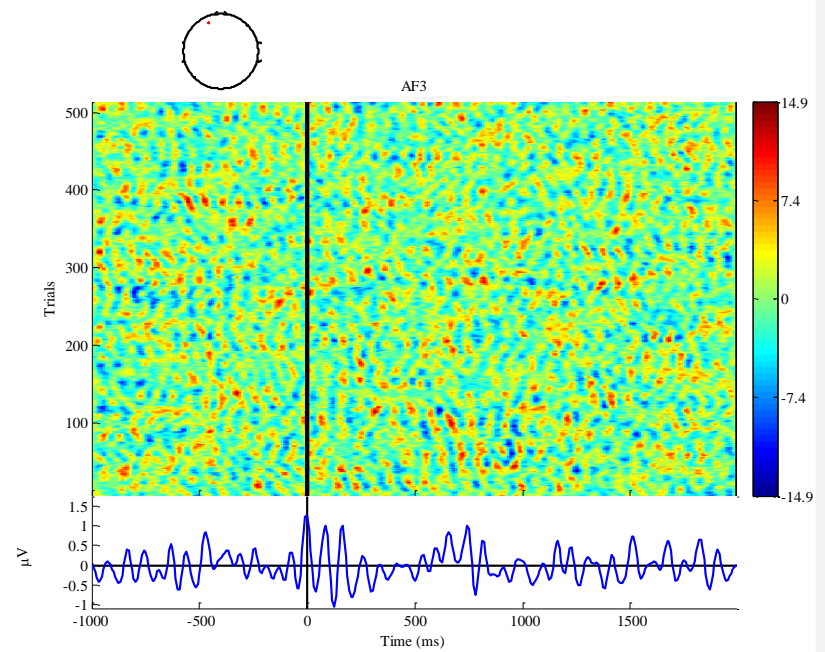(a) The F3 (blue) and AF4 (green) ERP responded to the target auditory event.

(b) The AF3 (blue) and AF4 (green) ERP from the non-target event.
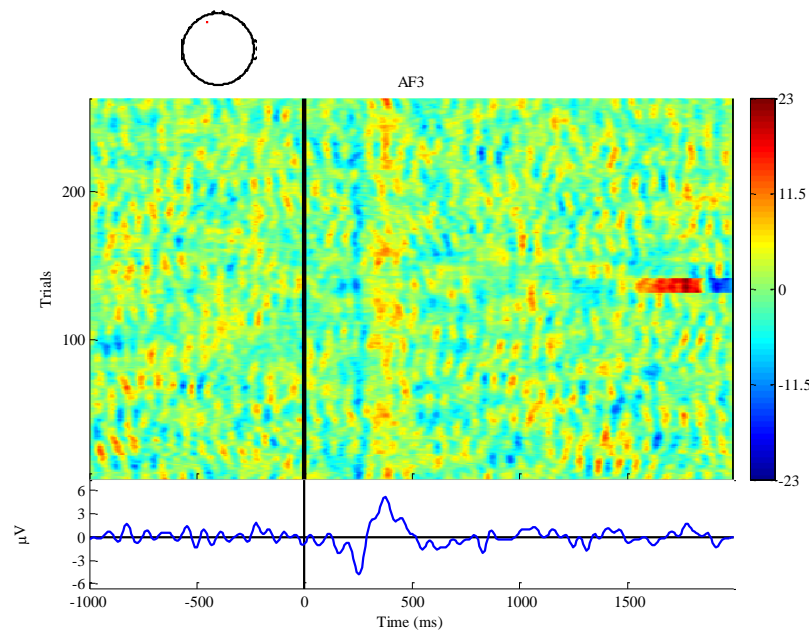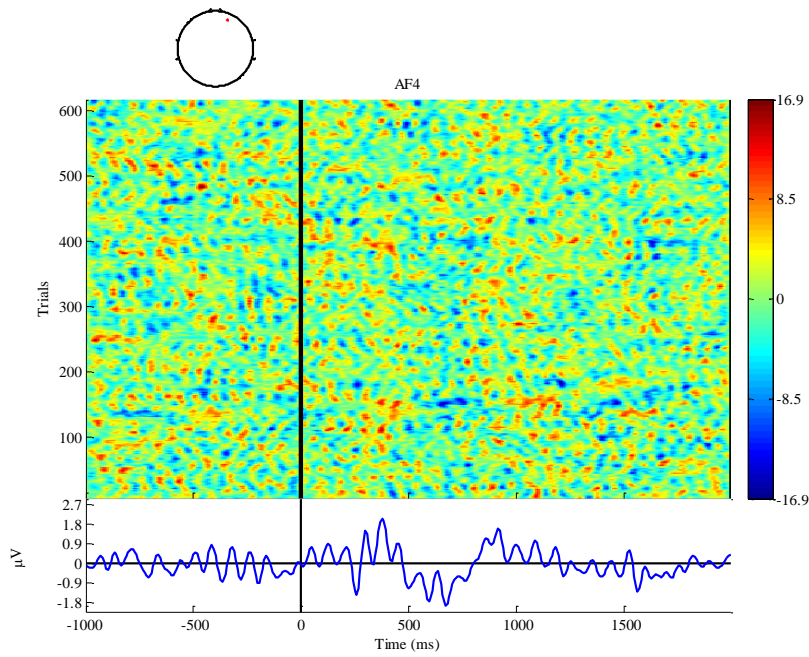
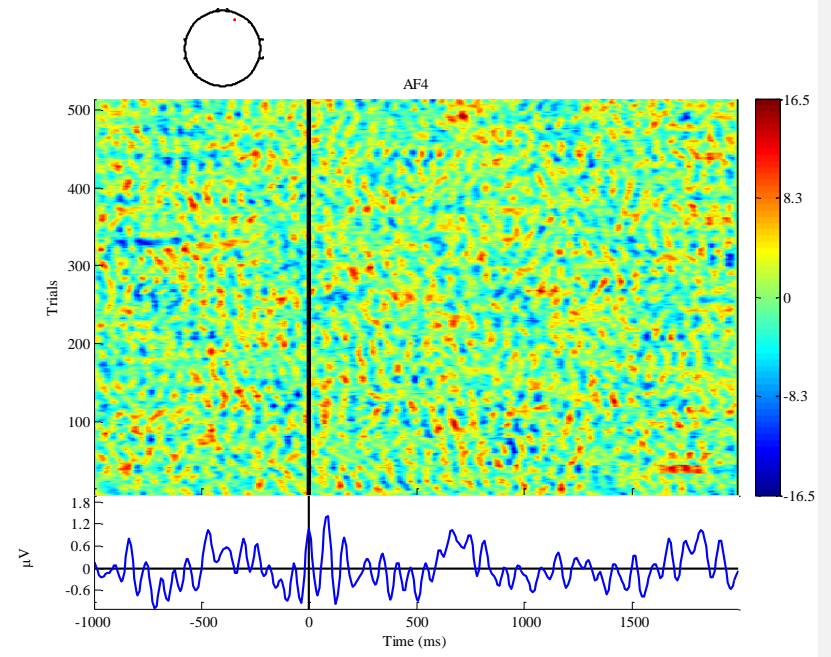(c) The AF3 ERP image responded to the target auditory event.
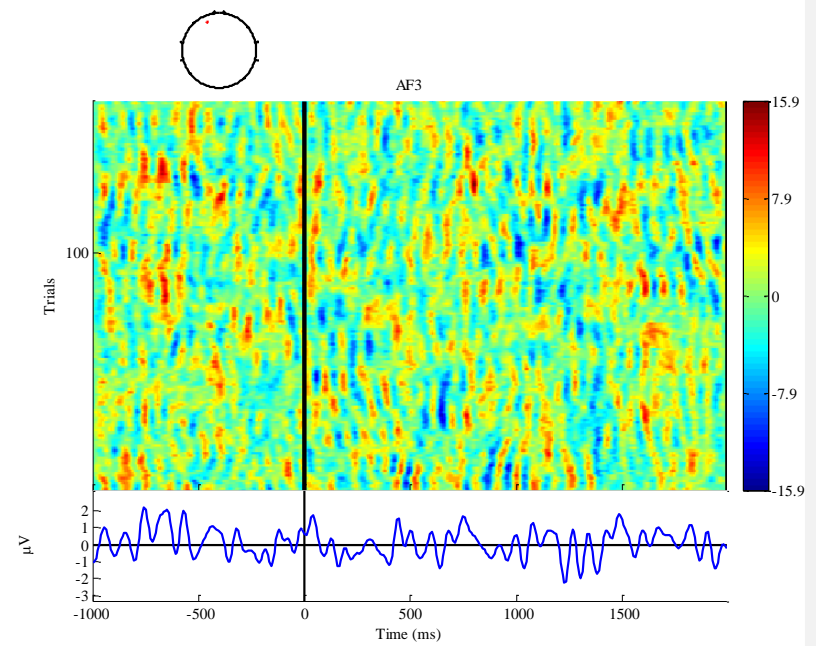
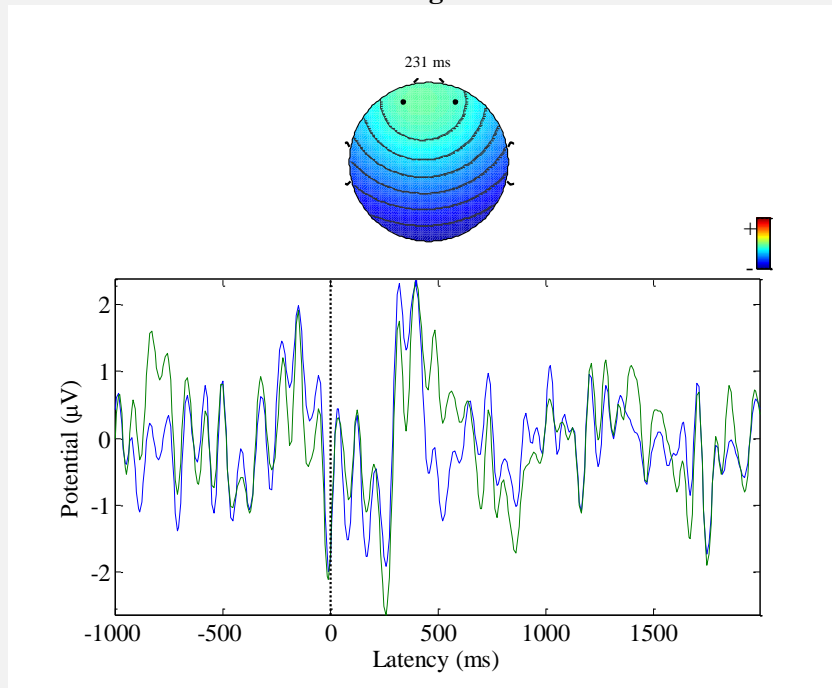(d) The AF3 ERP image responded to the non-target event.
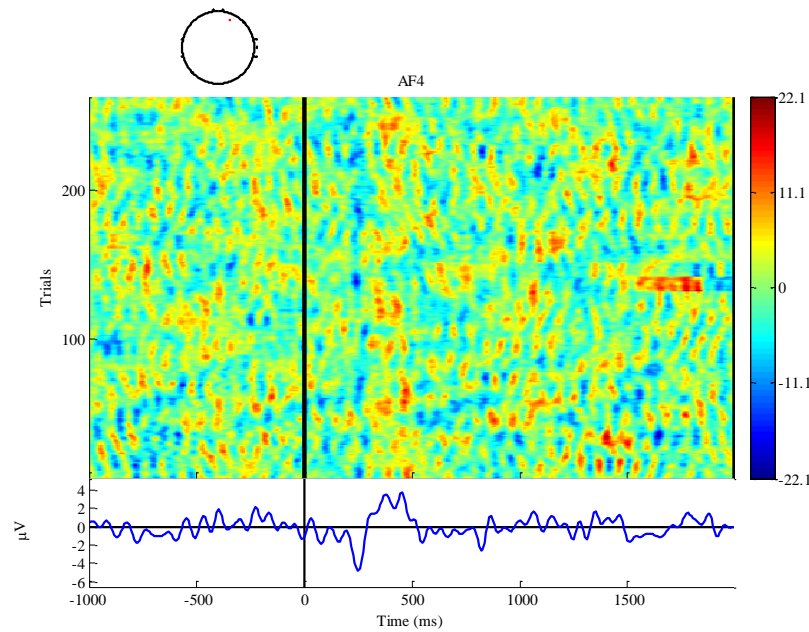
(e) The AF4 ERP image responded to the target auditory event.
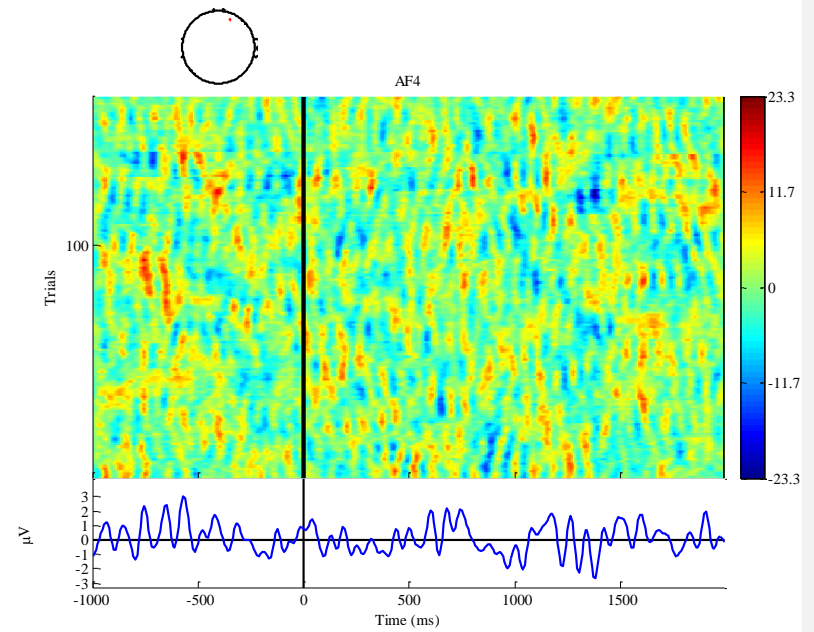
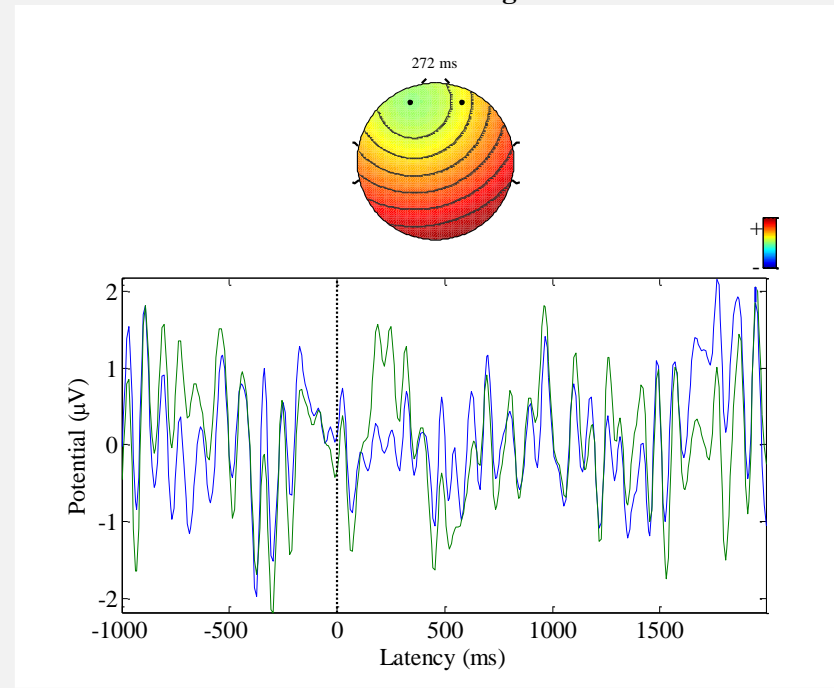(f) The AF4 ERP image responded to the non-target event.

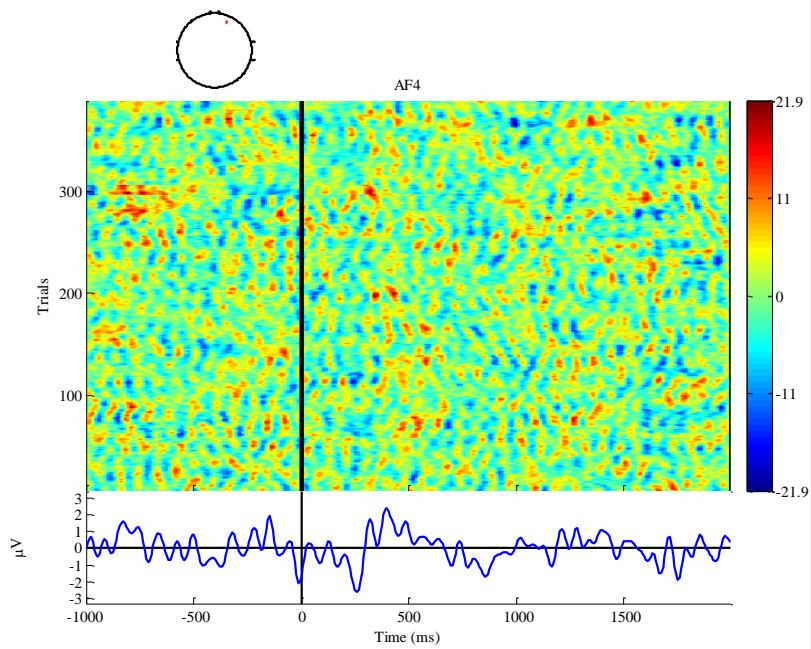Figure Appendix.4 The comparison between targets and non-target response for experiment 1.

(a) The AF3 (blue) and AF4 (green) ERP responded to the target auditory event.

(b) The AF3 (blue) and AF4 (green) ERP from the non-target event.

(c) The AF3 ERP image responded to the target auditory event.

(d) The AF3 ERP image responded to the non-target event.

(e) The AF4 ERP image responded to the target auditory event.

(f) The AF4 ERP image responded to the non-target event.

Figure Appendix.5 The comparison between targets and non-target response for experiment 2.

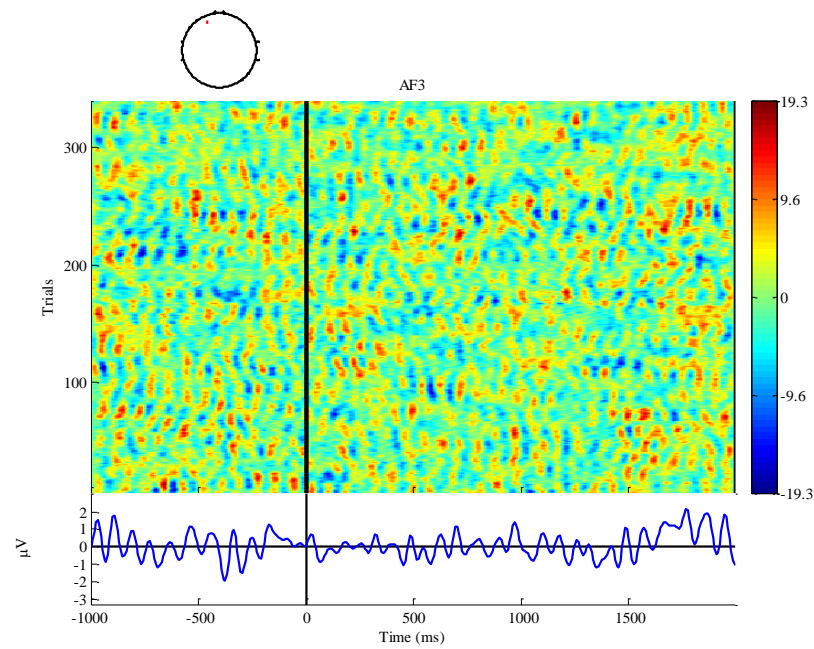(a) The AF3 (blue) and AF4 (green) ERP responded to the target auditory event.

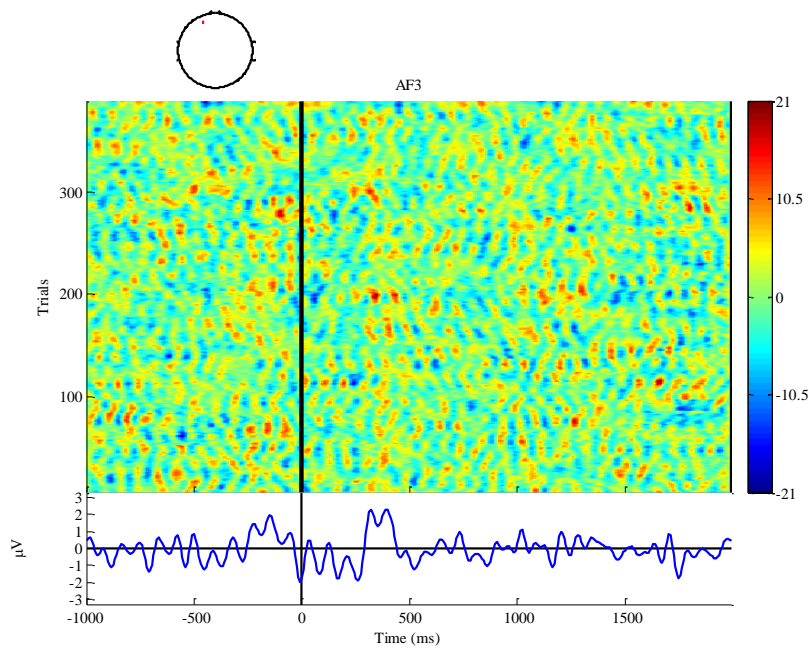(b) The AF3 (blue) and AF4 (green) ERP from the non-target event.

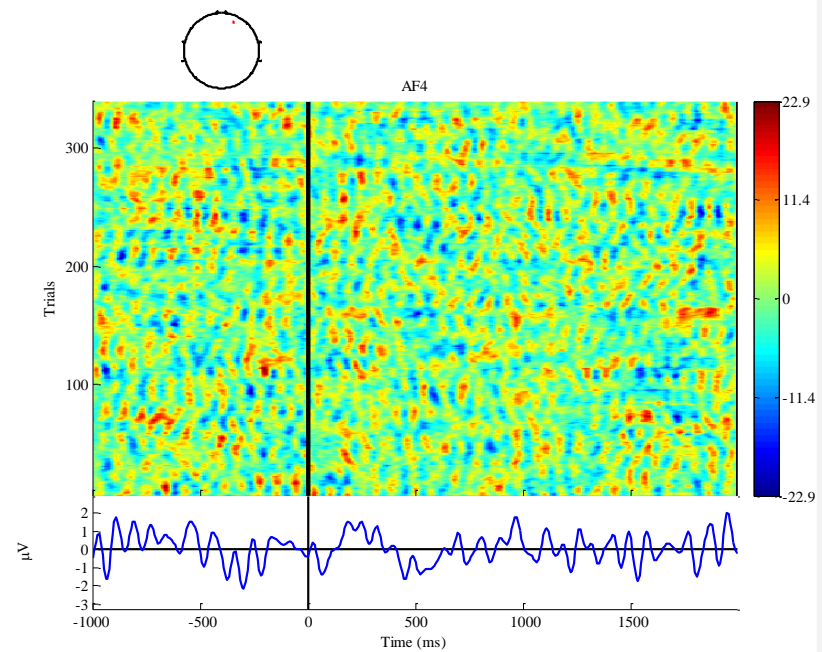(c) The AF3 ERP image responded to the target auditory event.

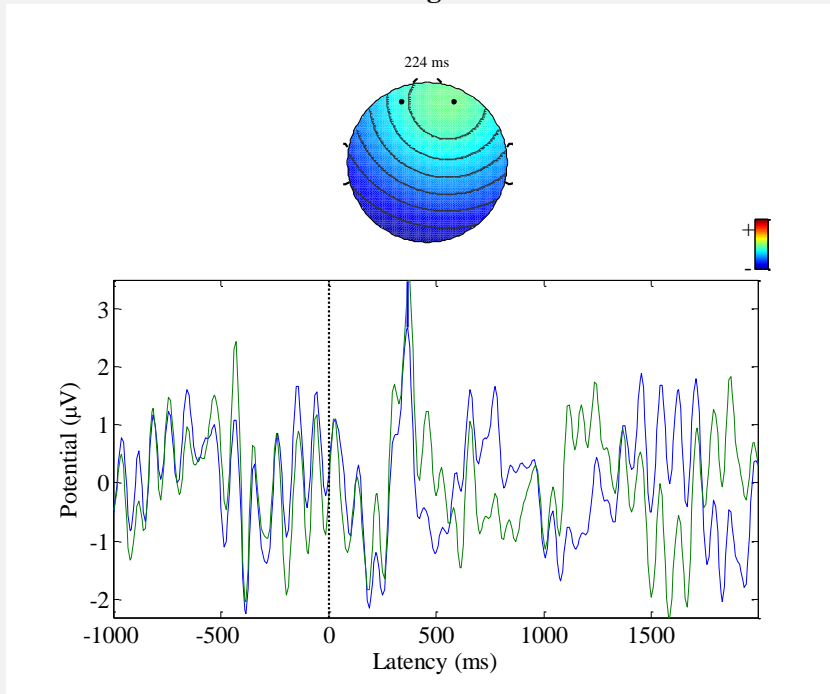(d) The AF3 ERP image responded to the non-target event.

(e) The AF4 ERP image responded to the target auditory event.

(f) The AF4 ERP image responded to the non-target event.

Figure Appendix.6 The comparison between targets and non-target response for experiment 3.

Target

(a) The AF3 (blue) and AF4 (green) ERP responded to the target auditory event.

Non-target

(b) The AF3 (blue) and AF4 (green) ERP from the non-target event.

(c) The AF3 ERP image responded to the target auditory event.

(d) The AF3 ERP image responded to the non-target event.

(e) The AF4 ERP image responded to the target auditory event.

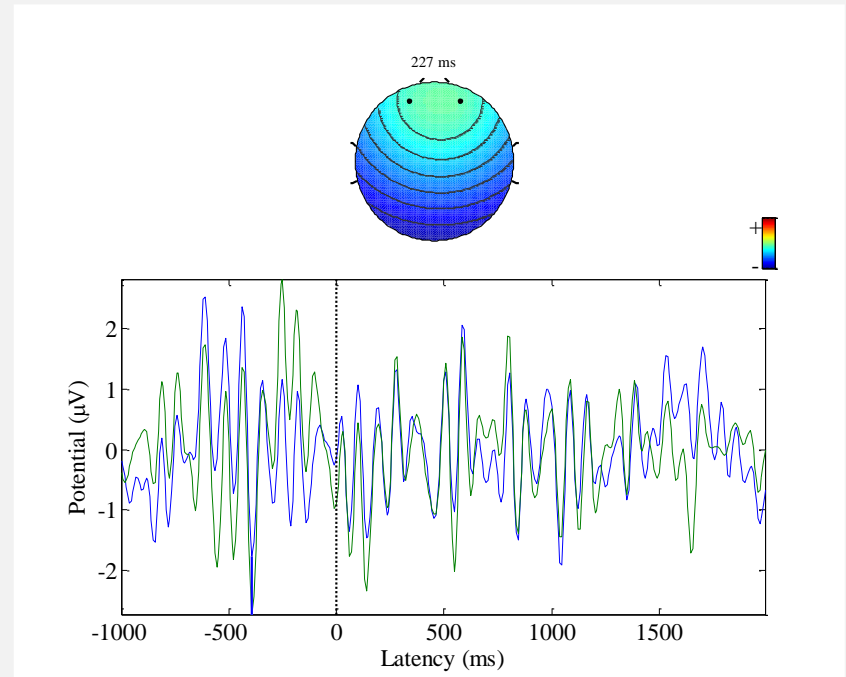(f) The AF4 ERP image responded to the non-target event.

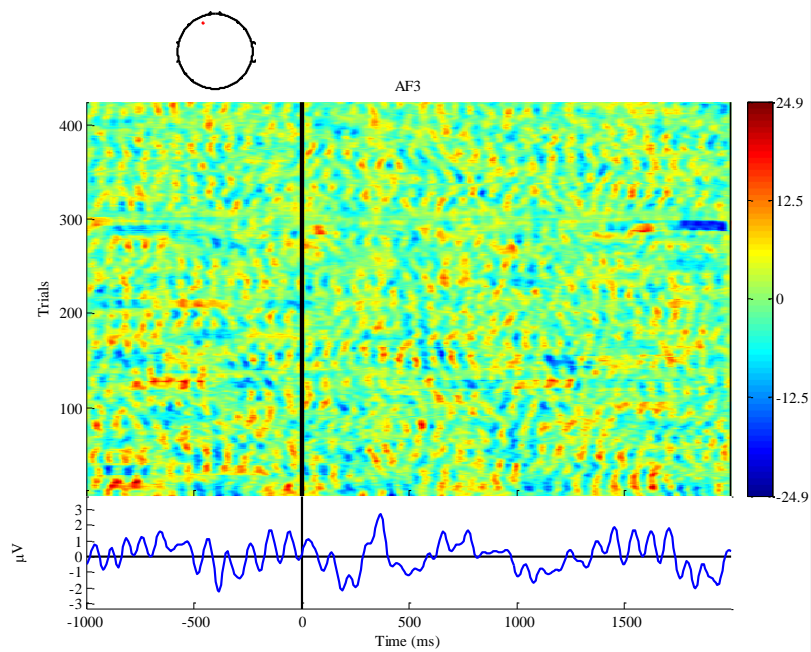Figure Appendix.7 The comparison between targets and non-target response for experiment 4.

(a) The AF3 (blue) and AF4 (green) ERP responded to the target auditory event.
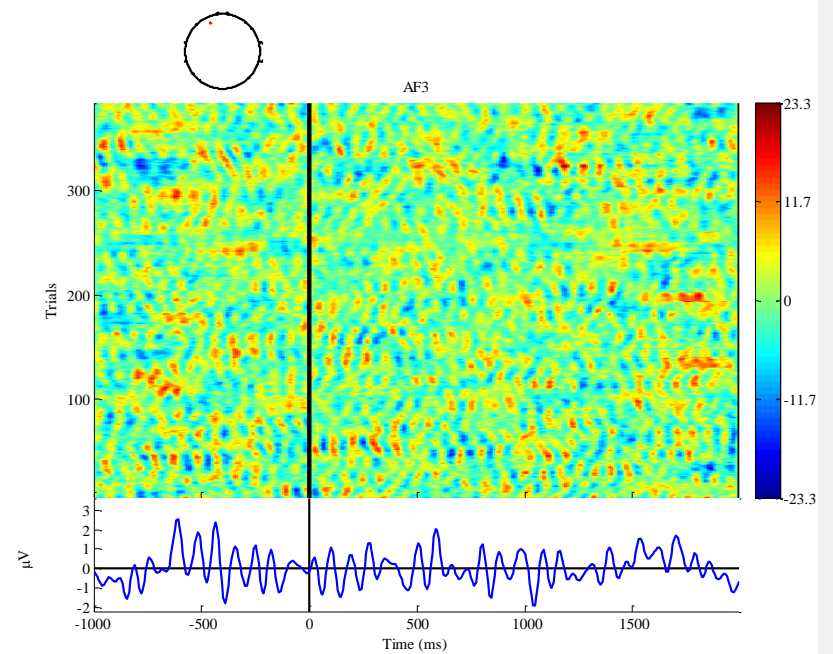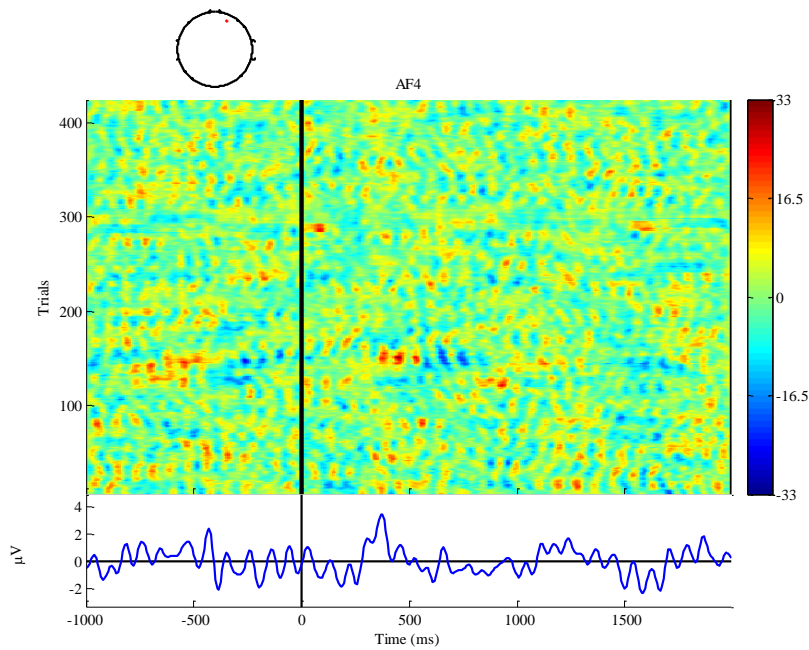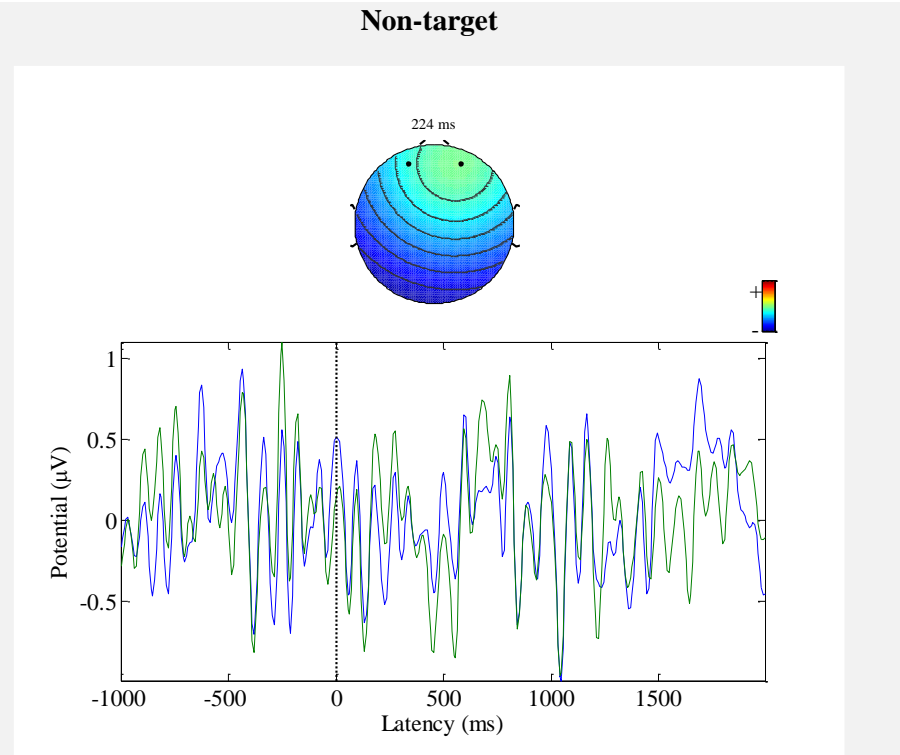

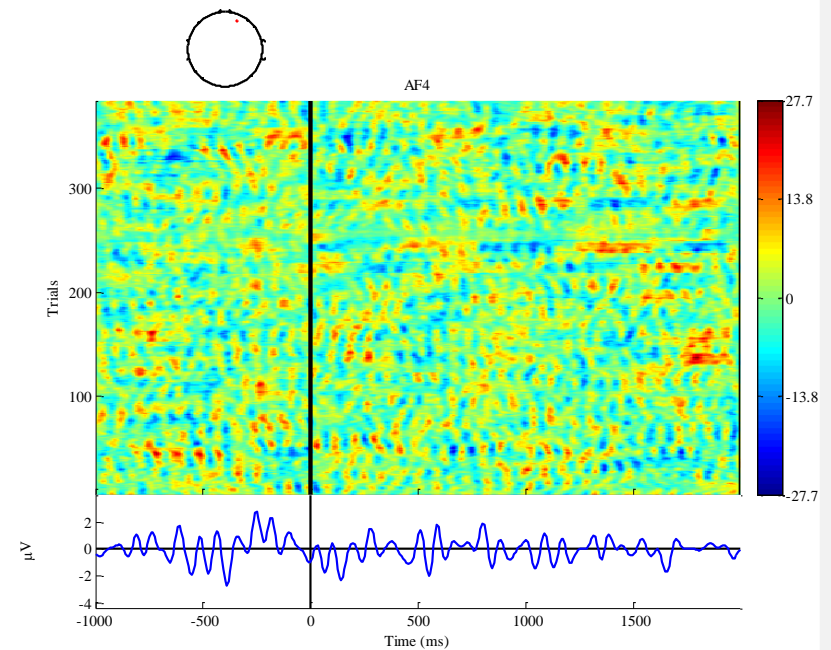(b) The AF3 (blue) and AF4 (green) ERP from the non-target event.
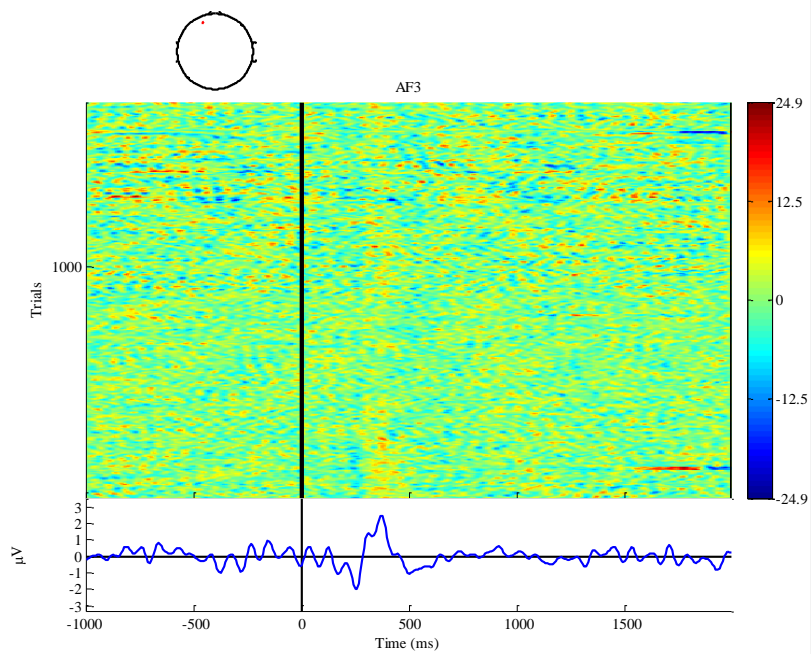
(c) The AF3 ERP image responded to the target auditory event.
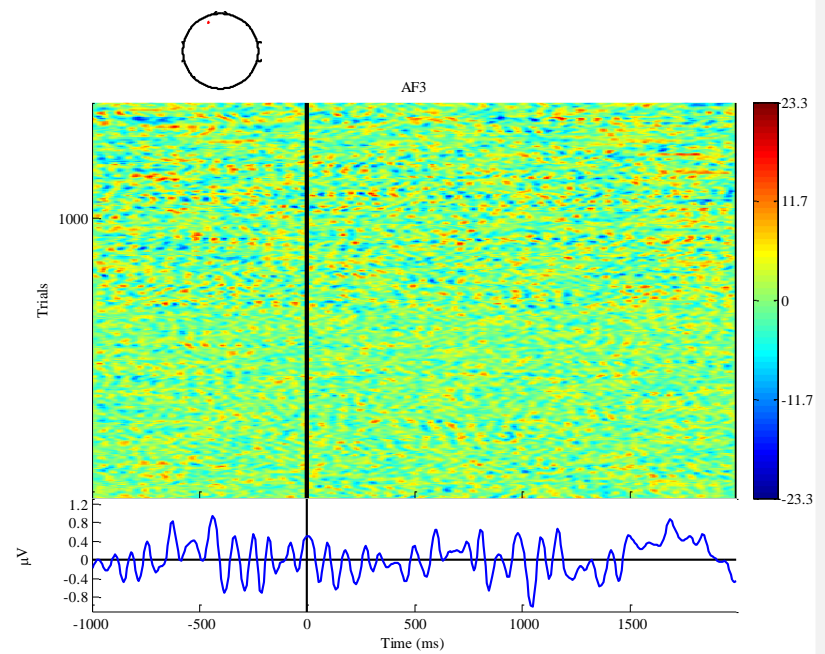
(d) The AF3 ERP image responded to the non-target event.
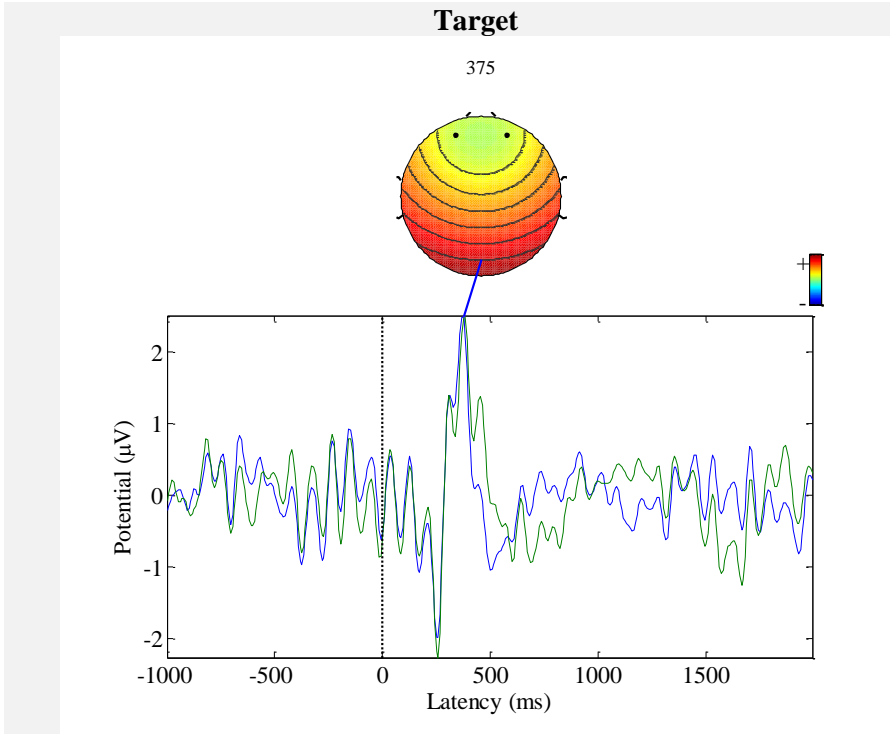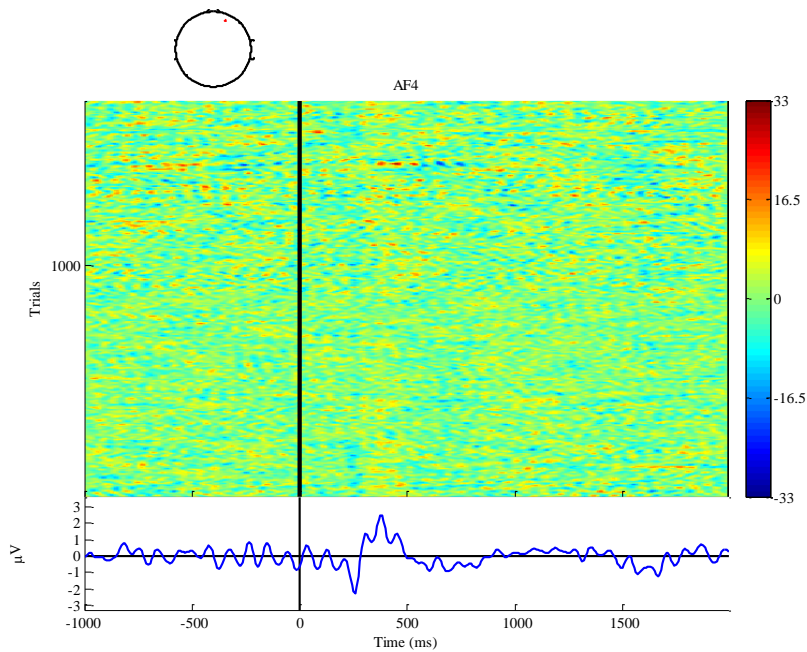
(e) The AF4 ERP image responded to the target auditory event.
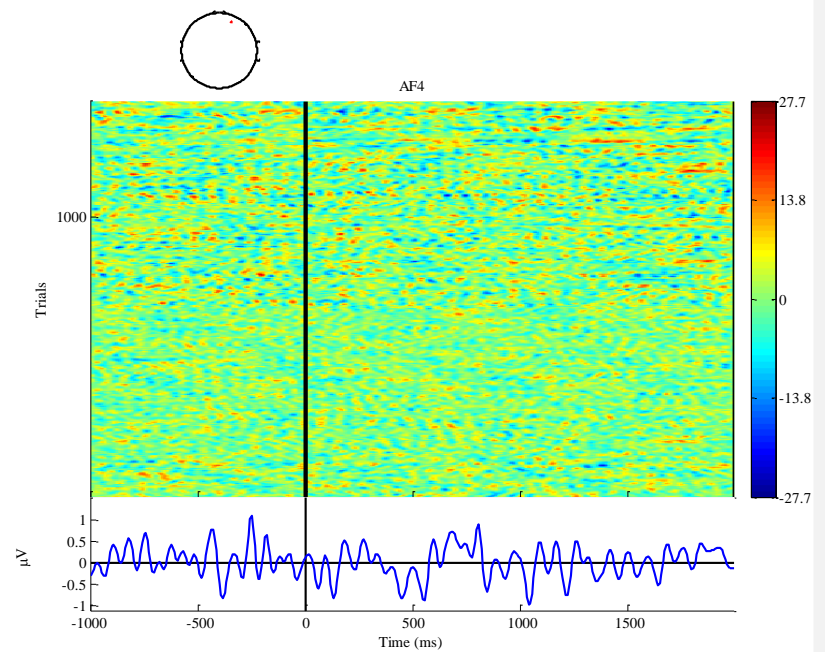
(f) The AF4 ERP image responded to the non-target event.

Figure Appendix.8 The comparison between targets and non-target response from all the 4 experiments.
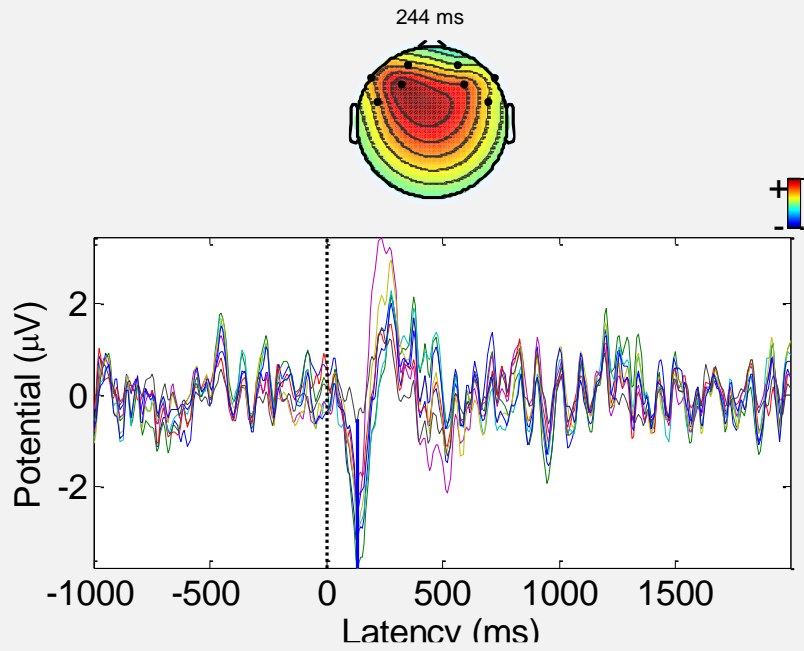
(a) Target (the ERP responded to a mouse click)
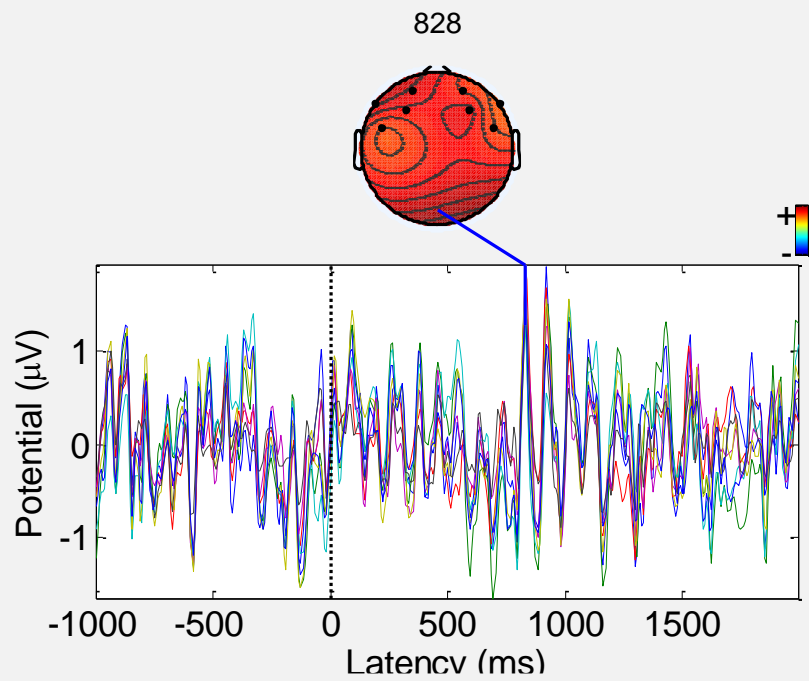
(b) Non-target

Figure Appendix.9 The brain responses to (a) target and (b) non-target (experiment 1).
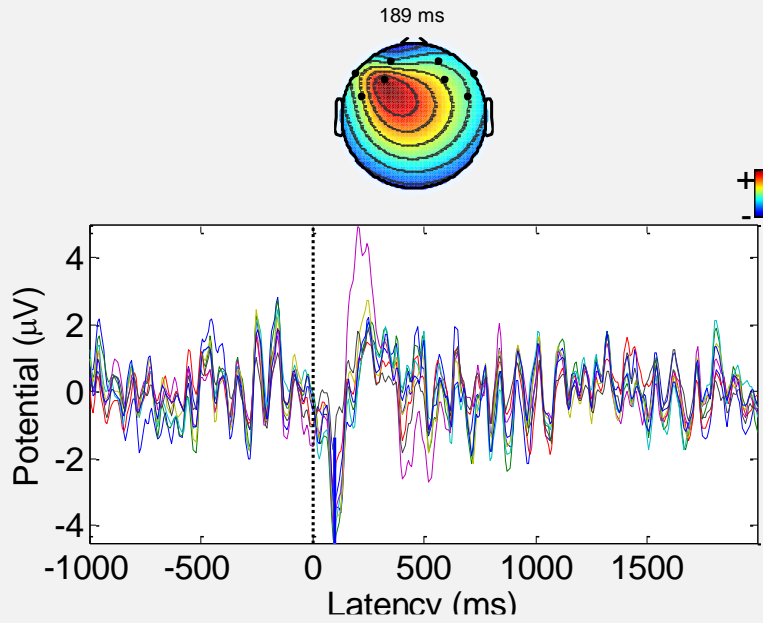
(a) Target (the ERP responded to a mouse click)
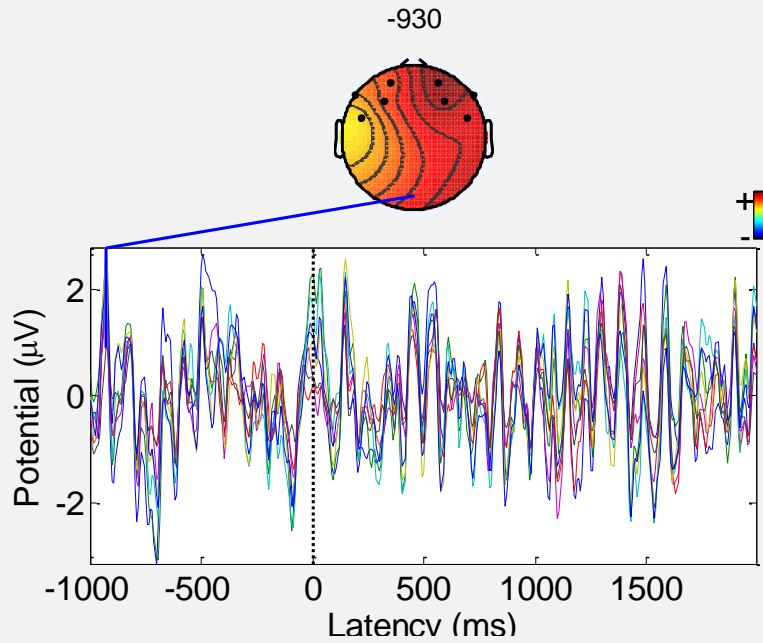
(b) Non-target

Figure Appendix.10 The brain responses to (a) target and (b) non-target (experiment 2).
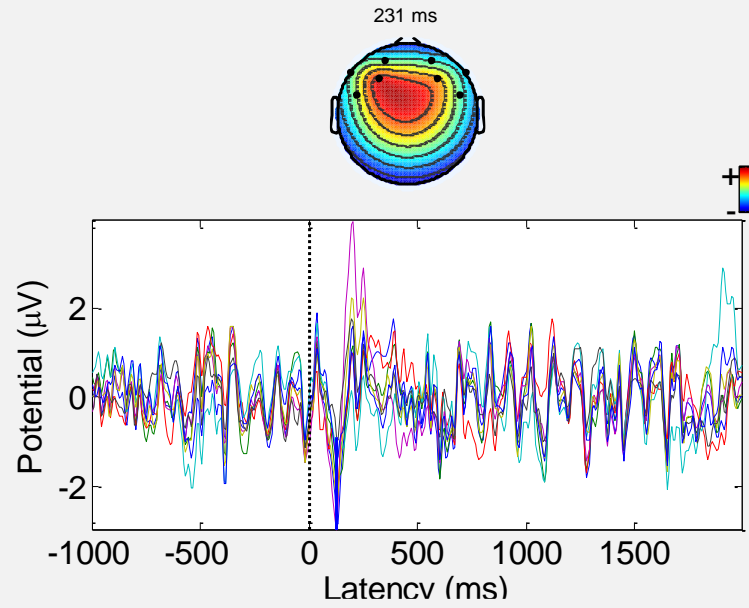
(a) Target (the ERP responded to a mouse click)
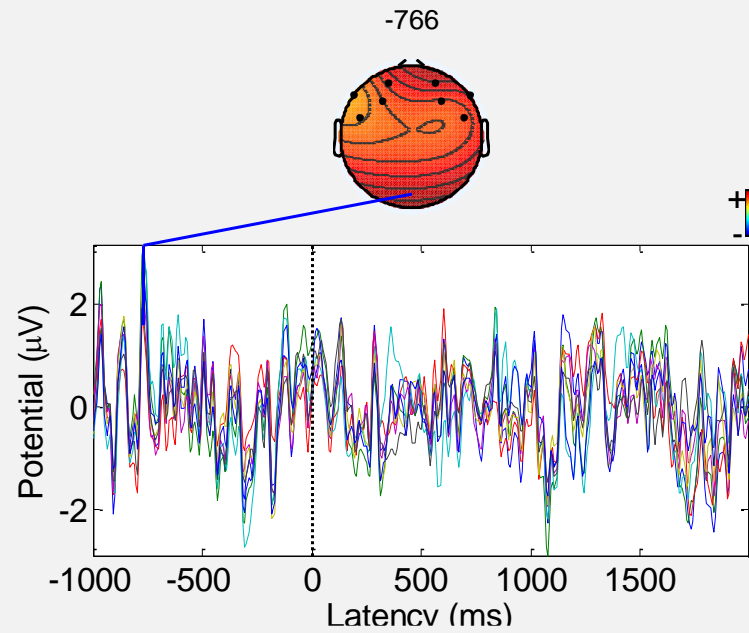
(b) Non-target

Figure Appendix.11 The brain responses to (a) target and (b) non-target (experiment 3).
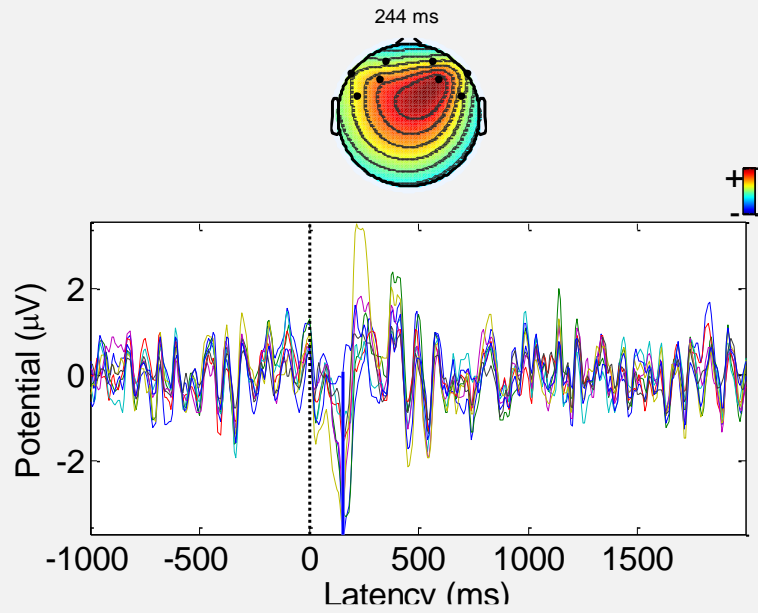
(a) Target (the ERP responded to a mouse click)
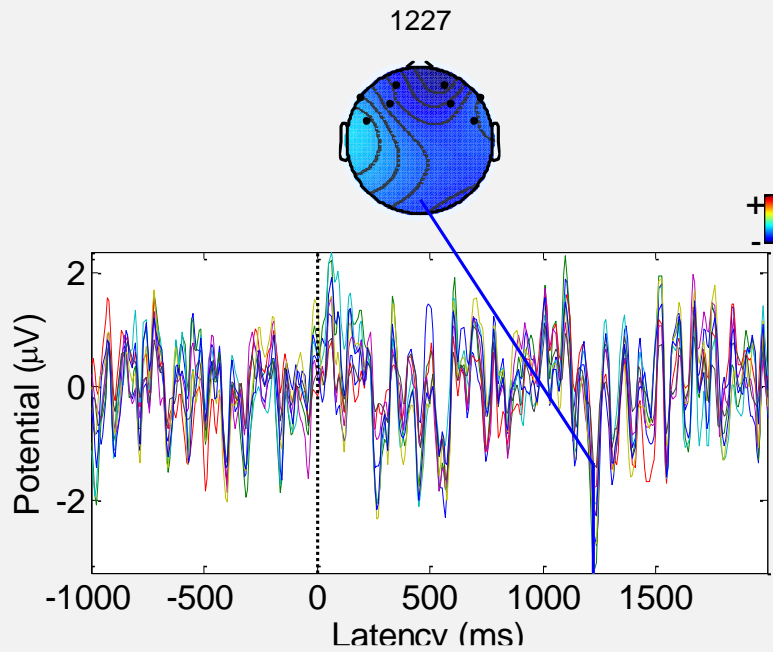
(b) Non-target

Figure Appendix.12 The brain responses to (a) target and (b) non-target (experiment 4).

I. The modelling results based on each of the target hitting task performance indicators (RT, MT, DT, MA, HA, IP)

I.1 RT modelling result

10-time-10-fold average classification accuracy when using reaction time (RT) as a performance indicator

■ Average training accuracy   □ Average testing accuracy

Figure Appendix.13 The 10-time-10-fold cross validation results for RT as a performance indicator.

Table Appendix.1 The confusion matrix of the RT classification model with a single hidden neuron.

		Predicted Class		
		Low	High	
Actual Class	Low	588 (TP) 26.0%	351 (FN) 15.5%	62.6% (TPR) 37.4% (FNR)
	High	545 (FP) 24.1%	775 (TN) 34.3%	58.7% (TPR) 41.3% (FNR)
		51.9% (TNR) 48.1% (FPR)	68.8% (TNR) 31.2% (FPR)	60.3% (AC) 39.7% (Error)
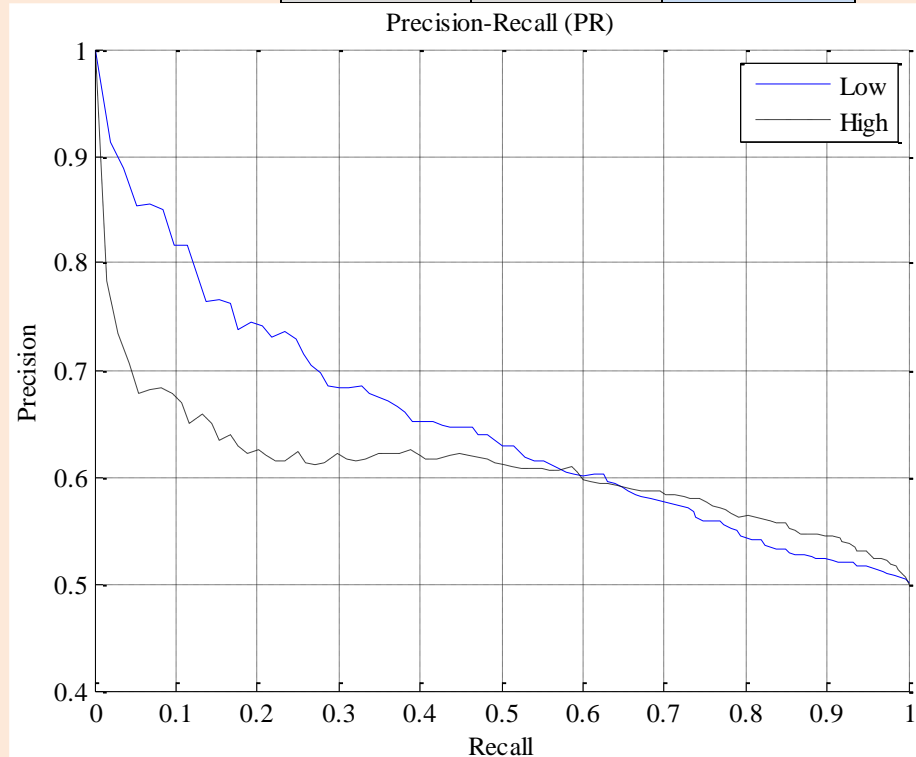
(a) The precision-recall curve from the RT model training.
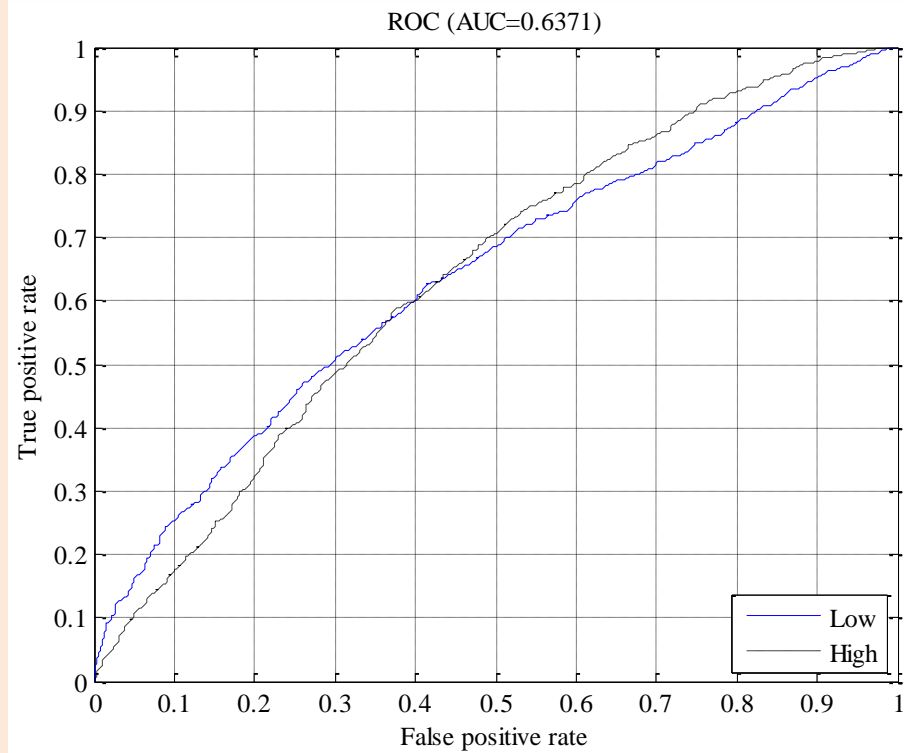
(b) The ROC curve from the RT model training.

Figure Appendix.14 The RT model training performance curves (a) PR curve (b) ROC curve.

Table Appendix.2 The confusion matrix of the RT blind test classification model with a single hidden neuron.

		Predicted Class		
		Low	High	
Actual Class	Low	72 (TP) 28.3%	51 (FN) 20.1%	58.5% (TPR) 41.5% (FNR)
	High	55 (FP) 21.7%	76 (TN) 29.9%	58.0% (TPR) 42.0% (FNR)
		56.7% (TNR) 43.3% (FPR)	59.8% (TNR) 40.2% (FPR)	58.3% (AC) 41.7% (Error)

(a) The precision-recall curve from the RT model blind testing.

(b) The ROC curve from the RT model blind testing.

Figure Appendix.15 The RT blind testing performance curves (a) PR curve (b) ROC curve.

I.2 MT modelling result

10-time-10-fold average classification accuracy when using movement time (MT) as a performance indicator

☐ Average training accuracy   ☐ Average testing

Accuracy (%)

Number of hidden neurons

Figure Appendix.16 The 10-time-10-fold cross validation results for MT as a performance indicator.

Table Appendix.3 The confusion matrix of the MT classification model with the 2 hidden neurons.

		Predicted Class		
		Low	High	
Actual Class	Low	955 (TP) 42.3%	135 (FN) 6.0%	87.6% (TPR) 12.4% (FNR)
	High	175 (FP) 7.7%	994 (TN) 44.0%	85.0% (TPR) 15.0% (FNR)
		84.5% (TNR) 15.5% (FPR)	88.0% (TNR) 12.0% (FPR)	86.3% (AC) 13.7% (Error)
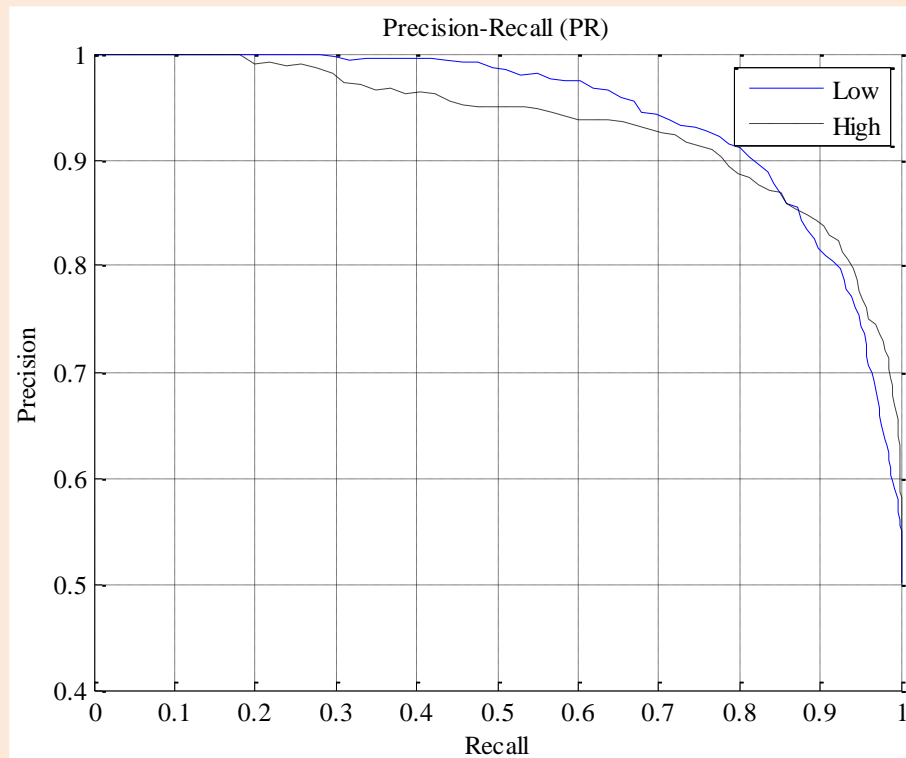
(a) The precision-recall curve from the MT model training.
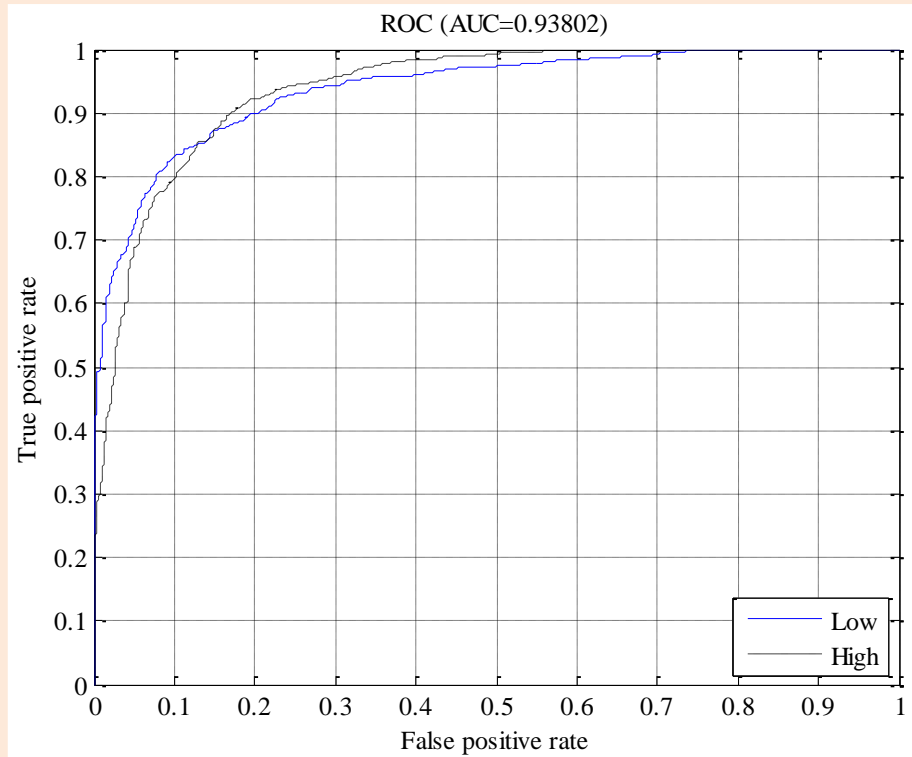
(b) The ROC curve from the MT model training.

Figure Appendix.17 The MT model training performance curves (a) PR curve (b) ROC curve.

Table Appendix.4 The confusion matrix of the MT blind test classification model with the 2 hidden neurons.

		Predicted Class		
		Low	High	
Actual Class	Low	92 (TP) 36.2%	36 (FN) 14.2%	71.9% (TPR) 28.1% (FNR)
	High	35 (FP) 13.8%	91 (TN) 35.8%	72.2% (TPR) 27.8% (FNR)
		72.4% (TNR) 27.6% (FPR)	71.7% (TNR) 28.3% (FPR)	72.0% (AC) 28.0% (Error)

Precision-Recall (PR)

(a) The precision-recall curve from the MT model blind testing.

ROC (AUC=0.86199)
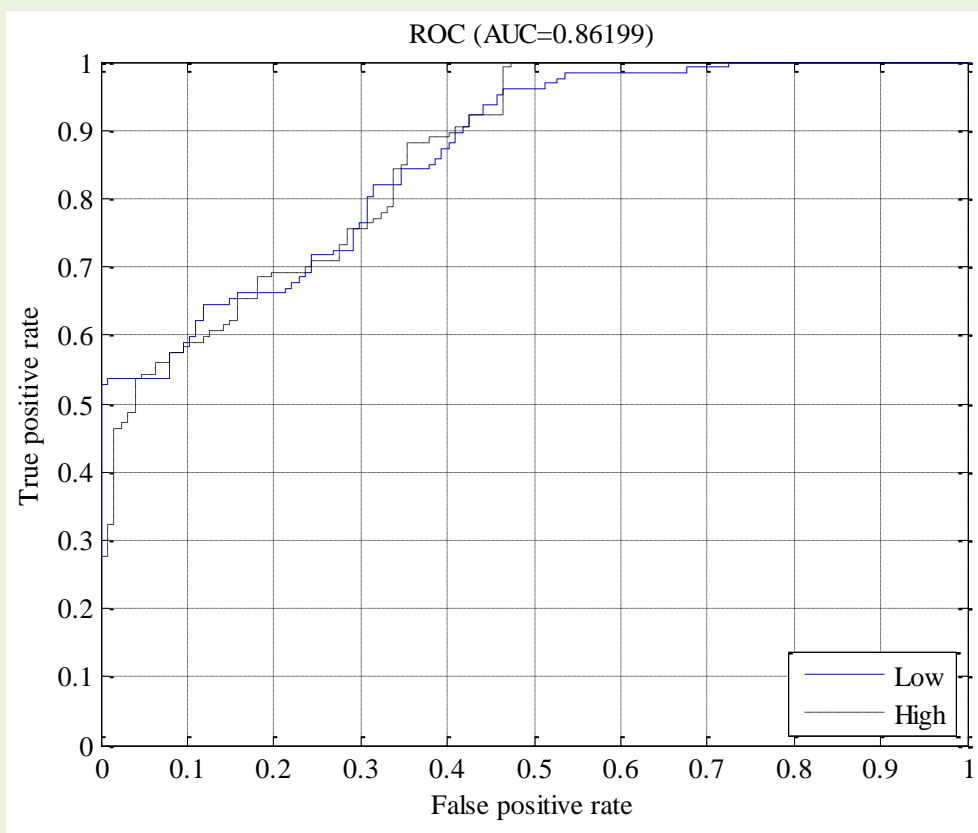
(b) The ROC curve from the MT model blind testing.

Figure Appendix.18 The MT blind testing performance curves (a) PR curve (b) ROC curve.
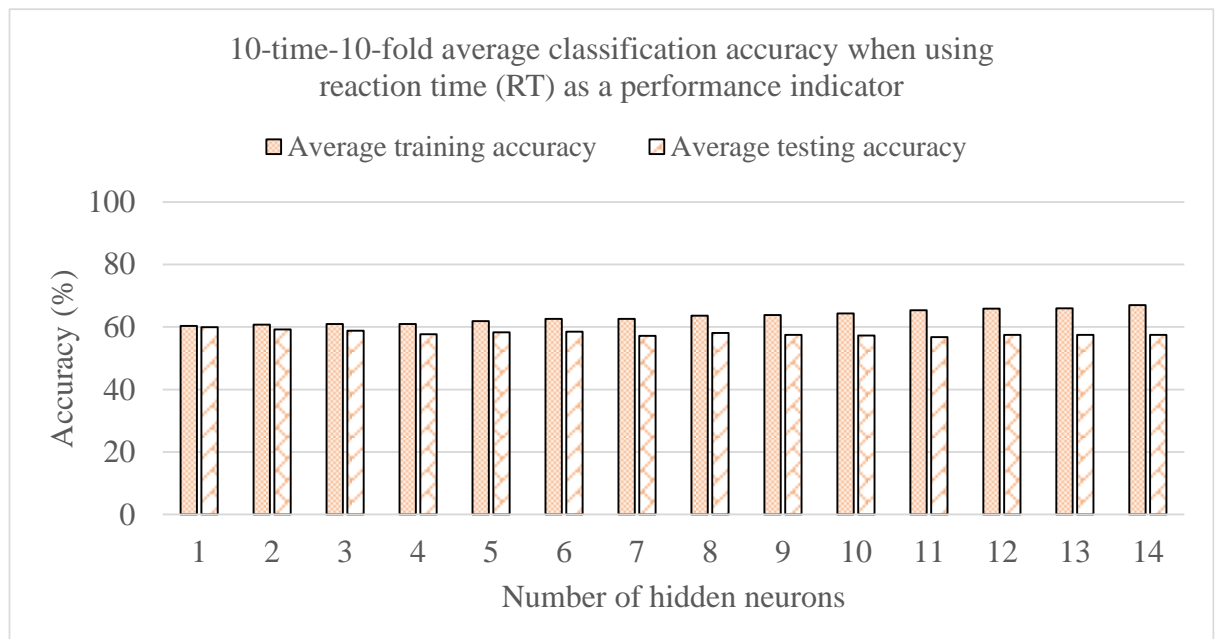
I.3 DT modelling result
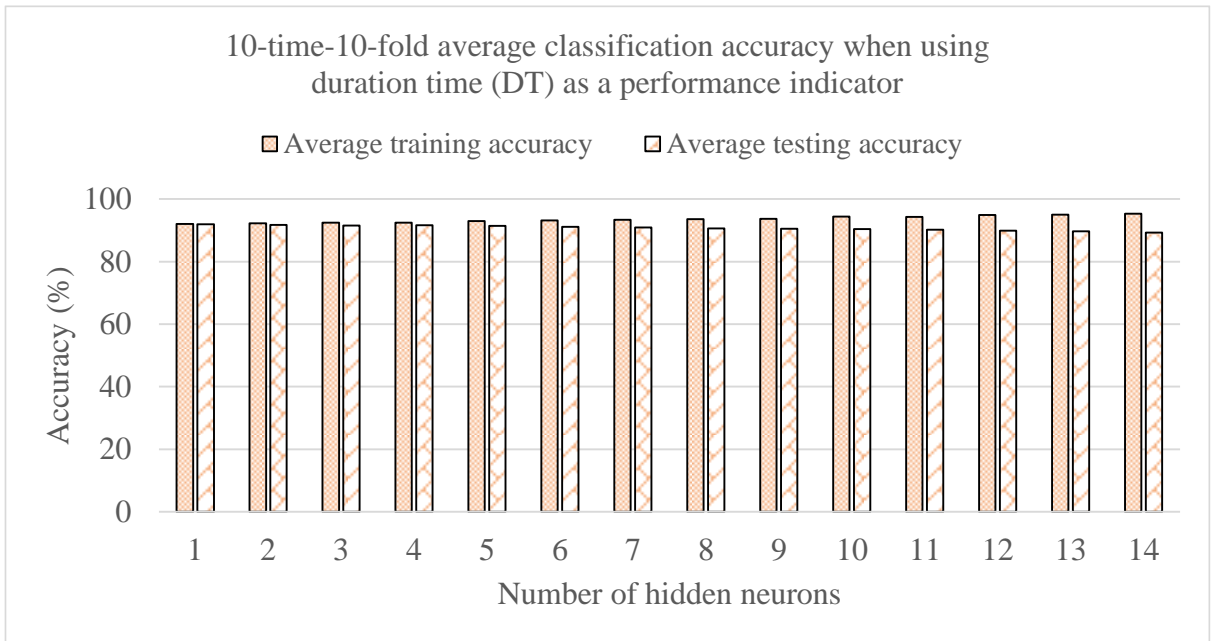
Figure Appendix.19 The 10-time-10-fold cross validation results for DT as a performance indicator.

Table Appendix.5 The confusion matrix of the DT classification model with a single hidden neuron.

		Predicted Class		
		Low	High	
Actual Class	Low	1040 (TP) 46.0%	86 (FN) 3.8%	92.4% (TPR) 7.6% (FNR)
	High	92 (FP) 4.1%	1041 (TN) 46.1%	91.9% (TPR) 8.1% (FNR)
		91.9% (TNR) 8.1% (FPR)	92.4% (TNR) 7.6% (FPR)	92.1% (AC) 7.9% (Error)
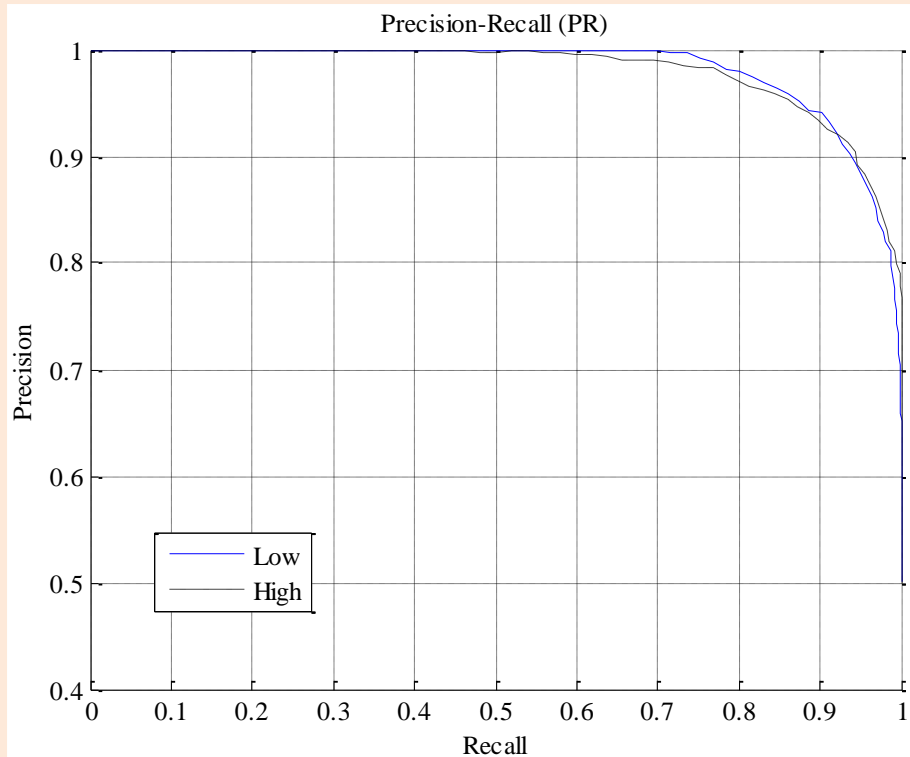
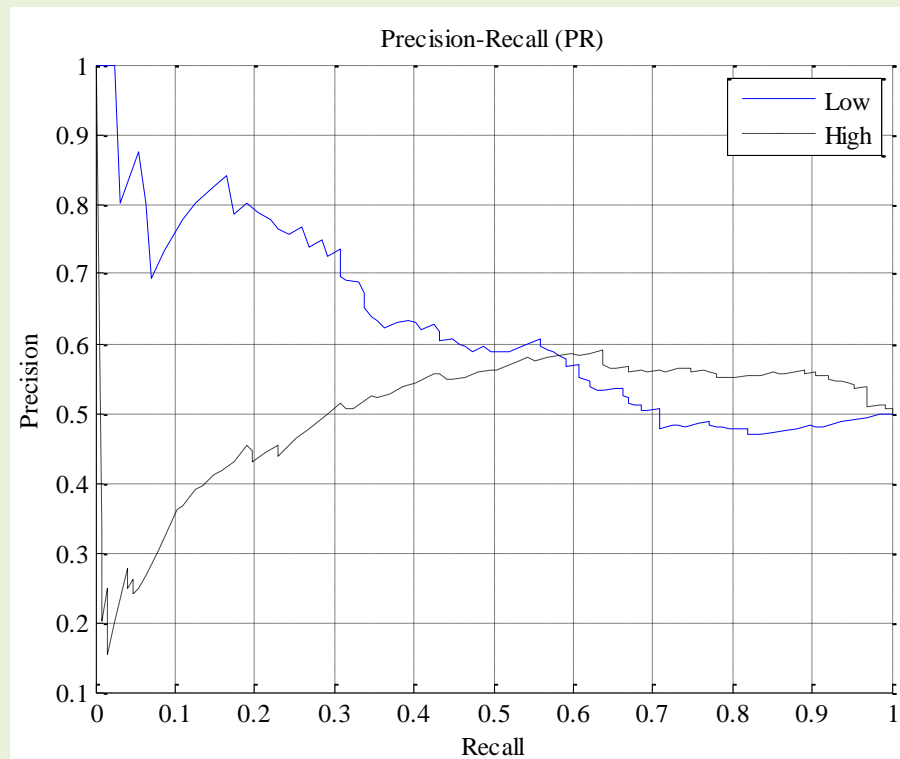(a) The precision-recall curve from the DT model training.
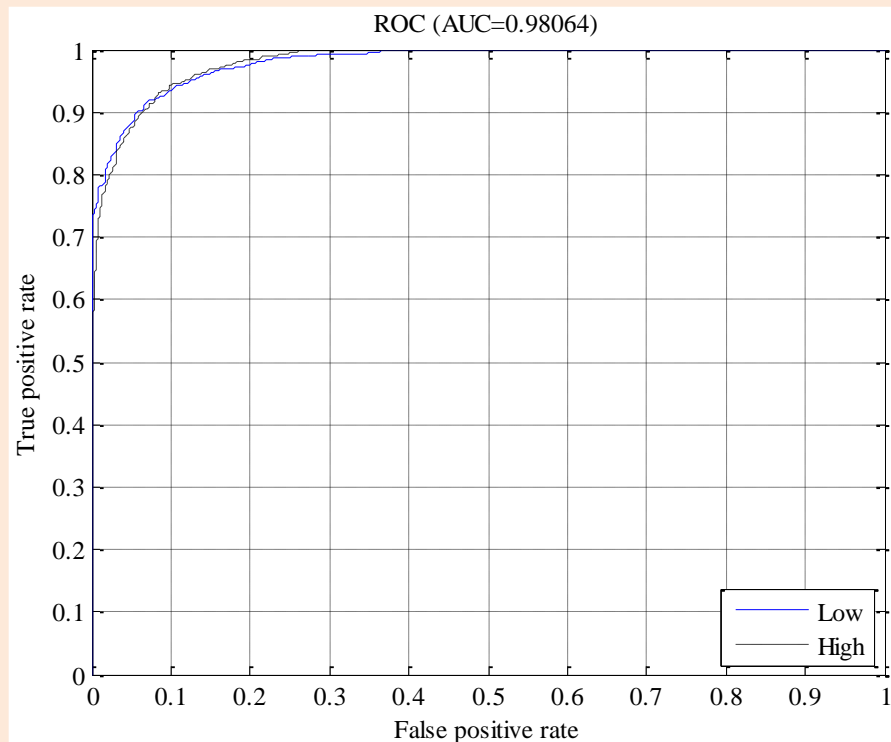
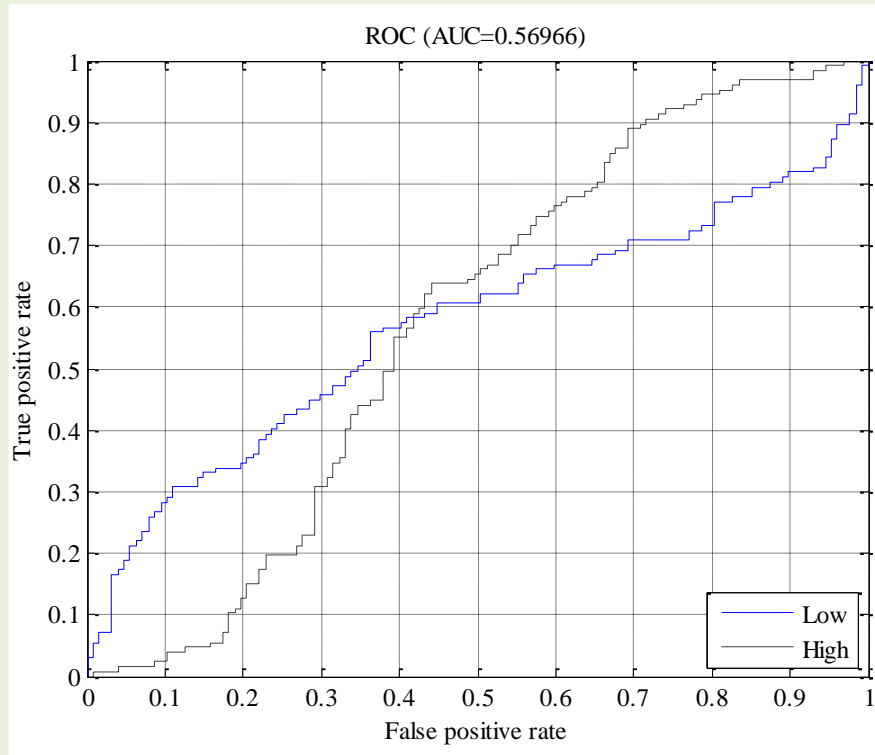(b) The ROC curve from the DT model training.

Figure Appendix.20 The DT model training performance curves (a) PR curve (b) ROC curve.

Table Appendix.6 The confusion matrix of the DT blind test classification model with a single hidden neuron.

		Predicted Class		
		Low	High	
Actual Class	Low	93 (TP) 36.6%	32 (FN) 12.6%	74.4% (TPR) 25.6% (FNR)
	High	34 (FP) 13.4%	95 (TN) 37.4%	73.6% (TPR) 26.4% (FNR)
		73.2% (TNR) 26.8% (FPR)	74.8% (TNR) 25.2% (FPR)	74.0% (AC) 26.0% (Error)

(a) The precision-recall curve from the DT model blind testing.

ROC (AUC=0.8809)

(b) The ROC curve from the DT model blind testing.

Figure Appendix.21 The DT blind testing performance curves (a) PR curve (b) ROC curve.
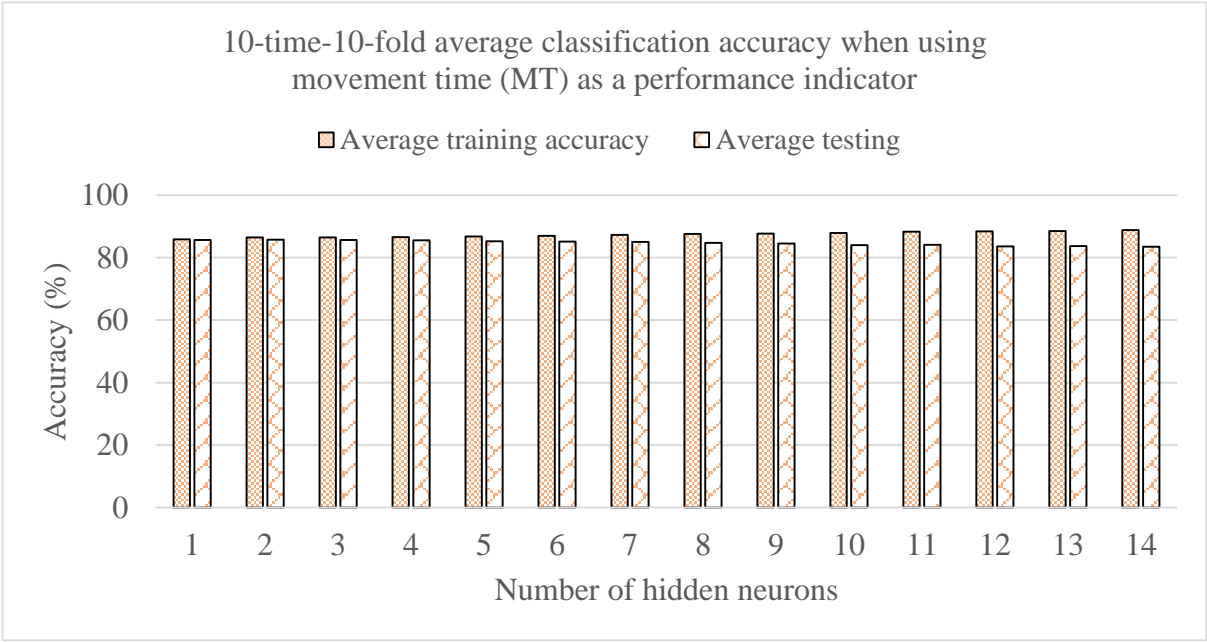
I.4 MA modelling result
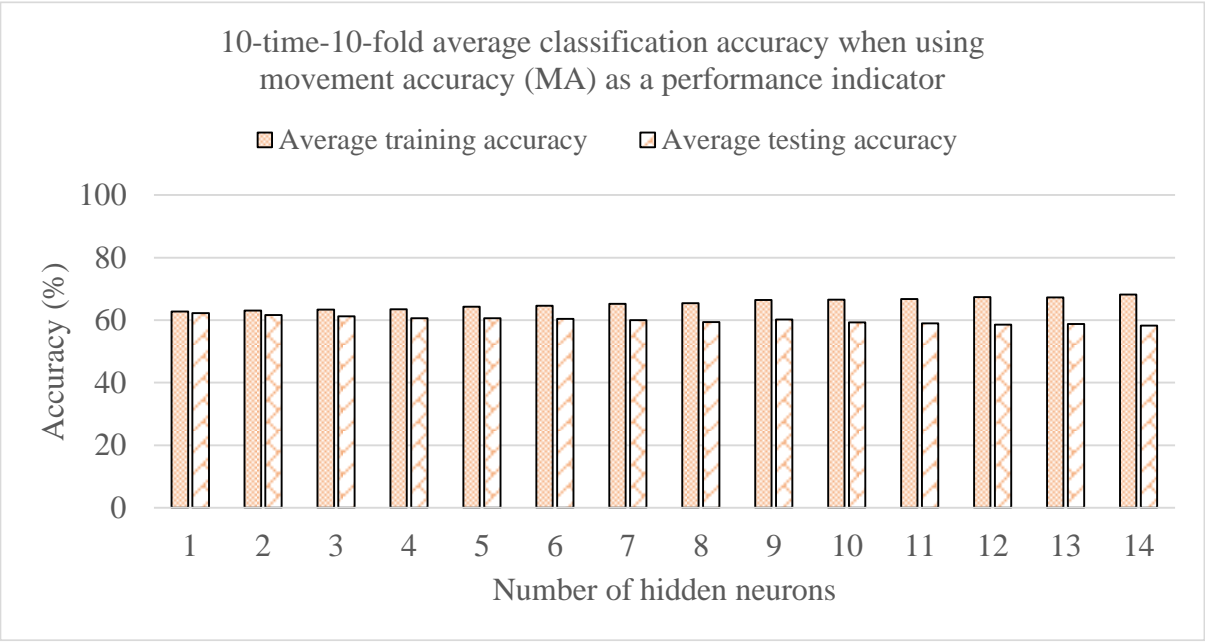
Figure Appendix.22 The 10-time-10-fold cross validation results for MA as a performance indicator.

Table Appendix.7 The confusion matrix of the MA classification model with a single hidden neuron.

		Predicted Class		
		Low	High	
Actual Class	Low	678 (TP) 30.00%	388 (FN) 17.20%	63.6% (TPR) 36.4% (FNR)
	High	452 (FP) 20.00%	741 (TN) 32.80%	62.1% (TPR) 37.9% (FNR)
		60.0% (TNR) 40.0% (FPR)	65.6% (TNR) 34.4% (FPR)	62.8% (AC) 37.2% (Error)
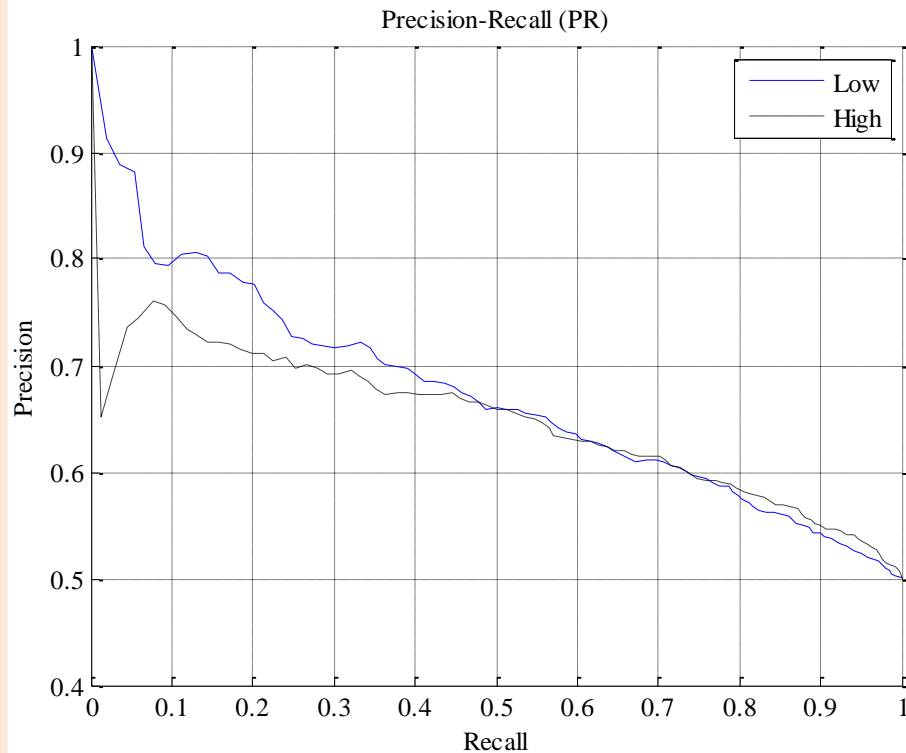
(a) The precision-recall curve from the MA model training.
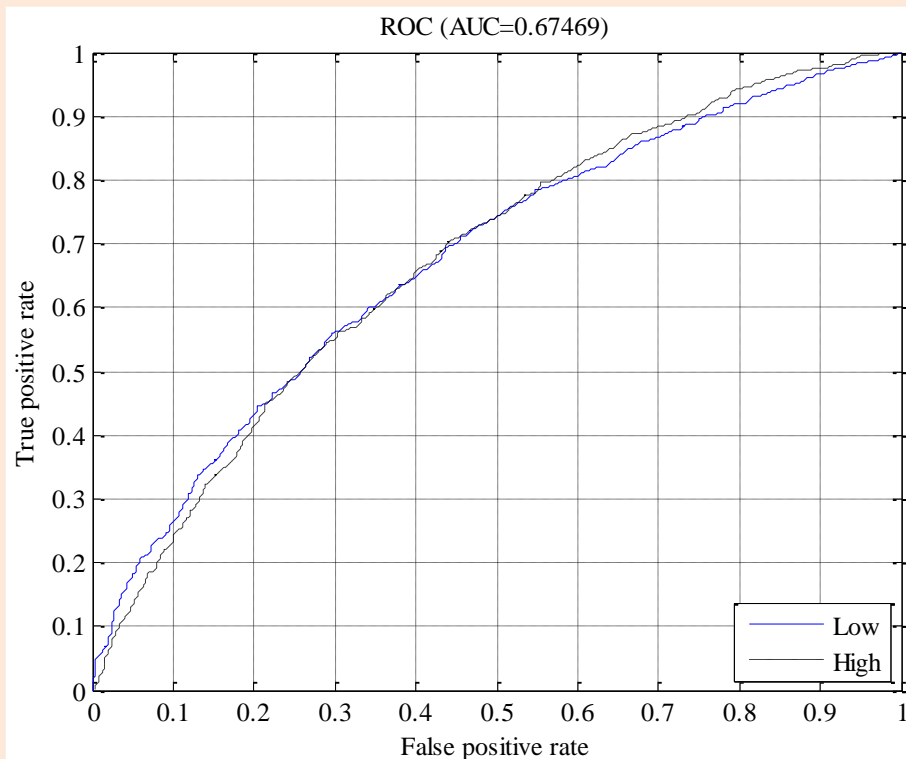
(b) The ROC curve from the MA model training.

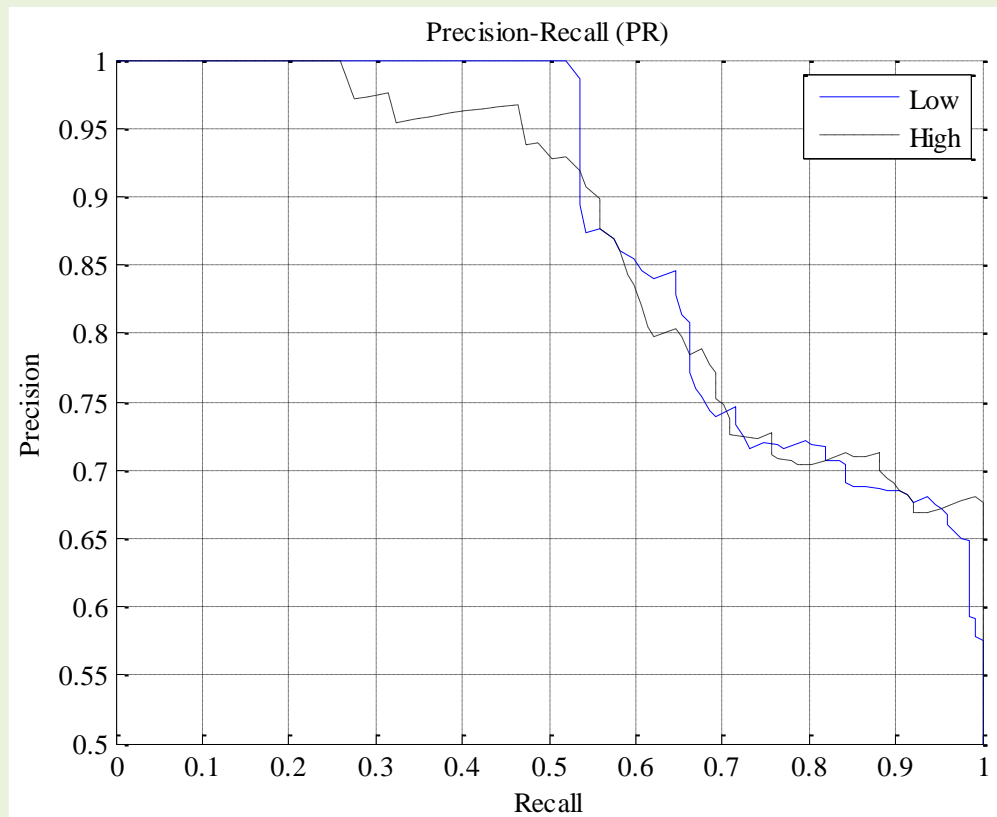Figure Appendix.23 The MA model training performance curves (a) PR curve (b) ROC curve.

Table Appendix.8 The confusion matrix of the MA blind test classification model with a single hidden neuron.

		Predicted Class		
		Low	High	
Actual Class	Low	81 (TP) 31.90%	38 (FN) 15.00%	68.1% (TPR) 31.9% (FNR)
	High	46 (FP) 18.10%	89 (TN) 35.00%	65.9% (TPR) 34.1% (FNR)
		63.8% (TNR) 36.2% (FPR)	70.1% (TNR) 29.9% (FPR)	66.9% (AC) 33.9% (Error)
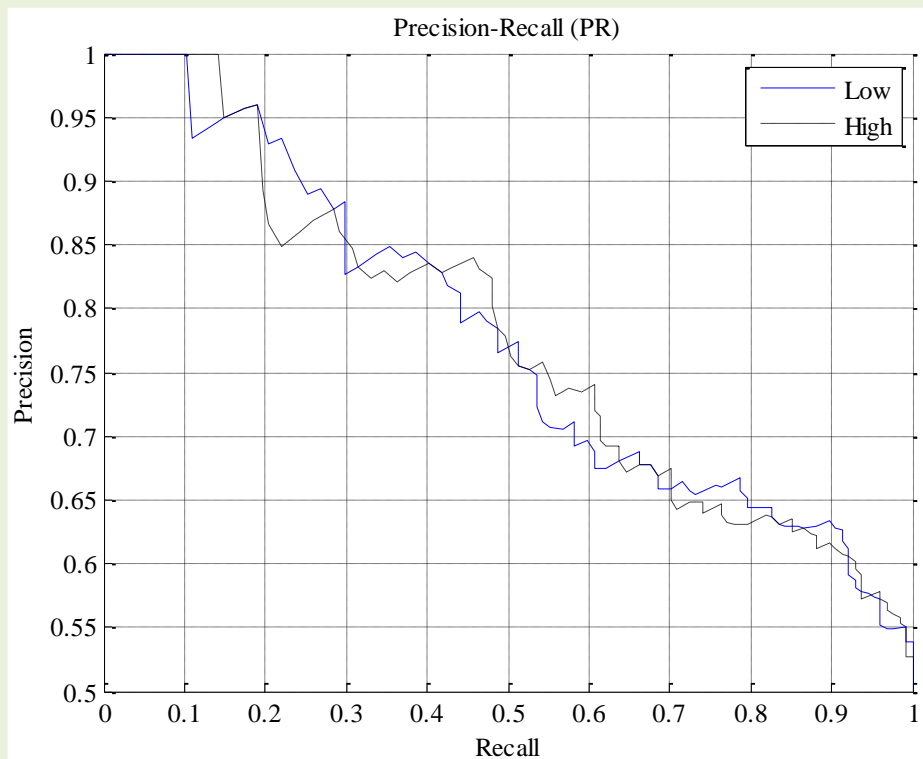
Precision-Recall (PR)

(a) The precision-recall curve from the MA model blind testing.
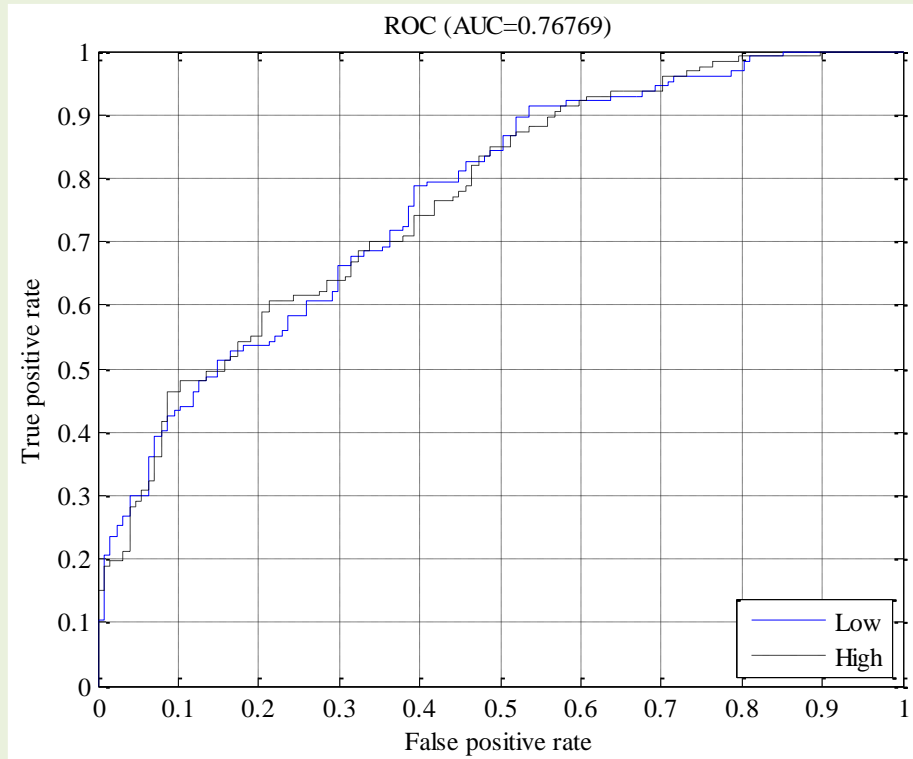
(b) The ROC curve from the MA model blind testing.

Figure Appendix.24 The MA blind testing performance curves (a) PR curve (b) ROC curve.

I.5 HA modelling result

10-time-10-fold average classification accuracy when using hit accuracy (HA) as a performance indicator

☐ Average training accuracy ☐ Average testing accuracy

Figure Appendix.25 The 10-time-10-fold cross validation results for HA as a performance indicator.

Table Appendix.9 The confusion matrix of the HA classification model with 8 hidden neurons.

		Predicted Class		
		Low	High	
Actual Class	Low	731 (TP) 32.3%	423 (FN) 18.7%	63.3% (TPR) 36.7% (FNR)
	High	408 (FP) 18.0%	699 (TN) 30.9%	63.1% (TPR) 36.9% (FNR)
		64.2% (TNR) 35.8% (FPR)	62.3% (TNR) 37.7% (FPR)	63.2% (AC) 36.8% (Error)
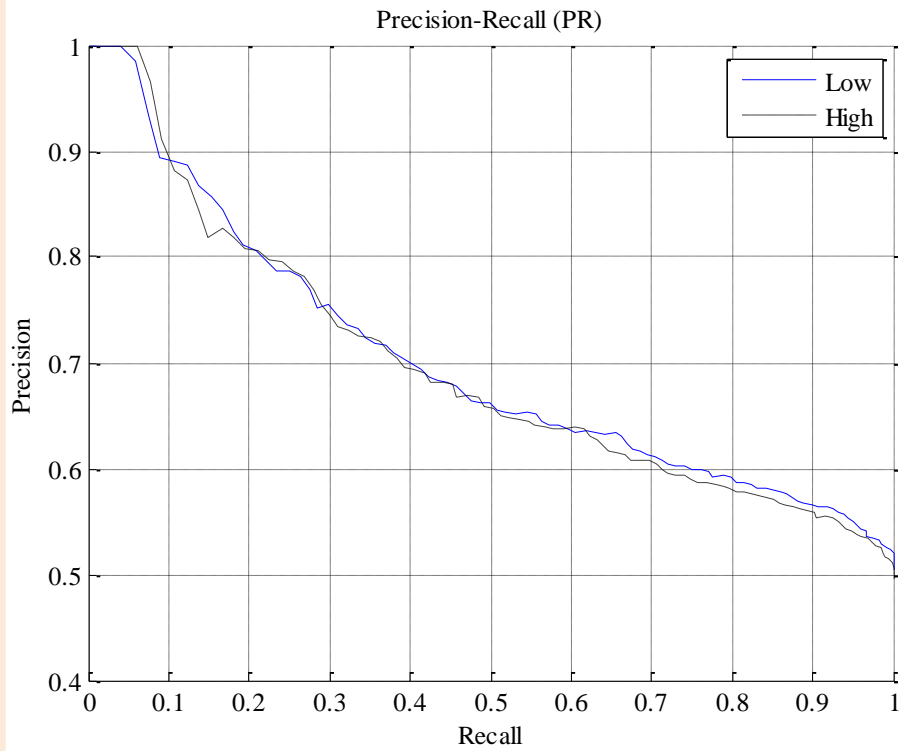
(a) The precision-recall curve from the HA model training.
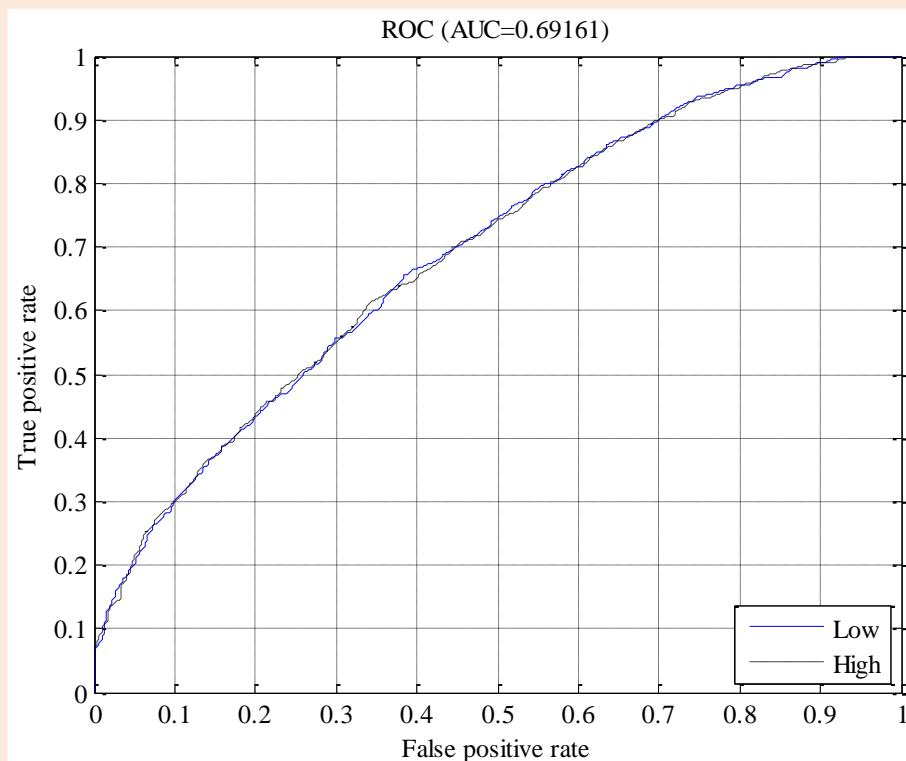
(b) The ROC curve from the HA model training.

Figure Appendix.26 The HA model training performance curves (a) PR curve (b) ROC curve.

Table Appendix.10 The confusion matrix of the HA blind test classification model with 8 hidden neurons.

		Predicted Class		
		Low	High	
Actual Class	Low	86 (TP) 34.1%	58 (FN) 23.0%	59.7% (TPR) 40.3% (FNR)
	High	41 (FP) 16.3%	67 (TN) 26.6%	62.0% (TPR) 38.0% (FNR)
		67.7% (TNR) 32.3% (FPR)	53.6% (TNR) 46.4% (FPR)	60.7% (AC) 39.3% (Error)
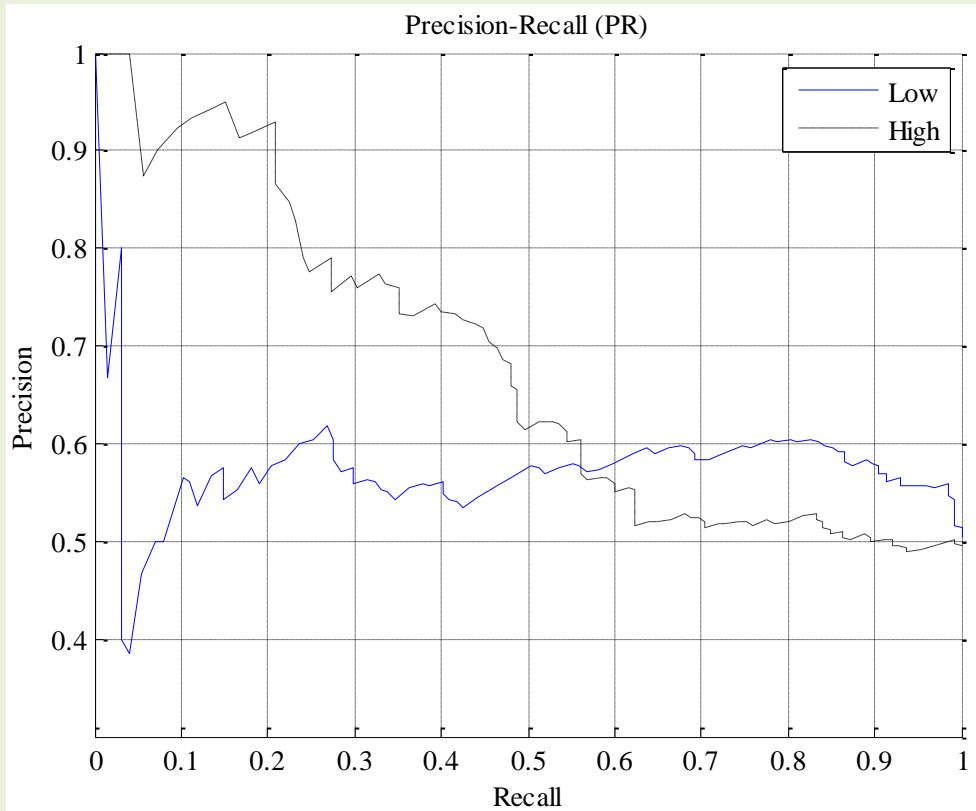
(a) The precision-recall curve from the HA model blind testing.
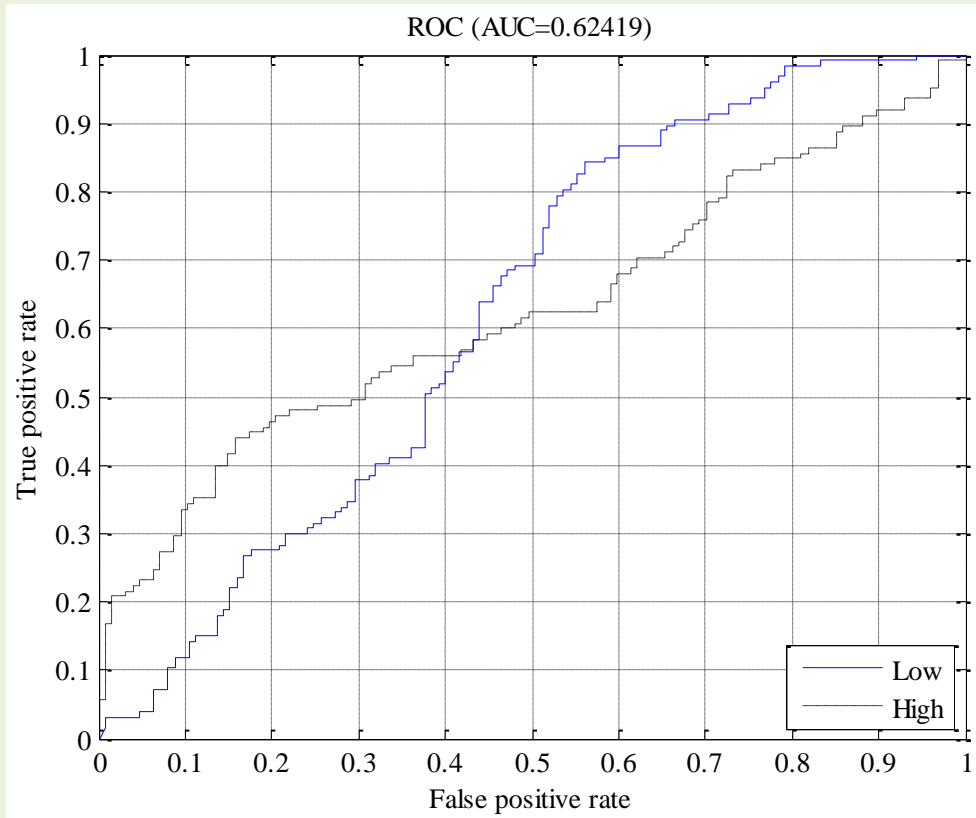
(b) The ROC curve from the HA model blind testing.

Figure Appendix.27 The HA blind testing performance curves (a) PR curve (b) ROC curve.

I.6 IP modelling result

10-time-10-fold average classification accuracy when using Fitts index of performance (IP) as a performance indicator

Figure Appendix.28 The 10-time-10-fold cross validation results for IP as a performance indicator.

Table Appendix.11 The confusion matrix of the IP classification model with the 6 hidden neurons.

		Predicted Class		
		Low	High	
Actual Class	Low	761 (TP) 33.7%	321 (FN) 14.2%	70.3% (TPR) 29.7% (FNR)
	High	370 (FP) 16.4%	807 (TN) 35.7%	68.6% (TPR) 31.4% (FNR)
		67.3% (TNR) 32.7% (FPR)	71.5% (TNR) 28.5% (FPR)	69.4% (AC) 30.6% (Error)
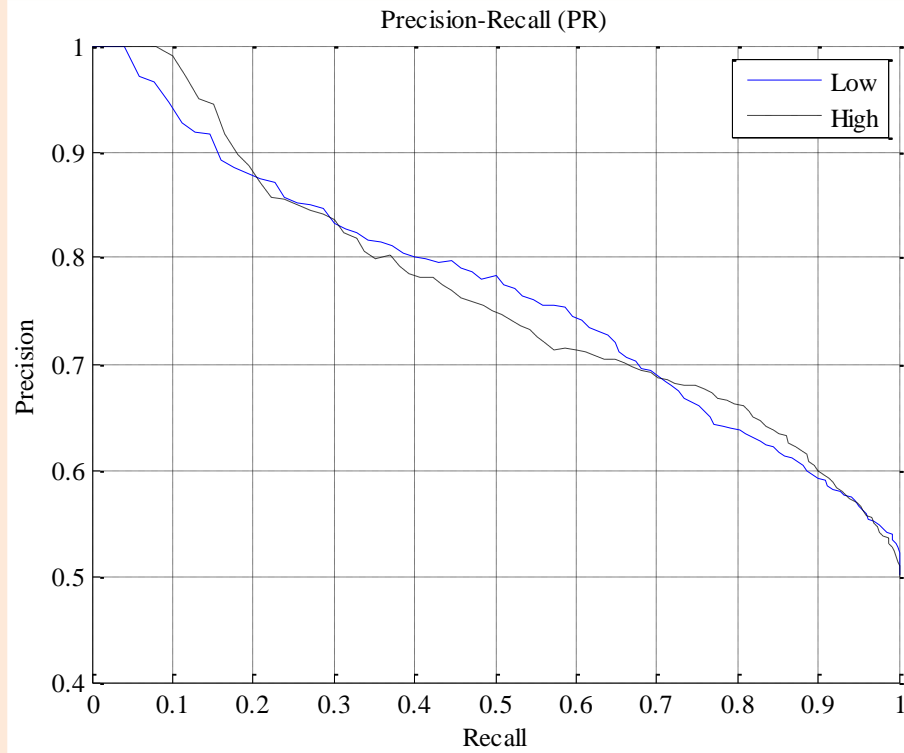
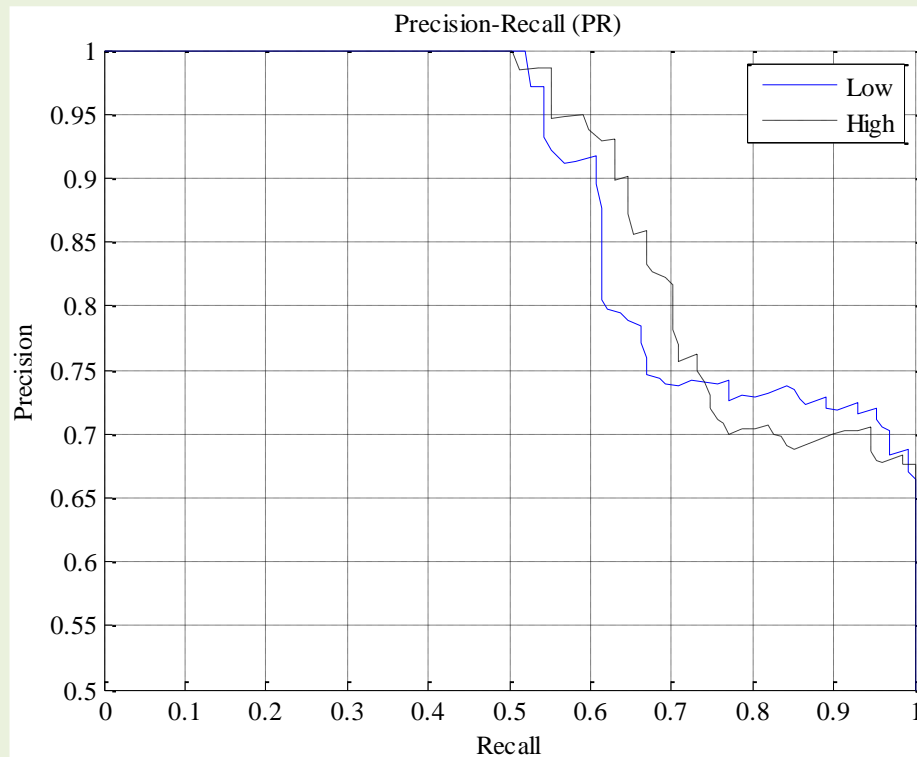(a) The precision-recall curve from the IP model training.
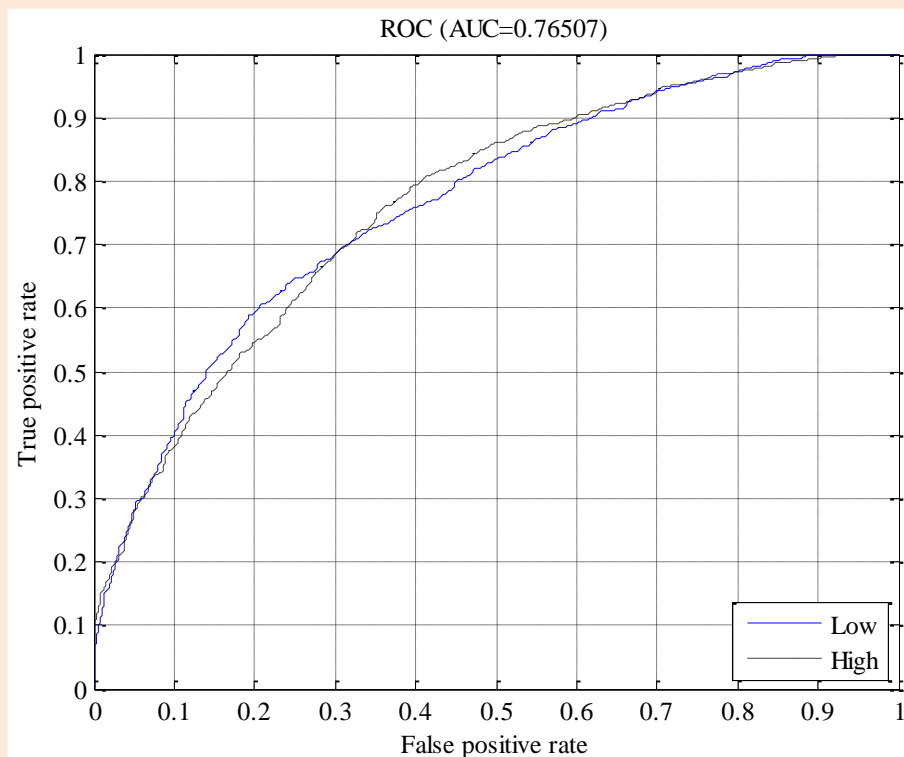
(b) The ROC curve from the IP model training.

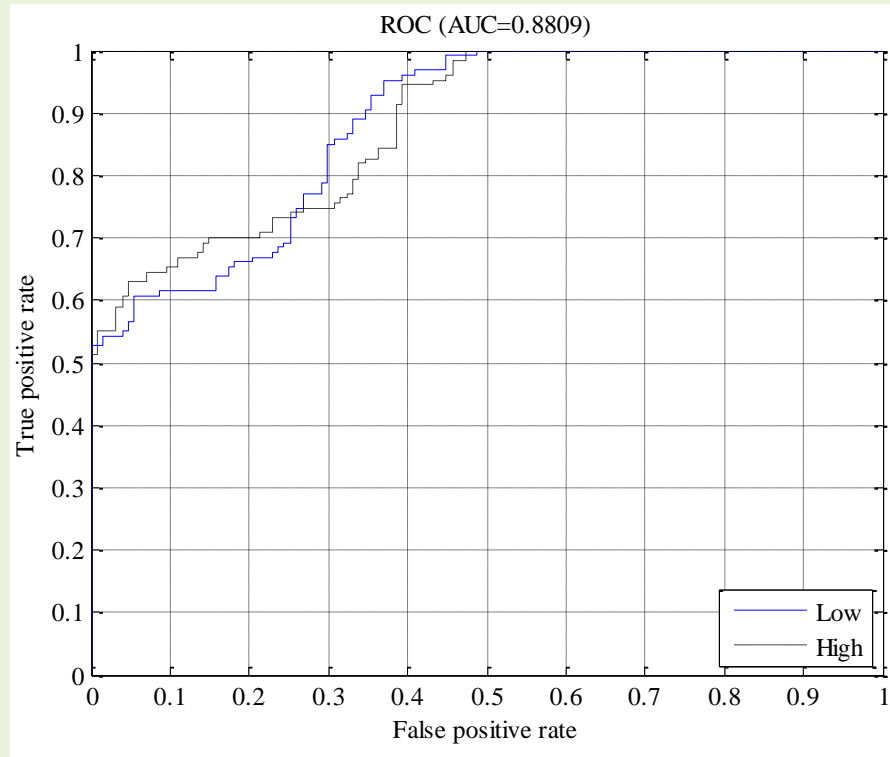Figure Appendix.29 The IP model training performance curves (a) PR curve (b) ROC curve.

Table Appendix.12 The confusion matrix of the IP blind test classification model with the 6 hidden neurons.

		Predicted Class		
		Low	High	
Actual Class	Low	77 (TP) 30.3%	44 (FN) 17.3%	63.6% (TPR) 36.4% (FNR)
	High	50 (FP) 19.7%	83 (TN) 32.7%	62.4% (TPR) 37.6% (FNR)
		60.6% (TNR) 39.4% (FPR)	65.4% (TNR) 34.6% (FPR)	63.0% (AC) 37.0% (Error)
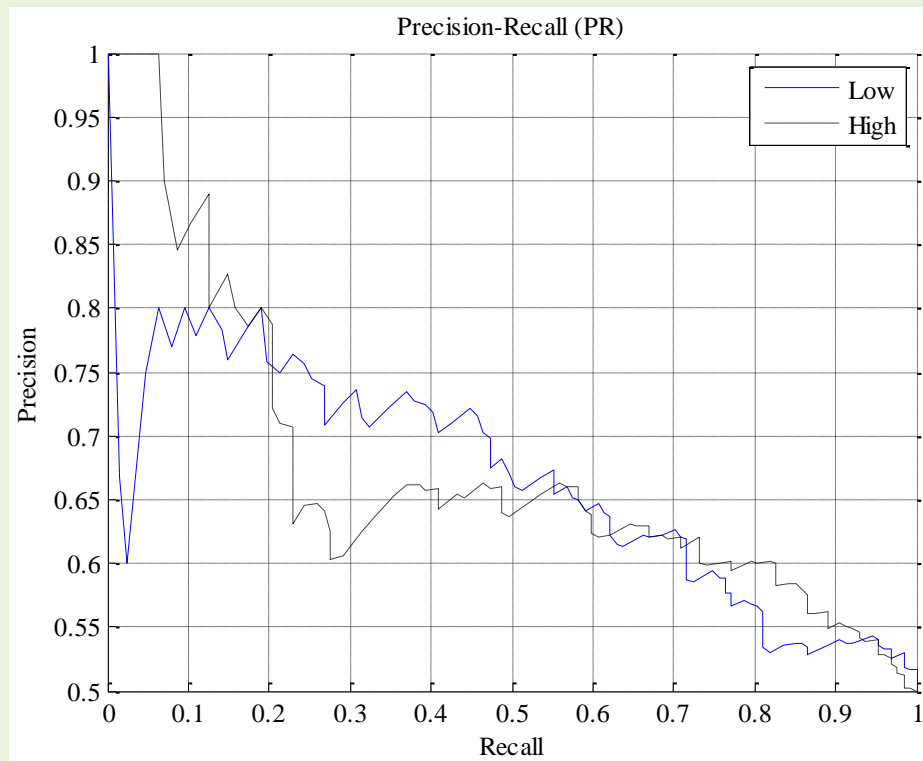
Precision-Recall (PR)

(a) The precision-recall curve from the IP model blind testing.
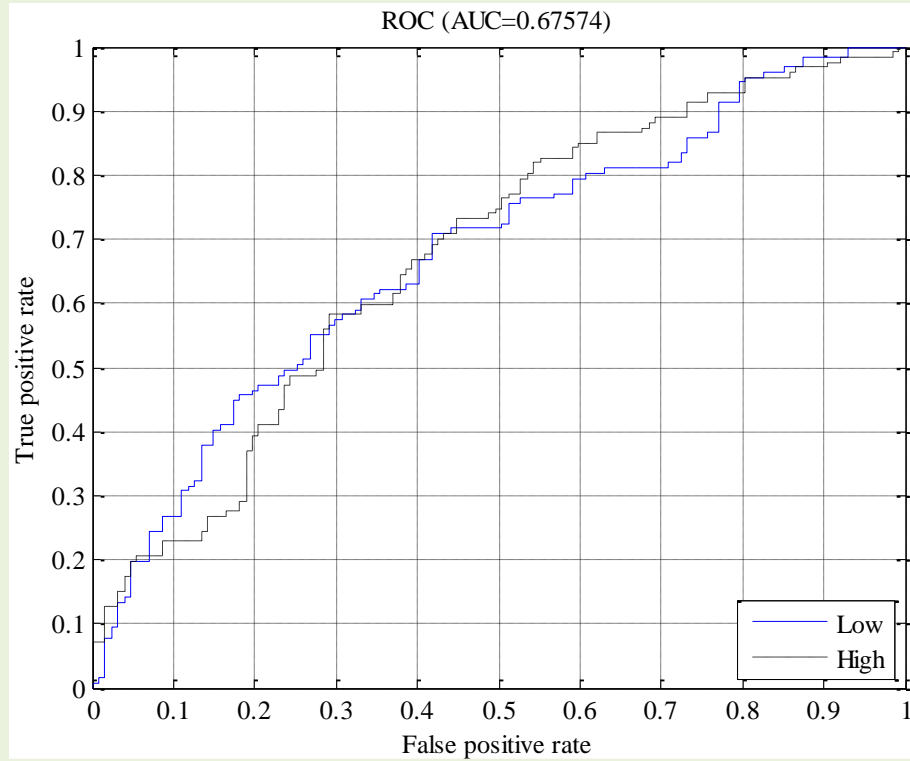
(b) The ROC curve from the IP model blind testing.

Figure Appendix.30 The IP blind testing performance curves (a) PR curve (b) ROC curve.

J. Copy of publications
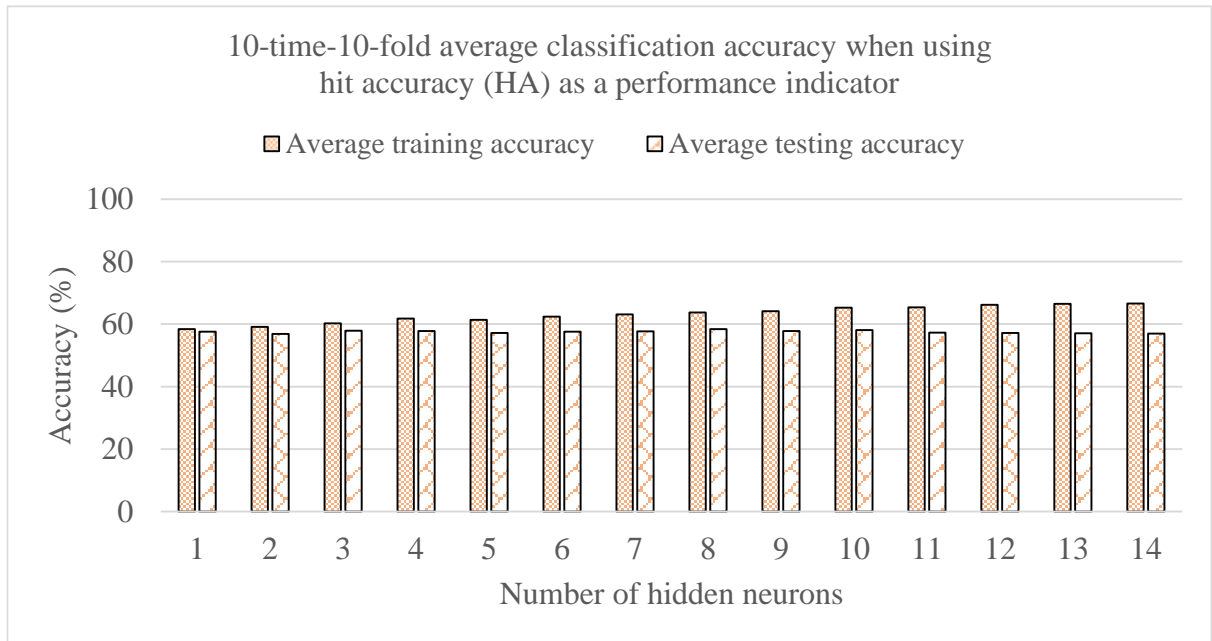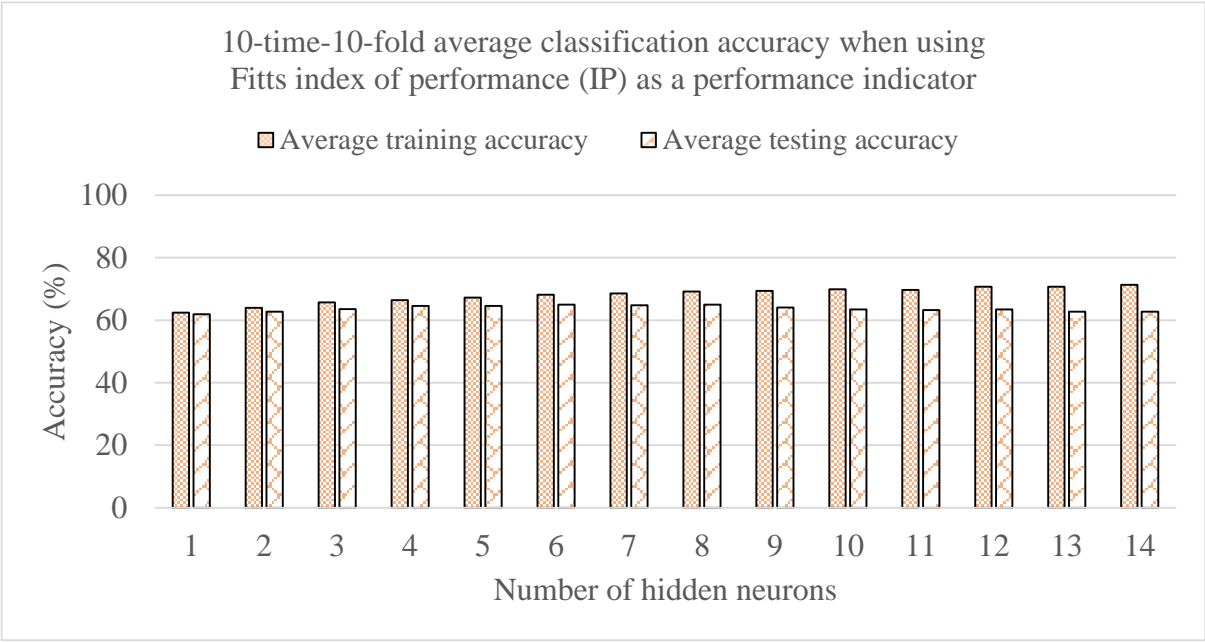
Real time Virtual Simulation of an Underactuated Pendulum-Driven Capsule System

Keattikorn Samarnggoon and Hongnian Yu

Abstract— In this paper, a real time virtual simulation framework which is the foundation for studying human adaptive mechatronics (HAM) is proposed. This framework allows researchers to interact and experiment with the system in real time. Thus, motion control patterns can be identified and learned with, for example, a heuristic strategy. The prototype is developed with an underactuated pendulum-driven capsule robot model. Motion control patterns are identified and presented. The experimentation results demonstrate the proposed concept.

Keywords-human adaptive mechatronics, pendulum capsule robot, underactuated systems, virtual environment, real time system (key words)

I. INTRODUCTION

Human adaptive mechatronics (HAM) is defined as an intelligence human machine system in which the system can be self-adapted intelligently based on the current user competency level to obtain optimum performance [1–5]. To achieve the HAM requirements, there must be several mechanisms working together. The main components of a HAM system are human operators, the intelligent discrimination of operator actions, competency evaluation metrics, human machine interaction mechanisms, and the machine system.

The work presented in this paper is a part of HAM research which covers a real time virtual system for understand the functions of human operators in HAM which has many invaluable advantages. This kind of virtual simulation systems running in real time allows researchers to experiment with dynamic of the modelled system in an immediate and interactive manner. Robotic researchers usually design mechanical systems by modelling mathematical relation of system parts but there exists troublesome to find control patterns for human operating a robot. This issue can be overcome by the help of real time virtual simulation systems. Motion control patterns could be identified by trial and error (heuristic) experimentation strategies using this virtual system. Moreover, apart from the robot mechanical simulation itself, dynamics of the environment can also be integrated into the simulation, for examples, different frictions of ground areas, dynamic of fluid while controlling robot movements, and capsule bots moving on a simulated deformable surface in medical application robotics.

Virtual training is also capable with this real time simulation based on the human-in-the-loop concept of mechanical systems. Training scenarios can be implemented with little effort or at no cost. Measurement of performance improvements can also be done from the feedback within the environments. This allows users to practice as much as they want. As a result, the user learning curve could be improved drastically. Regarding training environment with virtual real time simulation, it is a novel concept called human adaptive mechatronics that could further help optimise the learning curve of a user while training by its assisting behaviours.

The main contributions of the paper are
- Proposing a real time virtual human and machine interactions framework. The proposed framework will be a basis for development and realisation of the HAM concept.
- Developing a human heuristic learning strategy for learning motion control patterns.
- Conducting the experimental tests to demonstrate the framework and the HAM concepts.

II. RELATED WORKS

Human is considered the main component of the HAM systems because the aim of this system is a combination of an automatic control and adaptive manual control system which is operated by humans. Normally, humans are complex and unpredictable, but if they are involved in a goal oriented task, it is possible to recognise their intentions. Human has been long studied in many related fields e.g., neurophysiological, neuroscience, cognitive science, and psychophysical. In neuroscience study, Haynes and colleague successfully read human covert intention by decoding brain images from various sections simultaneously [6], [7]. The pattern recognition technique is used in decoding those human intentions by discriminate patterns from spatial information from various brain activity areas. This method of using spatial brain information is claimed to be more accurate than analysing only specific area of the human brain. The reason is that when human performing an activity, several of brain areas are working together according to its functions. Additionally, human intentions are influenced from personal experiences. This is indicated by Blakemore and Decety analysis of the evidences of brain activity [8]. The evidences show that when human perceive biological motions there exists brain activity that try to simulate these motions internally. As a consequence, this internal simulation would reflect as intentions in future actions. This basically works in the same way as training activity to improve personal experience.

Human has good abilities to learn, predict, and process information. However, these capabilities are depended on individual. A task that is performed by different persons might return different results because of individual ability. Individual ability is usually denoted by word 'skill' and the outcome from using skill to perform an action is called 'performance'. Learning capability is another magnificence aspect of human being in which humans have learnt to improve their skills and as an overall result i.e., overall

performance improvement. The most important part that ruled all of these capabilities is the thinking inside the human brain. Consequently, as mentioned earlier, internal thinking would reflect out as the intentions to do a specified task. This intended output actions could be identified by pattern recognition techniques. The intention recognition is also considered as part of the HAM system.

For the intelligent machine to serve or adapt to human appropriately, it needs to know human intentions by estimating from various kinds of related information. Fortunately, sensor technologies have advanced significantly along with the matured field of pattern recognition. These two combinations are essential for online human intention recognition. Observations and measurements from sensors are the inputs to pattern recognition algorithms to identify or estimate human intention at time. There exist numbers of information to be monitored and measured which is depended on the type of tasks. For examples, patterns of force signals exert on an arm gripper are recognised to discriminate human operator actions when performs industrial weight loading operation using Hidden Markov Models [9], motion and velocity pattern profiles are the information used to classify human actions in telemanipulation tasks [10]. The identified actions are useful for switching among virtual fixture models which help in different mode of operations. Once the machine has ability to identify human intention in which step the human operator is performing. It is functionality of the next component of the HAM system to evaluate how well the performing competency.

The aim of competency evaluation is to measure how well the operator is performing a step of the task so that the next component of the HAM system can make adaptations for assisting the operator. A generic performance evaluation framework, human performance index (HPI), is proposed in [11]. The framework consists of two layers of evaluation. The first layer is the collection of performance variables that evaluate raw competency of actions. The second layer is the weighted conditional integral of those variables in the first layer for specific area of measurement e.g. speed, and accuracy. This layer is called performance criterions. Final performance conclusion, HPI, is then weighted and accumulated from the second layer values. On the other hand, this HPI measurement concept can be viewed as grading evaluation in education such as school. Evaluations such as paper works, examinations, and attendance are scored. These scores are weighted with different percentage values according to its importance. The subject's grade is calculated from these values. Grading point average (GPA) is finally calculated from weighted credits of each subject. Therefore, the HPI is viewed as the GPA while performance criterions are viewed as subjects, and raw evaluations are viewed as those scorings. In addition, this HPI framework could be used in two modes, open form and closed form. The open form is located at the second layer in which these performance criterions can be used in any applicable future closed form. The closed form is located at the final

accumulation evaluations, HPI or GPA. Performance criterions such as speed and accuracy are the example of competency measurement metric. This metric is a basis for the next step of the HAM system, adaptive tuning.

Intelligent adaptation of the HAM system is tuned based on current operator competency. There are two types of adaptation i.e., passive and active adaptation. Tuning parameters inside the machine without interfering the operator is a passive adaptation [12]. An active adaptation works in the opposite way. It actively assists the operator by, as an example, pushing small amount of force to the controller grip to help achieving the aimed intention easily [13–15].

The basis system model for this paper is an underactuated modelling approach and a 6-step motion control strategy to develop a desired driving profile studied in [16].

Underactuated mechanical systems are a system that has less control inputs than degrees of freedom of the system to be controlled. This system may also occur in a full actuated system because it losses some freedom of control due to some reasons such as accident or system failure.

III. PROPOSED REAL TIME VIRTUAL SIMULATION SYSTEM
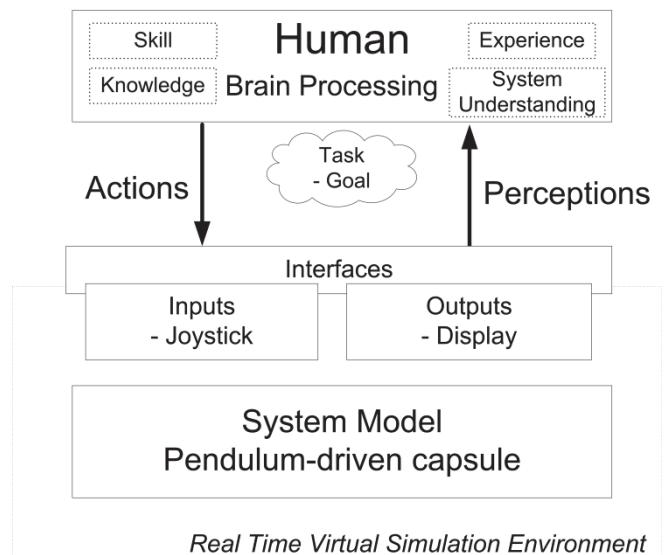
Figure 1. Diagram of the proposed real time virtual simulation based on HAM.

In this paper, the framework for the human machine controlling system in real time virtual simulation environment is proposed. Fig.1 shows a diagram and components of the system. The human operator interacts with a real time virtual simulation via the provided interfaces while perceiving information from the controlling system through a display monitor. It is the human operator's brain that processes information and orders the muscles to take actions to control an interface to manipulate the machine for accomplishing the desired task. Information is retrieved through various perception channels, e.g., eyes looking at meaningful data on the display screen, ears hearing the alert sound signal, and feeling of touching control interfaces. The human operator then observes, interprets, and processes this information and reacts with

appropriate actions with the aimed goal in mind. Overall, these activities can be viewed as a human-in-the-loop control scheme and they are working together to be a system. Lacks of one of these components could cause the system failure.

The human block in the proposed framework diagram (Fig.1) acts as a controller that controls the underlying virtual simulation system. Loop of brain processing, perceptions, and actions that related to the human block is performed simultaneously. To control the system, the human operator first needs to know the goal of the controlling task. Then, the control strategy is planned to reach the goal. For example, the heuristic strategy is one of many strategy selections. Based on the planned strategy, series of actions are performed repeatedly. Outcome of each action may not be as planned but it can be adapted according to the situation because of adaptability of human. This process can be viewed as a learning process to control the system. It is individual skills that affect all blocks in the human related loop i.e., skill for perceptions, skill for information processing, and skill for conducting actions. These inputs (perceptions), outputs (actions), and internal flows (brain activities) work as a control system that interacts with the underlying virtual simulation environment.

There is a 'task' block located in conjunction between a human controller and the system (Fig.1). Task understanding is needed to be given first so that the human operator is able to plan actions ahead in mind. For example, the given task as controlling a robot to the right, an operator might think ahead about how to control to reach the given goal. Thus, it is very important to describe the task goal to the human operator.

The proposed real time virtual simulation environment needs software components to compose the system. These components are responsible to simulate the dynamical system, in this case the pendulum-driven capsule robot, to interface with the input system, to render the outputs to the display interface, and in the future functionalities; to recognise human intention and to calculate assisted tuning parameters and forces. The blocks component of this simulation environment from the software architecture point of view is shown in Fig.2.

Software architecture design for this proposed system in Fig.2 is designed centred on the following system functional requirements: 1) simulating dynamics in real time, 2) allowing the user to interact with the simulated dynamic via some controlling interfaces, 3) displaying adequate information for the user to perceive, 4) recognising and adapting the system behaviour based on the current user's competency, and 5) logging and saving experiment data for future analysis. It starts with initial conditions and enters the main simulation loop with the aimed sampling time step. The simulation loop continues running until the software is terminated. Inside of the simulation loop, there are particular components executing to serve the whole functionalities of this virtual system. The ordinary differential equation

solver, ODE Solver block, is used for solving ordinary differential equations with the implemented method and algorithm. The equations are based on the mathematical model of the mechanical system. The input system is responsible to handle an interface between the human operator and the virtual system. The input values from the device are transformed into the model's input at every single step of simulation loops. The display output is drawn by the underlying graphic rendering system to visualize the simulating environment. Additional features such as the log system and the real time oscilloscope alike, the graphing system are essential for analysing immediate simulating values as well as logged values for later analysis. Realisation of HAM cannot be achieved without the following components; adaptation computation based on human intention and its corresponding competency, adaptation computation which is divided into passive and active tuning (Shaded blocks in Fig.2).
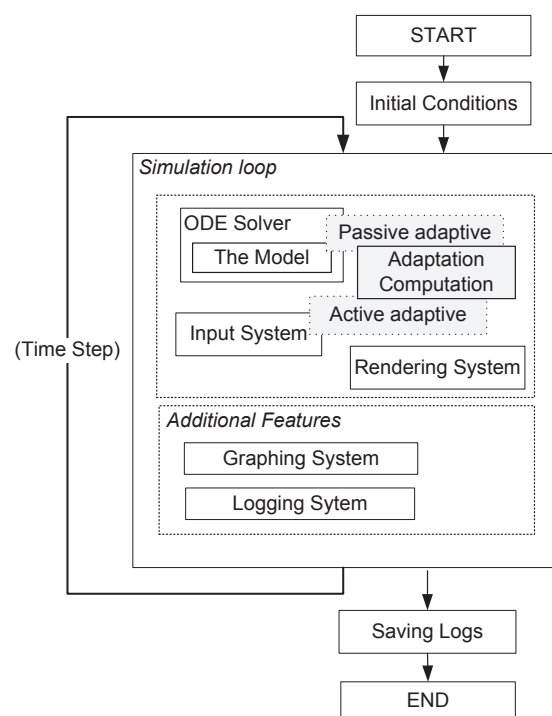
Figure 2. The software architecture.

IV. MODEL OF THE DYNAMICAL SYSTEM

The schematic diagram of the underactuated pendulum-driven capsule system [16] shown in Fig.3 is adopted as a machine to the proposed virtual simulation system. M is mass of a capsule body. The mass m is on the top of the weightless link L. The link can rotate 360 degrees around the centre. One dimensional movement is defined by a position denoted by x and friction f is modelled to point in an opposite direction of the body movement base on the Coulomb's friction model. The system is driven only by the force from the movement of the ball which is exerted by input torque τ and its moving momentum that causes forces.

The movement is possible because of both pendulum force and surface friction force.

From Fig.3, the ball position is defined in terms of cart position x at the centre as shown in equation (1). Then, the ball position equation is differentiated to get velocity and acceleration as in equations (2) and (3) respectively.

$$ball\ position = (x - Lsin\theta)\hat{\imath} + (Lcos\theta)\hat{\jmath} \qquad (1)$$
$$ball\ velocity = (\dot{x} - L\dot{\theta}cos\theta)\hat{\imath} - (L\dot{\theta}sin\theta)\hat{\jmath} \qquad (2)$$
$$ball\ acceleration = (\ddot{x} - L\ddot{\theta}cos\theta + L\dot{\theta}^2sin\theta)\hat{\imath} -$$
$$(L\ddot{\theta}sin\theta + L\dot{\theta}^2cos\theta)\hat{\jmath} \qquad (3)$$

Equation (3) and Newton's law of motion give forces from motion of pendulum ball in both x and y directions as follows.

$$F_{bx} = -m\ddot{x}_b \text{ , and } F_{by} - mg = m\ddot{y}_b$$

$$F_b = \begin{bmatrix} F_{bx} \\ F_{by} \end{bmatrix} = \begin{bmatrix} -m\ddot{x} + mL\ddot{\theta}cos\theta - mL\dot{\theta}^2sin\theta \\ mg - mL\ddot{\theta}sin\theta - mL\dot{\theta}^2cos\theta \end{bmatrix}$$

Also, the input torque to the joint is calculated as follows.

$$\tau = (-mLcos\theta)\ddot{x} + (mL^2)\ddot{\theta} - mgLsin\theta$$
$$F_{bx} - f = M\ddot{x} ; \quad where \quad f = \mu Nsgn(\dot{x})$$
$$N = Mg + F_{by}$$
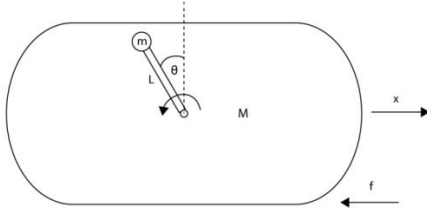
Figure 3. Pendulum-driven capsule system.

From above equations, we have

$$\ddot{x} = \frac{f\sigma_1 + \ddot{\theta}Lmcos\theta - \dot{\theta}Lmsin\theta}{M + m} \qquad (4)$$
where $\sigma_1 = -g(M + m) + \dot{\theta}^2Lmcos\theta + \ddot{\theta}Lmsin\theta$

$$\ddot{\theta} = \frac{Lmcos\theta\ddot{x} + \tau + gLmsin\theta}{L^2m} \qquad (5)$$

Equations (4) and (5) are the system equations with the single control input torque τ.

V. IMPLEMENTATION OF REAL TIME SIMULATION

To conduct real time simulation, the forth order Runge Kutta numerical approximation method of ODEs [17] is used. From the system model (4) and (5), we have

$$\dot{v} = \frac{(2M + 2m)(\sigma_2 + \mu S\sigma_3) - \omega^2Lmsin\theta}{(M + m)(2M + m - mcos2\theta - \mu Smsin2\theta)} \qquad (6)$$
$$where\ \sigma_2 = \frac{cos\theta(\tau + gLmsin\theta)}{L}$$
$$and\ \sigma_3 = \frac{gLmsin^2\theta + \tau sin\theta}{L} - g(M + m) + \omega^2Lmcos\theta$$

$$\dot{\omega} = \frac{(2M + 2m)(\tau + gLmsin\theta - \sigma_4)}{L^2m(2M + m - mcos2\theta - \mu Smsin2\theta)} \qquad (7)$$

$$where\ \sigma_4$$
$$= \frac{Lmcos\theta(\mu S(Mg + mg - \omega^2Lmcos\theta) + \omega^2Lmsin\theta)}{M + m}$$
$$\dot{x} = v \qquad (8)$$
$$\dot{\theta} = \omega \qquad (9)$$
where $S = sgn(\dot{x})$

Equations (6), (7), (8), and (9) are then solved by the forth order Runge Kutta numerical approximation algorithm.

An implementation of this real time virtual simulation system is developed using the industry leading application programming interface named Microsoft XNA and C# programming language. Sampling time is chosen at 10ms although it might change depending on the system performance but the system implementation is coded to compensate the issue by using elapsed time of each loop as a time step. The system parameters are as follows; M=0.5kg, m=0.05kg, L=0.3m, g=9.81m/s^2, μ=0.01 N*m/s.

The proposed real time virtual simulation system is controlled by the gaming joystick. The only system input is the amount of torque applied to the joint. The amount of torque can be varied by pushing an analogue stick in which its value is range between -1.0 and 1.0 N. In this case, the mapping is straightforward i.e. [-1.0, 1.0], value from an analogue stick is mapped to the input torque, τ, to drive the underactuated pendulum-driven capsule robot. However, it is noticed that the aimed system time step is 10ms. Therefore, the torque pushed by the joystick in real time is applied to the system at every time step of the system loop.

The screenshot of the simulation display is shown in Fig.4 when the system is simulated. The capsule body and its inner swinging shaft with the attached pendulum ball are displayed for the user to observe the capsule robot. Also, additional features for output information data are shown as online oscilloscope like a graphing system for both user observation and validation purposes.

Observations and manual controls are an inevitable couple in the human-in-the-loop control system. The proposed online simulation system displays necessary information on the monitor for observation while the user control amount of input torque via a joystick is shown in Fig.4. The user has an assigned task in mind while observing the pendulum movement on the screen and react to the dynamic behaviour of the system in real time to achieve desire control motions. In this case motion is in one dimensional movement i.e. moving to the left or vice versa.

Both input and output raw data during runtime experimentation of controlling are logged and saved for further analysis. Angle θ, angular velocity ω, capsule position x, capsule velocity v, and input torque τ are those variables that have been recorded. Also, an extra variable such as sign (sgnẋ) of the friction term is logged for more

clarification and validation of the implemented friction model.

VI. LEARNING OF MOTION CONTROL PATTERNS

One of the useful functionality of the real-time simulation system is apparent for heuristic strategy experimentation. In the following section, searches and results of motion control patterns for the pendulum-driven capsule system are presented. Control characteristics were experimented by the heuristic strategy. Ability to control this dynamical system is depended on the user's skill and understanding of the system. However, once understood, control characteristics can be identified and used as a pattern of control strategy.
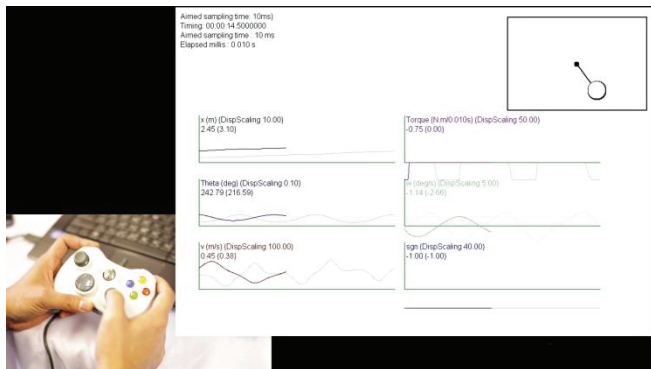
Figure 4. User using the joystick to control virtual simulation system.

The system initial values θ, ω, x, v, and τ are 180 degrees, 0 rad/s, 0 m, 0 m/s, and 0 N.m/s respectively. At the beginning the system stays still with the pendulum shaft and the ball lying straight down. When a small torque is applied, the pendulum begins to swing and the capsule start to move to the left and to the right repeatedly according to forces from the ball and the surface friction model as shown in Fig.5. The capsule is unintentionally displaced to the right by small torque after it finally comes to the steady state.

After several tries to control movement of the pendulum-driven capsule, the control strategy is developed. The system begins at the steady state and is intentionally controlled using the identified control patterns to move a capsule to the left and then to the right (Appendix 1). The identified control patterns to move a capsule by an input torque is summarised by the following strategies.

Step 1) Generate a torque by pushing the joystick to allow the pendulum to swing freely around, and then release the joystick (Fig.6).

Step 2) If one wants to move the capsule to the left, while the pendulum is freely swinging to the left side, the human operator needs to push the torque backward suddenly only in an appropriate short period of time. Moving to the right is done in the opposite way (Fig.7).

More precisely, to move to the left, the user needs to push the torque in the middle of rising or falling of angular velocity. In other words, one needs to push the torque at the edge of sine curves. These torque control strategies allow the user to control the pendulum driven capsule in the desired directions.
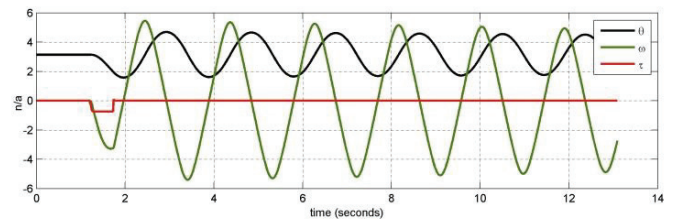
Figure 5. Single pushed torque.
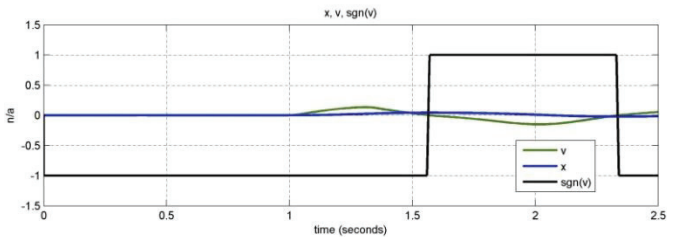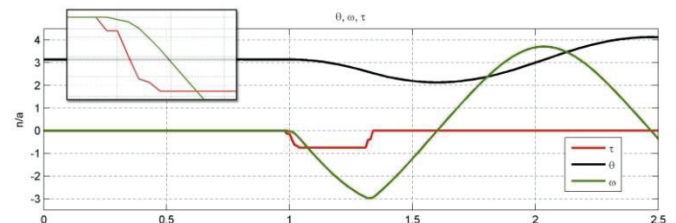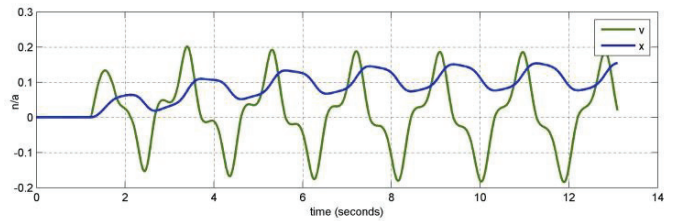
Figure 6. Control characteristics for step 1.
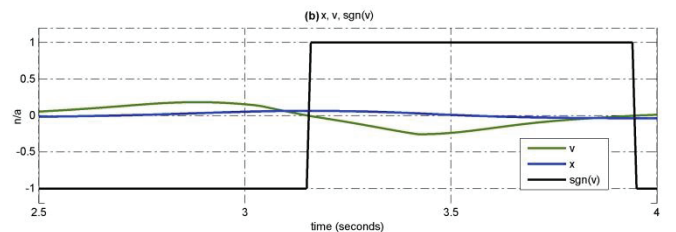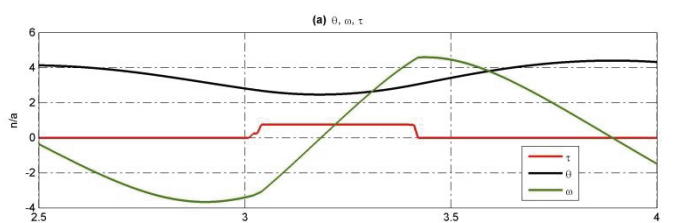
Figure 7. Control characteristics for step 2.

VII. CONCLUSIONS AND FUTURE WORK

A framework of the human-in-the-loop control scheme using real time virtual simulation has been proposed. The software architecture and implementation of the underactuated pendulum-driven capsule robot system have been developed. Usefulness of real time simulation is apparent because of an interactivity nature of this type of systems. The system dynamic model can be realised experimentally. As a result, systematic motion control patterns can be identified. The system also exposes an important of human controlling ability. Different user controlling skills appear to be an important factor in the human-in-the-loop system control. The human controlling skill is depended on user's perceptions, brain processing of particular circumstances, and control actions. Overall performance of the system is another aspect compared to user skills that control the system.

The identified patterns of motion control for the joint torque seem similar to a walking cycle of human. The inverted bottom half circle of leg movements is shown in Fig.8. For example, given that desired movement is to move to the right, at first push the pendulum to swing freely from A to B and vice versa. At the moment that the pendulum ball nearly reaches point B, the torque should add in the opposite way. This will make the capsule move to the right because of both pushed torque and friction. This is working in the same way as human walking habits.
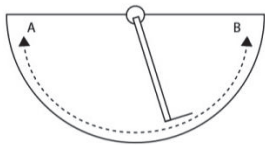
Figure 8. Human walk cycle.

In future works, closed loop control of an underactuated pendulum-driven capsule robot and a more complex model of double underactuated pendulum-driven robot [18] will be implemented as well as realization of an assisting control system based on human adaptive mechatronics. Also, the important adaptive mechanisms that would affect and optimise the learning curve of training will be experimented.

REFERENCES

[1] S. Suzuki, "Human Adaptive Mechatronics," *Industrial Electronics Magazine, IEEE*, vol. 4, no. 2, pp. 28–35, 2010.

[2] H. Yu, "Overview of human adaptive mechatronics," in *Proceedings of the 9th WSEAS International Conference on Mathematics & Computers In Business and Economics*, 2008, pp. 152–157.

[3] F. Harashima and S. Suzuki, "Human adaptive mechatronics-interaction and intelligence," in *Advanced Motion Control, 2006. 9th IEEE International Workshop on*, 2006, pp. 1–8.

[4] "Guest Editorial," *Proceedings of the Institution of Mechanical Engineers, Part I: Journal of Systems and Control Engineering*, vol. 225, no. 6, pp. 705–708, 2011.

[5] "Editorial," *International Journal of Modelling, Identification and Control*, vol. 4, no. 4, pp. 299–303, 2008.

[6] J. D. Haynes and G. Rees, "Decoding mental states from brain activity in humans," *Nature Reviews Neuroscience*, vol. 7, no. 7, pp. 523–534, 2006.

[7] J. D. Haynes, K. Sakai, G. Rees, S. Gilbert, C. Frith, and R. E. Passingham, "Reading hidden intentions in the human brain," *Current Biology*, vol. 17, no. 4, pp. 323–328, 2007.

[8] S. J. Blakemore and J. Decety, "From the perception of action to the understanding of intention," *Nature Reviews Neuroscience*, vol. 2, no. 8, pp. 561–567, 2001.

[9] V. Fernandez, C. Balaguer, D. Blanco, and M. A. Salichs, "Active human-mobile manipulator cooperation through intention recognition," in *Robotics and Automation, 2001. Proceedings 2001 ICRA. IEEE International Conference on*, 2001, vol. 3, pp. 2668–2673.

[10] W. Yu, R. Alqasemi, R. Dubey, and N. Pernalete, "Telemanipulation assistance based on motion intention recognition," in *Robotics and Automation, 2005. ICRA 2005. Proceedings of the 2005 IEEE International Conference on*, 2005, pp. 1121–1126.

[11] T. Parthornratt, R. Parkin, and M. Jackson, "Human performance index–a generic performance indicator," *Proceedings of the Institution of Mechanical Engineers, Part I: Journal of Systems and Control Engineering*, vol. 225, no. 6, pp. 721–734, 2011.

[12] K. Tervo, "Human Adaptive Mechatronics Methods for Mobile Working Machines," Doctoral thesis, Department of Automation and Systems Technology, Aalto University, Espoo,Finland. 2010.

[13] K. Furuta, Y. Kado, S. Shiratori, and S. Suzuki, "Assisting control for pendulum-like juggling in human adaptive mechatronics," *Proceedings of the Institution of Mechanical Engineers, Part I: Journal of Systems and Control Engineering*, vol. 225, no. 6, pp. 709–720, 2011.

[14] S. Suzuki and F. Harashima, "Assist control and its tuning method for haptic system," in *Advanced Motion Control, 2006. 9th IEEE International Workshop on*, 2006, pp. 374–379.

[15] S. Suzuki, K. Kurihara, K. Furuta, and F. Harashima, "Assistance control on a haptic system for human adaptive mechatronics," *Advanced Robotics*, vol. 20, no. 3, pp. 323–348, 2006.

[16] H. Yu, Y. Liu, and T. Yang, "Closed-loop tracking control of a pendulum-driven cart-pole underactuated system," *Proceedings of the Institution of Mechanical Engineers, Part I: Journal of Systems and Control Engineering*, vol. 222, no. 2, pp. 109–125, 2008.

[17] J. C. Butcher and J. Wiley, *Numerical methods for ordinary differential equations*, vol. 2. Wiley Online Library, 2008.

[18] Y. Liu, H. Yu, and S. Cang, "Modelling and motion control of a double-pendulum driven cart," *Proceedings of the Institution of Mechanical Engineers, Part I: Journal of Systems and Control Engineering*, vol. 226, no. 2, pp. 175–187, 2012.

Appendix 1
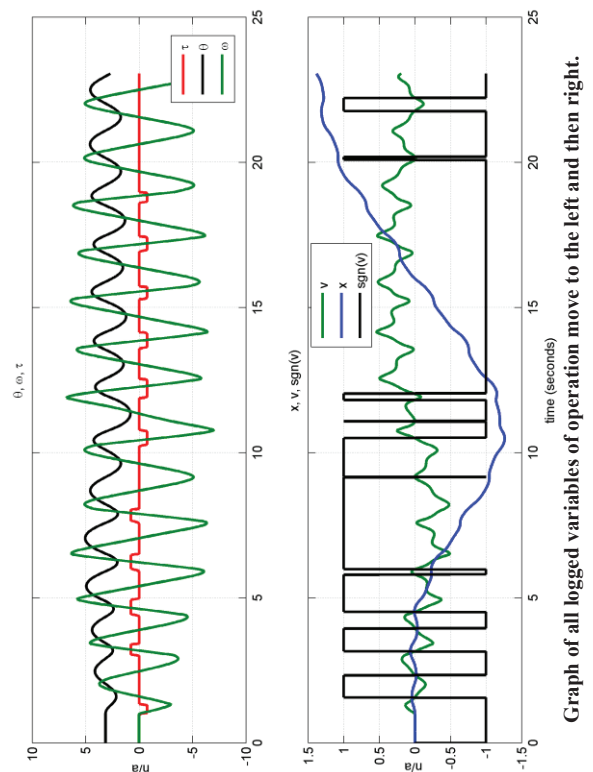
Graph of all logged variables of operation move to the left and then right.

A Physical Mobile 2-Dimensional Inverted Pendulum-Driven Capsule System

Keattikorn Samarnggoon*

College of Arts Media and Technology, Chiang Mai University
Huaykeaw Rd., T.Suthep, A.Muang, 50200 Chiang Mai, Thailand
Faculty of Computing, Engineering and Science
Staffordshire University, Beaconside, Stafford ST18 0DF
Email: K.Samarnggoon@staffs.ac.uk
*Corresponding author

Hongnian Yu

School of Design, Engineering and Computing
Bournemouth University, Fern Barrow, Poole, Dorset BH12 5BB
Email: yuh@bournemouth.ac.uk

Abstract: In this paper, we build a physical 2D inverted pendulum-driven capsule system for the human adaptive mechatronics (HAM) study purpose. We conduct the empirical studies on the pendulum angle rotation profile to drive the capsule system using four types of control input cycles. The results show that the capsule system moves according to the used type of control input with difference speed and accuracy performance in 2D space. The movements aiming at a straight line is faster and more accurate than the movement with the specified initial angles.

Keywords: *Human adaptive mechatronics (HAM), Capsule System, Inverted Pendulum, Robotics*

1   Introduction

An inverted pendulum-driven (IPD) cart or capsule system has been intensively studied recently because of its remarkable unique characteristics. One of the particular unique features is that it can move without external moving parts, which means it is minimally invasive for applications such as the human body diagnosis in medicine (endoscopy), tube inspection, and slippery surface movement. Moreover, it is an underactuated system which is the system whose independent inputs is less than its degree of freedom (DoF). It is in contrast to the fully actuated system which has equal or more actuators compared to the DoF (Liu and Yu, 2013; Spong, 1998). Even though in the fully actuated system, an underactuated situation could occur if failure of any actuator happens.

Yu (2008a) investigated a six-step tracking control law for a 1D IPD capsule. A further improved control method called 'switch control' was proposed by Yu (2008b). However, those studies are based on a single pendulum rotation in a fixed plane which implies that the possible movement is in one direction only. Liu (2012) studied a double IPD cart to allow movement in 2D space with the identical principle. Moreover, a similar underactuated mechanism using inner mass movement to displace a capsule robot without legs was also studied in (Li, 2006; Liu, 2008a; Liu, 2008b; Yu, 2011).

This paper presents an alternative implementation of a single IPD capsule system which is able to change the plane of rotation of the pendulum rather than fixed. The change of the plane of the pendulum rotation implies that the force exerted on the capsule base is also changed which allows the system to move in the direction which differs from a straight line. The paper presents the requirement, design, configuration, implementation and experimental results of a physical mobile 2D IPD capsule system. This system is intended to be used in HAM to study the human function as a controller to learn to use this uncommon system which is slightly difficult to control. A preliminary study on virtual simulation was conducted in (Samarnggoon and Yu, 2012).

2   Requirements, Design, Configuration, and Implementation

This section presents the requirements, configuration and implementation of the physical mobile 2D IPD capsule system.

2.1 The Requirements

The following requirements are summarised based on the modelling by Yu (2008a) plus requirements for the HAM experiment on human control skill (Samarnggoon and Yu, 2012).

The pendulum: 1) The pendulum rotation range is 1800 with a mass attached on its far end; 2) The rotation speed is quick enough to respond the control input; *The base of the capsule body*: 3) The base can rotate around z-axis to allow the change of rotation plane of the inverted-pendulum located above; *Overall system requirement:* 4) The system mobility is required to avoid spring effect on the electrical wirings. Thus, it requires battery powered and wireless controlled.

2.2 The Design and Configuration

The sketch capsule system shown in Figure 1 consists of the base which is a flat surface and has no external moving parts, the rotatable plate on top of the base which attached to the pendulum. The plate can rotate within -900 and 900 (β angle). The pendulum is rotated by angle. The coordinate of the plate is denoted by x, y, and z while the capsule coordinate is denoted by X, Y, and Z. The capsule weight is M while the pendulum weight is m.
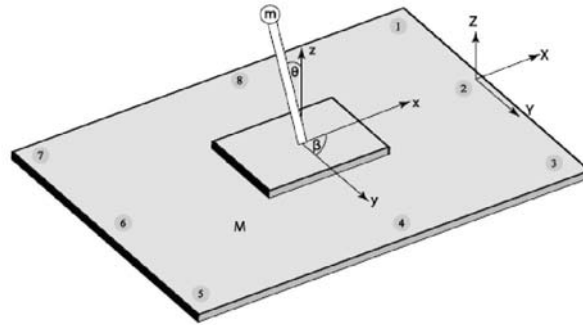
Figure 1 sketch diagram of the design of the capsule system.

The microcontroller unit in Figure 2 is an Arduino connected to two servo motors through the analogue input/output pins, A1 and A2. The serial communication Tx and Rx pins are connected to the corresponding pins on the XBee wireless communication unit. The PC is connected to another XBee unit which allows wireless communication between them. The PC acts as a controller which can be either automatically or manually (a joystick) controls the capsule robot. In this study, the pre-generated control cycles are used as the control signals.
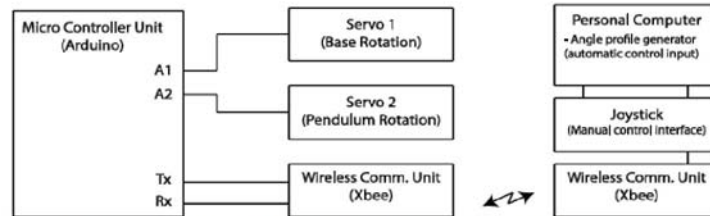
Figure 2 schematic diagram of the system configuration.

2.3 The Implementation

Figure 3 shows the hardware implementation of the capsule robot system.
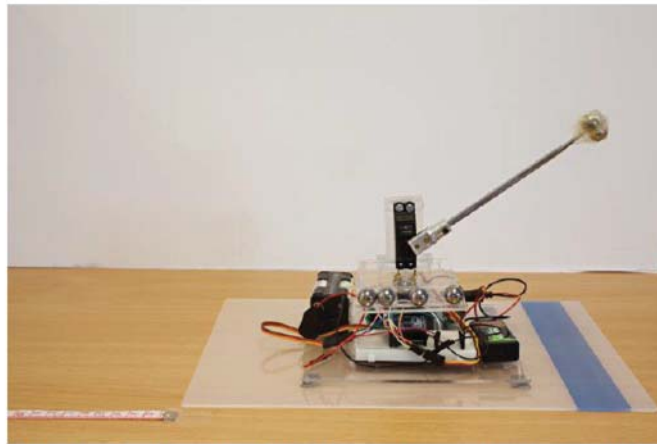
Figure 3 a photograph of the physical capsule robot prototype.

The bottom parts comprise of a Plexiglas plastic capsule base attached with the MCU, XBee, batteries, and Servo1. Servo 1 connects between the capsule base and the upper plate. The upper plate is attached to Servo2 for the pendulum rotation. The attachment of Servo1 and the upper plate allows the upper plate to be rotated around the z-axis (Figure 1) which can change of the plane of rotation of the pendulum. In other words, in Figure 1 at the initial settings, $\beta=00$, the pendulum is rotated about the y-axis. When the upper plate is rotated either toward non-zero $+\beta$ or $-\beta$ angle, the axis of rotation of the pendulum is changed.

The requirement for Servo1 is that it can rotate quickly enough to respond to the human hand movement on the joystick otherwise it will frustrate the operator due to the delay. Thus, the GoTech servo model GS-D9257 is chosen which provides the speed of 0.07s/600 and the stall torque at 4.2 kgcm, which is proper to tolerate torque of the pendulum rotation. Thus, it can rotate at the speed of 1.16ms per degree. Moreover, an additional advantage from this servo is its lightweight (26g). However, this servo has the limited range of 1200. The base servo is Power HD model HD-1705MG with 17.5g, 2.0 kgcm stall torque, and speed at 0.05s/600. The microcontroller unit (MCU) is an Arduno Uno R3. The wireless module is XBee model XB24-Z7PIT-004. The MCU is powered by 9v battery while the 2 servos are powered by a separated 6v battery.

3   The Experimentation

The experiment aimed at finding the feasibility of an automatic control of the capsule system commanded via the wireless communication between the PC and the mobile capsule in a 2D space. 4 types of angle profiles (the slow and fast swing, and the simple switch control) were used to control the capsule in this experiment (Yu, 2008a). The parameters for the total time for a cycle, slow swing time, fast swing time and the range of swing angles for each of the profile are shown in Table 1. Generally, there are two sets of angle range i.e. full range (I and II) and half range (III and IV). Within the same set, they are divided into two different swing frequencies.

Table 1 the parameters for each of cycle type.

Type	Total cycle time (Seconds)	Frequency (Hertz)	Slow swing time (Seconds)	Fast swing time (Seconds)	θ Angle Range (Degrees)
I	0.875	1.14	0.850	0.025	60 to -60
II	0.450	2.22	0.425	0.025	60 to -60
III	0.450	2.22	0.425	0.025	60 to 0
IV	0.250	4	0.225	0.025	60 to 0

The physical capsule was placed on a wood table top. This means it is the surface friction between wood and Plexiglas plastic. Calibration tape was attached to the table top as a reference axis and distance metric for the position tracking software (Figure 3). A small black dot was marked on the capsule base as a position tracking point. The position tracking software, Tracker, was used to track the position of the capsule (Brown, 2009). A digital single lenses reflex attached with macro lenses was used when capturing the video record of the capsule which gives minimal distortion to the plane of the capsule movement.

There are eight experiments conducted in this paper. The abbreviation E followed by the number of the experiment is used. For example, E1 stands for the first experiment while E2 stands for the second experiment and so on. The four types of control input cycle were applied to control with the initial capsule settings shown in Table 2.

Table 2 the settings for each of the experiment trial.

Experiment	β (Degree)	Input Cycle Type
E1	0	I
E2	0	II
E3	0	III
E4	0	IV
E5	45	I
E6	-45	I
E7	45	IV
E8	-45	IV

4   Results

Prior to the experiments, the total mass and weight distributions of the capsule are measured with M= 420g, m=42g. The eight points of weight distribution around the base are measured using the calibrated Flexiforce force sensor (Hollinger, 2006). Refer to Figure 1 the following are weight measured from each point; 1)142g, 2)200g, 3)196g, 4)300g, 5)194g, 6)236g, 7)158g, and 8)214g. It is normal that the weight distribution varies because the placements of hardware on top of the capsule base.

The capsule displacement results for all of the eight experiments are illustrated in Figure 4. The X and Y trajectories are illustrated using thin solid line (blue colour) and thick solid line (red colour) respectively. The capsule displacement performance is summarised in Table 3. The error between the aimed angle and the actual capsule trajectory is calculated and shown on the most right column.

Table 3 average speeds, desired and actual heading direction.

Experiment (and type of input)	Average X Speed (cm/s)	Average Y Speed (cm/s)	Desired Direction (Initial β) (degree)	Actual Direction (degree)	Error (degree)
E1 (I)	0.0744	-0.0033	0	2.53	2.53
E2 (II)	0.4400	-0.0593	0	7.67	7.67
E3 (III)	0.2678	-0.0341	0	7.25	7.25
E4 (IV)	0.3611	-0.0524	0	8.25	8.25
E5 (I)	0.0420	-0.0209	45	26.45	18.55
E6 (I)	0.0654	0.0142	-45	-12.25	32.75
E7 (IV)	0.1634	-0.0675	45	22.44	22.56
E8 (IV)	0.3156	0.0210	-45	-3.80	41.20

5   Discussions

The capsule straight line displacements controlled with input cycle of type I, II, III, and IV started with the desired initial angle β equal to zero (Table 3, E1 to E4) move with a slight angle error of 2.53, 7.67, 7.25, and 8.25 degrees correspondingly. The E1 is controlled with an input cycle of type I while E2 is controlled with an input cycle of type II. Both types of control input are based from the same range of pendulum rotation angle except the different in the swing frequency i.e. type II is higher than type I.

For a straight line movement, it is obvious that the average capsule speeds from the same set of pendulum rotation range with the higher pendulum swing frequency are faster than the lower ones i.e. the average capsule speed from E2 (II) and E4 (IV) are faster than E1 (I) and E3 (III) respectively. However, this does not apply across the different sets of the two angle ranges. E4 (IV) which was controlled with a higher frequency of 4 Hz with a half range gives lower average capsule speed than E2 (II) which was controlled from a full range with a lower frequency of 2.22 Hz.

The attempts to control the capsule system displacement with the

initial β angle at +450 and -450 are E5 (I) and E7 (IV), E6 (I) and E8 (IV) respectively. E5 (I) which controlled by the input control cycle type I make the capsule displacement towards the desired 450 direction with the error of 18.550 while the opposite E6 (I) also make progress towards the desired direction with the higher direction error of 32.750. The average speed of E6 (I) is slightly faster than that of E5 (I). E7 (IV) and E8 (IV) were controlled with the half range rotation type of input control cycle IV. The results from E7 (IV) and E8 (IV) have the same trend as E5 (I) and E6 (I) i.e. the direction error and the speed. E7 (IV) which aims at +450 makes smaller directional error of 32.750 compared to 41.200 from E8 (IV). However, the average speed from E8 (IV) is faster than from E7 (IV). This agrees the same trend from E5 (I) and E6 (I). These trends confirmed with the weight distributions across the capsule base. The direction towards the lighter weight gives faster capsule displacement i.e. point 1 compared to point 3 (Figure 1). Also, the total weight for the above parts of the capsule system is lighter.
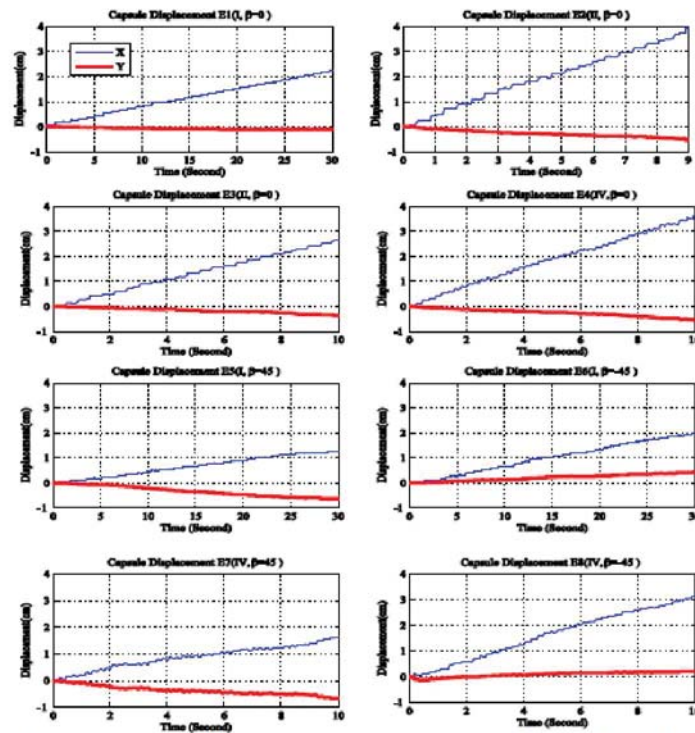
Figure 4 capsule displacement results from experiment E1 to E8.

6   Conclusions and Future Works

We conducted the experiments to control the physical capsule system in a 2D space. Although the displacements at ±450 β angle are not accurate as desired, it can move at an angle rather than only a straight line. A straight line movement is quite accurate with small error. This hardware prototype could be improved further by using precision manufacturing to build the system with more accurate for mass balance as in the same way as wheel balance in vehicular system like car, truck, and motorcycle.

The contributions of this paper are as follows. A physical system prototype of the capsule robot can displace in a 2D space by changing the plane of pendulum rotation. Two main pendulum angle profiles with different cycle timings are adopted from the references for a control

signal commanded over wireless communication channel. The empirical studies on the feasibility of the capsule system to displace in a 2D space have been conducted.

This capsule hardware system will be the platform to study a human control function in HAM. The system has some degrees of difficulty to control which is a good point to study the human learning function and to measure a skill performance from a number of subjects which is the main concern of HAM to build a system that can adaptively adjust to a skill level of user performance.

References

Brown, D., 2009. Tracker video analysis and modeling tool. Open source, physics 4.

Hollinger, A., Wanderley, M.M., 2006. Evaluation of commercial force-sensing resistors, in: Proceedings of International Conference on New Interfaces for Musical Expression. Citeseer.

Li, H., Furuta, K., Chernousko, F.L., 2006. Motion generation of the capsubot using internal force and static friction, in: Decision and Control, 45th IEEE Conference On. pp. 6575–6580.

Liu, Y., Yu, H., 2013. A survey of underactuated mechanical systems. IET Control Theory and Applications 7, 1–15.

Liu, Y., Yu, H., Cang, S., 2012. Modelling and motion control of a double-pendulum driven cart. Proceedings of the Institution of Mechanical Engineers, Part I, 226, 175–187.

Liu, Y., Yu, H., Wane, S., Yang, T., 2008a. On tracking control of a pendulum-driven cart-pole underactuated system. International Journal of Modelling, Identification and Control 4, 357–372.

Liu, Y., Yu, H., Yang, T., 2008b. Analysis and Control of a Capsubot, in: Proceedings of the 17th World Congress, The International Federation of Automatic Control, Seoul, Korea, pp. 756–761.

Samarnggoon, K., Yu, H., 2012. Real time Virtual Simulation of an Underactuacted Pendulum-Driven Capsule System, in: Control , UKACC International Conference On. Presented at the United Kingdom Automatic Control Council (UKACC), IEEE, Cardiff, pp. 568–573.

Spong, M.W., 1998. Underactuated mechanical systems, in: Control Problems in Robotics and Automation. Springer, pp. 135–150.

Yu, H., Huda, M.N., Wane, S.O., 2011. A novel acceleration profile for the motion control of capsubots, in: Robotics and Automation (ICRA), 2011 IEEE International Conference On. pp. 2437–2442.

Yu, H., Liu, Y., Yang, T., 2008. Closed-loop tracking control of a pendulum-driven cart-pole underactuated system. Proceedings of the Institution of Mechanical Engineers, Part I, 222, 109–125.

Yu, H., Yang, T., Liu, Y., Wane, S., 2008. A further study of control for a pendulum-driven cart. International Journal of Advanced Mechatronic Systems 1, 44–52.

Human Skill Performance to Control an Underactuated Pendulum-Driven Capsule System

Keattikorn Samarnggoon[1], Shuang Cang[2], Hongnian Yu[3], Mohammad S. Hasan[1], Tobias Flämig[4]

[1]Faculty of Computing, Engineering and Science, Staffordshire University, Beaconside, Stafford ST18 0AD, UK
[2]School of Tourism, Bournemouth University, Fern Barrow, Poole, Dorset BH12 5BB, UK
[3]Faculty of Science and Technology, Bournemouth University, Fern Barrow, Poole, Dorset BH12 5BB, UK
[4]Baden-Wuerttemberg Cooperative State University, 70174 Stuttgart, Germany

Abstract — **This paper investigates human learning and skill performance to control an underactuated pendulum-driven capsule system within an interactive virtual simulation environment. A number of experiments is conducted with 9 participants who learned to control the capsule using a physical joystick. The results show differences in learning and skill performance among the participants. Right-handed and left-handed participants achieve their highest trial on the opposite side of their handedness. The high learners tend to achieve great final performance whereas the moderate learners produce stable low or moderate performance. The variance of the displacements achieved appears to be a learning indicator while the high frequency of joystick oscillation at the right portion and interval gives high performance results.**

Keywords-human factor; human adaptive mechatronics; virtual simulation; human skill; human learning

I. INTRODUCTION

Although advances in technology have evolved a machine to become more autonomous/automated, many machines still require human operators to operate and interact with them either fully manual, semi-manual, or supervisory controls especially in human centred machine such as lower limbs walking support structure for elderly or disabled, prosthesis, wheelchair etc. As a consequence, human control behaviour and performance have become the main focus in human adaptive mechatronics (HAM) research.

A HAM concept aims to improve a machine with the capability to adjust itself based upon the performance level of the human user [1], [2], [3], [4], [5]. The main idea behind HAM comes from that humans can learn to operate machines. In contrast, it is interesting to develop a machine that could learn to provide assistance to its user based on an individual skill performance. To achieve this type of machine, several methods and techniques such as human behaviour study, pattern recognition of the human operator actions, human skill performance evaluation during the machine operation, the interaction model between human and machine, the machine system modelling are being studied.

Human machine control performance and evaluation are the important HAM components because they provide a basis for the machine to give the appropriate adjustment and assistant. Without the knowledge of human operation performance, the machine would have no information for the adaptive adjustment

and assistant. In this paper we investigate human learning and performance to control an underactuated pendulum-driven capsule system within an interactive virtual simulation environment.

The paper is organised into the following sections. A review of the related works is presented in Section II. The proposed human interaction model appears in Section III. The experimentation procedures and settings are presented in Section IV. The results from the experiments are summarised in Section V. The discussion and conclusion are presented in Section 0 and VII, respectively.

II. RELATED WORKS

Human skills have been long studied in a number of classical research fields e.g. psychology, sports, human factor engineering etc. [6], [7], [8]. However, there exist few studies on the human skill performance evaluation when operating a machine according to the HAM concept.

In a research area called haptic shared control (HSC) several studies have focused on human sharing control simultaneously with the machine. A special haptic force feedback device has been employed to help assist human driver in a car lane keeping task which proven to reduce the control activity by 16% [9], [10]. A performance and training enhancement by applying HSC to give a virtual force field a.k.a. 'virtual fixture' has proven to improve the performance. However, for a training enhancement it is ineffective because the operator tend to rely on the existence of the shared assistance [11].

Rasmussen divided the human performance behaviour into three levels i.e. skill, rule, and knowledge [12]. At the skill level behaviour, manipulations by humans are merely based upon voluntary movements, which behave like an automated action without consciousness. Those actions are extremely integrated, smooth, and can hardly be decomposed into elements without careful attention. This human low-level skill phenomenon is also confirmed in the study of professional musicians such as violinists and cellists who are hardly able to specifically describe the components to their performance [13]. At the rule level behaviour, the human use the stored rules, know-how, or instruction to control their actions. In other words, control is ruled by past successful experiences either from personal or vicarious/indirect experiences. At the highest level, knowledge level behaviour usually occurs in unfamiliar situations because previous experiences, rules, or know-how cannot be applied

directly. Critical thinking, problem solving strategy and a modified plan of actions are tested against the desired goal heuristically.

In [14], four approaches to human performance modelling; information processing, control theory, task network, and knowledge based are studied for a number of useful applications e.g. in system design, system development, and system evaluation. Having a human performance model has many benefits such as reducing risk, cost, and danger prior to the actual system implementation.

A brain monitoring system to investigate voluntary motion is studied to reveal the relation between brain activation area and skilled motion [15]. A near-infrared spectroscopy (NIRS) brain monitoring technique is used while the participants are asked to perform a drawing task by looking at the mirror instead of looking at the paper directly. The proposed index is used to evaluate and classify the skill levels into three categories high-skilled (HS), middle-skilled (MS), and low-skilled (LS). High-skilled persons show that there is activation in a premotor cortex (PMC) and supplementary motor area (SMA) during the early phase of the task performance which decreases gradually later on as an indicator of becoming a normal skilled action.

Discrete operator's hands movement during machine console operation have been investigated to evaluate the operator performance in [16], [17]. Fitts' law is applied and validated in the study for the task which has partly visual feedback such as machine console operation [18]. The machine console operation is considered as partly visual feedback because it does not intensively require perception through the eye. The outcome indicates that it is possible to use discrete hand motion to estimate skill level of the machine operator. In other words, there is a difference in the sequences of hand movement between novice and expert operators. A novice seems to prone to unnecessary sequence of motions while the expert motions are optimised. In addition, eye gaze tracking is applied to gather the operator eyes gaze while performing machine console operation [19].

A human performance index (HPI) is a method to evaluate human operator performance by scoring the chosen performance variables such as speed and accuracy variables and then applying multilayer weighting criteria to obtain the performance index value [20]. The method is validated using an on screen mouse target hitting task to measure a user's time taken to reach a circle target on the screen, an average time used across the number of trials, a cursor path accuracy, and an accuracy on the clicked target. The Fitts' law is also applied in this study to validate the speed-accuracy trade-off of the task.

The work presented in this paper follows the concept from [21] which provides an interactive virtual simulation environment to allow human interaction with the system based on the HAM principle. In the previous work, a single human operator has learned heuristically to control and identify the possibilities of angle profile pattern of the virtual pendulum-driven capsule system. In this work, a number of subjects participate in this work allow performance measurement analysis from their heuristic learning and control trials.

III. HUMAN OPERATOR AND CAPSULE SYSTEM

In this section, a human operator interaction model with the capsule system is proposed and the details of the pendulum-driven capsule system are presented.

A. Human-capsule system interaction model

Fig. 1 shows the human-capsule system interaction model in this study. The model consists of 4 building blocks which pass the control information throughout system paths. The human operator is given the goal of the task to be performed. The internal processing of human brain processes the provided information and takes action via the joystick interface to control the pendulum-driven capsule system. The joystick actions then translate into the inverted pendulum angle. A proper rotation of the inverted pendulum will drive the capsule system towards desire direction. However, this rotation is the main control that the individual human operator has to learn. The appearance of pendulum orientation and capsule position on the display acts as the feedback information to the human operator eyes to be perceived and react. Then, it is returned to the human operator internal processing to process the information and make progress to the capsule position as required by the given task goal.
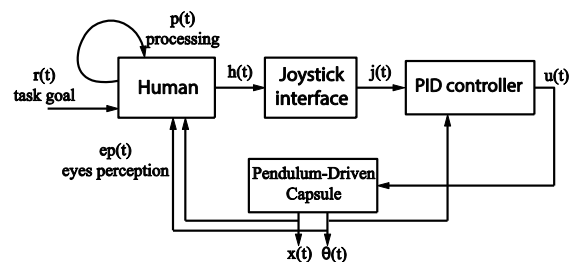

Figure 1 The human interaction model with the pendulum-driven capsule system.

Fig. 1 contains time-varying variables passing the information throughout the system paths. $r(t)$ is the reference or the given task goal, $p(t)$ is an internal processing of an individual human brain, and $h(t)$ is the result of an internal brain processing output as a hand motion to control the joystick interface. $j(t)$ is the output from the joystick which is generated by the human operator hand movement, $u(t)$ is the control output from the PID controller to the pendulum-driven capsule simulation according to the desired angle. $\theta(t)$ and $x(t)$ are outputs from the simulation model which appear on the screen of the virtual simulation platform and they act as feedback to the human operator visual perception. $ep(t)$ is the simulation output information plus any external disturbances such as environmental distractions and unrelated activities on the screen.

B. The pendulum-driven capsule model and simulation

The schematic diagram of a pendulum-driven capsule model is shown on Fig. 2. The model is adopted from [22] with additional proportional-integral-differential (PID) controller applied to control the input torque to achieve the desired angle of the pendulum. In other words, the same mathematical model in [21] is applied with additional PID controller. The PID controller constants – kP, kI, kD are 0.7, 0.7, and 6.0, respectively. The control output gain factor is 10. Table I shows the parameters for the pendulum-driven capsule system. Fig. 3 shows the 3D simulation of the model that is used for the experimentation.
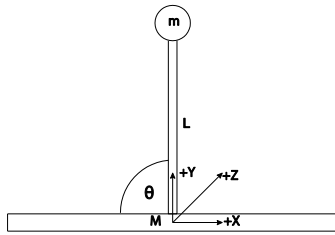
Figure 2 The pendulum-driven capsule system model.

TABLE I. THE CAPSULE SYSTEM PARAMETERS

Ball mass (kg)	Capsule mass (kg)	Shaft length (m)	Surface friction coefficient	Gravity constant (m/s²)
0.2	0.5	0.3	0.5	9.81

IV. THE EXPERIMENT

The experiment is designed to investigate the human operator learning and skill performance when operating the pendulum-driven capsule system. This capsule system is chosen because it has a number of unique features [23], [24]. It is an underactuated mechanism, which can be used to avoid benefit from past experience. A direct control of the angle of the pendulum requires hand motion skill to swing the pendulum at the right oscillation and timing to initiate the capsule robot to displace. As a consequence, it requires both learning and skill to operate this system.

As described in the interaction model, a joystick is used as the interaction interface for the human operator to operate the system. Fig. 4 shows the joystick and the corresponding axis used to control the angle of the pendulum directly. The direct angle control means that when the joystick is pushed towards negative x direction it will rotate the pendulum angle of the capsule system to left hand side which means toward the positive 90 degrees of the pendulum-driven capsule model (Fig. 2). A screenshot of the 3D simulation of the pendulum-driven capsule system is shown on Fig. 3. The sampling interval was at 10 milliseconds.

The given control task in this experiment is a direct pendulum angle control to displace the capsule to the specified direction i.e. left or right. A human controller has full control over the desired angle of the pendulum by pushing the joystick handle. The effect of pushing the handle will cause the capsule to move erratically back and forth. This is normal because of the mechanism of the inverted pendulum-driven capsule system. However, it is controllable for the intended displacement direction.

Each session of the experiment for each participant contained learning sessions prior to the actual performance trials. The actual trials consist of 6 trials separated into 3 trials for right and 3 trials for left movement. There is no time limitation for the learning session while the actual trial is limited to 20 seconds a session which means a participant has to control the capsule to the specified direction as far as possible within the provided time limit.
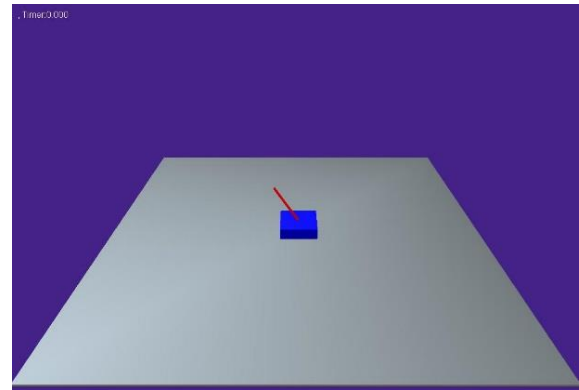

Figure 3 The screenshot of the simulation platform.

Figure 4 The joystick control interface and the axis uses to control the pendulum angle.

Nine participants ages between 21 and 50 attended this experiment. Each of them agreed and signed the consent form prior to the experiment session. The participants have different personal attributes such as ages, handedness, and knowledge about principles related to the machine which could influence the control learning and performance.

V. RESULTS

This section summarises the results from the experimentation conducted by nine participants. They have been labelled as P1 to P9 in Figure 5. The 'R' and 'L' letter indicate right or left movement task followed by a trial number in Figure 5. For examples, 'R1' stands for the first right trial, 'R2' for the second right trial, and so on. Each of the participants did perform the experiment for 'R1' to 'R3' and 'L1' to 'L3' produced a total of 54 trials for the entire experimentation from the nine participants.

The participant's attributes and knowledge regarding the theory related to the capsule system has been shown in Table II. Eight of them are male and seven of them are right handed while the other two are left handed for handedness. All of them know Newton's law of motion which is a basis to this capsule system model and almost all of them know about a pendulum. However, approximately half of them know an inverted pendulum and only three of them understand the principle on the inverted pendulum. None of the participants has tried this experimentation platform before.

Table III shows the results – learning time prior to the actual performance, average displacement achieved and average speed. A total absolute displacement and a total average speed are also calculated to see an overall performance of each participant. The absolute value of final capsule position for each of the trial for every participant is plotted and shown on Fig. 5.
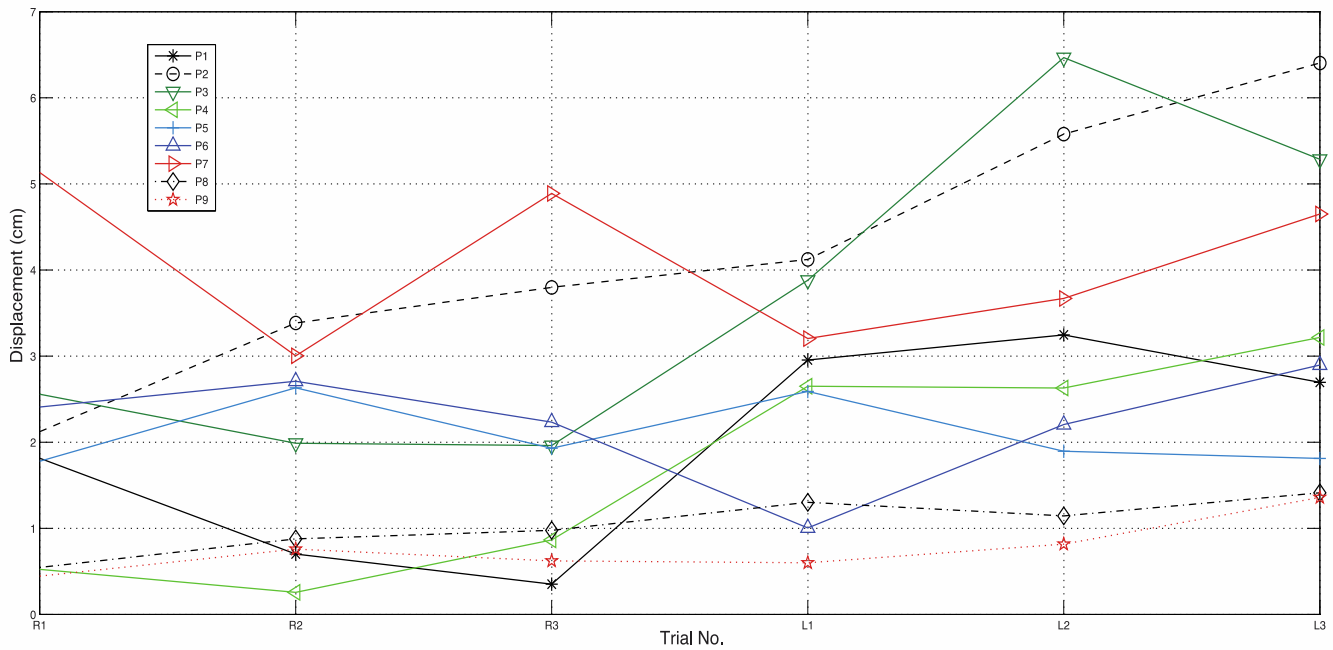
Figure 5 The absolute value of final capsule position.

TABLE II. THE PARTICIPANTS ATTRIBUTES AND KNOWLEDGE

P	G	A	H	N	Pe	IPe	IpeP	TBF
P1	M	31-35	Right	Y	Y	N	N	N
P2	M	36-40	Right	Y	Y	Y	N	N
P3	F	31-35	Right	Y	Y	N	N	N
P4	M	21-25	Right	Y	N	N	N	N
P5	M	26-30	Left	Y	Y	N	N	N
P6	M	26-30	Right	Y	Y	Y	N	N
P7	M	41-45	Left	Y	Y	Y	Y	N
P8	M	46-50	Right	Y	Y	Y	Y	N
P9	M	26-30	Right	Y	Y	Y	Y	N

P=Participant Identity, G=Gender, A=Ages, H=Handedness, N=Knowledge on Newton law of motion, Pe=Knowledge on pendulum, IPe=Knowledge on inverted pendulum, IPeP=Knowledge on inverted pendulum principle, TBF=Has the participant tried this experiment before

TABLE III. LEARNING TIME, AVERAGE DISPLACEMENT, AND AVERAGE SPEED

P	LT (sec)	Avg R Dis (cm)	Avg R Spd (cm/s)	Avg L Dis (cm)	Avg L Spd (cm/s)	Tot. ABS Dis (cm)	Tot. Avg Spd (cm/s)
P1	78.79	0.89	0.045	-2.90	-0.145	11.38	0.95
P2	100.76	3.07	0.154	-5.34	-0.267	25.22	2.10
P3	212.9	2.12	0.106	-5.15	-0.257	21.79	1.82
P4	260.8	0.53	0.026	-2.81	-0.141	10.02	0.84
P5	141.97	2.07	0.104	-2.06	-0.103	12.39	1.03
P6	318.09	2.42	0.121	-2.02	-0.101	13.33	1.11
P7	98.88	4.31	0.216	-3.82	-0.191	24.41	2.03
P8	97.51	0.77	0.038	-1.26	-0.063	6.09	0.51
P9	586.88	0.60	0.030	-0.90	-0.045	4.50	0.38

P=Participant identity, LT=Learning time, Avg R Dis=Average right displacement, Avg L Dis=Average left displacement, Avg R Spd=Average right speed, Avg L Spd=Average left speed, Tot. ABS Dis=Total absolute displacement gained, Tot. Avg Spd=Total average absolute speed (cm/s)

VI. DISCUSSIONS

In this section, interpretation of the results concerning learning and skill performance in the context of the capsule system control task is discussed.

According to Table III the amount of learning time (LT) does not reflect the performance of the actual trials. The best total absolute displacement achieved belongs to 'P2' who took 100.76s for learning time while 'P9' used 586.88 to learn to control the robot but the total absolute displacement achieved for 'P9' is the worst among all participants. This indicates that the participant 'P9' spent a large amount of time to figure out how the capsule system works but could not acquire sufficient skill to control the capsule system.

The skill performance indicator is a final position of the capsule achieved within the time limitation of 20 seconds for a trial. As shown on Fig. 5 the highest performances belong to 'P2-L3' and 'P3-L2'. It is apparent that the best performer, P2, also exhibits the highest total average speed at 2.10 cm/s (Tot. Avg Spd) as shown on Table III. 'P2' shows consistent performance. The lowest trial belong to 'P4-R2', however, the total average speed is on a moderate level at 0.84 cm/s.

Fig. 6 shows the average absolute speed for right and left control task. It is interesting that almost all of the right-handed participants gained more speed on the control task for the given left hand side movement task. Likewise, the left-handed participants, 'P5' and 'P7' achieved more speed on their right hand side tasks. This could be an effect of hand grasping orientation on the joystick control interface. This interesting fact conforms to performance achieved by the best trial which belongs to the left movement task by right handed participant 'P2-L3', while the maximum displacement achieved from left handed participants belongs to the right movement task 'P7-R1'.
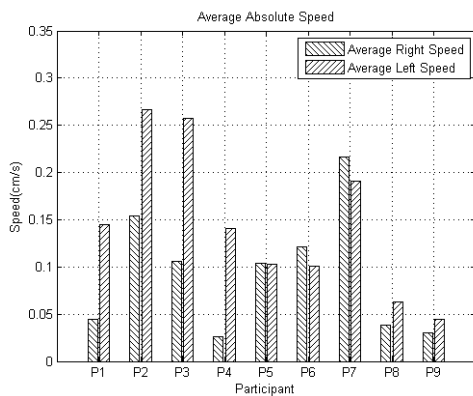
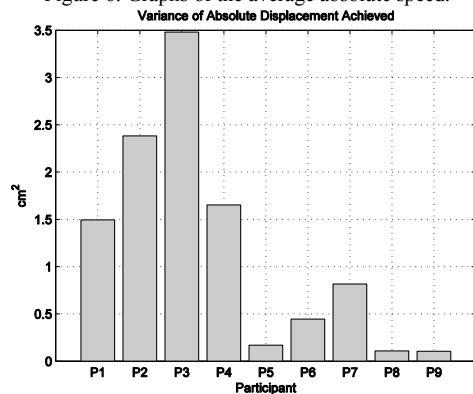Figure 6. Graphs of the average absolute speed.

Figure 7. Variance of absolute displacement for each participant.

The variance of the absolute displacement achieved for each participant is calculated and is shown in Fig. 7. This value indicates consistency of performance for each of the participant across the performance trials. It could be used as a 'learning index'. For example, the participant 'P3' gained the highest learning performance because the first three right side trials (Fig. 5) are not very well but in the next three left trials the participant achieves almost as long displacement as the highest displacement achieved by 'P2'. This interpretation method is also applied to the participant 'P4' who gained a high learning performance indicator (variance). Although the participant 'P7' achieved good performance across all of the trials, the variance is relatively low. This means there was not much learning gained by this participant.

Fig. 8 shows the control input characteristics of two best and two worst trials from all of 54 trials. The two best trials from the participant 'P2-L3' and 'P3-L2' are shown on Fig. 8 (a) and Fig. 8 (b), respectively. The worst two performance trials are from participant 'P4-R2' and 'P1-R3' which are shown in Fig. 8 (c) and Fig. 8 (d), respectively.

The frequency characteristic of the control input from Fig. 8 shows clues for the high performance trials. The control inputs with high frequency i.e. around 1 Hz or more are from both of the highest trials, 'P2-L3' and 'P3-L2'. Also, this frequency is performed and maintained across the performance trials. In other words, it is performed at consistent frequency across the trials. In contrast, the low skill performer exhibits low frequency action, inconsistent across the trial. These control input characteristics were performed by 'P4-R2' and 'P1-R3'.

VII. CONCLUSIONS AND FUTURE WORKS

Human learning and skill performance to control an underactuated pendulum-driven capsule system is studied in this paper. The human interaction model with the capsule system is proposed to explain the flow of control data and information throughout the system paths. The experimentation is carried out with 9 participants to study their learning and skill to control the capsule system. These participants exhibit different learning strategies, control strategies, and performance outcomes.

In this study, the learning time used prior to the actual performance does not reflect the actual trial sequences. However, the variance of the displacements achieved across all trials indicates the learning achievement. The final displacement of the capsule and the corresponding average speed are skill performance indicators. It appears that the participant who is able to oscillate the control input at high, consistent frequency, and at the appropriate portion on the joystick x-axis has achieved relatively high performance.

Although the angle control pattern generated by human operator differs from the 6 steps control strategy in [22] the pattern successfully drives the capsule system forward, it is not a perfect trajectory as in automatic control. This is normal as a human being who can heuristically learn and apply knowledge at the facing circumstance to solve the problem but does not need to be mathematically/objectively perfect as in the automation.

In future works, an analysis of the time series of the control input will be studied to utilise the details of the participants hand control behaviour on the joystick interface, for example similarity, trend and seasonality of the control input. In addition, future experiment will include biometric measurement such as eye gaze, body movement, and surface brain activity during the participants control activity. These measurements will give a deeper understanding of the human learning, skill performance, and control behaviour on the robot system control task under the HAM concept.

REFERENCES

[1] Harashima, F. and Suzuki, S., "Human adaptive mechatronics-interaction and intelligence," in *Advanced Motion Control, 2006. 9th IEEE International Workshop on*, 2006, pp. 1–8.

[2] S. Suzuki, "Human Adaptive Mechatronics," *Industrial Electronics Magazine, IEEE*, vol. 4, no. 2, pp. 28–35, 2010.

[3] S. Suzuki, H. Igarashi, H. Kobayashi, T. Yasuda, and F. Harashima, "Human Adaptive Mechatronics and Human-System Modelling," *Int J Adv Robotic Sy*, vol. 10, no. 152, 2013.

[4] H. Yu, "Guest Editorial," *Proceedings of the Institution of Mechanical Engineers, Part I: Journal of Systems and Control Engineering*, vol. 225, no. 6, pp. 705–708, 2011.

[5] H. Yu, "Editorial," *International Journal of Modelling, Identification and Control*, vol. 4, no. 4, pp. 299–303, 2008.

[6] G. Wulf, *Attention and motor skill learning*. Human Kinetics, 2007.

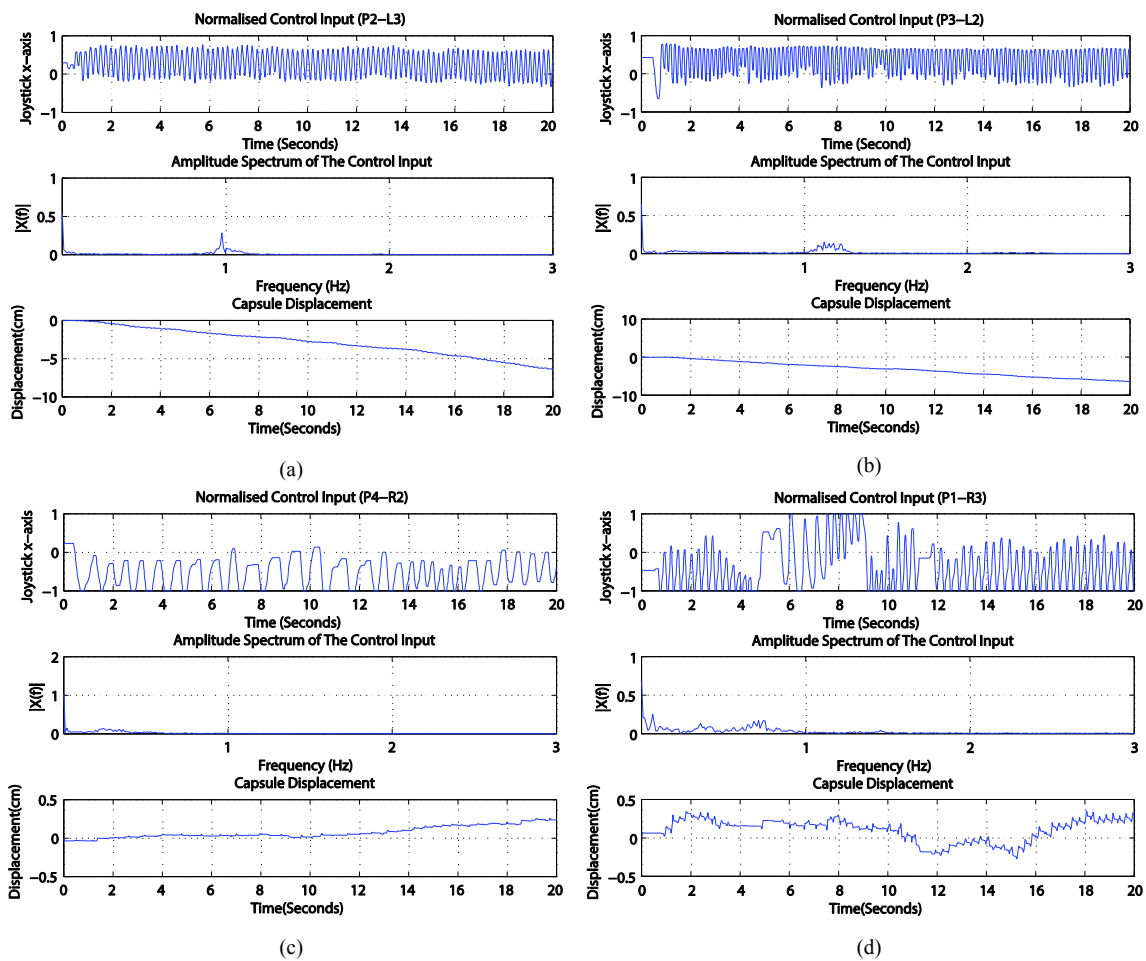[7] M. D.Robb, *The dynamics of motor-skill acquisition*. Prentice Hall New Jersey, 1972.

Figure 8 Graphs show normalised control input from the joystick, the frequency characteristics, and the capsule displacement.

[8] W. H. Edwards, *Motor Learning and Control: From Theory to Practice.* Cengage Learning, 2010.

[9] M. Mulder, D. A. Abbink, and E. R. Boer, "Sharing Control With Haptics: Seamless Driver Support From Manual to Automatic Control," *Human Factors: The Journal of the Human Factors and Ergonomics Society*, 2012.

[10] D. A. Abbink, M. Mulder, and E. R. Boer, "Haptic shared control: smoothly shifting control authority?," *Cognition, Technology & Work*, pp. 1–10, 2012.

[11] M. K. O'Malley, A. Gupta, M. Gen, and Y. Li, "Shared control in haptic systems for performance enhancement and training," *TRANSACTIONS-AMERICAN SOCIETY OF MECHANICAL ENGINEERS JOURNAL OF DYNAMIC SYSTEMS MEASUREMENT AND CONTROL*, vol. 128, no. 1, p. 75, 2006.

[12] J. Rasmussen, "Skills, rules, and knowledge; signals, signs, and symbols, and other distinctions in human performance models.," *Systems, Man and Cybernetics, IEEE Transactions on*, vol. 13, no. 3, pp. 257–266, 1983.

[13] K. Furukawa, S. Igarashi, K. Ueno, T. Ozaki, S. Morita, N. Tamagawa, T. Okuyama, and I. Kobayashi, "Modeling human skill in bayesian network," *Linkoping Electronic Articles in Computer and Information Science*, vol. 7, p. 012, 2002.

[14] B. M. Huey, S. Baron, and D. S. Kruser, *Quantitative modeling of human performance in complex, dynamic systems*. National Academies Press, 1990.

[15] S. Suzuki, H. Kobayashi, and F. Harashima, "Brain monitoring analysis of skill on voluntary motion," in *Control, Automation and Systems, 2007. ICCAS'07. International Conference on*, 2007, pp. 1178–1182.

[16] S. Suzuki and F. Harashima, "Skill Evaluation from Observation of Discrete Hand Movements during Console Operation," *Journal of Robotics*, vol. 2010, pp. 1–13, 2010.

[17] S. Suzuki and F. Harashima, "Analysis of machine operation skills using hand discrete movement," in *Emerging Technologies and Factory Automation, 2008. ETFA 2008. IEEE International Conference on*, 2008, pp. 2824–2829.

[18] P. M. Fitts and M. I. Posner, "Human performance," 1967.

[19] J. Kolodko, S. Suzuki, and F. Harashima, "Eye-gaze tracking: an approach to pupil tracking targeted to FPGAs," in *Intelligent Robots and Systems, 2005.(IROS 2005). 2005 IEEE/RSJ International Conference on*, 2005, pp. 344–349.

[20] T. Parthornratt, R. Parkin, and M. Jackson, "Human performance index– a generic performance indicator," *Proceedings of the Institution of Mechanical Engineers, Part I: Journal of Systems and Control Engineering*, vol. 225, no. 6, pp. 721–734, 2011.

[21] K. Samarnggoon and H. Yu, "Real time Virtual Simulation of an Underactuacted Pendulum-Driven Capsule System," in *Control (CONTROL), 2012 UKACC International Conference on*, Cardiff, 2012, vol. 2012, pp. 568–573.

[22] H. Yu, Y. Liu, and T. Yang, "Closed-loop tracking control of a pendulum-driven cart-pole underactuated system," *Proceedings of the Institution of Mechanical Engineers, Part I: Journal of Systems and Control Engineering*, vol. 222, no. 2, pp. 109–125, 2008.

[23] Y. Liu and H. Yu, "A survey of underactuated mechanical systems," *IET Control Theory and Applications*, vol. 7, no. 7, pp. 1–15, Feb. 2013.

[24] M. W. Spong, "Underactuated mechanical systems," in *Control Problems in Robotics and Automation*, Springer, 1998, pp. 135–150.